THE DOME FIRE OBSIDIAN STUDY:

INVESTIGATING THE INTERACTION OF HEAT, HYDRATION, AND GLASS GEOCHEMISTRY

BY

ANASTASIA STEFFEN

B.A., Anthropology, Washington University, 1986
M.A., Anthropology, University of New Mexico, 1992

DISSERTATION

Submitted in Partial Fulfillment of the
Requirements for the Degree of

Doctor of Philosophy
Anthropology

The University of New Mexico
Albuquerque, New Mexico

July, 2005

DEDICATION

This dissertation is dedicated to Fred and Mary Trembour. You are my role models.

ACKNOWLEDGEMENTS

First, I acknowledge the strong intellectual guidance and partnership offered by my dissertation chair, Dr. Ann Ramenofsky. I thank the members of my committee, Lawrence Straus, Bruce Huckell, Ed Bedrick, and, especially, Richard Hughes, for all their contributions throughout this process. For their help from the Anthropology Department office, I thank Erika Gerety, Mary Rhodes, Carla Sarracino, and Yolanda Nieto.

The fieldwork and labwork phases of this project would not have been possible without the help of Shawn Penman, Rachel Steffen, Phil LeTourneau, Ethan Geidraitus, Katerina Vaitkus, Gerry Raymond, and Tod Roberts. John Phillips provided excellent field and specimen photography. Help with GIS, software, and facilities was provided by Ken Cannon and Ralph Hartley of the Midwest Archaeological Center, Matt Dooley, and Jerry Gleason of the Bio-Optics Lab at U. of O. in Eugene.

As with any interdisciplinary project, I benefited from technical assistance from individuals from a broad range of disciplines. I thank Richard Hughes (Geochemical Research Laboratory, Jamie Gardner and Fraser Goff (Los Alamos National Laboratory), Gordon Moore and Shawn Whaley (Arizona State University), Nelia Dunbar and Jim Barker (New Mexico Tech), H. R. Westrich and Ron Loehman (Sandia National Laboratory), Are Tsirk, and Robert L. Smith. Here at UNM, numerous people at the Earth and Planetary Sciences Department have been invaluable, especially Mike Splide, Gary Smith, John Husler, Chip Shearer, and Tobias Fischer. None of these generous folks are responsible for any errors I've made in my interpretations or applications.

In the realm of obsidian and fire effects, several individuals have been a source of encouragement, inspiration and assistance, including Yuichi Nakazawa, Krista Deal, Tom Origer, Janine Loyd, Craig Skinner, Carol Winkler, and Ron Towner. Of course, everything I know about lithic technology I learned from Peter Ainsworth. Most of all, I thank Fred Trembour for his thoughtful advice, creativity, and willingness to nurture my interest in obsidian and heat. And I thank Mary Trembour for her support in Fred's name, as well as the extraordinary spirit she has shared with me and my tribe.

This project was made possible by funding from the Canon National Parks Science Scholars Program. Without the generous support of this fellowship program, I would never have been able to conduct the diverse analyses I was able to pursue. Thank you to Gary Machlis for leading this program. Additional funding and logistical support was provided by the Santa Fe National Forest (SFNF) Heritage Resources Program (which funded the pilot project), the SFNF Jemez District, the Valles Caldera National Preserve, Sigma Xi, and the Student Research Allocations Committee of the Graduate and Professional Student Association at UNM. Thank you to Mike Bremer, Rita Skinner, Phil Neff, John Peterson, Rory Gauthier, Cynthia Herhahn, Kay Beeley, Mike Elliott, and Steve Chomko.

It takes a village to complete a dissertation and I am deeply grateful to all of my friends and family who have given me support along the way. Ann Ramenofsky has been more than just an advisor to me: she, along with her family Tom, Ben, and Kate, have provided fellowship and a sense of home for me along this long journey. Shawn Penman, Beth Bagwell, Beth Mohr, Phil LeTourneau, Jeremy Kulisheck, Kathy Helton, Jill Hazelton, and Rachel and Lora Steffen all helped to keep me going and in good cheer.

Surely the best part of a hard project is to look back on it fondly. With Nathan, my partner in patience and joy, I look forward to now just looking back fondly as we get on with the rest of life.

THE DOME FIRE OBSIDIAN STUDY:

INVESTIGATING THE INTERACTION OF HEAT, HYDRATION, AND GLASS GEOCHEMISTRY

BY

ANASTASIA STEFFEN

ABSTRACT OF DISSERTATION

Submitted in Partial Fulfillment of the
Requirements for the Degree of

Doctor of Philosophy
Anthropology

The University of New Mexico
Albuquerque, New Mexico

July, 2005

THE DOME FIRE OBSIDIAN STUDY:
INVESTIGATING THE INTERACTION OF HEAT,
HYDRATION, AND GLASS GEOCHEMISTRY

by

Anastasia Steffen
B.A., Anthropology, Washington University, 1986
M.A., Anthropology, University of New Mexico, 1992
Ph.D., Anthropology, University of New Mexico, 2005

ABSTRACT

This research integrates the analysis of obsidian geochemistry with investigation of the effects of forest fires on obsidian artifacts in surface assemblages. The first component of this project investigated the nature of heat altered obsidian at a prehistoric quarry site following the 1996 Dome Fire in the Jemez Mountains of northern New Mexico. Burned artifacts were examined to discern indicators of heat alteration in obsidian and to measure the impact of the fire on obsidian hydration (OH) bands. Descriptive categories developed to encompass a range of fire effects are provided here as a tool for identifying heat-altered obsidian in archaeological contexts. Measurement of obsidian hydration in artifacts collected from across the site demonstrate substantial loss and alteration of OH information, as well as positive correlation of OH loss/alteration with degree of burn severity.

The second component of the project investigated the role of obsidian geochemistry in fire effects, especially obsidian vesiculation. Intrasource and intersource geochemical analyses of obsidian trace element composition were integrated with analysis of major/minor elements, and with analysis of the water content as a volatile

constituent. Results show elemental homogeneity among the Dome area Obsidian Ridge/Rabbit Mountain obsidians of the Cerro Toledo Rhyolite (CTR), demonstrate a cogenic relationship among geographically separate CTR deposits, and confirm that these obsidians are chemical distinct from Valles Rhyolite (VR) glasses at Cerro del Medio. Analyses of obsidian water content using loss-on-ignition (LOI) and infrared spectroscopy (FTIR) demonstrate the efficacy of both techniques for archaeological applications. Water contents were found to be low in VR samples, but high and variable in CTR samples. These results accord with the expectation of higher and more variable water contents in glasses from pyroclastic deposits, as compared with lower water contents in obsidians from extrusive volcanic contexts. This study provides a new example in which obsidian water content is high and variable within a single chemical type. This example provides support for the inclusion of water content as a compositional variable in the OH dating model and demonstrates the utility of integrating analysis of both elemental and volatile composition into archaeological practices of obsidian geochemical analyses.

TABLE OF CONTENTS

LIST OF FIGURES xv
LIST OF TABLES xix
CHAPTER 1 INTRODUCTION 1
1.1. Organizational Structure of the Dissertation 8
1.2. Hypotheses and Analytical Methods 8
CHAPTER 2 BACKGROUND 13
2.1. Study Area 13
Study Area: Setting 13
Study Area: Geology 14
Study Area: Geology 15
Cerro Toledo Rhyolite in the Dome Area 18
Cerro Toledo Rhyolite as a Larger Geologic Unit 19
Study Area: Archaeology at Capulin Quarry and the Dome Obsidian Quarries 21
Study Area: Environment and Fire History 25
2.2. Research Context 28
History of Obsidian Fire Effects Research in Archaeology 28
Issues in Obsidian Fire Effects Research in Archaeology 29
Types of Archaeological Studies of Forest Fire Effects on Obsidian 31
Review of Previous Results in Archaeological Obsidian Fire Effects Studies 32
The Current Study in Research Context 40
CHAPTER 3 OBSIDIAN FIRE EFFECTS 42
3.1. Methods 47
Collection of specimens within the forest fire area 47
1. Sampling between burned and unburned area of site 47
2. Sampling among vesiculation clusters 48
3. Sampling within area with dispersed moderate and severe burning 49
Examination of obsidian fire effects 51
Reconnaissance for fire effects outside Capulin Quarry 52
3.2. Descriptions of Macroscopic Obsidian Fire Effects 55

Fire effects descriptive categories 56
Matte finish 57
Surface sheen 58
Additive sheen 58
Altered sheen 60
Fine Crazing 61
Deep Surface Cracking 64
Vesiculation 66
Incipient bubbles 69
Fire fracture 72
Other obsidian fire effects 76
Discussion of obsidian fire effects 79
CHAPTER 4 OBSIDIAN HYDRATION ANALYSES 81
4.1. Assemblage-Scale Analysis of Obsidian Hydration in Artifacts from Areas of Capulin Quarry with Variable Burn Severity 82
Obsidian Hydration Analysis Methods Used 82
Selection of Specimens 83
Obsidian Hydration Analysis of the Burned Assemblage 84
4.2. Specimen-Scale Analysis of Obsidian Hydration Analysis of Five Individual Burned Specimens from Capulin Quarry 90
Intensive obsidian hydration analysis 91
Specimen 1691-54. 94
Specimen 1691-55. 95
Specimen 1691-53. 96
Discussion of Specimens 1691-53, 54, & 55. 97
Specimen 1691-02. 99
Discussion of Sections 4.1 and 4.2 104
4.3. Analysis of Fire Effects and Obsidian Hydration in Artifacts from Controlled Sample Unit SU1 105
Sample Unit Collection Strategy 107
Examination of Fire Effects in Collected Artifacts 107

Obsidian Hydration Analysis of SU1 Specimens 111
Results of OH Analysis in SU1 Specimens 115
Discussion of OH Analysis Results 119
CHAPTER 5 GLASS-WATER INTERACTIONS 121
5.1 Obsidian Composition 124
Composition in the Development of Obsidian Hydration Dating 125
5.2. Challenges to OHD Methodology 129
Implications for the Methodology of OH Dating 130
5.3. Value of Measuring Water Content 131
How Does Water Vary In Obsidian? 134
Obsidian Water Content and Vesiculation 137
5.4. Cerro Toledo Rhyolite as a Case Study in Obsidian Water Content 139
CHAPTER 6 ELEMENTAL COMPOSITION ANALYSES 143
6.1. Trace Element Geological Baseline ED-XRF Analysis for Cerro Toledo—Dome (CTD) Obsidian 145
Dome Area Geological Context: "Obsidian Ridge" & the Cerro Toledo Rhyolite. 145
Trace Element Compositional Analysis 149
Geological Sampling for Elemental Composition Analyses within CTD 150
Selection of samples 153
Analytical Methods: ED-XRF Elemental Composition Analysis 155
Results: Intrasource ED-XRF Trace Element Composition Analysis for CTR-Dome 156
6.2. Intrasource WD-XRF Analyses of Major and Minor Elemental Composition for Cerro Toledo–Dome (CTD) Obsidians 161
Analytical Methods: WD-XRF Elemental Composition Analysis & Iron Analysis 161
Selection of samples 164
Results: Intrasource WD-XRF Element Composition Analysis for CTR-Dome 164
Discussion of WD-XRF trace element results 165
Discussion of WD-XRF minor and major element results 168
Discussion of WD-XRF trace vs. minor and major element results 172

6.3. Intersource WD-XRF Analyses (& ED-XRF) of Elemental Composition for Cerro Toledo Dome (CTD), Cerro Toledo Northeast (CTN), and Cerro Del Medio (CDM) Obsidians 175
Selection of samples 177
Results: Intersource WD-XRF and ED-XRF Composition Analyses for CTD, CTN, and CDM Obsidians 181
Discussion of Results: Intersource Composition Analyses for CTD, CTN, and CDM 184
1. Are obsidians from CTR (CTD and CTN) sufficiently distinguishable from CDM obsidians? 184
2. Are obsidians in the Cerro Toledo Rhyolite geological unit (CTD & CTN) compositionally similar? 187
Trace Elements Within the Cerro Toledo Rhyolites (CTD & CTN) 187
Major and Minor Elements Within the Cerro Toledo Rhyolites (CTD & CTN) 192
Trace Elements Within the Valles Rhyolite (CDM) 194
3. Are CTD obsidians more or less variable in composition than the comparison obsidians? 196
Chapter Summary 199
CHAPTER 7 WATER CONTENT ANALYSES: LOI and FTIR METHODS 200
7.1. Measuring water content in rhyolite glass 200
Archaeological analyses of obsidian water content 202
7.2. Loss-on-ignition (LOI) Analysis Methods 204
7.3. Fourier Transform Infra-Red Spectroscopy (FTIR) Analysis Methods 207
FTIR analysis of calibration standards and obsidian "unknowns" 208
Discussion of FTIR water content results for calibration standards 225
CHAPTER 8 WATER CONTENT ANALYSES: RESULTS FOR JEMEZ OBSIDIANS 227
8.1. LOI & FTIR Analysis of Water Content in Obsidian from CTD, CTN & CDM 227
Selection of samples 227
Results: FTIR & LOI Analyses of Water in Obsidian from CTD, CTN, & CDM.. 229
LOI Results and Discussion 230

FTIR Results and Discussion 238
8.2. Comparison of LOI and FTIR Analyses of Water Content in Obsidian to Assess Accuracy of LOI Analysis..... 242
8.3. Conclusions: Comparison of the LOI and FTIR Techniques for Archaeological Applications 246
8.4. Conclusions: Interpreting the LOI and FTIR Analyses of Water Content..... 247
CHAPTER 9 CONCLUSIONS 253
Summary of Research and Results..... 253
Applications and Implications..... 258
Fire and the Formation of the Archaeological Record 258
Fire and the Management of Cultural Resources 260
The Validity of Archaeological Methods of Obsidian Analysis 265
LIST OF APPENDICES..... 269
APPENDIX A. Unpublished results of laboratory heating of hydrated obsidian, by Fred W. Trembour..... 270
APPENDIX B. Fractography analysis of fire fractures, by Are Tsirk..... 278
APPENDIX C. Unpublished data on experimental vesiculation of artificially hydrated silica glass; experiments conducted by H. R. Westrich, Sandia National Laboratory..... 326
APPENDIX D. ED-XRF Analyses: Original Letter Reports and Data from R. E. Hughes, Geochemical Laboratory..... 333
APPENDIX E. Experimental Heating of Obsidian with Known Water Contents 352
APPENDIX F. ED-XRF and WD-XRF Tables: Elemental Composition Data by Specimen..... 355
REFERENCES 367

LIST OF FIGURES

Figure 1-1. Vesiculated obsidian nodule 2
Figure 2-1. Location Maps of Jemez Mountains in New Mexico. 14
Figure 2-2. Jemez Lineament and Miocene to Holocene volcanic fields (from Ander et al. 1981). 15
Figure 2-3. Geology of the Valles caldera, from Smith, Bailey, and Ross (1970) "Geologic Map of the Jemez Mountains, New Mexico". 16
Figure 2-4. Geology of the obsidian-bearing deposits in the Dome area, from Goff, Gardner, and Valentine (1990) "Geology of St. Peter's Dome area, Jemez Mountains, New Mexico". 17
Figure 2-5. CTR deposits shown on shaded relief plotted from 10m DEM.. 20
Figure 2-6. Obsidian quarries and lithic scatters recorded by the SFNF in the Dome area demonstrating overlap with exposures of Cerro Toledo Rhyolite (Qct/Qctt from Smith et al. 1970) 22
Figure 2-7. Larson et al. (1988:142, Figure 12.2) site map for AR 03-10-03-1691 (Capulin Quarry) showing their recommendations for site preservation based on results of subsurface testing. 24
Figure 2-8. Fire history of large fires in the Jemez Mountains, 1950s through 2004; data from SFNF fire GIS layer. 26
Figure 2-9. Fire severity map of the Dome Fire (data reflects combined SFNF and BNM post-fire interpretation). 27
Figure 3-1. Partially vesiculated obsidian flakes from Capulin Quarry (Specimens 1691-02 and 1691-51, dorsal surface; inset box is ventral surface of 1691-51) 42
Figure 3-2. Capulin Quarry following the Dome Fire. 43
Figure 3-3. Vesiculation Cluster 3 around partially burned stump; box in lower right is a closer view of vesiculated pieces shown in upper left (October 1997)..... 44
Figure 3-4. Capulin Quarry Site Map. 46
Figure 3-5. G. Raymond recording artifact attributes and position within 50 cm-x-50 cm sample unit at Cluster 3 (red-and-white grid square in photo center)..... 49
Figure 3-6. View SW to NE across Sample Unit 1 (SU1) 5 m-x-5 m collection unit; orange string lines mark 1 m-x-1 m grid (November 2001). 50

Figure 3-7. Collection of artifact and non-artifact obsidian specimens within a 1 m-x-1 m unit in SU1 (Subunit H1). 50
Figure 3-8. Characteristics of burning, vegetation, recent disturbances, and distribution of tuff blocks and gravel were sketched prior to collection within 1 m-x-1 m units in SU1. 51
Figure 3-9. Campfire outside the Dome Fire burn area where vesiculated obsidian has been found in this and a nearby campfire ring consistently each time monitored between 1996 and 2004..... 53
Figure 3-10. Additive surface sheen 59
Figure 3-11. Altered surface sheen. 60
Figure 3-12. Altered surface sheen as apparent on non-artifact specimen OR-SH501 from Obsidian Ridge Quarry AR 03-10-03-2360 (LA82485). 61
Figure 3-13. Fine crazing. 62
Figure 3-14. Fine crazing on dorsal surface of the partially vesiculated flake specimen 1691-02. 63
Figure 3-15. Fine crazing with two very different appearances. 63
Figure 3-16. Deep surface cracking on specimen GS02-11. 64
Figure 3-17. Deep surface cracking. 65
Figure 3-18. Deep surface cracking / stretched crazing. 66
Figure 3-19. Complete vesiculation 66
Figure 3-20. Vesiculated flake 67
Figure 3-21. Vesiculation: fully and partially vesiculated artifacts. 68
Figure 3-22. Vesiculation as shown in SEM secondary-electron images of vesiculated obsidian 69
Figure 3-23. Incipient bubbles in specimen 1691-53 70
Figure 3-24. Incipient bubbles 71
Figure 3-25. Incipient bubbles 71
Figure 3-26. Fire fracture 72
Figure 3-27. Fire fracture. 74
Figure 3-28. Dissimilarity in obsidian color and translucency in specimen 1691-02. 77
Figure 3-29. Blistered surface on a non-artifact nodule from Capulin Quarry 79

Figure 4-1. Proportion of intact/measurable hydration bands in unburned and burned areas at Capulin Quarry..... 86
Figure 4-2. Distribution of intact/measurable hydration bands by degree of burning..... 86
Figure 4-3. Distribution of diffuse hydration bands by degree of burning..... 88
Figure 4-4. Five partially vesiculated flakes: Specimens 1691-51, 52, 53, 54, and 55 92
Figure 4-5. Ventral and dorsal views of specimen 1691-02 with OH measurements 100
Figure 4-6. Hydration bands on heat-caused vesicles on specimen 1691-02 102
Figure 4-7. Sample Unit 1 is a 5 m-x-5 m grid with 25 1 m-x-1 m subunits..... 108
Figure 4-8. Relative frequencies of fire effects observed in SU1 artifacts..... 110
Figure 4-9. Proportion of intact/measurable hydration bands in SU1 artifacts with no visible fire effects (NAFE) and with fire effects..... 116
Figure 4-10. Proportions of intact obsidian hydration (OH), diffuse hydration (DH), and no visible bands (NVB) in SU1 artifacts, comparing between artifacts with and without fire effects. 117
Figure 4-11. Proportions of intact obsidian hydration (OH), diffuse hydration (DH), and no visible bands (NVB) in SU1 artifacts, comparing among NAFE artifacts and those with crazing and vesiculation..... 118
Figure 4-12. Proportions of intact OH, diffuse hydration (DH), and no visible bands (NVB) in crazed and vesiculated artifacts from SU1..... 119
Figure 6-1. Smith, Bailey, and Ross (1970) map of Dome area geological units. 147
Figure 6-2. CTD sample locations included in this study, shown on the Goff et al. (1990) map of Dome area geological units (not to original scale) 148
Figure 6-3. Area map of CTD geological sampling locations..... 151
Figure 6-4. XY plot of oxidation states of iron (Fe_2O_3 and FeO) in CTD samples..... 171
Figure 6-5. Map of CTD, CTN, and CDM geological sampling locations plotted on 10m DEM shaded-relief map. 176
Figure 6-6. Map of CTN and CDM geological sampling locations plotted on 10m DEM shaded-relief map. 180
Figure 6-7. Bivariate plots of XRF data for trace elements Y / Nb, Zr / Rb, & Zn / Ti. 185
Figure 6-8. XYZ plots of XRF trace elements Ti / Zn / Zr and Rb / Nb / Y. 186

Figure 6-9. Geology of the Toledo Embayment area, from Gardner & Goff (1996:227). 190
Figure 6-10. CTN sampling locations with outlines from the Gardner & Goff (1996) map units. 190
Figure 6-11. WD-XRF major and minor elements Na / Ca and Total Iron / Mn plotted on XY graphs. 193
Figure 6-12. Map of Cerro del Medio showing J. Gardner's preliminary geological units on 10m DEM shaded relief. 194
Figure 6-13. XY plot of Fe_2O_3 and FeO values for CDM, CTD and CTN/CTNo samples (data from titration analysis). 197
Figure 7-1. Comparison of FTIR spectra, stacked to show peaks. 214
Figure 7-2. Comparison of FTIR spectra showing actual absorbances. 214
Figure 7-3. Illustration of peak measurement using 0.65% & 2.71% standards. 216
Figure 7-4. Details of calculation method for measuring peak height minus background, using 2.71% calibration standard at 5200cm^{-1} H_2O peak as example..... 218
Figure 7-5. Comparison of OH and H_2O concentrations in standards with differing total water content. 221
Figure 7-6. Comparison of FTIR results and expected values for standards..... 225
Figure 8-1. Mean plots and scatter plots of total LOI measures of 55 obsidian samples from CTD, CDM, CTN, and CTNo 231
Figure 8-2. Histograms of total LOI, H2O-, H2O+ measures of 55 obsidian samples by source: CTD, CDM, CTN, and CTNo 232
Figure 8-3. Histogram of total LOI for CTD samples; created with 15 classes to accentuate possible bimodality. 236
Figure 8-4. Scatter plot of total FTIR measures of 20 obsidian samples from CTD, CDM, CTN, and CTNo. 241
Figure 8-5. Comparison of LOI and FTIR water content results by individual sample 243
Figure 8-6. Comparison of LOI and FTIR water content results by individual sample showing source and obsidian color (brown glasses shown in red). 244

LIST OF TABLES

Table 2-1. Geological units mentioned in the text. 18
Table 2-2. Obsidian hydration analysis of obsidian artifacts burned in the Henry Fire (from Origer 1996:81-82, compiled from Tables 28-30). 33
Table 2-3. Trembour (1990:175) results of laboratory heating of hydrated obsidian. 35
Table 2-4. Unpublished results of laboratory heating of hydrated obsidian by Trembour. 36
Table 2-5. Skinner et al. (1997:12, Table 2) results of laboratory heating of hydrated obsidian 37
Table 2-6. Effects observed on obsidian specimens in Buenger (2003) muffle furnace laboratory heating experiments. 39
Table 2-7. Research questions posed by Skinner et al. (1997:14). 40
Table 4-1. Obsidian hydration analysis of artifacts at Capulin Quarry collected from areas with differing degrees of burn severity. 84
Table 4-2. Obsidian hydration analysis of five partially vesiculated flakes from Capulin Quarry. 93
Table 4-3. Hydration band measurements in multiple cuts on Specimen 1691-02. 101
Table 4-4. Items collected from the eight subunits in SU1 109
Table 4-5. Obsidian hydration analysis of 87 SU1 artifacts and added artifacts. 112
Table 5-1. Obsidian elemental composition as weight % oxide (Macdonald et al. 1992). 124
Table 5-2. Relationship of water content and vesiculation in artificially hydrated silicate glasses 138
Table 5-3. Obsidian water content values reported in the literature for New Mexico obsidians 142
Table 6-1. Elemental compositional analyses and samples used. 144
Table 6-2. Intrasource geological sampling locations: Cerro Toledo—Dome (CTD). .. 152
Table 6-3. Summary of mean ED-XRF values for each element across all CTD samples (not differentiating among locations). 157
Table 6-4. ED-XRF trace element summary values for CTD samples by location. 158
Table 6-5. Constituents measured in the whole rock and iron analyses. 163

Table 6-6. Grouped mean WD-XRF values for trace elements across all CTD samples (not differentiating among locations). 165
Table 6-7. WD-XRF trace element values for CTD samples by location. 167
Table 6-8. Grouped mean WD-XRF values for major and minor elements across all CTD samples (not differentiating among locations). 168
Table 6-9. WD-XRF major and minor element values for CTD samples by location. .. 169
Table 6-10. Comparison of WD-XRF and ED-XRF analyses results for CTD samples. 173
Table 6-11. Intersource Comparison: Geological samples from three different geological contexts used for multiple XRF compositional analyses 177
Table 6-12. Intersource Geological Sampling Locations: Cerro Toledo—Northeast (CTN), and Cerro del Medio (CDM) [see Table 6-2 for CTD locations]..... 179
Table 6-13. ED-XRF data for all individual specimens from CDM and CTN (see notes at bottom for id of mapped geological unit in far right column). 182
Table 6-14. ED-XRF summary values for all three source areas (CTD, CTN, CDM). 182
Table 6-15. WD-XRF trace element summary values for all three source areas (CTD, CTN, CDM). 183
Table 6-16. WD-XRF minor and major element summary values for all three source areas (CTD, CTN, CDM) 183
Table 6-17. WD-XRF and ED-XRF trace elements in all CTN samples. CTN is not split into two groups..... 188
Table 6-18. WD-XRF and ED-XRF trace element summary values for all three source areas 188
Table 6-19. WD-XRF minor and major element means for all three source areas (CTD, CTN, CDM) 192
Table 6-20. Major and minor elements measured by WD-XRF. Data includes only sample size, means, and CV values for CDM, CTD, and CTN (from Table 6-16). 196
Table 6-21. CV and means for CTD and CDM samples with and without mahogany specimens. 198

Table 7-1. Identification of wavenumber and water species investigated by transmission FTIR in this study (table follows King et al. 2002:1084, Table 4) 215
Table 7-2. Calculation method used for measuring FTIR peak heights. 217
Table 7-3. Averaged FTIR results and calculation of water content for seven standards. 219
Table 7-4. Comparison of FTIR outcomes with differing values of density (ρ) 220
Table 7-5. Un-averaged FTIR data for calibration standards 222
Table 7-6. Difference between FTIR results and expected values for calibration standards..... 225
Table 8-1. Samples used in LOI and FTIR analyses. 228
Table 8-2. Summary of LOI measures of H_2O-, H_2O+, and Total LOI for 55 obsidian samples from CTD, CDM, and CTN. 229
Table 8-3. Individual specimen LOI measures of H_2O-, H_2O+, and Total LOI for CTD, CTN, and CTN samples (plus one each samples from outside sources). 230
Table 8-4. Comparison of total LOI means among differing combinations of sources using Kruskal-Wallis, F-test, and T-test statistics..... 234
Table 8-5. ANOVA of total LOI means for CTD, CDM, CTN, and CTNo (n=55)..... 234
Table 8-6. Post-hoc multiple comparison for total LOI among CTD, CDM, CTN, and CTNo (n=55) using Bonferroni adjustment. 234
Table 8-7. Summary of LOI measures of H_2O^-, H_2O^+, and Total LOI for 52 obsidian samples from CTD, CDM, and CTN; specimens CDM-304, GS7B-1, and GS8-1 are excluded 237
Table 8-8. Water content as measured by FTIR and LOI for 20 CTD, CTN, and CDM obsidian samples 239
Table 8-9. Means of FTIR measures of H_2O and OH for 20 CTD, CDM, and CTN obsidian samples;(ε) from Ihinger and Stolper 1994. 240
Table 8-10. Summary of FTIR measures of H_2O and OH for 20 CTD, CDM, and CTN obsidian samples; (ε) from Ihinger and Stolper 1994. 240
Table 8-11. Comparison of Mean Total Water Content. 242
Table 8-12. Individual FTIR measures (i.e. replicated measures at multiple locations on an individual specimen);. 250

Table C-1. Calibration standards: Average values for all 9 elements measured on EPMA. 329
Table C-2. Westrich data as scanned 10/2004 330
Table E-1. Description of heated specimens including LOI water content and results .. 354
Table E 2. Additional composition data on heated specimens 354
Table F- 1. 1998 Analysis: ED-XRF ppm values for trace elements and element weight percent values for K and Ca, CTD only (data by individual specimen). 356
Table F-2. 2004 Analysis: ED-XRF ppm values for trace elements and element weight percent values for K and Ca, includes all three source areas: CTD, CTN, and CDM (data by individual specimen) [shaded rows are excluded samples]. .. 357
Table F-3. WD-XRF ppm values for trace elements (data by individual specimen). 360
Table F-4. WD-XRF oxide weight percent values for major and minor elements (data by individual specimen). 362
Table F-5. WD-XRF computed element weight percent and ppm values for selected major and minor elements (data by specimen). 364
Table F-6. WD-XRF summary of means for computed element weight % and ppm values for selected major and minor elements. 366

CHAPTER 1
INTRODUCTION

For ten days in April and May of 1996, the forest fire known as the Dome Fire burned out of control in the Jemez Mountains of northern New Mexico. The severity of the fire was intensified by serious drought conditions and high winds; by the time this major forest fire was brought under control, over 16,000 acres of Ponderosa pine and mixed-conifer forest had burned on the Santa Fe National Forest and in the adjacent Bandelier National Monument. During routine archaeological survey by SFNF archaeologists following the fire, a startling phenomenon was discovered at Capulin Quarry (LA23961), one of the numerous obsidian procurement sites that populate this obsidian-rich landscape: pieces of obsidian were burned into unrecognizable frothy masses of bubbled glass (Figure 1-1). Our surprise at encountering this extraordinary "vesiculated" obsidian and curiosity about the potential causes of this remarkable transformation of the natural glass prompted the questions that inspired this dissertation. How hot must a fire burn to cause this response? Is the damage at Capulin Quarry as unusual as it initially appeared? If so, why did it occur at this location during this fire? If not unusual, why is obsidian vesiculation not well known to archaeologists? What was responsible for the variable fire effects observed on obsidian across the site? What effects were there on the obsidian hydration bands of artifacts burned during the forest fire? How should archaeologists interpret such an extreme impact to this assemblage, and what lessons could be learned to better preserve the archaeological record?

These questions about the Dome Fire and the obsidian fire effects observed at Capulin Quarry have a number of broader implications for our understanding of the formation of the archaeological record, for the validity of archaeological methods of obsidian analysis, and for the management of cultural resources. This research addresses these three areas by exploring variation in two realms: 1) in macroscopic and microscopic fire effects on obsidian artifacts, and 2) in the composition of obsidian in geological deposits in the Dome area. The contemporary forest fire and its consequences are used as a case study of potential fire alteration occurring in both modern and past events of heat exposure.

Figure 1-1. Vesiculated obsidian nodule

This research seeks to understand the role of forest fires as an agency of change in the formation of the archaeological record. Forest fires are a component of the forest ecology in which prehistoric quarry assemblages become archeological deposits. When fires alter artifacts within these deposits, this heat response is a component of the general glass-environment interaction in which obsidian hydration occurs. I use the circumstance of extreme heat effects during a forest fire as an opportunity to investigate the conditions of water absorption exploited for chronometric goals in the obsidian hydration dating method. In this sense, the extreme case offers the occasion to reconsider the "normal" in both the processes and assumptions of obsidian hydration as an archaeological dating method.

First, the unexpected appearance of vesiculated obsidian is a reminder that glass is not an inert substance, but rather a material in dynamic interaction with the environment. Second, the potential for loss of hydration rinds in artifacts exposed to the heat of a forest fire demonstrates that glass hydration is not the unidirectional uptake of water, but rather the net balance attained in an on-going loss/gain interaction occurring at artifact surfaces (e.g., Ambrose 1998). Finally, variation in fire effects observed across the expanse of the forest fire raises questions about the assumption of compositional homogeneity across the entirety of these obsidian-bearing geological deposits conventionally understood to be a single geochemical source. This study takes a cue from each of these considerations, with a research design constructed to address various assumptions integral to the

methodology of archaeological obsidian analyses. This research has the following objectives, with the details of each objective explained further in this and later chapters:

1. Identify how archaeologists may recognize fire effects on obsidian artifacts by describing the variability in fire effects observed at Capulin Quarry.
2. Evaluate the impact of forest fires for obsidian hydration dating by examining the presence and characteristics of hydration rinds in burned artifacts associated with greater and lesser degrees of burn severity across Capulin Quarry.
3. Consider the role of obsidian elemental composition for variable fire effects, especially vesiculation, by measuring major, minor, and trace element composition within the Cerro Toledo Rhyolite obsidian-bearing deposits burned during the Dome fire, and then comparing elemental composition to nearby obsidian sources to assess intrasource vs. intersource compositional variation.
4. Develop an appropriate archaeological methodology for measuring water in obsidian by testing alternative techniques for determining obsidian water content.
5. Determine the variation of volatile composition within this geochemical source by measuring obsidian water content within the Cerro Toledo Rhyolite and comparing to water content measured in nearby obsidian sources.

These five objectives together contribute to the broader goals and applications of this research: 1) to understand how fires alter archaeological assemblages and the obsidian hydration chronometric information contained in the artifacts, 2) to provide baseline information needed to better preserve these assemblages, and 3) to potentially improve an important chronometric technique by enhancing our understanding of the role of glass composition in the obsidian hydration process.

These objectives address two broad problem areas: the description and analysis of fire effects on obsidian, and the analysis of obsidian composition. The first is a topic that has only recently received focused attention in the archaeological community. Contemporary archaeological fire research began with the 1977 La Mesa Fire which occurred in Bandelier National Monument immediately adjacent to the area burned in the 1996 Dome Fire. La Mesa was the first forest fire in which systematic post-fire archaeological investigations were conducted (Traylor et al. 1979, republished in 1990), including the first in-depth investigation of fire effects on obsidian (Trembour 1979,

1990). Little additional research was conducted on the topic until the late 1980s and early 1990s, when an increase in the number, size, and severity of forest fires throughout the western United States, as well as growth in the use of controlled forest fires, prompted a sharp increase in concern by federal cultural resource managers about how natural and prescribed fires affected archaeological assemblages in western forests, where geological obsidian sources occur and where obsidian artifacts are a substantial component of archaeological assemblages. The focus of this research is the potential of fire to affect hydrated artifact surfaces and the implications for obsidian hydration dating (OHD).

The relevant connection between fire and obsidian hydration is heat. Since the inception of archaeological interest in OHD, two main factors, among several others, have been known to affect the process of obsidian hydration: temperature and chemical composition of the obsidian (Friedman and Smith 1960). Developing a robust model of obsidian hydration requires an understanding of the differential roles of these factors in affecting the rate at which hydration occurs, and thus how the measured hydration band might be interpreted for archaeological dating (e.g., Ambrose 1976; Ericson and Berger 1976; Ericson et al. 1976; Friedman et al. 1994, 1997; Jackson 1984; Ridings 1991, 1996; Trembour and Friedman 1984). Temperature--usually considered in terms of ambient temperature and effective hydration temperature--has been considered an especially important factor in the process and rate of hydration in the early development (e.g., Friedman and Long 1976; Ericson 1975; Trembour and Friedman 1984) as well as more recent application of OHD (e.g., Ridings 1991, 1996).

Obsidian hydration begins when a fresh surface is created on a piece of obsidian, such as when a flake is removed during core reduction, at which time the glass begins to absorb water gradually. As a dating technique, OHD depends on measurement of the depth of that hydration layer to estimate the interval during which the hydration band (also called the rim or rind) has formed. The technique involves microscopic examination of thin sections removed from the edges of the item, and measurement of the width (i.e., depth, thickness) of the hydration band in microns. On a given item, a wider/deeper band would indicate a longer hydration interval, and thus a longer interval of time since that surface was created. However, high heat has the potential to "reset" the

obsidian hydration clock: when an artifact is subjected to high heat, the band is modified or lost, the estimation of original interval is compromised, and the hydration process again may begin or be renewed on these altered surfaces (Friedman and Smith 1960; Friedman and Trembour 1983; Trembour 1979, 1990; Trembour and Friedman 1984).

In this study, the two broad problem areas, obsidian fire effects and obsidian composition, are linked by the roles of temperature and composition in the obsidian hydration model. Upon discovery of the vesiculated obsidian within the Dome Fire burn area, there were two possibilities to explain this uncommon obsidian fire effect: either the fire burned unusually hot, or the obsidian responded in an unusual manner, or both. In effect, these two possibilities presented alternative hypotheses to be investigated. I chose to focus on the second: the role of the material (glass) in variable and extreme response to the heat of the fire. Examining the role of fire is much more complicated, first because fire is a process that occurs as a series of events, and second because the outcomes of heat exposure can only be understood with sufficient knowledge about the material on which that process acts.

The first step in this study was to conduct a pilot project[1] (Steffen 2002) to determine whether the obsidians in the deposits exposed throughout the Dome area (and burned during the Dome Fire) were homogenous when measured using standard archaeological obsidian sourcing analysis. X-ray fluorescence (ED-XRF) analysis of obsidian samples from several locations indicated that there was no difference in trace element composition in glasses from across the deposit (see Chapter 6), and provided no evidence for intrasource trace or minor element variability that would explain the variation in forest fire effects observed within the Dome Fire (Steffen 2002:169-172). Furthermore, simple preliminary laboratory heating experiments demonstrated that samples having the same trace element profile responded quite differently to heat, with some specimens vesiculating at lower temperatures than others (Steffen 2002:171-173). Clearly, trace element homogeneity did not tell the whole story and some other factor

[1] Obsidian geochemical data from this pilot project (Steffen 2002; originally published in an edited volume of obsidian fire effects articles: Loyd et al. 2002) are included here in Chapter 6. The study also included description of macroscopic fire effects (included here in Chapter 3), investigation of variable effects to obsidian hydration in artifacts at Capulin Quarry (included here in Chapter 4), and preliminary laboratory heat experimentation and investigation of heat effects for x-ray fluorescence (ED-XRF) analysis.

must contribute to vesiculation as a response to extreme heat. I was unable to find studies in the archaeological literature conducted to establish compositional causes of vesiculation or variable fire effects in obsidian artifacts.[2] Instead, the geological literature provided the most likely candidate for a compositional factor capable of lowering the temperature for glass vesiculation: water.

It is well known in igneous petrology and geochemistry that water can lower the temperature at which a solid melts (e.g., Winter 2001:120-126). However, igneous petrology discussions usually focus on water in a melt rather than in the resulting tephra, with little consideration of water extant in a silicate glass like obsidian. The geological literature has an entirely different focus than that needed to immediately answer the question posed here: does the amount of water in obsidian lower the temperature at which vesiculation occurs in response to external heat as from a forest fire? Instead, geochemical discussions of the volatile component (dominated by H_2O and to a lesser degree CO_2) in obsidian composition focus on using investigations of obsidian to infer the amount of water or other fluids or gasses present in magma prior to or during an eruptive event. The details of how water occurs in obsidian are addressed in Chapter 5, but it is important to note here that while the geological literature provides essential information on the composition of natural glasses, primary research was necessary to measure the amount of water in obsidians in the study area and to evaluate the potential for variation in water content in these obsidians prior to determining if variation in water content could be responsible for variation in obsidian response to high heat, especially vesiculation. If water content can vary independently from trace element composition, then this could explain the variation in heat response found in the preliminary heating experiments. A substantial portion of this dissertation pursues this hypothesis.

Trace element profiles are the established means of defining a geochemical source or chemical group (*sensu* Hughes 1998a) for archaeological determination of obsidian artifact provenance. This sourcing is linked directly to the methodology of obsidian hydration dating where hydration rates determined for specific artifacts are then correlated to that geochemical source, and an explicit assumption is made that the trace

[2] The most directly relevant fire effects study is by Nakazawa (1998), but his focus is on alterations in the surface appearance of burned artifacts and chemical aspects of organic material burned with the obsidian.

element grouping also represents major and minor element composition (Friedman et al. 1997: 312-313), and by extension all other compositional variation relevant for hydration rate. If, however, intrasource variation is found in volatile (water) composition, then the link between trace element homogeneity and total obsidian compositional homogeneity may be more complex. The implication for obsidian hydration dating is that if the water content of obsidian affects the rate at which the glass surface hydrates, then variation in water content within a geochemical source would be relevant for establishing rates of hydration for that source, which possibly could be expressed as a range of rates rather than a single rate.

The role of variation in obsidian water content for OHD has been pursued extensively by Stevenson and colleagues (Stevenson et al. 1993, 1996, 1998, 2000, 2001, 2004), who argue that the "intrinsic" water content of obsidian is an integral component of the obsidian hydration process: under similar conditions, water-rich glasses can be expected to hydrate at a faster rate than obsidians with less water (Stevenson et al. 1996:235-236). However, direct measurements of water content in obsidians sampled from across a geological source area has been published in only one case study, at the Coso volcanic field in California (Stevenson et al. 1993). All other studies by Stevenson and colleagues are *applications* of the intrinsic water content approach to analyze specific archaeological assemblages, and these lack investigation of multiple samples across geochemical sources and/or water is measured only indirectly using density determinations. The work conducted at Coso, however, is important because it demonstrates the potential for widely varying water content (0.31 to 2.34 weight % H_2O, as measured by infrared spectroscopy) at obsidian quarries within this volcanic field and at locations previously identified as having homogenous trace element profiles. Without regard to the utility and accuracy of the intrinsic water content approach for determining specific hydration dates, the results of the study at Coso indicate the potential for water content variation to occur within geochemical sources and thus support the investigation of intrasource variation in water content at other obsidian deposits.

1.1. Organizational Structure of the Dissertation

This dissertation integrates an investigation of obsidian compositional variation with obsidian fire effects. These two problem areas are linked by obsidian hydration dating. In the section below, I present the hypotheses to be tested in both problem areas, and introduce the methods used to investigate microscopic and macroscopic fire effects and elemental and water content analyses of obsidian. In the first half of this study (Chapters 2 – 4), macroscopic fire effects are described at the scale of individual specimen and then examined in correlation with microscopic effects on obsidian hydration rinds both at the scale of individual specimens and as distributed across Capulin Quarry in areas of differing burn severity. In the second half of the study (Chapters 5 – 8), I investigate a broad range of compositional variables (trace, minor, and major elements, and water content) in obsidian from geological deposits across the Dome area and from other obsidian sources within the Jemez Mountains. Then I evaluate the role of water content in obsidian as it relates to vesiculation and the OHD method. Included in this investigation is a comparison of alternate techniques for measuring water content in obsidian and an evaluation of their utility for archaeological applications. In the concluding chapter (Chapter 9), I summarize the results obtained for both problem areas, and discuss the relevance of the results for identifying and interpreting fire effects from contemporary and prehistoric fires, for cultural resource management in circumstances where both wildfires and controlled forest fires present challenges to preservation of the archaeological record, and for the role of obsidian water content in compositional analyses and the obsidian hydration dating method.

1.2. Hypotheses and Analytical Methods

In Part I, direct observation of obsidian fire effects (in Chapter 3) provides the descriptive baseline needed to develop and test hypotheses concerning the effects of heat exposure for obsidian hydration in burned artifacts (Chapter 4). As discussed in Chapter 2, there is no pre-existing comprehensive set of systematic categories that can be applied to obsidian artifacts to identify fire effects on artifacts, to make generalizations about the co-occurrence of multiple fire effect attributes, or to identify correlations between the presence of specific fire effect attributes and altered obsidian hydration

bands. Chapter 3 provides this set of descriptive categories, as developed through visual examination of artifacts from Capulin Quarry as well as low and high magnification with optical and scanning electron (SEM) microscopy. Characteristics of fire effect trait categories such as crazing, sheen, and vesiculation are communicated through narrative description and by photographic images. Additional investigation included a fractographic analysis by A. Tsirk of fracture surfaces thought to be associated with fire fracture (Appendix B). The co-occurrence of multiple traits is investigated in Chapter 4, first at the scale of individual specimen, and then at the scale of assemblage by looking at multiple artifacts collected from a 5-x-5-m sample area to determine the frequency and prevalence of combinations of traits.

With visible fire effects organized in descriptive categories, it is possible in Chapter 4 to test hypotheses about the correlation of observable fire effects and heat alteration of obsidian hydration (OH). Obsidian hydration analysis was conducted by T. Origer on artifacts collected across Capulin Quarry. Artifacts for OH analysis were selected from areas where no burning was apparent as well as from a variety of burn contexts within the area of the Dome Fire to reflect differing degrees of burn severity. Artifacts were also collected from within a 5-x-5-m sample area with moderate to severe apparent burn severity and where observed fire effects were widely variable. Artifacts with and without observable fire effects were analyzed for presence and absence of OH as well for evidence of intact but altered OH rims. Origer's analyses provided not only the usual measurement of OH rim width, but also description of aberrations from normal OH appearance as well as photographic documentation of diffuse (altered) rims and OH rims present on vesicles caused by fire exposure.

If visible fire effects co-occur with alteration and loss of hydration bands, then identification of the presence of observable fire effect attributes serves as a reliable indicator of present or past OH alteration, and macroscopic examination of samples proposed for OH dating provides an easy means to assess the potential of heat interference in the chronometric utility of an artifact or assemblage. If OH alteration is found to occur even where no macroscopic effects are present, then the role of heat exposure in altering the hydration information in obsidian assemblages is more difficult to detect.

One goal of this research is to assess the pervasiveness and uniformity of forest fire OH effects in an assemblage. At Capulin Quarry, where a contemporary fire has burned in a mosaic of severity, the potential for variation in OH effects is demonstrated simply by observing differences in burn intensity across the site. However, such direct observation is not possible for prehistoric assemblages and buried assemblages, where a fire history with potentially numerous events cannot be reconstructed. The Dome Fire has provided an opportunity to answer a number of questions with implications for any obsidian-bearing assemblage in a forested area. What proportion of an assemblage has alteration of OH? Does that proportion vary depending on visible contexts of burning? Does the proportion of OH alteration correlate with the pervasiveness of fire effects visible on obsidian artifacts? If the proportion of OH alteration or loss can be estimated, then it is possible to quantify the expected or observed adverse effect of modern wildfires for cultural resources management of an archaeological landscape subjected to forest fires. This information also may be projected into the past, enabling assessment of whether specific fire effects that have the potential to persist over time on an artifact (e.g., crazing) can serve as reliable evidence of past OH alteration. If alteration of OH can be linked closely with presence or absence of specific fire effect traits, those traits can serve as good candidates for proxy evidence of previous fire alteration in the extant OH observed in an artifact, thus providing evidence that the OHD information available from that artifact is unlikely to inform on the date of manufacture of the piece.

In Part II, the scope of investigation shifts from the scales of artifact and site to the geological landscape in which the Dome Fire occurred. The obsidian-bearing deposits in which the quarries burned by the Dome Fire occur are part of the Cerro Toledo Rhyolite, and are well known as the single geochemical source known variously as Obsidian Ridge, Rabbit Mountain, or Cerro Toledo Dome. Geological samples were collected from across this entire geological deposit to assess intrasource geochemical homogeneity. Trace, minor, and major element composition were measured using two x-ray fluorescence (XRF) techniques, energy dispersive (ED-XRF) and wavelength dispersive (WD-XRF). The results of these analyses are reported in Chapter 6. Artifacts subjected to OH analysis also were analyzed using ED-XRF.

The first goal of the geological sampling was to establish whether the Cerro Toledo Dome (CTD) obsidians could correctly be considered a "geochemical source" as defined by trace element homogeneity. The hypothesis that the deposits might not be a single geochemical source was rejected in the pilot project study (Steffen 2002), a conclusion further support by the additional sampling reported here. With CTD defined as homogenous geochemical source as defined by trace-element composition, what other compositional components could contribute to the variation in fire response observed throughout the Dome Fire? The first hypothesis tests whether the CTD obsidians are variable in their minor and major element composition, as compared to their trace element composition (Chapter 6). The second hypothesis tests whether the water content in CTD glasses is higher or more variable than usually expected in obsidian (Chapters 5 and 8). Two methods were used to measure water content in the geological obsidian samples: simple loss-on-ignition (LOI) and Fourier-transform infrared spectroscopy (FTIR). The methodologies of each technique are described in Chapter 7. Variability in water content as measured by LOI and FTIR is compared to variation in trace, minor, and major elemental composition (measured by ED-XRF and WD-XRF in Chapter 6).

Chapter 5 provides the geological background (from igneous petrology, geochemistry, and volcanology) needed to assess the nature and origin of intrasource vs. intersource compositional variation in obsidian. Here I also consider how obsidian composition plays a role in the glass-environment interactions central to the obsidian hydration dating model. I also address why water content has not been a focus in previous OHD research and consider recent advances in obsidian hydration dating that strongly support (explicitly or implicitly) the relevance of obsidian water content. If water content is an important variable in the rate of obsidian hydration, understanding how it varies within and among the many diverse obsidian sources used by prehistoric groups may hold a key to improving the performance of OHD as a chronometric technique.

To increase the robustness of the comparison among compositional components (volatiles vs. elements), and to put these comparisons into broader perspective, geological obsidian samples from two other source areas in the Jemez Mountains also are included. These include smaller sample sets from obsidian-bearing deposits at Cerro Toledo

Northeast (CTN, also of the explosive-origin Cerro Toledo Rhyolite) and Cerro del Medio (CDM, of the Valles Rhyolite, a more recent extrusive obsidian source in the center of the Valles caldera). After first determining whether CDM and CTN can be considered different geochemical sources from CTD, I test the hypothesis that the CTD obsidians burned in the Dome Fire are both higher and more variable in water content than glasses from these nearby source areas. The differing volcanic histories of the three obsidians (CTD, CTN, and CDM) are considered as a potentially productive topic for understanding the causes and origin of variation in obsidian water content. The results obtained are then discussed in terms of the role of water content for vesiculation as a fire effect, and the implication of high and variable water contents for obsidian hydration dating and source-specific hydration rates as defined by trace element homogeneity.

In sum, this dissertation begins with investigation of the event of a forest fire, creates the descriptive language needed to measure the unfamiliar phenomena that resulted, and pursues quantification of macroscopic and microscopic variation in heat effects to evaluate the potential chronometric impact of forest fires. These considerations are then integrated with a geochemical investigation of obsidian composition to understand how variation in such fire effects may occur and to re-examine the reliability and validity of the obsidian hydration dating model. This is an interdisciplinary dissertation that is unabashedly methodological in nature: the focus throughout is on the archaeological record rather than on the prehistoric people who contributed to the formation of the record. However, the analyses pursued and the arguments developed all contribute directly to the tools used by archaeologists to measure when in prehistory people created the assemblages under study, how the archaeological record has been transformed until the present, and how archaeologists can succeed in preserving sites and deposits in forested environments.

CHAPTER 2
BACKGROUND

This chapter provides background information on the archaeology and geology of the study area, with particular attention to the large quarries that occur at surface exposures of artifact-quality obsidian within the Dome area in the Jemez Mountains of northern New Mexico. A brief discussion is provided of the environment and fire history of the study area to provide spatial and temporal context for the Dome Fire and the effects to obsidian artifact assemblages that are the focus of this study. The second half of the chapter is a review and history of previous archaeological research on obsidian fire effects. Here I identify central issues common to prior studies and summarize the results of these studies. This provides a context for how the goals of the current study were developed, and shows how the results obtained here will contribute to our scant knowledge concerning this peculiar transformation of the archaeological record.

2.1. Study Area

Study Area: Setting

The Dome Fire was named for the St. Peter's Dome area in the Jemez Mountains. The Dome area is located in the San Miguel Mountains on the southeast side of the Valles caldera in north-central New Mexico southwest of Los Alamos and northwest of Santa Fe (Figure 2-1). Topography in the Dome area is characterized by rugged and incised landscapes with flat sloping mesas created by numerous uplifted sedimentary blocks, volcanic domes, and large pyroclastic deposits associated with the Valles caldera and earlier volcanic eruptions. The Pajarito Plateau, widely known as an area rich in Ancestral Puebloan archaeological sites, is located outside the study area to the east.

High elevations in the Dome area occur at several mountain peaks and range from 9940 feet (3030 m) above mean sea level (amsl) at Rabbit Mountain to the north, and 8460 feet (2580 m) amsl at the lookout near St. Peter's Dome toward the south. On the gently southeast sloping mesas, elevations range from about 8800 feet (2684 m) amsl at the north end of the area, to 7000-6500 feet (2135-1980 m) amsl at the south end. The Dome area is drained by deeply incised drainages in Frijoles, Capulin, Sanchez, and

Cochiti Canyons. Bandelier National Monument (BNM) is located on the east side and the Jemez District of the Santa Fe National Forest (SFNF) is on the west. Outside the Dome area are the Valles Caldera National Preserve (VCNP) on the north and Los Alamos National Laboratories (LANL) to the northeast.

Figure 2-1. Location Maps of Jemez Mountains in New Mexico.

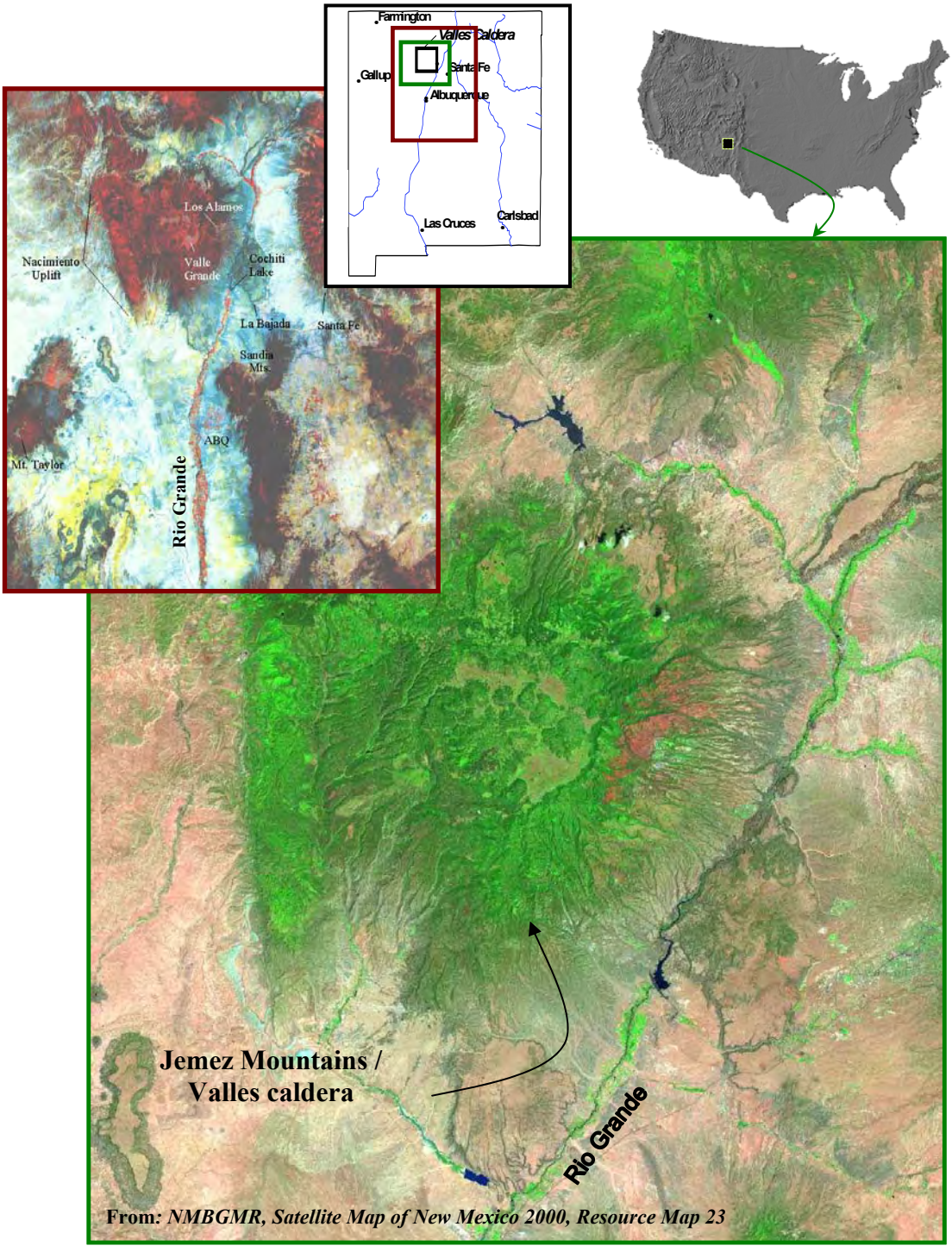

Study Area: Geology

The Jemez Mountains are located at the intersection of the Rio Grande rift and the Jemez lineament (Aldrich 1986), an elongated distribution of volcanically active areas stretching from northeast New Mexico southwest into Arizona (Figure 2-2).

Figure 2-2. Jemez Lineament and Miocene to Holocene volcanic fields (from Ander et al. 1981).

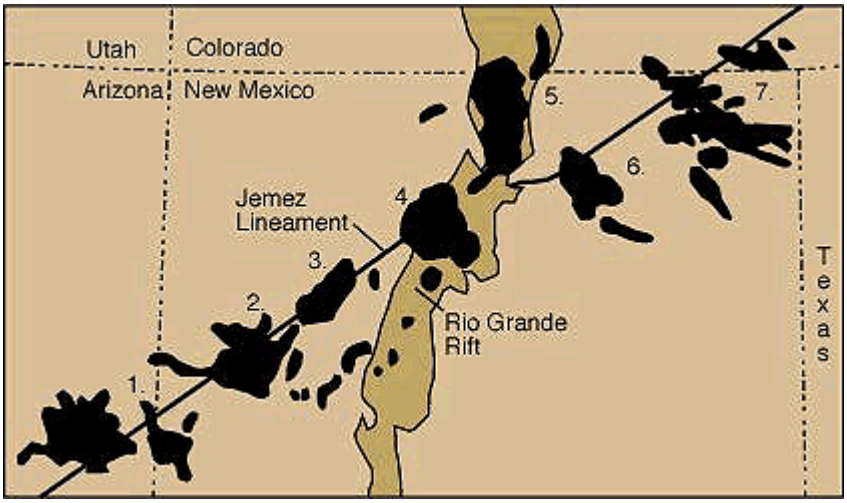

1. Springerville 3. Mount Taylor 5. Taos 7. Raton-Clayton
2. Zuni-Bandera 4. Jemez Mountains 6. Ocate

USGS 7.5 quadrangle geological maps are available for only one of the four quadrangles that encompass the Dome area (Frijoles Quad: Goff et al. 2002) and mapping is underway for the Bland, Canada, and Cochiti Dam USGS 7.5 quadrangles. Thus the two geological mapping references for the obsidian-bearing deposits in the Dome area are the 1970 geological map of the Jemez Mountains (Smith et al. 1970) (Figure 2-3) and the 1990 geological map of the Dome area (Goff et al. 1990) (Figure 2-4).

The landforms in the Dome area were created by some of the most recent as well as much older volcanic episodes in the Jemez volcanic field (see Table 2-1 for geological units noted here). The older Tertiary domes that rise above the Quaternary mesas include those from the Keres group (such St. Peter's Dome and Boundary Peak of the Paliza Canyon Formation [Tpa, using nomenclature of Smith et al.1970; see Figure 2-3], and Rabbit Hill and Cerro Picacho of Bearhead Rhyolite [Tbi])—and from the Polvadera Group (such as the unnamed peak east of Rabbit Mountain [sometimes called Scooter Mountain] of the Tschicoma Formation [Tt]).

Figure 2-3. Geology of the Valles caldera, from Smith, Bailey, and Ross (1970) "Geologic Map of the Jemez Mountains, New Mexico". The identification of CTR locations discussed in the text is added. Map as shown is not to original (1:125,000) scale.

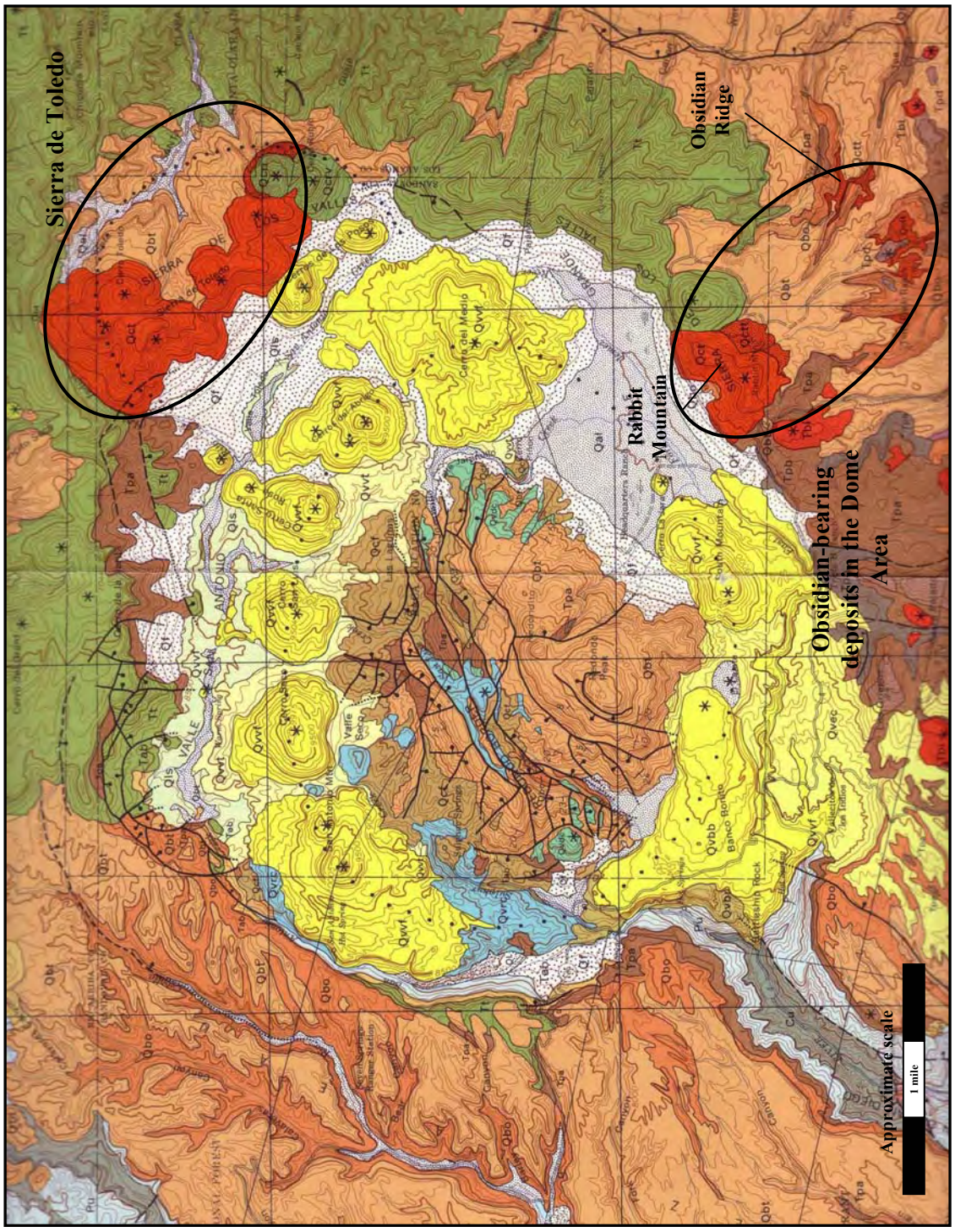

Figure 2-4. Geology of the obsidian-bearing deposits in the Dome area, from Goff, Gardner, and Valentine (1990) "Geology of St. Peter's Dome area, Jemez Mountains, New Mexico". The identification of quarry locations discussed in the text is added. Map as shown is not to original (1:24,000) scale.

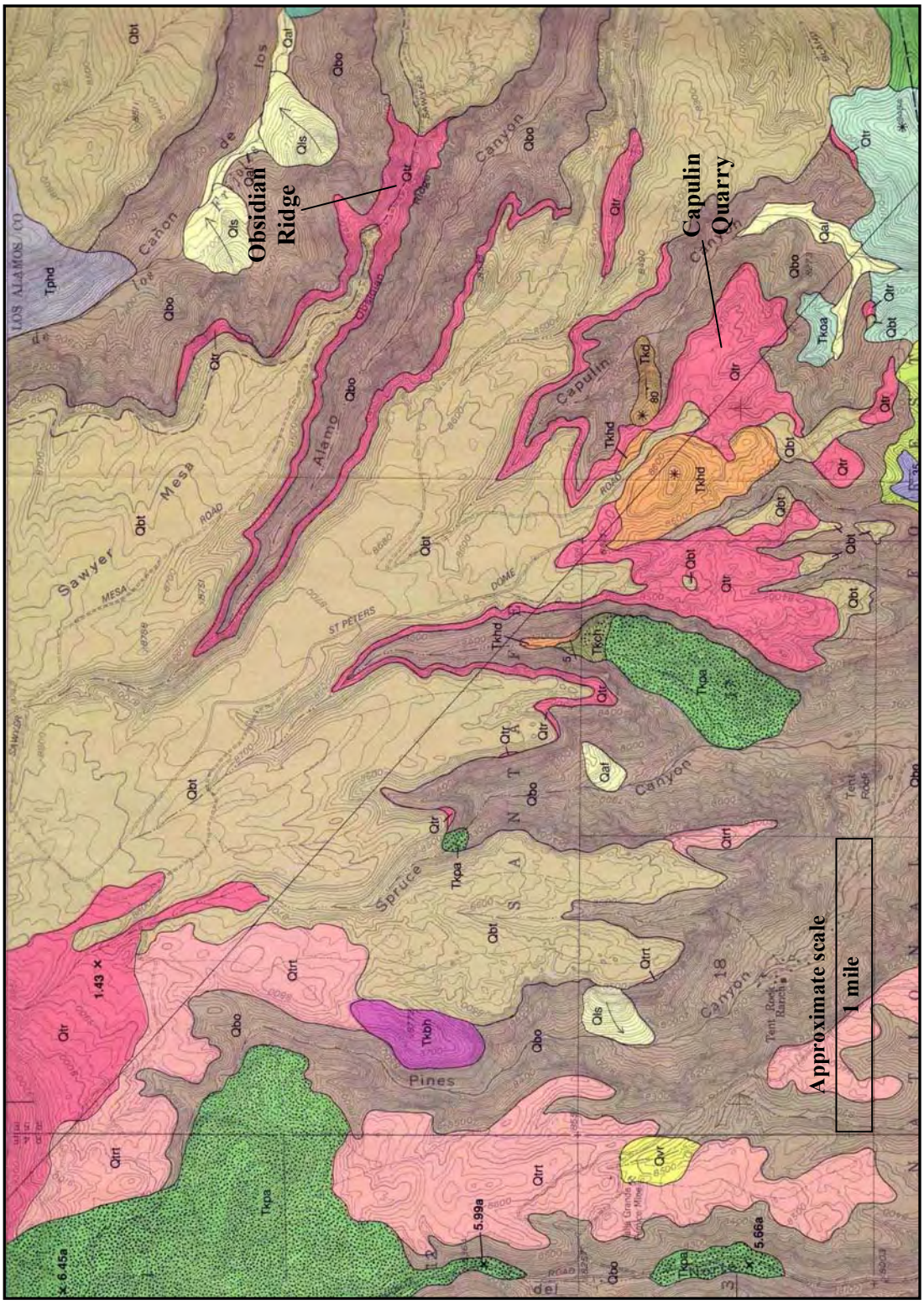

The younger southeast sloping mesas, however, are formed by relatively recent pyroclastic deposits of the Tewa group and are associated with the two Quaternary caldera eruptions known as the Valles and the Toledo calderas that produced the Bandelier tuffs (Qbt and Qbo in Figures 2-3 and 2-4). These layers of variably welded ash-flow tuffs and ash-fall pumice, are known as the Tshirege member (Qbt, Upper) and the Otowi member (Qbo, Lower) of the Bandelier tuff, and date to approximately 1.22 and 1.61 million years ago (mya), respectively (Spell et al. 1996).

Table 2-1. Geological units mentioned in the text.

Period	Smith et al. 1970 abbr.	Goff et al. 1990 abbr.	Group	Geological unit
Quaternary	Qvvf		Tewa	Valles Rhyolite
Quaternary	Qbt	Qbt	Tewa	Tshirege member, Bandelier tuff (Upper)
Quaternary	Qct/Qctt	Qtr/Qtrt	Tewa	Cerro Toledo Rhyolite
Quaternary	Qbo	Qbo	Tewa	Otowi member, Bandelier tuff (Lower)
Tertiary	Tt		Polvadera	Tschicoma Formation
Tertiary	Tbi		Keres	Bearhead Rhyolite
Tertiary	Tpa		Keres	Paliza Canyon Formation

Cerro Toledo Rhyolite in the Dome Area

Sandwiched between the two Bandelier tuff members is the Cerro Toledo Rhyolite (CTR), the geological unit that bears the high-quality obsidian best known to archaeologists as Obsidian Ridge obsidian. The large prehistoric obsidian procurement archaeological sites ("quarries") are located where the Cerro Toledo Rhyolite deposits are exposed below the Upper and above the Lower Bandelier tuffs. These exposures can occur as broad expanses on top of the mesas, or as an enclosed layer in canyon sidewalls below the mesas. No other obsidian-bearing deposits are known to occur in the Dome area, despite the fact that Tertiary formations noted above (e.g., Bearhead Rhyolite) are known to have obsidian-bearing deposits in other areas of the Jemez Mountains (e.g., Baugh and Nelson 1987).

All exposures of artifact-quality obsidian in the Dome area are thought to be associated with what Goff et al. (1990) call the Rabbit Mountain rhyolite of the Cerro Toledo Rhyolite. Rabbit Mountain is located at the northwest end of the Dome area and this complex of volcanic domes—described as a flank eruption by Goff and others—is the source of the tephra deposits in which the obsidian occurs. The Rabbit Mountain

rhyolite is described as "Black, very aphyric obsidian to white, devitrified rhyolite; contains no visible phenocrysts; may display spherulitic flow banding..." with an age of 1.43 (±0.04) million years as established by potassium-argon dating (Goff et al. 1990). As shown in Figure 2-4, there are two parts of the deposit, indicated as Qtr and Qtrt by Goff et al. (1990). These units are comparable to but do not correspond exactly with the Qct and Qctt units (Figure 2-3) mapped by Smith et al. (1970; with Qctt described as including "hot avalanche deposits from the Rabbit Mountain center"). The Qtr deposits "form domes, flows, and flow breccias that thin to south and east, and have a maximum thickness of about 50 meters; Qtrt consists of mixed ash-fall and ash-flow deposits" (Goff et al. 1990, also citing Heiken et al. 1986; see also Gardner et al. 1986). The larger obsidian clasts of toolstone quality are found in Qtr, with smaller less-suitable obsidian in Qtrt. The exposure known as "Obsidian Ridge" (see Figure 2-3) is located in Qtr, as are all the other large quarry areas in the Dome area.

Cerro Toledo Rhyolite as a Larger Geologic Unit

The Cerro Toledo Rhyolite also occurs outside the Dome area (Figure 2-5). Although not well-known to archaeologists (cf., Newman and Nielsen 1985), artifact-quality obsidian occurs in CTR deposits in the Sierra de Toledo in the northeastern quadrant of the Valles caldera. Compositional and volcanic relationships between these northeastern CTR obsidians and the better known Dome area CTR deposits are of interest in this study in order to understand the petrogenesis of any potential compositional variation within the Dome area obsidian deposits. In other words, understanding the geologic knowledge of the entirety of the CTR will inform on the origin and composition of obsidians within and among differing obsidian source and quarry locations in the Dome and Sierra de Toledo areas. A review of the current geological understanding of CTR in the Sierra de Toledo follows.

The Cerro Toledo Rhyolite is composed of a sequence of pyroclastic activity and dome building that occurred in the interval between the large ignimbrite eruptions of the Valles and Toledo caldera collapses (Heiken et al. 1986; Spell et al. 1996; Stix et al. 1988). Recent mapping of the geological landforms of the Sierra de Toledo by Gardner and Goff (1996), and geochronological analyses by Spell et al. (1996) address the

somewhat confusing relationships among the domes. To summarize, several CTR domes occur within the Toledo embayment. Two domes (East and West Los Posos) were previously mapped as part of the Valles Rhyolite (e.g., Smith et al. 1970), but now are considered part of CTR (Heiken et al. 1986; Self et al. 1986). While the Toledo embayment was originally thought by some (e.g., Smith et al. 1970) to define part of the

Figure 2-5. CTR deposits shown on shaded relief plotted from 10m DEM. CTR locations are modified from Smith et al. 1970, with re-classification to CTR of previous Qvvf domes (Warm Springs Dome, Cerro Trasquilar, East and West Los Posos: Heiken at al. 1986; Self et al. 1986) and Tbi dome (Justet 1996; Justet and Spell 2001:249).

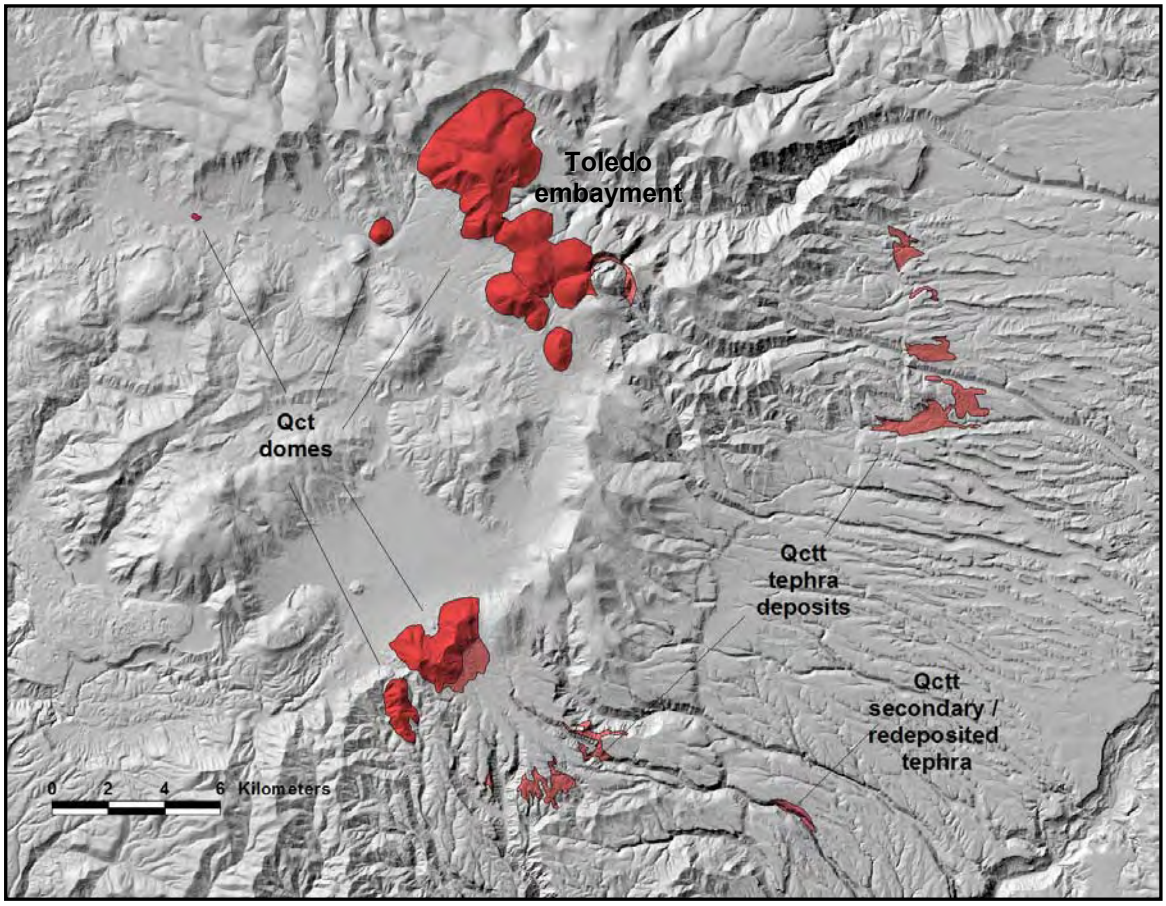

caldera outline formed in the Toledo eruption, more recent analyses argue that the two calderas were nearly spatially coincident (Goff et al. 1984) and that the Toledo embayment has other regional structural controls and may have formed as some other kind of collapse associated with the development of the Toledo caldera (Gardner and Goff 1996). With this interpretation, the domes in the area of the Toledo embayment have multiple origins (Stix et al. 1988) and include 1) those associated with intracaldera

ring fracture dome building within the Toledo caldera (i.e., the two Los Posos Domes and Cerro Trasquilar), and 2) those associated with the development of the embayment (i.e., Cerro Toledo, Turkey Ridge, Indian Point, Pinnacle Peak). However, these two categories do not group by age, with earlier and later geochronological dates included in each category (Stix et al. 1988). Rabbit Mountain, in the Dome area, groups geochemically with domes within the Toledo embayment, and has an age that is similar to Cerro Toledo (Stix et al. 1988:6130).

The Cerro Toledo Rhyolite is of interest to geologists because it contains information on the evolution of the volcanic system and magma chamber in the interval between the two large caldera forming eruptions. For this archaeological study, that geological discussion is important because it addresses the origin of potential variation within CTR obsidians. Spell et al. (1996) point out that while there is little variation in major and minor elements within the CTR rhyolite samples analyzed, there is greater variation in trace element composition among different dome and tephra deposits. They interpret this and other evidence to indicate relative complexity in the evolution of the magma system and variation in the differentiation of the erupted magmas, including magma replenishment event(s) and tapping of separate magma bodies during the 380,000 year interval between the caldera eruptions (Spell et al. 1996:267-268). Applied to the current study, these possibilities indicate potential mechanisms for the origin of variation in elemental and volatile composition among the CTR obsidian deposits, and suggest that greater or lesser variation in volatiles would likely correlate to the presence or absence of trace element variation within or among CTR obsidian deposits. Other mechanisms for the introduction of variation in volatile composition, such as those associated with the nature of explosive eruption processes, are discussed in Chapter 5.

Study Area: Archaeology at Capulin Quarry and the Dome Obsidian Quarries

Capulin Quarry (LA 23961; also known by the SFNF site number AR 03-10-03-1691) is an area of obsidian procurement and reduction located atop a large exposure of Qtr obsidian-bearing pumice and rhyolite-tuff deposits. The quarry is located on the top and side slopes of a NW-SE trending ridge just to the south and west of Capulin Canyon and immediately east of Forest Road 289 (Figure 2-6). Boundaries for the site are

difficult to define because the quarry-reduction deposits are coincident with an expansive exposure of obsidian-bearing deposits with variable surface expressions concealed or exposed by differences in slope, landform, vegetation, soil erosion, and sedimentation. Using the relative distribution of high density surface artifacts as the criteria for site boundaries, the site measures at least 1000 m NW/SE by 400 m NE/SW, with an area of about 21 hectares (~52 acres).

Figure 2-6. Obsidian quarries and lithic scatters recorded by the SFNF in the Dome area demonstrating overlap with exposures of Cerro Toledo Rhyolite (Qct/Qctt from Smith et al. 1970). Sites in the text are labeled by SFNF site number (e.g., 03-1691).

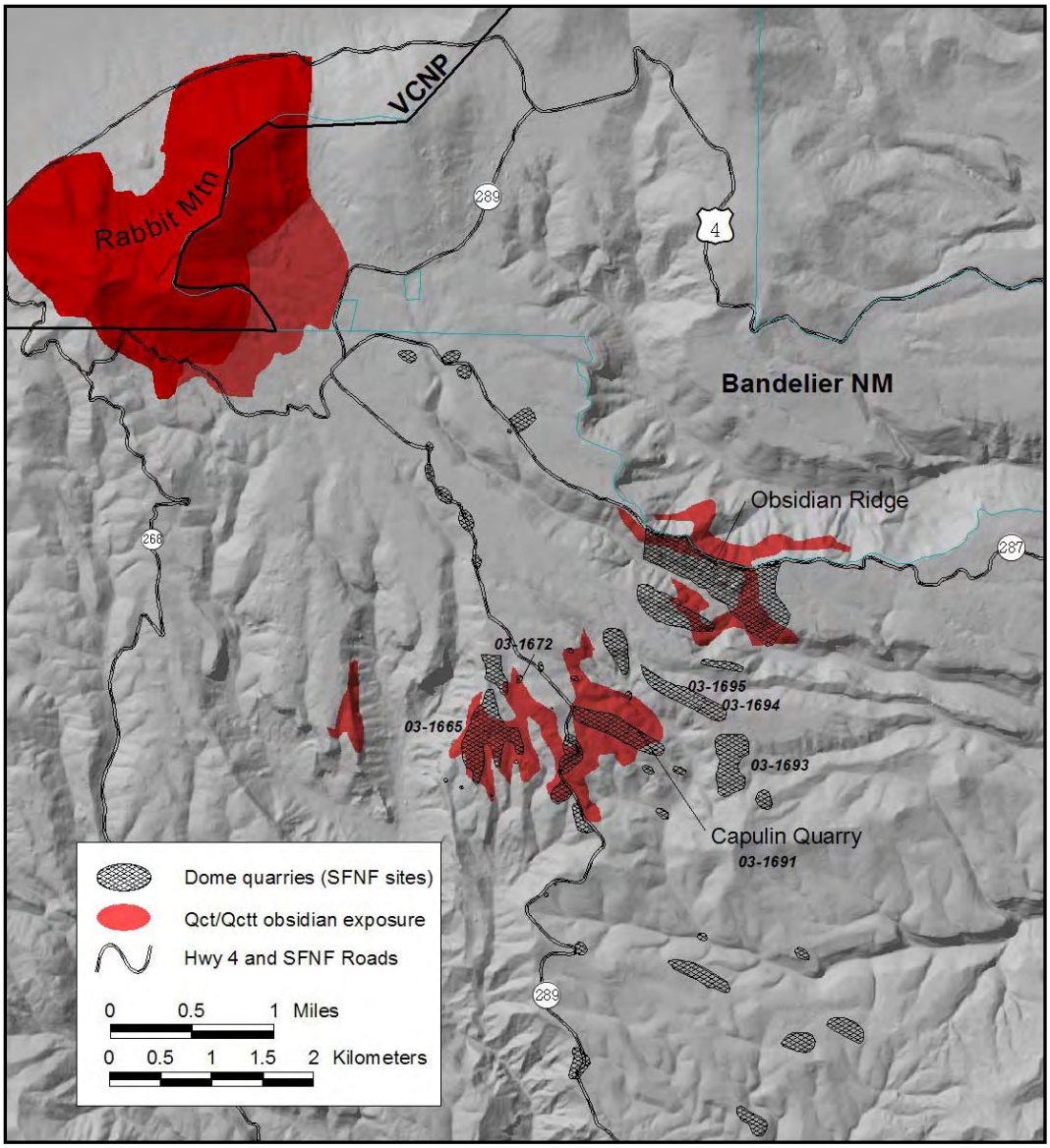

Capulin Quarry was originally defined for SFNF management purposes largely as a surface deposit. An important aspect of the quarry sites in the Dome area is that due to the shallow forest soils and their location in primarily erosional settings along ridgetops, these quarries occur on "the surface" as defined from a variety of perspectives, including geological, archaeological, pedogenic, and topographic surfaces as well as the contemporary landscape surface. As such, an abundant assemblage is available to past and present natural archaeological transformations, such as forest fires, that occur at the surface. Further, the non-stratified character of these archaeological deposits, along with their lack of otherwise ubiquitous cultural features such as fieldhouses and pueblos, defy the familiar conventions of site documentation, evaluation, and preservation in the Jemez region.

Questions about how site boundaries should be defined, what constitutes site "significance", and how the Dome quarry deposits should be protected given their expanse and apparent assemblage redundancy, were the subject of extensive consideration and reconsideration by USFS cultural resource managers throughout the 1980s (e.g., Cartledge 1987; Muceus 1982; Smith 1984; see also Moore 1987). Despite these efforts, the conclusions reached in the 1980s are not fully satisfactory. For example, subsurface testing in the late 1980s at Capulin Quarry (Larson et al. 1988) was used to redefine the boundaries to one portion of the site where subsurface and potentially stratified deposits were demonstrated to occur (Figure 2-7). This resulted in a reduction of the fully protected area of the site to that subset of the site in which "pockets of buried cultural material have been identified which have significant information potential (Larson et al 1988:140)." In the case of Capulin Quarry only approximately 20% of the site was recommended for full protection under these criteria (Figure 2-7), and the area of the current study was excluded. This focus on intact subsurface deposits as a criterion for significance of archaeological deposits led also to recommendations for the removal from management consideration of five other quarry/lithic reduction sites in the Dome area; as shown in Figure 2-6 (see sites noted by SFNF site number on this map), four of these five sites are large and extensive quarry deposits.

Figure 2-7. Larson et al. (1988:142, Figure 12.2) site map for AR 03-10-03-1691 (Capulin Quarry) showing their recommendations for site preservation based on results of subsurface testing. Only the stippled area was "recommended for avoidance or further data recovery". The area of focus in the current study is identified here as an oval outline of red short-dashes. Other modifications from the original figure include scale reduction and bolder shading.

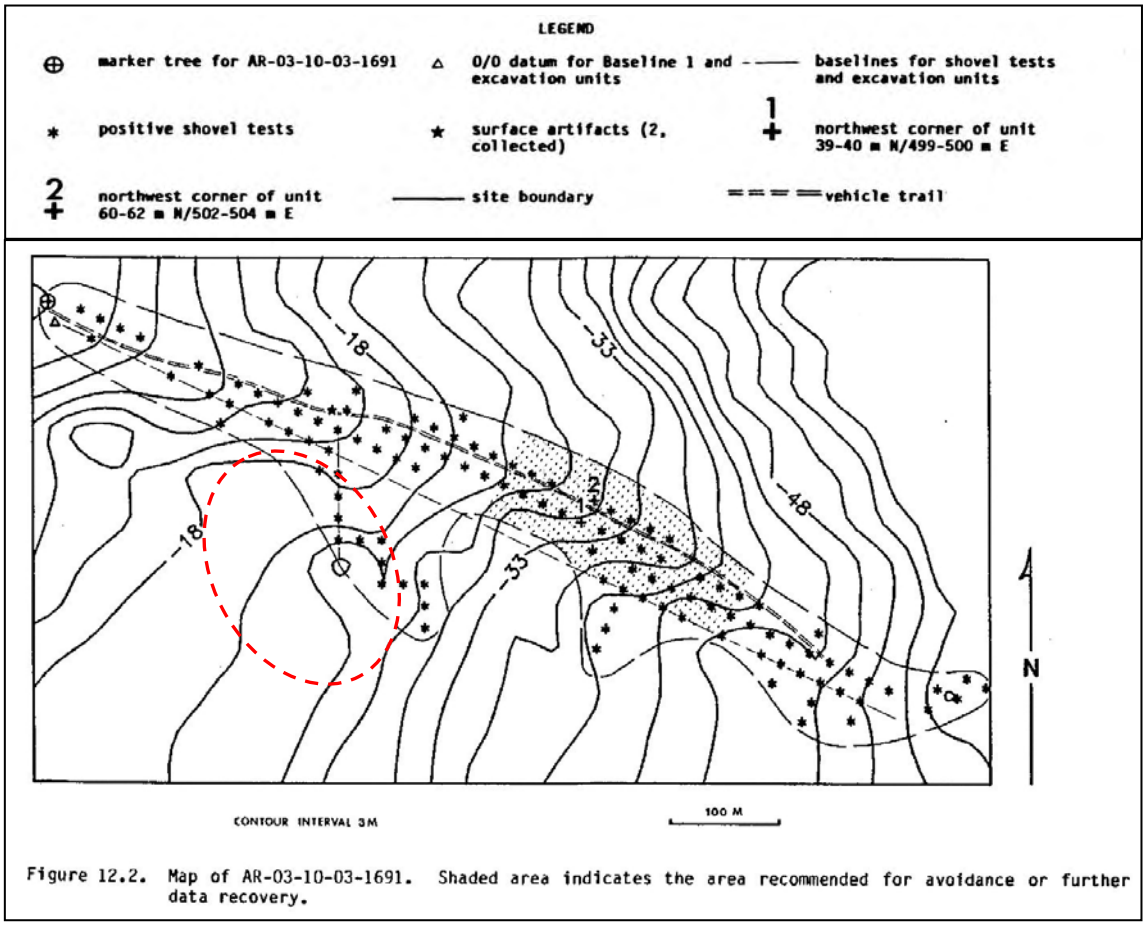

Figure 12.2. Map of AR-03-10-03-1691. Shaded area indicates the area recommended for avoidance or further data recovery.

It is difficult to see how such sites could be considered to "have no further significant information potential" (Larson et al. 1988:140) unless the interpretation of significance places a heavy emphasis on the value of subsurface deposits and devalues the information potential of shallow or surface deposits. The current study at Capulin Quarry demonstrates one obvious value of assemblages on the contemporary surface: they provide a window into how transformations of the surface archaeological record may have occurred in the past, including the alteration of surface assemblages by forest fires.

Study Area: Environment and Fire History

Elevation at Capulin Quarry ranges from 8300 to 8500 feet (2530 to 2592 m) amsl. Overstory vegetation in the area is dominated by Ponderosa pine with some spruce and fir. Understory vegetation includes grasses, Gambels oak, and New Mexico locust. Average annual precipitation is 18-23 inches (46-58 cm), with most coming in summer months during the July-August "monsoon" rains. Climate on the east side of the Jemez Mountains is described in Touchan et al. (1996) as follows:

> The length of the frost-free growing season in Los Alamos is 157 days, or around five months (Bowen 1989). July is the warmest month at Los Alamos, with a mean temperature of 28ºC (82ºF), and January is the coldest month, with a mean temperature of -1.6ºC (29ºF). The annual precipitation ranges from about 30 cm (12 inches) at the lowest elevations to about 90 cm (35 inches) at the highest elevations. Yearly precipitation is bimodal, with maxima in winter (December-January) and summer (July-August). Winter precipitation falls primarily as snow, with average accumulation of about 130 cm (51 inches). This moisture has its origin in eastern-moving storms from the Pacific Ocean. Summer precipitation results from a southeasterly wind pattern that typically transports moisture from the Gulf of Mexico to New Mexico. This moisture, combined with strong heating, produces and unstable atmosphere that leads to convective storms. Forty percent of the total annual precipitation falls in July and August during the height of the summer rainy season. ([Touchan et al. 1996:34-35]; *conversion to (ºF) and (inches) added*)

Most forest fires on the east side of the Jemez Mountains occur during the summer "monsoon" season and are caused by lightning. In a study at Bandelier National Monument, 86% of fires were found to have been started by lightning, with most occurring June through August (Foxx and Potter 1978).

Examination of fire scar patterns by Touchan et al. (1996) to reconstruct fire history in the Jemez Mountains included sampling locations within the Capulin Quarry site. Their results indicate that the norm for pre-1900 fire regimes are low-intensity forest fires occurring at high frequencies in Ponderosa pine forests and somewhat lower

frequency in mixed-conifer forests. The fire return interval for major fires in the area of Capulin Canyon was estimated at 6.5 to 7.5 years (Touchan et al. 1996:41; using WMPI as the calculation), which fits with estimates for modern (pre-1900) return intervals in other Ponderosa pine forests in the Southwest (Swetnam and Baisan 1996). The Jemez study noted a pattern between precipitation and fire in Ponderosa pine forests: a drier than normal winter-spring season immediately preceded fire occurrence, but wetter seasons occurred in the preceding two years—allowing for the buildup of fuels by the vegetation grown during those wetter seasons (Touchan et al. 1996). The Dome Fire occurred in 1996 under just these conditions, as did the Cerro Grande fire in 2000 (Figure 2-8).

Figure 2-8. Fire history of large fires in the Jemez Mountains, 1950s through 2004; data from SFNF fire GIS layer. Small-scale inset map was prepared by the SFNF.

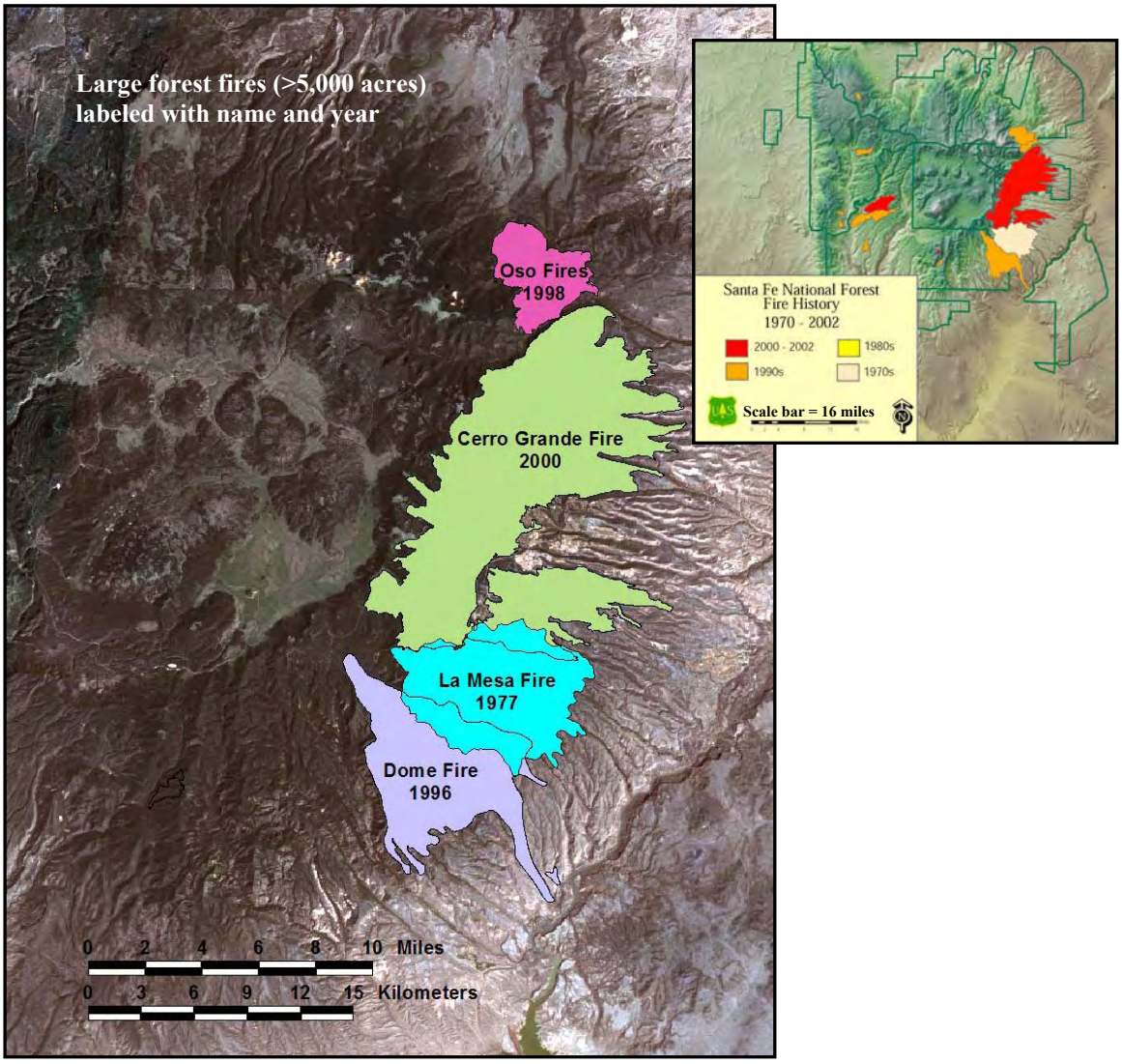

The Dome Fire (~16,500 acres / 6,680 ha) was a human-caused fire, ignited during conditions of extreme drought by an unextinguished campfire on April 25, 1996. This was the second recent large fire in the southeast Jemez Mountains (Figure 2-8), preceded by the La Mesa Fire (~15,500 acres / 6,275 ha) in 1977. The Oso Fire Complex followed in 1998 (~6,500 acres / 2,630 ha) and the Cerro Grande Fire in 2000 (~43,000 acres / 17,415 ha). All of these large fires were human-caused (Baldwin et al. 2002) and occurred early (April through June) in the fire season. The two-year return interval of the three most recent of these large fires further distinguishes the recent three decades from the preceding fire history of the Jemez Mountains.

Figure 2-9. Fire severity map of the Dome Fire (data reflects combined SFNF and BNM post-fire interpretation).

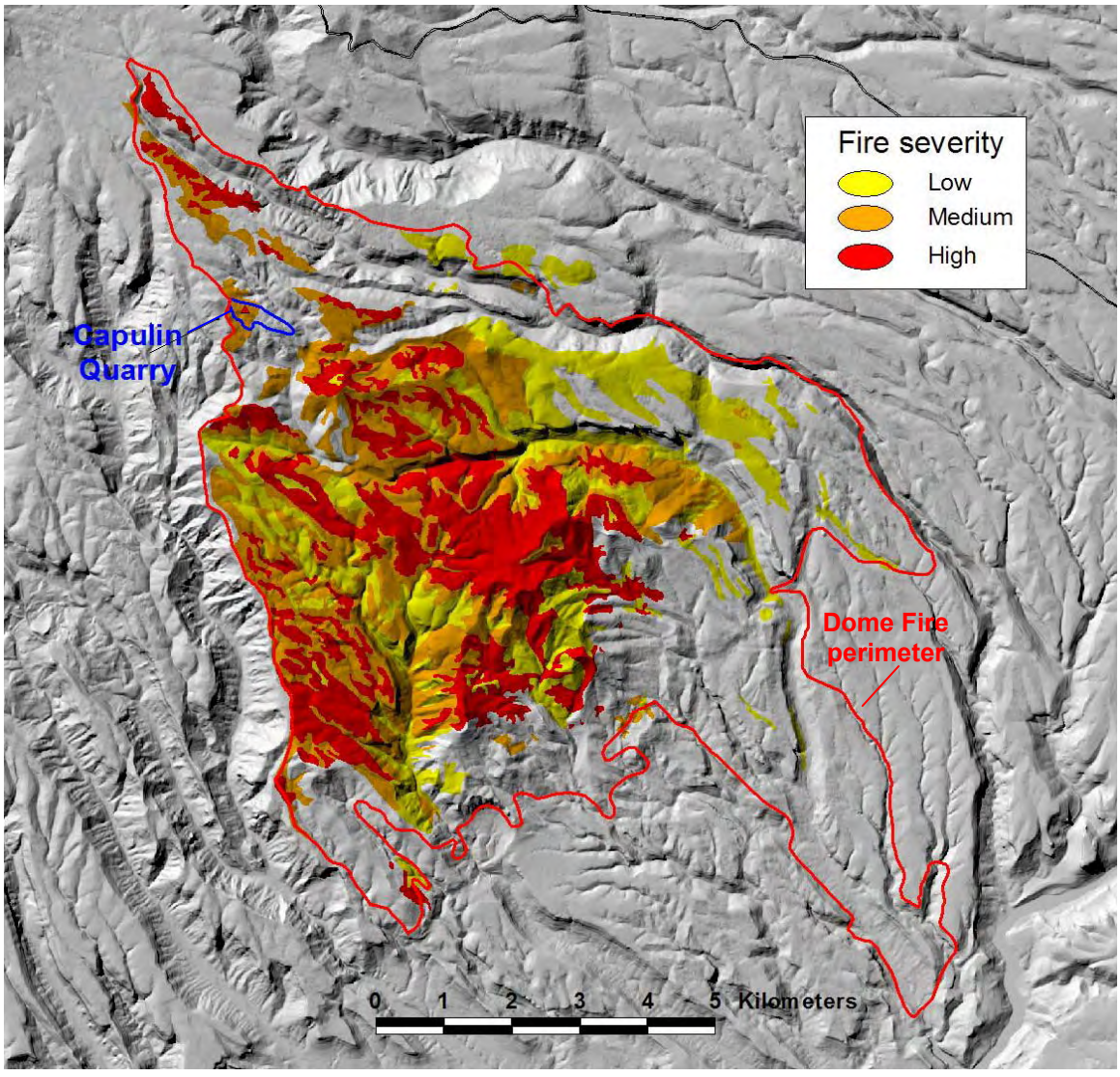

The early occurrence in the fire season, the large size, and the frequency of the three most recent forest fires on the east side of the Jemez bolsters the interpretation that the Dome, Oso, and Cerro Grande Fires demonstrate unusual fire incidence. Livestock grazing, logging, and fire suppression are all factors that contribute to changes in fire regime in the Jemez Mountains and other southwestern forests. The frequency and severity of forest fires in the Southwest has increased since the turn of the century. Large fires such as these three are occurring "unnaturally" more often, and "extensive (> 100 ha) stand-replacing fires rarely (if ever) occurred in pure, southwestern Ponderosa pine forest before the middle of the 20th century (Allen 2001:32)." Thus, the Dome Fire as a whole probably represents a worst-case scenario for forest fire effects to archaeological assemblages in the Jemez Mountains. Whether this is similarly the case in the portion of the Dome Fire area that includes Capulin Quarry is less certain, although mapping of burn severity (Figure 2-9) by the SFNF and BNM (National Park Service 1996) indicates medium burn severity on all or part of Capulin Quarry, including the portion of the site where the vesiculation clusters occur.

2.2. Research Context

History of Obsidian Fire Effects Research in Archaeology

Contemporary archaeological fire research began with the 1977 La Mesa Fire, which occurred in Bandelier National Monument immediately adjacent to (and overlapping with) the area burned in the 1996 Dome Fire (Figure 2-8). Because La Mesa was the first forest fire in which archaeologists were deployed to protect cultural resources during an active wildfire, and it was the first fire for which systematic post-fire investigations were conducted, the La Mesa Fire study (Traylor et al. 1979, republished in 1990) is recognized as a landmark in the investigation of fire impacts to cultural resources (Cartledge 1996:210). The La Mesa Fire study also is important because it included the first in-depth investigation of fire effects on obsidian (Trembour 1979, republished in 1990). Trembour's study has endured as the premier research on obsidian fire effects, and serves as a basis for the current study.

Archaeologists have become increasingly involved in forest fire research, and interest in fire effects on obsidian has been growing throughout the 1990s. Prior to 1999 there were about a dozen studies that discussed the effects of fire on obsidian artifacts (Anderson and Origer 1997; Davis et al. 1992; Deal 1997; Green et al. 1997; Linderman 1991, 1992; Nakazawa 1998; Origer 1996 [in Lentz et al. 1996]; Origer and Anderson 1994; Skinner et al. 1997; Trembour 1990). In 1999 several new studies were presented in a Society for California Archaeology symposium, and later assembled into an edited volume (Loyd et al. 2002). This volume presents the most salient compilation of in-depth obsidian fire effects studies available in the archaeological literature, and is now the main reference available on the topic. This volume also provides a comprehensive review of current obsidian fire effects studies (Schroder 2002), updating the inventory of earlier archaeological fire effects studies provided by Duncan (1990). Another excellent review of forest fire effects to lithic artifacts is being published as part of the USDA Rainbow Series on Fire Effects to Cultural Resources (Deal 1999).

Issues in Obsidian Fire Effects Research in Archaeology

The central problem driving obsidian fire effects research is the potential of fire to affect obsidian hydration analysis. Nearly all of the in-depth studies of obsidian fire effects focus on the effects of fire for hydrated artifact surfaces. The connection between forest fires and obsidian hydration (OH) is high temperature. Temperature has long been included as a relevant variable in determining the rate of obsidian hydration for dating (e.g., Friedman and Long 1976; Ericson 1975; Trembour and Friedman 1984; see also Ridings 1991, 1996 for a more recent consideration of the role of temperature and climate), but usually is considered in terms of environmental temperature and effective hydration temperature. Environmental temperature can be contrasted to high-temperature heat exposure in terms of "primary" versus "secondary" hydration (*sensu* Freter 1993:286). Effective hydration temperature is a primary hydration variable because it is involved in the hydration process. Exposure to high heat is a secondary hydration variable because it affects an existing hydration rim rather than the process of hydration. Sources of high heat include forest fires as well as grass fires (Picha et al. 1991), swidden

agriculture (Freter 1993; Friedman and Trembour 1983), kilns, cremations or ritual burning (Hatch et al. 1990; Stevenson et al. 2004), and hearths (Nakazawa 1998).

However, the distinction between primary and secondary hydration variables becomes less clear when considering whether heat exposure affects subsequent hydration. While the ability of high heat to "dry out" the previously hydrated layer is intuitively obvious, the processes involved in that "dehydration" and subsequent rehydration are complex and poorly understood (Ambrose 1976, 1998; Hatch et al. 1990; Loyd 2002; Trembour 1990). Increasing our understanding of how these processes occur in high heat conditions may prove valuable for improving our understanding of the obsidian hydration process at ambient temperatures.

Another on-going concern in OHD is how ambient temperature is experienced by artifacts on the surface versus those in buried deposits (see recent review by Beck and Jones 1994). Because forest fires occur primarily at the surface, the distrust of OHD for surface obsidian is especially relevant. However, exposure of artifacts to contemporary fires on a contemporary surface is not unique to the present: such surface exposure is similarly likely to have occurred if now-buried artifacts exposed on past surfaces were subject to prehistoric fires. This problem of unknown surface/subsurface history of assemblages is inherent in the OHD method; but, as Beck and Jones (1994:53-54) point out, the validity of OHD for surface artifacts is not necessarily less than for subsurface artifacts because this difficulty is intrinsic to any interpretation of the archaeological record (Dunnell and Dancey 1983; Foley 1981). Witnessing contemporary fire effects to obsidian assemblages simply demonstrates the principle.

Generally, OHD is better accepted where interpretation of obsidian hydration results is of relative rather than "absolute" temporal relationships (e.g., Beck and Jones 1994; Jackson 1984; Layton 1973; Tremaine and Fredrickson 1988). Use of OHD for relative rather than quantitative estimates of age allows for an assumption of constant variability in key parameters such as effective hydration temperature, tolerates the treatment of assemblages as palimpsests, and can avoid application of potentially problematic equations for hydration rate calculation. However, as a secondary hydration variable, heat exposure may diminish the utility of OHD even for relative comparisons if,

for example, the consequences of a given forest fire (past or contemporary) are variable across a burned site.

Types of Archaeological Studies of Forest Fire Effects on Obsidian

Archaeological studies of fire effects fall into three categories: post-fire studies initiated subsequent to wildfires, field experiments conducted as part of prescribed burning, and laboratory experimentation. Each type of study offers different opportunities and has specific limitations, as explored further in the review of previous study results, below. Buenger (2003) summarizes the important variables in archaeological forest fire effects as: 1) fuel type, 2) fuel load, 3) fire behavior, 4) proximity of artifacts to fuels, and 5) artifact class. In reviewing the literature, the variables that have been the focus of research attention in assessing fire effects for obsidian as a class of artifacts are described as temperature, duration of heating, fuel load and fuel type, apparent burn intensity, burning conditions, and exposure (i.e., surface versus subsurface). Only apparent burn intensity and exposure can be readily assessed in post-fire studies, while field and laboratory experimentation allows the replication, control, or manipulation of other variables such as temperature, duration of heating, fuel load and fuel type, burning conditions, and exposure.

All archaeological investigations of fire effects can be understood as conducted at one of two analytical scales: 1) the combined impact of fire to OH rims in an assemblage, and 2) the expression of fire effects on individual specimens. Studies at the scale of assemblage are much more common than studies at the scale of specimen. No prior studies have been conducted (except Steffen 2002) that examine the effects of forest fires on obsidian hydration at the scale of specimen; all studies at this scale involve only description of visible fire effects (see Chapter 3). Most of the numerous assemblage-scale studies, as discussed below, focus on how fire affects obsidian hydration dating. A few examine how heat exposure may alter analysis of chemical composition (Shackley and Dillian 2002, Steffen 2002) or glass density (Jones 2002).

Review of Previous Results in Archaeological Obsidian Fire Effects Studies

Taken as a whole, obsidian fire effect studies show definitively that forest fires can have a measurable and chronometrically significant effect on OH rims. The initial results found by Trembour (1990) in his 1979 study have been observed in several subsequent studies. When exposed to heat, obsidian hydration rims will develop a more diffuse hydration front--with continued exposure and increased temperature, the hydration band can expand in width and then become fully obliterated.

While actual percentages vary somewhat among the studies, all are consistent in showing altered or lost obsidian hydration bands for some proportion of burned assemblages. In some assemblages as little as 10-20% of the burned artifacts retain detectable bands or non-diffuse hydration rims (Skinner et al. 1997; Anderson and Origer 1997; respectively). There can also be striking differences between artifacts resting on a burned surface (with 35% retention of rims) and artifacts from below the surface (with 86 to 95% retention of rims) (Trembour 1990). In another study (Linderman 1991, 1992), none of the surface artifacts retained measurable hydration after exposure to slash pile burning, while three of the artifacts (~10%) placed just below the surface (3.5 cm) did retain measurable hydration.

A **post-fire study** following the Henry Fire (Lentz et al. 1996) is of particular interest here because it occurred in the southwestern quadrant of the Jemez Mountains on Holiday Mesa, where obsidian artifacts could have derived from the Cerro Toledo Rhyolite source areas investigated in the current study.[1] Obsidian hydration analysis of 10 obsidian artifacts (Origer 1996) from Henry Fire sites with variable degrees of burning (lightly, moderately, and heavily burned, as determined in part by observing characteristics of ground charring) indicate variable alteration of OH bands that correlates partially with degree of burning at the site and partially with surface vs. subsurface exposure (Table 2-2). Light burning had minimal effect to OH (100% intact OH), moderate burning yielded intact measurable OH in 66% of specimens, and heavy burning yielded undamaged OH in only 33% of specimens (Origer 1996:82).

The fact that the "control" artifact collected from an apparently unburned site (see Lab # 2 core flake, bottom row of Table 2-2) did not have intact hydration and showed

[1] No geochemical sourcing was conducted on obsidian artifacts in the Lentz et al. 1996 study.

macroscopic and microscopic evidence of damaged surfaces is important. It demonstrates one of the difficulties of post-fire studies and a central concern for any study of the archaeological record of past and present fire effects: the burning of forests is a recurring process that creates multiple opportunities for heat exposure to assemblages and for individual specimens to experience repeated heat exposure. Assessing the effects to artifacts from a known forest fire must also take into account that observed effects actually may be from prior events.

Table 2-2. Obsidian hydration analysis of obsidian artifacts burned in the Henry Fire (from Origer 1996:81-82, compiled from Tables 28-30).

Lab # & Artifact Type	Surface / subsurface	Burning at site	Mean OH thick (µ)	Macroscopic condition of surface(s)	Microscopic condition of surface(s)
3 angular debris	Surface	Light	2.4	good	good
6 projectile point	Stratum 1	Light	6.1	good	good
1 core flake	Surface	Light	1.8	good, shiny undamaged	good
8 multidirectional core	Surface	Moderate	DH ~2.9	good	slightly damaged
9 core flake	Stratum 1	Moderate	2.2	good	moderately damaged
4 core flake	Surface	Moderate	1.5	good	slightly damaged
7 core flake	Surface	Heavy	2.5	dull dorsal, good ventral	one or more damaged surfaces
10 angular debris	Stratum 1	Heavy	DH	good	no obvious damage
5 core flake	Surface	Heavy	NVH	good dorsal, dull ventral	one or more damaged surfaces
2 core flake	Surface	Unburned / Control	NVH	dull damaged surfaces	damaged surfaces

One of the greatest benefits of post-fire studies is that they afford a view of actual variability in fire effects under the conditions of real forest fires and authentic archaeological assemblages. However, the variables of burning and the actual conditions of artifacts prior to the recorded occasion of heat exposure cannot be known. In prescribed burn field experiment studies, how burning occurs can be controlled or known, and artifact conditions can be recorded and/or manipulated.

Recent **prescribed burn studies** control the fuel loading to which assemblages are subject (e.g., Benson 2002; Deal and McLemore 2002; Green et al. 1997; Halford and

Halford 2002; Solomon 2002). Where fuel loads and actual ground temperatures could be estimated or measured in these studies, the proportion of hydration rims lost in an assemblage was higher in the higher fuel loads and lower with lighter fuels.

As additional variables are added to the design of prescribed burn studies, new questions are raised. Such variables include duration of heat exposure and season of burning (Deal and McLemore 2002). The results of the Deal and McLemore (2002) study show a strong influence of lengthened heat exposure, with hydration rim losses (from 33% to 78%) occurring in all the fuel types, at relatively low burn temperatures, and even in subsurface samples.

Other questions posed by results of recent prescribed burn field experiment studies include spatial variation in surface fire effects. A study by Halford and Halford (2002) in a sagebrush steppe community in Mono County, California, demonstrates spatial variation in fire effects at a surprisingly fine scale, where hydration band alteration varied in artifacts distributed within spatial scales as small as 1 m^2. Another recent study (Solomon 2002) shows hydration losses at anomalously low temperatures (< 100°C), indicating that there may be some other as yet unidentified variable(s) that interact(s) to lower the temperature at which OH rims are affected. Differences in raw material between the studies is certainly one variable whose relevance is not yet understood, although results of experimental heating studies by Solomon were interpreted to indicate that variation in material source did not play a role in the results she obtained (Solomon 2002:84).

To summarize thus far, the role of post-fire studies has been to establish the kinds of empirical variation in effects possible following forest fires, while the role of field experimentation with prescribed or controlled burning has been both to evaluate the contribution of alternate variables and to introduce new variables with previous unrecognized relevance. Both kinds of studies address the complexity of heat effects in the setting of actual forest fires. In contrast, the role of laboratory heating experiments is to systematically simplify the equation in order to determine the constants that can be assumed amid the range of uncontrolled or unknown variables.

Experimental laboratory studies of heat alteration of existing obsidian hydration rims (Hatch et al. 1990; Skinner et al. 1997; Solomon 2002; Trembour 1990)[2] allow analysis of how temperature and duration of heat exposure affect artifacts under controlled conditions. Trembour's 1979 La Mesa fire study was the first such laboratory investigation of heat alteration of OH rims (Trembour 1990:175-77). Several pieces of the same hydrated artifact were subject to heat exposure of one hour at various temperatures between 170°C and 760°C in a muffle furnace. He observed that with increased heat exposure there was a diminution in the sharpness of the hydration boundary, an increase in the width or depth of the hydration band with "diffusion", and eventual loss of the hydration band (Table 2-3). Trembour also noted the development of thermal crazing at 540°C, and "vesiculation" of the obsidian at temperatures above 750°C. The obsidian used was from a "South American" source, and Trembour (1990:177) notes that experiments on glasses from other sources had similar results although with some variation in the temperatures at which alteration occurred.

Table 2-3. Trembour (1990:175) results of laboratory heating of hydrated obsidian.

Heating Temperature (1 hr duration)	**Observed effect/alteration**
Untreated	A uniform rind of about 10.7 µm depth, of white color in both plain and polarized light, and with sharp interface line separating hydrated from unhydrated obsidian.
170°C, 220°C and 350°C	Progressively more tinting of the rind to grey or violet in plain light, lessening of rind brilliance in polarized light, increasing broadening and blurring of the interface "line", inward travel of the "line" to deeper positions to a maximum of about 20%. These phenomena are attributed to diffusion and stress-relief with rising temperatures. At about 350 degrees centigrade, efforts to fix the position of the interface for measurement become unfeasible.
430°C	At about 430 degrees centigrade virtual thermal obliteration of all traces of rind and inner boundary took place.
540°C	First appearance of thermal crazing on the obsidian surfaces whether they are external and fresh, internal, or hydrated. The onset temperature is quite sharp. The cracks are very shallow and tend to form an intersecting network visible with a magnifying handglass.
760°C	Beginning of melting and vesiculation of the test piece body; conversion to a frothy mass by escaping volatiles.

In addition to results published with the La Mesa Fire study, Trembour also conducted additional unpublished heating experiments to investigate the temperature at

[2] Another experimental laboratory study of heat effects that included obsidian is by Bennett and Kunzmann (1985). The study is not discussed here because the authors did not include alteration of OH in their investigations, and because the document is marked "Preliminary: Not for Citation or Publication".

which crazing and vesiculation occurred in obsidian artifacts from various obsidian sources. The results of one set of such experiments are shown here in Table 2-4 (Trembour, personal communication 1996), with the full description included in Appendix A. These results are especially informative because they provide an assessment of the relationship between crazing and vesiculation in a variety of obsidians. Trembour's unpublished results (Appendix A) also show the data he used to conclude (Friedman and Trembour 1983:545) that the formation of crazing occurs at higher temperatures than does alteration of hydration rinds (i.e., above 540°).

Table 2-4. Unpublished results of laboratory heating of hydrated obsidian by Trembour (see Appendix A).

Obsidian Source	Crazing Temp.		Vesiculation Temp.	
	°F.	**°C. conv.**	**°F.**	**°C. conv.**
Popayon, Columbia:				
Artifact "X"	1000	538	1400	760
River Pebble, RN2	1800	588	1500	815
Soil Pebble, RQ	1100	593	1550	843
River Pebble, RM1	>1600	>871	>1600	>871
El Zamorano, Honduras:				
River Pebble	1100	593	1550-1600	843-871
(USGS) Mexico 1	<1150	<621	<1260	<682
(USGS) 3419-8B	<1150	<621	<1150	<621
" 3419-17D	>1550	>843	>1550	>843
Obsidian Cliff, Wyo.:				
nat. fragment	>1550	>843	>1550	>843
El Chayal, Guatemala:				
nat. fragment	>1550	>843	>1550	>843

More recent heating experiments by Skinner et al. (1997:10-13) essentially replicated Trembour's published results with heating of one hour at six temperature intervals between 100°C and 600°C (Table 2-5). After heating to 300°C for one hour, significant alteration of the diffusion front was observed. When heated at 400°C, the diffusion front is lost and the hydration band is no longer measurable. When heated to 500°C and above, the hydration band has disappeared. The artifact used in this study was from the Newberry Volcano geochemical source in central Oregon.

Table 2-5. Skinner et al. (1997:12, Table 2) results of laboratory heating of hydrated obsidian. Six sections of a single Newberry Volcano Flow obsidian artifact were heated for 60 minutes to six different temperatures.

Oven Temp	Hydration Rim before heating	Hydration Rim after heating	Comments
100° C	3.2 ± 0.1 µm	3.1 ± 0.1 µm	No change in the rim width or rim appearance.
200° C	3.2 ± 0.1 µm	3.4 ± 0.1 µm	Slight increase in rim width; diffusion front remains clearly defined.
300° C	.2 ± 0.1 µm	5.4 ± 0.0 µm	Hydration rim becomes very diffuse; diffusion front becomes very indistinct and difficult to measure.
400° C	3.2 ± 0.2 µm	None	Extremely diffuse rim is only marginally recognizable and could easily be missed; absolutely no sign of a diffusion front remains.
500° C	3.2 ± 0.1 µm	None	No visible hydration rim.
600° C	3.2 ± 0.1 µm	None	No visible hydration rim.

A similar study conducted by Hatch et al. (1990) on an artifact of El Chayal obsidian from Guatemala returned results generally in agreement with those of Trembour (1990) and Skinner et al. (1997). In a study designed to address the potential effect of cremation fires on obsidian hydration in artifacts in Hopewell assemblages, they observed expansion of the hydration band when heated at temperatures from 100°C to 400°C (heating for 20 minutes), and progressive decrease in the hydration band from 500°C to 900°C (Hatch et al. 1990: 473-4). In this experiment, however, the hydration band was not lost even at the highest heating temperature. In a similar experiment reported briefly in Stevenson et al. (2004:562), hydration rim(s?) were lost after heating for twenty minutes at 400°C.

In all of these studies, the duration of heating was one hour or less. Solomon (2002) obtained somewhat surprising results in a laboratory heating experiment where relatively low temperatures were used (100°C to 300°C) when heating durations were extended to 12 hours. Obsidian hydration bands were altered or lost in 75% of specimens at 200°C when heated for 12 hours, but only in 20% of specimens when heated for 2 hours. At 300°C, 100% of bands became diffuse after 1.3 hours heating and all were altered after 12 hours heating (20% diffuse, 80% no visible band). These results suggest that smoldering fires could have significant OH effects even if the maximum temperatures reached remain low. Interestingly, alteration or loss of hydration bands was greater and more consistent in samples placed on sand than in those placed in crucibles.

However, another variable, type of obsidian, could contribute to the outcome. The 90 samples used in the experiments were from four California obsidian sources (Borax Lake, Mt. Konocti, Napa Valley, and Annadel, with sourcing based on visual identification). The report indicates that source had no effect on outcome (Solomon 2002:84) but the report does not identify source of specimen in the presentation of data/results.

The final experimental study to be discussed (Buenger 2003) is the most recent and is the first study to fully combine field and lab experimentation in analysis of obsidian fire effects. Buenger conducted controlled laboratory experiments a number of different kinds of artifact material types, including obsidian, using 1) a muffle furnace, and 2) a large combustion chamber within an environmentally controlled wind tunnel. By using the wind tunnel, Buenger is the first researcher to replicate actual fire conditions and to study wildland fire intensities under a variety of fuel loads, fuel placement relative to artifacts, and wind velocities. He recorded not only ambient temperatures during burning, but also monitored actual artifact temperatures on upper and lower surfaces, and compared air vs. soil heat flux. Unfortunately, heat effects on obsidian were not the focus of the study: only two obsidian artifacts per trial were included in the muffle furnace and in the wind tunnel trials, and obsidian hydration effects were not part of the research design. No source is given for the obsidian used.

Buenger's muffle furnace heating experiments provides some new information relevant for describing fire effects. Table 2-6 shows his results of laboratory heating of obsidian in a muffle furnace (Buenger 2003:132-170, especially Table 3.1, pages 168-170). He observed metallic sheen occurring upon heating to 400°C and above, and surface crazing occurring at temperatures from 600°C and above (except for one case of crazing at 400°C). Most interesting, another effect Buenger observed commonly was "enhancement of pre-existing cracks" or "enhanced radial fracture lines". As he discusses, this effect is to existing "radial fracture lines" originally produced during knapping, where "Under thermal stress, these lines appear to increase in length, width, and presumably depth (Buenger 2003:225)." This effect also was observed during wind tunnel trials where more detailed information was available on actual artifact temperature, rates of heating and cooling, and differences in the experience of upper and lower artifact surfaces.

Table 2-6. Effects observed on obsidian specimens in Buenger (2003) muffle furnace laboratory heating experiments (includes two obsidian types, with two specimens—one from each source—used in each temperature run).

Temp °C	**Obsidian1** black with fine gray banding, unspecified source	**Obsidian2** black, red, and translucent, unspecified source
100°	None	None
200°	Increased luster	Increased luster
300°	Increased luster	Increased luster
400°	Metallic sheen Light enhancement of pre-existing cracks Light fine surface crazing	Metallic sheen Light enhancement of pre-existing cracks
500°	Metallic sheen Light enhancement of pre-existing cracks	Metallic sheen Light enhancement of pre-existing cracks
600°	Metallic sheen Light enhancement of pre-existing cracks Light fine surface crazing	Metallic sheen Light enhancement of pre-existing cracks Light fine surface crazing
700°	Metallic sheen Light enhancement of pre-existing cracks Light fine surface crazing	Metallic sheen Light enhancement of pre-existing cracks Light fine surface crazing
800°	Metallic sheen Moderate enhancement of pre-existing cracks Light fine surface crazing	Metallic sheen Moderate enhancement of pre-existing cracks Light fine surface crazing
900°	Metallic sheen Moderate enhancement of pre-existing cracks Moderate fine surface crazing	Metallic sheen Moderate enhancement of pre-existing cracks Light fine surface crazing
1000°	Metallic sheen Moderate enhancement of pre-existing cracks Moderate fine surface crazing Heavy vesiculation	Metallic sheen Moderate enhancement of pre-existing cracks Light fine surface crazing

Buenger (2003:226) infers that it is likely that enhancement of "radial fracture lines" develops under conditions "where obsidian is subjected to precipitous and brief heating above 500°C." This seems like an accurate interpretation. Temperature differentials within a specimen would lead to thermal stresses and strains that could conceivably extend the secondary fracturing associated with these fracture marking, enhancing their appearance (Tsirk, personal communication 2005). What Buenger is calling "radial fracture lines" are fracture markings known to fractographers as a form of "twist hackle" (Fréchette 1990:9, 21; see also Chapter 3). Such twist hackles, if further deformed (as by thermal stress due to expansion or unequal stresses), could conceivably become enhanced in appearance due to stretching. That enhancement of "radial fracture lines" has not previously been described by researchers of obsidian fire effects (including the current study) is not surprising. While such features can be detected by

fractographers even without examination prior to heating (Tsirk, personal communication 2005)[3], they likely would be observed by archaeologists only when artifacts were carefully examined both before and after heating. Buenger's (2003) study included this unusual attention to, and documentation of, detail among all the artifacts included in his study. Overall, Buenger's study sets a new standard for archaeological fire effects studies, and makes particularly effective use of the wind tunnel combustion chamber. Future research of this kind that is focused on obsidian fire effects and that includes analysis of alteration of obsidian hydration has the potential to be extraordinarily productive.

The Current Study in Research Context

Five questions for further research on obsidian fire effects were posed by Skinner et al. (1997). These are listed in Table 2-7 along with examples of studies that explicitly address the research question.

Table 2-7. Research questions posed by Skinner et al. (1997:14).

Questions for further obsidian fire effects research	Examples of recent (post-1995) studies that explicitly address the research question
1. What visual or petrographic (microscopic) indications of fire exposure are retained by obsidian artifacts or other artifacts or features found at archaeological sites?	Buenger 2003 Nakazawa 2002
2. What types of vegetation and fuel loads are necessary to reach temperatures capable of erasing or altering obsidian hydration rims?	Benson 2002 Deal and McLemore 2002 Green et al. 1997 Halford and Halford 2002
3. What variables can significantly ameliorate the effects of fire, e.g., depth of burial of an artifact?	Anderson and Origer 1997 Skinner et al. 1997
4. How much heat over what period of time is required to affect or erase hydration rims?	Origer et al. 1997 Hatch et al 1990 Solomon 2002
5. What effect does the chemical composition of the glass have upon rim survivability during heating, i.e., are temperature effects source-specific?	Solomon 2002

[3] Tsirk observes (personal communication 2005): "The stresses causing the enhancement of the twist hackles are different from those that led to the formation of the markings. The microscopic details of the enhanced twist hackles are therefore likely to differ from those of the normal formation of the markings. It is thus conceivable that detection of the enhancement might be possible without seeing the markings before a fire."

As shown, the fifth question in Table 2-7 concerns the role of obsidian composition in OH alteration. Only one example (Solomon 2002) can be found in the recent literature (post-1995), and preceding that, only Trembour's unpublished research (Appendix A) explicitly addresses this question. The current study was designed to fill this gap by investigating the role of obsidian composition in heat alteration of obsidian by forest fires.

To place the current research into the context of previous research, this is a post-fire study that focuses on the effects of fire on obsidian artifacts occurring on the surface. This research explores and describes macroscopic variation of fire effects, and then considers microscopic effects to obsidian hydration in artifacts at a variety of scales: within an assemblage and across a site, as well as within individual specimens. Finally the role of obsidian composition in variable fire effects is investigated by conducting intensive analyses of elemental and volatile composition of obsidian from within the Cerro Toledo Rhyolite obsidian in the Dome area where the Dome Fire occurred, and from alternate obsidian source locations with similar and dissimilar geologic origins. The contribution of this study to archaeological forest fire research will be an in-depth analysis of obsidian fire effects at multiple scales and degrees of resolution, married to obsidian geochemical analyses relevant for further enhancing the development and application of the obsidian hydration model.

CHAPTER 3
OBSIDIAN FIRE EFFECTS

In an archaeological discovery experience that does not often occur in actual professional circumstances, the unexpected phenomenon of extreme fire-altered obsidian was first encountered by the author and another Santa Fe National Forest archaeologist during routine post-fire survey for closure of roads in mid-July 1996, five weeks after the Dome Fire started. Initially it was not clear what the peculiar pumice-looking pieces were that we discovered amid the obsidian artifacts and nodules densely covering the ground along and below the ridgetop at Capulin Quarry. That the phenomenon was fire-altered obsidian only became evident once obsidian artifacts were found that had clearly discernible flake morphology compromised by bubbling and bloating (Figure 3-1). These partially vesiculated flakes served as a keystone to decode the bloated pieces that lacked identifiable artifact attributes.

Figure 3-1. Partially vesiculated obsidian flakes from Capulin Quarry (Specimens 1691-02 and 1691-51, dorsal surface; inset box is ventral surface of 1691-51)

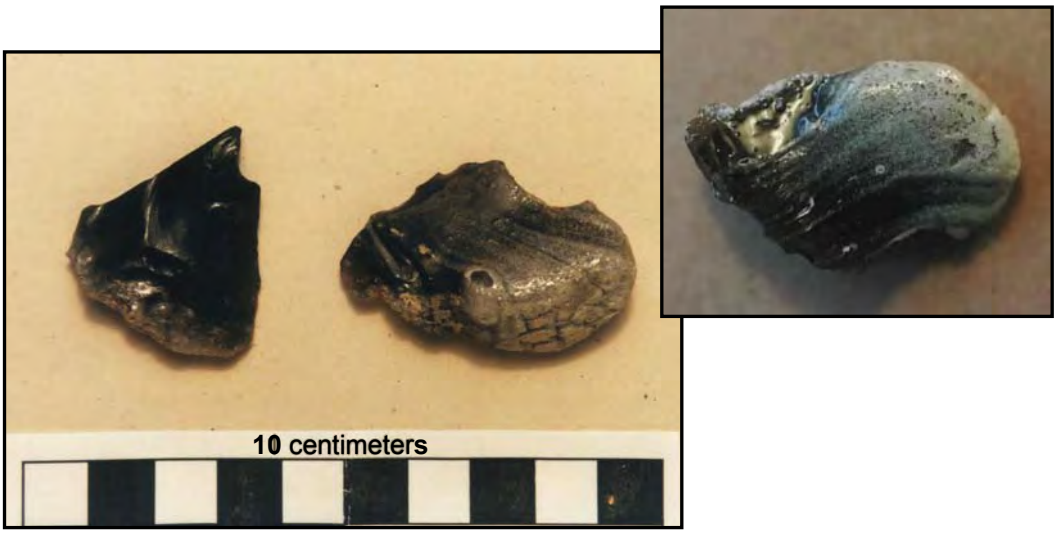

Once the vesiculated obsidian was recognized as not a normal product of volcanic or igneous petrogenesis, the "clusters" of vesiculated obsidian then drew our attention to the extent and distribution of archaeological fire effects at Capulin Quarry. These clusters are areas up to 2 m in diameter with concentrations of whitened and puffy

obsidian that, at the time they were first discovered, stood out as loci of light-colored material in conspicuous contrast to the blackened soil background.

Figure 3-2. Capulin Quarry following the Dome Fire. Photos taken in July 1996 on the day the vesiculated obsidian was first discovered in the burned portions of this quarry site: (a) view from near ridgetop facing west toward upper end of southwest-facing bowl in which high burn severity and locations of vesiculated obsidian were observed (E. A. Giedraitis in photo right); (b) appearance of a "cluster" of vesiculated obsidian around stump burnout at Capulin Quarry (the elongated light-colored features are exposed roots). Note in both (a) and (b) that the only remaining ground cover is fallen pine needles (post-fire), new generation of annuals, or partially combusted larger fuels—all original organic material was burned during the forest fire. The mortality of the standing trees visible in the foreground of (a) eventually reached 100% tree loss in the first year following the fire.

Figure 3-3. Vesiculation Cluster 3 around partially burned stump; box in lower right is a closer view of vesiculated pieces shown in upper left (October 1997).

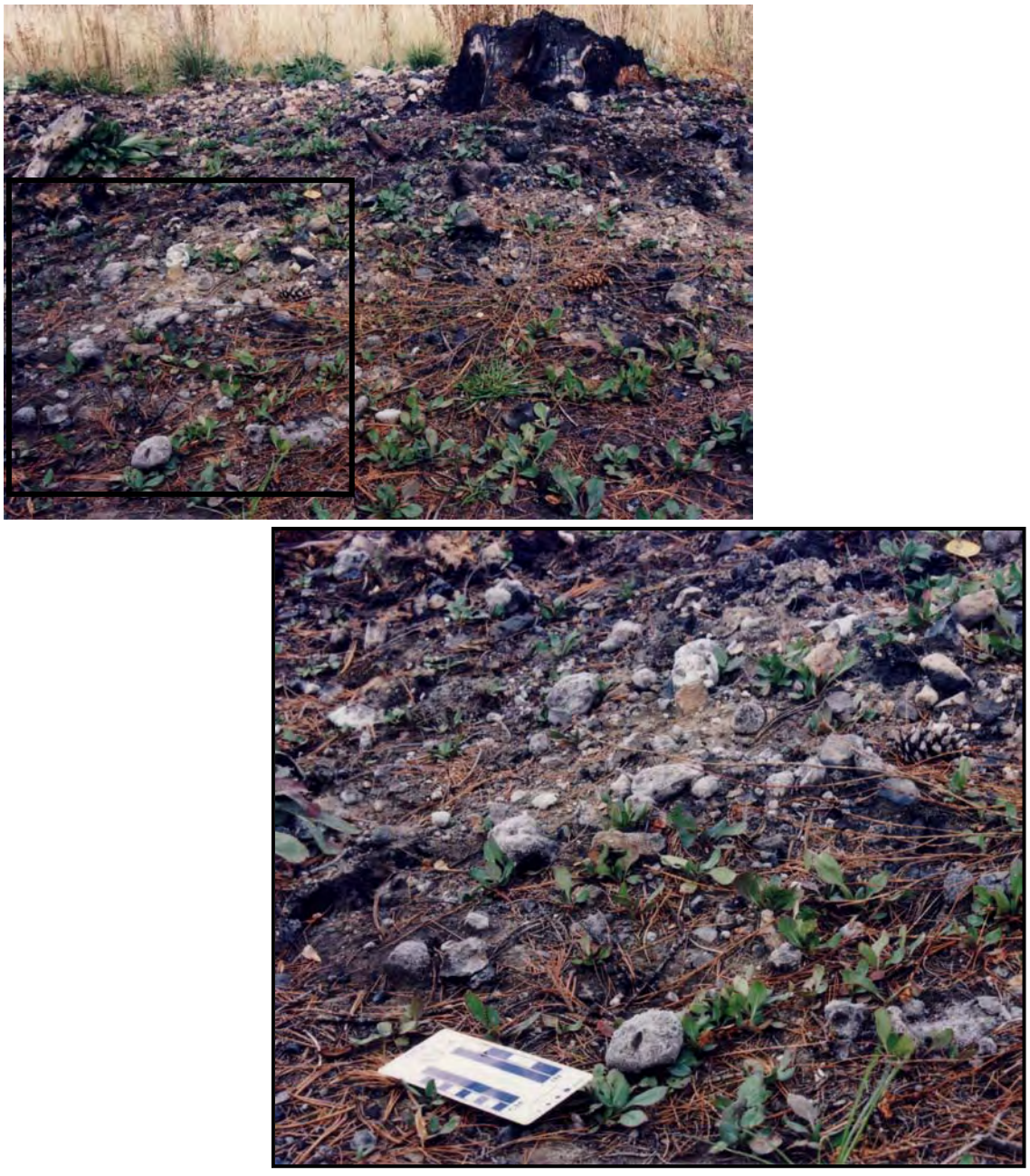

Several clusters were found to occur around burned-out stumps (Figures 3-2 and 3-3), and most of the twelve clusters mapped for this project are relatively evenly spaced in the severely burned portion of the site (Figure 3-4). Chances are good that additional unrecorded clusters occur at the site, as their visibility is surprisingly low where the soils were not charred black. Furthermore, our success in locating the vesiculated materials decreased significantly over time with the successful germination of grasses seeded into the Dome Fire burn area as part of post-fire rehabilitation.

Burning within the Capulin Quarry site was variable in severity. Along most of the ridgetop and on the sideslopes where the dense exposures of natural obsidian and obsidian artifacts occur, burning was mostly of high and moderate severity, but there are some patches of light burning. Areas of light burning were found in several locations: around the perimeter of the quarry, at the western edge of the ridge (where a wide road--Forest Road 289--served as a firebreak), and on the eastern end (the tip of the main northwest-to-southeast-trending ridge along which the obsidian-bearing geological deposit outcrops). There are few kinds of archaeological materials at the quarry other than obsidian, but some hammerstones observed within the burn area had fire-blackening and sooting, and several of the few chert artifacts seen at the site exhibit the classic fire-crazing and potlidding well-known for this material type (Purdy 1974, 1975; Purdy and Brooks 1971).

In the 100-x-100-m area of the site where the largest concentration of vesiculated obsidian clusters occurred, the burning was nearly uniformly severe: all surface organic materials were consumed to expose mineral soil, and standing trees suffered greater than 80 percent mortality with most exhibiting some degree of direct burning. There were numerous root burn-outs, and several examples of tuff boulders with heat spalling. The topographic location of this portion of the site makes it a good candidate for intense wildfire impact: it is a southwest-facing bowl below a narrow ridge that drops steeply to the north into the deeply incised upper reaches of Capulin Canyon. More dispersed occurrences of vesiculated obsidian were also found on the northwest-to-southeast-trending ridge that bounds this bowl to the east, and in a southeast-facing draw between that ridge and the main ridge.

Figure 3-4. Capulin Quarry Site Map.

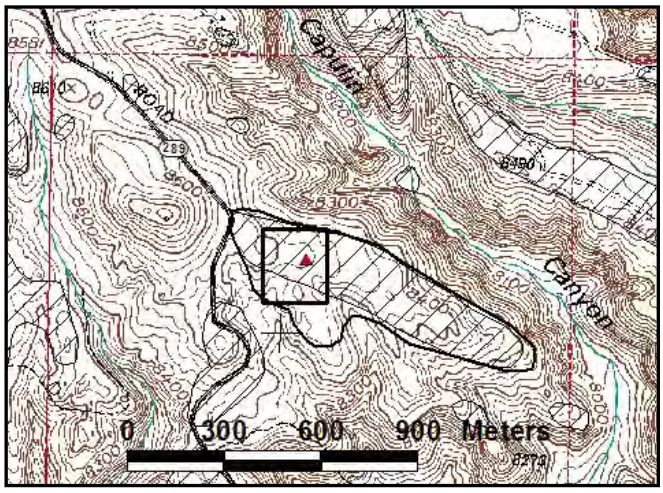

Capulin Quarry / LA 23961
SFNF AR 03-10-03-1691

←Topographic map is from Bland 7.5' Quadrangle (SFNF primary base series).

↓ Site map corresponds with inset rectangle and was created from ~600 total station mapping points; only features discussed in text are included.

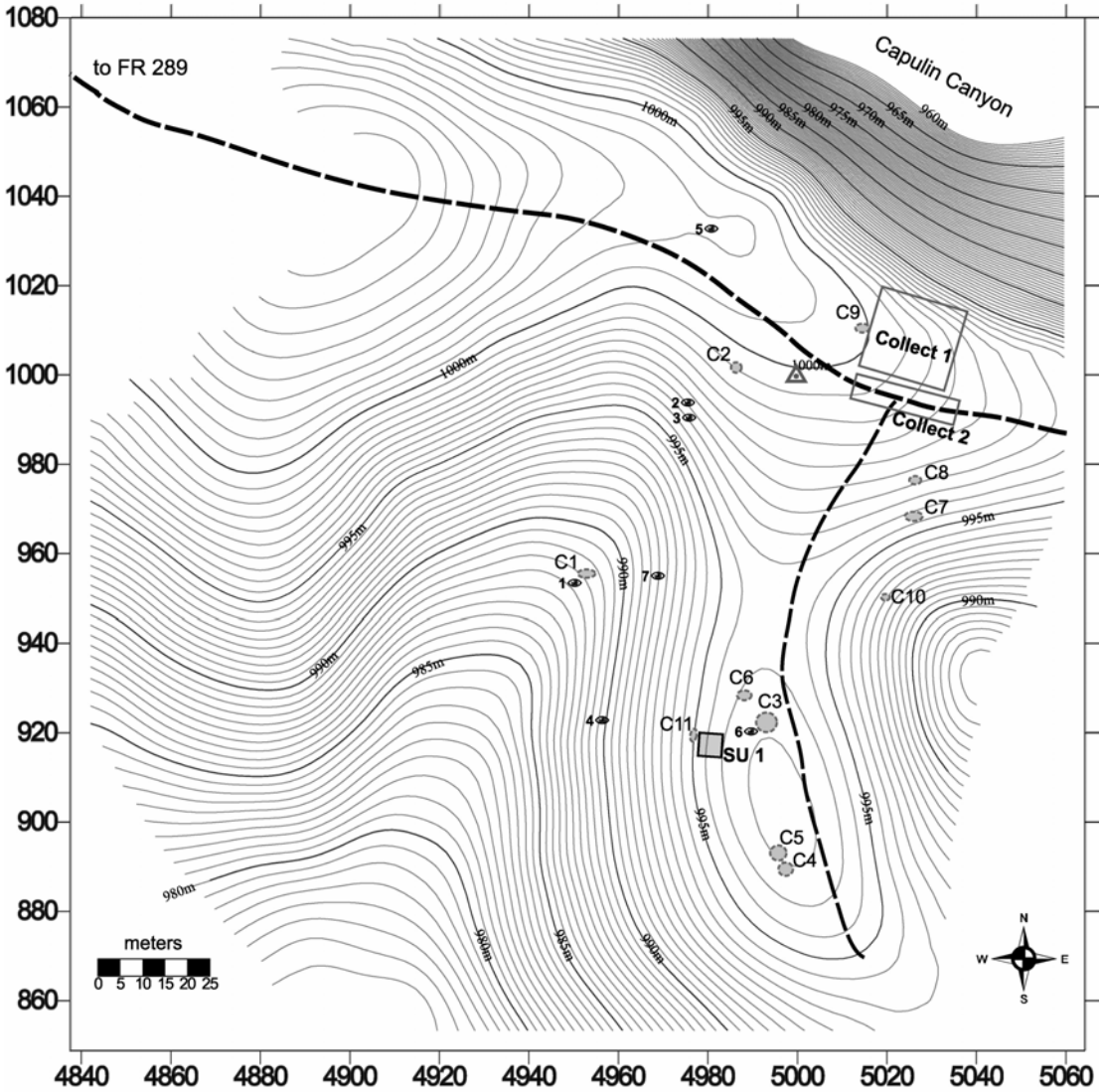

▲ Primary mapping datum, located at UTM E 372055.2, N 3961795.4, using Trimble GeoXT (PDOP 4.3, with differential correction, NMERI base station, 10/4/2004); elevation at datum is 2586m (8484 feet) amsl (from 10m DEM); labelled contour levels are arbitrary wth reference to mapping datum at 1000m.

Contour intervals = 0.5m
Bold contours at 5m intervals
C5 = vesiculation cluster
4👁 = photo point

3.1. Methods

Fieldwork at Capulin Quarry included mapping and collection of obsidian artifacts and raw material samples. Shawn Penman and the author mapped the site using a Sokkia total station (Figure 3-4). Topography, modern features, areas of burning, and the distribution of the clusters of vesiculated obsidian in the burned portions of the site were mapped. The locations of several photo points were also documented. Photo-documentation of site erosion and the recovery of vegetation at the site was conducted from certain photo points at regular intervals of at least every six months (and usually more often) through the first three years following the fire, and at irregular intervals after 1999 (usually 1-2 times per year) until 2003.

Collection of specimens within the forest fire area

Artifacts were collected from burned and unburned parts of the site using both judgmental and systematic approaches. Decisions about how to collect and select artifacts for analysis were greatly aided by discussions with Fred Trembour, Richard Hughes, and Tom Origer. Three surface collections were conducted to recover burned artifacts at increasing finer spatial resolution. Materials collected from all three sampling areas were employed in OH analyses to determine whether and how obsidian hydration rinds were affected. In addition, materials collected from the third area, Sample Unit 1 (SU1)—the 5 m-x-5 m grid—were used to compare among variable macroscopic effects, and between macroscopic and microscopic (OH) effects.

1. Sampling between burned and unburned area of site

This "judgmental" sample was conducted to compare burned vs. unburned materials broadly across the site. Specimens were selected arbitrarily from across the surface within two large collection areas. This collection was intended to be "neutral" with regard to obsidian fire effects: no attempt was made to select for or against apparent fire-alteration in these specimens. "Collect 1" was located **within** the burned area and measures approximately 20 m-x-20 m. "Collect 2" was located **outside** of the burned area and measures approximately 20 m-x-10 m. Finding an area in the site that was truly "not burned" was difficult. As a result, "Collect 2" includes materials from within a road

judged to have not experienced direct fire exposure. Because it was difficult to judge burning in this two-track where fuels would already have been absent, the assessment of no burning may not be entirely accurate.

Across the site, additional judgmental sampling included collecting and mapping individual specimens that were of particular interest (e.g., as especially good examples of certain fire effects or raw material visual appearance), or to increase the total sample of partially vesiculated flakes.

2. Sampling among vesiculation clusters

This systematic collection compared artifacts from areas with different degrees of apparent burn severity across the site, with reference to the location of clusters of vesiculated obsidian. Specimens were collected from within and near three vesiculation clusters (Clusters 2, 3, and 7). One set of specimens (Unit 1) was collected from within a 50-x-50-cm grid placed to include an area of dispersed vesiculated materials (not dense enough to warrant the term cluster). In each case, all artifacts >2 cm were collected after recording their location within a 50-x-50-cm grid and photographing the burned materials in situ (Figure 3-5).

In the obsidian hydration analyses presented in Chapter 4, these two collection areas were combined to create categories of burn severity designated by proximity to the vesiculation clusters. The categories created represent the full range in the "burn mosaic" observed at Capulin Quarry. The four categories thus provide an ordinal distribution across the degrees of burn severity observed across the entire site. In decreasing order of burn severity they are:

- *in cluster*: within a maximum 1 m diameter central core of vesiculation clusters;
- *near cluster*: within 2 m of the center of a cluster;
- *burn area*: specimens were collected from throughout the burned portions of the site but not in proximity to clusters;
- *unburned*: specimens were collected from within the quarry but in an area not burned during the Dome Fire.

Figure 3-5. G. Raymond recording artifact attributes and position within 50 cm-x-50 cm sample unit at Cluster 3 (red-and-white grid square in photo center). The 5 m-x-5 m systematic collection area is located on the slope in the left background of photo; photo faces southwest (April 1997).

3. Sampling within area with dispersed moderate and severe burning

The final sample area is a 5 m-x-5 m grid ("Sample Unit 1, SU1") placed in an area adjacent to a cluster of vesiculated obsidian, and included dispersed artifacts that were visibly fire-affected. The goal was to provide a sample that is representative of the full range of heat effects expected where there is high and moderate severity of burning but where not all artifacts are necessarily affected. Collection across an area 5 m-x-5 m provides a larger sample size than can be collected in a single small unit and affords examination of effects across a larger contiguous area.

Within this 5 m-x-5 m grid, all surface artifacts >2 cm were collected within each of the 25 1 m-x-1 m units (Figure 3-6). In addition, all obsidian that appeared to be fire-fractured was collected. Finally, non artifacts were collected if they exhibited signs of fire alteration such as crazing and vesiculation. Collected specimens were etched with a small mark on the side facing up (Figure 3-7).

Figure 3-6. View SW to NE across Sample Unit 1 (SU1) 5 m-x-5 m collection unit; orange string lines mark 1 m-x-1 m grid (November 2001).

Figure 3-7. Collection of artifact and non-artifact obsidian specimens within a 1 m-x-1 m unit in SU1 (Subunit H1). All collected artifacts were etched on up-facing surface (November 2001).

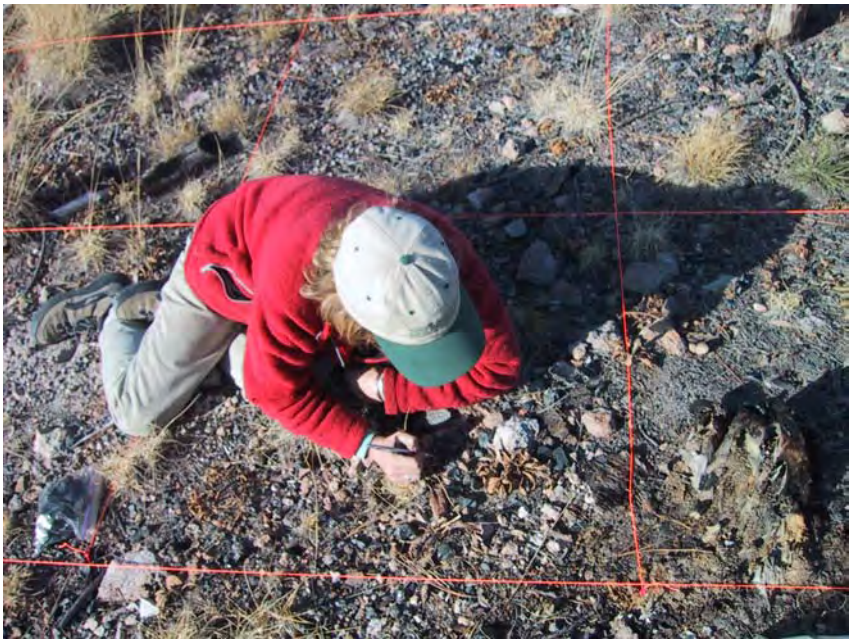

Figure 3-8. Characteristics of burning, vegetation, recent disturbances, and distribution of tuff blocks and gravel were sketched prior to collection within 1 m-x-1 m units in SU1. The red-and-white 50 cm-x-50 cm mapping square is located in the SW quadrant of Subunit F1 (November 2001).

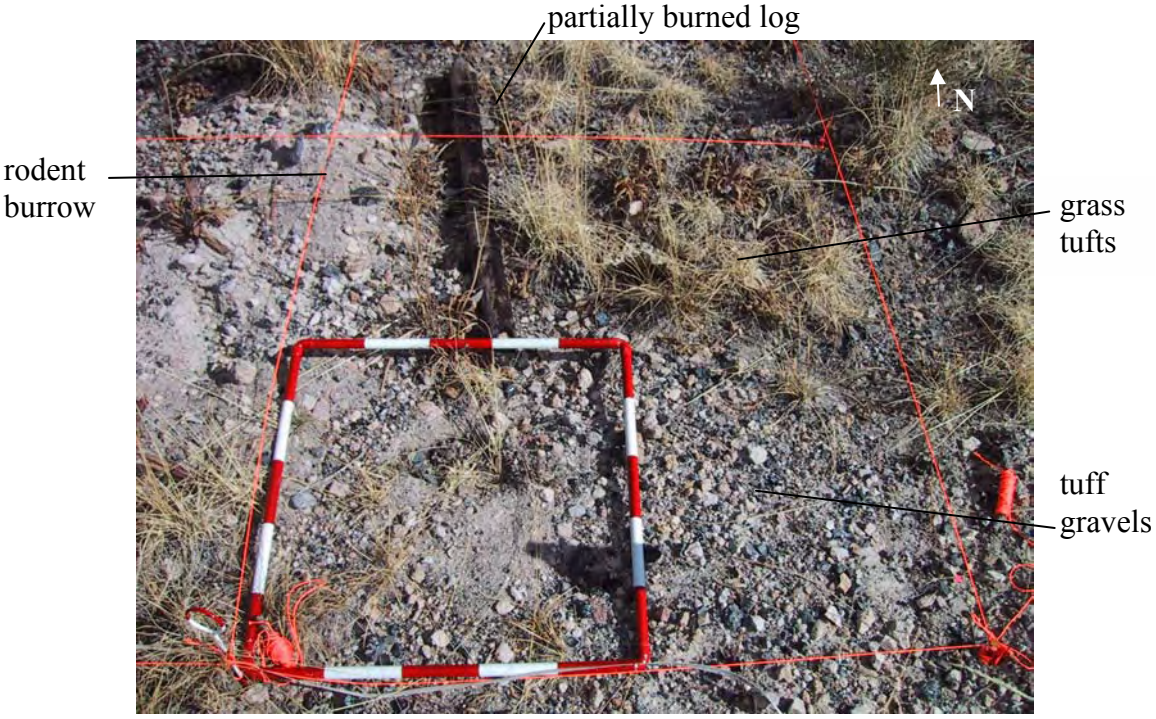

Prior to collection, each unit was photographed and a sketch map was made of the presence and distribution of existing vegetation (e.g., tufts of grass) and insulating materials (e.g., large tuff blocks, concentrations of smaller tuff gravels), and any indicators of burning (e.g., partially consumed logs, scorched tuffs) or post-fire disturbances (e.g., rodent burrowing) (Figure 3-8). The total number of artifacts recovered in this manner turned out to be startlingly more abundant than the number actually needed for analysis, so only a sample of the total was subject to obsidian hydration analyses (see below). All artifacts and non-artifacts, however, were systematically examined for potential fire effects.

Examination of obsidian fire effects

After collection, all specimens from Capulin Quarry were closely examined to identify whether any macroscopic fire effects could be observed. This inspection was conducted using the naked eye, assisted in some cases with a 10x hand lens and/or a

magnifying lamp. As part of the process of learning to accurately identify fire effects, some artifacts were examined under a dissecting microscope at magnifications up to 50x. It was determined during the examination process that the fire effects described in Chapter 4 are most reliably detected with 10x hand lens magnification, rather than with no magnification, and can be best seen under incandescent or natural light. However, all fire effects described here as "macroscopic" are *visible* without magnification once the analyst is familiar with their appearance. Fluorescent light without any additional incandescent or natural light seems to be the least favorable lighting condition.

Before sending specimens for XRF and OH analysis, raw material appearance and observed fire effects were recorded and each specimen was photographed. Specimens were submitted for XRF and OH analyses along with these observations and accompanied by specimen photographs. When the XRF and OH analyses were conducted, Hughes and Origer marked on the photographs the exact locations sampled. This step was important for understanding possible relationships between the analytical results obtained and the nature and location of macroscopic fire effects. In several cases, multiple XRF readings or OH cuts were needed to better measure the potential role of variable fire effects on individual specimens; in these cases, the information recorded on specimen photographs proved to be especially useful.

Specimens collected from the 5 m-x-5 m grid were examined in the same way but also were sorted by size and by whether they were artifacts, fire-fractured non-artifacts, or unfractured non-artifacts. Any cores (unshaped and bifaces) or otherwise modified flakes (e.g., shaped scrapers or flakes with edge-utilization) were noted. The overwhelming majority of items collected from the units within the 5 m-x-5 m grid, however, are simply un-modified flakes or fractured obsidian.

Reconnaissance for fire effects outside Capulin Quarry

From 1997 to 1999 non-systematic survey was conducted throughout the area burned in the Dome Fire to determine whether there were other locations with concentrations of obsidian fire effects, especially vesiculation, outside Capulin Quarry. Several other instances of vesiculation were found both within and outside the Dome Fire burn area, although nowhere did this fire effect occur in as large an area or with so many

dense clusters as observed at Capulin Quarry. Multiple pieces of vesiculated obsidian were found at Obsidian Ridge (which experienced back-burning during Dome Fire suppression), in a location outside the Dome Fire where prescribed burning occurred in the early 1990s, at a stump burned by a lightning strike on Rabbit Mountain, within the burn zone of another smaller forest fire (the 1998 Cochiti Fire), and most revealing, within recent campfire rings at a location outside of the Dome Fire (Figure 3-9). In all of these cases (except, perhaps, in the Cochiti Fire area where burn severity was not specifically assessed), the burning conditions that resulted in obsidian vesiculation would be considered anything but extreme.

Figure 3-9. Campfire outside the Dome Fire burn area where vesiculated obsidian has been found in this and a nearby campfire ring consistently each time monitored between 1996 and 2004: (a) R. Steffen at campfire ring; (b) view within campfire ring showing oxidized tuff blocks, burned bone, and vesiculated obsidian, with quarter for scale; (c) burned bone and vesiculated obsidian from within campfire (November 2001).

An additional site with obsidian fire effects (e.g., crazing, deep cracking, surface sheen, and vesiculation) also was found outside the Dome area at a small rockshelter site (LA82757) within the Valles Caldera National Preserve on the southeast side of Cerro del Medio (north of the current project area). There are two factors that make this find particularly interesting. First, the site is located outside the CTR-Dome source area and instead near Valles Rhyolite primary or secondary Cerro del Medio source areas (see Chapters 2 and 6 for additional discussion of the CDM source area). Second, the site was found by archaeological surveyors trained to recognize the fire effects described later in this chapter. Further, the site had previous been recorded and tested (Acklen 1993) without any documented recognition of heat alteration to obsidian at the site. While it is possible that a forest fire event occurred at the site after testing, this is unlikely. The recognition of the attributes of heat altered obsidian in 2002 at the site by archaeologists trained to identify these effects provides confirmation that obsidian fire effects, while subtle, can be reliably identified in archaeological assemblages once made known to trained professionals.

In sum, the results of my reconnaissance for other locations like Capulin Quarry indicate that the obsidian fire effects observed at this site are unusual in extent but not in kind. Archaeologists' lack of collective knowledge of the existence of obsidian vesiculation probably stems from a lack of familiarity with the appearance of this extreme fire effect rather than an actual rarity of the phenomenon in assemblages affected by forest fires. My conclusion is that at least three factors are required to consistently and reliably document obsidian altered in forest fires. These factors are: 1) conditions of sufficient heat to cause alteration (which may not require extraordinarily high burning temperatures or duration of exposure), 2) field personnel able to recognize the phenomenon when encountered, and 3) an abundance of obsidian material subjected to the sufficient conditions of heat alteration. In other words, obsidian fire effects are not likely to be recognized in the field unless there are conspicuous alterations of obsidian, and this is much more likely to occur when there are large quantities of glass on the surface available to be altered. If only a fraction of a given assemblage is affected, and if assemblages do not have high frequencies of obsidian, the results on the ground may not

be noticed. Finally, field survey immediately after burning will increase greatly the likelihood that forest fire effects to obsidian are accurately recorded.

3.2. Descriptions of Macroscopic Obsidian Fire Effects

In this section I describe the range of visible fire effects observed on obsidian artifacts at Capulin Quarry. This variation is grouped into several categories, and much of the text here is similar to information presented previously (Steffen 2002:163-165). The fire effects described here include the unusual and eye-catching vesiculation, and the more familiar obsidian sheen and relatively well known fire fracture, as well as subtle and less familiar attributes such as obsidian crazing and subsurface bubbling.

There is a need for a standardized set of definitions of the characteristic attributes found on burned obsidian (Deal and McLemore 2002:32; Kelly 2002:13; Skinner et al. 1997:14). As noted in Steffen (2002:163), standardized descriptions would have several benefits. They would facilitate communication among researchers, aid archaeologists in recognizing fire effects when encountered in the field or lab, and increase documentation of the occurrence of fire alteration. Increased recognition and documentation of obsidian fire effects will expand our knowledge of variation in burned assemblages, and result in a better understanding of how prevalent the occurrence of fire alteration of obsidian is in contemporary fires and in prehistory. If accurate identification and description can become commonplace in routine examination of obsidian artifacts, then the question of whether there has been prior heat exposure in assemblages will be raised more often. This can improve the selection of specimens submitted for obsidian hydration dating, expand inquiry into the issue of fire and heat as a post-depositional transformation of assemblages, and potentially broaden the research contexts in which the question of heat-alteration is considered.

Only two previous studies, by Trembour (1979, 1990) and Nakazawa (1998, 2002), provide the kind of systematic description that archaeologists need. Both Trembour's and Nakazawa's descriptions are based on field observations as well as heating experiments. While Trembour's descriptions were simple and did not include photographs (Trembour 1990:175; see Table 2-3 in Chapter 2, this work), they were the

only widely available descriptions available until the recent publication of the Loyd et al. (2002) volume in which Nakazawa's and Steffen's descriptions and photographs also were published. Nakazawa had earlier (1998) provided description and photographs, but this work was an unpublished M.A. thesis at Hokkaido University. The thesis, while written in English, was not known or available in the United States except as an abstract (see Loyd 1999:4).

Lack of access to systematic descriptions of visible obsidian fire effects has hampered communication among researchers of obsidian forest fire effects. An example of this problem can be found in the immediate research context of forest fire effects in the Jemez Mountains. Two post-fire archaeological studies near the current research area are the Henry Fire study (Lentz et al. 1996) and the Bandelier National Monument (BNM) Dome Fire studies (Elliott 1999; Elliott et al. 1998; Ruscavage-Barz 1999; Schub and Elliott 1998). While systematic descriptions of fire effects on lithic artifacts are included in both the Henry and BNM Dome Fire studies, these descriptions are oriented toward the fire effects apparent in chert artifacts, and the counts (frequencies) in tables of fire effects observed in these studies do not distinguish between the material types (i.e., chert, basalt, rhyolite, and obsidian) of lithic artifacts on which they occur. Thus, while it is clear that the intention of these researchers is to describe the effects of fire for obsidian artifacts, the systematic descriptive terminology used (e.g., potlidding, spalling, luster, crazing, in Lentz 1996) appears more suited to heat effects on chert artifacts, while those effects peculiar to obsidian required *ad hoc* descriptions (e.g., melting, re-liquification, styrofoam, popcorn, in Elliott 1999; Elliott et al. 1998; Ruscavage-Barz 1999; Schub and Elliott 1998). These observations on the use of terminology are not meant as criticism of these authors, but rather underscore the inadequacy of the available language for describing obsidian fire effects.

Fire effects descriptive categories

The goal of the descriptive categories provided here is to create a suite of descriptions that are inclusive of the full range of obsidian fire effects observed at Capulin Quarry and other Dome area sites following the Dome Fire. The eight categories include *matte finish*, *surface sheen (additive and altered)*, *fine crazing*, *deep surface*

cracking, *vesiculation*, *incipient bubbles*, and *fire fracture*. These categories build on Trembour's (1990) descriptions, with reference to Nakazawa's (1998, 2002), and are expanded from Steffen (2002). Additional kinds of fire effects or variations of these effects may occur on obsidian but were not evident in the Dome Fire specimens examined for this study. It is hoped that the suite of descriptions presented here will provide a baseline for archaeologists describing obsidian heat effects, and that these can be augmented or improved by others conducting intensive examinations of assemblages where there are differences in material characteristics or conditions of heat exposure that may create additional or differing expressions of obsidian heat alteration.

The order of presentation of the categories in the list below is arbitrary and does not imply any sequential relationship among the fire effects or how they develop on obsidian during a fire. The only two categories that are considered linked are fine crazing and deep cracking (with the latter developing from the former). Further, the *categories* are mutually exclusive (except as noted for crazing and cracking) but can and do occur concurrently on the same piece.

Matte finish

Matte finish is a dulling of one or more artifact surfaces. This may look like "weathering" or a lusterless patina. While often creating a dusty or soiled appearance, the dulling of the surface is not changed by wiping or rubbing. Depending on the nature of the source material, matte finish may appear similar to the primary cortex. Under low magnification, the surface may have an appearance of shallow pitting or roughness. Matte finish is difficult to capture in photographs, so no figure is provided here.

Matte finish is a broadly inclusive, wholly descriptive category that does not imply an understanding of how it was caused. It includes the characteristic “dulled” surfaces reported by Bennett and Kunzmann (1985) but is not intended to include a chalky patina that is described in several studies and was observed at Capulin Quarry. This build-up of a light-colored substance on the surface was not included in this category, or in other categories, because such patina development could be caused by other processes independent of heat exposure. Matte finish also likely includes what has been called “oxidation” of obsidian surfaces (e.g., Davis et al. 1995:37), although that

term implies undemonstrated knowledge of the mechanism that produces the dulled appearance. Matte finish probably is similar also to Nakazawa's (1998) "decrease in vitreousness", and appears similar to his Type 1c alteration (2002) where dulling of the surface results from tiny surface cracks.

Nakazawa's (1998) investigation into the role of matrix surrounding obsidian specimens when heated is particularly useful in understanding the dulling appearance in matte finish. He found that the dulling of surfaces increased with higher temperatures, longer duration of heating, and, especially, with the presence of wood ash in contact with specimen surfaces. The illustrations included in his study (Nakazawa 1998:25-30) match well with the dulled appearance observed on artifacts at Capulin Quarry that are included here in the category of matte finish.

Surface sheen

Surface sheen is a change in the reflective quality of the glass surface that appears as a metallic-like luster. The surface is less glassy and more metallic or burnished in appearance. This is one of the most widely recognized obsidian fire effects but its cause has been unclear. Examination of the sheen using optical microscopy and scanning electron microscope [SEM] shows that surface sheen is actually two different phenomena. One kind of sheen (additive) is caused by organic buildup (Figure 3-10) and the other kind of sheen (altered) involves a physical change in the surface (Figures 3-11 and 3-12).

Additive sheen

Additive sheen has the characteristic "gun-metal" appearance commonly observed on burned obsidian. This additive material appears under low and high magnification as a coating or residue (Figure 3-10: b-d). In qualitative x-ray microanalysis of such surfaces using an energy-dispersive x-ray spectrometer (EDS) in the SEM, high values of carbon are indicated. Buenger (2003:60) describes "an adhesive brown combustive residue" that occurs on a variety of burned artifact materials. Buenger's discussion appears to provide a satisfying explanation for the cause of additive sheen:

> The combustive residue deposit is a highly nitrogenous condensate tar that forms on cool surfaces (i.e., artifacts) during a fire (Yokelson et al. 1997). This deposit

> ranged in color from golden brown to black depending on the extent of combustion of the tar deposit. The charred portions of organic specimens represent the byproduct of the pyrolysis and partial combustion of those materials, particularly wood specimens. DeBano et al. 1998:23, refer to this as "char", a substance that is neither an intact organic compound nor pure carbon. In the instance of condensate tar deposition on artifact surfaces, it is likely that under natural conditions these deposits will weather from the surfaces of artifacts over time. In the laboratory, these deposits can be removed via vigorous scrubbing with water and a pumice soap solution. [Buenger 2003:60]

In the case of obsidian where there are no combustibles intrinsic to the artifact, there is no charring of the artifact and the condensate tar is wholly a residue deposited on the surface of the glass. A duff ground cover dominant in pine needles, as at Capulin Quarry, provides a rich source of pitch for deposition onto artifacts during the burning of a forest fire.

Figure 3-10. Additive surface sheen: (a) complete specimen 1691-1 (photo taken prior to OHD cut); (b) close-up showing optical magnification of sheen at location of OHD cut on specimen edge (note tarry globules visible in upper right); (c) secondary-electron image of residue on artifact surface (no scale recorded for this SEM image which was obtained at 500x magnification); (d) obsidian hydration cross-section shows no visible hydration and weathering or residue on exterior of obsidian surface (obsidian is located in lower left while upper right is the resin matrix of the OH slide; no magnification recorded for OH images, normal light, photography by T. Origer).

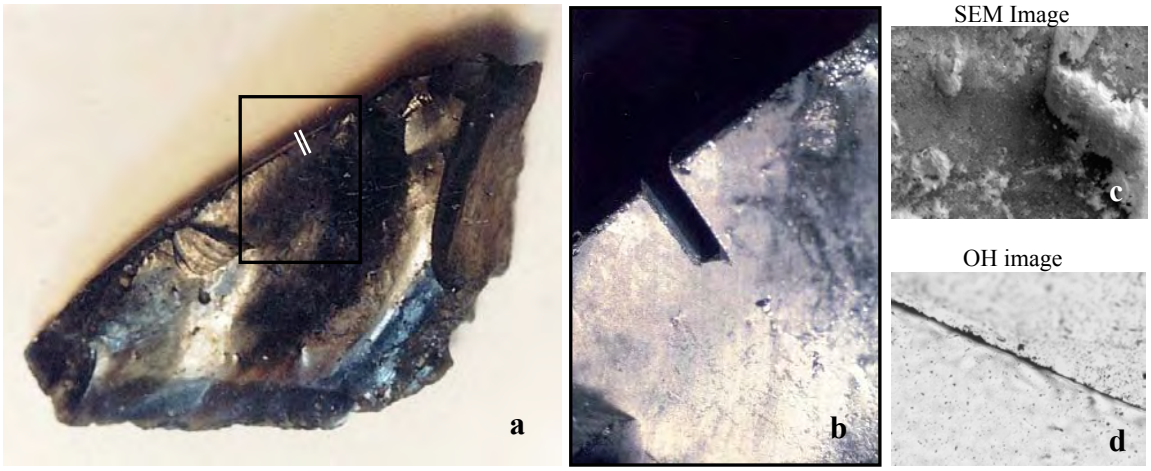

Altered sheen

In comparison, altered sheen is more silvery and reflective in appearance, and has a crinkly texture rather than the smoother burnished appearance of additive sheen (Figures 3-11 and 3-12). My examinations under high and low magnification indicate that in this kind of sheen the change in the reflective properties of the glass surface is caused by physical alteration of the surface by shallow (<10 microns) crazing and, in some cases, the formation of very small bubbles (see Figure 3-11:b). The specimens illustrated in Figures 3-11 and 3-12 demonstrate that altered sheen can vary across the surface of the glass depending on the underlying textures within the glass, although this is not a necessary characteristic of altered sheen. Altered sheen appears to match Nakazawa's (1998) "tiny bubbles", as well as his description of Type 1c alteration (2002).

Figure 3-11. Altered surface sheen, which appears as banding due to variability within the glass: (a) artifact specimen 1691-12; (b) OH image showing small bubbles below surface of glass (no scale, normal light, photography by T. Origer); (c) close up of sheen surface (originally 10x magnification); (d) further close up of sheen surface showing irregular texture of surface, and spalling at inclusion where "sheen surface" has been lost leaving unaltered glass (originally 25x magnification).

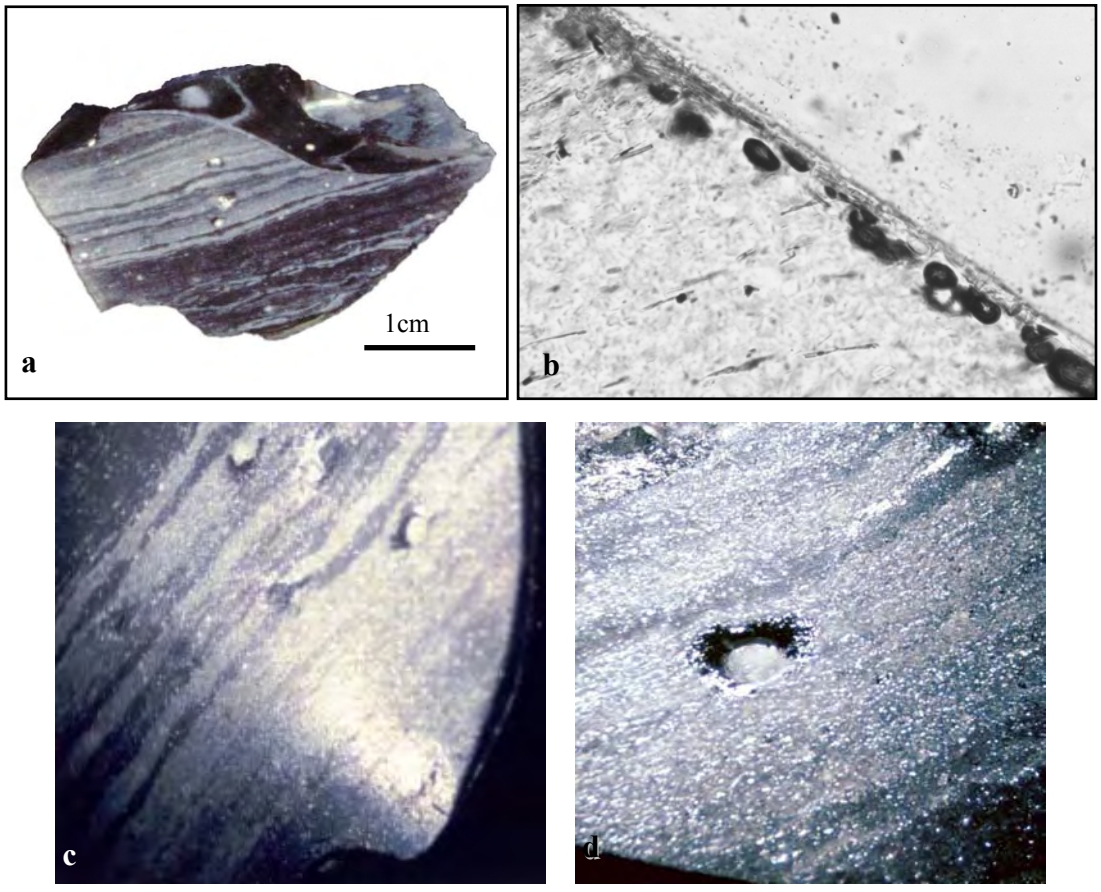

Figure 3-12. Altered surface sheen as apparent on non-artifact specimen OR-SH501 from Obsidian Ridge Quarry AR 03-10-03-2360 (LA82485): (a) 25x magnification; (b) 40x magnification, view corresponds with location of circle in (b).

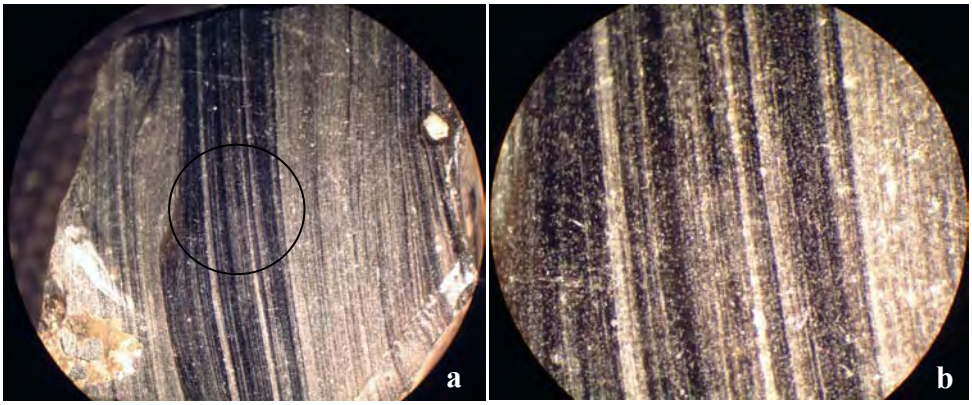

Fine Crazing

Fine crazing describes a delicate network of shallow cracks on fresh fractures or artifact surfaces (Figures 3-13 through 3-15). The crazing occurs across entire individual surfaces, but not necessarily on all of the specimen's surfaces. The crazing that I observed on burned obsidian at Capulin Quarry is quite unlike the kind of crazing that occurs on burned chert artifacts. Obsidian crazing is extremely shallow and is clearly a phenomenon that occurs only at the very surface. By contrast, chert crazing is caused by *internal* fracturing (including potlidding) expressed at the surface as cracking (Purdy 1974, 1975; Purdy and Brooks 1971). The causes of fine crazing in obsidian are probably similar to the surface crazing seen in silica glazes on high-fire ceramics, and as such may be a result of cooling processes and/or differential thermal expansion rather than the kind of material failure observed in chert crazing.

Fine crazing in burned obsidian overlaps somewhat in appearance with radial fracture lines that develop during detachment from a core. However, obsidian crazing can be readily distinguished from radial lines because crazing forms a network of interlocking or closed polygons (Figures 13-15) and radial lines do not. In the specimens I have examined, crazing also can be expressed in ways that fracture associated with removal from a core could not; this includes fine-line networks on ventral flake surfaces that are continuous across eraillure scars. Crazing can be easy to spot or very difficult to recognize, sometimes requiring a hand lens to identify. I have observed that crazing

more frequently is apparent on obsidian glasses that have smooth surface textures and/or that are clear rather than opaque. This may be because it is easier to identify crazing on the surfaces of fully aphyric glasses rather than because of actual variation in the occurrence of crazing among differing materials.

Figure 3-13. Fine crazing: (a & b) specimen 1691-SU1-I31, 6.3x and 40x magnification; (c & d) specimen 1691-26, 6.3x and 25x magnifications [both close up views (b & d) are at center of 6.3x images]; (e) alternate view of specimen 1691-26 [compare to (c)].

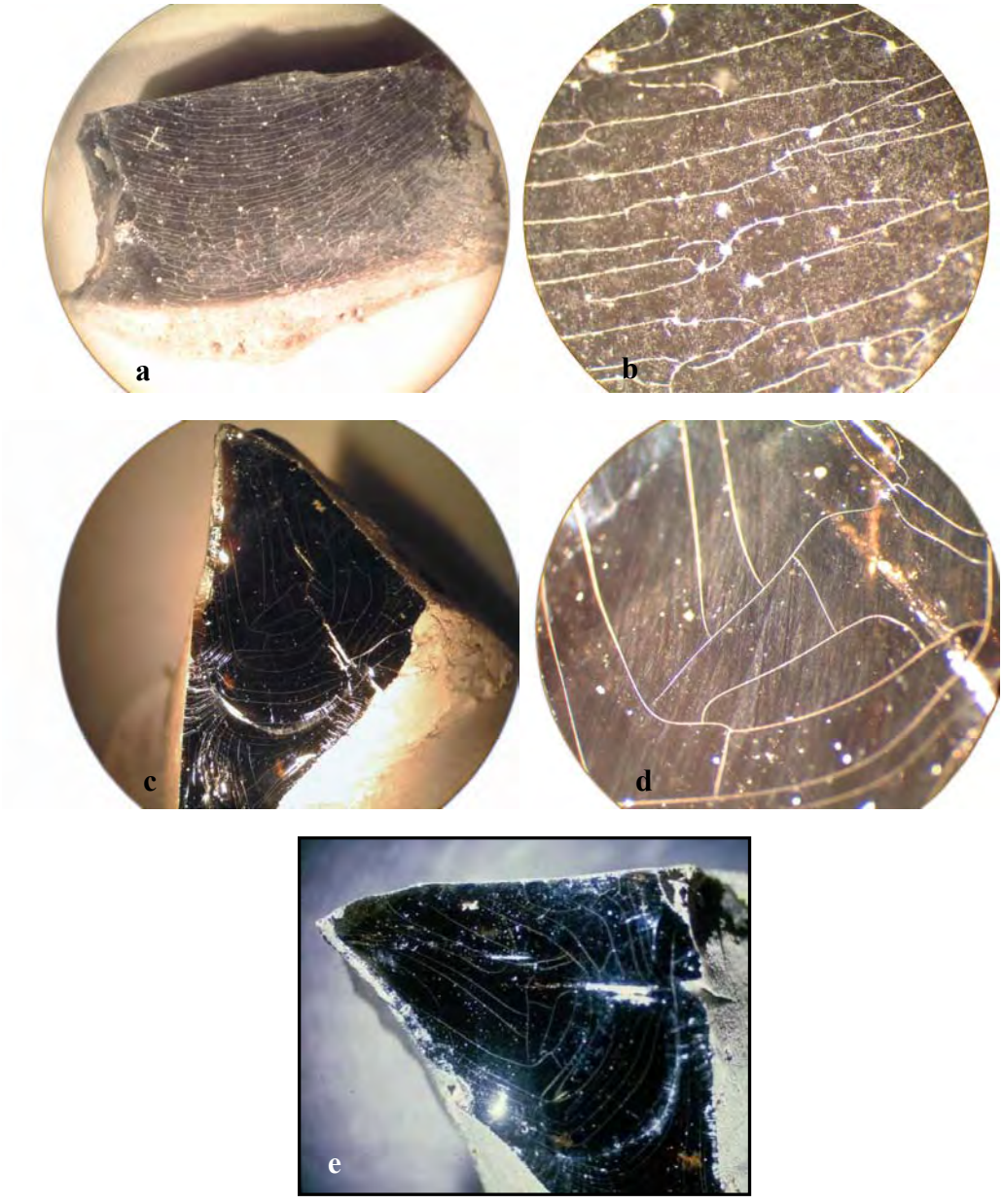

Figure 3-14. Fine crazing on dorsal surface of the partially vesiculated flake specimen 1691-02: (a) 8x magnification; (b) 30x magnification taken at center of image (a). Crazing lines appear to be somewhat altered by deformation from partial vesiculation.

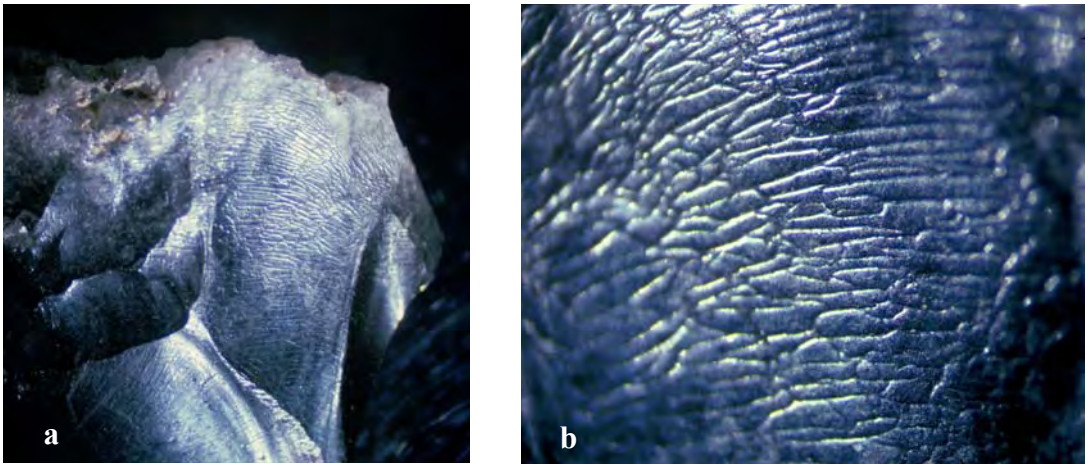

Figure 3-15. Fine crazing with two very different appearances: (a) semi-enclosed polygons on ventral surface of opaque obsidian specimen 1691-53 (see Figure 3-23, below); (b) fine crazing on translucent glass specimen from Colombia to illustrate the appearance of crazing where lines on multiple surfaces are apparent through nearly transparent glass (specimen provided by F. Trembour).

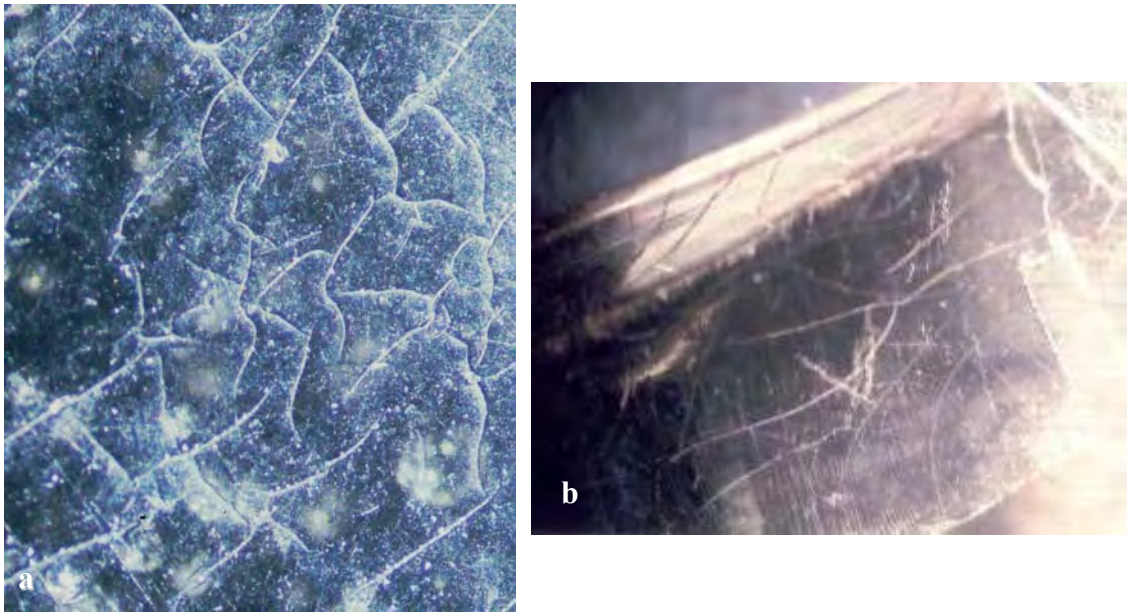

Deep Surface Cracking

Deep surface cracking describes artifact surfaces that are split by shallow crevices that extend below the immediate surface of the artifact (Figure 3-16). These cracks are deeper than fine crazing and create a roughened surface that can be detected tactilely.

Figure 3-16. Deep surface cracking on specimen GS02-11 illustrates deep cracking on ventral surface of partially vesiculated flake, note simple crazing in lower right which grades into cracking with increased proximity to the vesiculation on the left (originally 6.6x magnification).

Most of the deep surface cracking that I observed can be understood as an extension of surface crazing or an effect subsequent to fine surface crazing. This often occurs in conjunction with deformation of the artifact, such as by vesiculation. Based on observations made during heating experiments and examination of specimens through SEM imaging (Figure 3-17), my impression is that deep cracking is not a separate phenomenon from fine surface crazing, but rather is caused by stretching of a finely-crazed surface when expansion of the glass occurs with bubbling, vesiculation, or other plastic deformation. New cracks can be created when extreme deformation occurs with vesiculation (as shown in Figure 3-17:e), but this seems only to occur in extreme cases of vesiculation, and not where deep cracking is observed on otherwise intact artifacts. Stretched crazing can be seen even on the surface in areas of full vesiculation (Figure 3-18).

Figure 3-17. Deep surface cracking. (a) Specimen 1691-51, and sequence of SEM images that illustrates progressive stretching with deformation of artifact due to the bloating of vesiculation. Sequence of (b-e) images begins on left: (b) fine crazing; (b) crazing altered to upraised cracks; (d) stretching of cracks; (e) smoothing/flattening of cracks, with new emergence of splitting independent of the original crazing (scale bar in lower left corner of SEM images is 200 microns).

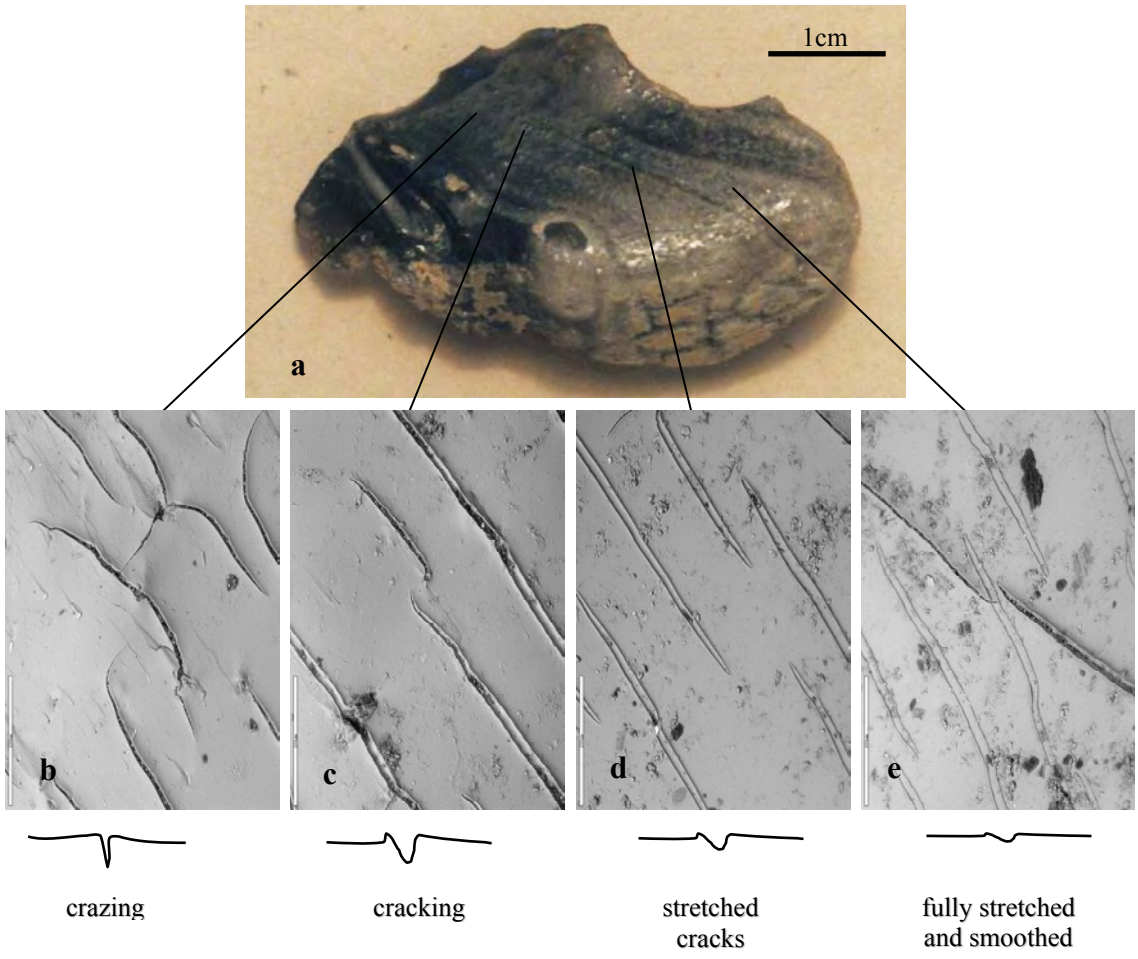

Figure 3-18. Deep surface cracking / stretched crazing. View is in an area of full vesiculation at the vesiculated edge of specimen 1691-SU1-J5C: (a) originally 6.3x magnification; (b) originally 40x magnification.

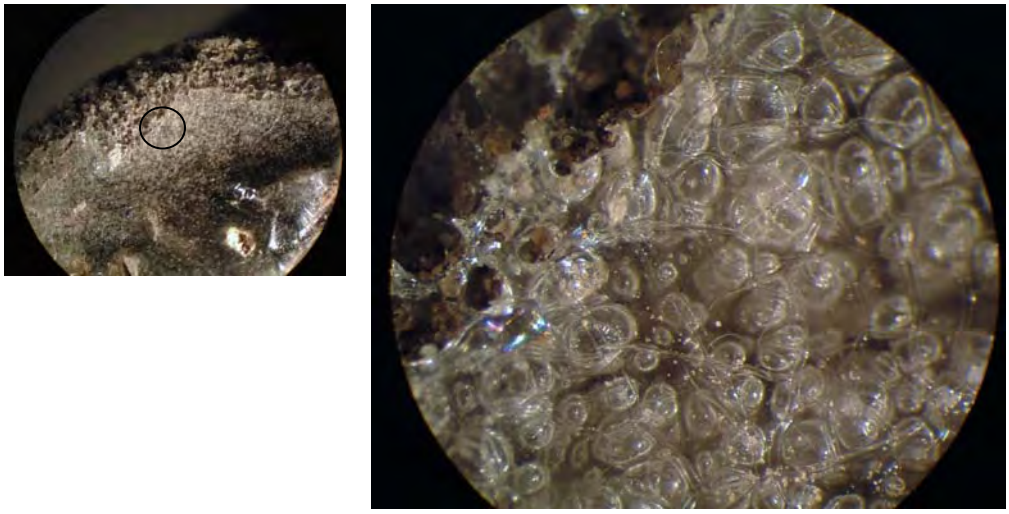

Vesiculation

Vesiculation is expressed as the formation of abundant and interconnected bubbles throughout the interior and at the surface of the glass object as a result of heating that, in turn, causes deformation and an increase in object volume or size (Figures 3-1, 3-14, 3-16, 3-17, 3-19, 3-20, and 3-21, see also Chapter 4). As established in informal

Figure 3-19. Complete vesiculation: views of fully and partially vesiculated nodules and artifacts* in situ *(a and b). Note that the partially vesiculated flake above knife in (b) is specimen 1691-03; (photos by J. C. Phillips, October, 1996).

heating experiments, this "puffing" occurs without an actual appreciable decrease in total weight, although there is the illusion that the piece is much more lightweight than before it expanded. Specimens can be either completely or partially vesiculated and vesiculation may or may not alter the form of the artifact. One case I observed is a fully vesiculated flake that despite being completely bloated still retained all of the flake characteristics needed to determine the ventral and dorsal surfaces, orient the proximal and distal ends of the flake, and observe the location of cortex that existed on the flake before it was burned (Figure 3-20). In other cases, vesiculation renders an item unrecognizable. In particular, thin flakes tend to curl upward and can end up looking just like pieces of packing foam. Despite lacking a shiny ("glassy") surface and having lost the ability to fracture conchoidally, vesiculated obsidian is still glass. This fact is demonstrated by the characteristic "clink" the deceptively soft-looking and pillowy pieces make when dropped on a hard surface.

Figure 3-20. Vesiculated flake: dorsal and ventral views of a fully vesiculated obsidian flake retaining recognizable flake morphology (proximal end is up, distal end is down).

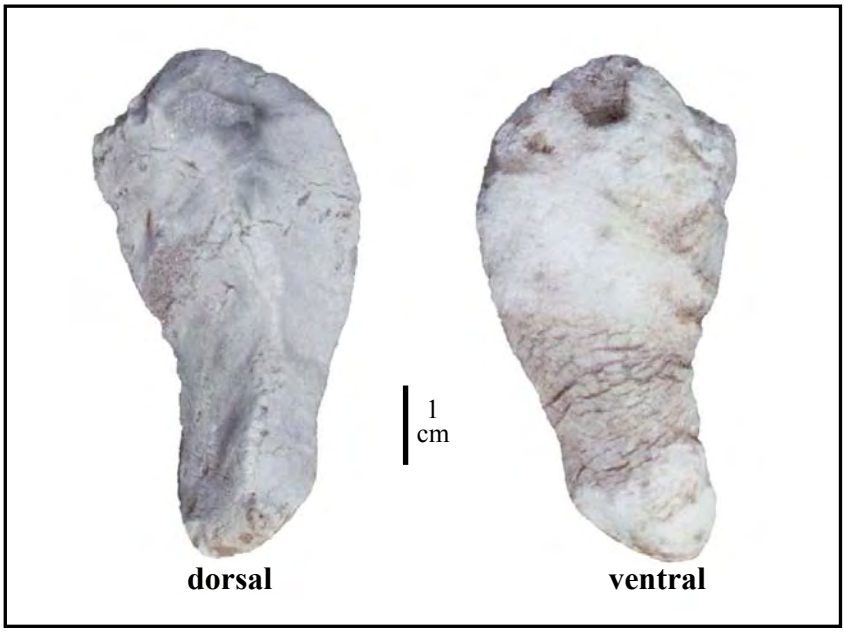

Figure 3-21. Vesiculation: fully and partially vesiculated artifacts (clockwise from upper left: unnumbered specimen, 1691-06, 1691-03, unnumbered specimen).

"Vesiculation" is the term used by Trembour (1990). Nakazawa's (1998) term for the phenomenon is "explosion" of the glass. These terms are similar to what is meant by the geological term "vesicularity", which refers to the relative volume of bubbles (vesicles) in the glass that form in association with the pyroclastic processes that produced the deposit. As used here, "vesiculation" refers to vesicles in obsidian created as a response to heat exposure unrelated to the original formation of the clasts (see Trembour 1990). Figure 3-22 shows SEM images of vesiculation in artifacts burned in the Dome Fire. Figure 3-22:b-d show vesicles on a flat surface embedded in epoxy and polished for SEM analysis, while Figure 3-22:a shows an unmodified vesiculated surface. The latter three views are intermediate between full vesiculation and incipient bubbles; full vesiculation was difficult to capture in the SEM because the fragile glass walls of bubbles did not hold up well to sample preparation and polishing.

Figure 3-22. Vesiculation as shown in SEM secondary-electron images of vesiculated obsidian: (a) unmodified surface of specimen 1691-02 (materials within vesicles are soil particles); (b, c, & d) flat polished surfaces of vesiculated obsidian from specimen 1691-50.

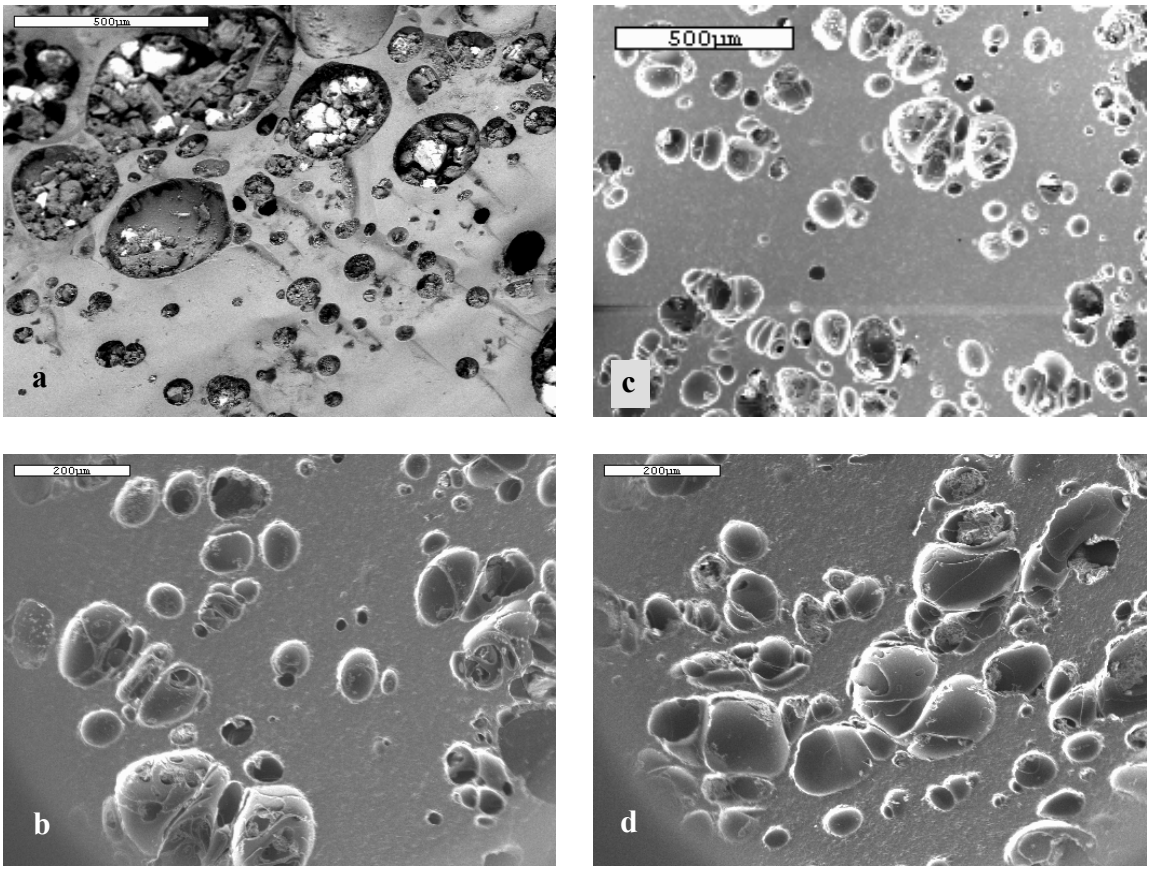

Incipient bubbles

Incipient bubbles describe individual bubbles that have developed below the subsurface, but without the abundance, density, and interconnectedness of vesiculation (Figure 3-23). There is no appreciable deformation because the internal bubbles are not developed sufficiently to compromise the shape of the glass matrix.

These subsurface bubbles are observed more frequently in clear obsidian than in cloudy or opaque obsidian, perhaps because subsurface bubbles are easier to see when the glass is more transparent, and can be more readily apparent when there is light transmitted through translucent or semi-translucent glass (Figure 3-24). Another

Figure 3-23. Incipient bubbles in specimen 1691-53. Image illustrates incipient bubbles (upper center) adjacent to vesiculation (right), as visible on the ventral surface of a crazed and partially vesiculated flake

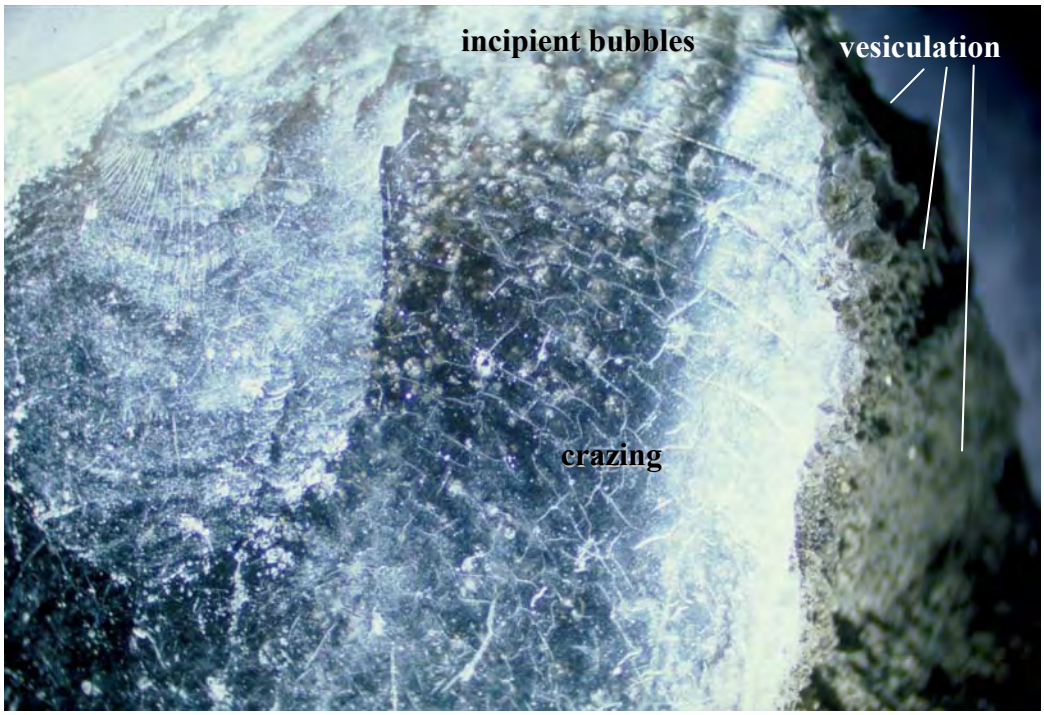

possibility is that cloudy glasses contain more precursors for bubble formation (e.g., internal inclusions such as microlites, phenocrysts, or zenolith particles). In other words, if cloudy materials have more loci for bubble nucleation, the result would be more and smaller bubbles. Under conditions leading to vesicle formation, more loci for bubble formation may predispose a specimen to vesiculation rather than the more "incomplete" alteration represented by incipient bubbles.

Incipient bubbles have been observed to follow banding or other characteristics visible in the glass (Figure 3-25), lending support to the inference that the formation of bubbles is influenced by compositional or textural characteristics of the glass. This observation was an important influence in examining possible compositional causes for variable expression of vesiculation in obsidians found in the Cerro Toledo Rhyolite deposits affected by the Dome Fire.

Figure 3-24. Incipient bubbles. Image of specimen 1691-3 showing incipient bubbles apparent when viewed with light transmitted through the glass (originally 6.6x magnification). Other views of this specimen without transmitted light (e.g., Figures 3-18 & 3-20) show that incipient bubbles are not always immediately apparent.

Figure 3-25. Incipient bubbles. Image illustrates variation in bubble formation corresponding to banding in the glass (specimen GS2002-12 at 6.6x magnification).

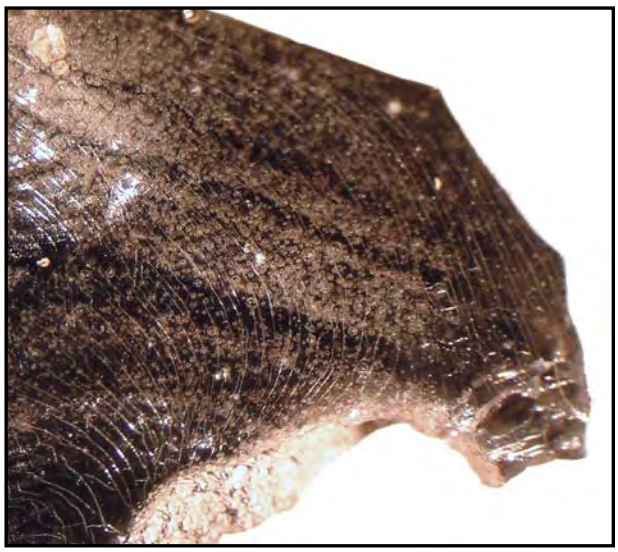

Fire fracture

Fire fracture describes rapid fracture through the body of the artifact or nodule that can look similar to intentional lithic reduction but that initiates from within the item rather than at a margin or edge from an externally applied force (Figure 3-26). As such, fire fracture is similar to potlidding, but at Capulin Quarry fracture rarely was expressed in the lens-shapes characteristic of potlidding. Obsidian fire fracture in the Dome Fire nearly always involved breakage of whole objects, and never occurred as potlids "popping-off" of the nodule or artifact (in contrast to Lentz et al. 1996:70, Figure 33).

Figure 3-26. Fire fracture: (a) fire fractured pieces; (b) refit of fire fractured pieces.

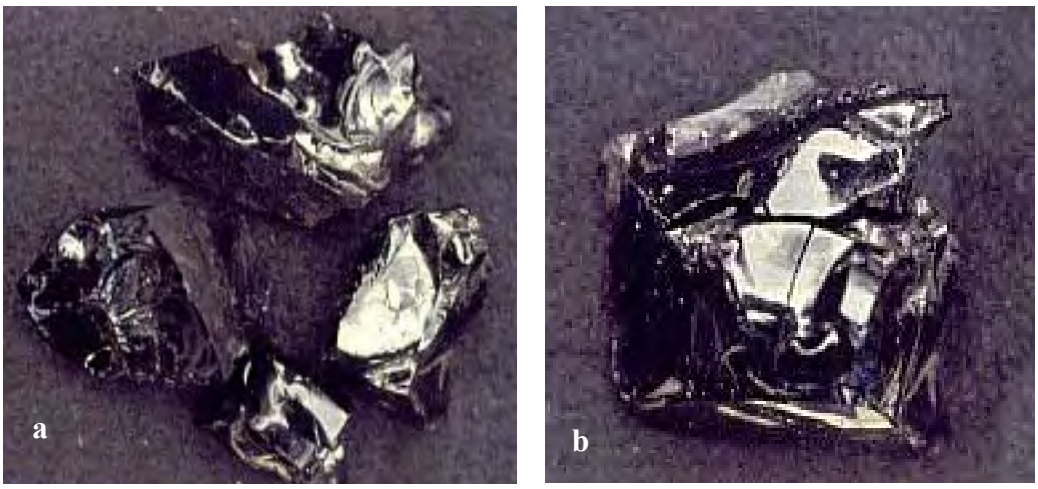

Distinguishing fire fracture from intentional lithic reduction can be difficult at first, but characteristic features emerge with continued examination. Fire fracture has ripples, as in conchoidal fracture, but lacks a bulb of percussion--the attribute of applied-force fracture so characteristic of human-induced flaking. Because fire fracture initiates from within rather than at or near the edges of a nodule, all edges of a fire fractured piece are margins or terminations--there is no proximal end. Many fractures seem to initiate at an inclusion of some kind, such as a phenocryst, that can be seen near the center of the fracture surface. In many cases tiny "gullwings" point back to this center initiation[1].

[1] The term “gull wing” not only is descriptively apt, it is an actual fractographic term. Fréchette (1990:10-15) identifies gull wings as primary Wallner lines, and includes gull wings in the broader generic category of rib marks.

These faint v-shaped markings look like a minute disturbance in the fracture path akin to the pattern that a smooth current of water makes as it flows around a rock in a stream.

For a lithic analyst at a quarry site, adding fire fracture to the complexity of reduction information already in abundance in such assemblages can be bewildering. The most disorienting aspect of fire fracture in these assemblages is that fire-fractured materials do not conform to the most basic distinction made in lithic technology--the essential contrast of core vs. flake expressed by positive and negative flake/scar relationships. A fire fractured nodule breaks into many pieces, none of which are actual flakes or cores.

Fire fracture specimens from Capulin Quarry were examined by fractographer Are Tsirk, and a brief report of his findings is included here as Appendix B. He observed several characteristic markings of fire fracture surfaces, as described and illustrated in his report. Any markings that are peculiar to fire fracture, and concomitantly unusual for intentional human fracture as in knapping, are of particular interest for the current study because such characteristics may be useful as attributes to identify the occurrence of fire fracture surfaces and to distinguish fire-fractured pieces from actual artifacts. Tsirk concludes that three of four (if not all) of the specimens he examined likely were not produced by knapping. Features of particular interest are certain kinds of mist and hackle, mist-lines, mist-hackle configurations, as well as parabolas and fracture branching. Figure 3-27:c&d illustrates mist and parabolas. Tsirk observes that these fracture markings do not occur often in knapping fracture[2], but they are common on the specimens Tsirk examined and were frequently observed by the author on the numerous fire fractured pieces examined for this study.

I observed the appearance of dulled patches (mist) and elongated lines radiating out from the interior of fracture surfaces (parabolas) frequently on surfaces from specimens from Capulin Quarry I believe to be caused by fire fracture. Without magnification, areas of mist appear as dull spots on the fire fracture surface. While I had noticed these dull areas in my examinations, I had not suspected that these features were

[2] It is important to note, however, that Tsirk is clear that determining that the attributes he observed were caused by thermal stress (as opposed to some other form of non-knapping fracture such as accidental breakage) was not possible without additional examination of specimens and further experimental investigations.

fracture markings (I assumed they were areas of residue or abrasion). However, once I was introduced to the appearance of mist, these attributes were not difficult to identify. Tsirk concludes that such features, as well as other less readily identifiable attributes discussed in his report, occur at high fracture velocities that are extremely rare in knapping, except in accidental breakages which initiate at or near an edge of the fracture surface. The presence of mist and parabolas appear to be good indicators of fire fracture, especially where they are in association with fractures that appear to initiate at inclusions interior to the specimen (i.e., well away from the surfaces).

Figure 3-27. Fire fracture: (a) nodule with four fire fractured pieces that fully refit; (b) exploded view of fire fracture pieces (arrows in [a] and [b] point to the piece shown in close up views); (c) fire fracture surface showing inclusion (lower center) near which fracture appears to have initiated (originally 6.3x magnification); (d) fire fracture surface showing trailing extensions or parabolas which point back to origin of fracture (originally 16x magnification).

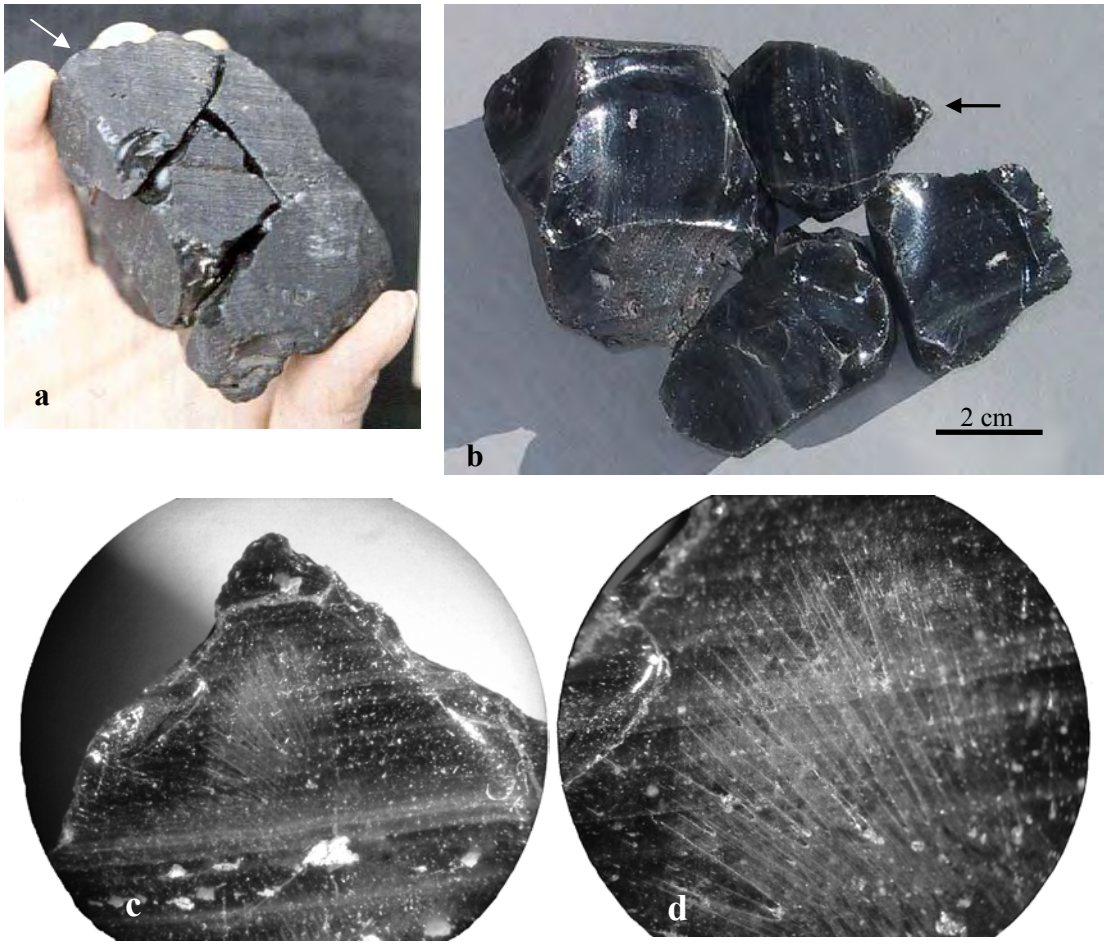

Determining what visual characteristics are appropriate for identifying the presence of fire fracture, as distinguishable from other sources of fracture, is aided by understanding how fire fractures may occur from thermal stress. In Appendix B, Tsirk determines that at least some of the characteristics he observed in the fire fracture specimens indicate fracture from thermal stresses that occurred during "heat-up rather than cooling" (see Appendix B, Section 6). In addition, Tsirk offers the following remarks for consideration:

> When a specimen is subjected to an external heat source, its outer parts will have more thermal expansion because they are at higher temperatures. As a result, the inner parts of the specimen will be in tension and its outer parts in compression. That is, the outer parts of the specimen tend to or actually do pull apart its inner portion. Since the mechanism involves differential thermal expansion, the magnitude of the tensile stresses developed depends on the rate of heating. The mechanism described is for the specimen being heated up. Upon cooling, the situation is reversed, with tensile stresses developing instead at the outer surface or surfaces. In principle, it is thus possible to get fire fractures initiating at surface with sufficiently rapid cooling. This was not observed with the specimens considered in this research. (Tsirk, personal communication 2005)

Characteristics frequently observed in what I believe are fire fractures include, as noted above, the lack of bulbs of percussion, presence of only fracture terminations, and unclear status of "negative" versus "positive" flake/flake scar relationships. Additional characteristics are a ring-shape to the outline of fracture surfaces, and a tendency of fracture surfaces to extend beyond the fracture plane. The latter gives the appearance that the fracture swooped around an edge or corner of the specimen to remove a small portion of the other side of the nodule. In contrast, intentional knapping fracture (with the exception of plunging termination as in overshot flakes) tends to terminate at the end of the mass of the piece rather than running over onto the adjacent edge.

The main challenge for the reliability and validity of fire fracture identification is that other non-human (i.e., non-intentional, non-knapping) agents and circumstances may be responsible for fractures that I examined in broken nodules and pieces at Capulin Quarry. Further examination, experimentation, and fractographic analysis will be needed

to differentiate with complete certainty between fractures caused directly by forest fires and those caused by frost fracture and other factors that might contribute to thermal stress failure, such as internal stresses that are residual from the original circumstances of obsidian petrogenesis. For now, the characteristics believed to be indicative of fire fracture, as described, here are inferred from examining hundreds of examples from Capulin Quarry that possess these redundant features. This examination included not only individual pieces but also focused on examples of refitted nodules with multiple pieces broken in a manner that clearly could not have been from knapping (e.g., Figure 3-27:a-b). Thus, while the descriptions provided here are not definitive, I am confident that they represent relevant aspects of fire fracture appearance and can serve as a baseline for continued observation and description.

Other obsidian fire effects

Two other kinds of obsidian alteration by heat were observed at Capulin Quarry in addition to those described in the eight categories. These include 1) an alteration of obsidian color and translucency, and 2) surface blistering. Because these were found in only single individual specimens, they are not described here as categories but are interesting enough to warrant brief mention.

Specimen 1691-02 is a partially vesiculated flake that also has crazing and incipient bubbles (see Figures 3-1 & 3-14, above; see also discussion of this artifact in Chapter 4, section 4.2). The artifact at first appears to be black opaque obsidian, but unusual colors in the flake were first noticed when examined under an optical microscope with transmitted light. One half of the flake (nearest the vesiculated edge) is translucent and medium to light grey, while the other half of the flake is opaque and brown (Figure 3-28). There is no abrupt demarcation between these two visual variants within the glass; instead they grade into each other rapidly with some feathering of the opaque brown material into the translucent grey. While neither visual variant is uncommon in obsidian from this source, their combination on one flake is unusual.

Figure 3-28. Dissimilarity in obsidian color and translucency in specimen 1691-02: (a) partially vesiculated flake (at approximately actual size) showing apparent black color of glass under normal light; (b) view (originally at 6.6x magnification) showing differences in the appearance of the glass visible with transmitted light that correspond to vesiculated and unvesiculated areas of the flake.

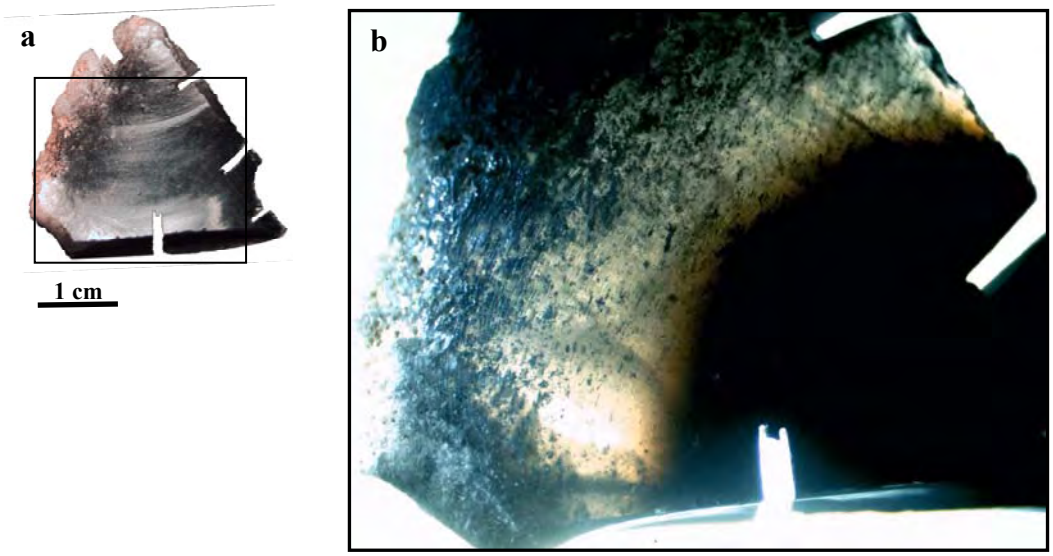

The different colors in the glass correspond spatially with the expression of fire effects (where incipient bubbles and vesiculation occur only on the translucent end of the flake), which raises the question of whether the observed material variation is associated with heat alteration—either as cause or effect. To test whether differences in the glass might be the cause of differences in fire effects, X-ray fluorescence analysis (ED-XRF) was conducted of vesiculated (clear) and unvesiculated (opaque brown) parts of the glass and the results showed differences in the trace elements detected[3] (Steffen 2002:195). However, the ED-XRF results were similar to those seen in several samples for vesiculated vs. unvesiculated specimens, suggesting that the irregularity of vesiculated surfaces or changes in composition associated with vesiculation are more likely to be responsible for variable ED-XRF than that differences in the glass contributed to the variable fire effects in specimen 1691-02. To test the alternate possibility that heat

[3] All elemental values (except Sr) were slightly higher in the vesiculated/clear area than in the unvesiculated/brown area, with a particularly high elemental value for Zn. In that study, high Zn values appear to associate with vesiculated glass; this is probably an artifact of the ED-XRF analysis technique rather than evidence of actual compositional changes or differences (Steffen 2002).

caused the observed differences in the glass, simple laboratory heating experiments were conducted on five samples of brown obsidian from locations in the CTR-Dome obsidian-bearing deposits. Three of the five materials changed from opaque brown to translucent grey or pale grey-brown when heated to temperatures above 800°C, while two did not change color or translucency[4]. While not conclusive, the heating experiment results support the inference that the differences in obsidian color and translucency observed in specimen 1691-02 demonstrate a fire effect in which the appearance is altered in a particular kind of brown obsidian present in the CTR-Dome quarries.

The second anecdotal fire effect observed at Capulin Quarry is surface blistering on a non-artifact nodule (Figure 3-29). The nodule has a variable covering of what appears to be bubbled glass, giving the outer surface of the piece an appearance akin to having been deep-fried in oil. It is possible that the bubbled outer covering is some kind of additive material or residue on the exterior, but examination under an optical microscope better supports the interpretation that the blistered surface is part of the original glass. What is intriguing about the piece other than its curious appearance is the possibility that the bubbled outer material is the result of vesiculation of a hydrated layer or cortex of the glass. If so, it might be an extension of the surface bubble layer illustrated in Figure 3-11:b where the outward appearance of the glass in that case was altered surface sheen. The idea that a hydrated outer glass layer could vesiculate while the underlying unhydrated glass remains unaffected accords with the potential role for glass water content in obsidian vesiculation.

[4] Four of the five materials included in the heating experiments are glass samples also analyzed in Chapters 6 and 8. The two samples that did not change color or translucency are CTD5-307 and CTD12-302. The three samples that changed from opaque to clear are CTD5-309, CTD8S-302, and an unnumbered specimen not included in the petrology samples analyzed. Both samples that did not change color or translucency are fully opaque milk-chocolate brown glasses with a "plastic" texture. In contrast, the glasses that changed color are the type of brown glass that appears to be a non-translucent black in hand specimen with a tobacco brown color visible on edges when held to the light (i.e., the brown color is only visible when the glass is very thin). These two kinds of glass appear to be quite different in color, texture and light-transmitting characteristics, and the latter three samples are much closer to specimen 1691-02 than the former two.

Figure 3-29. Blistered surface on a non-artifact nodule from Capulin Quarry: (a) bubbling of surface; (b) discontinuous and less pronounced bubbling on surface with variability apparently corresponding to underlying material (e.g., swirls) (both originally 6.6x magnification).

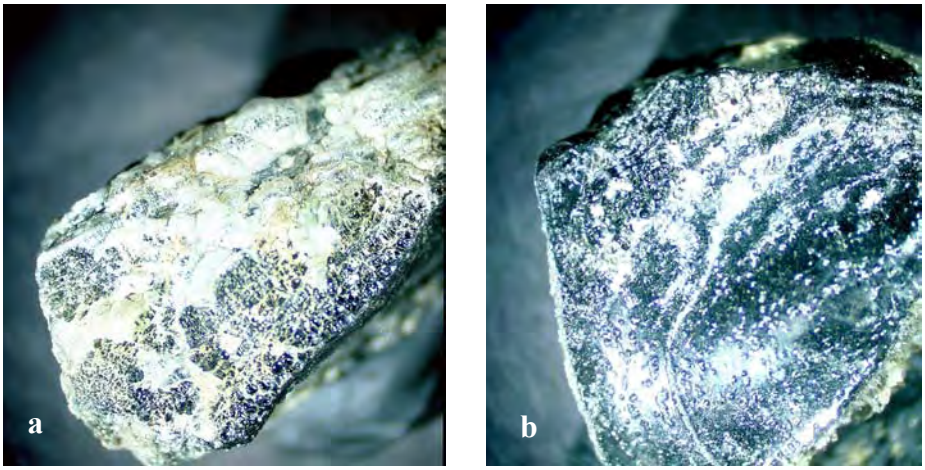

Discussion of obsidian fire effects

The macroscopic fire effects described above are readily observed on obsidian artifacts and hand specimens. Except for full vesiculation (which renders the objects very fragile and susceptible to both mechanical and chemical weathering) and additive surface sheen caused by organic residue (which is subject to loss over time with exposure to the environment), these attributes can be expected to preserve well in the archaeological record. Therefore, partial vesiculation, incipient bubbles, and surface crazing and cracking all can be used as indicators not only of heat exposure during contemporary fires but also as evidence of past heat exposure.

As observed many years ago (Friedman and Trembour 1983), crazing is particularly promising for use in recognizing past fire alteration. Crazing can be expected to preserve well on burned artifacts because the alteration is entirely surficial (i.e., it does not compromise the body of the specimen) and therefore should not enhance or accelerate deterioration of a specimen. Further, there is some experimental evidence that crazing does not occur until temperatures are reached that are higher than those expected to alter and obliterate pre-existing obsidian hydration bands (Friedman and Trembour 1983). The implication is that hydration bands measured on a crazed surface--or even on the

crazing crack that extends into the surface--could be inferred as post-dating the fire exposure that caused the crazing (Trembour, personal communication 1997). Thus, crazed artifacts would provide ideal surfaces to explore the potential of obsidian hydration dating for estimating how long ago the fire exposure occurred (Friedman and Trembour 1978).

Determining the conditions under which each fire effect occurs is outside the scope of this dissertation. However, providing systematic descriptions of these easily recognized and persistent macroscopic attributes of fire alteration will enable the exploration of their co-occurrence with alteration of obsidian hydration rinds on artifacts with these macroscopic fire effects. In the next chapter, artifacts from Capulin Quarry are examined to evaluate the impact of the forest fire for OH dating information in the burned assemblage, both in terms of the degree of observed burn intensity at variable collection locations and in terms of the macroscopic fire effects observed on specimens.

CHAPTER 4
OBSIDIAN HYDRATION ANALYSES

The potential of consequences of forest fires for obsidian hydration dating of artifact assemblages is the primary concern motivating archaeologists to consider the need for protection of sites from wildfires and controlled burning. As discussed in Chapter 2, the extreme physical alteration of obsidian observed at Capulin Quarry is remarkable and outside the expected, but the potential for microscopic alteration of obsidian hydration within such assemblages is not. Further, the possibility that past fires, in history and prehistory, may have altered the chronometric information available in an assemblage raises concerns about the reliability and validity of the OH dating technique. Previous research has shown that forest fires do alter OH bands. However, whether past or contemporary exposure to forest fires actually has an impact on the sum of OH information in the assemblages that archaeologists sample when utilizing the technique, and thus whether this factor is relevant for research outcomes when employing OH dating, are separate questions that must be evaluated beyond the observation that alteration does occur. These are questions about the method (*sensu* Dunnell 1971), as opposed to the technique, of obsidian hydration dating.

The first two sections (4.1 and 4.2) of this chapter introduce the goals of the OH analyses, and include investigation of potential heat alteration in OH at Capulin Quarry. The focus here is whether or not alteration of OH occurred following the Dome Fire, whether OH effects are variable depending on burn severity context, and whether OH alteration co-occurs with the most extreme fire effect observed, vesiculation. These analyses are conducted at two analytical scales: examination of the entire assemblage (Section 4.1) and examination of individual specimens (Section 4.2). The entirety of Sections 4.1 and 4.2 were previously published as part of the pilot project (Steffen 2002) on which much of this dissertation is based. In Section 4.3, attention is turned toward quantifying variation in observed macroscopic fire effects and assessing the co-occurrence of these macroscopic effects with microscopic OH alteration, as expressed among artifacts collected from within a controlled sample unit (SU1).

4.1. Assemblage-Scale Analysis of Obsidian Hydration in Artifacts from Areas of Capulin Quarry with Variable Burn Severity

Measuring the effect of the Dome Fire on hydration bands on artifacts at Capulin Quarry has two purposes. The first is to evaluate the impact of the forest fire at a site where the most extreme kind of fire effect--vesiculation--is observed in abundance. Assuming that this extreme response is evidence of high heat, it makes sense that this site would experience substantial impact to hydration bands, and also that the greatest proportion of hydration band alteration or loss would occur on artifacts in close spatial association with vesiculated materials. These assumptions are evaluated at the scale of assemblage (Section 4.1) by comparing OH analysis results among artifacts distributed across the site in areas with varying degrees of burning intensities and differing amounts of obsidian fire effects. Early in the assemblage-scale OH analysis there were indications that some artifacts did not conform to the intuitive expectation that the presence of vesiculation meant the absence of hydration bands. Therefore, the second purpose of the assemblage-scale OH analysis is to provide a background for examination of peculiarities in the relationship between artifact vesiculation and hydration band alteration that occur at the scale of specimen (Section 4.2).

Obsidian Hydration Analysis Methods Used

Hydration band analyses were undertaken by Tom Origer at the Sonoma State University Obsidian Hydration Laboratory, using techniques outlined in the following condensed version of his description. Thin sections were reduced by manual grinding with a slurry of #500 silicon carbon abrasive to thicknesses determined by the "touch" technique and "transparency" test, then mounted with coverslip using Lakeside Cement. Extant hydration bands were measured with a strainfree 60 power objective and Bausch and Lomb 12.5 power filar micrometer eyepiece on a Nikon petrographic microscope. Six measurements were taken at several locations along the edge of each thin section, and these measures as well as the calculated means were provided as data. The hydration measurements produced have a range of ± 0.2 microns due to normal limitation of the equipment. Origer recorded observations regarding the quality (condition) of the

hydration bands, noting particularly the external edges where fire effects would be. Also, Origer videotaped several thin sections and photographed examples of especially interesting features observed in association with fire effects including sheen, crazing, and vesiculation. The photographic slides and the three videotapes are an invaluable resource--both for developing an understanding of microscopic heat effects and as a communication tool (see Figures 3-10 & 3-11 in Chapter 3, and Figure 4-6, below).

Selection of Specimens

The selection and examination of specimens was an iterative process between Origer, Hughes, and myself, with samples processed in several batches[1]. Specimens were selected to represent a full range of the fire effects observed at Capulin Quarry, as well as differences in raw material appearance and texture, and differences in the reduction aspects of the artifacts (e.g., to include cores and flakes--and less identifiable reduction items--representative of the variety in reduction apparent in the quarry assemblage). X-ray fluorescence analysis was conducted on most of the specimens included in the hydration analysis. Table 4-1, below, lists OH results by specimen and also indicates whether XRF measurements were taken.

In total, examination of hydration surfaces was conducted for 58 obsidian specimens from Capulin Quarry. These included both artifacts (n=46) and non-artifacts (n=11), with the majority of non-artifacts being pieces with either fresh or older fire fracture surfaces. In numerous cases, multiple cuts were made per specimen, often to provide information on the most altered as well as the least altered portions of the item. This produced more than one hydration band measurement per item. Multiple outcomes also were obtained when differing hydration bands could be detected within a single thin section. Thus the number of OH observations (n=91) well exceeds the number of items examined.

The analyses presented here include only artifacts (i.e. no non-artifacts) collected from Capulin Quarry, and provide a summary of these data to address three questions:

[1] The completed microslides are curated in the Sonoma State University Obsidian Hydration Laboratory under File numbers 98-H1772, 98-H1730, 99-H1848, 99-H1855, and 99-H1857.

1) do hydration bands appear to have been altered by the fire within the burned areas of the site?;

2) are there differences in apparent alteration depending on the degree of burning evident where the artifacts were collected?;

3) does alteration of hydration bands necessarily co-occur with vesiculation of obsidian artifacts?

Obsidian Hydration Analysis of the Burned Assemblage

Table 4-1 lists hydration observations for 41 artifacts collected at a variety of locations within Capulin Quarry. Only eight specimens (20 percent) are from unburned areas, while 33 specimens (80 percent) are from various burned areas of the site. The categories used to describe differences in burning severity are listed in Chapter 3. To re-state, locations within the burned areas of the site are grouped by proximity to the vesiculation clusters. They are either "in cluster" (within the maximum 1 m diameter central core of vesiculation clusters), "near cluster" (within 2 m of the center of a cluster), or "burn area" which indicates that the specimens were collected from throughout the burned portions of the site, without proximity to clusters.

Table 4-1. Obsidian hydration analysis of artifacts at Capulin Quarry collected from areas with differing degrees of burn severity.

XRF [a]	Spec#	03-1691 Location	Burn Exposure (severity)	Observed Fire Effects[b]	Origer Notes[c]	Band Cond[d]	Band Measures[e]	Item Qty	#Cuts/ Bands[f]
✓	1691-01	burn area	burn area	sheen	wea	nvb	none	1	1
✓	1691-02	burn area	burn area	craz, vesic	none	ok	2.8, 3.4, 4.8, 5.8, 6.0, 6.3, 6.4	1	7
✓	1691-03	burn area	burn area	craz, vesic	wea	dh	none	1	2
✓	1691-4A	by Clust 1	burn area	sheen	wea	nvb, ok	none, 1.1	1	2
✓	1691-05	in road	unburned		none	ok	2.5	1	1
✓	1691-06	in Clust 2	in cluster	craz, vesic	none	nvb	none	1	1
✓	1691-07	in Clust 2	in cluster	craz, vesic	wea	dh, nvb	none	1	2
✓	1691-08	in Clust 2	in cluster	craz	wea	dh	none	1	1
✓	1691-10	in Clust 3	in cluster	craz, vesic, sheen	wea	dh	none	1	1
✓	1691-14A	in Clust 7	in cluster	craz	wea	dh	none	1	2
✓	1691-14B	in Clust 7	in cluster		wea	dh	none	1	1
	1691-17	Unit 1	near cluster		2 bands	dh	~3.4	1	2
✓	1691-18	Unit 1	near cluster		none	nvb	none	1	1

Table 4-1. Continued: Obsidian hydration analysis of artifacts at Capulin Quarry

XRF [a]	Spec#	03-1691 Location	Burn Exposure (severity)	Observed Fire Effects [b]	Origer Notes [c]	Band Cond [d]	Band Measures [e]	Item Qty	#Cuts/ Bands [f]
	1691-19	Unit 1	near cluster	sheen	wea	nvb	none	1	1
	1691-20	Unit 1	near cluster		2 bands	ok	4.8, ~5.7	1	2
✓	1691-22	Unit 1	near cluster		wea	nvb	none	1	1
✓	1691-27	in Clust 2	in cluster	craz, vesic	none	dh	none	1	1
✓	1691-28	in Clust 3	in cluster	craz, vesic	wea	dh	none	1	2
	1691-29	in Clust 3	in cluster	craz, sheen, fract	wea	dh	none	1	2
✓	1691-31	Collect 1	burn area		none	dh	none	1	1
	1691-32	Collect 1	burn area		none	ok	5.1	1	1
✓	1691-33	Collect 1	burn area		none	dh, ok	none, 5.6	1	2
	1691-34	Unit 1	near cluster		wea	dh	none	1	1
✓	1691-35	Collect 1	burn area		none	nvb	none	1	1
✓	1691-36	Collect 1	burn area	craz, sheen	none	nvb	none	1	1
	1691-37	Collect 1	burn area		none	dh	~10.3	1	1
	1691-38	Collect 1	burn area		none	ok	1.2	1	1
✓	1691-39	Collect 1	burn area		none	nvb	none	1	1
	1691-40	Collect 1	burn area		wea	ok	5.7	1	1
✓	1691-41	Collect 1	burn area		wea	dh	none	1	1
✓	1691-42	Collect 2	unburned		none	ok	1.5	1	1
	1691-43	Collect 2	unburned		wea	ok	3.3	1	1
	1691-44	Collect 2	unburned		wea	ok	5.1	1	1
✓	1691-45	Collect 2	unburned		wea	dh, ok	none, 1.6	1	2
	1691-46	Collect 2	unburned		none	ok	3.8	1	1
✓	1691-47	Collect 2	unburned		none	nvb, ok	none,5.3, 5.3, 5.9	1	4
	1691-48	Collect 2	unburned		none	nvb	none	1	1
	1691-49	burn area	burn area		2 bands	dh, ok	none, 2.9	1	2
	1691-50	burn area	burn area	craz, vesic	wea	dh	none	1	4
	1691-106	burn area	burn area		none	ok	1.7	1	1
	1691-107	burn area	burn area	sheen, fract	none	dh	~4.3	1	1
							Totals:	41	64

[a] Check mark indicates specimens were included in X-ray fluorescence analysis.

[b] Macroscopic fire effects observed on specimens correspond with those described in Chapter 3:
sheen = altered or additive surface sheen vesic = vesiculation
craz = fine surface crazing or cracking fract = fire fracture

[c] Observations made during OH analysis: wea = weathering of surface was noted;
2 bands = two measurable bands were observed within one cut.

[d] Band condition as assessed during hydration band measurement:
ok = normal measurable hydration band;
dh = diffuse hydration (not measurable);
nvb = no visible band.

[e] Mean values of six measurements made for each band, in microns; approximate estimates of diffuse bands are indicated by "~".

[f] Number of thin section cuts examined per specimen, including total number of bands observed where multiple bands were present for a single cut.

Comparing between burned and unburned areas of the site (Figure 4-1), specimens with hydration bands are present in a much higher relative frequency in the unburned areas (seven specimens; 87.5 percent) than in the burned areas (nine specimens; 27.3 percent). As shown in the cross-tabulation in Figure 4-1, the statistical test does not support independence between the degree of burning and the presence of intact hydration in these artifacts.

Figure 4-1. Proportion of intact/measurable hydration bands in unburned and burned areas at Capulin Quarry.

	OH not present	OH present
Burned	24	9
Unburned	1	7
Pearson's Chi-square 9.82, df=1, p=.002		

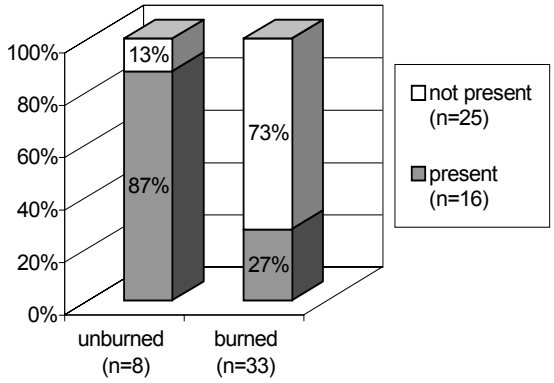

Further, comparing among the areas with different degrees of burning (Figure 4-2), the distribution of specimens without measurable bands present follows the pattern expected: the relative frequency of specimens with bands is highest in the unburned areas of the site, decreases in the general burned areas and near clusters, and is lowest within clusters.

Figure 4-2. Distribution of intact/measurable hydration bands by degree of burning.

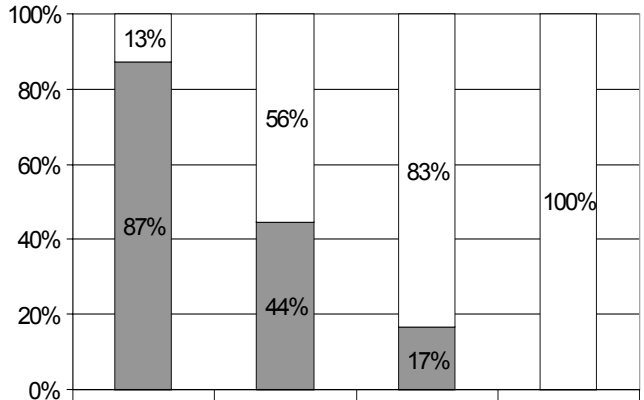

	unburned	burn area	near cluster	within cluster
band not present	1	10	5	9
band present	7	8	1	0

To summarize Figure 4-2, there does appear to be an inverse relationship between the proportion of bands present and the degree of burning the artifacts experienced. This figure shows the relative frequencies of specimens with bands present versus bands not present in each of the four burning categories. In the unburned areas, the relative frequency of artifacts with bands present is highest: seven of eight artifacts (87.5 percent) have measurable bands. In contrast, no artifacts exhibit measurable hydration bands within the "in cluster" areas where evidence of burning is most severe. In between, artifacts with bands present represent 44 percent and 17 percent in the general "burn area" and in the "near cluster" areas, respectively. This relationship between burn severity and alteration of OH bands is statistically significantly using the Chi-square test (15.14, df=3, p=.002). Overall, the results show a trend toward decreasing presence of measurable hydration bands with increasing degree of burning. This apparent trend is statistically significant as tested using the directional measure Somers' d (-0.547, p<.001) in SPSS.

So far, this discussion considers only whether measurable bands are present but cannot conclude with certainty that absent bands are the result of fire-alteration. An additional line of evidence, the distribution of diffuse hydration, can be used to support that interpretation. Trembour (1990) and other researchers (e.g., Deal and McLemore 2002; Hatch et al. 1990; Origer, personal communication; Skinner et al. 1997) have recognized the occurrence of diffuse hydration and the potential for its use in identifying heat exposure. Figure 4-3 compares relative frequency within each burn category of three groups of artifacts: 1) those with no visible hydration present, 2) those with at least one surface with diffuse hydration (ignoring the condition of other bands on these specimens), and 3) those with intact, measurable hydration bands present and without any incidence of diffuse hydration. The results suggest that the presence of diffuse hydration bands correlates with degree of burning. The proportion of specimens with diffuse hydration increases with degree of burning, while the proportion of specimens with only non-diffuse bands present decreases.

Figure 4-3. Distribution of diffuse hydration bands by degree of burning.

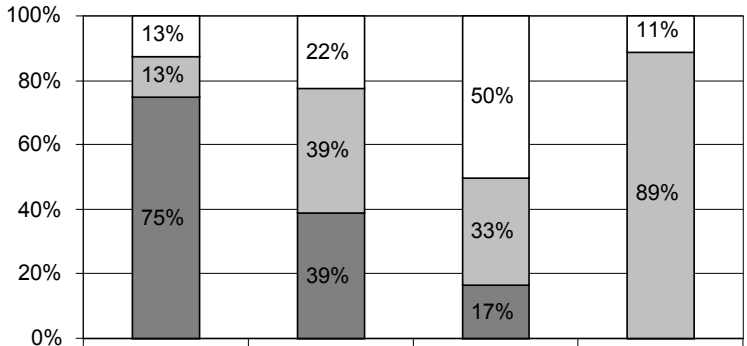

	unburned	burn area	near cluster	in cluster
no visible hydration	1	4	3	1
diffuse hydration present	1	7	2	8
hydration band(s) present but none diffuse	6	7	1	0

The pattern evident in Figure 4-3 agrees with the results reported by Trembour (1990) in his analysis of experimental heating effects on hydrated obsidian. Trembour describes a progression of heat response in experimental specimens where the hydration rind under polarized light changed in color, then showed "increasing broadening and blurring of the interface 'line'", followed by "virtual obliteration of all traces of the rind and its inner boundary" (Trembour 1990:175). The results shown in Figure 4-3 do indicate higher relative frequencies of diffuse hydration occurring in artifacts associated with areas of greater severity of burning at Capulin Quarry.

The information on diffuse hydration presented in Figure 4-3 is complex and difficult to interpret, but does invite speculation. Obviously, the proportion of artifacts with diffuse hydration increases with degree of burning, ballooning to 89 percent of artifacts from the "in cluster" contexts. A more complicated pattern can be seen in the relationship between artifacts with diffuse hydration present and artifacts with no visible hydration. As shown in this figure, the proportion of specimens with no visible hydration decreases substantially among the "in cluster" artifacts; making it appear that artifacts with diffuse hydration not only replace artifacts with hydration bands present, they also seem to replace some proportion of artifacts with no visible hydration. This may be an oddity of this assemblage--a good possibility given the small sample size in the analysis. However, one interpretation is that diffuse hydration can result from a process at least

partially independent of the hydration band that occurred on that surface prior to heat exposure. This would run counter to the perception that diffuse hydration occurs solely as the result of expansion of extant hydration into the body of the glass. It might be that diffuse hydration could also result from a process of water diffusion that is responding directly to heat, or that might even involve introduction of "new" water into the glass surface. One way to evaluate this alternative is to directly measure the concentration of water with depth below the glass surface. Anovitz et al. (1999) discuss the measurement of depth versus concentration profiles of water in glass using secondary ion mass spectrometry (SIMS). Application of SIMS analysis to burned or experimentally-heated obsidian artifacts might be a productive exercise, with the potential to provide information useful not only for interpreting heat-alteration of hydrated artifacts, but also for increasing knowledge about glass hydration processes[2]. If so, artifacts with diffuse hydration bands in burned (and unburned) obsidian assemblages should not be ignored nor should their existence be treated only as a spoiler for obsidian hydration dating. Reporting the occurrence of diffuse hydration in standard OH analyses, regardless of whether fire effects are an explicit subject of the study, would assist in determining how common and how widespread is the phenomenon.

To summarize, the results of the obsidian hydration analyses of artifacts from the burned quarry support the interpretation that the Dome Fire altered hydration bands on artifacts burned during the fire. Not only is the proportion of artifacts with measurable bands present much lower in the burned areas compared to unburned areas, the results also indicate that the proportion of bands present decreases with each increase in the severity of burning at this site. The occurrence of diffuse hydration in the assemblage appears to follow a similar pattern, with a high frequency of artifacts with diffuse hydration in the most severely burned parts of the site and a low frequency of diffuse hydration on artifacts from unburned parts of the site. Use of diffuse hydration as an indicator of heat exposure seems to work well in this case. However, the information

[2] In an article (Steffen 2002) published after this section was originally written, Stevenson et al. (2004) conducted SIMS analysis of hydration profiles on pieces of obsidian that had been heated prior to inducing hydration. Their application is only indirectly applicable to the present circumstances but their results suggest that SIMS can be used productively to illustrate differences in the appearance of hydration associated with heat exposure.

about diffuse hydration obtained here is difficult to interpret and would be best used to suggest future study rather than to draw conclusions.

Overall, it is clear that the Dome Fire created conditions sufficient to alter the obsidian hydration information contained in artifacts at Capulin Quarry: over 85 percent of unburned artifacts have intact measurable hydration bands, compared to less than 30 percent of artifacts in the burned areas. This study joins the body of archaeological fire effects literature showing that forest fires can and do alter obsidian hydration bands, and therefore can have a measurable, redundant, and potentially significant effect on the chronometric potential of obsidian hydration data in burned assemblages. However, the implications of these results for managing and interpreting the archaeological record are not necessarily so clear. Although the information in this and other similar studies will be useful to inform decisions about whether these fire effects constitute a "negative impact" or an "adverse effect", such management decisions are independent of these findings.

4.2. Specimen-Scale Analysis of Obsidian Hydration Analysis of Five Individual Burned Specimens from Capulin Quarry

In the obsidian hydration analysis in Section 4.1 the emphasis was on assessing the extent of fire alteration of hydration bands in the entire assemblage, especially as expressed depending on variation in the severity of burning across the site. In this section I examine how alteration of hydration bands is expressed depending on macroscopic fire effects on specific obsidian artifacts. Do specimens that are vesiculated still retain measurable hydration bands? Are hydration bands retained in specimens with crazing? First, I review briefly the data presented in the assemblage analysis above (Section 4.1) to assess relationships among vesiculation, crazing, and hydration bands. Second, I discuss the results of an "intensive" hydration analysis of several partially vesiculated artifacts that Origer conducted to augment the assemblage analysis.

As shown in Table 4-1 above, there are eight artifacts with vesiculation. All but one of these specimens either have no visible hydration band (nvb) or have only diffuse

hydration (dh). Therefore, in this sample almost no artifacts with vesiculation have intact hydration bands. It appears that the heat exposure that resulted in vesiculation reached or surpassed the heat exposure required to alter or obliterate hydration. The one exception is specimen 1691-02. This particular artifact has a number of unusual obsidian hydration characteristics, and will be discussed in detail below. As for specimens with crazing, the results are similar to those with vesiculation. Except for specimen 1691-02, all artifacts with crazing have no visible hydration or only diffuse hydration. Note that eight of the twelve artifacts with crazing also have vesiculation--so the condition of hydration bands would be expected to be poor. However, the results are the same for the four artifacts with crazing but without vesiculation: none have measurable hydration. It is a reasonable inference that, as with vesiculation, artifacts with crazing experienced heat exposure capable of altering hydration bands. For this sample, the presence of either crazing or vesiculation is sufficient evidence to anticipate a lack of measurable hydration.

The one specimen that differs from this generalization is 1691-02. This artifact has vesiculation, crazing, incipient bubbling, and some deep cracking yet still has intact measurable hydration bands on all the surfaces examined. Further, the hydration band measurements obtained are quite complicated. As shown in Table 4-1, all of the bands on this artifact are intact and distinct, with band widths ranging from 2.8 to 6.4 microns (including several intervals represented along the way). These unexpected results were in part responsible for the specimen analysis I will discuss now. Because the results obtained for specimen 1691-02 are so complicated and challenging to explain, a full description of that artifact is saved until the end of this section.

Intensive obsidian hydration analysis

After considering the results obtained in the overall assemblage analysis and especially for 1691-02, I returned to the site in February 1999 to find and collect additional examples of partially vesiculated flakes. It was important to obtain specimens with identifiable artifact form that had well-developed vesiculation in combination with intact or nearly-unaltered portions of the glass. Four new artifacts (1691-52 through 55) were judgmentally collected, and these were submitted to Origer for analysis along with

another good example of partial vesiculation on a flake (1691-51) that had been collected in July 1996. XRF analysis was not conducted on these five flakes.

Figure 4-4. Five partially vesiculated flakes: Specimens 1691-51, 52, 53, 54, and 55 ("v" marks areas of vesiculation).

All five of the flakes (Figure 4-4) have moderate vesiculation (enough to expand or swell part of the body of the flake), and all but one (1691-54) have clearly observable crazing. Multiple cuts were made on each artifact in order to examine the parts of each flake that had greater and lesser fire alteration visible (except for 1691-51 where a single cut was made to crosscut both vesiculated and unvesiculated parts). Origer's examination of the OH on these five flakes was especially careful and provided more information about band condition and the nature of diffuse hydration than is usual in OH analysis. As a result, the observations collected for each specimen are especially detailed and, consequently, more complicated. Summary results of OH analysis of the five partially vesiculated flakes are presented in Table 4-2. Discussion of additional details follows below.

Table 4-2. Obsidian hydration analysis of five partially vesiculated flakes from Capulin Quarry.

Spec#	03-1691 Location	Burn exposure	Observed Fire Effects	Origer Notes	Band Cond	Band Measures	Item Qty	#Cuts/ Bands
1691-51	by Cluster 2	near cluster	vesic, craz	none	dh	none	1	1
1691-52	by Cluster 1	near cluster	vesic, craz	wea	dh	none	1	3
1691-53	area of Cluster 2	burn area	vesic, craz	wea, 2 bands	dh, ok	none, 1.5, ~2.1	1	3
1691-54	burn area	burn area	vesic, slight craz	wea	dh, ok	none, 5.8	1	2
1691-55	burn area	burn area	vesic, craz	wea	dh	none, ~3.0	1	3
See notes for Table 4-1, above						Totals	5	11

Three outcomes of this analysis address the questions posed about potential alteration of obsidian hydration bands on artifacts with crazing and/or partial vesiculation. First, all five flakes have surfaces without measurable hydration. Second, all five flakes show diffuse hydration on at least one location. Finally, two flakes (1691-51 and 52) have no measurable hydration bands at any location, while three flakes (1691-53, 54, and 55) have *both* measurable and non-measurable hydration.

The first and greatest implication of these results is that heat exposure during the Dome Fire is shown to have caused alteration of hydration bands in all five flakes, but that partial vesiculation does not always indicate that alteration of hydration is complete across the whole specimen. Somehow, heat exposure that can cause vesiculation on one part of the artifact does not necessarily affect the entire specimen equally or evenly. This is surprising, especially after watching how vesiculation occurs during lab experiments: in the bench furnace, specimens being heated first glowed red for some time before vesiculation occurred. Intuitively, it is difficult to imagine how hydration bands could remain on a specimen that had reached such a high temperature. One possibility is that the three flakes that have intact hydration were partially buried, or were exposed to an intense heat source from one direction only. In any case, the implication is that during a fire an artifact can lose all hydration information in one portion while retaining some kind of hydration in another.

These results for the five flakes differ from the larger analysis of the burned assemblage. In that sample all but one of the artifacts with vesiculation and/or crazing

was found to be without measurable hydration. Two sampling factors may help to account for finding a higher proportion of intact hydration bands in this set of five specimens. First, the partially vesiculated flakes were collected specifically because they were expected to have a greater chance for variable hydration. Second, multiple cuts were taken on each of these samples at locations selected with the purpose of encountering the greatest range of variation in hydration bands that might occur. In other words, more cuts, strategic placement of cuts, and specially chosen specimens will likely increase the chances for finding all possible results. Better recognition of the full range of fire effects may help guide decisions about how hydration analysis cuts are placed on pieces that have been exposed to fires.

Describing how heat alteration varies across a specimen requires more detailed examination than is usually undertaken in a standard obsidian hydration analysis. I wanted to understand precisely how hydration was retained when in association with macroscopic fire effects. How close could hydration bands be to vesiculated areas and still be measurable? Did diffuse hydration vary according to proximity of vesiculation and crazing? Here I describe in detail each of the three specimens (1691-53, 54, & 55) that retained hydration bands. These brief summaries include the macroscopic fire effects on each flake, placement of cuts, and a review of the observations made during microscopic OH examinations. The descriptions are presented not in specimen number order, but rather according to my perception of the complexity of results.

Specimen 1691-54.

This is a complete flake or a fragment of a core (the morphology is slightly warped by vesiculation). The glass is opaque and dark grey with faint flow banding and occasional tiny speckles. When collected, the artifact had the dorsal surface up and the ventral surface down. Fire effects are different on each side of the flake, with the ventral surface nearly free of macroscopic effects. This surface of the flake is fully intact with almost no vesiculation-except at small portions of the edges at each end of the flake. Crazing is not visible on the ventral surface. On the dorsal surface, however, vesiculation occurs at each end of the flake and along a dorsal ridge. Vesiculation is well developed at each end of the flake, resulting in exposure of fragile vesicles that are now broken and

abraded. However, along the dorsal ridge much of the vesiculation is less developed and occurs just below the "skin" of the surface, creating a smooth surface with intact vesiculation preserved beneath. Many areas of the dorsal surface have crazing, but rather than the network of fine lines found on the other specimens, there is instead cracking on the flake that appears to be caused by deformation of the piece (and consequent stretching).

Obsidian hydration cuts were made at the mid-section of the flake (Cut 1) and at one end (Cut 2). In both cases, the cuts included mostly unvesiculated glass. Hydration was observed on all surfaces of the cross-sections but varied greatly between cuts: one has a measurable hydration band and the other does not. Cut 1, located at the mid-section of the flake in the least vesiculated part of the specimen, had measurable hydration along all surfaces, measuring an average of 5.8 microns. For this cut, there were no effects of heat exposure apparent during the OH examination. In contrast, Cut 2 exhibited no measurable hydration or had diffuse hydration. Diffuse hydration also was observed on two vesicles, with several other bubbles having no hydration. Interestingly, Origer describes differences in the diffuse hydration depending on proximity to vesiculation--with fainter and more diffuse hydration on the dorsal surface, and brighter, darker diffuse hydration further from the vesiculated part of the flake.

Specimen 1691-55.

This is a nearly complete flake with a portion broken from the distal end. The material is opaque and dark grey with flow banding, occasional tiny speckles, and one larger inclusion apparent on the dorsal surface. When collected the dorsal side of the artifact was facing up. Fire effects are similar on each face of the flake, and include vesiculation at the proximal end of the flake that is apparent on both sides but somewhat more developed on the dorsal surface. There also is a small area of vesiculation on the distal tip. At the proximal end, the vesiculation has broken through the surface, but elsewhere the vesiculation is beneath the "skin" of the surface. Both faces have crazing, and on both faces the crazing is much more apparent nearest to the vesiculation. Crazing is also apparent on the broken surface where the end of the flake snapped off, and this

surface appears to have some sheen as well. Away from vesiculated areas, crazing is difficult to detect and probably is absent.

Three obsidian hydration cuts were made on this flake. One cut (Cut 1) is located at the distal end of the flake and well away from any vesiculation. Two cuts (Cut 2 & 3) are located at the proximal end of the flake within and adjacent to the vesiculated glass. The results of OH analysis do not follow any clear pattern. Despite differences in the location of the cuts relative to macroscopic fire effects, all three cuts show diffuse hydration or no visible bands. However, the hydration bands were in better condition at Cuts 1 & 2 making it possible to estimate the hydration band width at 3.0 microns. Further, hydration band condition does not correlate with one or another side of the artifact as greater diffusion or absence of bands occurs on either the dorsal or the ventral surface depending on which cut is examined. Therefore, neither the proximity to vesiculation and crazing nor the side of the artifact have apparent correlation with hydration band condition on this specimen.

Specimen 1691-53.

This is a complete flake of translucent black obsidian with fine flow banding that is apparent only with transmitted light. The glass has no inclusions. When collected the dorsal surface of the flake was down, and the unvesiculated portion of the distal end was slightly buried. Fire effects include full vesiculation on one unburied corner of the flake, and crazing covering the ventral surface with little to no crazing on the dorsal side. This specimen also is an excellent example of incipient or subsurface bubbling (see Chapter 3, Figure 3-23). Bubbles occur just below the surface and deep into the glass, beginning very small and increasing in size and density with proximity to the vesiculated area until they grade into full vesiculation. Because the glass is translucent, it is possible to see that the subsurface bubbling is unevenly distributed inside the glass: more bubbles occur along the internal flow bands. This is a phenomenon that is present in specimens 1691-54 and 55 but is even more apparent and readily observable in this flake. The significance of differential bubbling or vesiculation along flow banding is that it suggests that there are differences in heat response that correspond with some kind of

compositional, textural, or structural variation within the glass of an individual specimen or nodule.

Three cuts were made on this specimen and they are numbered Cuts 2, 3, & 4 (a Cut 1 was planned but not undertaken; although awkward, the original numbering is used here to correspond with the OH laboratory records). Two cuts (Cuts 2 & 3) are located adjacent to the vesiculated portion of the flake and included areas with bubbles. In both cases, hydration is diffuse, with slightly less diffuse hydration on the ventral surface allowing an estimate of approximately 2.1 microns hydration depth on that surface. Also observed in Cut 2 are vesicles with diffuse hydration. The third cut (Cut 4) is located away from vesiculation and bubbling and had different results. Here the ventral surface had a distinct measurable hydration band (1.5 microns), while the dorsal surface had un-measurable diffuse hydration.

In part, these are the results expected: the areas nearest the vesiculation and bubbling have the worst band condition, while the area furthest from vesiculation has a measurable hydration band. Also, the cut with measurable hydration (Cut 4) is located on the part of the flake that was buried when the specimen was collected. What is surprising is that the greatest alteration of hydration is observed on the surface that was facing up when collected (ventral) rather than the dorsal surface which was resting on the ground. One explanation is that the artifact was not in the same position during the fire as it was when collected. Another interesting aspect to the OH observations on this specimen is the greater width of diffuse hydration (approximately 2.1 microns; Cuts 3 & 4) compared to the intact hydration band (1.5 microns; Cut 4). This matches Trembour's (1990) observation that the hydration band deepens as it becomes more diffuse in response to heat.

Discussion of Specimens 1691-53, 54, & 55.

To summarize, the OH results on these specimens show that there are general relationships between the macroscopic fire effects and the expression of hydration on these partially vesiculated flakes. On flakes where intact hydration bands are retained, they are located on parts of the specimen where macroscopic fire effects are least apparent or are absent. However, despite the relative distance from vesiculation and

crazing, the areas with intact hydration are nonetheless quite close to fire effects in absolute terms. On specimen 1691-54, the location with the intact (5.8 microns) hydration band is less than five millimeters from vesiculated glass. On specimen 1691-53, the intact (1.5 microns) hydration band is more than 200 mm from the closest vesiculation. However, at that cut, the opposing face of the flake--where only diffuse hydration was observed--is only nine millimeters at the thickest part of the cut, placing intact and diffuse hydration very close together indeed.

This intensive examination also offers new information on the nature of diffuse hydration. First, the analysis shows there can be a direct relationship between the proximity of vesiculation and the degree of diffusion (as observed on specimen 1691-54). However, on another specimen (1691-55), less diffuse hydration occurs at the two locations (Cuts 2 & 3) that are closest to vesiculation, while more diffuse hydration occurs at the cut furthest from extant vesiculation[3]. Second, the results show that diffuse hydration can occur in direct association with vesiculation. This occurs in all three of these specimens, as well as on 1691-51 and 52 (see Table 4-2, above).

Finally, the direct association of diffuse hydration and vesiculation is expressed most enigmatically where there are actual vesicles with diffuse hydration (as on specimens 1691-53 and 54). In these cases (e.g., Figure 4-6, below), bubbles below or at the surface of the glass exhibit hydration along their internal bubble surfaces (i.e. on the interior of the bubble). This is difficult to explain because if the vesicles were caused by heat, how did the diffuse hydration occur so rapidly after the fire? There seem to be two possibilities. First, the vesicles are inherent in the glass (i.e. are not caused by heat exposure) and had hydration prior to the fire; when the artifact was heated, the existing hydration on the bubble surface became diffuse. Second, the vesicles were caused by heat exposure during the fire, and the diffuse hydration occurred through some process that is different than the process described by Trembour (1990). I would prefer the former explanation because it is simpler. Unfortunately, that explanation it is not

[3] The distal end of specimen 1691-55 is broken. This seems to offer the possibility that a vesiculated part of the artifact could have snapped off. If so, this would mean that Cut 1 was, in fact, close to vesiculation. I suspect this is not the case because 1) there is crazing on the break surface, and 2) at the other tip of the break, vesiculation curls around slightly onto the break surface. Thus, if the end of the flake did break off, it had to have done so during the fire to allow the opportunity for these fire effects to occur on the new surface.

supported because in these specimens the vesicles clearly appear to be heat-caused bubbles--created as part of vesiculation and not inherent to the glass. It is possible to identify hydration on vesicles that are inherent to the glass. One example did occur in the artifacts analyzed from Capulin Quarry. This is specimen 1691-05, a biface collected from a roadbed where it was protected from the fire. On this specimen the hydration band on the vesicle is distinct and unaltered, measuring 6.0 microns (the same as the hydration on the specimen exterior). If the vesicles with diffuse hydration on specimens 1691-53 and 54 are not inherent to the glass, this leaves the second, perplexing option: that the vesicle hydration occurred upon or after heating through some other process than inward "diffusion" of extant hydration. Perhaps alternate explanations can be devised, or the model described by Trembour can be augmented or clarified to include the phenomenon of diffuse hydration on heat-caused vesicles.

Turning to the final artifact in this "intensive" analysis, specimen 1691-02 offers a good contrast to these five partially vesiculated flakes. For this artifact, an entirely different set of explanations apply: most likely, this flake was burned during a fire that occurred long before the Dome Fire.

Specimen 1691-02.

This artifact is a nearly complete flake with a flake break or snap at the distal end (Figure 4-5). The flake is relatively thin and the dorsal surface is covered with shallow multidirectional flake scars; this appears to be a biface reduction flake. It is difficult to describe the obsidian. One half of the flake (nearest the vesiculated edge) is translucent and medium to light grey. The other half of the flake is opaque and brown. There is no apparent demarcation between these two visual variants within the glass; instead they grade into each other rapidly with some feathering of the brown material into the translucent grey. While neither visual variant is uncommon in obsidian from this source, their combination on one flake is unusual. Experimental heating of similar obsidians, as discussed in Chapter 3, determined that the unusual appearance of this glass is the result of heat exposure.

Figure 4-5. Ventral and dorsal views of specimen 1691-02 with OH measurements (in microns).

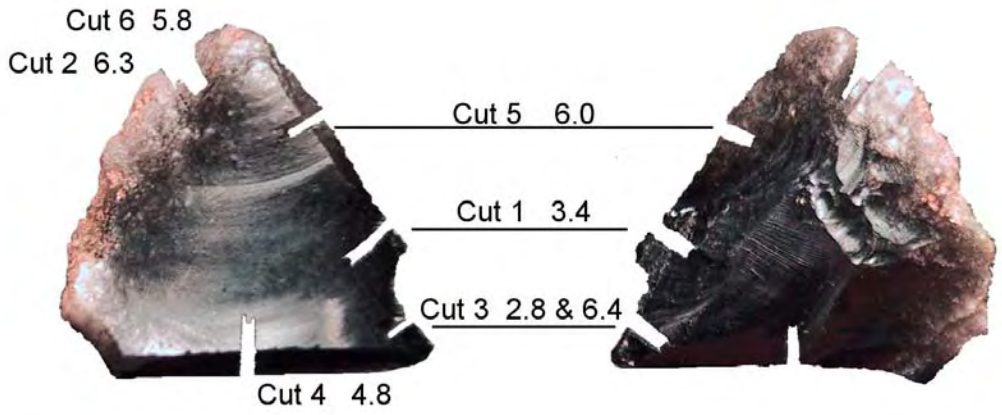

The specimen was collected from within the burned area of the site but in a roadbed that probably experienced relatively little heat exposure during the Dome Fire. Unfortunately, no information was recorded on the position of the flake when it was collected (it was one of the first artifacts removed from the site, prior to systematic documentation and collection). This specimen has several fire effects. It is vesiculated from the platform down along one edge, with incipient bubbles at the gradual boundary of the vesiculation. It is important to note that the vesiculation had to have occurred after the flake was detached from a core. This is certain because the vesiculation "wraps around" onto both the ventral and dorsal surfaces, and occurs on both the interior and exterior surfaces of the platform. Much of the vesiculation is contained within the "skin" of the surface, and only breaks through to expose the vesicles at the most exterior part of the vesiculated flake margin. Vesiculation is only observed in the translucent grey portion of the flake; the opaque brown portion has no vesiculation. Crazing occurs across the entirety of both faces, and is expressed most strongly nearer to the vesiculated portion. There does not appear to be crazing on the surface of the distal flake break.

Table 4-3. Hydration band measurements in multiple cuts on Specimen 1691-02 (all measurements are in microns).

Cut Number	Observed Fire Effects	Ventral Band	Dorsal Band	Other Measurements
1	crazing	3.4	3.4	
2	vesiculation	6.3	6.3	6.3 = bands on vesicles
3	crazing	2.8	2.8	6.4 = band on damaged area where dorsal and ventral surface converge
4	crazing on flake surfaces, none on flake break	4.8	4.8	4.8 = band on flake break surface
5	vesiculation	6.0	6.0	
6	vesiculation	5.8	5.8	

Six obsidian hydration cuts were made on this flake (Table 4-3, see Figure 4-5, above). This is the most on any of the specimens in this study, and certainly a high number for any analysis. Despite this abundance, there is no redundancy in the results: each cut yielded different obsidian hydration band widths. Clearly, this makes the OH results for this artifact complicated, but the results are also significantly different from the other burned specimens in this study in two ways. First, there is no diffuse hydration on this flake. All of the five partially vesiculated flakes included in the intensive OH analysis, and all but one of other seven vesiculated specimens in the burned assemblage OH analysis, have diffuse hydration. Second, this specimen has vesicles with hydration--but in this case, these are intact, measurable hydration bands (Figure 4-6). The other burned specimens with hydration on vesicles, 1691-53 and 54, have only diffuse hydration. The conclusion I draw from these two pieces of evidence--no diffuse hydration and intact hydration on heat-caused vesicles--is that the fire effects on specimen 1691-02 may be from an earlier fire. In other words, the flake did not burn during the Dome Fire, and did burn in a fire some time in the past.

Figure 4-6. Hydration bands on heat-caused vesicles on specimen 1691-02: (a) hydration on vesicle surface (6.3 microns)--note that hydration band only occurs on the exposed vesicle; (b) hydration on exterior artifact surface and on vesicle surface (6.3 microns)--note hydration bands lining the walls of the crack or "canal" that connects the artifact surface to the vesicle. (Microphotograph by T. Origer)

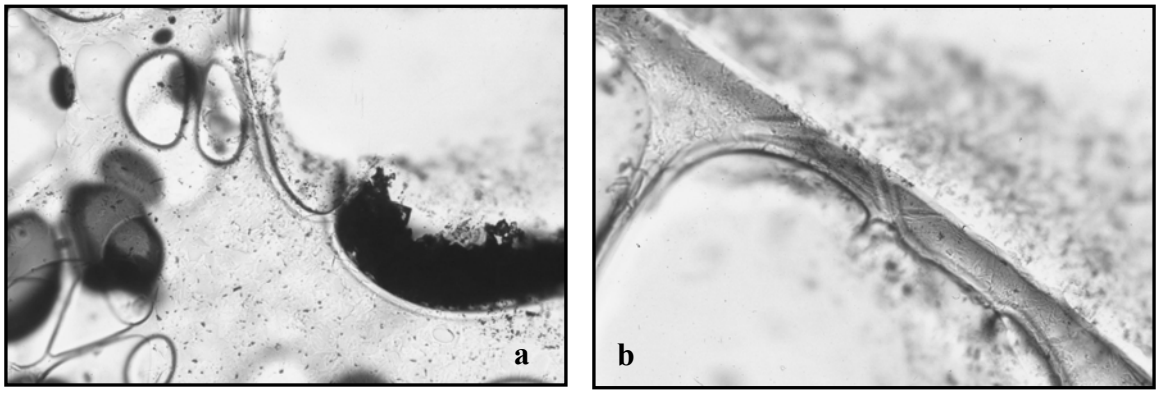

If the artifact was burned in the past rather than in the recent fire, this helps somewhat with the interpretation of the OH results obtained in the multiple cuts. The measurements presented in Table 4-3 suggest there are two groups of hydration band width measurements. The three cuts made in vesiculated areas of the artifact (Cuts 2, 5, & 6) have band measurements that range from 5.8 to 6.3 microns, and this includes the band width of 6.3 microns on vesicles in Cut 2. The three cuts made in the unvesiculated parts of the artifact (Cuts 3, 1, & 4), have band measurements of 2.8, 3.4, and 4.8 microns, respectively. The band widths in the vesiculated areas are the widest and are roughly similar, while the band widths in the unvesiculated areas are narrower but relatively diverse.

No standard obsidian hydration interpretations can be made from this suite of measurements. The greatest band widths occur in the vesiculated areas, so the normal interpretation would require this portion of the flake to be the oldest. Narrower band widths occur on the rest of the flake, in the unvesiculated portions, which would indicate that they are younger. However, the technological information is straightforward on this flake. Except for the flake break at the distal end, this is a flake without significant post-detachment modification. Because the vesiculation occurs on the platform and bulb of percussion, as well as on top of the proximal dorsal scars behind the platform, this means that the heat exposure that resulted in vesiculation occurred after all of these surfaces

were created--after the flake was detached from the core. All the dorsal scars overlap as if they were made while the flake was still attached to the core, and none of the dorsal scars initiate on the flake edges (i.e. all of the dorsal scars were there before the flake was created). Finally, the band width on the distal flake break is 4.8 microns, which is greater than the band widths on the nearest flake surfaces (2.8 and 3.4, in Cuts 3 and 1, respectively). One additional observation also eludes technological explanation. On Cut 3 there are two bands: one measuring 2.8 microns (on both the dorsal and ventral surfaces) and one measuring 6.4 microns (which occurs on a small portion of the edge of the flake where the two surfaces converge). In the OH thin-section, the area appears weathered. Under lower magnification of the hand specimen (e.g., 20x), this area has a rough appearance that at first glance looks like microfracture associated with edge chipping but on closer examination is not normal edge damage but rather a craggy irregular surface. I think this damaged area is the result of vesiculated glass spalling off--perhaps a "sloughing" off of vesiculated glass or a separation of the surface along a plane of shallow incipient bubbles (for example, as expressed on specimen 1691-12 and illustrated in Chapter 3, Figure 3-11).

This set of observations leads to two conclusions about the obsidian hydration history of this artifact. First, none of the usual explanations about sequential removal can explain the differences in the band widths across the flake. In fact, in every cut the measurements on the dorsal and ventral surfaces are identical (Table 4-3), thus excluding the most important indicator that a flake has been modified at a time more recent than when the flake was originally created. The distal flake break should either have the same band width as the adjacent surfaces (if it occurred at or near the time of flake detachment), or have a narrower band width (if it occurred after the flake was created). Second, even applying what we know about fire alteration to obsidian hydration bands does not provide an obvious alternate post-fire obsidian hydration history, and raises many more questions than can be answered. If the fire simply "reset" the obsidian hydration clock on this artifact, why do the hydration bands vary so much across the piece? Why are the bands at the vesiculated locations less variable than the bands in the unvesiculated areas?

I can speculate about how heat exposure could account for certain band widths or groups of OH results, but I cannot yet formulate a coherent explanation to explain the

combined hydration analysis results across the entire specimen. For example, one possibility to explain the wider bands in vesiculation-area cuts is that they represent the manner in which diffuse hydration hydrated after the episode of heat exposure--where the hydration band was widened during heating and with re-hydration became distinct again at this increased width. Or, the wider bands in the vesiculation-area cuts show that post-fire re-hydration occurs at a different rate where heat alteration of obsidian is extreme. This might apply also to explaining the diverse band widths in the unvesiculated areas.

In summary, the obsidian hydration results obtained for specimen 1691-02 are unusual and puzzling, and cannot readily be explained in terms of the artifact's technological history, speculation as to its fire history, or compositional disparities in the piece. A satisfactory explanation for the obsidian hydration on specimen 1691-02 will require a more complete understanding of how obsidian hydrates following significant heat exposure. For now, however, an important implication of these results is the recognition that obsidian does form hydration bands after substantial heat exposure, and that these bands can be intact and measurable. Any obsidian hydration analysis that includes fire altered artifacts will benefit from not only from an informed attempt to identify any macroscopic fire effects that evidence past heat exposure, but also a thorough or "intensive" obsidian hydration analysis that includes multiple cuts. Such analyses could change the overall interpretation of the OH information in a burned assemblage, and more importantly for now, will contribute to our understanding of past heat alteration and subsequent hydration of obsidian artifacts.

Discussion of Sections 4.1 and 4.2

The obsidian hydration analysis of the burned and unburned assemblage at Capulin Quarry (Section 4.1) produced results that are relatively straightforward. There is clear evidence that heat exposure during the Dome Fire altered obsidian hydration bands in the burned specimens, and that the proportion of specimens without measurable hydration increased with the degree of burning in this sample. The results also suggest that the presence of diffuse hydration could be used as an indicator of recent exposure to heat. However, when the scale of analysis is shifted from the assemblage to the specimen (Section 4.2), the results are more complex. While crazing and vesiculation are

associated with both the presence of diffuse hydration and a lack of measurable hydration, the "intensive analysis" of several partially vesiculated flakes showed that within a specific specimen a single hydration cut might not represent all of the hydration information--or the range of relationships between macroscopic and microscopic fire effects--on that artifact. Finally, one specimen in the analysis, 1691-02, appears to be an example of an artifact burned during an earlier fire, and then re-hydrated in a way that is not yet understood. This artifact illustrates both that new kinds of obsidian hydration information may exist on artifacts burned in past or prehistoric fires, but that there is much that must be learned before beginning to develop any potential for using obsidian hydration dating to estimate the age of past fire exposure on such artifacts.[4]

Use of OH analysis of burned obsidian artifacts as a tool in constructing fire histories was an early hope of this study, effectively dashed by the complexity of results obtained in the pilot project (i.e., Sections 4.1 and 4.2). With OH results this variable, much more would need to be known to pursue any systematic use of altered hydration and subsequent re-hydration as a method for measuring the interval that had passed since alteration occurred. Instead, these OH results and the concomitant composition analyses in the pilot project (see Chapter 6) served to focus attention in this research on understanding: 1) variation in heat effects (both macroscopic and microscopic), and 2) determining the role of potential composition variability in obsidian glass-environment interactions (including both hydration loss and gain). The remainder of this chapter addresses the former.

4.3. Analysis of Fire Effects and Obsidian Hydration in Artifacts from Controlled Sample Unit SU1

The examination and analysis of obsidian samples collected in SU1 has two goals. The first is to describe systematically the expression of the three most prevalent fire effects observed in artifacts at Capulin Quarry following the Dome fire: vesiculation,

[4] The portion of this chapter that is the pilot project, previously published in Steffen (2002), ends with this paragraph.

crazing, and fire fracture. By collecting specimens systematically and completely within a gridded sample area, it is possible to describe how the fire effect attributes are expressed on all pieces in the surface assemblage that was exposed to fire. The relative proportions of affected to unaffected artifacts can be assessed, frequencies among each of the three fire effects can be quantified and compared, and the distribution of fire effects across the 5 m-x-5 m area can be examined. The second goal is to determine how obsidian hydration data (microscopic alteration) co-occurs with the expression of observable fire effects (macroscopic alteration). The analyses conducted in the pilot project (Section 4.1 and 4.2) clearly confirm the hypothesis that the conditions reached at Capulin Quarry during this recent forest fire were sufficient to substantially alter hydration in artifacts in the assemblage, and that the alteration expressed as diffuse hydration and lack of visible hydration bands was greater in samples collected from locations with greater evidence of burn intensity. However, only a non-judgmental sample can provide a view of the proportions of visible fire effects, and the correlation with OH alteration, that is representative of the quarry assemblage.

To review from Chapter 2, Sample Unit 1 ("SU1") is a 5 m-x-5 m grid placed in an area adjacent to a cluster of vesiculated obsidian located on a west-southwest facing slope of a ridge in the southeast portion of the site. This area was selected because the apparent burn severity was moderate to severe, ground visibility was high, and post-fire disturbance appeared minimal. The sampling unit is located adjacent to vesiculation cluster 11 (located at the northwest corner of SU1) and no vesiculated artifacts were observed within the sample unit prior to collection. The goal was to collect a sample of all artifacts (with or without visible fire effects) that is representative of the full range of heat effects where there is high and moderate severity of burning but where not all artifacts are necessarily affected. Systematic collection across the 5 m-x-5 m gridded sample unit provides a greater assemblage sample size than can be collected in a single smaller area, affords examination of effects across a larger contiguous area than was collected previously, and provides a representative sample of all artifacts subjected to burning—whether or not macroscopic fire effects are observed on the items collected. Collection of non-artifacts with evidence of fire effects, especially fire fracture, provides

a comparative sample of severity of fire alteration that is independent of artifacts collected.

Sample Unit Collection Strategy

Within the 5 m-x-5 m grid, all surface artifacts >2 cm were collected within each of the 25 1 m-x-1 m subunits (see Figures 3-6 through 3-8 in Chapter 3). In addition, all obsidian items that appeared to be fire-fractured were collected, and other non artifacts were collected if they exhibited signs of fire alteration such as crazing and vesiculation. Collected items were marked on the side facing up by inscribing a small mark with a glass-etching pen. Prior to collection, each subunit was photographed and a sketch map was made of the presence and distribution of existing vegetation (e.g., tufts of grass), insulating materials (e.g., large tuff blocks, concentrations of smaller tuff gravels), any indicators of burning or lack of combusted materials (e.g., partially consumed logs, scorched tuffs), or post-fire disturbances (e.g., rodent burrowing). Photographs were made of all subunits before collection was begun. In a few subunits, where variability was noted in the intra-subunit distribution of fire effects, artifacts were collected within 50 cm-x-50 cm quadrants to increase the spatial resolution; resulting data within these quadrants could later be grouped by subunit as needed.

Examination of Fire Effects in Collected Artifacts

As soon as collection was initiated, it became clear that the total number of artifacts and non-artifacts recovered in this manner was much more abundant than the number actually needed for analysis. No final total was computed but it is estimated that several-thousand items were collected within the 5 m-x-5 m sampling unit. To create a manageable sample size for close examination of potential fire effects on every specimen, a systematic sampling strategy was devised to select eight $1m^2$ subunits (Figure 4-7). The selected subunits are F1, F3, F5, H2, H4, J1, J3, and J5. This provides a 32 percent (8 of 25 subunits) sample that is broadly distributed across the sampling unit, with spacing of the eight selected subunits designed so that no subunit is adjacent to another.

Figure 4-7. Sample Unit 1 is a 5 m-x-5 m grid with 25 1 m-x-1 m subunits. The eight 1 m-x-1 m subunits included in the artifact analysis are shown as shaded squares.

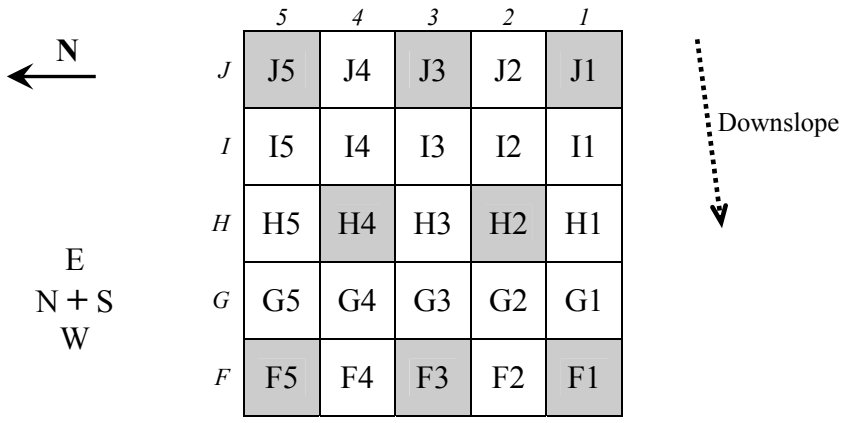

After collection, all specimens from the eight subunits in SU1 were closely examined (with and without a 10x hand lens, a magnifying lamp, and in some cases a binocular microscope with up to 50x magnification) to identify whether any macroscopic fire effects could be observed and to confirm that non-artifacts collected as having fire fracture were indeed fire-fractured items. Some specimens were rejected during this examination either because they did in fact have fire fracture surfaces, or because they were not actual artifacts; such rejected specimens are not included in the totals used.

For artifacts where macroscopic fire effects could be observed, a hierarchical method was used to sort artifacts into categories. This method creates simplified categories that are not mutually exclusive by observed fire effect (however, to address the complexity of co-occurring fire effects, this information was noted outside of the sorting process). In order of hierarchy, these categories are: artifacts with vesiculation, with crazing, and with fire fracture. In all cases where vesiculation was observed, some kind of crazing was also observed-so no attempt was made to record this co-occurrence categorically. The category of vesiculation thus subsumes crazing, and all artifacts with vesiculation are sorted into the "artifacts with vesiculation" category. Where crazing was observed (and vesiculation was not), items were sorted as "artifacts with crazing". For those artifacts where both crazing and fire fracture was observed a count was maintained but no category was created. Finally, artifacts with only fire fracture were sorted into the "artifacts with fire fracture" category; none of these artifacts had also crazing or vesiculation (if they had, they would have been sorted into a higher category). Items

were further subdivided into 1 cm size sub-categories (>7cm, <7cm, <6cm, <5cm, <4cm, <3cm, and <2cm) and weights of artifacts in each size sub-category were recorded. In the discussion that follows, only total counts by subunit are considered.

Table 4-4. Items collected from the eight subunits in SU1. Includes all artifacts (with and without fire effects) and non-artifacts with fire fracture. The table is designed to show subtotals within various groupings (separated by double lines) and associated percentages (column totals and percent totals are designated with italics).

Sub unit	Total items[1]	Non–artifacts w/FF	All artifacts	Artif w/o fire effects	Artif w/fire effects	Artif w/FF	Artif w/craz	Artif w/vesic	All items w/fire effects[2]	All items w/o fire effects[3]
J5	82	32	50	29	21	12	3	6	53	29
J3	185	80	105	79	26	18	8	0	106	79
J1	62	22	40	29	11	10	1	0	33	29
H4	160	48	112	75	37	25	12	0	85	75
H2	273	85	188	159	29	16	11	2	114	159
F5	206	63	143	112	31	24	7	0	94	112
F3	33	12	21	19	2	2	0	0	14	19
F1	22	10	12	6	6	4	2	0	16	6
	1023	*352*	*671*	*508*	*163*	*111*	*44*	*8*	*515*	*508*
	% within groups	34.4%	65.6%	75.7%	24.3%	68.1%	27.0%	4.9%	50.3%	49.7%
			100.0%		*100.0%*			*100.0%*		*100.0%*

Sub unit	Total items[1]	Non–artifacts w/FF	All artifacts	Artif w/o fire effects	Artif w/fire effects	Artif w/FF	Artif w/craz	Artif w/vesic	All items w/fire effects[2]	All items w/o fire effects[3]
J5	8.0%	9.1%	7.5%	5.7%	12.9%	10.8%	6.8%	75.0%	10.3%	5.7%
J3	18.1%	22.7%	15.6%	15.6%	16.0%	16.2%	18.2%	0.0%	20.6%	15.6%
J1	6.1%	6.3%	6.0%	5.7%	6.7%	9.0%	2.3%	0.0%	6.4%	5.7%
H4	15.6%	13.6%	16.7%	14.8%	22.7%	22.5%	27.3%	0.0%	16.5%	14.8%
H2	26.7%	24.1%	28.0%	31.3%	17.8%	14.4%	25.0%	25.0%	22.1%	31.3%
F5	20.1%	17.9%	21.3%	22.0%	19.0%	21.6%	15.9%	0.0%	18.3%	22.0%
F3	3.2%	3.4%	3.1%	3.7%	1.2%	1.8%	0.0%	0.0%	2.7%	3.7%
F1	2.2%	2.8%	1.8%	1.2%	3.7%	3.6%	4.5%	0.0%	3.1%	1.2%
	100.0%	*100.0%*	*100.0%*	*100.0%*	*100.0%*	*100.0%*	*100.0%*	*100.0%*	*100.0%*	*100.0%*

[1]Includes 1) all artifacts and 2) all non-artifacts with fire fracture: does not include items rejected during examination as not belonging to either of these two categories.

[2]Includes artifacts with various fire effects and non-artifacts with fire fracture.

[3]Includes only the items collected (all artifacts and all non-artifacts with fire fracture): many, many more non-artifact obsidian nodules were present within units.

The total number of items examined from the eight subunits (n=1023) includes 352 artifacts, and 671 non-artifacts with fire fracture (Table 4-4, Figure 4-8). Of all artifacts collected, just under 25 percent (n=163) have observable vesiculation, crazing, or fire fracture, while 508 (75.7 percent) have no visible fire effects (NAFE). The most common fire effect in artifacts was fire fracture (n=111; 68.1 percent), followed by crazing (n=44; 27.0 percent) and vesiculation (n=8; 4.9 percent). Figure 4-8 shows proportional totals of artifacts with and without fire effects, and in each of the three categories.

Figure 4-8. Relative frequencies of fire effects observed in SU1 artifacts: (a) artifacts with fire effects, and artifacts with no apparent fire effects (NAFE) as proportion of all artifacts collected (n=671); (b) relative frequencies of vesiculation, crazing, and fire fracture as percent of all artifacts with fire effects (n=163); (c) Venn diagram showing schematic view of co-occurrence of these attributes.

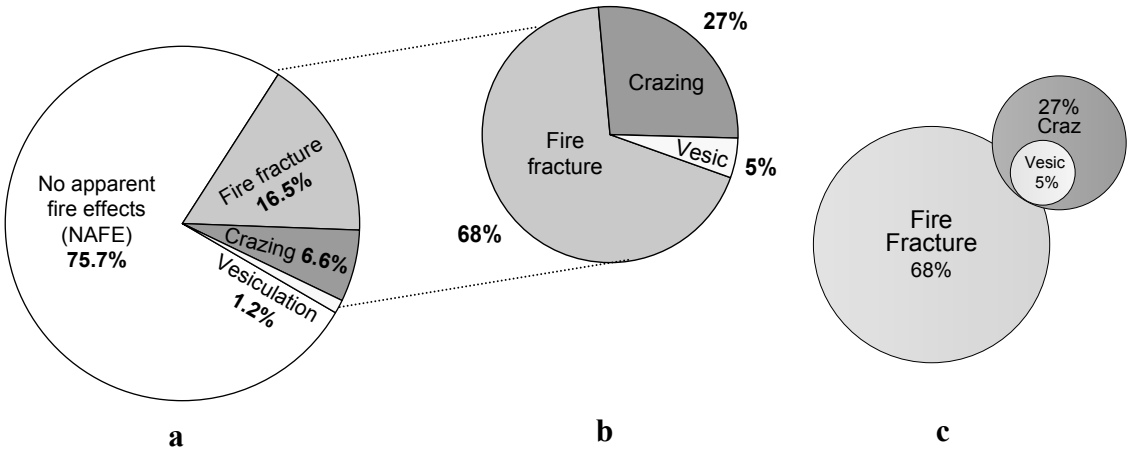

The Venn diagram in Figure 4-8:c is a schematic representation of co-occurrence of the three fire effect attributes. It illustrates that a small proportion of fire fractured artifacts have crazing (8 of 111, 7.2 percent), a larger proportion of crazed artifacts (8 of 44, 18.2 percent) exhibit fire fracture, a quarter of all vesiculated artifacts have both crazing and fire fracture (2 of 8, 25 percent), and all vesiculated artifacts have some crazing. In other words, the hierarchy used to create sorting categories reflects both the relative frequency of each attribute occurring in this assemblage, and an increasing intensity of fire alteration. Trembour (1990; see also Appendix A) established that where crazing occurs it does so prior to reaching the conditions (i.e., heat, duration) required to

cause vesiculation. Fire fracture probably does not occur along the same continuum because it likely involves relationships among the surface to volume ratio of an item, heat, duration, and the rapidity of heating and cooling (Bennett and Kunzmann 1985; Buenger 2003; Tsirk, Appendix B). However at the scale of assemblage, as represented in SU1, the relative co-occurrence of these three fire effects appears to represent an increase in the intensity of macroscopic fire alteration, and perhaps reflects the nature and degree of fire or heat exposure during the event of the burn. This could have implications for how obsidian hydration bands experience alteration during forest fire exposure.

Obsidian Hydration Analysis of SU1 Specimens

There are two goals of this OH analysis. The first is to assess whether artifacts with observable effects are more likely to have alteration of obsidian hydration than artifacts with no visible fire effects (NAFE). The second is to determine if there is any correlation between specific macroscopic fire effects and OH alteration.

These questions can be stated more formally as hypotheses. The first hypothesis is that artifacts without observable fire effects are more likely to have intact obsidian hydration bands and are less likely to have diffuse hydration. The second hypothesis is nested within the first: artifacts with the specific fire effects of crazing and vesiculation are less likely to have intact obsidian hydration, and are more likely to have diffuse hydration (DH) and no visible bands (NVB). In the specimens analyzed from SU1, NAFE artifacts are expected to have greater relative frequencies of intact hydration and a smaller proportion of OH bands that are diffuse or not visible. Artifacts with crazing and vesiculation are expected to have lower relative frequencies of intact hydration and a higher proportion of OH bands that are diffuse or not visible.

The methods used to select SU1 obsidian artifacts for obsidian hydration analysis are guided by these questions and the goal of obtaining a sample that is representative of the overall assemblage at Capulin Quarry. Two groups of artifact were submitted from each 1 m-x-1 m subunits included in the examination of fire effects (above): 1) all artifacts with crazing or vesiculation, and 2) a sample of six artifacts with no apparent fire effects. The six NAFE specimens were chosen to be equivalent among the subunits, and represented apparent variation in obsidian material, artifact size, artifact thickness, and

technological characteristics observed throughout the sampling unit. Most NAFE artifacts included in the six-per-subunit controlled sample are flakes or partial flakes and several thicknesses and sizes are represented. Other artifacts include cores and core fragments, and flakes on nodules (see Table 4-5, below).

Thus the NAFE sample size is fixed within the sample unit (six artifacts per subunit), while the sample of artifacts includes all such specimens found within each subunit. The intention in the first case is to represent the overall quarry assemblage, and in the second case to represent the totality of crazed and vesiculated artifacts within the sample area. This unbalanced sampling strategy is warranted by the need to include sufficient crazed and vesiculated specimens despite their small quantity within the subunits (see Table 4-4 and discussion, above), as well as to represent the much larger quantity of NAFE specimens found within subunits.

The obsidian hydration analysis was again conducted by T. Origer, now of Origer's Obsidian Laboratory, using the same techniques described in Section 4.1. As learned in the intensive analysis of OH in individual specimens (Section 4.2), partially vesiculated artifacts can have multiple OH outcomes on a single specimen. Therefore, multiple OH cuts were made on several of the fire effects specimens. In retrospect, it would have been prudent to conduct such multiple OH analyses on some of the NAFE artifacts but this was not done; all NAFE artifacts have only a single OH cut. OH analysis results originally were recorded by individual OH cut, and are summarized by specimen in Table 4-5.

Table 4-5. Obsidian hydration analysis of 87 SU1 artifacts and added artifacts.

XRF[a]	Spec	Artifact	Fire effects?	Fire effects[b]	SU1 OH[c]	Other notes on specimen	Band Measures[d]	OH cuts[e]	# of OH Results[f]
	J5-01	flake	N	nafe	SU1		NVB, 3.4	1	2
	J5-03	flake	N	nafe	SU1		1.5	1	1
	J5-04	flake	N	nafe	SU1		DH	1	1
	J5-06	flake	N	nafe	SU1		8.6	1	1
	J5-07	flake	N	nafe, FF: fits J5-8	SU1		DH	1	1
	J5-08	flake	N	nafe, FF: fits J5-7	SU1		DH	1	1
	J5-09	flake	Y	craz	SU1		DH	1	1
✓	**J5-B10**	flake	Y	vesic, craz	SU1	vesic flake, special OH	DH, DH, 1.1, DH, DH, DH	5	6

Table 4-5. Continued: SU1 Obsidian hydration analysis.

XRF[a]	Spec	Artifact	Fire effects?	Fire effects[b]	SU1 OH[c]	Other notes on specimen	Band Measures[d]	OH cuts[e]	# of OH Results[f]
	J5-C11	flake	Y	vesic, craz	SU1	vesic flake, special OH	DH	1	1
✓	**J5-D12**	flake	Y	vesic, craz	SU1	vesic flake, special OH	5.0, 5.0	2	2
✓	**J5-E13**	flake	Y	craz, FF, vesic	SU1		1.1, NVB	1	2
✓	**J5-G15**	flake	Y	craz	SU1		1.2, NVB	1	2
	J3-01	flake	N	nafe	SU1		DH	1	1
	J3-03	core frag	N	nafe	SU1		DH	1	1
	J3-04	flake	N	nafe	SU1		DH	1	1
	J3-06	bipolar core frag	N	nafe	SU1		DH	1	1
	J3-07	flake	N	nafe	SU1		3.3	1	1
	J3-08	flake	N	nafe	SU1		1.1, 4.9	1	2
	J3-09	core	Y	craz	SU1		4.6, DH;~ 7.2	1	2
	J3-10	flake	Y	craz, FF	SU1	flake surfaces are weathered; fresh surf is FF	DH	1	1
	J3-11	flake	Y	craz	SU1		5.9	1	1
	J3-12	flake	Y	craz	SU1		DH	1	1
	J1-01	flake	N	nafe	SU1	similar to Polv Pk obsid	DH	1	1
	J1-03	flake	N	nafe	SU1		DH	1	1
	J1-04	flake	N	nafe	SU1		DH	1	1
	J1-06	flake	N	nafe	SU1		6.2, 8.0, DH	1	3
	J1-07	flake	N	nafe	SU1		DH	1	1
	J1-08	flake	N	nafe	SU1		DH	1	1
✓	**J1-10**	flake/core frag	Y	vesic, craz	SU1	vesic flake, special OH	3.4, 4.8, 7.2, 7.3, 10.1, 10.1, 11.4, 11.5	4	8
	H4-01	flake	N	nafe	SU1		DH;~ 6.5 DH;~ 3.2	1	2
	H4-03	flake	N	nafe	SU1		DH, DH;~ 3.2	1	2
	H4-04	flake	N	nafe	SU1		5.8	1	1
	H4-06	flake	N	nafe	SU1		NVB	1	1
	H4-07	flake	N	nafe	SU1		DH	1	1
	H4-08	flake	N	nafe	SU1		DH	1	1
	H4-09	flake	Y	craz	SU1		1.9, DH	1	2
	H4-10	flake	Y	craz	SU1		DH	1	1
	H4-11	flake	Y	craz	SU1		DH	1	1
	H4-12	flake	Y	craz	SU1	linear craz, poss usewear	DH	1	1
	H4-13	flake	Y	craz	SU1		3.7	1	1
	H4-14	flake	Y	craz	SU1		1.7	1	1

Table 4-5. Continued: SU1 Obsidian hydration analysis.

XRF[a]	Spec	Artifact	Fire effects?	Fire effects[b]	SU1 OH[c]	Other notes on specimen	Band Measures[d]	OH cuts[e]	# of OH Results[f]
	H2-01	flake	N	nafe, 1 FF surf	SU1		DH	1	1
	H2-03	flake	N	nafe	SU1		DH, NVB	1	2
	H2-04	flake	N	nafe	SU1		NVB	1	1
	H2-06	flake	N	nafe	SU1		DH	1	1
	H2-07	flake	N	nafe	SU1		DH	1	1
	H2-08	flake	N	nafe	SU1		DH;~ 6.2	1	1
✓	**H2-10**	flake	Y	vesic	SU1	vesic flake, special OH	DH, DH, DH	3	3
	H2-12	flake	Y	poss. vesic, craz	SU1		DH	1	1
	H2-13	flake	Y	craz, FF	SU1		DH	1	1
	H2-14	flake	Y	craz, poss. FF	SU1		DH, 1.3	1	2
	H2-15	flake	Y	craz	SU1		3.3	1	1
	H2-16	flake	Y	craz, FF	SU1	fits with H-18 at FF break	DH	1	1
	H2-18	flake	Y	craz	SU1	fits with H2-16 at FF break	DH	1	1
	F5-01	flake	N	nafe	SU1		DH	1	1
	F5-03	flake	N	nafe	SU1		DH	1	1
	F5-04	flake	N	nafe	SU1		DH	1	1
	F5-06	flake	N	nafe	SU1	heavily coated	1.1, DH	1	2
	F5-07	core	N	nafe	SU1		DH	1	1
	F5-08	flake	N	nafe	SU1		NVB	1	1
	F5-09	flake	Y	craz	SU1		DH	1	1
	F5-10	flake	Y	craz	SU1		NVB	1	1
	F5-11	flake	Y	craz	SU1		DH	1	1
	F5-12	flake	Y	craz	SU1		DH	1	1
	F5-13	flake	Y	craz	SU1		DH	1	1
	F3-01	flake	N	nafe	SU1		DH	1	1
	F3-03	flake	N	nafe	SU1		DH	1	1
	F3-04	flake	N	nafe	SU1		DH;~ 6.0	1	1
	F3-06	flake	N	nafe	SU1		4.3	1	1
	F3-07	flake	N	nafe	SU1		1.1, NVB	1	2
	F3-08	flake	N	nafe	SU1		6	1	1
	F1-01	flake/nodule	N	nafe-FF	SU1		2.6	1	1
	F1-03	flake	N	nafe	SU1		DH	1	1
	F1-04	flake	N	nafe	SU1		DH	1	1
	F1-06	flake (brown)	N	nafe	SU1		1.3	1	1
	F1-07	flake	N	nafe	SU1		1.2	1	1

Table 4-5. Continued: SU1 Obsidian hydration analysis.

XRF[a]	Spec	Artifact	Fire effects?	Fire effects[b]	SU1 OH[c]	Other notes on specimen	Band Measures[d]	OH cuts[e]	# of OH Results[f]
	F1-08	flake	N	nafe	SU1		7.1	1	1
	F1-09	flake	Y	craz, poss FF	SU1	blue-brown obsid	4.1	1	1
	F1-10	flake	Y	craz	SU1		6.4, 10.6	1	2
✓	**601**	biface frag	N	nafe	Add	biface, nafe, special OH	NVB, DH;~ 8.4, NVB	2	3
✓	**603**	biface frag	Y	craz	Add	biface, crazing, special OH	DH, DH	2	2
	604	flake	Y	vesic, craz	Add	vesic flake, heavily coated, special OH	DH, DH, DH, DH, DH	5	5
	H2-09	flake	N	nafe	Add	blue-brown obsid	NVB	1	1
✓	**I4-01**	flake	Y	vesic, craz	Add	vesic flake, special OH	1.8, DH, 1.4, 1.7, DH, DH	3	6
	J1-09	biface frag	N	nafe	Add	glass has bubbles (non-fire)	7.0, DH	1	2
✓	**J4-01**	flake	Y	vesic, craz	Add	vesic flake, special OH	DH, 1.8, DH, DH, DH	4	5
✓	**J5-F14**	biface frag	N	nafe	Add	biface, nafe, special OH	1.2, 1.2, NVB, 1.1, NVB	3	5
			Y = 35 *N = 52*		*SU1=79* *Add= 8*			*110*	*138*

[a] Check mark indicates X-ray fluorescence analysis was conducted on specimen (see Appendix D).

[b] Macroscopic fire effects observed on specimens correspond with those described in Chapter 3:
sheen = altered or additive surface sheen vesic = vesiculation nafe = no apparent fire effects
craz = fine surface crazing or cracking fract = fire fracture

[c] Whether specimen was included in the controlled sampling of SU1: SU1 = yes; Add=added specimen
Observations made during OH analysis: wea = weathering of surface was noted;
2 bands = two measurable bands observed within one cut.

[d] Mean values of six OH measures for each band (OH in microns) and/or hydration condition assessed during analysis: DH = diffuse hydration (not measurable) NVB = no visible band
DH;~x.x = diffuse hydration followed by estimated measurement

[e] Number of thin section cuts examined per specimen

[f] Total number of bands observed where multiple bands were present for a single cut.

Results of OH Analysis in SU1 Specimens

The total sample of artifacts from SU1 submitted for OH analysis (n=79) includes 48 artifacts with no visible fire effects (six samples each from eight subunits), and 31 artifacts with the fire effects of vesiculation or crazing. To approximate the analysis conducted for the pilot project (Section 4.1, see Figure 4-1), I first looked at whether artifacts had any intact measurable obsidian hydration present in any OH cut, regardless of whether diffuse hydration (DH) or no visible bands (NVB) were present in any OH cut (Figure 4-9). As noted in Section 4.1, OH artifacts include those that have intact

measurable bands present and have no indication of diffuse hydration, DH artifacts include those with diffuse hydration present without regard to any other hydration results on the item, and NVB artifacts include those with no visible hydration in any cut.

The general results are as expected: the low proportion of intact obsidian hydration supports the interpretation that OH was altered in the fire. The specific results, however, are surprising: artifacts with and without intact OH are nearly equally represented in artifacts with and without fire effects. The first hypothesis immediately can be rejected.

Figure 4-9. Proportion of intact/measurable hydration bands in SU1 artifacts with no visible fire effects (NAFE) and with fire effects.

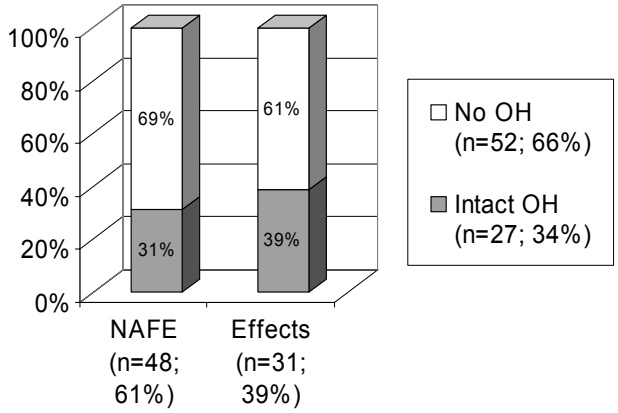

On the one hand, these results are surprising because they are counter to the expectation that the absence of observable fire effects indicates less likelihood of heat-exposure sufficient to alter hydration. On the other hand, these results accord well with results obtained in the pilot project. In this earlier component of the current study, artifacts collected from the "burn area" (Figure 4-1) are artifacts combined from the general burn area and from near and within vesiculation clusters (Figure 4-2). These three degrees of burn severity characterize the burn context of SU1 from which the current specimens were collected. In fact, the range of burn severity at this location was part of the reason for its selection. In the earlier sample, 27 percent of specimens in the burn area specimens had intact OH (Figure 4-1); this is similar to the 34 percent intact OH when NAFE and fire effects specimens are combined. It appears that it is neither impossible nor even unusual for OH alteration to occur in individual specimens without

the concomitant development of observable macroscopic fire effects. While the analyses that follow provide more detail about the presence of intact OH, diffuse hydration, and no visible bands, and how obsidian hydration results vary among artifacts with and without crazing and vesiculation, this determination remains the summary finding of the SU1 OH analysis (see end of the chapter).

Figure 4-10. Proportions of intact obsidian hydration (OH), diffuse hydration (DH), and no visible bands (NVB) in SU1 artifacts, comparing between artifacts with and without fire effects.

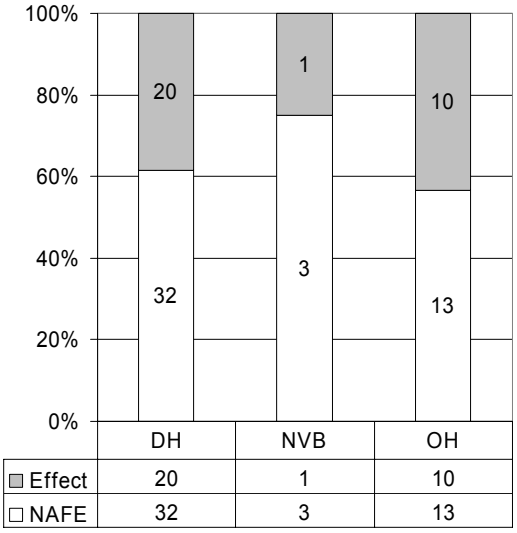

	DH	NVB	OH
Effect	20	1	10
NAFE	32	3	13

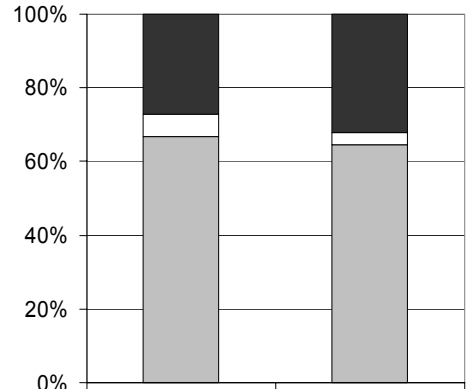

	0 NAFE	1 Effect
OH	27.1%	32.3%
NVB	6.3%	3.2%
DH	66.7%	64.5%

Figure 4-10 shows the proportions of intact hydration, diffuse hydration, and no visible bands in the SU1 specimens. Again the results are counter-intuitive, with NVB more common in NAFE artifacts than in those with observable fire effects, and intact OH equally common in artifacts with fire effects than in those without. Diffuse hydration, which may serve as an indicator of heat alteration, occurs in a high proportion of all artifacts (n=52; 65.8%) and is equally common in NAFE and fire effects artifacts. The high frequency of diffuse hydration in SU1 artifacts weakens the possibility that the low proportion of intact OH in these artifacts is due to some factor other than heat exposure.

Turning to the second hypothesis, Figure 4-11 shows the relative frequencies of artifacts with crazing, vesiculation, and no apparent fire effects. As with the tests of the first hypothesis, the results obtained in SU1 artifacts are unquestionably counter to the results expected, but given the results seen thus far there are no great surprises. Intact

OH is equally or less common in NAFE artifacts as in those with crazing or vesiculation. The second hypothesis, that asserted the likelihood of lower intact OH and higher NVB and DH in crazed and vesiculated samples, can be rejected.

Figure 4-11. Proportions of intact obsidian hydration (OH), diffuse hydration (DH), and no visible bands (NVB) in SU1 artifacts, comparing among NAFE artifacts and those with crazing and vesiculation.

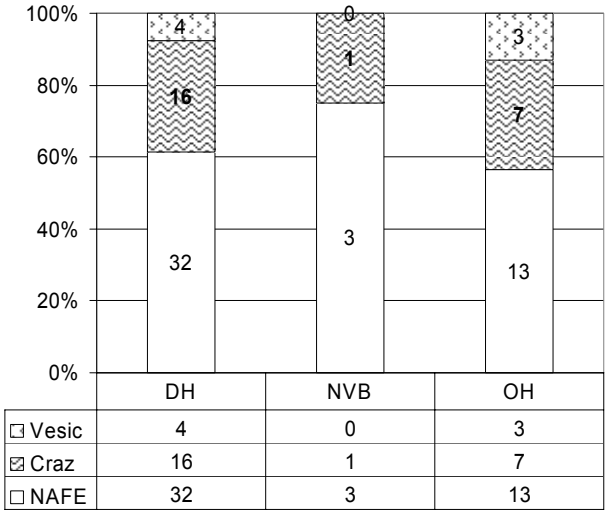

	DH	NVB	OH
Vesic	4	0	3
Craz	16	1	7
NAFE	32	3	13

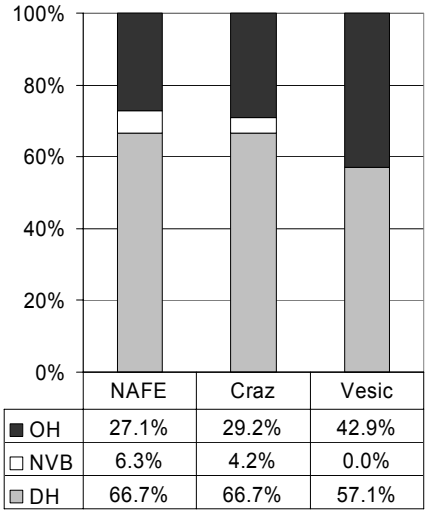

	NAFE	Craz	Vesic
OH	27.1%	29.2%	42.9%
NVB	6.3%	4.2%	0.0%
DH	66.7%	66.7%	57.1%

Finally, examination of only the artifacts with fire effects shows that in the SU1 sample, artifacts with crazing and with vesiculation do retain intact measurable hydration (Figures 4-11 & 4-12). Intact hydration is present in 29.2 percent (n=7) of crazed artifacts and 42.9 percent (n=3) of vesiculated artifacts. These are very high proportions, especially in comparison with results obtained in the pilot project study (Section 4.2) where very few crazed and vesiculated specimens retained OH. Closer examination of the data suggests that in the fire effects artifacts with intact hydration, two of the three vesiculated artifacts and two of the seven crazed artifacts also have one or more NVB results, or have possible diffuse hydration present (i.e., where the width of OH is greater than would be expected, suggesting diffuse hydration with the appearance of intact OH). While these observations change the relative frequencies of intact OH on fire effects artifacts, they do not resolve the differences between the current results and those obtained in the pilot project study.

Figure 4-12. Proportions of intact OH, diffuse hydration (DH), and no visible bands (NVB) in crazed and vesiculated artifacts from SU1.

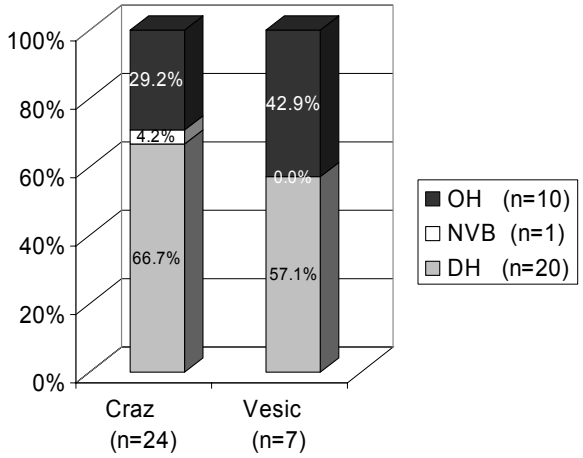

Discussion of OH Analysis Results

The OH analyses presented here (Section 4.1 – 4.3) show that obsidian artifacts at Capulin Quarry experienced substantial alteration of OH bands from the Dome Fire. The frequency of intact OH is lower and the incidence of absent OH is higher in artifacts in spatial association with areas of moderate and severe burning, and also where there are concentrations of artifacts with macroscopic evidence of heat exposure such as crazing and vesiculation. Further, these relative frequencies co-occur with variable proportions of diffuse hydration, indicating that DH may serve as a valid indicator of heat exposure. These characteristics are demonstrated in the artifacts analyzed from SU1 where artifacts with and without fire effects all have a high frequency of non-intact or diffuse hydration. Overall, portions of the Capulin Quarry assemblage from areas of moderate and severe burning have been shown to be subject to alteration of a substantial proportion of their artifacts, indicating that fire exposure exemplified by the Dome Fire can have a broad impact on the OH information contained in surface artifacts.

One surprising result of the SU1 analysis, counter to expectation and to the results observed in the Section 4.2 analysis, is that alteration of hydration bands does not appear to always co-occur neatly with the presence or absence of crazing and vesiculation on a given artifact. This means that, at the scale of specimen, the presence of vesiculation and crazing are not diagnostic for lost OH, and the absence is not diagnostic for no-effect to

OH. Macroscopic examination of each artifact cannot be relied upon to identify those artifacts with OH alteration or to rule out OH alteration. Macroscopic fire effects traits do, however, identify assemblages where lost or altered OH is present.

Another important outcome of the OH analyses is the discovery of variable hydration in individual specimens where multiple OH cuts were employed (Section 4.2). Partially vesiculated flakes were found to have various expressions of absent or diffuse hydration, as well as intact measurable hydration. Most surprising is the observation (made by T. Origer) of hydration bands on heat-caused vesicles. At the least, this intensive analysis of individual specimens demonstrates that different OH may be observed if different portions of the same burned artifact are examined. More puzzling are the questions raised about how both hydration loss and reuptake proceeds in heated obsidian. What these analyses cannot answer is whether there is any chronometric utility of the OH that is intact on artifacts with fire effects. The analysis of multiple OH cuts on specimen 1691-02 demonstrates that intact OH on this piece does not seem to correspond with outcomes on a "normal" artifact. Based on the results found in this study, I would cast doubt on the use of OH measurements on any artifact with vesiculation, and would be uncomfortable with such measurements on artifacts with crazing.

CHAPTER 5
GLASS-WATER INTERACTIONS

This chapter serves as a bridge between the first and second half of the dissertation. The descriptive chapters in Part I demonstrate the variability of heat alteration in obsidian observed as a result of the Dome Fire. In Part II, I pursue several analyses to determine the potential role that obsidian composition may play in that variability. This chapter provides the background for my focus on glass composition and argues for the archaeological relevance of measuring water content as part of a comprehensive analysis of obsidian composition for obsidian hydration dating, as well as for fire effects research. As I investigate in Chapter 8, the water content of the obsidian deposits burned during the Dome Fire is one alternate explanation for why the extreme fire effects, most notably vesiculation, occurred here. In Chapter 6, I measure elemental composition to understand the variation in obsidian composition present in these same geological deposits. These integrated analyses of compositional variation will inform future research into the full range of causes for differential fire alteration of obsidian artifacts, including the prospect of water hydration/diffusion models sufficient to explain the unexpected complexity of alteration and loss of hydration bands as observed in Chapter 4. Most broadly, the compositional analyses in Part II of this dissertation contribute to the continuing development of the obsidian hydration dating method by demonstrating variation in a compositional variable, obsidian water content, that in current OHD methodology is treated essentially as a constant.

The broad context of the discussion in this chapter is the nature of the interaction of glass and environment. As a naturally formed volcanic glass, obsidian is subject to a wide variety of transformational processes of direct or indirect interest to archaeologists. These processes range from the cooling that occurs immediately after eruption, to solar bombardment when resting on an exposed surface, to etching caused by contact with acidic soils when buried, to fracture of a nodule caused by a percussion blow wielded in prehistory by a human testing for material quality, to colluvial transport down a slope when dislodged by an ungulate. The diversity of these processes demonstrates that archaeological analyses of the toolstone obsidian are inherently interdisciplinary. The

prominence of geological and materials science background and analyses in Part II of this dissertation is merely an amplification of that norm.

In this study I focus on two processes that transform obsidian: the hydration of rhyolitic glass at time-scales measured in centuries and millennia, and the episodic heating of the same obsidian when exposed to elevated temperatures reached during forest fires. The two processes vary in temporal scale: additive hydration is gradual and continuous, while transformations that occur during fire exposure are episodic, brief, and subject to varying periodicity and amplitude depending on the changing fire ecology of the forest setting. The two processes also may differ in how uniformly they operate across spatial scales. The process of obsidian hydration occurs at rates that are relatively uniform across a landscape, but that may be influenced by the ambient temperature, relative humidity, and chemical conditions at a given local setting. However, as demonstrated in Chapter 4 and in previous fire effects research discussed in Chapters 2 and 4, fire exposure occurs at a spatial scale at or below the landscape inside the boundaries of a forest fire, with variations well below the scale of landform.

I focus on what these two disparate processes have in common: the internal material characteristics of the obsidian subject to gradual hydration or rapid exposure to heat. In the glass-environment equation, intrinsic or internal variables are those that are part of the material and not the environment (Ericson 1988). Understanding the material that is subject to the two processes is a reasonable prerequisite to explaining fire alteration and hydration because both involve environmental variables that will act upon the material. While this is an obvious approach to take in understanding fire effects, it is somewhat counter-intuitive in considering hydration because much of the focus in the obsidian hydration literature of the last two decades has been on environmental variables that affect hydration rates such as ambient temperature, relative humidity, and soil chemistry.

I chose to examine the full range of chemical composition[1] for four reasons. The first, as noted above, concerns the self-evident primacy of internal variability in obsidian:

[1] The most obvious type of materials analysis of obsidian is examination of chemical composition, but there were other possibilities for investigation that I could not pursue in this study. Prominent among these are the texture of the glass, which encompasses inclusions (i.e., the presence and orientation of microlites, spherulites, micro-crystalline inclusions, and xenolith particles), as well as the presence and density of

understanding the causes of variation in fire effects must begin with extensive prior knowledge of the material affected before it is possible to understand the complex processes of fire exposure. This composition-focused approach has not been pursued in previous research on fire effects to obsidian (see review in Chapter 2). Second, variation in water content is an excellent candidate as a cause of variability in vesiculation as an outcome of fire exposure. It was this possibility that caused me to initiate this examination of glass composition. Third, throughout the development of obsidian hydration dating, obsidian composition has been recognized as a central variable. Regardless of differences in how considered, composition must play some role in any formulation of hydration rates and the calculation of artifact age. Finally, as I will discuss, recent developments in the methodology of obsidian hydration dating have brought to the forefront the role of composition, specifically water content, in the modeling of obsidian hydration and the practice of OHD.

While this project began as an inquiry into whether obsidian water content plays a role in the effects of fire on obsidian artifacts, I soon recognized that investigating this question intersected with an emerging factor in obsidian hydration chronometry research: the role of obsidian water content for obsidian hydration rates (e.g., Stevenson et al. 1993, 1996, 1998), and the modeling of obsidian hydration as concentration-dependent diffusion (e.g., Anovitz et al. 1999, 2004; Riciputi et al. 2002). Conducting intrasource and intersource analyses of the full range of obsidian elemental composition in conjunction with an analysis of water content is both more inclusive and more in-depth than previously could be justified for either goal alone. By combining the two goals I was able to pursue baseline composition information otherwise unavailable and address important questions in both fire effects and obsidian hydration research.

In the next three chapters I will investigate the composition of obsidian contained in the deposits exposed to the Dome forest fire. My goal is to establish whether there is compositional variation within the Cerro Toledo Dome (aka Obsidian Ridge/Rabbit Mountain) obsidians where the Dome fire burned, and to use the two other obsidians for comparison to evaluate variation within and between the geological deposits. I begin my

---

bubbles, and overall porosity and micro-fracturing. Additional factors worthy of future investigation are the relative size of nodules, and clues to cooling history in the configuration of external surfaces.

examination of obsidian composition by measuring trace elements, a type of analysis that has become standard in archaeological sourcing studies. I then veer from current practice to measure also the broad spectrum of minor and major elements. Finally I step out of convention to examine whether there is variation in the main volatile constituent, water, in these artifact-quality obsidians.

In this chapter, I review how obsidian composition has been treated in the development of OHD and then turn to recent proposals to substantially alter that methodology. These broad changes involve a compositional role for obsidian water content in OHD modeling and practice. I discuss how this volatile constituent may vary in obsidian, and close the chapter with the presentation of the current research as a case study in measuring water content as part of an inclusive analysis of obsidian composition.

5.1. Obsidian Composition

Obsidian is a silicic glass of volcanic origin. As a *glass* it is without crystalline structure and the term *obsidian* usually is reserved for glasses high in silica (e.g., >70%, Macdonald et al. 1992). In addition to silica, the major elements are Al, Na, K, Ca, Mg, Fe, all in combination with O as oxides. In a review of worldwide sub-alkalic obsidians (i.e., higher in silica, lower in alkalis), which include most of the obsidians of interest to archaeologists, Macdonald et al. observed the following compositional ranges:

Table 5-1. Obsidian elemental composition as weight % oxide (Macdonald et al. 1992).

Oxide	Weight %
SiO	70 - 77.5%
Al_2O_3	11.4 – 16.3%
Fe_2O_3	0.1 – 3.3%
FeO	0.1 – 2.6%
Mg	<0.0005 - >1.0%
Ca	0.2 – 4.6%
Na_2O	2.7 – 5.9%
K	0.6 – 6.6%

Titanium, lead, manganese, and barium all may occur as minor elements (i.e., 0.1 – 1%), and numerous other elements occur as trace elements (i.e., <0.1%). Obsidian also contains volatiles retained after degassing of the magma during eruption and cooling. The main volatile in obsidian is water, with smaller amounts of carbon dioxide. Because

the discussion of water in obsidian is complex and requires further context, it will be taken up in a later section.

Composition in the Development of Obsidian Hydration Dating

The obsidian hydration dating (OHD) method measures the depth of diffusion of water into fresh glass surfaces as a means for estimating the interval since the creation of that surface. In introducing the new technique to the archaeological community, Friedman and Smith (1960) demonstrated an unusual exchange of information between the disciplines of geology and archaeology. Not only were they bringing to archaeology their geochemical observations about a toolstone of importance in prehistory, they also had employed artifacts, and archaeological knowledge about the age of assemblages, to address geochemical questions about the nature of water in obsidian and whether hydration occurred at recent timescales and under normal atmospheric conditions (Friedman and Smith 1960). The observations that eventually were applied to hydration dating of obsidian artifacts were made as part of research to distinguish between pre- and post-eruptive origin of water found in rhyolitic glasses, to determine that perlite was a glass that had become hydrated after eruption, and to distinguish meteoric water in obsidian from water in the magma prior to eruption (Friedman and Smith 1955, 1958; Friedman et al. 1963, 1966; Ross and Smith 1955). Clearly, questions about water in the composition of obsidian—as hydrated water versus juvenile water (i.e., of magmatic origin)—have been an integral part of OHD from the beginning.

In the original presentation of the method, Friedman and Smith (1960) identified a variety of potential factors governing the rate at which hydration occurs: time, temperature, chemical composition, and relative humidity, with burning and erosion of the glass surface included as factors that could alter observable hydration layers. Using Freter's (1993:286) categorization of primary vs. secondary hydration variables, composition is a primary variable. Primary variables directly affect the rate of the additive hydration process and include, along with chemical composition, effective hydration temperature, relative humidity, and soil acidity/pH, and (adding to Freter's list) chemical dissolution of surfaces (e.g., Ambrose 1976, 1998). These factors must be considered in estimating the rate of hydration. Secondary hydration variables include exposure to burning or heat, spalling due to mechanical strain, and artifact reutilization.

While the last of these is an issue of sample selection and archaeological interpretation, the former two are factors that like chemical dissolution can effectively subtract from the depth of the hydration layer.

The methodological objective of OHD for archaeological dating is to estimate relative or absolute age of artifacts from optical measurements of a hydration layer that has developed from the interplay of the sum of these additive and subtractive factors. The various approaches to OH dating undertaken in the four decades since its introduction can be sorted into three broad categories: relative, empirical, and experimental (Freter 1993). Relative dating involves only comparison of measured hydration layers, while empirical and experimental approaches tackle in various ways the problem of formulating the rate of hydration to estimate the actual age represented by those measured layers.

All three approaches, relative, empirical, and experimental, must consider obsidian composition in some way. Hull's (2001) recent review evaluating the performance of differing approaches to OH dating in North America demonstrates how this is accomplished in each approach. Relative OH dating of artifacts (e.g. Beck and Jones 1994; Fredrickson 1984) addresses compositional variation by attempting to control for different sources: different hydration thicknesses are compared only among artifacts which are grouped by source (determined by visual means or by geochemical analyses of composition). Empirical approaches (e.g. Hall and Jackson 1989) derive hydration rates by cross-dating OH measurements to the context of assemblages, features, or sites that have been dated by other methods. Chemical composition is addressed by explicitly designating these hydration rates as "source-specific" (Kimberlin 1976; Michels and Tsong 1980:427), thus holding chemical composition constant at the scale of geological source or flow as established by geochemical characterization of trace element composition (Hughes 1982, 1988). Hull (2001) makes a powerful case for the practical performance of archaeologically-based source-specific modeling of hydration rate where effective hydration temperature is included in the equation.

Experimental approaches use laboratory results to create, evaluate, or demonstrate OH rates by inducing hydration in accelerated time at elevated temperatures. Chemical composition can be addressed in two ways. One holds constant the geological source of

the obsidian(s) on which induced hydration experiments are performed resulting in source-specific experimental hydration rates. The second includes specific details about the chemical composition of the obsidian(s) in a model used in developing hydration rates. To convert from accelerated lab time to archaeological time, experimentation utilizes mathematical equations that account for the interaction of temperature, activation energy, and time to extrapolate rates of hydration applicable to archaeological conditions. However, because of the logical association of experimentation with modeling, it is not immediately apparent from the literature that experimentation does not necessarily involve modeling the role of composition in the hydration process. In fact, most experimental studies that employ induced hydration address composition in the same manner as relative and empirical approaches: by holding constant the source of artifacts under study to create source-specific induced hydration rates.

In other words, regardless of the type of approach and regardless of the importance asserted for composition in nearly every presentation of obsidian hydration dating, in-depth study of the functional role of chemical composition in the obsidian hydration model is not a part of the preponderance of obsidian hydration research in the four decades since its introduction. Over two decades ago, Michels and Tsong (1980; see also Ericson 1988; Friedman and Trembour 1983) observed this inattention to chemical composition in understanding hydration and hydration rates, and they championed (and later pursued) a reassertion of compositional analysis. Still, the body of OH research that includes analysis of minor and major elements in the formulation of hydration rates is small and mostly limited to nascent efforts that have not been developed further (e.g. Ericson 1981, 1988; Ericson and Berger 1976; Ericson et al, 1976; Friedman and Long 1976; Findlow et al. 1975; Kimberlin 1976).

In seeking guidance to select those major and minor elements that might play a role in obsidian hydration *and* in heat alteration I was unable to find a clear statement available in the current archaeological literature that describes the relationship between the elemental composition of rhyolitic glass and variation in rates of hydration. Instead three early articles (Ericson and Berger 1976; Ericson et al. 1976; Friedman and Long 1976) and two that are somewhat more recent (Michels and Tsong 1980; White 1988) have been most useful for this purpose.

Friedman and Long proposed a "chemical index" that quantified the role of relative weight percents of SiO_2, CaO, MgO, and H_2O^+. They posited that greater calcium and magnesium decrease the hydration rate, while greater silica increases the rate (Friedman and Long 1976:347). The equation implies also that H_2O^+ decreases the rate, although this is not stated.[2] Michels and Tsong (1980:429) note that components including CaO, MgO, Al_2O_3 and TiO, have the potential for passivation, or inhibition of chemical process, which I interpret as decreasing the hydration rate. Ericson and Berger (1976) offer three other formulations that quantify: 1) the relationship of alumina and alkali concentrations (a chemical structural factor zeta describing ratios of Al_2O_3 with alkalis, CaO, Na_2O, and K_2O), 2) the ratio of silicon to oxygen or the initial water content of the glass, and 3) the specific volume of the glass.

The function of the variables identified by these researchers follows from the structure of glass. In silicate melts Si-O and Al-O bonds are linked together to form polymerized networks (Winter 2001:46). In obsidian, Na, K, Ca, Mg, and Fe (ferrous) all can act as network modifiers (White 1988) as can H_2O, while Al can act either as a network modifier or network former (Ericson et al. 1976). As such, all are reasonable candidates as elements to consider for both the hydration and the vesiculation of obsidian. White (1988) provides a concise and simple summary of glass structure (see also Stevenson et al. [1998:183] for a slightly more accessible rephrasing of White's description):

> The basic building block of silicate glasses is the silica tetrahedron. In pure silica glass each tetrahedron shares all corners with adjacent tetrahedra to form a three-dimensional framework. All oxygens on the corners of the tetrahedra are shared between adjacent silicons and are called "bridging oxygens". Large ions of low valence are known as network modifiers. In obsidians and most other natural glasses these are the oxides of sodium, potassium, calcium, magnesium, and ferrous iron. Addition of the network modifiers has the effect of depolymerizing the network. The Si-O-Si bonds are broken and there are created a certain number of "non-bridging oxygens" with a formal negative charge. These

[2] The equation for the chemical index proposed by Friedman and Long (1976) is:

$$SiO_2 - 45(CaO + MgO) - 20(H_2O^+)$$

> coordinate the network modifier ion in such a way that local charge balance is maintained. [White 1988:227]

While the mechanisms of water diffusion into this structure are far from fully understood, the general principle applies that network modifiers may alter the rate at which water, as H_2O and/or OH, can diffuse into the glass. Likewise, these components: Na, K, Ca, Mg, ferrous iron, and water all could affect how hydrated glass is dehydrated when heated during a fire or how the rapid release of water occurs during vesiculation. For this reason I include analysis of these major and minor elements in my examination of compositional variation in Jemez obsidians.

5.2. Challenges to OHD Methodology

At the recent turn of the century two bold challenges were issued to practitioners of the obsidian hydration dating method (Anovitz et al. 1999; Stevenson et al. 2000). Here I briefly introduce both articles, and then later discuss in further detail the research each article represents.

The first challenge was a debut presentation of the archaeological analysis of hydration depth profiling using SIMS, or secondary ion mass spectrometry (Anovitz et al. 1999). The authors argued that problems with the performance of OHD in archaeological applications, particularly those in Mesoamerica, are "due, in part, to use of inappropriate analytical techniques and an improper model of the hydration process" (Anovitz et al. 1999:735). In particular they disputed both the optical measurement of the hydration layer and how the diffusion process is treated in standard OHD models. In essence, by rejecting the basic measurement technique and the underlying models of standard OHD, Anovitz et al. (1999) were contesting not only the reliability but also both the empirical and abstract validity (*sensu* Ramenofsky and Steffen 1998:8-10) of the method and its units. While the occasionally-disparaging tone is unfortunate (as is the use of the phrase "failure of obsidian hydration dating" in the title), the article exhibits extraordinary interdisciplinary scholarship, and demonstrates the persuasive power of a fully reasoned argument.

The second challenge to OHD practitioners came from Stevenson et al. (2000) who identify four longstanding assumptions of standard OHD that they believe are

unwarranted. Restated in summary form, the four assumptions they believe to be erroneous are: 1) the direct association of geological source and hydration rate (i.e., source-specific hydration rates), 2) use of trace element uniformity as indication of uniformity in the minor and major elements that influence hydration; 3) inattention to the role of relative humidity, and 4) the validity of archaeologically-derived source-specific hydration rates. In contrast to the Anovitz et al. (1999) unheralded inauguration of the SIMS approach, the Stevenson et al. (2000) article can be seen as a culmination of a decade constructing the argument for the primacy of water content as the causal compositional variable in rates of obsidian hydration (e.g., Mazer et al. 1991; Stevenson et al. 1993, 1996, 1998). The bottom line in this approach is that water content is the compositional parameter that controls hydration rate. While Anovitz et al. (1999) confronted *how* hydration is measured and *how* hydration rates should be modeled, Stevenson et al. (2000) questioned *what* compositional variables should be measured, arguing that measurement of water content should replace analysis of elemental composition.

These two challenges to OHD are crucial for the current study at two very different levels. The first is the magnitude of the implications of each for the scientific methodology of obsidian hydration dating. Second, each approach provides support for the value of obsidian water content analysis in the on-going development of the method of obsidian hydration dating.

Implications for the Methodology of OH Dating

These two new approaches confront central methodological components of obsidian hydrations dating: 1) measurement, 2) modeling, and 3) parameters.

1) The SIMS approach (later termed ODDSIMS for "obsidian diffusion dating by secondary ion mass spectrometry"; Riciputi et al. 2002:1055), alters the method radically by changing the phenomenon measured. OHD measures optically the depth of hydration by observing the distance inward from the glass surface to a visible birefringence front caused by differential strain at the boundary between the hydrated and unhydrated glass. In contrast, SIMS estimates the concentration of water as a function of depth by measuring the volume of (secondary) hydrogen ions sputtered from a surface when

bombarded with (primary) ions. In other words, SIMS estimates the amount of water at increasing depth within the surface (the depth/hydration profile), while standard OHD estmates the depth to which water adsorption has swelled the glass.

2) The ODDSIMS approach postulates that only a concentration-dependent model of diffusion is appropriate for OH dating. The authors incorporate from research in glass physics and chemistry a sophisticated understanding of current models for the diffusion of water into a silicate glass or melt. Knowledge of water diffusion in glass research has grown enormously since the introduction of OHD in 1960, and the Anovitz et al. (1999) article brings the archaeological community fully up-to-date.

3) The intrinsic water method advanced by Stevenson et al. (2000) changes the key compositional parameters of OHD, advancing water content to the forefront and downgrading all other chemical compositional variables to inconsequential status. They argue that the amount of water in obsidian is the most important intrinsic variable determining the rate of hydration, and if water content can vary independent of elemental composition then there is no need to measure any other compositional variable and no need to use composition to identify the geochemical source of obsidian artifacts to formulate OH dates or age.

I see these shifts in measurement, modeling, and parameters as substantial perturbations in the "normal science" (Kuhn 1970) practice of the obsidian hydration dating method. It is reasonable at a time of methodological flux to 1) examine anew variables previously considered well known, and 2) expend new effort measuring variables not previously worth measuring. This is the methodological basis for including in my research design 1) analysis of elemental composition that encompasses trace, minor, and major elements, and 2) the measurement of obsidian water content.

5.3. Value of Measuring Water Content

The water content of obsidian is fundamental to both obsidian dating approaches issuing the challenge. While the role of water content is explicit in the intrinsic water content approach advocated by Stevenson and colleagues (Stevenson et al. 1993, 1996,

1998, 2000, 2004), it is only implicit in SIMS approach[3]. In the two earliest discussions of ODDSIMS obsidian dating (Anovitz et al. 1999; Riciputi 2002), the centrality of water concentration prior to formation of the hydration layer is not explicitly discussed or modeled. However, the most recent paper in this series of articles by the same four researchers (Anovitz et al. 2004) explicitly identifies investigation of the relevance of water in a given glass as one of eight types of data needed to complete application of the diffusion model. Finally, an alternate model for concentration-dependent diffusion model by a different set of researchers (termed ODDSIMS-SS, Liritzis and Diakostamatiou 2002) explicitly recognizes a role for structural water concentration by modifying the ODDSIMS model to include a variable that expresses water content as an initial condition in the model.

One issue made clear by that the work of these SIMS researchers is that it will not be possible to simply reach across disciplinary boundaries into igneous petrology, glass chemistry and physics, or industrial glass studies to immediately find models directly suitable for the archaeological objective of modeling temporal rates of water diffusion at environmental temperatures over centuries and millennia. The question of whether glass geochemists recognize a role for water content in diffusion modeling is settled quite definitively by Zhang at al. (1991:441): "It has been known for several decades that the chemical diffusion coefficient of "water" in silica glass and other compositionally simple silicate glasses increases strongly with the water content of the glass". However, Zhang et al. (1991:441-442) go on to indicate a lack of consensus about the "cause of this strong concentration dependence of water diffusion in amorphous silicates", and summarize three available models as:

1. related to the interdiffusion of cations and water molecules or hydronium ions;

[3] I should clarify that SIMS instrumentation can be used to measure depth of water diffusion (i.e., Stevenson 2001; Stevenson et al. 2004) without necessitating complex theoretical modeling of water diffusion or acceptance of the concentration-dependent diffusion models developed in Anovitz et al. (1999, 2004), Liritzis and Diakostamatiou (2002), or Liritzis et al. (2004). However, where I use "the SIMS approach" here, I am indicating this interest in modeling. Also, it has been a useful devise to use the Anovitz et al. (1999) and Stevenson et al. (2000) articles to represent two distinct approaches to obsidian dating. They are not, however entirely, independent, as seen in the co-authorship of two recent articles (Liritzis et al. 2004; Stevenson et al. 2004).

2. due to the depolymerization of the silicate network upon dissolution of water as hydroxyl groups;
3. related to the fact that water dissolves in melts and glasses as two major species, H2O molecules...and hydroxyl groups...with different diffusion coefficients.

Most studies of water diffusion in natural and synthetic silicate glasses are undertaken to understand water diffusion in melts. As discussed at length by Anovitz et al. (2004:317-320), modeling of the processes of water diffusion in silicates is significantly different at temperatures above the glass transition temperature (~400°C) than at lower environmental temperatures. They further point out that the glass transition temperature can be substantially lowered with increasing water content and that this consideration should be included in experimentation of induced hydration at elevated temperatures. In sum, theoretical modeling of water diffusion indicates a role for base water content, but how it functions within the various SIMS diffusion models has not yet been fully addressed.

Instead, compelling empirical support for the relevance of water in obsidian dating comes from studies by Stevenson and colleagues (Mazer et al. 1991; Stevenson et al. 1993, 1996; 1998). Most intriguing is the demonstration of high and variable water contents in obsidian samples collected from several quarry sites from the Coso volcanic field (Stevenson et al. 1993). Analysis of total water content on 155 samples, measured by infrared-spectroscopy (FTIR) and reported as the sum of OH and H_2O, obtained ranges of 0.31% to 2.34% (as averages of multiple samples from each quarry location). The results were important 1) because they demonstrated in an archaeological study a wide range and higher total water values than usually recognized in the OHD literature, and 2) because this heterogeneity in water content was found *within* flows that could be distinguished from each other by trace element analyses (Stevenson et al. 1993). The implication is that if water content is included in the formulation of hydration rates, or in the determination of the age of individual artifacts, these results would derive a range of rates or ages within a geochemical source rather than a single rate or age. Finally, research on OHD in New Zealand (Stevenson et al. 1996) added a key argument for the relevancy of water content in hydration dating: that it directly and systematically affects

the rate of hydration. To whit, the expectation is that under the same conditions of temperature and humidity, obsidians with higher water content should hydrate at faster rates than obsidians with low water content; likewise, over the same interval water rich obsidians will form deeper/wider hydration layers than water poor obsidians under the same conditions (Stevenson et al. 1996:235-236). The subsequent application of these expectations in induced hydration and/or archaeological dating studies (e.g., Rosen et al. in press; Stevenson et al. 1998, 2000, 2004) have been carried out with variable success.

To summarize, water content has been demonstrated to vary both within and between obsidian deposits characterized by elemental analysis as similar and dissimilar. For obsidian hydration dating the value of measuring if and how variation in water content occurs in artifact-quality obsidian is that there is both theoretical and empirical support for it being a relevant variable for the rate at which hydration occurs. That this potential influence may be systematic depending on high versus low water content, and that it may affect induced hydration rates and/or improve archaeological fit of calculated OH dates, adds to the relevance of understanding patterns in obsidian water content.

How Does Water Vary In Obsidian?

In the brief review summary of obsidian composition near the beginning of this chapter, discussion of obsidian water content was deferred until this section to provide a better context for discussion. With the exception of Stevenson and colleagues the preponderance of the obsidian hydration literature has not treated obsidian water content as a relevant constituent. Early on the role of water in hydration rates was noted by Friedman and Long (1976) and discussed by Ericson and colleagues (e.g., Ericson et al. 1976; Ericson and Berger 1976). The more recent OHD literature has treated obsidian water content much as if it does not vary. The customary treatment of water content, as exemplified by a check of several OHD review articles, is only a mention in the description of obsidian composition. Where a water content is quantified (e.g. Beck and Jones 2000; Glascock et al. 1998:18; Goffer 1980:82; Goeksu 1991:303; Michels and Tsong 1980:405; Pollard and Heron 1996:85) the range given is most often at or similar to the 0.1 to 0.3% range provided by Friedman and Smith (1960) in their introduction of

obsidian hydration dating[4]. In other words, the obsidian hydration literature has created and maintained the perception among archaeologists that water content in obsidian is low and does not vary.

How is the water content of obsidian described in disciplines outside archaeology? A cursory review of the most comprehensive discussion of composition in geologically common obsidians (Macdonald et al. 1992) leaves the initial impression that 1% is the maximum water content in obsidian. However, this actually is a compositional definition intentionally imposed on variation observed in rhyolitic glasses. In geologic research, the dominant interest in obsidian is as a non-crystalline relatively unaltered representative of rhyolitic melts and conditions in magma chambers. Thus, geological treatment of obsidian usually maintains a strict boundary between obsidian and hydrated glasses such as perlite, resulting in an upper limit of water content that is set low, perhaps arbitrarily too low, in order to avoid hydrated glasses. This is the case in the broad review conducted by Macdonald et al. (1992), where nearly all examples are at or below 1%, and water contents at or below 0.5% are most common. However, if you read the fine print, literally, Macdonald et al. (1992:2) indicate that nearly all examples of obsidians with water contents above 1% were intentionally *excluded* from the study in order to avoid secondarily hydrated glasses. They acknowledge (Macdonald et al. 1992:72-73) examples of water contents above 1%, and in some cases up to 3%, citing Dunbar and Kyle (1986), Eichelberger and Westrich (1983), Newman et al. (1985), O'Neil and Taylor (1985), and Taylor et al. (1983). To these I can add the following recent geological studies[5] with obsidian water contents up to 2.5% as measured by FTIR or K-F titration: Taupo, New Zealand (Dunbar and Kyle 1992), Red Hill, New Mexico (R. J. Stevenson et al. 1997), Newberry Crater, Oregon (Rust 2003), and Mono Craters, California (Newman et al. 1986, 1988; Rust et al. 2004; Zhang et al. 1991, 1997). This body of recent geological work supports the summary generalization Macdonald et al. (1992:69-73) made for obsidians with high water contents: they are not common, and

[4] This discussion is not intended to imply that Friedman and Smith's conclusion of 0.1-0.3% water content in obsidian is out of date. Friedman stands by this interpretation in much more recent discussions (e.g., Friedman 1989) arguing that obsidians with water contents greater than 0.3% are very rare and occur only in a few volcanic circumstances.

[5] Some of these studies are the subsequent, more complete, publications associated with the citations in Macdonald et al. 1992.

they are found in the "intrusive margins of domes, in dikes, or in clasts from pyroclastic deposits."

What are sources of variation in obsidian water content? The "juvenile" volatile content of a solid glass, like obsidian, is a remnant of the gas and fluid content of the melt prior to exsolution that occurs during explosive or extrusive eruption and subsequent cooling. The amount of water retained in the glass depends on a complex interaction among a number of variables and conditions including: 1) the amount of water originally in the melt, 2) the temperature at which the melt degasses, 3) where and how fragmentation of the magma occurs, 4) the pressure context and rate of cooling. Overall, high and variable water contents are more likely to result from explosive than extrusive volcanic activity. Thus, obsidians with higher water contents are most likely to be found as pyroclasts in tephra deposits that are the product of explosive volcanic activity, and are less likely to be found in association with the domes or viscous lava flows resulting from extrusive volcanic activity (e.g., as illustrated by Hughes and Smith 1993:82, Figure 2). Likewise, they are more likely to be found in block-and-ash deposits from pyroclastic surges and pyroclastic flows, as well as volcanic debris flows, avalanches, and lahars. Thus, these deposits often may be more broadly distributed across the landscape due to high fragmentation and dispersion associated with explosive eruptions. High and variable water content obsidians would be found less often as large boulders and more often in deposits characterized by obsidian on the smaller end of the range suitable for use in artifacts, such as in nodules sizes that fall within the pyroclast size ranges considered lapilli (>2 mm to 6 cm) and blocks or bombs (>6 cm).

If water content has been demonstrated to be high and variable in obsidian, why is it that archaeologists have not measured water content as part of OHD? First and foremost, the strong argument for how water content may be relevant for OHD has been made only recently. The perception that obsidian water content is low has been continually reinforced in both the archaeological and geological literature. And prior to the work of the SIMS researchers where the case is made only implicitly, the supporting argument for a role of water content in obsidian hydration has been slow to emerge. Second, water content in obsidian is difficult to measure. The accuracy of available methods has not been readily apparent to archaeologists, and many techniques are

expensive and destructive. Without a strong research motivation, measuring water content simply has not been worth the effort.

Obsidian Water Content and Vesiculation

I have not found in the geological literature any discussions of how obsidian clasts respond to events of high heat such as when exposed for forest fires. However, there is indirect support of a role for water content in vesiculation. Vesiculation of glass occurs as the nucleation and growth of bubbles in a glass that has softened from a brittle solid state. It is reasonable to treat vesiculation in obsidian clasts or fragments (including artifacts) as rapid release of volatiles akin to the degassing of magma. R. J. Stevenson et al. (1997:560) describes vesiculation as the diffusion of water into a vesicle coupled with the viscous flow of the melt. It is well-known in igneous petrology that the addition of water to silicate melts (i.e., in a magma chamber) lowers the temperature at which melt occurs (e.g., Winter 2001:120-121), so it is a simple extrapolation to suggest that higher water content in a silicate glass also lowers the temperature of transition from a solid to a melt. Chemical composition also could play a role in the vulnerability of glass to heat and to softening depending on the contribution of network modifiers (Na, K, Ca, Mg, and ferrous iron) with or without interaction with water present in the glass.

Geological experimental heating studies, conducted for other goals, provide evidence that the tendency of obsidian to vesiculate under high heat conditions is greater in glasses with higher water contents. Dunbar and Kyle (1992:136) observed that hydrated perlite samples began to degas slowly at very low temperatures (~200°C), while natural obsidian fragments did not degas until a much higher temperature (800°C), and then rapidly as a release of magmatic water by vesiculation rather than a slow diffusion of hydrated water as in the perlite (Dunbar and Kyle 1992:138). Zhang et al. (1997:3091) observed that natural obsidian glass samples with water contents above 2.7% vesiculated easily and interfered with their heating experiments. Similarly Zhang and Behrens (2000: 246) observed in heating experiments using a sealed vessel under pressure that high pressure was needed to prevent bubble growth. It is unclear, however, if these observations apply more to hydrated obsidians than to unhydrated obsidians.

Direct information on vesiculation in obsidian comes from a study on vesiculation processes in a high water content obsidian from Red Hill, New Mexico (R. J. Stevenson et al. 1997). A sample of obsidian with water content of 1.4% to 1.8% (the former as measured by FTIR, the latter as measured by LOI) subjected to experimental heating showed rapid water loss beginning at 616°C, indicating this was the temperature at which vesiculation was initiated for this glass.

The clearest evidence of the relationship between the duration of heating, temperature, and vesiculation in glasses of differing water contents is in unpublished data on heating experiments provided to me by H. R. Westrich. Appendix C presents data and graphs that demonstrate that in artificially hydrated silicate glasses, with water contents ranging from 0.65% to 4.50%, the duration of heat exposure leading to vesiculation is much shorter (i.e., more rapid) in glasses with higher water contents. The temperature at which the samples vesiculated is lower in glasses with higher water contents (Table 5-2):

Table 5-2. Relationship of water content and vesiculation in artificially hydrated silicate glasses (data from H. R. Westrich, see Appendix C).

Water content	Temperature of vesiculation
3.7% to 5.1%	450 – 600°C
2.7% to 3.0%	500 - 600°C
1.9% – 2.0%	650 – 750°C
~1.1%	650 – 900°C
0.65%	750 - 900°C

Glasses with the highest water content (3.7% to 5.1%) vesiculated at the lowest temperature range, 450 – 600°C, compared to 500 - 600°C for glasses with 2.7 – 3% water, 650 – 750°C for glasses with 1.9% – 2% water, and 650 – 900°C for glasses with 1.1% water, and for glasses with 0.65%. These data demonstrate that variability in the water content of obsidians should cause variable response in obsidians exposed to high temperatures in forest fires. Obsidians with higher water contents are more vulnerable to heat exposure, and can be expected to vesiculate during more brief exposures and at lower temperatures of exposure.

5.4. Cerro Toledo Rhyolite as a Case Study in Obsidian Water Content

The current research context provides an excellent opportunity for pursuing a better understanding of variation in obsidian water content. Cerro Toledo Dome (CTD) obsidians have a high potential for water contents that are high and variable. They occur in pyroclastic tephra associated with hot avalanche deposits from the Rabbit Mountain dome. Nodules are relatively small bombs, blocks, and lapilli, that are high in visual variation and that often have cortex attributes that indicate fragmentation occurred prior to cooling. Unfortunately, published information (Table 5-3) contributes little to the assessment of CTD obsidian water content because the data is very limited and difficult to use given the range of methods used to measure water and the different units for reporting water. Some water contents measured for CTD are high compared to other New Mexico obsidians, but the comparison is not very useful except as neutral evidence that previous measures do not indicate that CTD glasses are *not* unusually low in water content. I believe that the CTD obsidians offer a good case study to evaluate whether the results obtained for Coso obsidians (Stevenson et al. 1993) occur in this pyroclastic setting.

The occurrence of vesiculation in the CTD obsidian deposits burned during the Dome forest fire warrants the analysis of water content as well as a breadth of elemental compositional analyses that would be difficult to justify for standard geochemical sourcing questions. In contrast to Stevenson and colleagues who advocate abandoning the analysis of chemical composition when the focus turns to water content, I pursue a comprehensive analysis of composition. My goal is to evaluate *variation* across all three kinds of composition—trace elements, major and minor elements, and the volatile constituent water. I use trace element composition to establish whether or not the CTD obsidians represent a valid chemical group as defined for obsidian source characterization. Low variation in trace elements is evidence that all obsidian clasts originate from the same magma chamber. These data can be compared to the major and minor elements, as oxides SiO, Al_2O_3, CaO, MgO, Na_2O, K_2O, that compose the bulk of the glass and that may have the potential to affect hydration rates and vulnerability to heat alteration. Substantial variation in these elements is not expected, but this measurement monitors any potential for "functional" variation within the deposits and provides data for future

investigation of water – oxide interactions. Finally, I use two different techniques to measure obsidian water content; these provide data on the water content in the CTD obsidians and also an assessment of which techniques are appropriate and practical for archaeological application.

As my focus is on the potential variation in water content, comparison of multiple kinds of compositional data allows me to cross-evaluate the degree of variability in water content. Because of the importance of complex eruptive and cooling processes in the volatile constituents retained in obsidian, water content may have a higher potential to vary than does elemental composition. Trace elemental composition is controlled almost entirely by the composition of the magma chamber, while major and minor elements are controlled mostly by magmatic composition and minor processes of crystallization and devitrification during volcanic activity and during cooling. Volatile composition is determined by all of these factors as well by the degassing and fragmentation that occurs during the eruption processes. In explosive pyroclastic eruptions, rapid loss of pressure, degassing, and fragmentation all have the potential to introduce variation into the final glass product. Non-explosive extrusions of rhyolitic magma have less potential for variation in volatiles, especially where degassing occurs at higher temperatures.

The elemental and water composition of CTD glasses are compared to similar pyroclastic obsidians from the same geological unit but located in the Sierra de Toledo area in the northeast quadrant of the Valles caldera. I expect that these glasses will have similar trace element concentrations as the CTD obsidians, with the same possibility of variation in major and minor elements. I do not predict the water contents of these glasses as the volcanic history of these domes is less well known. I do, however, assume that these pyroclastic obsidians also have the generic potential to be high and variable. For contrast, I compare the CTD obsidians to samples from the Valles Rhyolite geological unit at Cerro del Medio in the center of the Valles caldera. Cerro del Medio is a complex dome with obsidian formed from extrusive volcanic activity. I expect that these obsidians are less likely to be high or variable in water content, and are more likely to have water contents in the range below 0.5% that is more common for obsidian.

These analyses will provide data on intrasource and intersource compositional variation usually unavailable for the same samples. These data could be used for

determination of hydration rate(s), but that application does not limit the design of the study. Comparison of obsidian water content among deposits of differing volcanic origins will inform on whether the context of explosive vs. extrusive volcanic activity is a relevant distinction for understanding how high or variable water contents may influence the performance of obsidian hydration dating of artifacts from obsidian deposits beyond the study area.

Table 5-3. Obsidian water content values reported in the literature for New Mexico obsidians. Entries should be compared only within studies (to keep constant the method of water content analysis and type of water measured).

Study	Method	El Rechuelos	Canovas Canyon	Cerro Toledo		Valles Rhyolite	Cerro No Agua	Bear Springs	Arroyo Hondo	Red Hill
Macdonald et al. 1992	data in appendix; measured by vacuum extraction	0.14% 0.14% 0.23%	0.18% 0.23%	0.32% 0.61%		0.14% 0.30% 0.30%	0.15% 0.91% ①			
				Obsidian Ridge			**Cerro No Agua**	**Bear Springs**	**Arroyo Hondo**	
Ross, C. S. and R. L. Smith 1955	weigh-heat-reweigh, or direct measure of H_2O as part of D/H determinations			0.35%			0.30%	0.35%	0.32% upper 0.33% lower	
		Polvadera Pk		**Obsidian Ridge**			**Cerro No Agua**			**Red Hill**
C. Stevenson & McCurry 1990	--probably LOI no info on method; id that measures made at NM Bur of Mines & Mineral Res, Socorro (except No Agua)	0.24%		0.44%			N: 0.03% S: 0.03% E: 0.04% W: 0.03% Whitson 1982			1.32%
		Polvadera Pk	**Apache Tear (loc?)**	**Rabbit Mtn**	**Obs Ridge**	**Cerro del Medio**				
C. Stevenson 1994 (in Wolfman 1994)	FTIR at 4500 peak only: OH^- (but unclear because but graphs say H_2O^+)	0.11%	0.10% 0.20%	0.24% 0.32% 0.55%	0.11% 0.24%	0.08% 0.14% 0.18%				
		Polvadera Pk		**Obsidian Ridge**						**Red Hill**
C. Stevenson et al. 1998 Table 81, p.186	FTIR citing NSE 1986 OH- only reported	0.24% OH-		0.24% OH-						0.89% OH-
										Red Hill
R. Stevenson et al. 1997	3 methods (1 sample) FTIR: Penfield tube: TGA:									1.5% $OH+H_2O$ 1.9% H_2O 1.8% H_2O

① Macdonald et al. 1992 note that adsorption in prepared samples is likely to have introduced error in the 0.91 measure.

CHAPTER 6
ELEMENTAL COMPOSITION ANALYSES

The analyses in this chapter address whether the Cerro Toledo Rhyolite obsidians a compositionally homogeneous group. This question of chemical uniformity is considered first in terms of trace element composition, then in terms of minor and major element composition. Further, the question is addressed at two scales: intrasource and intersource. The examination of obsidian composition in the deposits directly affected by the Dome Fire is central to this study of obsidian fire effects because glass composition is the most stable causal variable that can be pursued in understanding variability in the response of obsidian subject to forest fires. Unlike the dynamic processes of heating and cooling of fire as an agency in transforming the contents of the archaeological record, obsidian composition 1) can be directly measured in the present using techniques that are quantifiable and reliable, 2) remains relatively constant or is subject only to slow and gradual change over time, and 3) varies across the landscape at large scales that are controlled by relatively well known geological processes.

The goals of this chapter are to create a comprehensive data set to evaluate the relative evenness of obsidian composition across the landscape variably affected by the Dome Fire, to resolve methodological requirements for adequate sampling and analysis techniques used to understand the composition of relevant obsidian-bearing geological deposits, and to address the implications of intrasource versus intersource obsidian compositional variation in the study area for the broader archaeological research contexts of obsidian sourcing studies and obsidian hydration chronometry.

The chapter begins with the construction and evaluation of a geological baseline of obsidian trace element composition within the source area affected by the Dome Fire. This initial trace element analysis employs a familiar methodology of geological sampling and energy-dispersive x-ray fluorescence (ED-XRF) measurement to establish a baseline of trace element compositional across the Cerro Toledo Rhyolite (CTR) deposits in the Dome area (CTD). This is followed by a second stage of compositional analysis that integrates intrasource and intersource compositional analyses, and incorporates measurement of major and minor elements. This second stage also employs wavelength-

dispersive x-ray fluorescence (WD-XRF) measurement, and further analysis of iron content in the samples. Intersource comparisons are made for obsidians collected in the Cerro Toledo Northeast area (CTN) of the CTR geological unit but outside the Dome area, and at Cerro del Medio (CDM) which is in a non-CTR geological unit. Together these elemental analyses provide a foundation of chemical composition data for the next chapters, which examine the water content of the rhyolitic glasses and test the performance of multiple techniques for the measurement of that volatile component.

The structure of the analyses in this chapter is as follows (Table 6-1). The first section (6.1) describes intrasource ED-XRF analysis of obsidian trace element composition of samples from within the Dome area (CTD), including sample selection, analysis methods, and results. The second section (6.2) considers CTD intrasource composition using WD-XRF measures of trace, minor and major elements. Finally, the third section (6.3) presents an intersource composition analysis using both ED-XRF and WD-XRF on obsidians from three geological areas: 1) the Dome area (CTD) and 2) Northeast area (CTN) of Cerro Toledo Rhyolite, and 3) the Cerro del Medio area (CDM) of Valles Rhyolite. This third section includes description of sample selection and methods used for WD-XRF, LOI, and iron analyses, and compares results of the ED-XRF and WD-XRF major, minor, and trace element analyses among glass samples from the three geological areas.

Table 6-1. Elemental compositional analyses and samples used.

Chapter Section	Scale of analysis*	Analysis / data	Elements	Deposits	Samples used
6.1	Intrasource	ED-XRF	Trace and selected minor elements	within CTD glasses	CTD pilot=31 CTD 2004=23/30 n=53/61
6.2	Intrasource	WD-XRF	Major and minor elements	within CTD glasses	2004 data: CTD=35 n=35
6.3	Intrasource	WD-XRF & ED-XRF	Trace, minor, major elements	across CTRs (CTD and CTN) and among all (CTD, CTN, CDM)	2004 data: CTD=36 CTN= 8 CDM=12 n=56

*where "source" is equivalent to geological unit

6.1. Trace Element Geological Baseline ED-XRF Analysis for Cerro Toledo—Dome (CTD) Obsidian

In this section I employ energy-dispersive x-ray fluorescence analysis (ED-XRF) to characterize obsidian trace element composition **within** the Cerro Toledo Rhyolite (CTR) deposits in the Dome area. The analysis was conducted to provide a baseline profile of the trace element composition of obsidians collected from numerous locations throughout the Dome area Cerro Toledo Rhyolite deposits (i.e., Cerro Toledo--Dome [CTD] deposits of the CTR geological unit). Without knowing what variation might occur within the source, it is difficult to evaluate whether compositional variation may play a role in response of the obsidian to heat. The baseline analysis is a necessary first step to assessing potential variability in obsidian composition with the CTD glasses. By comparing ED-XRF measures of trace element (and selected minor element) composition in glass samples collected across the Dome area CTR deposits, the relative homogeneity of the deposit can be assessed. Further, if trace element composition is homogenous across the samples, then trace element composition can serve as a measure of intrasource and intersource variation against which other compositional variables, such as major and minor element composition and water content, can be compared.

Dome Area Geological Context: "Obsidian Ridge" and the Cerro Toledo Rhyolite

Quarries burned during the Dome fire are surface exposures of obsidian-bearing deposits of Cerro Toledo Rhyolite within the St. Peter's Dome area. These quarries are all considered to be "Obsidian Ridge" obsidian, which is named after one quarry location (Figure 6-1). As discussed in Chapter 2, the "Obsidian Ridge" source in the Jemez Mountains is familiar to Southwestern archaeologists--both anecdotally and through geochemical characterization. Trace element analyses to define a geochemical profile for this source are best known in the archaeological literature by the works of Newman and Nielsen (1985), Baugh and Nelson (1987), and, most recently, Glascock et al. (1999), as well as additional analyses (Macdonald et al. 1992; Stevenson and Klimkiewicz 1990; Stevenson and McCurry 1990). However, the combined total of geological samples included in these published analyses is about forty, and the manner in which sampling locations are identified does not allow an assessment of where samples were collected

and whether they are drawn from numerous locations across the geological deposit or were concentrated in only one or in a few locations. This lack of spatial precision renders the published data difficult to use for questions other than the one posed by the original authors: the establishment of a trace element profile or "fingerprint" associated with the best known archaeological quarry and geological source locations (primarily at Obsidian Ridge).

The previous investigations are not adequate to answer my questions about compositional homogeneity in Cerro Toledo Rhyolite glasses. To understand how glass composition might play a role in how fire effects vary among obsidian artifacts burned at multiple quarries in the Dome area, I require a more complete and extensive geological examination to address *variation across* rather than simply *similarity within* the deposits. To obtain the compositional information needed for this study requires that I expand the distribution of sampling locations, increase the number of samples analyzed, and measure a wider array of compositional variables.

Another problem in the published literature is the use of variable nomenclature: it often is not clear whether the previous investigations are all discussing the same deposits. While widely understood as a chemical group (*sensu* Hughes 1998a), this "source" is known alternately as Obsidian Ridge, Rabbit Mountain, or as the obsidian contained within the Cerro Toledo Rhyolite. In this study, I refer to all the obsidian bearing deposits in the Dome area as Cerro Toledo Dome (CTD) [1], because they occur within the larger geological unit known as Cerro Toledo Rhyolite (CTR). Part of this departure from using the more traditional "Obsidian Ridge" name is that once the Dome area is explored extensively on the ground, it becomes clear that the Obsidian Ridge location actually is a relatively minor source outcrop. Thus, while the familiar term "Rabbit Mountain/Obsidian Ridge" is suitable to identify some of the physiographic locations where the obsidian occurs, the term "Cerro Toledo Dome" is more appropriate for the source area because it identifies the geography and specifies the geological unit of Dome obsidians but is not restricted to certain physiographic locations.

[1] My use here of "Cerro Toledo Dome (CTD)" corresponds with my use of "Rabbit Mountain/Obsidian Ridge" in Steffen (2002).

My use of the "Cerro Toledo Dome" (CTD) identifies Cerro Toledo Rhyolite deposits from within the Dome area only. The ideal name for the obsidian source would be simply "Cerro Toledo" after the geological unit in which it is contained (see LeTourneau et al. 1997 for discussion). However, as discussed in Chapter 2 and later in this chapter (Section 6.3), other obsidian-bearing deposits of Cerro Toledo Rhyolite occur outside of the Dome area in the Sierra de Toledos in the northeast part of the Valles Caldera (Figure 6-1). Use of the term "Cerro Toledo" could inadvertently suggest an association with the geographical location of Cerro Toledo—the peak in the Sierra de Toledos—which is a part of the Cerro Toledo Rhyolite that has received little

Figure 6-1. Smith, Bailey, and Ross (1970) map of Dome area geological units. Locations discussed in the text added to the map (see also larger version in Figure 2-3).

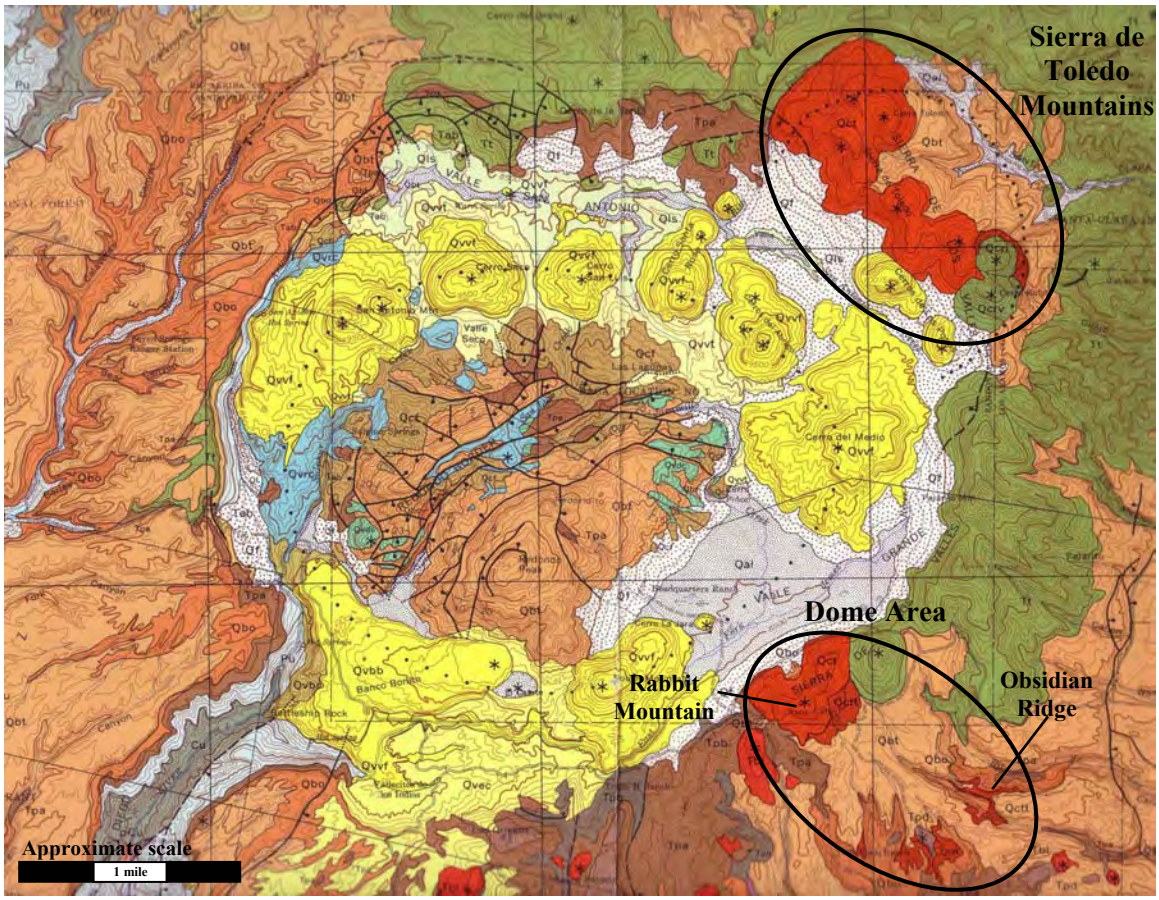

Figure 6-2. CTD sample locations included in this study, shown on the Goff et al. (1990) map of Dome area geological units (not to original scale). Sampling locations RM1, RM3 and RM4 are on Rabbit Mountain to the north of this map (see Figure 6-3, below, for all locations).

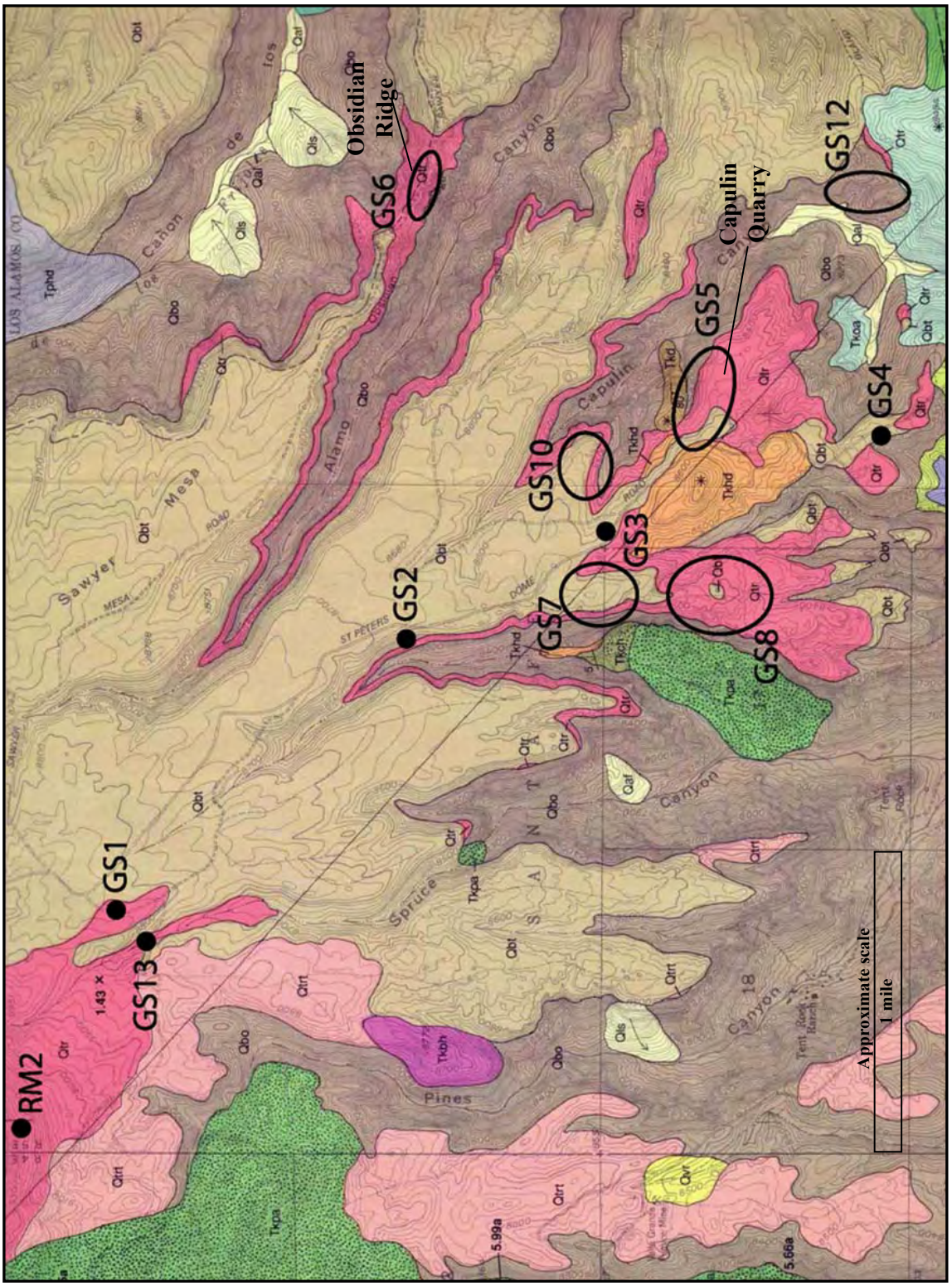

archaeological attention. I call this area "Cerro Toledo Northeast", CTN).[2] Understanding compositional relationships among the obsidians found in the Cerro Toledo Dome and Northeast areas is a central part of this inquiry into potential variation within the Cerro Toledo Rhyolite geological unit.

As discussed in Chapter 2, the Cerro Toledo Rhyolite is mapped as Qct (dark orange) and Qctt (dark orange with stipples) in the 125,000 scale map (Figure 6-1) by Smith, Bailey, and Ross (1970); this map provides the broad context of the CTR deposits. The more recent finer-scale geological mapping of the Dome area by Goff, Gardner, and Valentine (1990) at 1:24,000 (Figure 6-2) is more useful for archaeological understanding of the topographic distribution and geological relationships expressed in the outcrops associated with archaeological quarries. For these reasons I use Goff et al.'s rather than Smith et al.'s abbreviation throughout the text for obsidian-bearing geological deposits (Qtr) for the in the Dome area.

The Rabbit Mountain dome complex is located to the northwest of the Goff et al. (1990) mapping area and only a small segment of that dome is included on their map (see Figure 6-2, upper left corner). Larger obsidian clasts are found in Qtr (dark pink), while Qtrt (light pink) obsidian pieces tend to be much smaller and of little value as a toolstone. This is confirmed by field checking. I have visited nearly all the locations[3] mapped by Goff et al. (1990) as Qtr; artifact quality obsidian is abundant at all Qtr locations visited while little or no artifact quality obsidian occurs at the Qtrt locations I have visited. As discussed in Chapter 2, the Goff et al., map illustrates that Qtr deposits are exposed in many more locations than Obsidian Ridge, and that many of these locations are larger and have much broader surface expression than at that one well-known topographic location (see Figure 2-6 in Chapter 2).

Trace Element Compositional Analysis

ED-XRF analysis of trace elements was selected as the first analysis of obsidian geochemical composition because it is the standard tool used by archaeologists to define obsidian "sources" i.e., chemical groups, *sensu* Hughes 1998a). Establishing trace

[2] Compositional analyses of those obsidians from the CTR deposits in the Cerro Toledo Northeast (CTN) area are presented in Section 6.3.

[3] The only location outside of Rabbit Mountain I have not visited is the small area on a point above Tent Rock Ranch, just east of Spruce Canyon, on the east edge of Qtr.

element homogeneity within obsidians in a geological unit or at known locations for procuring tool-grade obsidian is an important component in geochemical sourcing studies of trade and exchange and a critical initial step for developing obsidian hydration dating for any specified kind of obsidian. Thus, while the ED-XRF analysis of trace elements presented here is relevant for the questions pursued in this research design, it also provides the data needed to align the current study with what is known about the Jemez Mountains obsidians. ED-XRF analysis of trace elements employs the analytical currency used throughout the literature; by defining the obsidian deposits in this study in these same units provides a comparative reference to the literature as well as a bridge for the data presented in each of the other compositional analyses considered in this study (i.e., WD-XRF analyses of minor and major elements, LOI and FTIR analyses of water content).

Much of the information and discussion included in this section were presented previously by the author (Steffen 2002) for a pilot project that served as the basis for this dissertation. The following treatment of geological sampling and ED-XRF analysis has been substantially expanded (with the number of samples doubled) to construct a comprehensive ED-XRF composition baseline for the Cerro Toledo—Dome obsidians. Additional field sampling was conducted, an entirely new set of 31 CTD samples were selected incorporating different attributes of nodule characteristics and, as discussed below, enhancements were made to the ED-XRF analysis design.

Geological Sampling for Elemental Composition Analyses within CTD

Geological sampling was undertaken with two purposes: 1) to investigate the relative homogeneity of, or potential variability in, obsidian composition from the Cerro Toledo Rhyolite deposits commonly known as the "Obsidian Ridge" source, and 2) to provide an accurate geological baseline for comparison among compositional variables and between burned and unburned samples. Several dozen obsidian samples were collected from 15 obsidian-bearing exposures of the Cerro Toledo Rhyolite geological unit (Table 6-2). Sampling was undertaken on several occasions from 1997 through 2003[4].

[4] Geological sampling trips were made in October 1997, May 1999, August 2000, November 2001, March, September, and November 2002, and June 2003, most often with the assistance of S. Penman.

Eleven of the fifteen sampling locations (Figure 6-3) selected for the current study are in the mapped Qtr deposits, as shown in Figure 6-2. Three locations (RM1, RM3, RM4) are outside the Goff et al. (1990) map area, but these locations on Rabbit Mountain would have been mapped as Qtr if included (F. Goff, personal communication, 2004).

Figure 6-3. Area map of CTD geological sampling locations.

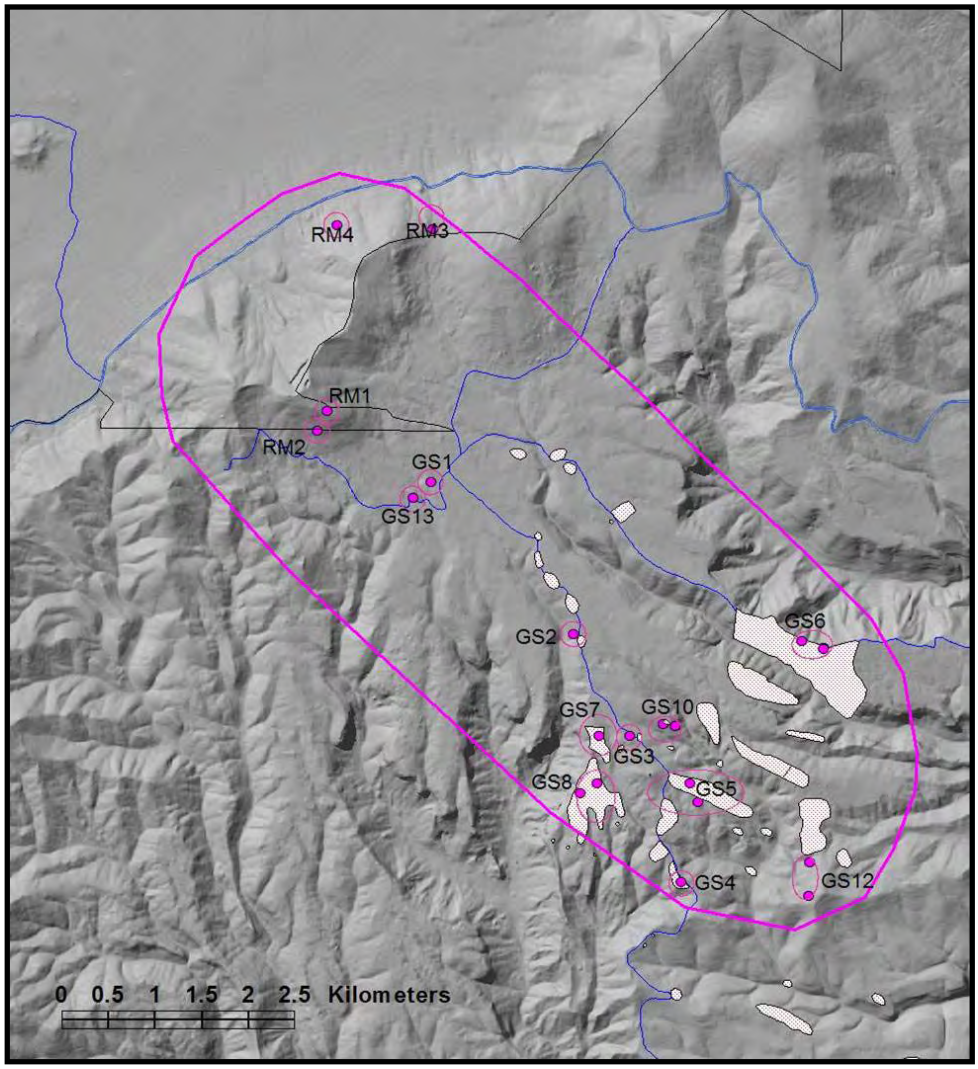

Table 6-2. Intrasource geological sampling locations: Cerro Toledo—Dome (CTD).

Geol Unit	Loc ID	UTM		Quarry site in the vicinity	Location description	In 1998 ED-XRF analysis	In 2004 ED-XRF analysis	In 2004 WD-XRF analysis
		Easting	Northing					
CTR: CTD	GS 1	369258	3965084	None	50m NW of FR 36; on a south facing slope	6	0	0
CTR: CTD	GS 2	370793	3963445	None	300m down a steep mesa slope below W side of FR 289	4	0	0
CTR: CTD	GS 3	371392	3962341	AR 03-10-03-1488 AR 03-10-03-1522 LA 24705	30m W of FR 289; in a cleared "safety zone" (site was extensively disturbed during suppression of the Dome Fire)	5	0	0
CTR: CTD	GS 4	371941	3960741	None	20m W of FR 289; between road and mesa edge	3	0	0
CTR: CTD	GS 5	372050	3961840	AR 03-10-03-1691 LA 23961	Capulin Quarry; large ridge E of FR 289	0	8	8
CTR: CTD	GS 6	373247 373472	3963352 3963284	AR 03-10-03-2360 LA 82485	Obsidian Ridge; in FR 287 atop narrow ridge	3	4	4
CTR: CTD	GS 7	371054	3962361	AR 03-10-03-1664 LA 55092	Along a flat ridgetop, on or near an abandoned road; very abundant obsidian	2	2	4
CTR: CTD	GS 8	371054	3961841	AR 03-10-03-1665 LA 55093	Along a flat ridgetop, on or near an abandoned road, very abundant obsidian	4	4	5
CTR: CTD	GS 10	371888 371763	3962450 3962467	AR 03-10-03-1401 LA 23922	At tip of ridge near head of Capulin Canyon	3	6	7
CTR: CTD	GS12	373327 373315	3960985 3960629	None	In road cut of FR 288D (closed), on NE facing slope; at the southeasternmost extent of Qtr	0	3	3
CTR: CTD	GS13	369083	3964891	None	Road cut on N side of FR 36, on S facing slope	0	0	1
CTR: CTD	RM1	368164	3965820	None	South facing slope on south flank of Rabbit Mountain, near ridge top	0	1	1
CTR: CTD	RM2	368058	3965613	None	South facing slope on south flank of Rabbit Mountain, midslope at VCNP/SFNF boundary	0	1	0
CTR: CTD	RM3	369289	3967776	None	At head of drainage on N side of saddle between Rabbit Mountain and Scooter Mountain	0	1	1
CTR: CTD	RM4	368262	3967819	None	North facing slope of Rabbit Mountain above Valle Grande, 300m north of Highway 4	0	1	1
					Total samples	30	31	35

In selecting geological sampling locations, diverse topographic settings were chosen to include easily accessed mesa surfaces as well more inaccessible locations on side slopes. Table 6-2 provides the description of each location (including UTM coordinates checked using a GPS unit with ±10 m accuracy) used in the geological

baseline study.[5] With two exceptions, the sampling locations are at least 150 m apart. Locations GS6a and GS6b are approximately 250 m apart but were given the same GS number because they are both located within the designated site area of Obsidian Ridge (LA82485). Similarly, GS5 includes an extensive area that corresponds with the entirety of Capulin Quarry (LA23961), and the UTM coordinates included in Table 6-2 are at the center. Elsewhere in the table pairs of UTM coordinates are given where the expanse of the sampling are was broad (i.e., GS6, GS10, GS12).

At each location, the natural nodules selected were clearly in geological context. In order to avoid materials transported to the area from some other source, sampling of the geological expression of obsidian-bearing deposits is improved if artifacts are avoided during geological sampling and when selecting specimens to include in a compositional analysis (but see also Glascock et al. 1998:23). In the Dome area it is difficult to avoid the overlap of geological exposures of obsidian-bearing deposits and archaeological sites. As noted in Table 6-2, many of the geological sampling locations are near documented archaeological quarry sites. Most of the samples analyzed in this ED-XRF baseline study are non-artifacts, but a few artifacts were included. I made the decision to include artifacts in a limited number of cases (six specimens: from GS 1, GS 2, and GS 4) in order to increase the number and spatial distribution of sampling locations. Data from the six artifacts analyzed as geological samples were included in the pilot project baseline ED-XRF sample because the results obtained do not indicate any chemical variation between the natural and artifact samples. No artifact specimens were included in the 2003/2004 composition analyses.

Selection of samples

ED-XRF analysis was conducted on 61 samples, including 30 samples from the pilot project (Steffen 2002) and 31 new samples. Samples selected for ED-XRF analysis are specimens intended to represent the wide range of visual diversity observed in the Cerro Toledo Dome obsidians. Appearance of obsidian samples include clear black, grey-and-black banded, opaque or cloudy light and darker greys and greenish greys

[5] Locations that do not appear on the table (e.g., GS9, GS11) were excluded from this geological baseline geochemical analysis because they are locations sampled specifically for burned obsidian. GS 9 is a prescribed burn location (outside the Dome Fire) where a single vesiculated obsidian artifact was recovered, and GS11 is a location within the Dome Fire where a few vesiculated pieces were found.

(some with small inclusions and some without), clear brown-black, opaque black (some of which have a "tobacco" color along thin edges when held up to the light), an opaque chocolate brown glass (sometimes with swirling of other brown or greenish colors), a grey-black material with a shimmering or sheen texture that looks like threads within the glass when the hand specimen is rotated in the light (this could be called pleochroic [Vierra 1993:161] or chatoyant in appearance, although neither term is technically accurate for glass). Specimens of brown glasses were especially common at the south end of the Qtr deposits (i.e., GS12). Mahogany specimens were observed rarely in the CTD deposits examined, and one sample of mahogany glass was analyzed from a collection location on Rabbit Mountain (i.e., RM3). While mahogany glasses have recently been recognized in Cerro del Medio obsidian deposits (e.g., LeTourneau and Steffen 2002), their presence in Jemez obsidian sources is not well documented.

After examining obsidian nodules from across the entire Cerro Toledo—Dome obsidian bearing deposits, I am convinced that there is little possibility of assigning a reliable visual characterization to CTD glasses because the actual variation is too great. This is in contradiction to customary field practice among many archaeologists working in the Jemez Mountains and throughout northern New Mexico who identify more or less diagnostic visual distinctions among the three best known sources: Cerro Toledo/Obsidian Ridge, Valles Rhyolite/Cerro del Medio, and El Rechuelos/Polvadera Peak. LeTourneau et al. (1997:28-29) provide an excellent concise summary of the "significant color differences among the sources" (see also Newman and Nielsen 1985:379, 381), but also demonstrate in blind tests comparing visual identification to XRF geochemical analyses that their actual success rate for correctly identifying Cerro Toledo/Obsidian Ridge obsidians using these color differences was very poor. They found that while success rates for correctly identifying Valles Rhyolite/Cerro del Medio and El Rechuelos/Polvadera Peak obsidians was quite good (>80 percent in each test), the success in correctly identifying Cerro Toledo/Obsidian Ridge specimens was 0 percent in each test. In another study, LeTourneau (2000:102) had similar outcomes: 33 percent success rate for Cerro Toledo Rhyolite, but 85 percent and 100 percent for Cerro del Medio and El Rechuelos, respectively. A recent study conducted by Schilz et al. (2004:227-8) replicated the visual identification criteria reported in Letourneau et al.

(1997) and found similarly poor results for reliable (and accurate) visual sourcing of Jemez obsidians. In eight specimens for which ED-XRF trace element sourcing was conducted by Hughes (2004a), four specimens (50%) were misidentified, including both of the Cerro Toledo/Obsidian Ridge specimens. Unfortunately, this means that this study succeeded in replicating the earlier 0% success rate in visual identification of Cerro Toledo/Obsidian Ridge obsidian. As the authors observe, "If these results are extrapolated to the entire inventory from the current project, visual identification may not be a reliable means of identification (Schilz et al. 2004:227)".

I believe the central difficulty for visual identification of Cerro Toledo/Obsidian Ridge obsidians demonstrated in these three studies is the broad visual variation inherent in CTD glasses; this variation is not readily apparent if only a few source outcrops are visited. As Schilz et al. (2004:228) observe of the disappointing outcome of their comparison of visual and geochemical sourcing, "This implies that individuals not intimately familiar with the three obsidian sources have less reliability with visual identification (Schilz et al. 2004:228)." I agree. Examination of obsidians across many CTD locations and at less well-known exposures, as conducted for this study, provides a different perspective on the overall visual characteristics of Cerro Toledo/Obsidian Ridge obsidian. Even the most customarily "reliable" visual identification of Jemez obsidian (e.g., Ridings 1991:80), that of the El Rechuelos/Polvadera Peak glasses (which tend to be cloudy and grey with abundant small white inclusions), comes into question when the observer becomes familiar with the array of obsidian visual variation present in the CTD geological deposits and discovers that similar obsidians are not uncommon at CTD locations. In sum, Cerro Toledo Dome obsidians are best characterized as having high variation in visual appearance and are not well suited to visual identification.

Analytical Methods: ED-XRF Elemental Composition Analysis

Trace element analysis for the geological baseline was conducted on 61 specimens by Richard Hughes, Geochemical Research Laboratory, during two episodes. The first analysis of 30 specimens was in 1998 for the SFNF pilot project (Hughes 1998b; see also Appendix D), as reported in Steffen (2002). The second analysis of another 31 samples was conducted in 2004 (Hughes 2004b; see also Appendix D). The two analyses

used similar procedures with slight changes in the 2004 analysis to include measurement of the minor elements K and Ca (and to exclude Zn and Ga). Elemental measures were reported in parts per million (ppm), except K, Ca, and total iron (as $Fe_2O_3^T$) which is reported in element weight percent. The following elements were included in each ED-XRF analysis:

1998: Zn, Ga, Rb, Sr, Y, Zr, Nb, Ba, Ti, Mn, $Fe_2O_3^T$, Fe/Mn ratio

2004: K, Ca, Rb, Sr, Y, Zr, Nb, Ba, Ti, Mn, $Fe_2O_3^T$, Fe/Mn ratio

The ED-XRF analyses were undertaken by Hughes using an energy dispersive x-ray fluorescence spectrometer. Further information on instrument, operating conditions, calibration standards, and detection limits are provided in Appendix D.

In the 2004 analysis, nine sample specimens[6] were removed from the analysis of ED-XRF results because physical conditions including poor reflection geometry, poor surfaces, or presence of inclusions at the surface had the potential to interfere with ED-XRF measurement. These nine were excluded from summaries of results but are included in the table of individual specimen results (Table F-2). Thus, 52 is the total number of samples included in this analysis of results.

Results: Intrasource ED-XRF Trace Element Composition Analysis for CTR-Dome

Summaries of trace element values generated for the 52 samples from 12 geological sampling locations are shown in Tables 6-3 and 6-4. Table 6-3 provides a summary of mean elemental values for all 52 samples across all 12 locations; Table 6-3 shows summary values by sample location. Element values are expressed in quantitative units using parts per million (ppm) for all elements except K, Ca and total iron $Fe_2O_3^T$ which are indicated by elemental weight percent. Data presented in the tables are organized by element and provide the sample minimum, maximum, mean, standard deviation, and coefficient of variation.

[6] The nine excluded specimens are as follows: CTD5-303, CTD5-307, CTD6-301, CTD7-302, CTD10-303, CTD10-306, CTD12-303, CTDRM-302, and CTDRM-304. Because only a single sample was included from locations RM2 and RM4, removal of the samples CTDRM-302 and CTDRM-304 effectively excludes both of the sample locations from the analysis, decreasing the total number of CTD locations from 14 to 12.

Table 6-3. Summary of mean ED-XRF values for each element across all CTD samples (not differentiating among locations).

Element	Unit	N	Minimum	Maximum	Mean	SD	CV (StDev/Mean) x 100
Rb	ppm	52	173	222	199.94	9.813	4.91
Sr	ppm	52	0	6	3.58	1.194	**33.38**
Y	ppm	52	54	67	59.40	2.809	4.73
Zr	ppm	52	153	178	164.60	5.737	3.49
Nb	ppm	52	77	96	86.40	3.626	4.20
Ba	ppm	0	nm	nm	n/a	n/a	n/a
Ti	ppm	52	285	513	420.75	41.317	9.82
Mn	ppm	52	385	767	625.06	56.080	8.97
$Fe_2O_3^T$	elem wt%	52	1.11	1.41	1.22	0.067	5.48
Zn	ppm	30	77	101	88.83	5.651	6.36
Ga	ppm	30	2	27	21.03	4.657	**22.14**
K	elem wt%	22	3.17	3.80	3.61	0.155	4.31
Ca	elem wt%	22	0.11	0.16	0.134	0.011	8.51

Given that all of the current samples were collected from within the Cerro Toledo Rhyolite, the results are as expected: Hughes's ED-XRF analyses of trace element composition determined that all of the CTR-Dome samples can be assigned to Obsidian Ridge (a.k.a. Cerro Toledo Rhyolite [Macdonald et al. 1992, Appendix 1, p. 148]; cf. Baugh and Nelson 1987, Table 1). Trace element values also match well with neutron activation analysis and X-ray fluorescence data for "Obsidian Ridge/Rabbit Mountain" published recently by Glascock et al. (1999). All samples can reliably be assigned (or "sourced") to this chemical group, using Hughes' criteria that all diagnostic mean measurements fall within 2 standard deviations of mean values for source standards (Hughes 1998b:1).

The relevance of these results for the current study is that they strongly indicate relative trace element homogeneity within the Cerro Toledo Rhyolite obsidians across various outcrops of the deposit in the Dome area (CTD) and despite broad visual variation in the samples analyzed.

Table 6-4. ED-XRF trace element summary values for CTD samples by location.

LOCATION		Rb ppm	Sr ppm	Y ppm	Zr ppm	Nb ppm	Ba ppm	Ti ppm	Mn ppm	$Fe_2O_3^T$ elem wt%	Zn ppm	Ga ppm	K elem wt%	Ca elem wt%
GS1	N	6	6	6	6	6	0	6	6	6	6	6	0	0
	Min	200	3	56	159	86	nm	420	597	1.19	81	19	nm	nm
	Max	213	4	63	175	90	nm	453	640	1.26	97	26	nm	nm
	Mean	206	4	60	167	88	n/a	435	614	1.215	91	22	n/a	n/a
	SD	5.68	0.55	2.48	5.42	1.55	n/a	10.76	14.61	0.0274	5.78	2.64	n/a	n/a
	CV	2.77	15.65	4.16	3.24	1.76	n/a	2.47	2.38	2.25	6.36	12.09	n/a	n/a
GS2	N	4	4	4	4	4	0	4	4	4	4	4	0	0
	Min	196	3	56	160	83	nm	421	581	1.17	88	2	nm	nm
	Max	212	4	62	168	89	nm	448	610	1.22	101	23	nm	nm
	Mean	203	4	59	164	86	n/a	436	598	1.203	93	18	n/a	n/a
	SD	7.18	0.58	2.50	3.30	2.50	n/a	11.47	12.12	0.0222	5.91	10.34	n/a	n/a
	CV	3.53	16.50	4.22	2.02	2.90	n/a	2.63	2.03	1.84	6.37	59.11	n/a	n/a
GS3	N	5	5	5	5	5	0	5	5	5	5	5	0	0
	Min	196	0	56	160	83	nm	417	575	1.15	87	17	nm	nm
	Max	207	4	60	170	89	nm	490	623	1.24	98	24	nm	nm
	Mean	202	3	58	164	87	n/a	445	597	1.192	92	21	n/a	n/a
	SD	4.72	1.52	1.48	3.65	2.68	n/a	27.76	19.21	0.0370	4.18	2.59	n/a	n/a
	CV	2.33	58.33	2.55	2.22	3.09	n/a	6.23	3.22	3.11	4.55	12.44	n/a	n/a
GS4	N	3	3	3	3	3	0	3	3	3	3	3	0	0
	Min	190	3	55	157	83	nm	413	571	1.15	81	18	nm	nm
	Max	193	4	58	160	84	nm	431	610	1.21	88	21	nm	nm
	Mean	192	3	56	158	84	n/a	424	590	1.173	85	20	n/a	n/a
	SD	1.53	0.58	1.53	1.73	0.58	n/a	9.87	19.55	0.0321	3.51	1.53	n/a	n/a
	CV	0.80	17.32	2.71	1.10	0.69		2.33	3.32	2.74	4.15	7.77	n/a	n/a
GS5	N	6	6	6	6	6	0	6	6	6	0	0	6	6
	Min	187	3	59	158	81	nm	285	648	1.20	nm	nm	3.17	0.11
	Max	218	6	66	175	96	nm	433	767	1.41	nm	nm	3.73	0.14
	Mean	203	4	61	169	88	n/a	372	699	1.300	n/a	n/a	3.505	0.127
	SD	12.11	1.37	2.53	6.72	5.28	n/a	58.03	42.69	0.0865	n/a	n/a	0.2125	0.0103
	CV	5.96	31.53	4.15	3.98	6.02	n/a	15.59	6.11	6. 65	n/a	n/a	6.06	8.15
GS6	N	6	6	6	6	6	0	6	6	6	3	3	3	3
	Min	188	3	56	159	77	nm	416	596	1.14	86	18	3.66	0.13
	Max	208	5	62	170	93	nm	460	680	1.26	92	27	3.76	0.16
	Mean	197	4	60	164	85	n/a	441	630	1.203	90	24	3.713	0.143
	SD	7.89	0.75	2.07	4.46	5.33	n/a	17.50	36.72	0.0423	3.21	4.93	0.0503	0.0153
	CV	4.00	19.54	3.46	2.72	6.27	n/a	3.97	5.83	3.51	3.59	20.84	1.36	10.66
GS7	N	3	3	3	3	3		3	3	3	2	2	1	1
	Min	190	3	54	158	81	nm	361	571	1.11	78	19	3.44	0.13
	Max	222	4	67	178	93	nm	363	695	1.39	87	23	3.44	0.13
	Mean	201	3.7	58.7	165	86	n/a	362	613.7	1.207	82.5	21	3.44	0.13
	SD	17.93	0.58	7.23	11.27	6.24	n/a	1.00	70.47	0.1589	6.36	2.83	n/a	n/a
	CV	8.90	15.75	12.33	6.83	7.26	n/a	0.28	11.48	13.16	7.71	13.47	n/a	n/a
GS8	N	8	8	8	8	8	0	8	8	8	4	4	4	4
	Min	191	3	55	156	81	nm	381	385	1.12	77	16	3.57	0.13
	Max	217	5	62	171	91	nm	513	682	1.33	87	27	3.66	0.14
	Mean	201	4	60	162	86	n/a	427	599	1.239	84	20	3.615	0.133
	SD	9.09	0.76	2.20	4.75	3.63	n/a	46.86	94.63	0.0666	4.69	4.79	0.0465	0.0050
	CV	4.53	18.90	3.70	2.92	4.22	n/a	10.99	15.80	5.38	5.58	23.64	1.29	3.77

Table 6-4. Continued: ED-XRF trace element summary values for CTD by location.

LOCATION		Rb ppm	Sr ppm	Y ppm	Zr ppm	Nb ppm	Ba ppm	Ti ppm	Mn ppm	$Fe_2O_3^T$ elem wt%	Zn ppm	Ga ppm	K elem wt%	Ca elem wt%
GS10	N	7	7	7	7	7	0	7	7	7	3	3	4	4
	Min	173	0	55	153	82	nm	389	589	1.14	84	24	3.62	0.14
	Max	212	5	65	173	90	nm	489	688	1.28	95	25	3.80	0.15
	Mean	195	3	59	166	87	n/a	436	631	1.216	88	24	3.705	0.143
	SD	12.86	2.16	3.35	7.23	2.73	n/a	38.27	39.53	0.0594	5.86	0.58	0.0806	0.0050
	CV	6.59	72.01	5.65	4.36	3.15	n/a	8.77	6.27	4.89	6.63	2.37	2.18	3.51
GS12	N	2	2	2	2	2	0	2	2	2	0	0	2	2
	Min	180	3	58	160	81	nm	346	652	1.21	nm	nm	3.38	0.12
	Max	208	5	64	167	85	nm	428	705	1.33	nm	nm	3.69	0.15
	Mean	194	4	61	164	83	n/a	387	679	1.270	n/a	n/a	3.535	0.135
	SD	19.80	1.41	4.24	4.95	2.83	n/a	57.98	37.48	0.0849	n/a	n/a	0.2192	0.0212
	CV	10.21	35.36	6.96	3.03	3.41	n/a	14.98	5.52	6.68	n/a	n/a	6.20	15.71
RM1	N	1	1	1	1	1	0	1	1	1	0	0	1	1
	Min	202	3	59	161	90	nm	419	654	1.21	nm	nm	3.77	0.14
	Max	202	3	59	161	90	nm	419	654	1.21	nm	nm	3.77	0.14
	Mean	202	3	59	161	90	n/a	419	654	1.210	n/a	n/a	3.770	0.140
	SD	n/a	n/a	n/a	n/a	n/a	n/a	n/a	n/a	n/a	n/a	n/a	n/a	n/a
	CV	n/a	n/a	n/a	n/a	n/a	n/a	n/a	n/a	n/a	n/a	n/a	n/a	n/a
RM3	N	1	1	1	1	1	0	1	1	1	0	0	1	1
	Min	195	4	59	167	89	nm	398	640	1.23	nm	nm	3.66	0.12
	Max	195	4	59	167	89	nm	398	640	1.23	nm	nm	3.66	0.12
	Mean	195	4	59	167	89	n/a	398	640	1.230	n/a	n/a	3.660	0.120
	SD	n/a	n/a	n/a	n/a	n/a	n/a	n/a	n/a	n/a	n/a	n/a	n/a	n/a
	CV	n/a	n/a	n/a	n/a	n/a	n/a	n/a	n/a	n/a	n/a	n/a	n/a	n/a
Total	N	52	52	52	52	52	0	52	52	52	30	30	22	22
all locs	Min	173	0	54	153	77	nm	285	385	1.11	77	2	3.17	0.11
	Max	222	6	67	178	96	nm	513	767	1.41	101	27	3.80	0.16
	Mean	200	4	60	165	83	n/a	421	625	1.224	89	21	3.609	0.134
	SD	9.81	1.20	2.81	5.73	3.63	n/a	41.32	56.08	0.0670	5.65	4.66	0.1555	0.0114
	CV	4.91	33.38	4.73	3.49	4.20	n/a	9.82	8.97	5.48	6.36	22.14	4.31	8.51

Another way to consider relative homogeneity is by applying some measure of variation. Following Hughes (1984:7), I use the coefficient of variation (CV), which is the standard deviation (SD) expressed as a percentage of the mean (Sokal and Rohlf 1981:59-60, SD/Mean*100)[7], as an indicator of relative variation of means among groups of samples while accounting for sample size and magnitude of measurement units.

[7] I did not apply the correction for small sample size indicated by Sokal and Rohlf (1981:59):

$$\text{Corrected CV} = \left(\frac{\text{SD}}{\text{mean}}*100\right) * \left(1 + \frac{1}{4n}\right)$$

because it did not change CV values substantially, and the unmodified CV equation is such an accessible concept. Using the modification added little to the analysis but added much to making CV seem complicated.

Higher CV values indicate greater variation. I use an arbitrary threshold of CV value 10 to identify CV values considered to have notably high versus low variation.

Overall the data in Tables 6-3 and 6-4 show low CV values expressed in nearly all elements.[8] CV values below 10 are obtained for all elements, Rb, Y, Zr, Nb, Ti, Mn, and $Fe_2O_3^T$, that can be well-measured in these samples and that are useful in discerning among sources when comparing results to values available in the published literature. This is what would be expected: the low CV values in these elements is simply another way of describing the high trace element homogeneity discussed above as low trace element variation. These low CV values accord with the Hughes' certainty in sourcing the samples to Obsidian Ridge (Appendix D). The low CV values can be seen in the data as summed across all locations (Table 6-3), and within each location (Table 6-4). In sum, the examination of CV supports the interpretation that there is no meaningful variation in the trace elements measured by ED-XRF analysis of these CTD samples.

One issue that arises in considering whether compositional variation exists within the CTD source obsidians is whether the ED-XRF technique for measuring composition might be affected by heat alteration of obsidian samples subject to burning in forest fires (e.g., Shackley and Dillian 2002). If heat temperatures can alter trace element geochemistry, then application of ED-XRF analyses (or any analysis of composition) to determine intrasource compositional homogeneity would need to take into consideration this potential for post-depositional transformation as a source of variation. For the pilot project I conducted two analyses to examine this issue (Steffen 2002). Both analyses support the conclusion that no appreciable alteration in trace element composition is detected with ED-XRF analysis. These results, as well as those of a similar study (Shackley and Dillian 2002), support use of XRF analysis in obsidian samples that could have a history of exposure to fire as long as fresh surfaces without gross heat alteration are used (for a counter example concerning Fe/Mn ratios see Jackson 1986).

In summary, this geological baseline analysis reveals no evidence in the trace elements and selected minor elements measured by ED-XRF for intrasource geochemical

[8] As Hughes (1984:7) points out in his discussion of CV for assessing source-specific elemental variation, it is not possible to determine from examination of CV alone whether observed variation in means is due to measurement error or actual compositional variation. In this case, the two high CV values, for Sr and Ga, are due to composition below the detection limits of the instrument (in the case of Sr) or other instrument-element issues (in the case of Ga).

variability in the CTD obsidians that would explain variation in the forest fire effects to obsidian observed within the Dome Fire. In other words, significant trace element variation was not found within this geological "source". This, of course, is not the same thing as saying there is no intrasource variation in glass composition, but rather identifies that if relevant variation exists it is not in the trace and selected minor elements measured, and it is not the kind of variation customarily measured by XRF for trace element sourcing of obsidian. In light of these results, two alternate analyses were undertaken to assess the potential for intrasource variation in other compositional constituents: the first to measure variation in minor and major elements using WD-XRF (Section 6.2), and second to measure obsidian water content (Chapters 7 - 8).

6.2. Intrasource WD-XRF Analyses of Major and Minor Elemental Composition for Cerro Toledo–Dome (CTD) Obsidians

Based on the overall lack of variation found in the trace element analysis reported in Section 6.1, I conducted a second compositional analysis to investigate potential variation in minor and major elements. For this purpose I used wavelength-dispersive x-ray fluorescence (WD-XRF) which is well-suited to measuring the full suite of minor and major elemental constituents of obsidian. The goals of this analysis are to 1) assess variation in elemental composition across a broader suite of elements, 2) further test whether there is compositional variation among different locations within the CTD area, and 3) compare whether major and minor elements exhibit the same degree of uniformity as do trace elements—as measured previously by ED-XRF and here again by WD-XRF. Thus, the goals are the same as for the previous trace element analysis, but now apply to minor and major elements. As in Section 6.1, this section addresses compositional data for samples only within the Cerro Toledo Dome (CTD) source area.

Analytical Methods: WD-XRF Elemental Composition Analysis and Iron Analysis

The WD-XRF analysis was conducted by J. Husler, Chemistry Laboratory, UNM Department of Earth and Planetary Sciences, on powdered obsidian samples using the following analytical methods. Husler's analyses included a "whole rock analysis", plus a

titration analysis to determine proportions of ferrous versus ferric iron. A whole rock analysis is a common approach in petrology, and simply means that the analysis is of the complete composition of the material, rather than an examination that focuses on only a portion (as in, for example, a mineralogical analysis that has the goal of distinguishing among minerals and phases rather than averaging across the differing constituents). This aspect of the analytical results is effectively no different than the ED-XRF analysis.

For analyses of obsidian composition, the important differences between WD-XRF and ED-XRF are: 1) WD-XRF is effective for measuring a suite of major and minor elements, while ED-XRF is best suited to measuring trace elements and only a limited number of minor elements, 2) WD-XRF is a destructive technique because it requires powdering of the samples, while ED-XRF is non-destructive technique that can analyze the unaltered surface of specimens, and 3) the practical accuracy of the two techniques is similar for the archaeological analysis of obsidian but measurements returned by WD-XRF tend to have higher precision (lower variation in values obtained). For customary archaeological sourcing studies, the need for destruction of at least a gram from a specimen is prohibitive for analysis of artifacts; however, for the current analysis of non-artifact geological samples, this was not a concern.

The whole rock analysis has two parts (Table 6-5): WD-XRF measurement of the major, minor, and trace elements listed below, and measurement of the volatile elements H_20 and CO_2 by loss-on-ignition (LOI). The volatile component is measured by LOI in the whole rock analysis in order to obtain a total that approximates 100%. I also added to this whole-rock analysis a determination of ferrous versus ferric iron concentration by titration. For simplicity, the titration analysis should be assumed as included wherever the "WD-XRF analysis" is referred to in this text. For the goals in this chapter, only the results of the WD-XRF and titration analysis of iron will be considered. The LOI results will not be considered until the next chapters LOI in which water content analyses are discussed but the LOI analysis is noted here because it is an intrinsic part of the whole rock analysis.

Table 6-5. Constituents measured in the whole rock and iron analyses.

Whole rock analysis
WD-XRF major and minor elements measured as oxide weight %:
SiO_2, TiO_2, Al_2O_3, $Fe_2O_3^T$, MnO, MgO, CaO, Na_2O, K_2O
WD-XRF trace elements measured as ppm:
Ba, Cr, Rb, Sr, Y, Zr, Nb, Co, Ni, Cu, Zn
Volatile constituents (LOI analysis):
H_2O^-, (H_20^++CO_2)
Iron analysis
Titration analysis of ferrous vs. ferric iron content:
FeO, Fe_2O_3

WD-XRF Analysis: As described by Husler, major and trace elements were determined using a Rigaku RIX-2100 wavelength-dispersive x-ray fluorescence spectrometer. The major elements were determined by fusing 1 g of (-)100 mesh sample with 9 g of lithium tetraborate at 1000º Celsius in a Pt-Au crucible for 15 minutes. The melt was poured into a Pt-Au mold and removed upon cooling. The analyses were made at 50 kV and 50 mA using a flow proportional counter for elements Si, Al, Ca, Mg, Na, K, P, and a scintillation counter for Fe, Mn, and Ti. The trace elements were determined by pressing to 20 tons a mixture of (-)100 mesh sample and boric acid binder in a ratio of 8.5 g sample to 1.5 g H_3BO_3. A scintillation counter was used as detector for all elements. Similarly prepared internationally recognized reference standard rocks (NIST, USGS, CCRMP, and NIM) were used for the calibration curves[9]. All procedures followed Connolly and Husler (1990). Original data was reported as oxide weight percent or ppm (see Table 6 - 5, above). No element-specific detection limits or estimates of error were reported by Husler (i.e., as provided by Hughes, see Section 6.1 and Appendix D).

Iron analysis: Ferrous iron was determined by dissolving a 0.5 g sample in sulfuric and hydrofluoric acids and titrating with standard potassium dicromate using sodium diphenylamine sulfonate as an indicator. Phosphoric acid was added to enhance the end point and boric acid was added to react with the excess hydrofluoric acid. Ferric oxide was determined by multiplying the ferrous iron (as FeO) by 1.1113 and subtracting

[9] The following standards were used in Husler's analyses: NIST (NBS 278 obsidian, NBS 688 basalt); USGS (BCR-1 basalt, G-2 granite, GSP-1 granodiorite, PCC-1 peridotite, DTS-1 dunnite, AGV-1 andesite), CCRMP (SO-1 through SO-4 soils), NIM (NIM-S syenite, and NIM-P peridotite).

this value from the total iron (as Fe_2O_3) found by the WD-XRF. Accuracy was checked by comparing to established NBS (NIST) and USGS certified values. The titration analysis compares Fe^{3+} to Fe^{2+}.

Selection of samples

The WD-XRF data discussed here are for 35 Cerro Toledo Dome samples.[10] In brief, the CTD specimens included in this sample are from locations GS 5 through RM4 (as listed in Table 6-2), except the specimen from RM2 which was inadvertently excluded. Overall the goal was to create a data set similar to that used in the initial ED-XRF analyses, with added locations further to the south (GS12), and to the north on Rabbit Mountain (RM1-RM4). Thus, the CTD samples here are the same 31 samples identified in Section 6.1 as from the 2004 analysis, plus the four samples (GS10, GS7-1, GS7B-1, and GS8-1) included in 1998 heating experiments (Steffen 2002); the specimens used here were not, of course, subjected to any heating. Other than as noted, there is complete overlap with the nodules used in this WD-XRF analysis and the 2004 ED-XRF analysis, and no overlap with the 1998 ED-XRF analysis.

Results: Intrasource WD-XRF Element Composition Analysis for CTR-Dome

Results are presented in three formats. Summaries of means of trace elements for the entire grouped CTD dataset (Table 6-6), and differentiated by location (Table 6-7), are presented first, followed by data for major and minor elements (grouped in Table 6-8 and location-specific in Table 6-9). Results by specimen are presented in Appendix F in Table F-3 (trace elements) and Tables F-4 and F-5 (major and minor elements). Note that conversions from oxide weight percent to elemental weight percent and ppm are provided for Ti, Mn, Ca, and K in Appendix F in Table F-5.[11]

[10] A full discussion of how samples were selected for the entire WD-XRF analysis is included in the following section (Section 6.3).

[11] Note also that three elements--Ti, Mn, and Mg--are included in the WD-XRF major and minor element table although they fall below the 0.1 weight percent threshold qualifying them as trace elements (i.e., where major elements are <1.0%, minor elements are 1.0% to 0.1%, and trace elements are >1.0% of any given total composition). This is demonstrated for Ti and Mn in Table F-5 where element weight percent and ppm values are shown. Ti oxide weight % values are borderline with values at the 0.1% boundary between minor and trace elements. Elemental weight % values show Ti as well below 0.1%. Nonetheless, inclusion of Ti, Mn, and Mg with the WD-XRF major and minor elements is a convention of data reporting for "whole rock analysis" and for that reason is maintained here.

Discussion of WD-XRF trace element results

The grouped WD-XRF trace element results for the 35 CTD samples (Table 6-6) indicate low CV values for six elements (Rb, Sr, Y, Zr, Nb, Zn) and very high variation for the remaining five elements (Ba, Cr, Co, Ni, Cu). It appears however, that measurement error is relevant for all five elements with high CV values. In the case of Ni and Co, the ppm values are all less than 6 ppm, which clearly indicates composition below the detection limits of the instrument. The other three elements--Ba, Cr, and Cu--have higher maximum values observed than for Ni and Co, but with zero values at the minimum of their range. These zero values are, in part, an artifact of my data analysis: where the original WD-XRF data listed ppm results as "<1 ppm", I inserted a zero value in order to conduct ratio scale descriptive statistics. I believe a zero value is appropriate for a ppm count less than 1. Therefore, data for elements Ba, Cr, Cu probably are exhibiting intrinsic variability but suffer from the same detection limits problem as noted for Ni and Co. In sum, there are no high CV values for trace elements in this analysis that are considered to be actual indicators of high variation in trace element composition. The WD-XRF analysis demonstrates low variation—high homogeneity—in trace element composition for 35 samples the representing Cerro Toledo Dome obsidian deposits.

Table 6-6. Grouped mean WD-XRF values for trace elements across all CTD samples (not differentiating among locations).

All CTD samples		ppm				
Element	**N**	**Minimum**	**Maximum**	**Mean**	**Standard Deviation**	**CV** (SD/Mean) x100
Ba	35	0	72	14.6	18.27	**124.92**
Cr	35	0	29	5.1	9.19	**179.76**
Rb	35	199	206	203.9	2.30	1.13
Sr	35	4	5	4.1	0.28	6.95
Y	35	63	66	65.2	0.98	1.51
Zr	35	171	179	176.6	2.56	1.45
Nb	35	138	148	145.1	2.51	1.73
Co	35	0	34	13.3	10.43	**78.18**
Ni	35	1	5	2.4	1.03	**43.49**
Cu	35	0	6	2.1	1.74	**83.35**
Zn	35	126	181	140.7	8.44	6.00

CV=(StDev/Mean) x 100

Low CV values for trace elements Rb, Y, Zr, Nb, and Zn are consistent with the high utility of these elements for discerning among chemical groups in the region. All

five elements fit with the first two components of the three-part equation for good "diagnostic" elements (Hughes 1993:204) for obsidian characterization studies: they appear to be well-measured by WD-XRF and they exhibit low relative variation within the grouped samples. Whether they perform well for the third component, high variability across multiple sources, will be examined in the third section (Section 6.3). Based on the results of ED-XRF analyses reported here in Section 6.1 and previous studies in the area (as discussed in Section 6.1), these trace elements can be expected to vary among different chemical sources sampled in the region.

In considering the low CV values of Rb, Sr, Y, Zr, Nb, and Zn, it is worth noting that they also reflect the high-degree of precision available with WD-XRF (where "precision" describes the clustering of data points). This is apparent in the narrow ranges of ppm values for all six elements. Note, however, that the high precision of WD-XRF does not necessarily equate to increased accuracy--which is governed by factors such as sample preparation, instrument calibration, operating conditions, and use of appropriate standards (see Hughes 1998a:107-109 for discussion of precision and accuracy in terms of reliability).

The second question to address is whether there is variation in trace elements among the sampling locations distributed across the CTD deposits. Examination of Table 6-7 does not indicate any such intrasource trace element variation. CV values and means for individual sampling locations are similar to summary CV and means.

Two elements, Sr and Zn, are somewhat more variable across locations (Table 6-7). For Sr, more variable CV values are not meaningful because of the narrow range of measured values (4-5 ppm). The summary values for Zn, however, are more interesting. Zn measurements have CV values ranging from 0.91 to 11.88 (with an average of 6.00), and means ranging from 137.8 to 153.8 ppm. I suspect, however, that the single high value of 181 ppm at GS6 (CTD6-306, Table F-3) is unduly affecting the dataset, and that this outlier exerts unwarranted influence on the general pattern among the samples. Overall, my conclusion is that there is little actual variation in trace elements across the CTD deposits sampled.

Table 6-7. WD-XRF trace element values for CTD samples by location.

CTD LOCATION		Ba ppm	Cr ppm	Rb ppm	Sr ppm	Y ppm	Zr ppm	Nb ppm	Co ppm	Ni ppm	Cu ppm	Zn ppm
GS05	N	8	8	8	8	8	8	8	8	8	8	8
	Min	0	0	200	4	64	172	141	0	2	0	138
	Max	72	17	206	4	66	179	147	22	3	6	142
	Mean	20.5	4.6	204.1	4.0	65.1	176.9	145.6	11.4	2.6	2.6	140.3
	SD	25.97	7.46	2.30	0.00	0.83	2.75	2.33	8.26	0.52	2.13	1.28
	CV	126.70	161.36	1.12	0.00	1.28	1.55	1.60	72.64	19.72	81.29	0.91
GS06	N	4	4	4	4	4	4	4	4	4	4	4
	Min	0	0	205	4	65	177	145	5	1	1	142
	Max	21	1	206	4	66	178	148	34	2	2	181
	Mean	10.5	0.3	205.3	4.0	65.5	177.8	146.3	17.0	1.8	1.5	153.8
	SD	8.66	0.50	0.50	0.00	0.58	0.50	1.26	13.64	0.50	0.58	18.26
	CV	82.48	200.00	0.24	0.00	0.88	0.28	0.86	80.22	28.57	38.49	11.88
GS07	N	4	4	4	4	4	4	4	4	4	4	4
	Min	0	0	200	4	63	171	141	0	1	1	127
	Max	25	27	205	4	66	178	147	29	5	5	143
	Mean	9.5	11.3	202.0	4.0	64.5	174.3	143.3	12.0	2.8	2.5	137.8
	SD	11.68	13.50	2.45	0.00	1.29	2.99	2.87	12.73	1.71	1.91	7.27
	CV	122.91	120.00	1.21	0.00	2.00	1.71	2.01	106.07	62.10	76.59	5.28
GS08	N	5	5	5	5	5	5	5	5	5	5	5
	Min	0	0	199	4	63	171	138	0	2	0	139
	Max	39	22	205	5	66	179	146	30	4	5	143
	Mean	17.2	9.0	202.8	4.2	64.6	176.0	143.4	14.8	2.6	2.4	140.6
	SD	17.22	11.87	3.03	0.45	1.14	3.39	3.71	12.99	0.89	2.07	1.52
	CV	100.15	131.94	1.50	10.65	1.76	1.93	2.59	87.76	34.40	86.40	1.08
GS10	N	7	7	7	7	7	7	7	7	7	7	7
	Min	0	0	200	4	64	172	142	0	1	0	139
	Max	60	19	206	5	66	179	147	23	3	3	144
	Mean	17.3	2.9	204.4	4.1	65.7	177.1	145.7	9.4	2.3	1.4	140.9
	SD	21.59	7.13	1.99	0.38	0.76	2.34	1.70	8.52	0.95	1.27	1.95
	CV	124.92	249.48	0.97	9.12	1.15	1.32	1.17	90.38	41.61	89.07	1.39
GS12	N	3	3	3	3	3	3	3	3	3	3	3
	Min	0	0	205	4	66	177	145	23	2	0	139
	Max	26	1	206	5	66	179	147	33	3	3	143
	Mean	8.7	0.3	205.3	4.3	66.0	178.0	146.0	28.3	2.3	1.3	141.0
	SD	15.01	0.58	0.58	0.58	0.00	1.00	1.00	5.03	0.58	1.53	2.00
	CV	173.21	173.21	0.28	13.32	0.00	0.56	0.68	17.76	24.74	114.56	1.42
GS13	N	1	1	1	1	1	1	1	1	1	1	1
	Min	0	29	199	4	63	172	140	13	5	6	140
	Max	0	29	199	4	63	172	140	13	5	6	140
	Mean	0.0	29.0	199.0	4.0	63.0	172.0	140.0	13.0	5.0	6.0	140.0
	SD	n/a	n/a	n/a	n/a	n/a	n/a	n/a	n/a	n/a	n/a	n/a
	CV	n/a	n/a	n/a	n/a	n/a	n/a	n/a	n/a	n/a	n/a	n/a
RM1	N	1	1	1	1	1	1	1	1	1	1	1
	Min	0	1	205	4	65	177	146	11	1	1	128
	Max	0	1	205	4	65	177	146	11	1	1	128
	Mean	0.0	1.0	205.0	4.0	65.0	177.0	146.0	11.0	1.0	1.0	128.0
	SD	n/a	n/a	n/a	n/a	n/a	n/a	n/a	n/a	n/a	n/a	n/a
	CV	n/a	n/a	n/a	n/a	n/a	n/a	n/a	n/a	n/a	n/a	n/a
RM3	N	1	1	1	1	1	1	1	1	1	1	1
	Min	2	0	204	4	65	177	146	7	1	1	126
	Max	2	0	204	4	65	177	146	7	1	1	126
	Mean	2.0	0.0	204.0	4.0	65.0	177.0	146.0	7.0	1.0	1.0	126.0
	SD	n/a	n/a	n/a	n/a	n/a	n/a	n/a	n/a	n/a	n/a	n/a
	CV	n/a	n/a	n/a	n/a	n/a	n/a	n/a	n/a	n/a	n/a	n/a

Table 6-7. Continued: WD-XRF trace element values for CTD samples by location

CTD LOCATION		Ba ppm	Cr ppm	Rb ppm	Sr ppm	Y ppm	Zr ppm	Nb ppm	Co ppm	Ni ppm	Cu ppm	Zn ppm
RM4	N	1	1	1	1	1	1	1	1	1	1	1
	Min	33	0	205	4	66	178	147	4	1	2	130
	Max	33	0	205	4	66	178	147	4	1	2	130
	Mean	33.0	0.0	205.0	4.0	66.0	178.0	147.0	4.0	1.0	2.0	130.0
	SD	n/a	n/a	n/a	n/a	n/a	n/a	n/a	n/a	n/a	n/a	n/a
	CV	n/a	n/a	n/a	n/a	n/a	n/a	n/a	n/a	n/a	n/a	n/a
Total	N	35	35	35	35	35	35	35	35	35	35	35
(all locs)	Min	0	0	199	4	63	171	138	0	1	0	126
	Max	72	29	206	5	66	179	148	34	5	6	181
	Mean	14.6	5.1	203.9	4.1	65.2	176.6	145.1	13.3	2.4	2.1	140.7
	SD	18.27	9.19	2.30	0.28	0.98	2.56	2.51	10.43	1.03	1.74	8.44
	CV	124.92	179.76	1.13	6.95	1.51	1.45	1.73	78.18	43.49	83.35	6.00

<u>Discussion of WD-XRF minor and major element results</u>

Turning to examination of major and minor elements measured by WD-XRF (Tables 6-8 and 6-9), with the exception of magnesium and iron all major and minor elements within the CTD samples are low in variation. This low variation is true not only for the sum of CTD samples (as shown in summary values, Table 6-8), but also among sampling locations: as shown in Table 6-9, there are no high CV values for samples at individual locations except for MgO and iron (measured as Fe_2O_3, FeO, and Total Fe).

Table 6-8. Grouped mean WD-XRF values for major and minor elements across all CTD samples (not differentiating among locations).

All CTD samples		Oxide wt%				
CTD	**N**	**Minimum**	**Maximum**	**Mean**	**Standard Deviation**	**CV** (SD/Mean)x100
SiO_2	35	74.83	76.94	76.231	0.54	0.71
TiO_2	35	0.076	0.084	0.0811	0.0014	1.69
Al_2O_3	35	11.72	12.58	12.046	0.17	1.38
Fe_2O_3	35	0.39	1.09	0.533	0.12	**22.31**
FeO	35	0.04	0.82	0.589	0.13	**22.02**
MnO	35	0.073	0.077	0.0751	0.0011	1.44
MgO	*34	0.03	0.09	0.052	0.02	**29.91**
CaO	35	0.41	0.42	0.412	0.004	0.99
Na_2O	35	4.07	4.40	4.297	0.06	1.31
K_2O	35	4.28	4.71	4.354	0.07	1.59
Total Fe (as Fe_2O_3)	35	1.05	1.48	1.180	0.11	**9.39**

*MgO value for CTD5-307 excluded because original WD-XRF analysis reported this value as "<0.01"

Table 6-9. WD-XRF major and minor element values for CTD samples by location.

CTD LOCATION		SiO_2 ox wt%	TiO_2 ox wt%	Al_2O_3 ox wt%	Fe_2O_3 ox wt%	FeO ox wt%	MnO ox wt%	MgO* ox wt%	CaO ox wt%	Na_2O ox wt%	K_2O ox wt%	Total Fe ox wt%
GS05*	N	8	8	8	8	8	8	7	8	8	8	8
	Min	75.09	0.08	11.73	0.44	0.55	0.074	0.030	0.41	4.23	4.31	1.10
	Max	76.94	0.08	12.26	0.76	0.74	0.077	0.070	0.42	4.40	4.37	1.33
	Mean	76.113	0.081	12.000	0.535	0.613	0.075	0.051	0.411	4.320	4.345	1.181
	SD	0.63	0.00	0.17	0.10	0.08	0.00	0.01	0.00	0.05	0.03	0.09
	CV	0.83	1.27	1.42	18.42	13.05	1.50	28.46	0.86	1.15	0.62	7.52
GS06	N	4	4	4	4	4	4	4	4	4	4	4
	Min	75.44	0.08	12.14	0.49	0.55	0.076	0.050	0.41	4.28	4.34	1.13
	Max	76.72	0.08	12.58	0.55	0.58	0.076	0.060	0.41	4.33	4.37	1.16
	Mean	76.198	0.082	12.300	0.513	0.568	0.076	0.057	0.410	4.305	4.355	1.141
	SD	0.58	0.00	0.19	0.03	0.01	0.00	0.00	0.00	0.02	0.02	0.01
	CV	0.76	0.71	1.57	5.13	2.64	0.00	8.48	0.00	0.48	0.40	1.15
GS07	N	4	4	4	4	4	4	4	4	4	4	4
	Min	75.70	0.08	11.91	0.50	0.57	0.074	0.040	0.41	4.27	4.28	1.13
	Max	76.48	0.08	12.13	0.55	0.72	0.076	0.070	0.42	4.32	4.35	1.35
	Mean	76.175	0.080	12.013	0.518	0.610	0.075	0.055	0.415	4.298	4.325	1.195
	SD	0.34	0.00	0.09	0.02	0.07	0.00	0.01	0.01	0.03	0.03	0.11
	CV	0.45	3.58	0.76	4.57	12.05	1.28	23.47	1.39	0.61	0.72	8.79
GS08	N	5	5	5	5	5	5	5	5	5	5	5
	Min	75.51	0.08	11.81	0.48	0.57	0.074	0.030	0.41	4.23	4.30	1.13
	Max	76.70	0.08	12.18	0.61	0.80	0.077	0.070	0.42	4.33	4.34	1.48
	Mean	76.274	0.081	12.020	0.516	0.668	0.075	0.054	0.414	4.296	4.324	1.264
	SD	0.47	0.00	0.14	0.06	0.11	0.00	0.02	0.01	0.04	0.02	0.17
	CV	0.61	1.04	1.15	11.01	16.85	1.46	33.64	1.32	0.97	0.35	**13.57**
GS10	N	7	7	7	7	7	7	7	7	7	7	7
	Min	74.83	0.08	11.72	0.40	0.49	0.073	0.030	0.41	4.18	4.29	1.10
	Max	76.83	0.08	121.8	0.60	0.73	0.077	0.064	0.42	4.35	4.38	1.32
	Mean	76.426	0.081	12.043	0.491	0.590	0.075	0.040	0.411	4.303	4.351	1.144
	SD	0.71	0.00	0.15	0.06	0.08	0.00	0.01	0.00	0.06	0.03	0.08
	CV	0.93	1.80	1.26	13.21	12.98	1.87	35.82	0.92	1.33	0.69	6.95
GS12	N	3	3	3	3	3	3	3	3	3	3	3
	Min	76.07	0.08	12.00	0.46	0.51	0.074	0.030	0.41	4.31	4.32	1.10
	Max	76.43	0.08	12.10	0.57	0.58	0.076	0.090	0.42	4.31	4.35	1.14
	Mean	76.253	0.082	12.067	0.513	0.547	0.075	0.060	0.413	4.310	4.337	1.120
	SD	0.18	0.00	0.06	0.06	0.04	0.00	0.03	0.01	0.00	0.02	0.02
	CV	0.24	0.71	0.48	10.73	6.42	1.53	50.00	1.40	0.00	0.35	1.79
GS13	N	1	1	1	1	1	1	1	1	1	1	1
	Min	76.26	0.08	11.92	0.57	0.82	0.074	0.040	0.41	4.27	4.32	1.48
	Max	76.26	0.08	11.92	0.57	0.82	0.074	0.040	0.41	4.27	4.32	1.48
	Mean	76.260	0.080	11.920	0.570	0.820	0.074	0.040	0.410	4.270	4.320	1.480
	SD	n/a	n/a	n/a	n/a	n/a	n/a	n/a	n/a	n/a	n/a	n/a
	CV	n/a	n/a	n/a	n/a	n/a	n/a	n/a	n/a	n/a	n/a	n/a

*MgO value for specimen CTD5-307 was excluded (original WD-XRF analysis reported this value as "<0.01")

Table 6-9. Continued: WD-XRF major and minor element values for CTD by location

CTD LOCATION		SiO_2 ox wt%	TiO_2 ox wt%	Al_2O_3 ox wt%	Fe_2O_3 ox wt%	FeO ox wt%	MnO ox wt%	MgO* ox wt%	CaO ox wt%	Na_2O ox wt%	K_2O ox wt%	Total Fe ox wt%
RM1	N	1	1	1	1	1	1	1	1	1	1	1
	Min	76.87	0.08	12.09	0.66	0.45	0.076	0.055	0.41	4.24	4.45	1.16
	Max	76.87	0.08	12.09	0.66	0.45	0.076	0.055	0.41	4.24	4.45	1.16
	Mean	76.870	0.083	12.090	0.660	0.450	0.076	0.055	0.410	4.240	4.450	1.160
	SD	n/a	n/a	n/a	n/a	n/a	n/a	n/a	n/a	n/a	n/a	n/a
	CV	n/a	n/a	n/a	n/a	n/a	n/a	n/a	n/a	n/a	n/a	n/a
RM3	N	1	1	1	1	1	1	1	1	1	1	1
	Min	76.20	0.08	11.95	1.09	0.04	0.076	0.061	0.41	4.07	4.71	1.13
	Max	76.20	0.08	11.95	1.09	0.04	0.076	0.061	0.41	4.07	4.71	1.13
	Mean	76.200	0.083	11.950	1.090	0.037	0.076	0.061	0.410	4.070	4.710	1.130
	SD	n/a	n/a	n/a	n/a	n/a	n/a	n/a	n/a	n/a	n/a	n/a
	CV	n/a	n/a	n/a	n/a	n/a	n/a	n/a	n/a	n/a	n/a	n/a
RM4	N	1	1	1	1	1	1	1	1	1	1	1
	Min	75.26	0.08	11.80	0.39	0.59	0.075	0.059	0.41	4.32	4.35	1.05
	Max	75.26	0.08	11.80	0.39	0.59	0.075	0.059	0.41	4.32	4.35	1.05
	Mean	75.260	0.080	11.800	0.390	0.590	0.075	0.059	0.410	4.320	4.350	1.050
	SD	n/a	n/a	n/a	n/a	n/a	n/a	n/a	n/a	n/a	n/a	n/a
	CV	n/a	n/a	n/a	n/a	n/a	n/a	n/a	n/a	n/a	n/a	n/a
Total	N	35	35	35	35	35	35	34	35	35	35	35
(all locs)	Min	74.83	0.08	11.72	0.39	0.04	0.073	0.030	0.41	4.07	4.28	1.05
	Max	76.94	0.08	12.58	1.09	0.82	0.077	0.090	0.42	4.40	4.71	1.48
	Mean	76.231	0.081	12.046	0.533	0.589	0.075	0.052	0.412	4.297	4.354	1.180
	SD	0.54	0.00	0.17	0.12	0.13	0.00	0.02	0.00	0.06	0.07	0.11
	CV	0.71	1.69	1.38	**22.31**	**22.02**	1.44	**29.91**	0.99	1.31	1.59	**9.39**

*MgO value for specimen CTD5-307 was excluded (original WD-XRF analysis reported this value as "<0.01")

Thus, except for Mg and iron, this WD-XRF analysis of major and minor element composition indicates compositional homogeneity across the CTD glasses. In part, these results can be expected given that major element variation in all obsidian is effectively constrained by the high percentage of silica (e.g., Macdonald et al. 1992:21). However it is notable that Ca, Na, and K exhibit very low variation within CTD, and exhibit average CV values below 2 across CTD and within sampling locations.[12]

What is most interesting for this analysis is the variation in magnesium and iron within CTD. For Mg, the summary CV for CTD is 29.91. FeO and Fe_2O_3 both have CV values greater than 22. These observed high CV values do not appear to be due to simple outliers or obvious measurement error. The possibility of error in data transcription was

[12] One odd observation is that the average CV for K across all CTD locations (CV 1.59) is higher than the highest CV at any individual location (CV 0.72 at GS7). I assume this is because the highest K value in the range (K_2O 4.71%) occurs at RM3 where the absence of multiple samples renders the CV not applicable.

ruled out. High CV values for Mg are present at several sampling locations, so the effect on average CV is even across the samples. In sum, Mg appears to be actually variable within the suite of CTD samples.

Many of these observations also hold for iron measured as Fe_2O_3, FeO, and total Fe. One contribution to the variation observed is a single outlier, CTDRM-303, that is unusual for a high value of Fe_2O_3 and low FeO. As shown in Figure 6-4, this specimen plots far outside the cluster for both oxidation states of iron. Note, however that the Total Fe value for this specimen is not unusual (Table F-4). Specimen CTDRM-303 is the only mahogany obsidian in the CTD samples, and the red color characteristic of this obsidian probably is caused by greater oxidation in the iron content (i.e., high Fe_2O_3).

Figure 6-4. XY plot of oxidation states of iron (Fe_2O_3 and FeO) in CTD samples.

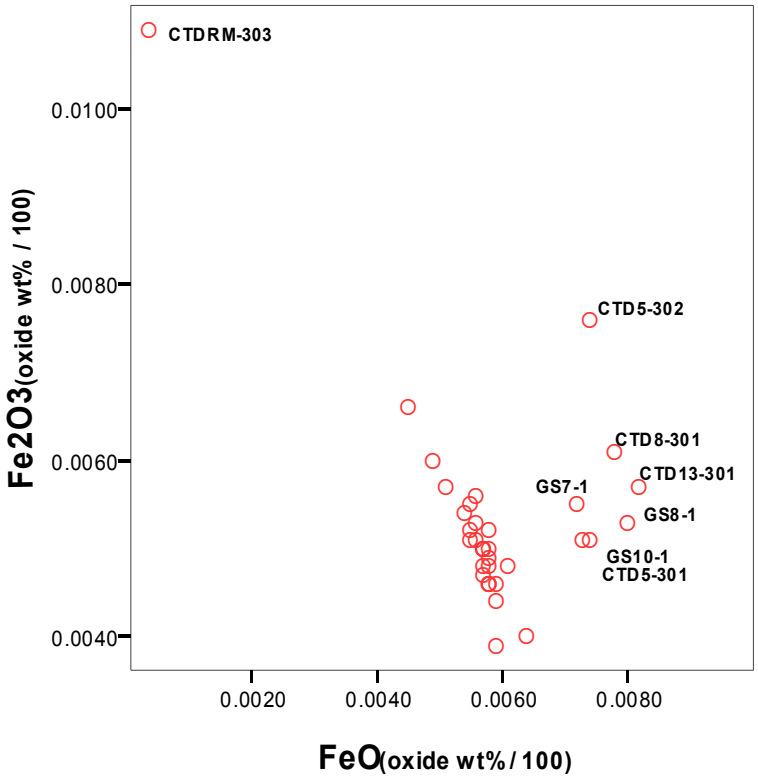

Figure 6-4 displays a potential pattern in the relationship of Fe_2O_3 and FeO. There may be an inverse correlation between the two oxidation states for about 80% of the samples, which are distributed in an intriguingly linear pattern on the left side of the

plot. The remaining seven samples (labeled by specimen number in the figure) are scattered on the right side of the plot (higher FeO). I did not perform a regression analysis or other statistical test to assess the potential for correlation as I have not found any link among these more scattered samples: they are from a variety of locations and do not include obvious visual characteristics anomalies such as unusual color.

While the potential association between Fe_2O_3 and FeO among certain samples could be investigated statistically, correlated values would not address the high CV values observed for Fe_2O_3 and FeO. One of the more interesting aspects of the puzzle presented by the iron results is that Total Fe (overall CV 9.39) does not vary as much as do Fe_2O_3 (overall CV 22.31) and FeO (overall CV 22.02). Relatively low variation in total iron also was reported in the ED-XRF analysis (measured as $Fe_2O_3^T$) as shown by CV values in Table 6-3. A pattern of inverse proportions for each oxidation state, as suggested in Figure 6-4, could produce the relatively lower variation in the summative value of Total Fe (i.e., the proportions are canceling each other out). Certainly the high variation in iron values expressed here, and potential patterns within and among the different iron measures, call for further investigation.

Discussion of WD-XRF trace vs. minor and major element results

The last question is whether major and minor elements exhibit the same degree of variation as do trace elements within the CTD samples. Considered in terms of all CV values for all elements in the WD-XRF analysis, trace elements have much higher CV values but, as discussed earlier in this section, many of these can be understood as caused by instrumentation and by the small amounts of certain elements in these samples. Where trace element ppm values do not occur at the lower end of detection limits (compare Ba, Cr, Co, Ni, Cu), and do not have ranges that are too restricted (compare Sr), variation is low among trace elements in a similar degree to most major and minor elements, as measured by the coefficient of variation. I conclude that the comparison of various CV results shows that major and minor elements have low overall variation, and that major and minor elements are similar to trace elements in having low variation within the CTD samples. The comparison of trace element variation to major and minor element variation appears to have been productive in demonstrating similar variation

among trace, minor, and major elements, illustrating that the variation observed for Mg and iron is higher than for other elements and thus may be measuring actual compositional variation within the samples.

It is also possible to compare WD-XRF and ED-XRF results to assess whether observed variation is actual rather than analytical. This comparison can be applied only to the elements included in both analyses (which excludes Mg), and requires that values from each analysis be in the same units (effectively excluding iron which I was unable to convert). Oxide weight percent results from the WD-XRF analysis were converted to ppm (Ti and Mn) or element weight percent (Ca and K).

Table 6-10. Comparison of WD-XRF and ED-XRF analyses results for CTD samples. Only elements measured in both analyses are included. All WD-XRF oxide wt % values (except Total Fe) are converted to element wt % or ppm, as appropriate.

	WD XRF results						ED-XRF results					
Element	**N**	**Min**	**Max**	**Mean**	****SD**	**CV**	**N**	**Min**	**Max**	**Mean**	****SD**	**CV**
Rb ppm	35	199	206	203.9	2.30	*1.13*	26	173	222	198.6	12.05	*6.07*
Sr ppm	35	4	5	4.1	0.28	*6.95*	26	3	6	4.0	0.92	***23.11***
Y ppm	35	63	66	65.2	0.98	*1.51*	26	54	67	59.7	3.12	*5.22*
Zr ppm	35	171	179	176.6	2.56	*1.45*	26	153	178	164.5	6.27	*3.81*
Nb ppm	35	138	148	145.1	2.51	*1.73*	26	77	96	85.8	4.26	*4.96*
***Ti** ppm	35	455	503	486.1	8.24	*1.69*	26	285	461	395.5	39.68	***10.03***
***Mn** ppm	35	565	596	581.4	8.35	*1.44*	26	385	767	646.1	72.22	***11.18***
***Ca** el wt%	35	0.29	0.30	0.295	0.003	*0.99*	26	0.11	0.16	0.134	0.0114	*8.51*
***K** el wt%/	35	3.55	3.91	3.614	0.057	*1.59*	26	3.17	3.80	3.609	0.1555	*4.31*
Total Fe (as Fe_2O_3)	35	1.05	1.48	1.180	0.11	9.39	26	1.11	1.41	1.240	0.0857	*6.91*
	oxide wt%, unable to convert to element wt%						*element wt %*					

* Ti, Mn, Ca, and K WD-XRF results were converted from oxide wt %.

As shown in Table 6-10, all the elements that can be compared directly have lower CV values in the WD-XRF results than in the ED-XRF results. This is an expected result because WD-XRF has generally higher precision than does ED-XRF (i.e., more tightly clustered outcomes, as illustrated in Figure 6-7, below), but this does not imply greater accuracy in the WD-XRF data. Differences in accuracy may be suggested by incomparability in actual values obtained by the two analyses are evident in the table, such as the much larger values for Nb in the WD-XRF data compared to the ED-XRF results. The differences demonstrated in Table 6-10 for Nb, Ti, and possibly Ca are cause for concern if these figures were to be used for source identification of artifacts. However, for the purpose of the current analysis which focuses on investigating variation

within the source, and where all comparisons of actual elemental values are from within a single analysis, the potential error in elemental values is of less relevance. The comparison demonstrates that there are no substantial differences in the variation exhibited in the data from each analysis.

In summary, examination of WD-XRF and ED-XRF measurement of elemental concentration and variation among CTD samples indicates that there is little actual variation in the composition of obsidians across the deposit, with the potentially significant exception of magnesium and iron. Use of the titration analysis to distinguish between oxidation states of iron suggests the possibility of intrasource compositional variation not usually investigated in standard archaeological obsidian sourcing studies. While total iron is universally measured in XRF and NAA studies of obsidian, and has potential for use as a diagnostic element in obsidian characterization (including Jemez Mountains sources; e.g., Baugh and Nelson 1987; Glascock et al. 1999:864, Fig. 2), differentiating the concentrations of Fe_2O_3 and FeO uncommon. The goal of the current analysis is largely investigative rather than conclusive, so the relevance of iron oxidation state in obsidian concentration is not certain. However, ferrous iron is a candidate to consider in understanding variable response of glass to heat exposure. As discussed in Chapter 5, Fe_2O_3 can act as a network modifier, possibly lowering the temperature of heat response in glass or influencing rate of diffusion by changing the oxygen-hydration bonding in the glass polymer.

6.3. Intersource WD-XRF Analyses (& ED-XRF) of Elemental Composition for Cerro Toledo Dome (CTD), Cerro Toledo Northeast (CTN), and Cerro Del Medio (CDM) Obsidians

This section considers obsidian elemental data collected from two obsidian-bearing areas geographically near to the CTD deposits. The purpose of the comparison is to determine whether obsidian deposits elsewhere in the Jemez volcanic system are more or less homogenous than the CTD glasses, enabling an assessment of the relative compositional homogeneity of CTD deposits. The selected comparison areas are at Cerro del Medio (CDM) in the center of the Valles caldera in the Valles Rhyolite geological unit, and Cerro Toledo Northeast (CTN) in the Sierra de Toledos in the Cerro Toledo Rhyolite deposits located in the northeast portion of the Valles caldera (Figure 6-5). The first area, CDM, was selected because it is geologically distinct from the Cerro Toledo Rhyolite (CTR) and thus should be dissimilar, and because it is recognizable to archaeologists. The second area, CTN, was selected for the opposite of those reasons: it is within the CTR unit and thus should be similar to CTD, and it is nearly unknown to archaeologists as a source for artifact quality obsidian (cf. Newman and Nielsen 1985). The comparison is further enhanced because Cerro Toledo Rhyolites (CTD and CTN) include primarily pyroclastic obsidians of explosive origin, while Cerro del Medio is an effusive source of obsidian. The former obsidians (explosive and pyroclastic, CTD and CTN) can be expected to have higher and more variable water contents, while the latter obsidians (effusive, CDM) can be expected to have lower and less variable water content.

Each set of sampling locations can be understood as geographic areas that overlap with geological units. However, as this sampling and analysis project demonstrates, the intersection of geography/landform and geology is not as well understood as might be expected given the importance of the Valles and Toledo caldera systems in the geological literature of the region and the history of volcanic geology, as well as the renown of the Jemez Mountains as an obsidian source in the archaeological literature.

This intersource analysis differs from the preceding intrasource analyses (Sections 6.1 and 6.2) in that it compares the Dome area obsidians (CTD) to glass samples from two other areas in the Jemez Mountains. Data presented in this section will be used to

answer three inter-related questions. First, are obsidians from CTR (CTD and CTN) sufficiently distinguishable from CDM obsidians? Second, are obsidians in the Cerro Toledo Rhyolite geological unit (CTD and CTN) compositionally similar? Third, depending on the coherence found in the CTD, CTN, and CDM source units, are CTD obsidians more or less variable in composition than the comparison obsidians? This section begins with a description of sampling at CDM and CTN, then addresses these three questions in the discussion of results.

Figure 6-5. Map of CTD, CTN, and CDM geological sampling locations plotted on 10m DEM shaded-relief map.

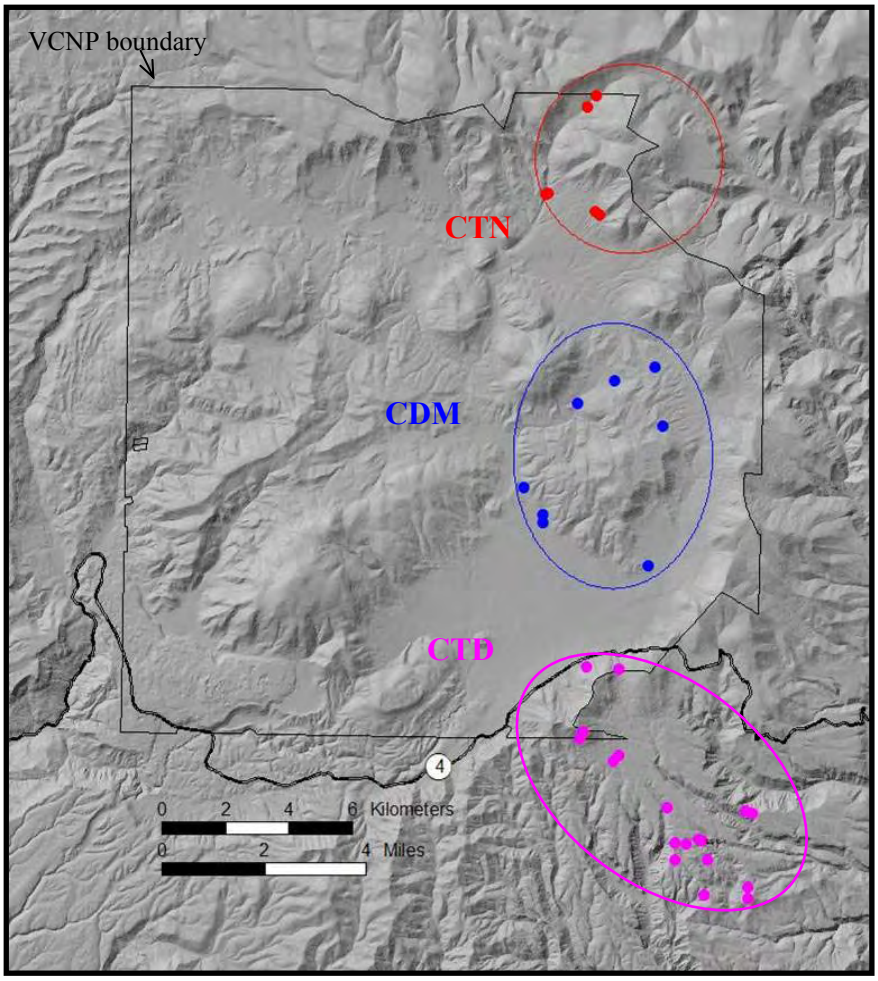

Selection of samples

This *intersource* analysis uses a set of 56 geological obsidian samples selected for comparison of multiple composition analyses (elemental composition--using both ED-XRF and WD-XRF--and water content--using LOI, FTIR, and SIMS) across the three geological contexts: two areas that occur within CTR, Cerro Toledo Dome (CTD) as discussed above in Sections 6.1 and 6.2, and Cerro Toledo Northeast (CTN), and a third location outside CTR, in the Valles Rhyolite: Cerro del Medio (CDM) (Figure 6-5).

The 56[13] obsidian specimens (Table 6-11) include 36 samples of Cerro Toledo Dome (CTD) obsidians, 8 samples from Cerro Toledo Northeast (CTN), and 12 Cerro del Medio (CDM) samples. The 36 CTD samples in this set are the same as those included in Section 6 2 (as "2004 ED-XRF") and include the four "1998 ED-XRF" samples included in the heat experiments (Steffen 2002).

Table 6-11. Intersource Comparison: Geological samples from three different geological contexts used for multiple XRF compositional analyses

Geological unit	Geographical sampling area	No. of Sampling Loci	Total samples available	Results used:	
				2004 ED-XRF	WD-XRF
Cerro Toledo Rhyolite (CTR)	**Cerro Toledo—Dome (CTD)**	14	36	*35/27	**35/ 35
Cerro Toledo Rhyolite (CTR)	**Cerro Toledo—Northeast (CTN)**	3	8	8 / 7	8 / 8
Valles Rhyolite (VR)	**Cerro del Medio (CDM)**	7	12	12 / 12	12 / 12
* 2004 ED-XRF analysis did not include sample CTD13-301 ** WD-XRF analysis did not include sample CTDRM-302				55 / 46	55 / 55
CTN sample excluded from ED-XRF results: CTN-303 CTD samples excluded from ED-XRF results: CTD5-303, CTD5-307, CTD6-301, CTD7-302, CTD10-303, CTD10-306, CTD12-303, CTDRM-302, CTDRM-304					

[13] Note that only 55 samples were actually used in the ED-XRF and WD-XRF analyses. This is because in each case one CTD sample (CTD13-301 for ED-XRF, and CTDRM302 for WD-XRF) had to be excluded because they were inadvertently left out of the group sent to each analyst. As noted in Section 6.1, several samples also were excluded from the analysis of ED-XRF results because the specimens had poor reflection geometry or other unsatisfactory conditions that were likely to compromise the ED-XRF measurements obtained. These samples are CTD5-303, CTD5-307, CTD6-301, CTD7-302, CTD10-303, CTD10-306, CTD12-303, CTDRM-302, CTDRM-304, and CTN-303. The total specimens included in the XRF analyses and the total specimen results used are shown in Table 6-11.

As shown in Figure 6-5, there are numerous sampling loci within each of the three geological sampling areas: CTD, CDM, and CTN (Tables 6-11 and 6-12). CTD samples include most of the Dome area collection locations described in Section 6.1 (Table 6-2). Ideally, the number of samples included from each source area should be equivalent, but the total of samples selected from the two comparison areas, CTN (n=8) and CDM (n=12) is more limited in number and spatial distribution. This is because the number of samples was restricted due to cost and the objectives of the analysis. That is, the goal here is to compare among source areas, and thus the resources that could be devoted to compositional analysis of the two "outside" source areas, CTN and CDM, were not as great as those available for the comprehensive baseline analysis pursued for the intrasource analyses of the Cerro Toledo Dome (CTD) obsidians. Further, the CTN and CDM sample areas are located within the Valles Caldera National Preserve (in the Sierra de Toledos and at Cerro del Medio) where access restrictions limited the range of available sampling locations as well as the number of samples collected.

CDM and CTN samples for this analysis (Tables 6-12) were collected[14] at sampling locations selected to represent broadly distributed locations (Figure 6-6) but access limitations in the VCNP restricted sampling only to easily accessed locations. Except location CDM 7, which is located near an old logging road accessible only on foot, all CTN and CDM sampling locations are near established in-use roads. Samples collected at CDM all occur in primary geological deposits--around the base or on Cerro del Medio--without significant transport from the location of their geological emplacement. The geological contexts of deposits sampled in CTN are less definitive. Some locations (CTN 3a and CTN 4) are within the drainage of the Rito de los Indios, indicating a potential for sampling of transported nodules. The other locations (CTN 1, CTN 2, CTN 3b, and CTN 5) are on side slopes and/or in small drainages with less potential for alluvial deposition but also the likelihood of colluvial transport. Overall, the depositional contexts of CDM samples are well-understood and the geological contexts are relatively clear, but both the depositional and geological contexts of CTN sampling locations are poorly understood.

[14] Geological collections were undertaken at CTN with P. LeTourneau in July 2001and at CDM with P. LeTourneau, F. Goff, and J. Gardner between August 2000 and October 2002.

Table 6-12. Intersource Geological Sampling Locations: Cerro Toledo—Northeast (CTN), and Cerro del Medio (CDM) [see Table 6-2 for CTD locations].

Geolog Unit	Loc ID	Easting	Northing	Quarry site in the vicinity	Location description	In 1998 ED-XRF analysis	In 2004 ED-XRF analysis	In 2004 WD-XRF analysis
CTR: CTN	CTN 1	368660	3981880	None	S facing slope in Sierra de Toledos along VCNP Road 10; below Turkey Ridge		1	1
CTR: CTN	CTN 2	368528	3981972	None	S facing slope in Sierra de Toledos along VCNP Road 10; below Turkey Ridge		1	1
CTR: CTN	CTN 3a	366985	3982503	None	In Rito de Los Indios drainage below Indian Point, possibly in alluvial/colluvial deposits, along VCNP Road I		1	1
CTR: CTN	CTN 3b	367040	3982550	None	In side drainage 75m E of Rito de Los Indios below Indian Point, possibly in alluvial/colluvial deposits, along unnamed logging road		2	2
CTR: CTN	CTN 4	368568	3985573	None	Upper Rito de Los Indios below unnamed dome W of Cerro Toledo, E of VCNP Road I, possibly in alluvial/colluvial deposits		1	1
CTR: CTN	CTN 5	368286	3985211	LA82581	Upper Rito de Los Indios below unnamed dome W of Cerro Toledo, in logging road 80m E of VCNP Road I, possibly in alluvial/colluvial deposits		2	2
					Total samples:	**0**	**8**	**8**
VR: CDM	CDM 1	369127	3976735	LA26919	North side of CDM base, along VCNP Road E on footslope above "Obsidian Valley"		1	1
VR: CDM	CDM 2a	366871	3972546	LA135612	South side of CDM base, north side of Valle Grande, along VCNP Road D		1	1
VR: CDM	CDM 2b	366881	3972308	LA135612	South side of CDM base, north side of Valle Grande, in deep erosion below stock pond		2	2
VR: CDM	CDM 3	366272	3973392	None	Southwest side of CDM base, in VCNP Road D and in drainage west of road		2	2
VR: CDM	CDM 4	370185	3970990	LA82577	Southeast tip of CDM base at south end of Rincon del Soldados and above Valle Grande, along VCNP Road D		1	1
VR: CDM	CDM 5	370392	3977161	None	North side CDM base, in eroded ditch off VCNP Road F		1	1
VR: CDM	CDM 6	367987	3976010	LA26916	Northwest side of CDM base, at Puerto de Abrigo saddle, along VCNP Road E		2	2
VR: CDM	CDM 7	370661	3975307	None	Northeast facing slope of CDM, in forested area		2	2
					Total samples:	**0**	**12**	**12**

Figure 6-6. Map of CTN and CDM geological sampling locations plotted on 10m DEM shaded-relief map.

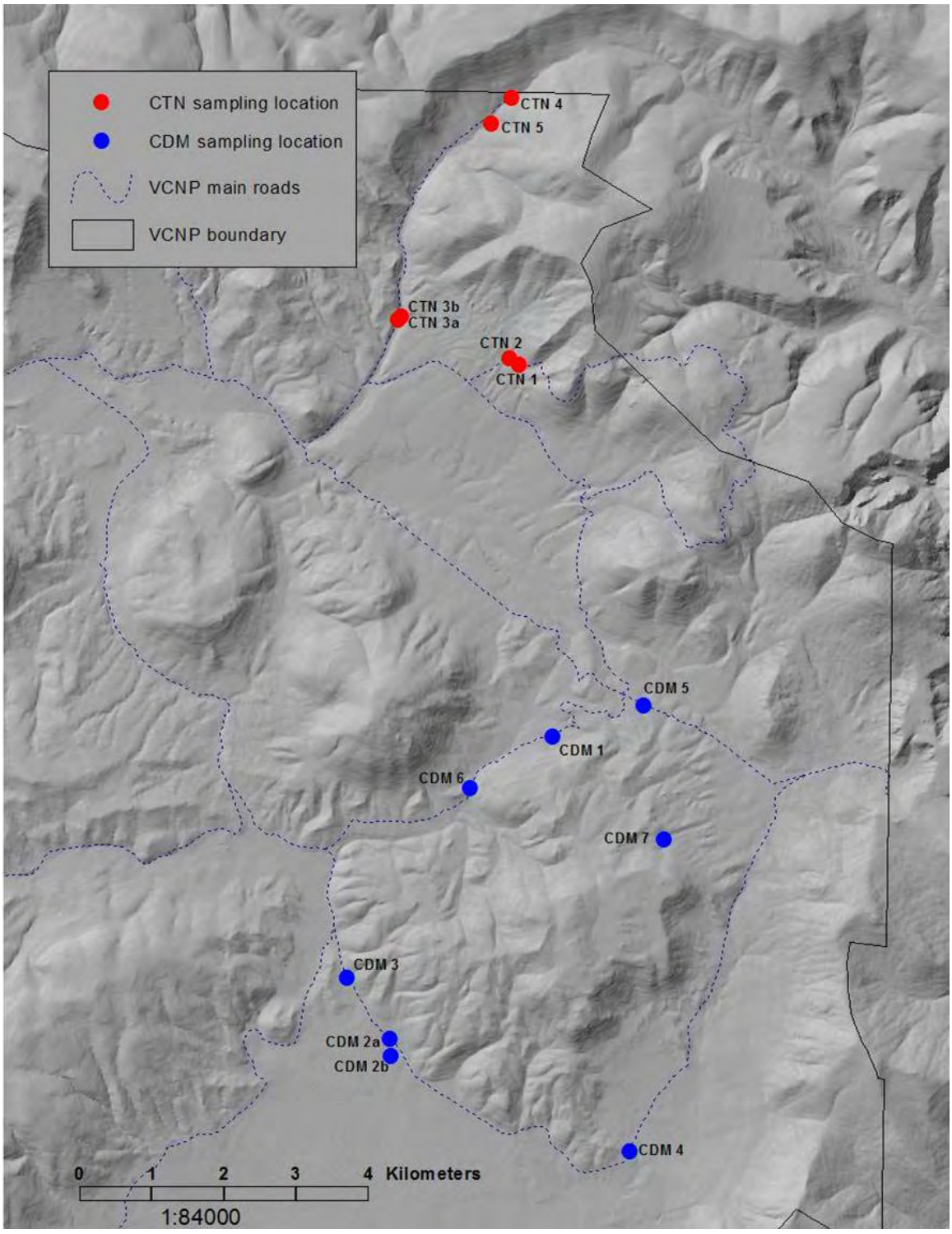

Results: Intersource WD-XRF and ED-XRF Composition Analyses for CTD, CTN, and CDM Obsidians

Results are presented in several formats. First, ED-XRF data for individual CDM and CTN specimens are presented below in Table 6-13 (these data are also in Table F-2). WD-XRF data for individual CDM and CTN specimens are more cumbersome and are presented only in Appendix F (Tables F-3 through F-5). Summary mean and CV values are presented for all three source areas (CTD, CTN, and CDM) in three tables: ED-XRF summaries are in Table 6-14, WD-XRF trace element summaries are in Table 6-15, and WD-XRF major/minor summaries are in Table 6-16.

To clarify the two XRF elemental analyses that are considered in this section, the major/minor elements measured by each XRF analysis are:

WD-XRF:	Major:	SiO_2, Al_2O_3, Na_2O, K_2O Total Iron
	Minor:	Fe_2O_3, FeO, CaO
ED-XRF:	Minor:	$Fe_2O_3^T$, Ca, K

The trace elements are:

WD-XRF:	Ba, Cr, Rb, Sr, Y, Zr, Nb, Co, Ni, Cu, Zn, plus Ti, Mn, Mg
ED-XRF:	Rb, Sr, Y, Zr, Nb, Ba, Ti, Mn,

Because Ti, Mn, and Mg are reported in WD-XRF as oxide weight percent (rather than ppm), they are included here with the major/minor element tables (Table 6-16 and Tables F-4 through F-6).[15] Calculated elemental weight percent and ppm values for Ti and Mn are presented in Tables F-5 and F-6.

The following additional information is useful for understanding the data tables. In Table 6-13 only, the geological sub-area in which each sampling location falls is noted in the far right column of the table. This information is true for the WD-XRF samples as well, but to save space the column is omitted from subsequent tables. For reasons explained later in this section, CTN samples have been split into two groups (CTN and CTNo) in the summary tables. In the table with individual specimen values (Table 6-13), the shaded row indicates a specimen that was intentionally excluded. In the tables with summary mean and CV values (Tables 6-14 through 6-16), the shaded row indicates CV values that have little meaning because the grouped sample size is too small (CTNo; n=2).

[15] See Footnote 11 in Section 6.2 for explanation of the treatment of minor vs. trace elements in the WD-XRF analysis.

Table 6-13. ED-XRF data for all individual specimens from CDM and CTN (see notes at bottom for id of mapped geological unit in far right column).

Loc ID	Sample ID	Rb ppm	Sr ppm	Y ppm	Zr ppm	Nb ppm	Ba ppm	Ti ppm	Mn ppm	$Fe_2O_3^T$ elem wt%	Fe/Mn ratio	K elem wt%	Ca elem wt%	REH ID	Geol Unit*
CDM 1	CDM-301	143	10	42	153	49	nm	541	462	1.09	27	3.82	0.21	CDM	LL
CDM 2a	CDM-302	157	10	44	160	50	nm	457	507	1.18	26	3.69	0.17	CDM	LL
CDM 2b	CDM-311	151	9	41	147	42	nm	416	510	1.20	25	3.52	0.17	CDM	LL
CDM 2b	CDM-312	152	6	38	146	49	nm	484	468	1.12	25	3.70	0.18	CDM	LL
CDM 3	CDM-303	156	6	40	156	47	nm	431	502	1.19	27	3.58	0.18	CDM	LL
CDM 3	CDM-308	151	40	41	150	44	nm	414	515	1.19	26	3.75	0.17	CDM	LL
CDM 4	CDM-304	150	9	40	152	50	nm	443	489	1.18	28	3.56	0.19	CDM	OL
CDM 5	CDM-305	161	6	41	158	48	nm	375	576	1.33	25	3.47	0.16	CDM	LL
CDM 6	CDM-309	150	6	45	162	51	nm	488	499	1.15	25	3.82	0.18	CDM	LL
CDM 6	CDM-310	153	9	42	155	53	nm	460	506	1.16	24	3.73	0.19	CDM	LL
CDM 7	CDM-306	148	7	40	153	52	nm	502	501	1.18	26	3.74	0.19	CDM	LL
CDM 7	CDM-307	138	10	37	144	43	nm	530	472	1.08	26	3.79	0.20	CDM	LL
CTN 1	CTN-301	149	8	47	133	65	nm	480	555	0.98	18	4.10	0.16	unk	TR
CTN 2	CTN-302	148	11	46	133	67	nm	468	547	0.99	18	3.74	0.15	unk	TR
CTN3a	CTN-303	188	6	62	148	80	nm	421	675	1.18	17	3.65	0.14	OR	IR
CTN 3b	CTN-304	201	4	57	156	88	nm	400	687	1.20	17	3.62	0.13	OR	IR
CTN 3b	CTN-305a	201	4	61	163	82	nm	554	531	1.27	19	3.52	0.12	OR	IR
CTN 4	CTN-306	193	4	65	158	87	nm	442	635	1.12	18	3.72	0.15	OR	IR
CTN 5	CTN-307	206	6	61	161	89	nm	405	673	1.24	20	3.59	0.14	OR	IR
CTN 5	CTN-308	202	4	63	168	91	nm	400	689	1.27	19	3.60	0.14	OR	IR

Shaded row indicates a specimen intentionally excluded from summaries because of unsatisfactory conditions (see Footnote 13).

***CDM geological units**: LL=Large Lobe OL=Oldest Lobe CM=Central Mountain

***CTN geological units**: TR=Turkey Ridge IP=Indian Point

Table 6-14. ED-XRF summary values for all three source areas (CTD, CTN, CDM). CTN is split into two groups (CTN and CTNo); bold numbers are CV values > 10.

SOURCE AREA		Rb ppm	Sr ppm	Y ppm	Zr ppm	Nb ppm	Ti ppm	Mn ppm	Fe_2O_3T elem wt%	K elem wt%	Ca elem wt%
CDM	N	12	12	12	12	12	12	12	12	12	12
	Min	138	6	37	144	42	375	462	1.08	3.47	0.16
	Max	161	40	45	162	53	541	576	1.33	3.82	0.21
	Mean	150.83	10.67	40.92	153.00	48.17	461.75	500.58	1.171	3.681	0.183
	SD	6.103	9.394	2.234	5.592	3.538	49.511	29.482	0.0640	0.1194	0.0142
	CV	4.05	**88.07**	5.46	3.66	7.34	**10.72**	5.89	5.47	3.24	7.79
CTD	N	26	26	26	26	26	26	26	26	22	22
	Min	173	3	54	153	77	285	385	1.11	3.17	0.11
	Max	222	6	67	178	96	461	767	1.41	3.80	0.16
	Mean	198.6	4.0	59.7	164.5	85.8	395.5	646.1	1.240	3.609	0.134
	SD	12.05	0.92	3.12	6.27	8.003	39.68	72.22	0.0857	0.1555	0.0114
	CV	6.07	**23.11**	5.22	3.81	4.96	**10.03**	**11.18**	6.82	4.31	8.51
CTN	N	5	5	5	5	5	5	5	5	5	5
	Min	193	4	57	156	82	400	531	1.12	3.52	0.12
	Max	206	6	65	168	91	554	689	1.27	3.72	0.15
	Mean	200.6	4.4	61.4	161.2	87.4	440.2	643.0	1.220	3.610	0.136
	SD	4.722	0.894	2.967	4.658	3.362	66.002	66.257	0.0628	0.0721	0.0114
	CV	2.35	**20.33**	4.83	2.89	3.85	**14.99**	**10.30**	5.15	2.00	8.38
CTNo	N	2	2	2	2	2	2	2	2	2	2
	Min	148	8	46	133	65	468	547	0.98	3.74	0.15
	Max	149	11	47	133	67	480	555	0.99	4.10	0.16
	Mean	148.50	9.50	46.50	133.00	66.00	474.00	551.00	0.985	3.920	0.155
	SD	0.707	2.121	0.707	0.000	1.414	8.485	5.657	0.0071	0.2546	0.0071
	CV	0.48	**22.33**	1.52	0.00	2.14	1.79	1.03	0.72	6.49	4.56

Shaded row indicates CV values that have little meaning because sample n=2

Table 6-15. WD-XRF trace element summary values for all three source areas (CTD, CTN, CDM). CTN is split into two groups (CTN and CTNo); bold = CV value >10.

values in ppm		Ba	Cr	Rb	Sr	Y	Zr	Nb	Co	Ni	Cu	Zn
CDM	N	12	12	12	12	12	12	12	12	12	12	12
	Min	nm	0	161	7	44	159	81	0	0	1	59
	Max	nm	14	164	8	46	167	83	30	2	5	82
	Mean	n/a	1.75	163.50	7.75	45.17	163.83	82.25	7.25	1.08	2.75	73.92
	SD	n/a	4.025	0.905	0.452	0.577	1.899	0.622	9.137	0.669	1.215	6.142
	CV	n/a	**230.03**	0.55	5.84	1.28	1.16	0.76	**126.02**	**61.71**	**44.20**	8.31
CTD	N	35	35	35	35	35	35	35	35	35	35	35
	Min	nm	0	199	4	63	171	138	0	1	0	126
	Max	nm	29	206	5	66	179	148	34	5	6	181
	Mean	n/a	5.11	203.89	4.09	65.17	176.60	145.06	13.34	2.37	2.09	140.69
	SD	n/a	9.193	2.298	0.284	0.985	2.558	2.508	10.432	1.031	1.738	8.439
	CV	n/a	**179.76**	1.13	6.95	1.51	1.45	1.73	**78.18**	**43.49**	**83.35**	6.00
CTN	N	6	6	6	6	6	6	6	6	6	6	6
	Min	nm	0	208	4	66	172	149	5	1	1	141
	Max	nm	1	209	4	67	175	151	38	3	8	144
	Mean	n/a	0.33	208.67	4.00	66.67	173.00	150.00	22.00	1.83	2.67	142.50
	SD	n/a	0.516	0.516	0.000	0.516	1.095	0.632	12.884	0.753	2.658	1.225
	CV	n/a	**154.92**	0.25	0.00	0.77	0.63	0.42	**58.56**	**41.06**	**99.69**	0.86
CTNo	N	2	2	2	2	2	2	2	2	2	2	2
	Min	nm	0	166	10	47	149	111	0	1	2	75
	Max	nm	0	167	11	48	152	111	4	1	3	84
	Mean	n/a	0.00	166.50	10.50	47.50	150.50	111.00	2.00	1.00	2.50	79.50
	SD	n/a	0.000	0.707	0.707	0.707	2.121	0.000	2.828	0.000	0.707	6.364
	CV	n/a	0.00	0.42	6.73	1.49	1.41	0.00	**141.42**	0.00	**28.28**	8.00

Table 6-16. WD-XRF minor and major element summary values for all three source areas (CTD, CTN, CDM). CTN is split into two groups (CTN & CTNo); bold=CV >10.

values in oxide wt%		SiO_2	TiO_2	Al_2O_3	Fe_2O_3	FeO	MnO	MgO	CaO	Na_2O	K_2O	Total Fe
CDM	N	12	12	12	12	12	12	11	12	12	12	12
	Min	75.73	0.10	12.28	0.41	0.07	0.054	0.050	0.47	4.14	4.52	1.11
	Max	77.40	0.10	12.71	1.04	0.75	0.056	0.120	0.48	4.21	4.66	1.68
	Mean	76.290	0.099	12.431	0.613	0.518	0.055	0.078	0.475	4.179	4.559	1.188
	SD	0.4591	0.0007	0.1562	0.2479	0.2138	0.0007	0.0171	0.0052	0.0198	0.0408	0.1721
	CV	0.60	0.73	1.26	**40.41**	**41.27**	1.21	**21.78**	1.10	0.47	0.89	**14.48**
CTD	N	35	35	35	35	35	35	34	35	35	35	35
	Min	74.83	0.08	11.72	0.39	0.04	0.073	0.030	0.41	4.07	4.28	1.05
	Max	76.94	0.08	12.58	1.09	0.82	0.077	0.090	0.42	4.40	4.71	1.48
	Mean	76.231	0.081	12.046	0.533	0.589	0.075	0.052	0.412	4.297	4.354	1.180
	SD	0.5379	0.0014	0.1656	0.1190	0.1297	0.0011	0.0154	0.0041	0.0564	0.0691	0.1108
	CV	0.71	1.69	1.38	**22.31**	**22.02**	1.44	**29.91**	0.99	1.31	1.59	9.39
CTN	N	6	6	6	6	6	6	6	6	6	6	6
	Min	75.21	0.08	11.83	0.44	0.43	0.075	0.057	0.41	4.30	4.29	1.10
	Max	76.53	0.08	12.35	0.63	0.60	0.077	0.070	0.42	4.34	4.34	1.13
	Mean	75.862	0.081	12.073	0.500	0.552	0.076	0.063	0.412	4.327	4.322	1.113
	SD	0.5712	0.0008	0.2240	0.0678	0.0611	0.0008	0.0056	0.0040	0.0151	0.0214	0.0103
	CV	0.75	1.01	1.86	**13.56**	**11.08**	0.99	8.87	0.98	0.35	0.49	0.93
CTNo	N	2	2	2	2	2	2	2	2	2	2	2
	Min	75.32	0.11	11.97	0.70	0.22	0.063	0.084	0.46	3.66	4.75	0.95
	Max	76.36	0.11	12.20	0.71	0.23	0.065	0.087	0.47	4.00	5.13	0.97
	Mean	75.840	0.113	12.085	0.705	0.225	0.064	0.086	0.465	3.830	4.940	0.960
	SD	0.7354	0.0007	0.1626	0.0071	0.0071	0.0014	0.0021	0.0071	0.2404	0.2687	0.0141
	CV	0.97	0.63	1.35	1.00	3.14	2.21	2.48	1.52	6.28	5.44	1.47

Discussion of Results: Intersource Composition Analyses for CTD, CTN, and CDM

The three questions posed at the beginning of this section are as follows. First, are obsidians from CTR (CTD and CTN) sufficiently distinguishable from CDM obsidians? The results obtained show that answering this first question is made more complex given the results of the second question: are obsidians in the Cerro Toledo Rhyolite geological unit (CTD and CTN) compositionally similar? The goal of these analyses is answering the third question: are CTD obsidians more or less variable in composition than the comparison obsidians? Answering this question depends on the coherence found in the CTD, CTN, and CDM source units, as established in the first two questions.

1. Are obsidians from CTR (CTD and CTN) sufficiently distinguishable from CDM obsidians?

This is a relatively standard kind of "sourcing" question. Comparison of XRF trace elements data shows that six trace elements (Ti, Rb, Y, Zr, Nb, Zn) are variably effective for discerning among CDM, CTD, and CTN samples (Figures 6-7 and 6-8).[16] Ellipses on the XY graphs (Figure 6-7) show the 95% confidence interval for intersection between the two trace elements plotted in each graph. The bivariate and XYZ plots (Figures 6-7 and 6-8) demonstrate that these six trace elements 1) can be used to graphically distinguish between the CDM and CTD samples, but 2) are problematic for the CTN samples. As expected, there are clear differences in trace elements between CDM and CTR glasses: the two CTR sources, CTN and CTD, can be distinguished from CDM based on trace element composition. However, the data and the plots show that there are both differences and similarities among the CTR glass samples (CTD and CTN). Of the eight CTN samples, six plot with the CTD samples for these trace elements, and two are markedly different than either CTD or CDM samples. In all three plots the red diamonds that do not fall within ellipses indicate the two CTN samples that differ from the other five CTN samples. These are the two samples grouped as CTNo in the data tables (Tables 6-14 through Table 6-16).

[16] Note that the bivariate plots in Figure 6-7 illustrate the greater precision of the WD-XRF data as shown by the tight clusters of data points, but also that the same cluster patterns are seen in both sets of XRF data.

Figure 6-7. Bivariate plots of XRF data for trace elements Y / Nb, Zr / Rb, & Zn / Ti.

WD-XRF Data (ppm)

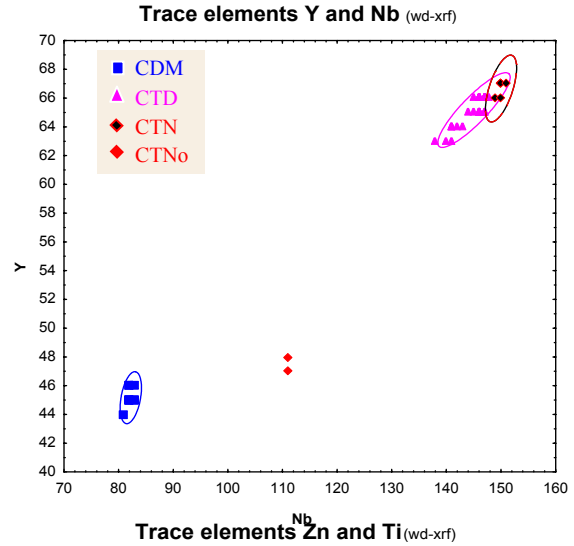

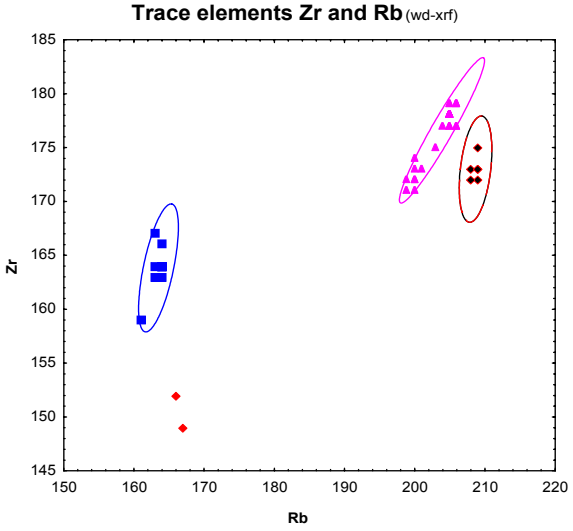

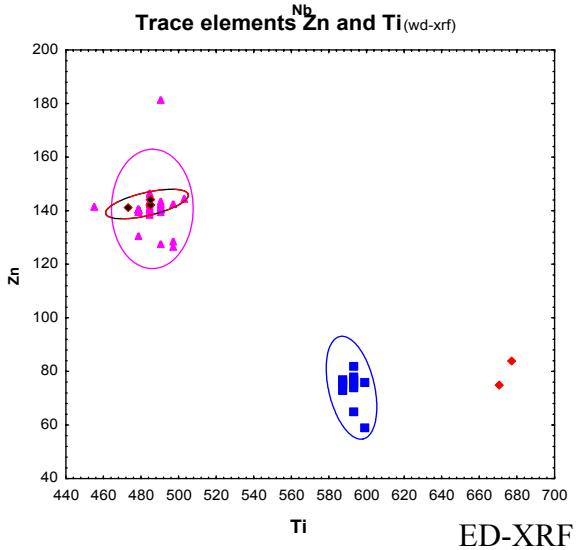

In the bivariate plots and the XYZ plots, blue squares represent CDM samples; while pink triangles and red diamonds represent CTR samples:

CDM samples = blue squares
CTD samples = pink triangles
CTN samples = red diamonds (black centers)

The two CTNo samples (as a subset of CTN) are shown as solid red diamonds

Ellipses in bivariate plots show the 95% confidence interval for the intersection of elements. Note that the number of samples is greater than is immediately apparent on some graphs because of the overlap of multiple data points.

ED-XRF DATA (ppm)

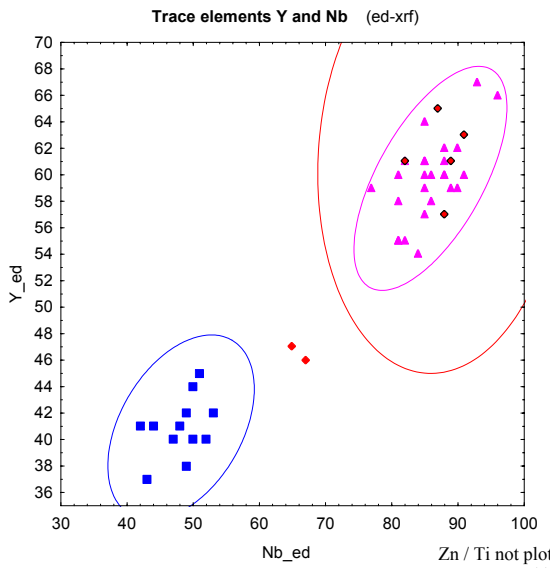

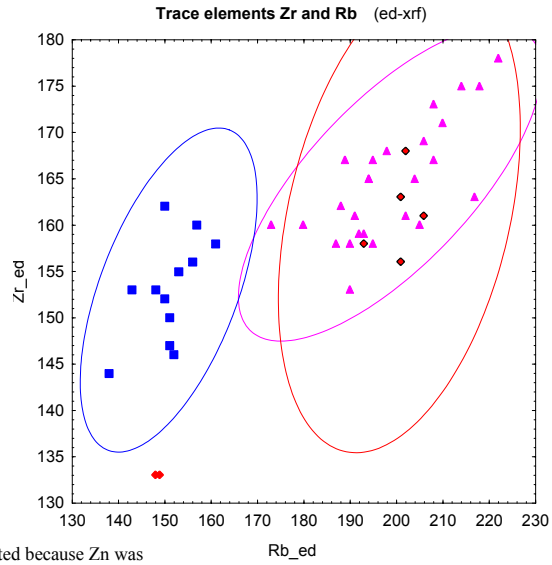

Zn / Ti not plotted because Zn was not measured in ED-XRF analysis

Figure 6-8. XYZ plots of XRF trace elements Ti / Zn / Zr and Rb / Nb / Y.

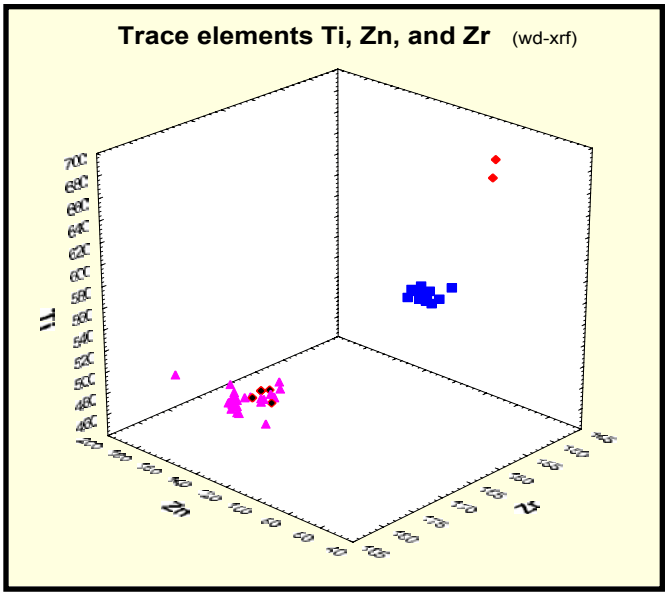

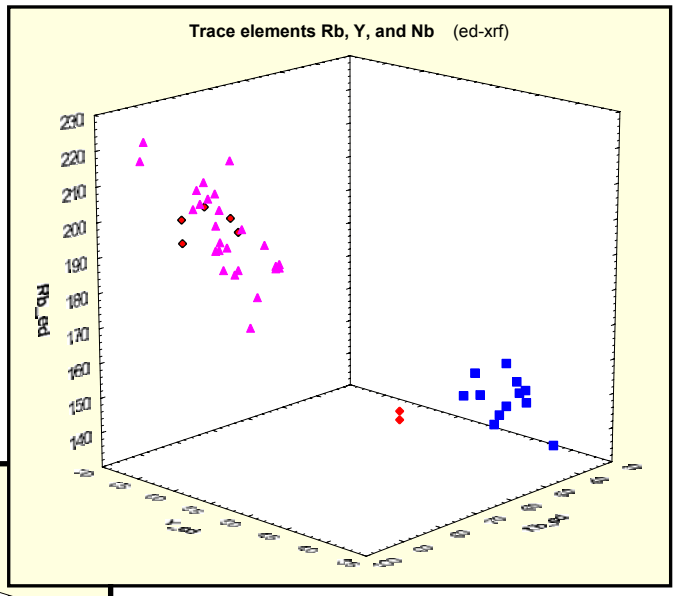

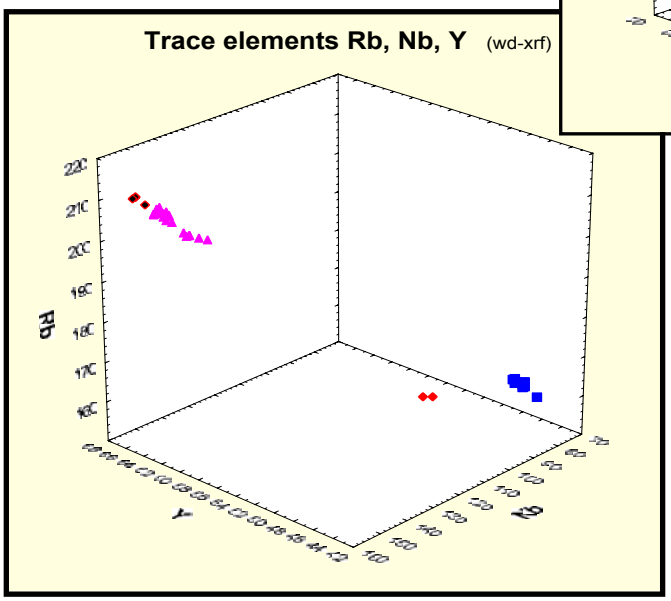

The broad conclusion that can reached is that trace element compositions of obsidians from the two Cerro Toledo Rhyolite sources are different than the Valles Rhyolite obsidian, CDM, except for two CTN samples which differ from both the CTD and the CDM trace element profiles. The more detailed conclusions that can be made from the data are discussed in the paragraphs that follow, addressing first the issue of compositional homogeneity within the Cerro Toledo geological unit.

2. Are obsidians in the Cerro Toledo Rhyolite geological unit (CTD and CTN) compositionally similar?

In this study the primary goal of all compositional analyses is to investigate potential variation within or among obsidian deposits to identify any factors that could affect obsidian hydration or how heat effects occur. Thus the initial examination of XRF data for CTN samples raised the possibility that intrasource variation within CTR might have been detected: two of the eight samples had measurable differences in elemental composition. This can be assessed by examining first trace elements and then minor and major elements.

Trace Elements Within the Cerro Toledo Rhyolites (CTD and CTN)

Table 6-17 shows the summary statistic outcomes—means, standard deviations, and CV values—for the six key trace elements when all CTN samples are combined. The combined CTN samples have high CV values—near or above 10—for all six elements (but less so for the element Zr). These high CV values could have been interpreted as indicators of high intrasource variation in these elements. Instead, I interpret the results to indicate that two samples, CTN-301 and CTN-302, represent a different geochemical profile than the other six CTN samples. The combined values in Table 6-17 can be compared to Tables 6-14 and 6-15 (or to Table 6-18, below, which shows ED-XRF and WD-XRF data extracted from Tables 6-14, 6-15, and F-6) in which CTN is split into CTNo (n=2) and CTN (n=5 or 6). Where the two samples are separated into CTNo (Tables 6-18), CV values are much smaller (below 10 in for all elements) for each subgroup than where combined (Table 6-17). Examination of these data and the associated bivariate and XYZ plots shows that compared to the rest of the CTN samples, the two CTNo samples are lower in Rb, Y, Zr, and Nb, and the WD-XRF data shows also that the CTNo samples are low in Zn and total iron.

Table 6-17. WD-XRF and ED-XRF trace elements in all CTN samples. CTN is <u>not</u> split into two groups; bold = CV value >10.

All CTN samples--without separating two samples as CTNo							
WD-XRF		Rb	Y	Zr	Nb	Ti	Zn
All CTN	N	8	8	8	8	8	8
	Min	166	47	149	111	473	75
	Max	209	67	175	151	677	144
	Mean	198.1	61.9	167.4	140.3	530.9	126.8
	SD	19.53	8.89	10.49	18.06	88.38	29.28
	CV	9.86	**14.36**	6.27	**12.88**	**16.65**	**23.10**
ED-XRF		Rb	Y	Zr	Nb	Ti	Zn
All CTN	N	7	7	7	7	7	nm
	Min	148	46	133	65	400	nm
	Max	206	65	168	91	554	nm
	Mean	185.7	57.1	153.1	81.3	449.9	nm
	SD	25.71	7.67	14.28	10.81	56.46	nm
	CV	**13.85**	**13.42**	9.32	**13.30**	**12.55**	nm

Table 6-18. WD-XRF and ED-XRF trace element summary values for all three source areas. CTN is split into two groups (CTN and CTNo); bold = CV value >10.

WD-XRF from Tables 6-15 & F-6		Rb	Y	Zr	Nb	Ti	Zn
CTN	N	6	6	6	6	6	6
	Min	208	66	172	149	473	141
	Max	209	67	175	151	485	144
	Mean	208.7	66.7	173.0	150.0	483.2	142.5
	SD	0.52	0.52	1.10	0.63	4.90	1.23
	CV	0.25	0.77	0.63	0.42	1.01	0.86
CTNo	N	2	2	2	2	2	2
	Min	166	47	149	111	671	75
	Max	167	48	152	111	677	84
	Mean	166.5	47.5	150.5	111.0	673.9	79.5
	SD	0.71	0.71	2.12	0.00	4.24	6.36
	CV	0.42	1.49	1.41	0.00	0.63	8.00
ED-XRF from Table 6-14		Rb	Y	Zr	Nb	Ti	Zn
CTN	N	5	5	5	5	5	nm
	Min	193	57	156	82	400	nm
	Max	206	65	168	91	554	nm
	Mean	200.6	61.4	161.2	87.4	440.2	nm
	SD	4.72	2.97	4.66	3.36	66.00	nm
	CV	2.35	4.83	2.89	3.85	**14.99**	nm
CTNo	N	2	2	2	2	2	nm
	Min	148	46	133	65	468	nm
	Max	149	47	133	67	480	nm
	Mean	148.5	46.5	133.0	66.0	474.0	nm
	SD	0.71	0.71	0.00	1.41	8.49	nm
	CV	0.48	1.52	0.00	2.14	1.79	nm

Separating CTN into two subgroups is supported not just by the data but also by the physiography of the sampling locations and known geological origins of the domes (Figure 6-10). CTN-301 and CTN-302 are located close together on a different landform than the other four sampling locations (Figures 6-6 and 6-10). CTN-301 and CTN-302 are located on the south side of the sampling area below what is known as Turkey Ridge, while the other CTN sampling locations are located to the west and north along or near the Rito de los Indios and below Indian Point (Figure 6-10).

The geological relationships of these Cerro Toledo domes are not well understood, and no 1:24000 geologic maps have yet been published. However, a recent analysis of the Toledo embayment by Gardner and Goff (1996) (Figure 6-9) supports the idea that the domes that compose Turkey Ridge are volcanically distinct from those at Indian Point and at Cerro Toledo (see also Spell et al. 1996). Samples collected from the four locations in or near the Rito de los Indios Canyon thus would derive from Indian Point or Cerro Toledo domes, while the two samples below Turkey Ridge are from a different vent dome (Figure 6-10).

This geological background helps to begin the search for the origin and association of the CTNo samples, but it should be noted also that the geochemical profile indicated by trace elements suggests a closer fit to Cerro del Medio than Cerro Toledo obsidians (Tables 6-14 and 6-15). This raises the possibility that the CTNo glasses should not be assumed automatically to be related to CTR deposits. For now, the CTNo are excluded from CTD, CTN, and CDM as a special case without known association.

It is possible that the CTNo samples represent a fully different chemical profile present in the Sierra de Toledo domes that has not been documented previously. Clearly, a sample of two specimens is not sufficient to define a new trace element profile, but even this small sample size is enough to demonstrate that the two obsidian samples obsidians do not fit with known profiles. These results are enough to raise, but not answer, the question of why a different profile of trace elements occurs in the Sierra de Toledos among deposits that are geographically close to deposits of the Cerro Toledo Rhyolite. To resolve this question, further sampling is needed (conducted with careful attention to the precise physiography of sampling locations) to increase the sample number and to define the extent of the area of deposits with these obsidians.

Figure 6-9. Geology of the Toledo Embayment area, from Gardner & Goff (1996:227).

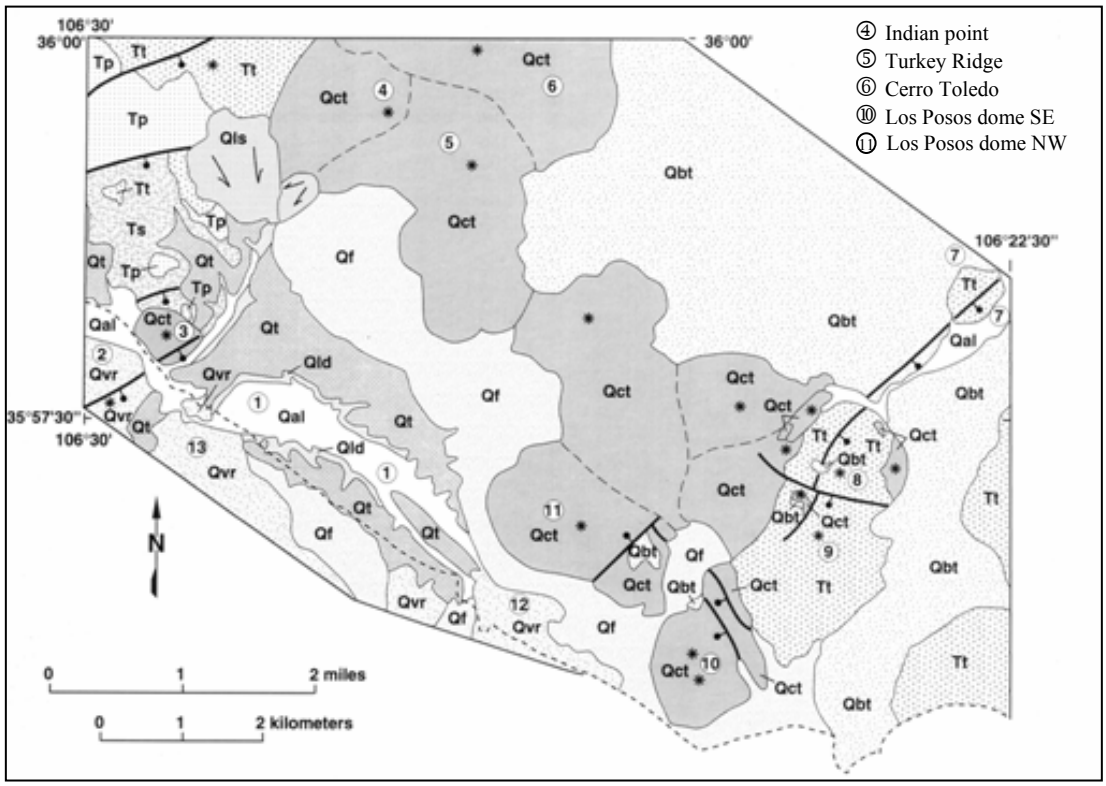

Figure 6-10. CTN sampling locations with outlines from the Gardner & Goff (1996) map units. Maps shown on (a) SFNF Primary Base Series topographic map (Valle Toledo and Polvadera Peak Quads) and (b) 10m DEM shaded relief.

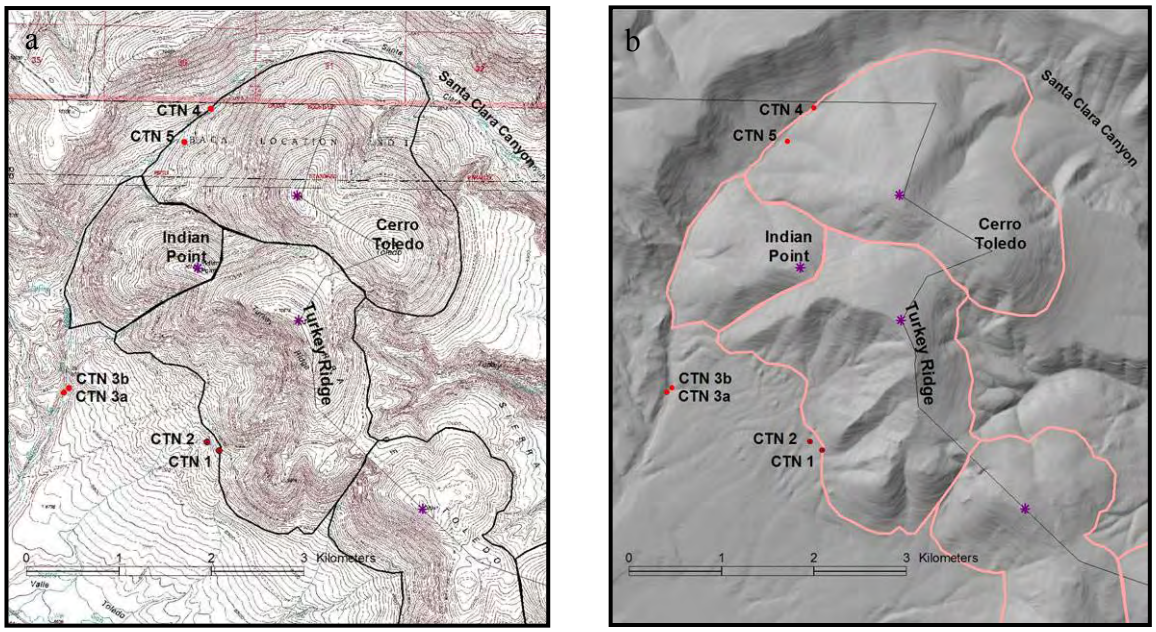

For this study, I am confident that the appropriate conclusion for the current data is that the two CTNo samples are distinct from the Cerro Toledo Rhyolite obsidians, and thus they do not indicate "intrasource" variation in CTR.

The second conclusion that can be drawn from the comparison of CTD and CTN results is that the Cerro Toledo obsidian chemical group (aka Obsidian Ridge) is expressed not at the scale of individual deposit, dome, or geographic feature, but at the scale of the geological unit. When the two differing samples are demarcated as a special case and not included automatically with CTN, it is clear that the Cerro Toledo Rhyolite obsidians are homogenous not just across the Dome deposits but also in the Northeast area outside of the Dome. This addresses the broader issue of archaeological sourcing for these deposits. The compositional analyses show clearly that there are glasses that share the Cerro Toledo trace element profile located outside the Cerro Toledo Dome area where the "Obsidian Ridge" chemical group was first recognized.

In other words, volcanic glasses of the "Obsidian Ridge" and "Rabbit Mountain" chemical type occur in these Northeast deposits of the Cerro Toledo Rhyolite geological unit far from the landforms of Obsidian Ridge or Rabbit Mountain. This is an important clarifying addition to the archaeological literature on obsidian sources in the Jemez Mountains. Others refer to deposits in Santa Clara Canyon outside the Valles caldera (Macdonald et al. 1992)[17] but *in situ* primary sources of Obsidian Ridge obsidian in the Sierra Toledos have been reported in the archaeological literature only by Newman and Nielsen (1985).[18,] It should not be assumed, therefore, that geological or artifact specimens with the Obsidian Ridge / Rabbit Mountain trace element geochemical profile originated from primary or secondary deposits related to the Dome deposits where Obsidian Ridge and Rabbit Mountain are located. For this study, the trace element results further strengthen the evidence that there is no variation in trace elements in the Cerro Toledo Rhyolite obsidian-bearing deposits, whether examined at the scale of the Dome area (as investigated in Sections 6.1 and 6.2, above) or at the scale of the CTR geological unit (as shown here in Section 6.3).

[17] See also unpublished website by Shackley (2002).
[18] There are other discussions of sources in geographic locations which potentially could be associated with Sierra Toledo domes (e.g., "Los Posos" and "Cerro Rubio" in Baugh and Nelson [1987] and "Cerro Pavo" in Glascock et al. [1999]) but the associated location description are too ambiguous to determine.

Major and Minor Elements Within the Cerro Toledo Rhyolites (CTD and CTN)

Turning to major and minor elements (Table 6-19), when these elements are considered patterns emerge that are similar to those observed in the trace elements. Looking at means for elements such as Mn, Mg, Ca, and K, samples from CTN cluster with CTD for all the samples except the two collected below Turkey Ridge (CTNo), with the latter two samples either unlike any other sources or more similar to CDM SiO_2 values, however, are distinctly different for all CTN samples as compared to either CTD or CDM samples, while Al_2O_3 is similar among all the CTR samples and notably different than CDM samples.

Table 6-19. WD-XRF minor and major element means for all three source areas (CTD, CTN, CDM). CTN is split into two groups (this is an abbreviation of Table 6-16).

oxide wt%		SiO_2	TiO_2	Al_2O_3	Fe_2O_3	FeO	MnO	MgO	CaO	Na_2O	K_2O	Total Fe
CDM	N	12	12	12	12	12	12	11	12	12	12	12
	Mean	76.29%	0.10%	12.43%	0.61%	0.52%	0.06%	0.08%	0.48%	4.18%	4.56%	1.19%
CTD	N	35	35	35	35	35	35	34	35	35	35	35
	Mean	76.23%	0.08%	12.05%	0.53%	0.59%	0.08%	0.05%	0.41%	4.30%	4.35%	1.18%
CTN	N	6	6	6	6	6	6	6	6	6	6	6
	Mean	75.86%	0.08%	12.07%	0.50%	0.55%	0.08%	0.06%	0.41%	4.33%	4.32%	1.11%
CTNo	N	2	2	2	2	2	2	2	2	2	2	2
	Mean	75.84%	0.11%	12.09%	0.71%	0.23%	0.06%	0.09%	0.47%	3.83%	4.94%	0.96%

CTNo samples also are notably different from all other chemical groups (CTD, CTN, and CDM) for iron and Na (Figure 6-11) as well as K. For iron, this may be an expression of the wide variation observed in FeO when a larger sample size is available (as discussed for CTD in Section 6.1, Figure 6-4). For Na, there appears to be a wide spread in the values of this element in the two CTNo samples, with the larger value nearing the range of the lower end observed in CTD samples. For K, the CTNo samples are simply much greater than any of the other source areas.

Figure 6-11. WD-XRF major and minor elements Na / Ca and Total Iron / Mn plotted on XY graphs.

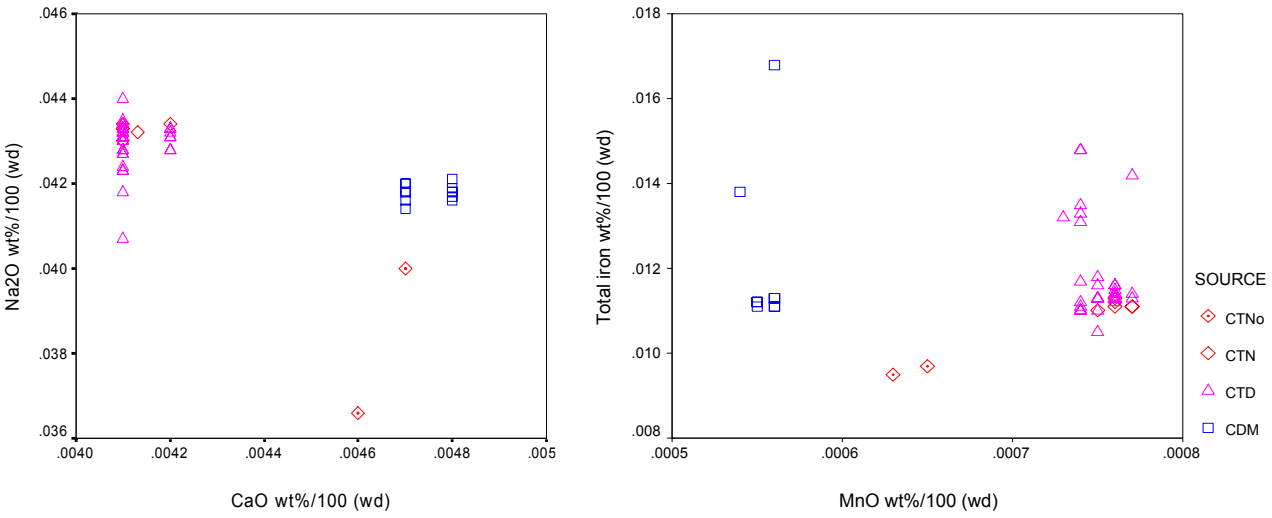

As pointed out by Hughes (2004b), without a larger sample size available for the CTNo samples it is difficult to make firm conclusions about this variant chemical profile. However, the results indicate that it is not a match for either CTD or CDM, that it does not group with the other CTN samples either (which fit with CTD), and that further sampling is strongly warranted for the areas below Turkey Ridge and throughout the Sierra de Toledos.

For the purpose of this study, it is sufficient to have determined that, except for the two unusual samples CTN-301 and CTN-302, the sum of all results of XRF analyses of elemental composition group CTD and CTN together into an internally coherent group obsidians from CTR that correspond with previous characterizations of CTD as a chemical group (i.e., usually referred to as "Obsidian Ridge"). The results reinforce the differentiation of these CTR glasses from obsidians occurring at Cerro del Medio, and point to the CTNo samples represented a variant geochemical profile that does not fit with the CTD, CTN, or CDM samples.

Thus, answers to the first two questions posed at the beginning of this section are clear but complex. First, obsidians sampled from within the CTR geological unit are compositionally similar except for two samples that appear to represent a compositional profile that is different enough to warrant pursuit of a new designation based on

elemental values observed and information known about the geology of the collection areas. Second, all CTR obsidian samples measured in this study are chemically distinct from CDM samples.

Trace Elements Within the Valles Rhyolite (CDM)

Before turning to the third question, which considers the internal variability of CTD glasses, it is worth considering briefly an issue of sampling with regard to the integrity of CDM as a chemical group. The XRF results obtained in this analysis accord well with previously published results for CDM (e.g., Baugh and Nelson 1987, Glascock et al. 1999, Macdonald et al. 1992) and confirm that the CDM outcrops sampled represent a chemical group when comparing trace elements such as Ti, Rb, Y, Zr, Nb, and Zn, and the minor element Ca.

Figure 6-12. Map of Cerro del Medio showing J. Gardner's preliminary geological units on 10m DEM shaded relief.

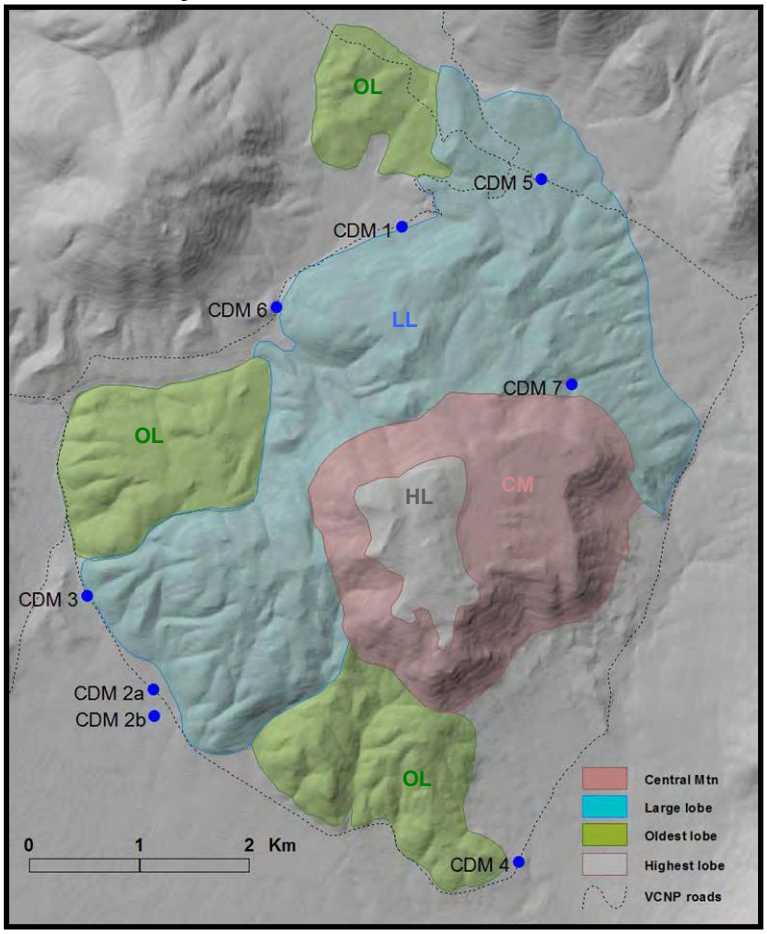

Source: Map by A. Steffen based on 2003 unpublished preliminary field mapping and interpretation by J. Gardner, Los Alamos National Lab

At first glance, it appears that the sampling locations used in this study are well distributed--with seven locations around the base of CDM and one location on the top (Figures 6-6 and 6-12). However, recent geologic mapping suggests that the history of dome development at Cerro del Medio actually is quite complex (see also Doell et al. 1968, as discussed in Baugh and Nelson 1987). Geological mapping on Cerro del Medio in 2001-2003 by J. Gardner, Los Alamos National Laboratory has produced preliminary results that indicate four distinct lobes on Cerro del Medio, probably ranging in age from 60,000 to 100,000 ya (J. Gardner, personal communication 2003). Using this information to compare with sampling locations (Figure 6-12), it turns out that despite the attempt at a representative distribution of sampling locations, seven of the eight locations are all on one of these lobes (i.e., except for CDM 4, located on the SE edge of CDM). Sampling only around the base—where there is direct access by drivable roads, and where most previous researchers also sampled—resulted in a biased and potentially non-representative sample.

This is an example of the difficulties inherent in achieving adequate sampling without sufficient geological background information. In this case, the information has only recently become available; future sampling can be informed by the results obtained by geologists currently mapping within the Valles caldera. For this study, the most important consideration is in how these results can be interpreted regarding compositional variation within the CDM chemical group. Intersource comparisons, and comparison of these results with previously published data for CDM, are less of a concern because the CDM chemical group was established using samples that likely sampled the Cerro del Medio landform and geological deposits in much the same manner as in this study. In effect, I sampled the same subset of variation that has been represented in the literature, and in this case the probable effect of non-representative sampling is biased toward internal homogeneity. In other words, it is likely that any error within my data is systematic bias toward geological uniformity. In sum, because of the small sample size and geological distribution of samples obtained, these data are not well suited to demonstrate the potential variation extant within all CDM glasses, but they are sufficient to independently corroborate the CDM chemical group at the locations that are best known and best represented in the published literature.

3. Are CTD obsidians more or less variable in composition than the comparison obsidians?

Finally, these examinations of the internal homogeneity of CTR obsidians from differing geographical areas (CTD vs. CTN) and the contrasts among the three areas (CDM, CTD, and CTN) enable answering the third and most important question of this section: are CTD obsidians more or less compositionally variable when compared to these nearby obsidian groups? This comparison is best made between CTD and CDM obsidian because these are the two groups in the analysis that have sufficient sample size. Among the trace elements measured with WD-XRF (Table 6-15), high CV values are observed for Cr, Co, Ni, and Cu. Reasons for this variation include differing forms of measurement error, as discussed in Section 6.1, and variation in these elements is not a particularly relevant consideration. In the ED-XRF data, trace elements Sr, Ti, and Mn all have high CV values. Sr can be disregarded because it is too near instrument detection limits. Ti has similar CV values for both CDM and CTD, while Mn more variable in CTD samples than in CDM samples (but not higher than CTN samples). Among major and minor elements, CV values are very high for Fe_2O_3, FeO, MgO, and WD-XRF data (Table 6-20, from Table 6-16) in both the CTD and CDM samples. Total iron is also high for the CDM samples (CV=14.5) and near 10 (CV=9.4) among the CTD samples. In sum, none of the major elements (i.e., SiO_2, Al_2O_3, Na_2O, K_2O) except total iron obtain CV values greater than 2, indicating low variation in major elements.

Table 6-20. Major and minor elements measured by WD-XRF. Data includes only sample size, means, and CV values for CDM, CTD, and CTN (from Table 6-16).

oxide wt%		SiO_2	TiO_2	Al_2O_3	Fe_2O_3	FeO	MnO	MgO	CaO	Na_2O	K_2O	Total Fe
CDM	N	12	12	12	12	12	12	11	12	12	12	12
	Mean	76.29%	0.10%	12.43%	0.61%	0.52%	0.06%	0.08%	0.48%	4.18%	4.56%	1.19%
	CV	0.60	0.73	1.26	**40.41**	**41.27**	1.21	**21.78**	1.10	0.47	0.89	**14.48**
CTD	N	35	35	35	35	35	35	34	35	35	35	35
	Mean	76.23%	0.08%	12.05%	0.53%	0.59%	0.08%	0.05%	0.41%	4.30%	4.35%	1.18%
	CV	0.71	1.69	1.38	**22.31**	**22.02**	1.44	**29.91**	0.99	1.31	1.59	9.39
CTN	N	6	6	6	6	6	6	6	6	6	6	6
	Mean	75.86%	0.08%	12.07%	0.50%	0 .55%	0.08%	0.06%	0.41%	4.33%	4.32%	1.11%
	CV	0.75	1.01	1.86	**13.56**	**11.08**	0.99	8.87	0.98	0.35	0.49	0.93

Magnesium and iron emerge as the most variable compositional constituent in both CTD and CDM samples (and in CTN samples as well). The most interesting facet

of the CV values observed in the WD-XRF (and iron titration analysis) is how much more variable Fe_2O_3 and FeO are compared to Total Fe. This matches with the low CV values for total iron (measured as $Fe_2O_3^T$) in the ED-XRF data (Table 6-14). I also do not know whether this is a product of measurement methods (i.e., where total iron is measured by XRF, whereas the valence states Fe_2O_3 and FeO are measured by titration) or if the variation is real. In these data, CDM samples are more variable than CTD samples, which may be a statistical result of a larger sample size for CTD.

Figure 6-13. XY plot of Fe_2O_3 and FeO values for CDM, CTD and CTN/CTNo samples (data from titration analysis).

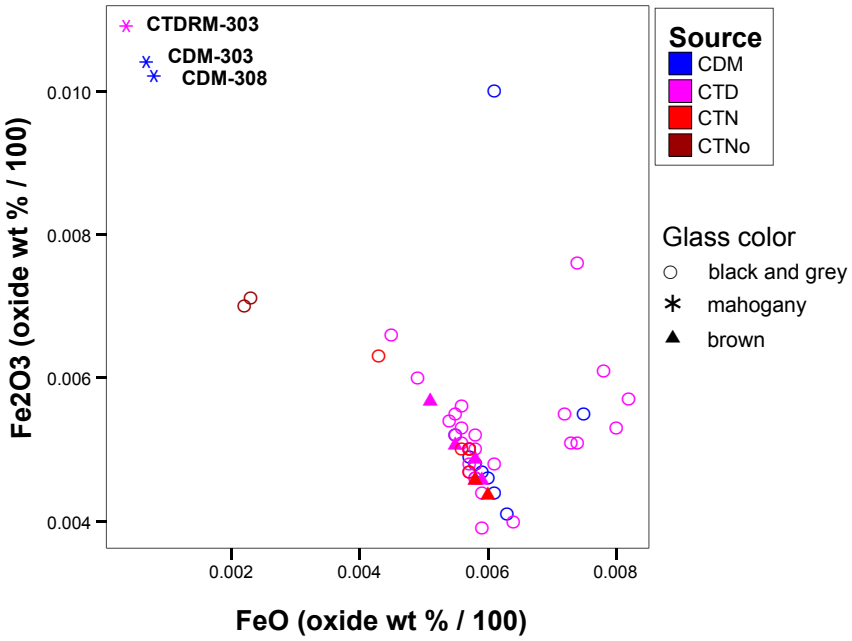

It does appear that a small number of the samples have a large influence in the range of iron values observed: these samples are mahogany colored glasses (CDM-303, CDM-308, and CTDRM-303). As shown as stars in Figure 6-13, the three mahogany samples greatly extend the lower range of FeO and the upper range of Fe_2O_3 for both CDM and CTD. Brown glasses (solid triangles) cluster with the other black and grey samples rather than the mahogany samples. Examination of Figure 6-13 further strengthen the pattern discussed in Section 6.1 for CTD alone, where Fe_2O_3 and FeO are inversely correlated except among those samples scattered on the right side of the graph (high FeO, variable Fe_2O_3).

As with CTD alone, the CDM mahogany samples appear to represent an extreme example of the inverse correlation between Fe_2O_3 and FeO; if so, removing the mahogany samples could lower the overall variation in iron in the source area populations. Table 6-21 demonstrates that removal of the three mahogany specimens does modify the CV values obtained: CV values do drop substantially for Fe_2O_3 and FeO—most dramatically in the case of FeO in the CDM samples. Note however, that Total Fe does not change substantially. In all these results suggest that mahogany samples contribute significantly to the iron variation observed in the CDM and CTD samples measured here. However, even when controlling for the effect of the mahogany samples, obsidians from the CTD and CDM source areas are more variable for iron content (however measured) than for all other major and minor elements. The results also indicate that all of the variation in iron observed here would not be measured by analysis of total iron alone. If valence state of iron content is significant in the response of obsidian to heat, or the process of hydration in obsidian, this variation would only be observed if analysis of Fe_2O_3 and FeO is conducted.

Table 6-21. CV and means for CTD and CDM samples with and without mahogany specimens.

with mahogany specimens					**without mahogany specimens**				
oxide wt%		**Fe_2O_3**	**FeO**	**Total Fe**			**Fe_2O_3**	**FeO**	**Total Fe**
CDM	N	12	12	12	CDM	N	10	10	10
	Mean	0.61%	0.52%	1.19%		Mean	0.53%	0.61%	1.20%
	CV	**40.41**	**41.27**	**14.48**		CV	**32.01**	9.09	**15.44**
CTD	N	35	35	35	CTD	N	34	34	34
	Mean	0.53%	0.59%	1.18%		Mean	0.52%	0.61%	1.18%
	CV	**22.31**	**22.02**	9.39		CV	**13.58**	**14.61**	9.49

In sum, the CTD source area samples are found to be variable for Mg and for iron. As measured by CV, the CTD samples are not more variable than the comparison source samples; CDM samples have CV values that are nearly as high (Mg) or higher (Fe_2O_3, FeO, and Total Fe) for elements for which high CV values were observed. Across the other elements that are well-measured by XRF, only Ti and Mn obtained high CV values and these are higher in CTD than in CDM.

Chapter Summary

1. Trace elements are homogeneous within the CTD deposits indicating that all the deposits in the Dome area are cogenetic.
2. Trace element composition is heterogeneous among the three source locations. Trace elements are similar in the CTD and most of the CTN samples, confirming the geological relationship of the separate geographic locations within the Cerro Toledo Rhyolite. The CDM samples have trace elements that effectively distinguish the Valles Rhyolite (VR) geological unit from the Cerro Toledo Rhyolite geological unit. Two CTN samples, grouped as CTNo, have trace element abundances that are dissimilar to both the CTR and CDM glasses. No geological relationships with CTR and VR can be determined at present for these CTNo samples.
3. Intersource comparison of major and minor elements among the source locations indicates little total rhyolitic variation among all the samples as a group, as expected for obsidians from the same volcanic field. The two CTNo samples have unusual values for some of these elements, further confounding their origin. Comparing CaO and MnO among the source locations, the three groups that are apparent: a) the two CTR obsidians (CTD and CDM), b) CDM, and c) CTNo, conform to the results of the trace elements.
4. Evaluation of internal homogeneity by comparison of CV values indicates higher variation only for MgO and two measures of iron: Fe_2O_3 and FeO. Total Fe has a high CV value only in the CDM samples. Mahogany samples contribute to the variation observed in Fe_2O_3 and FeO, but not in total Fe. Comparison among the source locations indicates that CTD samples are not more variable in iron and MgO, but that sample size differences may affect the comparison.
5. The results obtained for elemental composition will be compared to water content measures in Chapter 8 to evaluate whether variation in volatiles is similar to observed elemental composition variation.

CHAPTER 7
WATER CONTENT ANALYSES:
LOI and FTIR METHODS

Valid determination of water content in glass depends on selecting and developing appropriate techniques for measuring this volatile constituent in obsidian. This chapter provides detailed descriptions of the two methods, LOI and FTIR, used to measure water content in obsidians from the study area. Results obtained in the two water content analyses of obsidian samples from the Jemez Mountains are presented in Chapter 8.

Section 7.1 introduces the two methods used and provides a general discussion of archaeological water content analyses of obsidian. In Sections 7.2 and 7.3, details of how each analysis method was applied in this study are presented, along with information on analysis costs and tradeoffs for archaeological application. The degree of detail included in these sections will be of little interest other than to a practitioner seeking to undertake such analyses or to assess the approach taken in this study. Particular attention is given to FTIR sample preparation, instrument operation, and interpretation of raw data because the current application involved construction of new protocol and because these specifications affect both the feasibility of utilizing FTIR and the accuracy of FTIR results. As a test of my application, I present at the end of Section 7.3 the FTIR results I obtained on calibration standards with known water content (see Appendix C for description of calibration standards). I believe that both LOI and FTIR are techniques that have practical application for archaeologists. The information provided here can be used by archaeologists, or others without a technical background in geochemistry, to assess whether LOI or FTIR might be of use for their research and to gain entry into an unfamiliar literature on the subject.

7.1. Measuring water content in rhyolite glass

I use two methods to measure the water content of obsidian samples from variable sources in the Jemez Mountains. The goals of these analyses are 1) to measure the

amount of water in these glasses, 2) to observe the degree of variation in water content within and among the geochemical sources, and 3) to compare the effectiveness of the alternate techniques for determining obsidian water content, and the practicality of each for use by archaeologists. Unlike geochemical analyses used to measure elemental composition in obsidian, geochemical analyses to measure obsidian water content are not commonly applied or broadly understood by archaeologists. Selecting methods that are both effective for measuring water and appropriate for archaeological applications required some investigation into possible methods available in geology.

As discussed by Ihinger et al. (1994), there are four classes of techniques for measuring volatiles in geological materials: bulk extraction, energetic particle bombardment, vibrational spectroscopy, and phase equilibrium studies. I used two techniques in the current study[1]: loss on ignition (LOI), which is a bulk extraction technique, and Fourier transform infra-red spectroscopy (FTIR), which uses vibrational spectroscopy. Both techniques are appropriate for use on glass, and each employs instrumentation to which I had access or that could readily be conducted by others experienced with their use in obsidian. Briefly, LOI measures water content by heating a sample above 800ºC and measuring water content as the weight lost, while FTIR determines water content by measuring the proportion of light absorbed when transmitted through thin sections of obsidian. Each technique is described in further detail in Sections 7.2 and 7.3, respectively.

The discussion of LOI and FTIR methods in this chapter should be considered not only an explication of the techniques I used but also a consideration of the overall methodology of obsidian water content analyses for archaeological applications. Like geologists, archaeologists need a technique that is replicable on repeated applications and among users, that is inexpensive enough to allow analysis of multiple samples to address variation within and among sample groups, and that is affected least by other variables under consideration (e.g. glass composition). Unlike geologists, however, archaeologists are better served by less destructive techniques, and may not need a technique that

[1] I also employed a third technique, secondary ion mass spectrometry (SIMS), which uses energetic particle bombardment. I encountered problems in my application of SIMS, and therefore excluded this analysis from further discussion in the dissertation. However, I do believe that SIMS is a viable method for successfully measuring water in rhyolitic glasses and should be further explored by archaeologists.

produces results that are extremely precise or that can differentiate among water species. Archaeologists also may prefer a technique that can be undertaken by others, or that involves instrumentation that is readily accessible and is simple enough in application that it may be conducted and interpreted effectively without extensive training in geochemistry.

Archaeological analyses of obsidian water content

Previous archaeological research in obsidian water content is entirely dominated by C. Stevenson and co-workers (Mazer et al. 1991; Stevenson 1994, 2001; Stevenson and McCurry 1990; Stevenson et al. 1993, 1996, 1998, 2000, 2004; see also Stevenson n. d.). A review of his publications charts the path he has taken in seeking a suitable technique for measuring water in obsidian. The earliest study (Stevenson and McCurry 1990) measured H_2O^+ but does not indicate the technique used. LOI was used in the next study (Mazer, Stevenson, Ebert and Bates 1991)[2] with results reported as H_2O. His 1993 study of water content s of obsidian from the Coso range demonstrated a successful use of transmission FTIR to obtain water content values for a large number of obsidian samples (Stevenson et al. 1993). Citing concerns over the accuracy of FTIR in obsidians that are not fully transparent, Stevenson et al. 1996 used FTIR of a few clear samples to calibrate a curve for OH water content and glass density. From this point on, no further studies were made that measured FTIR in large number of geological samples. Three of his next studies employ FTIR to measure OH^-, H_2O, or total water (Stevenson 1994; Stevenson, Knaus, Mazer, and Bates 1993; Stevenson, Mazer, and Sheetz 1998), while two (including his most recent) use FTIR only to calibrate measurement of OH^- and H_2O^+ by density determination (Stevenson 2004; Stevenson, Sheppard, Sutton, Ambrose 1996). Finally, Stevenson provides the first use of photoacoustic infra-red spectrometry (IR-PAS) to measure hydration layers as depth of H_2O in conjunction with SIMS to determine hydration depth profiles (Stevenson 2001) but in this study intrinsic water content, as OH, was measured using the density determination method[3]. In sum, while Stevenson and

[2] Full listings of author names are provided in citations for the remainder of this paragraph so that the participants in each study, and cross-over among studies, can be identified easily.

[3] It is unfortunate that in this analysis of 27 obsidian specimens results of water content obtained by IR-PAS are not reported. The study either missed an excellent opportunity to cross-reference between density and IR methods, or results of this obvious comparison are excluded from the article.

colleagues have demonstrated the utility of transmission FTIR to obtain water content values for unknown obsidian samples (Stevenson et al. 1993), application of FTIR to all samples in a given study was largely abandoned in favor of the simpler density determination as calibrated by FTIR on a few representative samples (Stevenson et al. 1996).

As illustrated in this review, the methodology of Stevenson's studies has been complicated and can be confusing: Stevenson has switched among the variety of techniques discussed above and reports his water measures in a variety of forms: OH^-, OH, H_2O^+, H_2O, and total water. I surmise that much of the reason that Stevenson's work is difficult to use is that the primary goal of all his studies is to develop effective methods for measuring and interpreting obsidian hydration layers. This means that his reporting of water content analysis technique is subordinate to that OHD goal. As a result, it usually is not possible to compare water content results across his different studies and it is virtually impossible to replicate his methods. Except for the one well-reported study in which numerous samples were analyzed by FTIR (Stevenson et al. 1993) only partial information is provided on protocol, and water data is rarely presented at the scale of specimen and usually only in graphs or in tables designed for different purposes (i.e. to support the OH dates determined using water content as one variable among others in a hydration rate equation).

I am not convinced by conclusions expressed repeatedly about the ineffectiveness or inaccuracy of transmission FTIR in non-transparent glasses (Stevenson 2004:560; Stevenson et al. 1996:235, 1998:197). The geochemical study cited most often to support this concern (Newman et al. 1986) did not exclude non-transparent obsidians: "Most were not clear glasses but contained microvesicles and microphenocrysts. A few were banded with layers of clear and cloudy glass, and the latter probably the result of high concentrations of microvesicles" (Newman et al. 1527). A similar study of FTIR analysis of natural obsidians (Zhang et al. 1991) also used glasses with microphenocrysts and bubbles, and reported that this had "no major effect on experimental results" (Zhang et al. 1991:443). As discussed further below, I diminish the potential interfering effects of glass texture by using relative thin FTIR sample plates and by careful selection of FTIR beam locations on samples.

Much of the impetus in developing this dissertation research was to build on the work of Stevenson and colleagues by evaluating effective techniques for measuring water in obsidian. In the sections that follow I have sought to be as clear as possible about my application of the techniques so that they are replicable as well as open to critique. Likewise, in the presentation of results in the Chapter 8, I put forth each step in transforming raw data to interpretable outcomes. Implementing and evaluating the performance of the two analytical techniques I employed, LOI and FTIR, required fine tuning the protocol of FTIR as imported from geochemistry and comparing those results to the simpler LOI technique. The descriptions of methods that follow are detailed and lengthy in part to provide enough information to allow other researchers the opportunity to replicate, modify, or reject specific aspects of each of these techniques.

7.2. Loss-on-ignition (LOI) Analysis Methods

Loss on ignition is a bulk extraction technique that measures the loss of volatile constituents when powdered glass samples are heated to 800ºC. To summarize in simple terms, the glass sample is powdered, the powder is weighed and then heated to 100ºC to drive off adsorbed water (H_2O^-, the water trapped between mineral boundaries), and then weighed again before heating to 800ºC to drive off structural water (H_2O^+, bonded water) along with CO_2 and any organics. Subtraction of weight after final heating from original weight provides the LOI value. Thus "LOI" refers both to the technique for measuring water driven off on heating, and the calculated weight percent lost from an unheated to a heated specimen. As a value, LOI is the computed combined weight of H_2O^- plus H_2O^+ plus CO_2 and organics. In glasses, CO_2 and organics are vastly outweighed by water so that the resulting LOI value is generally treated simply as a measure of total water (here referred to in tables as Total LOI).

LOI sample selection and preparation: Because LOI is a bulk extraction technique that sums across all the volatile constituents of a glass sample, care was taken in selecting and preparing obsidian specimens for use in LOI. Materials with large spherulites and phenocrysts were avoided because these larger particles have the potential to hold more water than the surrounding glass matrix and could bias the water measures toward higher water content. Glass chips submitted for whole rock analysis were

selected from the parts of nodules with fewer large inclusions, and in some cases spherules and large phenocrysts were removed from the glass chips submitted. In some cases it was not possible to avoid all of these larger particles in glass materials. Nodules were broken into flakes and only those flakes from the interior of the nodule were used so as to avoid cortex. In some cases cortical areas were further removed using additional flaking or excision with a diamond saw. Cut or flaked materials were rinsed in tap water before submitting to the chemistry lab.

LOI procedures: The LOI analysis was conducted by J. Husler, Chemistry Laboratory, UNM Department of Earth and Planetary Sciences, on powdered obsidian samples as part of the whole rock analysis discussed in Chapter 6. The following is Husler's description of the material preparation, weighing, and heating techniques he used.

Volatile constituents of water and carbon dioxide were measured by comparing powdered sample weights before and after heating to determine loss-on-ignition (LOI). H_2O values were obtained by subtracting weight after heating from starting weight. The moisture content or absorbed moisture (H_20^-) was determined by weight loss on drying 0.5 g sample one hour in a Pt crucible at 105-115º Celsius. The H_2O^+ (combined moisture plus CO_2 plus organic matter) was determined by heating the sample an additional one hour at 1000º Celsius. That is, the value of H_2O^+ plus CO_2 is determined by adding to the LOI the amount of weight equivalent to the oxygen picked up from the FeO going to Fe_2O_3 at 1000º Celsius (1.1113 x weight of FeO minus original weight of FeO), with the FeO (ferrous iron) having been determined previously by dissolving 0.5 g sample in HF plus H_2SO_4 and titrating with potassium dichromate using sodium diphenylamine as an indicator. All procedures followed Connolly and Husler 1990.

I have some concern over certain aspects of laboratory procedures used in the LOI analysis of my samples. Specifically, Husler's description of analytical methods does not clearly specify the size of powder used in the process. This consideration is important if powders are allowed to adsorb water during the analysis or if stored for extended periods because smaller powders have greater relative surface area than do larger particle sizes. Careful sample handling requires that powders are stored in desiccators, and that weighing and heating are conducted soon after grinding to minimize opportunity for

adsorption (e.g., Newman et al. 1986; Westrich 1987). I feel confident that these handling specifications were followed, especially as I know that the powdering of samples preceded weighing and heating of samples by no more than hours, days, or a few weeks (depending on the sample), and samples were always properly stored in desiccators. However, if samples were ground to differing powder sizes, this could introduce variation in the final LOI results obtained. There may have been problems with variability in powder sizes when my samples were processed due to possible technician errors. It is not certain whether or not this occurred. Husler re-examined all of my samples once alerted to the potential procedural problems and conducted re-analyses in all cases that he determined appropriate. Therefore, while I am fairly confident that the LOI results are accurate, I cannot be completely certain that the results were not affected in some way by inconsistent preparation and handling by the lab technician.

Discussion of LOI: LOI offers a simple method for measuring water content in obsidians. Sample preparation is minimal and there are numerous lab practitioners with experience in its use. As discussed above, problems that can arise during application of LOI include inappropriate powdering of solid samples, use of inconsistent powder sizes, and failure to minimize the time between pulverizing of the glass and heating. The cost of LOI per sample is difficult to identify as it was included as part of the whole-rock analysis offered by the chemistry lab. The total cost for whole-rock analysis was $70 per sample including both LOI and WD-XRF analysis of major, minor, and trace elements. If WD-XRF results are desired in the application, as in this study, the cost of LOI can be considered to be low. The main disadvantage of LOI for archaeological applications is that it requires a relative large amount of material (0.5 to 1.0 g) and is fully destructive. Thus while very appropriate for geological material samples, LOI is not usually suitable for application to artifacts. It might be feasible to use LOI on debitage in cases such as obsidian quarry sites, where debitage is available for destructive analysis because it is both abundant and redundant in an archaeological assemblage. However, prehistoric artifacts with hydration rinds may alter the outcome by adding adsorbed water into the total weight lost (although this could be accounted for by carefully considering the proportions of total water contributed by $H2O^-$ versus $H2O^+$).

Overall, LOI could be considered an ideal technique for archaeologists to use for measuring water if it can be shown to be sufficiently accurate. The accuracy of LOI could not be tested independently here because no samples with known water content were available for LOI analysis. However, in this study, it will be possible to assess the accuracy and precision of LOI outcomes in the Jemez obsidian "unknown" samples by comparing LOI to FTIR results. This comparison will be undertaken in Chapter 8.

7.3. Fourier Transform Infra-Red Spectroscopy (FTIR) Analysis Methods

Infra-red spectroscopy is a vibrational spectroscopic technique that is well-established in geology for quantitative measurement of volatiles in silicate glasses (as discussed in Ihinger et al. 1994:71-73, 91-112). While Fourier transform infra-red spectroscopy (FTIR) is a less accurate method for measuring total water content compared to bulk techniques such as K-F titration and vacuum extraction, FTIR is highly suitable for measuring the concentrations of different water species (i.e., distinguishing between OH and H_2O).

There are two kinds of infra-red (IR) spectrometry: reflective and transmission IR techniques. In this study I employ transmission FTIR. Transmission IR spectrometry is well-known and used often for measuring water in glasses (e.g., Ihinger et al. 1994; King et al. 2002; Newman et al. 1986; Silver and Stolper 1989; Stolper 1982; Zhang et al. 1997). At present, reflective IR spectrometry for measuring water in low-water rhyolite materials is only experimental but has been demonstrated to work for CO_2 (Moore et al. 2000)[4].

Transmission IR spectroscopy works by passing a beam of infrared light through a thin glass sample of known thickness. In simple terms, water molecules in the glass are excited by energy at specific wavelengths in the infrared region of the spectrum causing absorbance. The beam is collected on the other side of the sample by a detector and any reduction in transmitted light intensity is the measured absorbance. Fourier transform IR spectrometers use an interferometer to compare a split light beam where one beam is directed through the sample; the difference in wavelengths received by the beam that

[4] It is possible that reflective FTIR could be a viable technique for obsidian artifacts (G. Moore, personal communication 2003). If so, it would have a great advantage over transmission FTIR for archaeological applications if it could be used directly on unaltered artifacts.

passes through the sample and the blank spectrum is an FTIR spectrum, specified to the spectral range used to measure water (Ihinger et al. 1994: 01-102). In the current application an IR microscope was used to focus the measured area on small areas of the obsidians samples (~3 – 5 mm).

For measuring water content in obsidian, FTIR offers the advantages of rapidity of measurement and concomitant minimization of instrument time and potential low cost. Also, it should be possible in the future to use FTIR directly on the same thin-sections removed for an obsidian hydration analysis. Finally, FTIR is a method that Stevenson has used (e.g., Stevenson et al. 1993, as discussed in Section 7.1): employing FTIR in my study provides continuity and comparison with the existing archaeological literature, and allows objective assessment of the strengths, weaknesses, and tradeoffs in using this technique.

The main drawback of the transmission IR technique is that it requires that a small cut sample be removed from the specimen (i.e., similar to obsidian hydration sample preparation), and involves double-sided polishing of parallel-sided glass chips. Sample preparation for transmission FTIR is always labor intensive or costly because it requires a high polish and precise control of sample thickness.

In sum, the most useful aspect of the FTIR technique for archaeologists is the ease, rapidity, and potential low-cost of the technique. In my application, I found that while use of the FTIR instrument is in fact easily learned, rapid, and inexpensive, the technique poses substantial difficulties and costs in sample preparation and in the processing and interpretation of raw data.

FTIR analysis of calibration standards and obsidian "unknowns"

FTIR sample preparation: FTIR sample preparation is very similar to the requirements of fluid inclusion sample preparation and requires double polished thin-sections. For the calibration standards, double polished thin sections were prepared by D. Mann, High Mesa Petrographics, by mounting into the glass chips into epoxy blocks to grind and polish one side before cutting into plates, then removing the surrounding epoxy from around the glass before cutting the final thin-section to a standard thickness. The sections were mounted as cut plates onto glass slides using Super glue, then ground and

polished on the second side. Both sides have a final finish of 0.05 microns. Super-glue is used for mounting to avoid heated adhesives and to ease removal of thin-sections from glass slides. Removal was achieved by soaking in acetone for up to 24 hours.

Geological obsidian samples from CTD, CTN, and CDM were prepared either by Mann, as above, or by Q. Sahratian at the Sample Preparation & Thin Section Laboratory, College of Mines and Earth Sciences, University of Utah by cutting a slice of the glass from samples chips I sent to him. Sahratian's preparation of the double polished thin-sections methods matched those of Mann, except that he cut a thin-section, polished the first side on a slide (rather than mounting in epoxy), then flipped the single-polished section to polish the second side. One difficulty encountered by this sample preparer was that the high polish on the samples made secure adhesion difficult, even with the use of Super glue. Because the glass plates were eventually to be removed from the slide to conduct FTIR analysis, the poor adhesion did not pose a problem for the current application.

The cost of this kind of sample preparation is relatively high compared to standard thin-section preparation. For preparation of the calibration standards (Mann), I paid $28.50 per sample for preparation of the calibration standards specimens. For preparation of the geological samples, Sahratian offered a much lower cost ($19 per sample) with comparable quality for preparation of the obsidian "unknowns". Preparation of the standards and unknowns is virtually the same, with the only discernible difference found in the more variable thickness in Sahratian's samples. It may be that Sahratian's poor control of thin-section thickness was due to not using the epoxy-mounting step that Mann used.

Thickness of FTIR sample plates: The usual approach to measuring water content in silicates would prescribe varying the plate thicknesses depending on the known or expected water content in the glass. In simple terms, the lower the concentration of water, the thicker the sample should be. The goal is to have a thin-section that is thick enough to allow light passing through the glass to be detected correctly where there are low water contents but not too thick so as to swamp detection on samples with higher water content. Setting multiple sample thicknesses was not appropriate for this study as this requires

foreknowledge of expected water contents, and thus imposes what may an unrealistic requirement for archaeological applications of the technique.

Therefore, working with Dr. G. Moore, Department of Chemistry and Biochemistry, Arizona State University, a standardized approach was devised for archaeological applications. We chose a sample plate thickness range of 150 to 180 microns (0.15 -0.18 mm) as a standard glass thickness appropriate for moderate to slightly higher rhyolite glass water content. Based on the available preliminary LOI analyses (which at that time were 0.6 to 1.8 wt % H_2O+ for Cerro Toledo and 0.3 wt % H_2O+ for Cerro del Medio obsidians), I estimated that the anticipated range of water contents was between 0.2 and 2.0 wt % H_2O+. Thus, we aimed for a plate thickness appropriate for the middle to upper end of that water range (e.g. 0.5 to 2.0 wt %). The motivation for this approach is that for this study it is most important first to accurately measure water above about 0.5%, and second to establish the upper limits of water content. Precise measurement below 0.5% is not needed as this can simply be considered very low water. Using these specifications, reporting of results would indicate, for example, that a specific low-water sample had "no greater than 0.5%" water, while another high-water sample had precisely "1.24 wt %" water. In other words, with the thickness selected there is a sacrifice of precision and accuracy on the low-water end in favor of reliability, precision, and accuracy on the high-water end for water contents above the specified threshold of 0.5%.

Another consideration in my selection of plate thickness is a concern, discussed earlier in this chapter, that non-transparent obsidians are inappropriate for transmission FTIR (Stevenson et al. 1993, 1996, 1998). However, I note that where sample thickness was reported in those studies (Stevenson et al. 1993:374; Stevenson et al. 1998:197) the FTIR plate thickness used was 1 mm. My use of substantially thinner plates (≤ 0.37 mm) decreases but does not eliminate the potential for interference of such inclusions. The plate thicknesses I use are similar to or less that those used in experiments (Newman et al. 1986:1535, Table 6; Zhang et al. 1991:443) in which good results were achieved in obsidians with microphenocrysts and bubbles.

Plate thicknesses of the calibration standards (prepared by Mann) were measured by G. Moore using a handheld digital micrometer. Average thicknesses in the calibration

standard plates range from 146 μ to 189 μ. However, plate thicknesses of the Jemez obsidian samples (prepared by Mann or by Sahratian) were much more variable than I requested from the two sample preparers. Thickness was estimated by averaging three measures from each plate taken in microns using a handheld Starrett No. 734 digital micrometer (courtesy of R. Loehman, Advanced Materials Lab, Sandia Laboratories). The samples prepared by Mann are more uniform (varying from 172 μ to 213 μ in average thickness), while those prepared by Sahratian are highly variable and range from 87 μ to 369 μ. I do not know why the preparation of these plates resulted in so much variation in thickness, but it may be that mounting the chips in epoxy for the first polish and then cutting the plate from the epoxy block allowed for greater control of thickness prior to the second polish.

For my application, which benefits from minimizing variation wherever possible, variable plate thicknesses are not ideal but do not compromise the analysis. In the calibration standards, the range of thickness is relatively low and suitable for the predetermined water contents (0.65% to 4.50%) although the thickness selected is high (i.e. thick) for water contents on the upper end of this range. For the unknowns where the range of plate thickness is substantially greater and where water contents were not known in advance, plate thicknesses at the higher and lower ends of the range could pose a problem if those samples have very low or very high water contents, respectively. A low-water sample that is on the thinner end (e.g. with a thickness of <100 μ) could produce absorbances that are very low. Conversely, a high water sample that is thicker could produce absorbances that are very high. The range of thickness in the twenty Jemez obsidian samples selected for the FTIR analysis is 175 μ to 369 μ which is a suitable range for the expected water contents using the absorbance peaks at 4500 cm^{-1} and 5200 cm^{-1}. Most importantly, the calculation of water content for each sample specifies the individual thickness of that plate, so overall variation does not affect the accuracy for a given plate.

Operation of the micro-FTIR instrument for analysis of obsidian water content: FTIR analysis was conducted by the author at Arizona State University (ASU), Center for Solid State Science (CSSS), with the assistance of G. Moore and S. Whaley (FTIR lab manager). The FTIR instrument work was conducted during two sessions. Analysis of

the seven calibration standards was conducted during the first session, June 12 – 13, 2003. Analysis of the 21 obsidian samples (unknowns) was conducted during the second session, November 18 – 20, 2003.

Analysis of each specimen takes approximately 20 - 30 minutes. However, with other setup and preparation activities the total average time per specimen was about one hour. With FTIR instrument time charged at $35/hour, and the added cost of plate preparation, the average cost per specimen was about $55/sample. With a larger number of samples and greater operator experience, this cost probably could be decreased to closer to $35/sample.

The FTIR spectrometer at ASU is a Bruker IFS 66 V/S bench-top Fourier transform IR spectrometer with evacuated optics. The instrument operates under <3 mbar vacuum with a high throughput Michelson interferometer with automatic alignment, a Kbr beamsplitter (Red) with a range of 7500-370 cm^{-1}, and a liquid nitrogen cooled MCT detector. Micro-FTIR analysis of all samples was conducted using an IR scope II microscope, with aperture set at 2.1. OPUS/IR software was used to operate the instrument and to create data output files. During analysis of the calibration standards, data was saved for 8000-600 cm^{-1} and each spectra was obtained with 64 scans. During analysis of the obsidian unknown samples, data was saved for 6000-600 cm^{-1} and each spectra was obtained with 128 scans. There is little difference between these two configurations; in the second session the number of scans was increased to improve data stability and accuracy, and the upper end of the spectra was truncated because values between 8000 and 6000 cm^{-1} would not be used in this water content analysis.

Micro-FTIR instrument analysis of each specimen involves placing the cleaned sample on a standard size holder in the microscope. For the calibration standards (which are smaller) the round opening in the holder is just less than 3 mm; for the larger unknown obsidian samples the opening is 5 mm. The optics on the microscope are used to examine the glass in the light path in order to avoid surface imperfections, as well as bubbles and microlites in the body of the glass. The latter was largely irrelevant in the synthesized glass standards, which have almost no inclusions and few bubbles. Five to eight locations were analyzed on each calibration standard with usually two replicates at each location.

In the natural obsidian unknown samples, seeking locations without obstructions was a significant part of the analysis process, and contributed substantially to the time needed per sample. The best possible locations were selected to have the least interference in the light path. Few of the obsidian specimens were found to have bubbles but many had microlites and a few have phenocrysts or other inclusions. Avoiding microlites in bands, swirls, and clusters was often difficult to achieve. In most cases it was possible to find relatively obstruction-free locations but for a few samples this was not possible. Careful notes were taken for each analysis location in order to account for the possible effect of obstructions. At least three locations were analyzed on each of the obsidian samples, with locations widely spaced across the specimen. Usually two replicates were taken at each location.

The OPUS/IR software functions by comparing a measured background (a blank spectrum recording how the instrument detects and collects the light transmission) to each sample reading (the FTIR spectrum with the specimen in the beam path). During both sessions the background was analyzed periodically--usually every hour or so. Background readings were taken by removing the sample holder from the microscope and taking a reading through air. Repeated and frequent background measures improve accuracy by accounting for any alteration in ambient moisture and temperature in the lab.

Processing and interpretation of FTIR analysis results: Output from each FTIR measurement consists of a text file with x and y coordinates to describe the curves and peaks along the resulting FTIR spectrum. To produce the graphic image of the spectra, text files were imported into a spreadsheet program (Excel) and then plotted as a line graph of the more than 3800 x-y coordinates in each file. Figures 7-1 & 7-2 show representative arrays for the seven calibration standards. In both of these graphs the spectra are normalized to plot systematically together on a single graph. In the first graph (Figure 7-1) the spectra for each standard are stacked to allow a good view of the shape of curves in each; the y-axis is left unlabelled.

Figure 7-1. Comparison of FTIR spectra, stacked to show peaks.

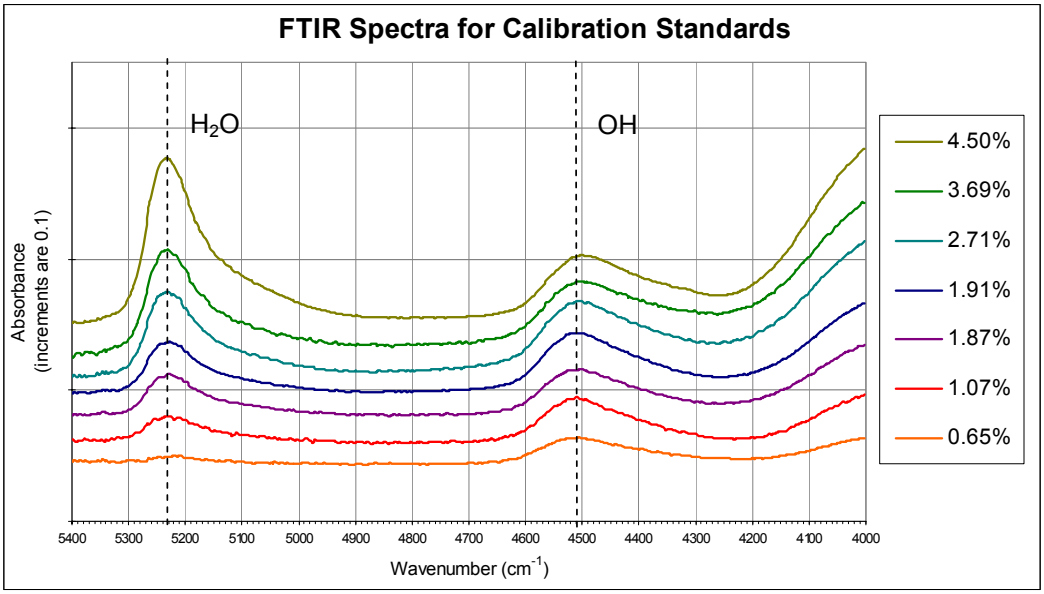

In the second graph (Figure 7-2) the spectra are placed in a similar position on the y-axis. Here the y-axis is labeled for increments of actual absorbance (A) and the relative relationships between peaks in each spectra can be compared.

Figure 7-2. Comparison of FTIR spectra showing actual absorbances.

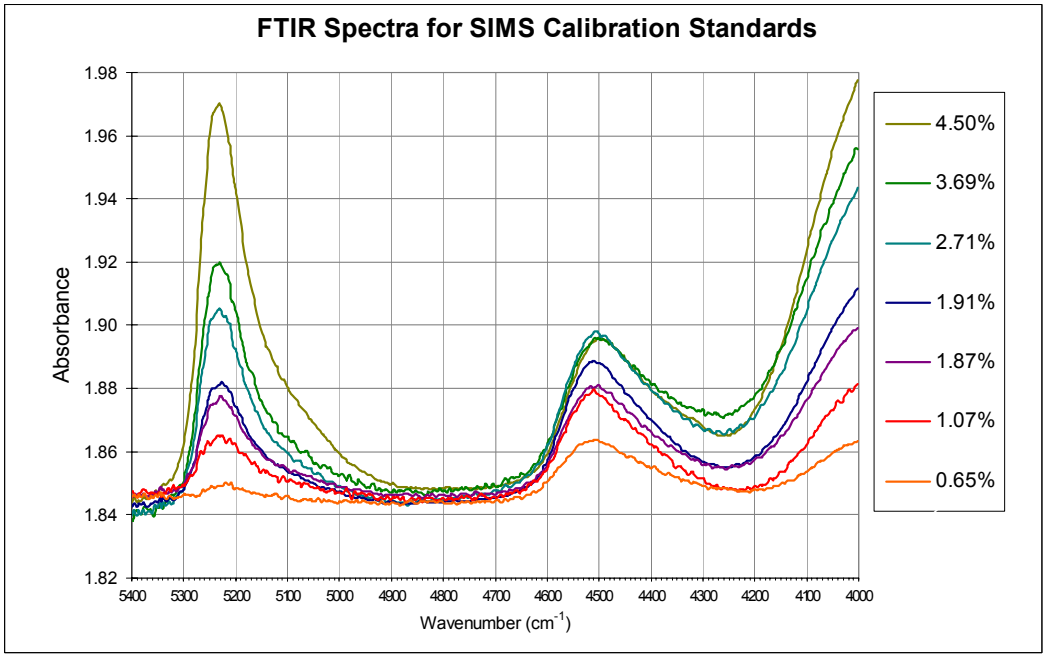

These graphs show only the array from 4000 to 5400 cm^{-1} because the absorbance peaks used for measuring water content in this study are at 4500 cm^{-1} and 5200 cm^{-1}. For these specimens, the actual peak locations are at about 4500 - 4510cm^{-1} and 5210 - 5230 cm^{-1} (shown as vertical dotted lines in Figure 7-1). The 5200 cm^{-1} peak is used to measure concentration of molecular water species dissolved in the glass (H_2O), and the 4500 cm^{-1} peak is used to measure OH, the hydroxyl concentration (see Table 7-1 below, from King et al. 2002:1084; also Ihinger et al. 1994:107). The combination of H_2O and OH describe the total water content in the glass. For this analysis, these peaks are used because they are well expressed for the sample thicknesses selected.

Table 7-1. Identification of wavenumber and water species investigated by transmission FTIR in this study (table follows King et al. 2002:1084, Table 4).

Wavenumber	Absorption band	Species	Vibration mode	Extinction coefficients (ε) used in this study (IS)*	Extinction coefficients (ε) alternate (NSE)**
4500	2.22µm	hydroxyl OH	Si-OH Al-OH	1.50	1.73
5200	1.91µm	molecular H_2O_{mol}	O-H stretch H-O-H band	1.86	1.61

*Ihinger & Stolper 1994 (in Ihinger et al. 1994:105,Table 2)

**Newman et al. 1986 (in Ihinger et al. 1994:105,Table 2)

Comparison among the shape and height of peaks in Figures 7-1 and 7-2 illustrates the relationship between H_2O and OH at differing total water contents. First, note how the spectra rise on the right side the graph with increasing water content; this is caused by peaks (off the graph) at 4000 cm^{-1}. Second, note that for the lowest water content (0.65%) the H_2O peak at 5200 cm^{-1} is lower than the OH peak at 4500 cm^{-1}, while with increasing water content this relationship is reversed. This demonstrates the expected relationship between H_2O and OH with increasing water content (McMillan 1994; Newman et al. 1986; Silver et al. 1990; Zhang et al. 1991). Compared to OH, H_2O content is relatively low in glasses with 1.0% or less total water content; with increasing total water content above 1.0%, the proportion of H_2O rises while OH remains more constant. This relationship between OH and H_2O is demonstrated at the end of this section with the results obtained for these calibration standards (Figure 7-6).

Determining water content from analysis of these spectra is not as straightforward as obtaining a simple single value from instrument output. The process involves measuring the difference between the background and the height of a peak, then using an

equation for calculation of species concentration. Use of the calibration equation is simple (see below), but judging by the available discussion of the techniques (Ihinger et al. 1994; Newman et al. 1986; King et al. 2000; Zhang et al. 1997) measuring peak height and subtracting background appears to be as much an art as a science. The general approach is to produce graphic images of the absorbance peaks (as in Figure 7-3) and then to use French curves to fit the baseline shape against adjacent peaks, then measure on the graphs the actual height of the peak from the baseline.

Figure 7-3. Illustration of peak measurement using 0.65% & 2.71% standards.

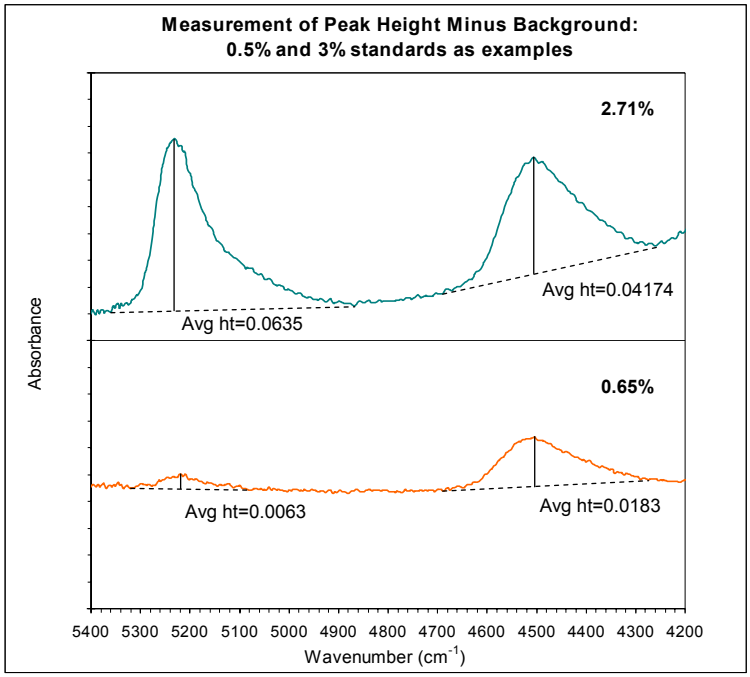

I found this graphic approach to be awkward, prone to imprecision, and unacceptably time-consuming. When measuring peak height for numerous samples with repeated measures, as in my study where analysis of 7 standards (n=70) and 21 unknowns (n=158) resulted in 228 arrays to be analyzed, the graphic approach is daunting to the point of inducing abandonment of FTIR. I suspect that where FTIR is used frequently and for measuring numerous samples, there either is some other technique available of which I am unaware, or the investigators are using the OPUS/IR software in a manner that makes it a more productive application.

I created a modified method that is not inherently graphic but seems to be as effective as the graphic approach and is far more efficient. All the arrays for a given standard or sample were imported into a single (Excel) spreadsheet with rows aligned; this places each x-value (wavelength) for each standard or sample on the same row in the spreadsheet (with the different arrays as the columns). The following process is summarized in Table 7-2 using the 0.65% and 2.71% standards as example arrays, as shown in Figure 7-3.

Table 7-2. Calculation method used for measuring FTIR peak heights.

		0.65% standard	***2.71% standard***
Goal	**Calculation**	**5200 cm^{-1}** H_2O (actual peak is 5210 - 5230 cm^{-1})	**5200 cm^{-1}**
Define left base of curve	Lowest point between 5400 and 5240	0.84491	0.90978
Define peak	Highest point between 5400 and 4900	0.85032	0.97539
Define right base of curve	Lowest point between 5220 and 4900	0.84313	0.91400
Determine arithmetic midpoint of baseline	Average of the two low points	0.84402	0.91189
Subtract midpoint of baseline from peak.	Highest point minus the average low point	0.00630	0.06350
Goal	**Calculation**	**4500 cm^{-1}** OH (actual peak is 4500 - 4510cm^{-1})	**4500 cm^{-1}**
Define left base of curve	Lowest point between 4700 and 4501	0.84383	0.91749
Define peak	Highest point between 4700 and 4200	0.86384	0.96821
Define right base of curve	Lowest point between 4500 and 4200	0.84717	0.93545
Determine arithmetic midpoint of baseline	Average of the two low points	0.84550	0.92647
Subtract midpoint of baseline from peak.	Highest point minus the average low point	0.01834	0.04174

I used a simple calculation formula to determine each y-value (absorbance) at the low points that define the base of each peak and at the peak (Figure 7-4). The two low points are then averaged to determine the arithmetic mean; this serves as a proxy for the baseline at the x-value of the peak (as described graphically in Figure 7-4 as the intersection of the vertical solid line with the dashed baseline). Subtracting the average

of the two low points from the height of the peak produces a measurement of the peak minus the baseline, which equals the height of the peak minus the background.

This approach appears to be equivalent to measuring from a straight line at the base as compared to using a French curve, which for these curves seems to be appropriate (see King et al. 2002 for discussion of other peaks where the French curve may be superior to use of a straight line). Using this calculation method, it is a relatively rapid process to obtain the height of the two peaks minus background for each of the text files imported from the OPUS/IR software.

Figure 7-4. Details of calculation method for measuring peak height minus background, using 2.71% calibration standard at 5200cm^{-1} H_2O peak as example.

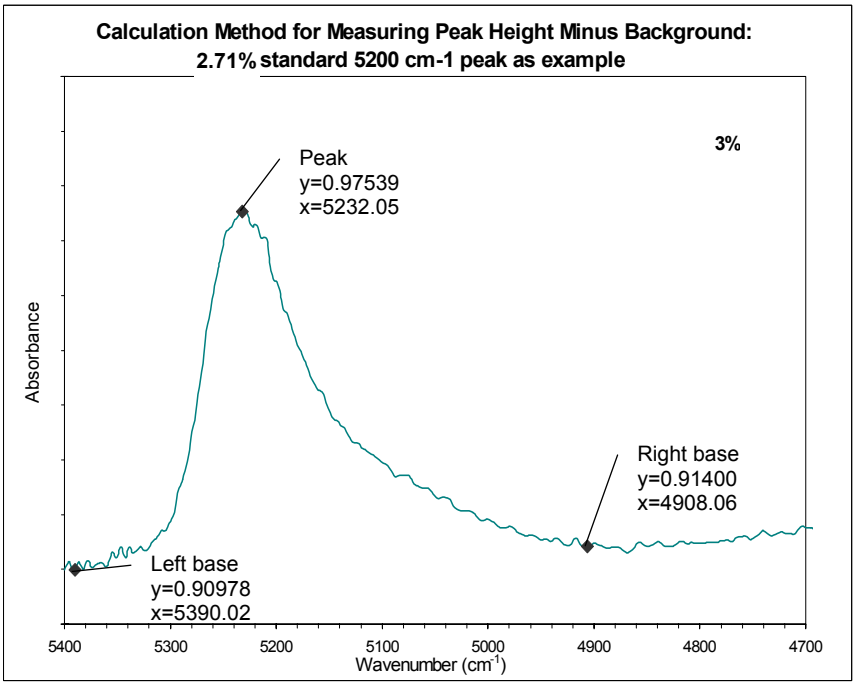

Calculation of water content from FTIR peak height: Calculating water species concentration from these results requires application of the following formula from Ihinger et al. 1994 (p. 107, Equation 15):

$$c = \frac{18.02 \times A}{d\rho\varepsilon}$$

solving for water content (c) as weight per cent H_2O contained within the glass, where absorbance (A) is measured as the maximum peak height after background subtraction, divided by the product of sample thickness in cm (d) and density in g/L (ρ), multiplied by

the extinction coefficient (ε) which is molar absorptivity in L/mol cm. Calculation of this formula is the step at which water content is computed, with A as the critical variable derived from the array produced by the FTIR instrument and OPUS/IR software. I conducted this calculation for A at the 4500 cm^{-1} and 5200 cm^{-1} bands, to obtain H_2O and OH concentrations, respectively, and then summed the results for total water content (Ihinger et al. 1994:108). My calculations are shown in Table 7-3 with the average total calculated water content (H_2O plus OH) shown in the far right column; un-averaged calculations are listed in Table 7-5.

Table 7-3. Averaged FTIR results and calculation of water content for seven standards.

FTIR results and calculation of water content for seven calibration standards (using **ε** from IS 1994)												
K-F total water	n	avg A 5230	avg A 4500	Thick (***d***) cm	Density (**ρ**) g/L	molar absorb (**ε**) for 5200	c 5200 (H_2O)	molar absorb (**ε**) for 4500	c 4500 (OH)	Avg calc H_2O conc from 5200	Avg calc OH conc from 4500	Avg comb H_2O plus OH
0.65%	3	0.006	0.020	0.01775	2303.4	1.86	0.0015	1.5	0.0060	0.15%	0.60%	0.75%
1.07%	10	0.021	0.033	0.01885	2314.6	1.86	0.0047	1.5	0.0092	0.47%	0.92%	1.39%
1.87%	10	0.031	0.030	0.01460	2289.5	1.86	0.0089	1.5	0.0107	0.89%	1.07%	1.96%
1.91%	9	0.040	0.040	0.01875	2282.5	1.86	0.0090	1.5	0.0112	0.90%	1.12%	2.02%
2.71%	5	0.063	0.041	0.01745	2270.7	1.86	0.0153	1.5	0.0124	1.53%	1.24%	2.77%
3.69%	13	0.080	0.037	0.01595	2255.7	1.86	0.0215	1.5	0.0125	2.15%	1.25%	3.40%
4.5%	3	0.125	0.039	0.01560	2229.8	1.86	0.0347	1.5	0.0134	3.47%	1.34%	4.81%

To obtain these results I made a series of decisions about, or manipulations of, each of the variables. **Absorbance** (A) is obtained from the interpretation of FTIR results for selected peaks (as described above). Sample **thickness** (*d*) is the average of three thickness measures across each standard plate.

Density (ρ) can be calculated from elemental composition, which I did using a complicated spreadsheet sent to me by G. Moore and devised by S. Newman. Newman's calculation uses eight elements (SiO_2, TiO_2, $Al2O_3$, FeO, MgO, CaO, Na_2O, and K_2O, which I had obtained from EPMA) plus H_2O to determine density. The density values I calculated for the seven standards (using Westrich's K-F values for H_2O) ranged from 2229.8 to 2314.6 g/L, as shown in Table 7-3.

Obviously, using known H_2O in the density calculation is circular where the goal is to measure water content. However, while I used the K-F titration water contents as reported by Westrich in the calculations shown in Table 7-3, I also checked to see how much the obtained outcomes differed depending on the H_2O value used in each calculation. In Table 7-4 I demonstrate how the results would have changed in density calculations if H_2O is set at extreme values of 0.01% and 10% for each standard. Clearly, while density does influence the final derived FTIR water content results, that influence is marginal within the goals of this analysis (e.g. variation for the 2% standard is no more than 10%). The error of using reported K-F water content values for calculation of density would have to be as high as the errors demonstrated in Table 7-4 (i.e. using 0.01% H_2O where 4.50% was correct, or 10% H_2O where 4.50% was correct) to substantially affect the outcome.

Table 7-4. Comparison of FTIR outcomes with differing values of density (ρ)

Standard	(Actual) FTIR combined H_2O + OH using obtained densities with K-F values for H_2O (**as in Table 7-3**)	(Hypothetical) FTIR combined H_2O + OH with density (ρ) set at value obtained with **H_2O at 0.01%**	(Hypothetical) FTIR combined H_2O + OH with density (ρ) set at value obtained with **H_2O at 10%**
0.65%	0.75%	0.74%	0.78%
1.07%	1.39%	1.38%	1.45%
1.87%	1.96%	1.94%	2.05%
1.91%	2.02%	2.00%	2.11%
2.71%	2.77%	2.73%	2.87%
3.69%	3.40%	3.32%	3.51%
4.5%	4.81%	4.64%	4.91%
Extinction coefficients used in these calculations are from Ihinger and Stolper 1994 (in Ihinger et al. 1994)			

The final variable in the equation, the **extinction coefficient** (ε), is specific to the band being measured and varies by the chemical composition of the sample. Different values for (ε) would be appropriate for rhyolites, andesites, and basalts. Values for (ε) have been developed for rhyolitic glasses (e.g. Newman et al. 1986) as a calibration process that compares FTIR results to known water values obtained through an independent method. The values for (ε) that I use ("IS": 1.86±0.05 for the 5200 cm^{-1} peak, and 1.50±0.05 for the 4500 cm^{-1} peak) are from Ihinger and Stolper 1994 (in Ihinger et al 1994, Table 2, p. 105), which is the most up-to-date reference for rhyolitic

glass I was able to find in the literature. I compared results (Table 7-5, far right columns) between the Ihinger and Stolper 1994 coefficients and the Newman et al. 1986 extinction coefficients (1.61±0.05 for the 5200 cm^{-1} peak, and 1.73±0.02 for the 4500 cm^{-1} peak). Results varied by 15% or less in the 0.65% to 1.91% standards, but were much more variable in the standards 2.71% and above. The differences in results with each set of coefficients is between calculated H_2O and OH values, which tend to cancel each other out for combined H_2O & OH in standards with 2.71% or less water. For most summaries, I will use the Ihinger and Stolper 1994 coefficients.

Comparison of H_2O and OH in the calibration standards: Results obtained for the seven calibration standards conform to the expected relationship between the water species OH and H_2O with increasing total water content, as discussed above regarding Figure 7-2. In Figure 7-5, the bars represent weight percent of OH and H_2O, while the symbol-line plots total water content. Above 1% total water content, OH weight percent does not increase while H_2O continues to increase, illustrating that H_2O is the water species that contributes most to the total water content above ~2% total water.

Figure 7-5. Comparison of OH and H_2O concentrations in standards with differing total water content.

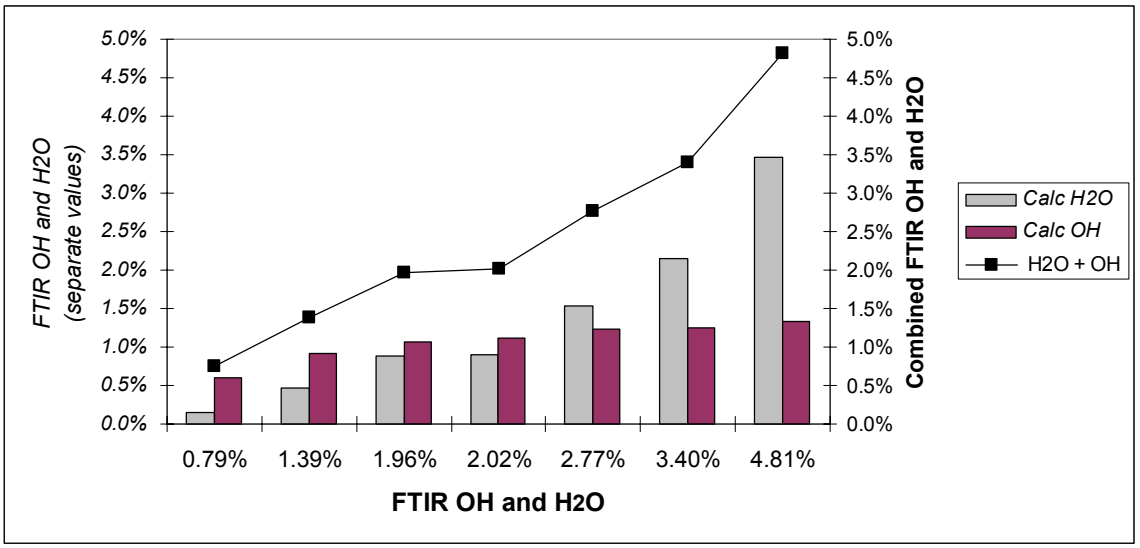

Table 7-5. Un-averaged FTIR data for calibration standards, showing calculations using extinction coefficients from Newman, Stolper, and Epstein. 1986 (NSE) and from Ihinger and Stolper 1994 (IS)

Table 7-5. Un-averaged FTIR data for calibration standards using differing extinction coefficients						Newman et al. 1986 (NSE) extinction coefficients					Ihinger & Stolper 1994 (IS) extinction coefficients					Difference between NSE and IS outcomes		
Calib Stand	Location	A 5200	A 4500	Thick (*d*) cm	Density (ρ)	(ε) at 5200	(ε) at 4500	NSE H_2O at 5200	NSE OH at 4500	NSE H_2O & OH	(ε) at 5200	(ε) at 4500	IS H_2O at 5200	IS OH at 4500	IS H_2O & OH	Diff NSE – IS H_2O	Diff NSE – IS OH	Diff NSE – IS H_2O & OH
0.65%	MV22-5-1-0	0.0063	0.0183	0.01775	2303.4	1.61	1.73	0.17%	0.47%	0.64%	1.86	1.5	0.15%	0.54%	0.69%	0.02%	-0.07%	-0.05%
0.65%	MV22-5-4-1	0.0068	0.0220	0.01775	2303.4	1.61	1.73	0.19%	0.56%	0.75%	1.86	1.5	0.16%	0.65%	0.81%	0.02%	-0.09%	-0.06%
0.65%	MV22-5-4	0.0058	0.0202	0.01775	2303.4	1.61	1.73	0.16%	0.51%	0.67%	1.86	1.5	0.14%	0.59%	0.73%	0.02%	-0.08%	-0.06%
0.65%	MV22-5-3-2	0.0067	0.0218	0.01775	2303.4	1.61	1.73	0.18%	0.55%	0.74%	1.86	1.5	0.16%	0.64%	0.80%	0.02%	-0.09%	-0.06%
0.65%	MV22-5-3-1	0.0066	0.0221	0.01775	2303.4	1.61	1.73	0.18%	0.56%	0.74%	1.86	1.5	0.16%	0.65%	0.81%	0.02%	-0.09%	-0.06%
0.65%	MV22-5-3-0	0.0067	0.0220	0.01775	2303.4	1.61	1.73	0.18%	0.56%	0.74%	1.86	1.5	0.16%	0.65%	0.80%	0.02%	-0.09%	-0.06%
0.65%	MV22-5-2-2	0.0059	0.0203	0.01775	2303.4	1.61	1.73	0.16%	0.52%	0.68%	1.86	1.5	0.14%	0.60%	0.74%	0.02%	-0.08%	-0.06%
0.65%	MV22-5-2-1	0.0061	0.0204	0.01775	2303.4	1.61	1.73	0.17%	0.52%	0.69%	1.86	1.5	0.14%	0.60%	0.74%	0.02%	-0.08%	-0.06%
0.65%	MV22-5-2-0	0.0058	0.0202	0.01775	2303.4	1.61	1.73	0.16%	0.51%	0.67%	1.86	1.5	0.14%	0.59%	0.73%	0.02%	-0.08%	-0.06%
0.65%	MV22-5-1-2	0.0061	0.0179	0.01775	2303.4	1.61	1.73	0.17%	0.46%	0.62%	1.86	1.5	0.14%	0.53%	0.67%	0.02%	-0.07%	-0.05%
0.65%	MV22-5-1-1	0.0066	0.0179	0.01775	2303.4	1.61	1.73	0.18%	0.46%	0.64%	1.86	1.5	0.16%	0.53%	0.68%	0.02%	-0.07%	-0.05%
1.07%	MV22-2A-2-1	0.0200	0.0332	0.01885	2314.6	1.61	1.73	0.51%	0.79%	1.30%	1.86	1.5	0.44%	0.91%	1.36%	0.07%	-0.12%	-0.05%
1.07%	MV22-2A-3-0	0.0214	0.0361	0.01885	2314.6	1.61	1.73	0.55%	0.86%	1.41%	1.86	1.5	0.48%	0.99%	1.47%	0.07%	-0.13%	-0.06%
1.07%	MV22-2A-3-1	0.0227	0.0349	0.01885	2314.6	1.61	1.73	0.58%	0.83%	1.42%	1.86	1.5	0.50%	0.96%	1.47%	0.08%	-0.13%	-0.05%
1.07%	MV22-2A-3-2	0.0223	0.0368	0.01885	2314.6	1.61	1.73	0.57%	0.88%	1.45%	1.86	1.5	0.50%	1.01%	1.51%	0.08%	-0.13%	-0.06%
1.07%	MV22-2A-5-0	0.0203	0.0322	0.01885	2314.6	1.61	1.73	0.52%	0.77%	1.29%	1.86	1.5	0.45%	0.89%	1.34%	0.07%	-0.12%	-0.05%
1.07%	MV22-2A-5-1	0.0199	0.0316	0.01885	2314.6	1.61	1.73	0.51%	0.75%	1.26%	1.86	1.5	0.44%	0.87%	1.31%	0.07%	-0.12%	-0.05%
1.07%	MV22-2A-5-2	0.0196	0.0323	0.01885	2314.6	1.61	1.73	0.50%	0.77%	1.27%	1.86	1.5	0.43%	0.89%	1.32%	0.07%	-0.12%	-0.05%
1.07%	MV22-2A-6-0	0.0217	0.0335	0.01885	2314.6	1.61	1.73	0.56%	0.80%	1.36%	1.86	1.5	0.48%	0.92%	1.40%	0.07%	-0.12%	-0.05%
1.07%	MV22-2A-6-1	0.0215	0.0336	0.01885	2314.6	1.61	1.73	0.55%	0.80%	1.35%	1.86	1.5	0.48%	0.92%	1.40%	0.07%	-0.12%	-0.05%
1.07%	MV22-2A-6-2	0.0220	0.0332	0.01885	2314.6	1.61	1.73	0.57%	0.79%	1.36%	1.86	1.5	0.49%	0.91%	1.40%	0.08%	-0.12%	-0.05%
1.07%	MV22-2A-2-2	0.0199	0.0317	0.01885	2314.6	1.61	1.73	0.51%	0.76%	1.27%	1.86	1.5	0.44%	0.87%	1.32%	0.07%	-0.12%	-0.05%
1.07%	MV22-2A-2-0	0.0205	0.0318	0.01885	2314.6	1.61	1.73	0.53%	0.76%	1.29%	1.86	1.5	0.45%	0.88%	1.33%	0.07%	-0.12%	-0.05%

Table 7-6. Continued: Un-averaged FTIR data for calibration standards

Table 7-5. Un-averaged FTIR data for calibration standards using differing extinction coefficients						Newman et al. 1986 (NSE) extinction coefficients					Ihinger & Stolper 1994 (IS) extinction coefficients					Difference between NSE and IS outcomes		
1.87%	MV22-19-1-0	0.0318	0.0308	0.0146	2289.5	1.61	1.73	1.06%	0.96%	2.02%	1.86	1.5	0.92%	1.11%	2.03%	0.14%	-0.15%	0.00%
1.87%	MV22-19-1-1	0.0316	0.0306	0.0146	2289.5	1.61	1.73	1.06%	0.95%	2.01%	1.86	1.5	0.91%	1.10%	2.01%	0.14%	-0.15%	0.00%
1.87%	MV22-19-1-2	0.0315	0.0308	0.0146	2289.5	1.61	1.73	1.05%	0.96%	2.01%	1.86	1.5	0.91%	1.11%	2.02%	0.14%	-0.15%	-0.01%
1.87%	MV22-19-4-0	0.0307	0.0295	0.0146	2289.5	1.61	1.73	1.03%	0.92%	1.95%	1.86	1.5	0.89%	1.06%	1.95%	0.14%	-0.14%	0.00%
1.87%	MV22-19-5-0	0.0311	0.0294	0.0146	2289.5	1.61	1.73	1.04%	0.92%	1.96%	1.86	1.5	0.90%	1.06%	1.96%	0.14%	-0.14%	0.00%
1.87%	MV22-19-8-1	0.0295	0.0294	0.0146	2289.5	1.61	1.73	0.99%	0.92%	1.90%	1.86	1.5	0.86%	1.06%	1.91%	0.13%	-0.14%	-0.01%
1.87%	MV22-19-8-2	0.0294	0.0295	0.0146	2289.5	1.61	1.73	0.99%	0.92%	1.91%	1.86	1.5	0.85%	1.06%	1.91%	0.13%	-0.14%	-0.01%
1.87%	MV22-19-9-0	0.0307	0.0296	0.0146	2289.5	1.61	1.73	1.03%	0.92%	1.95%	1.86	1.5	0.89%	1.06%	1.95%	0.14%	-0.14%	0.00%
1.87%	MV22-19-9-1	0.0304	0.0302	0.0146	2289.5	1.61	1.73	1.02%	0.94%	1.96%	1.86	1.5	0.88%	1.08%	1.96%	0.14%	-0.14%	-0.01%
1.87%	MV22-19-9-2	0.0303	0.0295	0.0146	2289.5	1.61	1.73	1.01%	0.92%	1.93%	1.86	1.5	0.88%	1.06%	1.94%	0.14%	-0.14%	0.00%
1.87%	MV22-19-4-2	0.0304	0.0295	0.0146	2289.5	1.61	1.73	1.02%	0.92%	1.94%	1.86	1.5	0.88%	1.06%	1.94%	0.14%	-0.14%	0.00%
1.87%	MV22-19-4-1	0.0310	0.0301	0.0146	2289.5	1.61	1.73	1.04%	0.94%	1.98%	1.86	1.5	0.90%	1.08%	1.98%	0.14%	-0.14%	0.00%
1.87%	MV22-19-2-0	0.0319	0.0282	0.0146	2289.5	1.61	1.73	1.07%	0.88%	1.95%	1.86	1.5	0.93%	1.01%	1.94%	0.14%	-0.13%	0.01%
1.87%	MV22-19-2-1	0.0314	0.0286	0.0146	2289.5	1.61	1.73	1.05%	0.89%	1.94%	1.86	1.5	0.91%	1.03%	1.94%	0.14%	-0.14%	0.00%
1.87%	MV22-19-8-0	0.0299	0.0297	0.0146	2289.5	1.61	1.73	1.00%	0.92%	1.93%	1.86	1.5	0.87%	1.07%	1.93%	0.13%	-0.14%	-0.01%
1.91%	MV22-7-1-0	0.0389	0.0385	0.01875	2282.5	1.61	1.73	1.02%	0.94%	1.96%	1.86	1.5	0.88%	1.08%	1.96%	0.14%	-0.14%	-0.01%
1.91%	MV22-7-2-0	0.0403	0.0410	0.01875	2282.5	1.61	1.73	1.05%	1.00%	2.05%	1.86	1.5	0.91%	1.15%	2.06%	0.14%	-0.15%	-0.01%
1.91%	MV22-7-2-1	0.0406	0.0402	0.01875	2282.5	1.61	1.73	1.06%	0.98%	2.04%	1.86	1.5	0.92%	1.13%	2.05%	0.14%	-0.15%	-0.01%
1.91%	MV22-7-2-1	0.0405	0.0408	0.01875	2282.5	1.61	1.73	1.06%	0.99%	2.05%	1.86	1.5	0.92%	1.15%	2.06%	0.14%	-0.15%	-0.01%
1.91%	MV22-7-3-0	0.0400	0.0406	0.01875	2282.5	1.61	1.73	1.05%	0.99%	2.03%	1.86	1.5	0.91%	1.14%	2.05%	0.14%	-0.15%	-0.01%
1.91%	MV22-7-3-1	0.0392	0.0402	0.01875	2282.5	1.61	1.73	1.03%	0.98%	2.00%	1.86	1.5	0.89%	1.13%	2.01%	0.14%	-0.15%	-0.01%
1.91%	MV22-7-4-0	0.0404	0.0388	0.01875	2282.5	1.61	1.73	1.06%	0.94%	2.00%	1.86	1.5	0.91%	1.09%	2.00%	0.14%	-0.14%	0.00%
1.91%	MV22-7-4-2	0.0408	0.0395	0.01875	2282.5	1.61	1.73	1.07%	0.96%	2.03%	1.86	1.5	0.92%	1.11%	2.03%	0.14%	-0.15%	0.00%
1.91%	MV22-7-5-2	0.0389	0.0388	0.01875	2282.5	1.61	1.73	1.02%	0.94%	1.96%	1.86	1.5	0.88%	1.09%	1.97%	0.14%	-0.14%	-0.01%
2.71%	MV22-8-9-0	0.0620	0.0402	0.01745	2270.7	1.61	1.73	1.75%	1.06%	2.81%	1.86	1.5	1.52%	1.22%	2.73%	0.24%	-0.16%	0.07%
2.71%	MV22-8-9-1	0.0620	0.0401	0.01745	2270.7	1.61	1.73	1.75%	1.05%	2.81%	1.86	1.5	1.52%	1.22%	2.73%	0.24%	-0.16%	0.07%
2.71%	MV22-8-9-2	0.0618	0.0401	0.01745	2270.7	1.61	1.73	1.74%	1.05%	2.80%	1.86	1.5	1.51%	1.21%	2.73%	0.23%	-0.16%	0.07%
2.71%	MV22-8-2-1	0.0635	0.0417	0.01745	2270.7	1.61	1.73	1.79%	1.10%	2.89%	1.86	1.5	1.55%	1.27%	2.82%	0.24%	-0.17%	0.07%
2.71%	MV22-8-2-2	0.0644	0.0423	0.01745	2270.7	1.61	1.73	1.82%	1.11%	2.93%	1.86	1.5	1.57%	1.28%	2.86%	0.24%	-0.17%	0.07%

Table 7-7. Continued: Un-averaged FTIR data for calibration standards

Table 7-5. Un-averaged FTIR data for calibration standards using differing extinction coefficients						Newman et al. 1986 (NSE) extinction coefficients					Ihinger & Stolper 1994 (IS) extinction coefficients					Difference between NSE and IS outcomes		
3.69%	MV22-2B-1-1	0.0780	0.0361	0.01595	2255.7	1.61	1.73	2.43%	1.05%	3.47%	1.86	1.5	2.10%	1.21%	3.31%	0.33%	-0.16%	0.17%
3.69%	MV22-2B-1-2	0.0774	0.0363	0.01595	2255.7	1.61	1.73	2.41%	1.05%	3.46%	1.86	1.5	2.09%	1.21%	3.30%	0.32%	-0.16%	0.16%
3.69%	MV22-2B-1-3	0.0760	0.0358	0.01595	2255.7	1.61	1.73	2.37%	1.04%	3.40%	1.86	1.5	2.05%	1.19%	3.24%	0.32%	-0.16%	0.16%
3.69%	MV22-2B-1-4	0.0760	0.0366	0.01595	2255.7	1.61	1.73	2.36%	1.06%	3.42%	1.86	1.5	2.05%	1.22%	3.27%	0.32%	-0.16%	0.16%
3.69%	MV22-2B-1-5	0.0775	0.0364	0.01595	2255.7	1.61	1.73	2.41%	1.05%	3.47%	1.86	1.5	2.09%	1.22%	3.30%	0.32%	-0.16%	0.16%
3.69%	MV22-2B-3-0	0.0748	0.0355	0.01595	2255.7	1.61	1.73	2.33%	1.03%	3.36%	1.86	1.5	2.02%	1.18%	3.20%	0.31%	-0.16%	0.16%
3.69%	MV22-2B-3-1	0.0765	0.0351	0.01595	2255.7	1.61	1.73	2.38%	1.02%	3.39%	1.86	1.5	2.06%	1.17%	3.23%	0.32%	-0.16%	0.16%
3.69%	MV22-2B-3-2	0.0781	0.0362	0.01595	2255.7	1.61	1.73	2.43%	1.05%	3.48%	1.86	1.5	2.10%	1.21%	3.31%	0.33%	-0.16%	0.17%
3.69%	MV22-2B-3-3	0.0842	0.0400	0.01595	2255.7	1.61	1.73	2.62%	1.16%	3.78%	1.86	1.5	2.27%	1.34%	3.60%	0.35%	-0.18%	0.17%
3.69%	MV22-2B-3-4	0.0856	0.0390	0.01595	2255.7	1.61	1.73	2.66%	1.13%	3.79%	1.86	1.5	2.31%	1.30%	3.61%	0.36%	-0.17%	0.18%
3.69%	MV22-2B-3-5	0.0850	0.0396	0.01595	2255.7	1.61	1.73	2.64%	1.15%	3.79%	1.86	1.5	2.29%	1.32%	3.61%	0.36%	-0.18%	0.18%
3.69%	MV22-2B-6-0	0.0821	0.0379	0.01595	2255.7	1.61	1.73	2.55%	1.10%	3.65%	1.86	1.5	2.21%	1.27%	3.48%	0.34%	-0.17%	0.17%
3.69%	MV22-2B-6-1	0.0838	0.0387	0.01595	2255.7	1.61	1.73	2.61%	1.12%	3.73%	1.86	1.5	2.26%	1.29%	3.55%	0.35%	-0.17%	0.18%
3.69%	MV22-2B-6-2	0.0833	0.0400	0.01595	2255.7	1.61	1.73	2.59%	1.16%	3.75%	1.86	1.5	2.24%	1.33%	3.58%	0.35%	-0.18%	0.17%
4.50%	MV22-21-5-1	0.1235	0.0390	0.0156	2229.8	1.61	1.73	3.97%	1.17%	5.14%	1.86	1.5	3.44%	1.35%	4.79%	0.53%	-0.18%	0.35%
4.50%	MV22-21-5-2	0.1232	0.0394	0.0156	2229.8	1.61	1.73	3.96%	1.18%	5.15%	1.86	1.5	3.43%	1.36%	4.79%	0.53%	-0.18%	0.35%
4.50%	MV22-21-5-3	0.1228	0.0387	0.0156	2229.8	1.61	1.73	3.95%	1.16%	5.11%	1.86	1.5	3.42%	1.34%	4.76%	0.53%	-0.18%	0.35%
4.50%	MV22-21-3-1	0.1289	0.0403	0.0156	2229.8	1.61	1.73	4.15%	1.21%	5.35%	1.86	1.5	3.59%	1.39%	4.98%	0.56%	-0.18%	0.37%

Discussion of FTIR water content results for calibration standards

The obtained mean FTIR total water values for the seven calibration standards (Table 7-6) are close in value to the expected K-F titration total water values for the standards from 0.65% to 2.71%, except for the high FTIR results obtained for the 1.07% standard. The two highest standards each deviate from expected by about .30%.

Table 7-8. Difference between FTIR results and expected values for calibration standards.

expected K-F water (Westrich)	*obtained* FTIR H2O + OH	*Difference of obtained from expected*
0.65%	0.75%	0.10 greater
1.07%	1.39%	0.32 greater
1.87%	1.96%	0.09 greater
1.91%	2.02%	0.11 greater
2.71%	2.77%	0.06 greater
3.69%	3.40%	0.29 lesser
4.50%	4.81%	0.31 greater

Figure 7-6. Comparison of FTIR results and expected values for standards

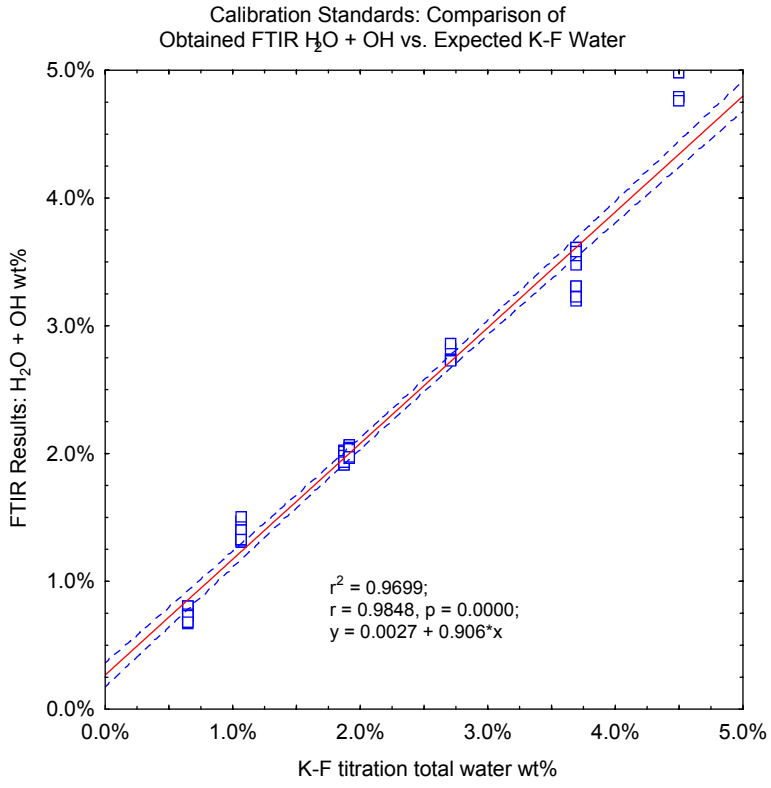

Figure 7-6 shows the plot of obtained and expected water values, with regression bands plotted for the .95 confidence level. The results show high correlation ($r=0.985$, $p<.001$) and the regression equation (Figure 7-6) indicates good linear fit ($r^2=.97$) with a y-intercept near zero. The poorer match of values for the two highest water content standards are expected because the calculation of extinction coefficients (ε) for the 5200 cm^{-1} and 4500 cm^{-1} absorption bands has been shown to yield the most precise results for water contents only up to 2% (Newman et al. 1986) or around 3% (Zhang and Behrens 2000; Zhang et al. 1997) in rhyolitic glasses.

This comparison of my FTIR results with the known water contents in the standards gives me high confidence in the sample preparation, instrument operation, choice of extinction coefficients, and calculation method used to measure peak height. Thus, I have equally high confidence in the results obtained from unknowns, as discussed in Chapter 8. This exercise using FTIR on specimens with water contents established independently by a different technique (K-F titration) addresses concerns expressed about FTIR (e.g., Friedman et al. 1997:331) and demonstrates in an archaeological study what is already fully established in geochemistry, that transmission FTIR can be an accurate method for measuring water content in obsidian. The utility of the technique in obsidians with microphenocrysts or bubbles can be evaluated during on-going use. The greatest limitation for archaeological applications is the cost/effort required for high-quality sample preparation, and the need to remove a small slice from an artifact. However, if the same glass sections removed for obsidian hydration analysis are used for FTIR analysis (with the additional preparation required), then FTIR adds no damage to specimens.

CHAPTER 8
WATER CONTENT ANALYSES:
RESULTS FOR JEMEZ OBSIDIANS

This chapter uses the LOI and FTIR analyses described in Chapter 7 to measure water content in the Jemez obsidians collected from CTD, CDM and CTN deposits. The two techniques are used to determine the water content in Dome CTD obsidians and to assess whether these glasses are more variable than the CDM and CTN comparison obsidians. A methodological component of the analysis compares the LOI analysis of more numerous samples (n=55) to FTIR analysis of a smaller subset (n=20) to evaluate the accuracy of the LOI results. The two techniques are found to obtain different results in terms of actual water content but similar results in terms of relative water content within and among the sources.

8.1. LOI and FTIR Analysis of Water Content in Obsidian from CTD, CTN and CDM

Selection of samples

The samples used in these two analyses of water content are drawn from the set of 55 obsidian samples used in the WD-XRF analysis as collected from the CTD, CDM and CTN sampling locations described in Chapter 6, and listed in Table 6-2 (CTD locations GS5 through GS13, RM1, RM3, and RM4), and Table 6-12 (CTN1-CTN5 and CDM1-CDM7).

LOI analysis is an integrated part of the whole rock analysis that included WD-XRF, so LOI was conducted on all 55 of the samples included in the WD-XRF elemental analysis in Chapter 6. LOI results by individual specimens were originally presented in a WD-XRF data table discussed in Chapter 6 (Appendix F, Table F-4). For comparison, two additional obsidian samples were included in the LOI analysis as independent "control" samples. These are one each samples from El Rechuelos (NM) and Glass Buttes (OR).

FTIR analysis was conducted on a subset of 20 of these 55 samples (Table 8-1). Overall the number of samples that could be analyzed with FTIR was restricted by the

experimentation time required to develop appropriate sample preparation, as well as scheduling limits involved in traveling to use the FTIR instrument. Selection of the FTIR samples emphasized diversity in CTD samples (n=15) because potential variation within the Dome obsidians is the focus of this study. Fewer samples were included from CTN (n=3; for comparison as another Cerro Toledo glass), and an even smaller number from CDM (n=2; for comparison as a non-Cerro Toledo glass from an extrusive volcanic context). At the time that FTIR samples were selected, the compositional differences later found within the CTN samples (see Chapter 6) were not known; by chance the three CTN samples include two with elemental composition like the CTD glasses, and one sample with the variant composition (CTNo).

The 15 CTD samples were selected to encompass a wide range of visual characteristics in the Dome obsidians, and thus include four brown glasses along with an assortment of the more common black and grey glasses. However, the CTD samples do not represent evenly the distribution of sampling locations (see Table 8-8, later in the chapter, for the CTD sampling locations represented). Seven locations are included but GS10 is overrepresented with five samples (33% of the CTD total samples). This occurred because of preference for examples of brown glasses (which are most common from the GS10 location) and for arbitrary reasons pertaining to when sample preparation was completed. Based on the analyses in Chapter 6 of elemental variation across CTD deposits, the uneven geographical representation is not expected to introduce bias into the analysis of water content.

Table 8-1. Samples used in LOI and FTIR analyses.

Geological unit	Geographical sampling area	Water content measures:	
		LOI	FTIR
Cerro Toledo Rhyolite (CTR)	**Cerro Toledo—Dome (CTD)**	35*	15
Cerro Toledo Rhyolite (CTR)	**Cerro Toledo—Northeast (CTN and CTNo)**	8	3
Valles Rhyolite (VR)	**Cerro del Medio (CDM)**	12	2
* LOI analysis did not include sample CTDRM-302		55	20

Results: FTIR and LOI Analyses of Water in Obsidian from CTD, CTN, and CDM

LOI results are discussed first to consider obsidian water content within the Cerro Toledo glasses and then are compared to water content in Cerro del Medio glasses. FTIR results are discussed second and are compared to LOI results. LOI and FTIR results are presented here in several tables. LOI summary results (minimum, maximum, mean, standard deviation, and CV) for H_20^-, H_2O^+, and total LOI are shown in Table 8-2; LOI values for each of the individual specimen are shown in Table 8-3. FTIR results will be presented later in Tables 8-8, 8-9, and 8-10.

Table 8-2. Summary of LOI measures of H_2O-, H_2O+, and Total LOI for 55 obsidian samples from CTD, CDM, and CTN.

LOI H_2O^-	N	*Min	*Max	Mean	SD	**CV
CTD	35	**0.00%**	**0.46%**	0.07%	0.00089	**120.11**
CDM	12	**0.00%**	0.31%	0.08%	0.00097	**119.58**
CTN	6	**0.00%**	0.16%	0.05%	0.00060	**129.56**
CTNo	2	**0.00%**	0.02%	0.01%	0.00013	**127.95**
Total	55	0.00%	0.46%	0.07%	0.00086	**122.98**

LOI H_20^+	N	Min	Max	Mean	SD	CV
CTD	35	0.28%	**1.85%**	0.99%	0.00329	**33.15**
CDM	12	**0.25%**	0.98%	0.45%	0.00199	**43.79**
CTN	6	0.98%	1.28%	1.12%	0.00105	9.39
CTNo	2	0.48%	0.49%	0.49%	0.00007	1.46
Total	55	0.00%	1.85%	0.85%	0.00387	**45.58**

Total LOI	N	Min	Max	Mean	SD	CV
CTD	35	0.28%	**1.79%**	0.93%	0.00321	**34.46**
CDM	12	**0.18%**	0.91%	0.40%	0.00195	**49.39**
CTN	6	0.92%	1.21%	1.06%	0.00104	9.83
CTNo	2	0.45%	0.47%	0.46%	0.00014	3.07
Total	55	0.18%	1.79%	0.81%	0.00364	**44.90**

*high-low range values shown in bold
** CV values ≥ 10 are shown in bold

Table 8-3. Individual specimen LOI measures of H_2O^-, H_2O^+, and Total LOI for CTD, CTN, and CTN samples (plus one each samples from outside sources).

Cerro Toledo Dome **CTD n=35**												
Specimen	**Source**	**Color***	**LOI H_2O-**	**LOI H_20+**	**Total LOI**		**Specimen**	**Source**	**Color***	**LOI H_2O-**	**LOI H_20+**	**Total LOI**
CTD5-301	CTD	0	0.180%	1.33%	1.25%		CTD10-301	CTD	0	0.001%	0.63%	0.56%
CTD5-302	CTD	0	0.220%	0.73%	0.73%		CTD10-302	CTD	0	0.170%	0.72%	0.66%
CTD5-303	CTD	0	0.001%	1.11%	1.11%		CTD10-303	CTD	0	0.001%	0.78%	0.72%
CTD5-304	CTD	0	0.040%	0.73%	0.67%		CTD10-304	CTD	0	0.020%	1.02%	0.96%
CTD5-305	CTD	0	0.060%	0.95%	0.89%		CTD10-305	CTD	0	0.075%	0.57%	0.52%
CTD5-307	CTD	b	0.001%	1.31%	1.24%		CTD10-306	CTD	0	0.015%	0.69%	0.63%
CTD5-308	CTD	0	0.090%	0.93%	0.86%		CTD12-301	CTD	b	0.020%	1.34%	1.28%
CTD5-309	CTD	0	0.100%	0.93%	0.87%		CTD12-302	CTD	b	0.160%	1.16%	1.10%
CTD6-301	CTD	0	0.039%	0.84%	0.78%		CTD12-303	CTD	b	0.060%	0.90%	0.84%
CTD6-302	CTD	0	0.060%	0.75%	0.69%		CTD13-301	CTD	0	0.130%	0.82%	0.73%
CTD6-303	CTD	b	0.150%	1.36%	1.30%		CTDRM-301	CTD	0	0.001%	0.40%	0.35%
CTD6-304	CTD	0	0.078%	0.74%	0.68%		CTDRM-303	CTD	m	0.060%	0.28%	0.28%
CTD7-301	CTD	0	0.020%	1.22%	1.16%		CTDRM-304	CTD	0	0.001%	1.38%	1.32%
CTD7-302	CTD	0	0.001%	1.04%	0.98%		GS10-1	CTD	0	0.018%	1.15%	1.07%
CTD8-301	CTD	0	0.020%	1.07%	0.98%		GS7-1	CTD	0	0.060%	1.38%	1.30%
CTD8-302	CTD	0	0.060%	0.76%	0.70%		GS7B-1	CTD	0	0.100%	1.85%	1.79%
CTD8S-301	CTD	0	0.080%	1.33%	1.26%		GS8-1	CTD	0	0.460%	1.36%	1.27%
CTD8S-302	CTD	0	0.040%	1.12%	1.06%							

Cerro del Medio **CDM n=12**						Cerro Toledo Northeast **CTN n=8**					
CDM-301	CDM	0	0.030%	0.38%	0.32%	CTN-301	CTNo	0	0.020%	0.49%	0.47%
CDM-302	CDM	0	0.080%	0.32%	0.24%	CTN-302	CTNo	0	0.001%	0.48%	0.45%
CDM-303	CDM	m	0.060%	0.29%	0.28%	CTN-303	CTN	0	0.001%	1.19%	1.14%
CDM-304	CDM	0	0.001%	0.98%	0.91%	CTN-304	CTN	b	0.060%	0.98%	0.92%
CDM-305	CDM	0	0.001%	0.33%	0.27%	CTN-305	CTN	0	0.036%	1.10%	1.03%
CDM-306	CDM	0	0.180%	0.42%	0.36%	CTN-306	CTN	0	0.020%	1.06%	1.00%
CDM-307	CDM	0	0.001%	0.42%	0.36%	CTN-307	CTN	b	0.001%	1.28%	1.21%
CDM-308	CDM	m	0.130%	0.48%	0.47%	CTN-308	CTN	0	0.160%	1.09%	1.03%
CDM-309	CDM	0	0.160%	0.50%	0.43%						
CDM-310	CDM	0	0.000%	0.66%	0.59%	Other Sources (1 specimen each)					
CDM-311	CDM	0	0.310%	0.25%	0.18%	El Rechuelos, NM		0	0.13%	0.37%	0.30%
CDM-312	CDM	0	0.020%	0.41%	0.34%	Glass Buttes, OR		0	0.04%	0.66%	0.56%

*Color: b=brown; m=mahogany; 0=grey or black

LOI Results and Discussion

As shown in Table 8-2 and illustrated in Figures 8-1 and 8-2, total LOI values across all samples range from a low of 0.18% to a high of 1.79%. H_2O^- values range from 0.00% to 0.46%, and H_2O^+ values range from 0.28% to 1.85%.

However, the high end of the total LOI and H_2O^+ measures are skewed by a single sample that I believe may be in error. The highest total LOI and H_2O^+ values, 1.79% and 1.85%, respectively, both derive from CTD specimen GS7B-1 (see Table 8-3). As shown in the mean plots in Figure 8-1, there is only one upper-end extreme value "*" among LOI value for the CTD samples—this is GS7B-1. GS7B-1 has the highest value for H_2O^+ (1.85%) but a relatively normal value for H_2O^- (0.10%). I strongly suspect that this extreme H_2O^+ value (and subsequent total LOI value) reflects some kind of error either during LOI calculation of the H_2O^+ values or in the treatment of the GS7B-1 sample during the LOI procedure or sample preparation. Certain samples were run multiple times by Husler's lab, and GS7B-1 was one of those; I am not comfortable accepting the LOI value for GS7B-1 as accurate.

Figure 8-1. Mean plots and scatter plots of total LOI measures of 55 obsidian samples from CTD, CDM, CTN, and CTNo

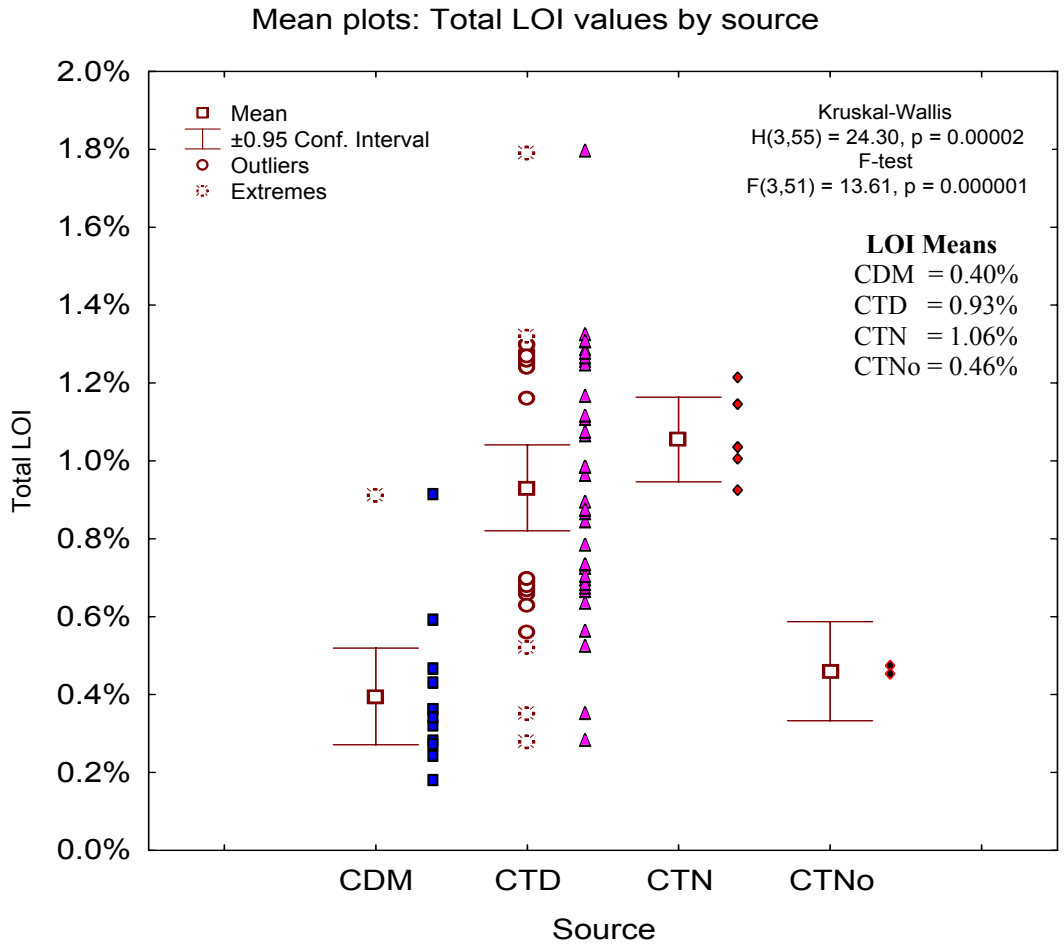

Figure 8-2. Histograms of total LOI, H_2O^-, H_2O^+ measures of 55 obsidian samples by source: CTD, CDM, CTN, and CTNo

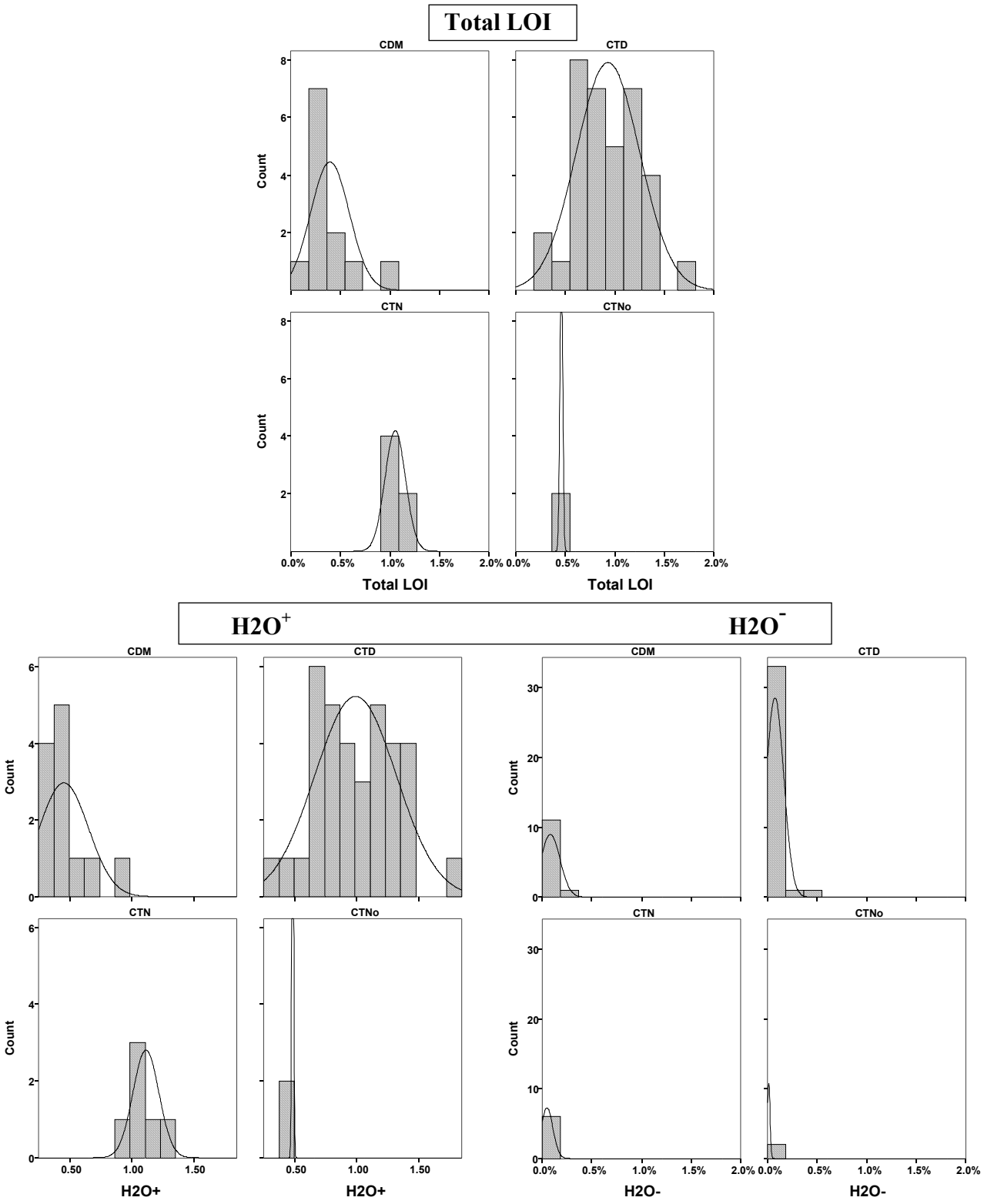

Comparison of results across the three measures of water content (H_2O^-, H_2O^+ and total LOI) provided by the LOI technique demonstrates differences in variation among these water measures. Adsorbed water, H_2O^-, has mean values ranging from 0.01% to 0.08% across the sources (Figure 8-2) with all results less than 0.20% except in three samples (CTD5-302, GS8-1, and CDM-311). While CV values for H_2O^- are very high (all at about CV 120 or above, Table 8-2) this variation contributes little to the overall variation in water content measured by total LOI because the actual H_2O^- weight % content is so low. Thus, in terms of effect on total water content, H_2O^- varies narrowly among the samples and across sources.

In contrast, H_2O^+, molecular water, and total LOI demonstrate real differences among the sources. Because of the minimal contribution of H_2O^- to the measured water content, H_2O^+ and total LOI are effectively the same measure and are used somewhat interchangeably throughout the remainder of this study. Total LOI is the principal LOI water content measure discussed in most comparisons here.

As illustrated with mean plots in Figure 8-1 and histograms in Figure 8-2, CTD and CTN, the two Cerro Toledo obsidians with the same XRF trace element profile (see Chapter 6), are notably higher in water content as measured by H_2O^+ and by total LOI. Mean total LOI values for CTD and CTN are 0.93% and 1.06%, respectively, compared to 0.40% and 0.46% for CDM and CTNo, respectively.

Mean total LOI values:	CTN	1.06%
	CTD	0.93%
	CTNo	0.46%
	CDM	0.40%

Comparisons of means across sources in several combinations using Kruskal-Wallis, F-test, and T-test statistics (Statistica 2001), as well as ANOVA and post-hoc multiple comparisons using a Bonferroni adjustment (SPSS 2002), support the interpretation of heterogeneity of means except between CTD and CTN samples (Tables 8-4 though 8-6). Because of the small sample size, CTNo obsidians (n=2) were excluded in several comparisons. In other words, the statistical tests support the interpretation that the means of each group are not different between CTD and CTN, but are different when comparing CTD and CTN to CDM. The LOI water contents in the Cerro Toledo obsidians are alike but different than the CDM obsidians.

Table 8-4. Comparison of total LOI means among differing combinations of sources using Kruskal-Wallis, F-test, and T-test statistics.

Comparison of means by source	Total LOI	Results
CTD/CDM/CTN/CTNo	KW p = .00002 F test p = .000001	Significant diff in means
CTD/CDM/CTN	KW p = .00002 F test p = .000001	Significant diff in means
CTD/CTN	T-test p = .3588	No significant diff in means
CDM/CTN	T-test p = .000001	Significant diff in means
CTD/CDM	T-test p = .000002	Significant diff in means

Table 8-5. ANOVA of total LOI means for CTD, CDM, CTN, and CTNo (n=55).*[1]

ANOVA Total LOI	Sum of Squares	df	Mean Square	F	Significance
Between Groups CTD/CDM/CTN/CTNo	.000	3	.000	13.612	**.000**
Within Groups CTD/CDM/CTN/CTNo	.000	51	.000		
Total	.001	54			

Table 8-6. Post-hoc multiple comparison for total LOI among CTD, CDM, CTN, and CTNo (n=55) using Bonferroni adjustment.

Source (I)	Source (J)	Mean Difference (I-J)*	Std. Error	Significance*	95% C.I. Lower Bound	95% C.I. Upper Bound
CDM	CTD	**-.005357**	.0009337	**0.000**	-.007920	-.002794
	CTN	**-.006596**	.0013956	**0.000**	-.010427	-.002765
	CTNo	-.000646	.0021318	1.000	-.006498	.005206
CTD	CDM	**.005357**	.0009337	**0.000**	.002794	.007920
	CTN	-.001239	.0012333	1.000	-.004624	.002147
	CTNo	.004711	.0020293	0.146	-.000859	.010282
CTN	CDM	**.006596**	.0013956	**0.000**	.002765	.010427
	CTD	.001239	.0012333	1.000	-.002147	.004624
	CTNo	.005950	.0022790	0.071	-.000306	.012206
CTNo	CDM	.000646	.0021318	1.000	-.005206	.006498
	CTD	-.004711	.0020293	0.146	-.010282	.000859
	CTN	-.005950	.0022790	0.071	-.012206	.000306

*Bold: The mean difference is significant at the .05 level.

[1] CTNo should have been excluded from this analysis; however, results without CTNo are substantively the same.

These LOI results match the expectation that the Cerro Toledo obsidian found within the area of the Dome Fire (CTD) is high in water content. That the CTN samples with the same XRF trace element profile as CTD also have similar mean water content was not a specific expectation of the experiment, but further supports the interpretation that obsidian-bearing deposits across the Cerro Toledo geologic unit can be characterized as containing high water content obsidian. However, the observed similarity in CTNo and CDM means is not interpreted the same way because the trace elements in each do not indicate geologic relatedness or similarity in origin.

Any interpretation must be treated with caution given the small sample size of CTNo, but the similarity in CDM and CTNo water content may be a reflection that they are alike because represent the more common range of water content values. This interpretation is supported by the LOI results available from the two additional samples included in the LOI analysis. The single samples from El Rechuelos (NM) and Glass Buttes (OR) also returned relatively low total LOI measures of .0.30% and 0.56%, respectively (Table 8-3).

Turning to consideration of variation in water content, three observations support the interpretation that CTD is more variable than CDM.

1) CTD samples have a broader range than do CDM samples.

2) While the CTD mean for total LOI is just under 1%, the range for CTD includes specimens with total LOI as low as 0.28% and as high as 1.38% (excluding the highest value that may be in error).

3) As illustrated in Figure 8-1, there are numerous outliers outside the 95% confidence interval. While the outliers are in part accounted for by the greater CTD sample size, this characteristic of the distribution of total LOI values support greater variation in the CTD obsidians.

Another (related) observation is that the CTD distribution for total LOI is platykurtic (having fewer items at the mean and more items in the intermediate regions; Sokal and Rohlf 1981:114) and suggests an underlying bimodal distribution. This potential bimodality is apparent in Figure 8-2, and can be accentuated by changing the number of classes in the frequency distribution. Figure 8-3 shows the total LOI histogram for CTD with fifteen classes (as compared to eleven classes in Figure 8-2),

with the number of classes selected specifically to enhance the bimodality of the frequency array.

Figure 8-3. Histogram of total LOI for CTD samples; created with 15 classes to accentuate possible bimodality.

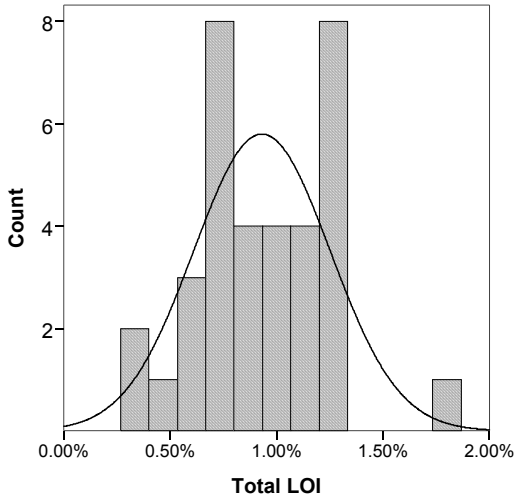

It is clear in both Figures 8-2 and 8-3 that the mean does not coincide with the mode, and Figure 8-3 shows the distribution with-literally-two modes. If this apparent bimodality actually describes an underlying two-part subdivision in the data, this finding might be an important component in explaining the high water content observed in the CTD samples. That is, the CTD deposits might have both obsidians with the "more common" lower water content and obsidians with a high water content, each normally distributed in frequency within the total assembly of obsidian nodules. Disappointingly, data exploration has not revealed any underlying correlations that might support or explain a two-part subdivision of the CTD samples. No correlations were found with other compositional variables or with sampling location.

Returning to consideration of variation in total LOI among the different sources, a final measure of variation, CV, surprisingly does not support higher variation in the CTD samples (Table 8-2). Both CTD and CDM have very high CV values (CV > 30) for H_2O^+ and total LOI, with CDM CV values somewhat higher. While the standard deviation of H_2O^+ and total LOI measures is higher for the CTD samples than other sources, comparison of CV values between CTD and CDM shows that samples from these two

sources have CV values that are similarly high within all three of the LOI measures of water (Table 8-2). Likely this is an artifact of the lower mean in CDM; the comparison of SD is probably more meaningful in this case.

To be certain that the standard deviation and CV values were not overly influenced by extreme values, I also computed summary values after dropping the specimens with the highest H_2O^+ and total LOI values from CDM and CTD (CDM304 and GS7B-1, respectively), as well as the specimen with the highest H_2O^- value (GS8-1, from CTD). Summary statistics without these three specimens are shown in Table 8-7. While CV values for CDM and CTD drop slightly in each LOI measure, especially for CDM, there are no substantial differences in means, standard deviations, or subsequent CV values when these extreme values are excluded. In terms of interpreting the CV values, CV values for CTD and CDM are similar even with this correction, indicating that the obsidian samples at CTD are highly variable but not more variable than samples from CDM.

Table 8-7. Summary of LOI measures of H_2O-, H_2O+, and Total LOI for52 obsidian samples from CTD, CDM, and CTN; specimens CDM-304, GS7B-1, and GS8-1 are excluded

LOI H_2O-	N	*Min	*Max	Mean	SD	**CV
CTD	33	**0.00%**	0.22%	0.06%	0.00060	**97.04**
CDM	11	**0.00%**	**0.31%**	0.09%	0.00098	**111.12**
CTN	6	**0.00%**	0.16%	0.05%	0.00060	**129.56**
CTNo	2	**0.00%**	0.02%	0.01%	0.00013	**127.95**
Total	52	0.00%	0.31%	0.06%	0.00069	108.71
LOI $H_2$0+	**N**	**Min**	**Max**	**Mean**	**SD**	**CV**
CTD	33	0.28%	**1.38%**	0.96%	0.00294	**30.77**
CDM	11	**0.25%**	0.66%	0.41%	0.00114	**28.22**
CTN	6	0.98%	1.28%	1.12%	0.00105	9.39
CTNo	2	0.48%	0.49%	0.49%	0.00007	1.46
Total	52	0.25%	1.38%	0.84%	0.00348	41.46
Total LOI	**N**	**Min**	**Max**	**Mean**	**SD**	**CV**
CTD	33	0.28%	**1.32%**	0.89%	0.00285	**31.88**
CDM	11	**0.18%**	0.59%	0.35%	0.00114	**32.79**
CTN	6	0.92%	1.21%	1.06%	0.00104	9.83
CTNo	2	0.45%	0.47%	0.46%	0.00014	3.07
Total	52	0.18%	1.32%	0.78%	0.00341	43.65
*high-low range values shown in bold ** CV values ≥ 10 are shown in bold						

In summary, the LOI analysis of 55 samples from CTD, CDM, CTN, and CTNo indicates that there are substantial differences among these groups as demonstrated graphically and as evaluated in terms of statistical significance using tests of homogeneity of means and analysis of variance. For this study, the importance of these results can be understood as follows:

1) CTD samples have higher overall water content as measured by total LOI, including numerous samples with total LOI higher than 1%. 14 of the 35 CTD samples (40%) are above 1% total LOI water content.

2) The Cerro Toledo obsidians CTD and CTN, are similar in having high water content, and can be distinguished statistically from lower water contents in the Cerro del Medio (CDM) samples. None of the CDM samples are greater than 1% for total LOI water content.

3) Measures of total LOI in CTD exhibits a broad range, and include lower water contents (such as those represented by CDM) as well as higher water contents.

4) CTD appears to be more variable than CDM using basic descriptive statistics. This is not supported by the observed CV values which are similarly high for both, but likely this is an artifact of the lower mean in CDM; the comparison of SD is probably more meaningful in this case.

The accuracy and utility of these results depends on the adequacy of the LOI technique for measuring obsidian water content. In the next analysis, a subset of 20 of these 55 samples are analyzed using FTIR, and the resulting FTIR results are used in Section 8.3 to evaluate the obtained LOI results.

FTIR Results and Discussion

Turning to FTIR analysis of water content, results for 20 samples from CTD, CDM, and CTN are shown in Table 8-8. LOI results also are shown in this table to allow comparison between these two methods for measuring water in the 20 samples included in the FTIR analysis. The values listed in Table 8-8 are the averages across multiple replicated measures on each specimen. Individual FTIR measures are listed in Table 8-12 at the end of this chapter. Tables 8-9 and 8-10 show summary values for FTIR

results by source. Table 8-9 is simply a subset of Table 8-10 intended to facilitate comparison of the means. The small sample size for sources other than CTD renders the summary statistics for CDM, CTN, and CTNo of little use. However, the means obtained for each source can be used, guardedly, to compare within the FTIR results as well to LOI results.

Table 8-8. Water content as measured by FTIR and LOI for 20 CTD, CTN, and CDM obsidian samples. H_2O and OH results are presented using extinction coefficients (ε) from Ihinger & Stolper 1994 (bold), with values using (ε) from Newman et al. 1986 included for comparison.[2]

				LOI			**FTIR (ε from IS 1994)**			FTIR (ε from NSE 1986)		
Source	Sample	Samp Loc	Color	H_2O^- (100ºC)	H_2O^+ (800ºC)	Total LOI	**H_2O (IS)**	**OH (IS)**	**H_2O & OH (IS)**	H_2O (NSE)	OH (NSE)	H_2O & OH (NSE)
CTD	CTD05-307	GS05	bt	0.001%	1.31%	1.24%	**0.79%**	**0.86%**	**1.64%**	0.91%	0.74%	1.65%
CTD	CTD06-301	GS06	0	0.039%	0.84%	0.78%	**0.23%**	**0.49%**	**0.72%**	0.26%	0.42%	0.69%
CTD	CTD06-302	GS06	0	0.060%	0.75%	0.69%	**0.13%**	**0.40%**	**0.53%**	0.15%	0.35%	0.50%
CTD	CTD07-302	GS07	0	0.001%	1.04%	0.98%	**0.30%**	**0.59%**	**0.90%**	0.35%	0.51%	0.87%
CTD	CTD10-301	GS10	0	0.001%	0.63%	0.56%	**0.16%**	**0.26%**	**0.42%**	0.19%	0.22%	0.41%
CTD	CTD10-302	GS10	0	0.170%	0.72%	0.66%	**0.12%**	**0.38%**	**0.50%**	0.14%	0.33%	0.47%
CTD	CTD10-303	GS10	0	0.001%	0.78%	0.72%	**0.14%**	**0.36%**	**0.50%**	0.16%	0.31%	0.47%
CTD	CTD10-305	GS10	0	0.075%	0.57%	0.52%	**0.09%**	**0.30%**	**0.39%**	0.10%	0.26%	0.37%
CTD	CTD12-302	GS12	b	0.160%	1.16%	1.10%	**0.99%**	**1.05%**	**2.04%**	1.15%	0.91%	2.06%
CTD	CTD12-303	GS12	b	0.060%	0.90%	0.84%	**0.84%**	**1.13%**	**1.97%**	0.97%	0.98%	1.95%
CTD	CTDRM-301	RM1	0	0.001%	0.40%	0.35%	**0.14%**	**0.18%**	**0.32%**	0.16%	0.16%	0.31%
CTD	GS10-1	GS10	0	0.018%	1.15%	1.07%	**0.13%**	**0.38%**	**0.51%**	0.15%	0.33%	0.48%
CTD	GS7-1	GS07	0	0.060%	1.38%	1.30%	**0.24%**	**0.59%**	**0.84%**	0.28%	0.52%	0.79%
CTD	GS7B-1	GS07	0	0.100%	1.85%	1.79%	**0.35%**	**0.68%**	**1.02%**	0.40%	0.59%	0.99%
CTD	GS8-1	GS08	0	0.460%	1.36%	1.27%	**0.34%**	**0.63%**	**0.97%**	0.39%	0.55%	0.94%
CTNo	CTN-302	CTN2	0	0.001%	0.48%	0.45%	**0.10%**	**0.14%**	**0.24%**	0.11%	0.12%	0.23%
CTN	CTN-304	CTN3b	t	0.060%	0.98%	0.92%	**0.52%**	**0.65%**	**1.17%**	0.60%	0.56%	1.16%
CTN	CTN-308	CTN5	0	0.160%	1.09%	1.03%	**0.21%**	**0.53%**	**0.74%**	0.24%	0.46%	0.70%
CDM	CDM-302	CDM2a	0	0.080%	0.32%	0.24%	**0.11%**	**0.24%**	**0.35%**	0.13%	0.21%	0.34%
CDM	CDM-304	CDM4	0	0.001%	0.98%	0.91%	**0.22%**	**0.63%**	**0.85%**	0.25%	0.55%	0.80%

[2] Table 8-8 shows FTIR results obtained using the two alternate extinction coefficients (ε) obtained from Ihinger and Stolper (1994) and Newman et al. (1986). As can be expected given the discussion of alternate extinction coefficients in Chapter 7, H_2O values calculated using ε from Ihinger and Stolper (1994) are lower than H_2O values calculated with ε from Newman et al. (1986), while OH values are the reverse. The total water values (H_2O plus OH) are similar, demonstrating that the effects of the differing coefficients are cancelled out when the water species are summed. Given the goals of the current study, no relevant differences are found in results using the alternate values of ε. Therefore, FTIR data presented hereafter all were computed using the Ihinger and Stolper (1994) extinction coefficients.

Table 8-9. Means of FTIR measures of H_2O and OH for 20 CTD, CDM, and CTN obsidian samples;* (ε) *from Ihinger and Stolper 1994.

Avg	n	Mean H_2O	Mean OH	Mean H2O+OH
CTD	15	0.33%	0.55%	0.88%
CDM	2	0.17%	0.44%	0.60%
CTN	2	0.36%	0.59%	0.95%
CTNo	1	0.10%	0.14%	0.24%

Table 8-10. Summary of FTIR measures of H_2O and OH for 20 CTD, CDM, and CTN obsidian samples;* (ε) *from Ihinger and Stolper 1994.

FTIR H_2O	N	Min	Max	Mean	SD	CV
CTD	15	**0.09%**	**0.99%**	0.33%	0.00290	**87.79**
CDM	2	0.11%	0.22%	0.17%	0.00073	**44.25**
CTN	2	0.21%	0.52%	0.36%	0.00218	**60.01**
CTNo	1	0.10%	0.10%	0.10%	n/a	n/a
Total	20	0.09%	0.99%	0.31%	0.00264	86.58

FTIR OH	N	Min	Max	Mean	SD	CV
CTD	15	0.18%	**1.13%**	0.55%	0.00286	**51.67**
CDM	2	0.24%	0.63%	0.44%	0.00276	**63.34**
CTN	2	0.53%	0.65%	0.59%	0.00085	**14.50**
CTNo	1	**0.14%**	0.14%	0.14%	n/a	n/a
Total	20	0.14%	1.13%	0.52%	0.00273	51.99

FTIR H_2O+OH	Min	Max	Mean	SD	CV
CTD	15	0.32%	**2.04%**	0.88%	0.00565	**63.93**
CDM	2	0.35%	0.85%	0.60%	0.00349	**58.08**
CTN	2	0.74%	1.17%	0.95%	0.00303	**31.85**
CTNo	1	**0.24%**	0.24%	0.24%	n/a	n/a
Total	20	0.24%	2.04%	0.83%	0.00524	63.11

The FTIR results show that CTD and CTN samples have higher mean total water contents than those from CDM and CTNo (0.88% and 0.95% compared to 0.60% and 0.24%, respectively).

Mean total FTIR values:	CTN	0.95%
	CTD	0.88%
	CDM	0.60%
	CTNo	0.24%

This is true also for water species H_2O and OH individually. H_2O ranges from 0.09% to 0.99%[3], with both ends of this range found in the CTD samples. OH ranges from 0.14% to 1.13%, with the highest value in CTD and the lowest in CTNo. Total FTIR (which is simply the sum of OH and H_2O) ranges from 0.24% to 2.04%, again with the highest value in CTD and the lowest in CTNo. Figure 8-4 illustrates the high variability in CTD sample values.

Figure 8-4. Scatter plot of total FTIR measures of 20 obsidian samples from CTD, CDM, CTN, and CTNo.

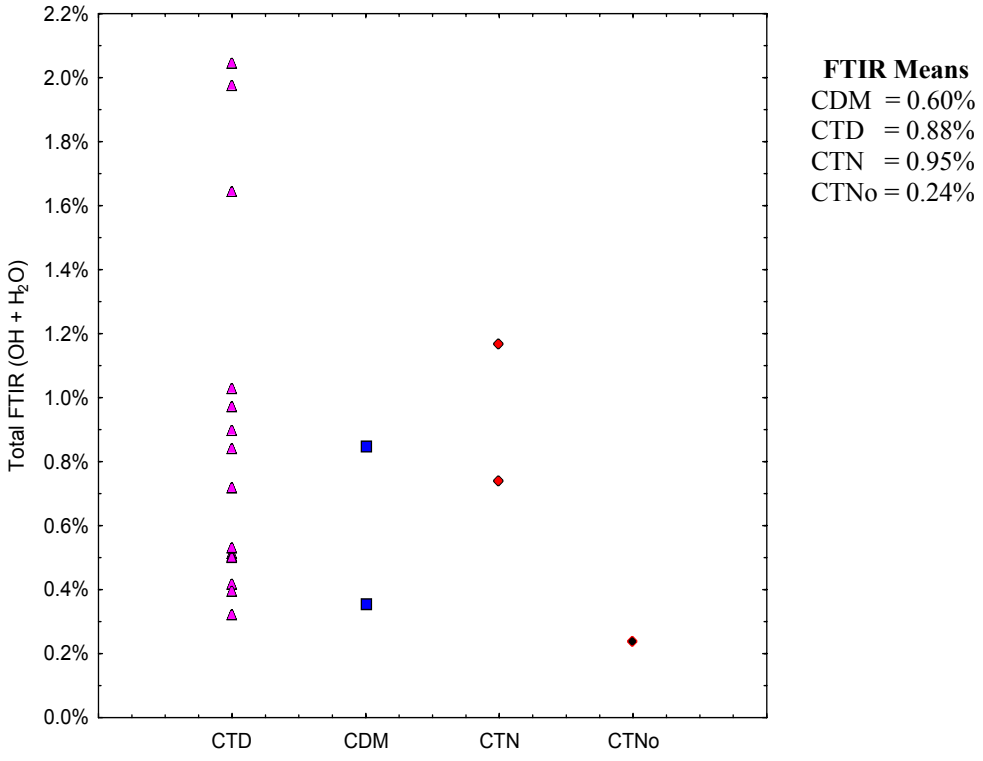

[3] Slight differences among individual and summary values in Tables 8-8, 8-9, and 8-10 are due to rounding.

Thus, ignoring for the moment the small and variable sample sizes among the four source areas, the FTIR results indicate that the two Cerro Toledo obsidians (CTD and CTN) are higher in water content than CDM and CTNo.

8.2. Comparison of LOI and FTIR Analyses of Water Content in Obsidian to Assess Accuracy of LOI Analysis

The FTIR results show the same pattern in relative obsidian water content among the source areas as observed in the LOI analysis. CTD and CTN have the highest water contents, and CDM and CTNo have the lowest. Comparison of ranges among the sources is not possible given the small sample sizes of CDM, CTN, and CTNo, but it is possible to observe that the FTIR water content values for CTD samples reproduce the broad spread observed in the CTD LOI measures (Figure 8-4; compare with Figure 8-1).

However, the two techniques do not replicate actual water content values obtained. As demonstrated by comparison of mean total water content values obtained by each technique (Table 8-11), total LOI values are higher than total FTIR for each group of samples except the CDM samples.

Table 8-11. Comparison of Mean Total Water Content.

Source area	Mean FTIR (H_2O + OH)	Mean LOI (Total LOI)
CTN	0.95%	1.06%
CTD	0.88%	0.93%
CDM	0.60%	0.40%
CTNo	0.24%	0.46%

As discussed in Chapter 7, FTIR is considered a more accurate technique than LOI for measuring obsidian water content. To assess the accuracy of the LOI analysis conducted on the complete set of 55 samples, I use the more accurate but more difficult FTIR technique to validate the use of the potentially less accurate but simpler LOI technique. This evaluation of method serves not only to estimate the quality of the water content data obtained in the LOI analysis in this study but also to weigh the utility of each technique for archaeological applications.

Overall, the total water content values obtained by LOI and FTIR are only in general agreement. Linear regression analysis comparing LOI and FTIR results for individual specimens (Figure 8-5) shows that with the entire dataset of 20 samples the relationship between the two measures is strong with a p-value significant at the .05 level (r^2=0.2921, p=0.0139). However there are four points that skew the distribution of FTIR measures toward higher water content values (CTD5-307, CTD12-302, CTD12-303, and less so, CTN-304). With the removal of these four points, the relationship between LOI and FTIR results is much stronger (r^2=0.7656, p=0.0000). In the regression equation for this modified dataset, the y-intercept is near 0 and the slope is closer to one (but at ~1.4x indicates that the LOI values are over-estimating water content).

Figure 8-5. Comparison of LOI and FTIR water content results by individual sample

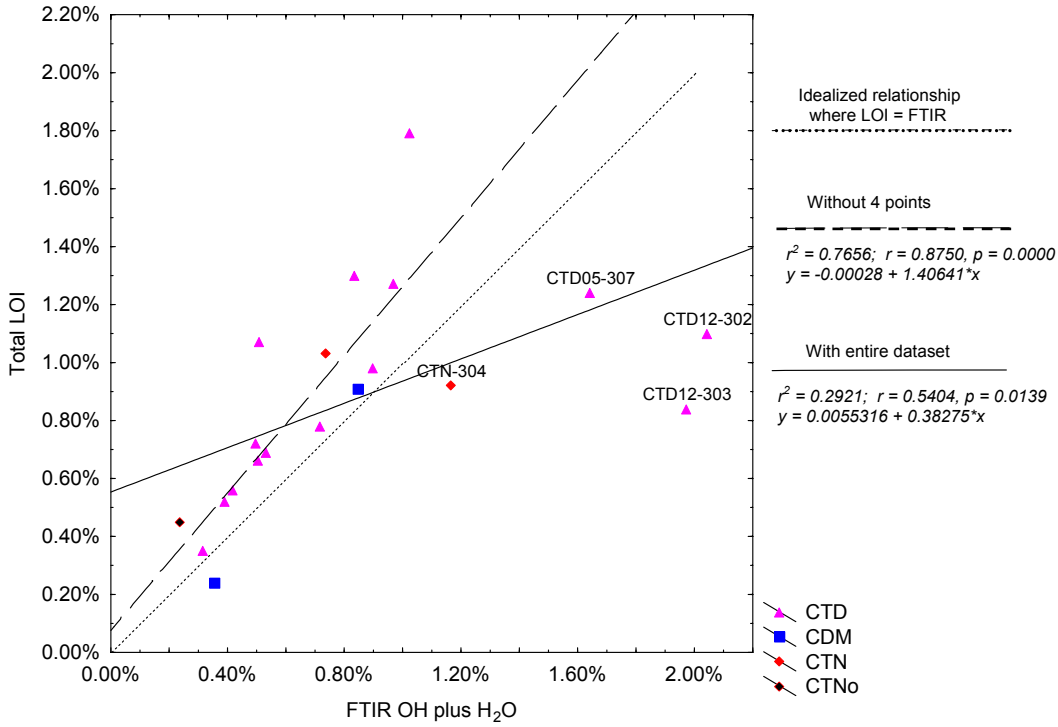

The influence of the four points on the regression relationship between LOI and FTIR raises the question of why these samples obtained such different FTIR outcomes. Examination of the specimens reveals that all four are brown glass while the remaining sixteen samples are black or grey (there are no mahogany samples in the FTIR subset).

Figure 8-6 shows the plot of these points coded for both obsidian color and source, and illustrates clearly that the LOI and FTIR measures correlate well in the black and grey obsidians but that the four brown samples measure much higher in the FTIR analysis than in the LOI analysis.

Figure 8-6. Comparison of LOI and FTIR water content results by individual sample showing source and obsidian color (brown glasses shown in red).

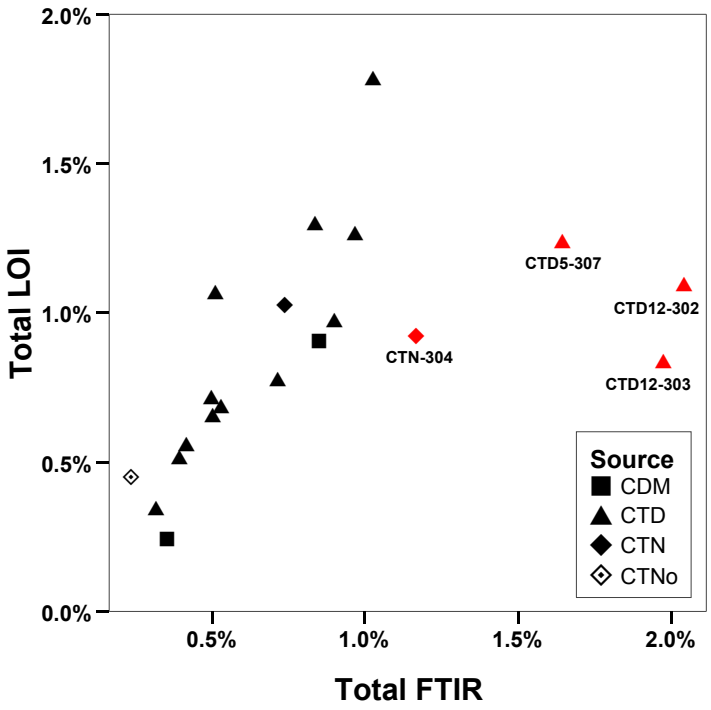

I believe that the FTIR measures for these four brown samples are incorrect, despite the overall superior accuracy of FTIR. I suspect two factors as contributing to these errors. The first concerns the translucency of the glass and the second is a specific observation about the FTIR results obtained for the four samples.

The translucency of the FTIR plates for three of the four samples (CTD12-302, CTD12-303, CTD5-307) is very low. These three samples have a remarkable appearance: while they tend to look fairly opaque-black in hand-specimen, they are brilliantly orange-brown in thin-section. Even in hand-specimens, though, the edges of flakes have a brown color when held to the light but only at the finest feather edge of the flake (i.e., light does not transmit through the glass except when quite thin). In addition to the unusual color,

compared to the other FTIR plates, these plates are more opaque in appearance when held up to the light. When under the FTIR microscope they were noticeably deeper in hue than the normal grey or black samples. This is not simply because they are thicker; plate thickness in the twenty samples ranges from 184 to 369 microns (Table 8-12) and these three samples are 184, 209, and 336 microns thick. Specimen CTN-304 breaks from this pattern; it also is orange-brown in color but it is more translucent and is not banded.

Because FTIR measures the absorbance of the infra-red beam as it passes through the glass, where there is greater absorbance (i.e., less passage of light) the water content is measured as higher. Any factor that interferes with passage of the infra-red beam through the glass increases absorbance. In these samples, absorbance was higher and therefore measured water content was higher.

Less translucent glasses may well have some factor that is altering and increasing the absorbance. It is not simply microlite density, however, as this varies among all the twenty samples analyzed, and is not necessarily greater in the brown glasses. However, in the three brown and banded samples (CTD12-302, CTD12-303, CTD5-307), it was particularly challenging to select locations for FTIR analysis on the specimen because of variability among bands in the translucency of the glass and presence of microlites. The resulting FTIR results are highly variable in these three samples (Table 8-12). It is possible that averaging across the samples is problematic in these samples—either because they are variable in water content across the different bands, or because there is some factor increasing the absorbance in the brown glass. Given the color, iron would be an obvious compositional factor, but examination of the data indicates that total iron, FeO, and Fe_2O_3 are not unusual in these samples. Examination of all the major elements showed no other obvious compositional differences.

The second observation is that the FTIR spectra for the four brown samples had a distinctive appearance. While many of the FTIR arrays had an upward tilt on the left (higher wavenumber), the four brown glasses had more pronounced uptilts (see Figure 7-1, Chapter 7, for examples of array appearance—those calibration standards did not have an uptilt to the left). Presumably the upward tilt indicates that there is a peak located at a higher wavenumber that is drawing up the spectra. I am not certain that this could contribute to the measurement of water in a sample but it seems possible that the

tilt could alter the subtraction of peak from background or might otherwise affect how the measured peak is expressed (see Chapter 7 for detailed discussion of subtraction and computation techniques used).

8.3. Conclusions: Comparison of the LOI and FTIR Techniques for Archaeological Applications

Whatever factors are affecting the FTIR analysis of the brown glasses, when these samples are removed from the analysis the relationship between the LOI and FTIR results is a strong one. It appears from the regression scatterplot in Figure 8-5 that the relationship is linear and that LOI measures tend to overestimate water contents compared to FTIR. Ideally, if the FTIR results are fully accurate and reliable, a function similar to the regression equation could be used to adjust LOI values.

The comparison of the results of the LOI and FTIR analyses indicates that the application of both techniques was successful. The results suggest that each technique may be better suited for archaeological applications depending on the goal:

1) LOI is cheap and readily accessible to archaeologists, but requires destruction of larger quantities of glass. Thus for analysis of artifacts it is a poor technique. However, for assessing the values and range of water contents at a geological source, it would be an appropriate technique to determine whether high water content obsidians are present. If high water content glasses are found using LOI, then the more accurate FTIR technique would be warranted.

2) FTIR is more difficult to use but is less destructive and more accurate. If it is used in conjunction with OHD analysis, it should be possible to use the OH thin section for FTIR plates with the added preparation after OH analysis is completed. Further analyses of larger samples of obsidian will assist in determining whether the problems found in the brown glasses in this study are widespread or an anomaly associated with these rather unusual glasses. For this reason, using two techniques together (e.g. FTIR paired with LOI, as in this study, or another technique such as K-F titration) is advised in further studies to detect or monitor such specific issues in the accuracy of FTIR.

8.4. Conclusions: Interpreting the LOI and FTIR Analyses of Water Content

It is clear from the LOI and FTIR results that the obsidian deposits in the Dome area include obsidians with a broad range of water contents. This range includes water contents that are similar to the comparison glasses and those that are substantially higher. If the CDM samples (as well as CTNo, El Rechuelos, and Glass Buttes samples) are taken to represent "normal" water contents, then Cerro Toledo samples (CTD and CTN) are shown to include obsidians with substantially higher water content.

Considering the results of both the LOI and FTIR analyses together, the summary conclusions of the water content analyses are as follows.

1) Dome (CTD) samples include obsidians that are relatively *higher* in water content than the sample group collected from nearby deposits at Cerro del Medio (CDM) or the few samples from CTNo, El Rechuelos, or Glass Buttes. Considering all the data and dropping specimens that appear suspect or in error, the range of water contents for CTD glasses in this study appears to be between 0.3% and 1.3%. This falls within the range of water contents reported in the geological literature, but exceeds the range of 0.1% to 0.3% frequently reported in the obsidian hydration dating literature or the <0.5% range reported as most common by Macdonald et al. (1992) (see Chapter 5).

2) It appears that the Dome obsidians also can be considered *more variable* as indicated by the broad range of water contents present in the CTD samples. The large sample size for CTD can be expected to better represent the actual range extant in the Dome obsidians, with the smaller sample size from Cerro del Medio potentially obscuring the full range there. However, the influence of sample size is unlikely to have yielded such skewed results; for comparison, any random sample of the CTD samples would be highly unlikely produce a range of results as low as those seen for CDM. The LOI and FTIR results together are strong evidence for high and variable water contents in the Cerro Toledo Dome obsidian deposits.

3) As a compositional constituent, water contents are more variable in the CTD and CDM samples than variability in elemental composition. Comparing the CV values obtained for LOI (CV~30) and FTIR (CV~60) to the CV values for elemental composition discussed in Chapter 6, the water content CV values are much higher than

the CV values obtained for the well-measured trace elements (CV~10) and the major and minor elements (CV<10) except for iron and magnesium which were shown to have CV values ~10 to 40. In other words, in these samples variation in water content is greater than the variation in most of the elements. Most importantly, water content appears to vary independently from the specific trace elements most often used to establish geochemical sources.

The third interpretation must be made carefully because it is important in two ways:

a) In these samples, the amount of variation in water content is shown to be independent of the amount of variation in elemental composition: water content is more variable. As discussed in Chapter 6, this is expected because obsidian water content can vary broadly depending on the variables and conditions of eruption and cooling, while elemental composition is determined primarily by the composition of the magma.

b) However, I demonstrate that the mean water content values are statistically different among samples from the geochemical sources that I confirmed in Chapter 6 *are* defined by trace elements (i.e., CTD-CTN vs. CDM). The water contents of Cerro Toledo obsidians are different than the Valles Rhyolite obsidians. This conclusion conforms with the expectation that the pyroclastic obsidians from the explosive volcanic source, CTD, are higher and more variable in water content than the obsidians from the extrusive source, CDM.

A critical implication of these results is that a trace-element-defined source, such as CTD or CDM, can be also "characterized" as having high vs. low water content, and more vs. less variation in water content.

My interpretation of these data are contrary to the recommendations made by Stevenson et al. (2000) that elemental composition should not be measured as part of obsidian hydration dating because water content can be variable. In contrast, I conclude that analysis of water content and elemental composition should be conducted in tandem. If the effort is made to measure water content variation in the obsidians at the "source" geological deposits, as in this study, then geochemical "sourcing" of an artifact by trace elements can indicate also whether that artifact comes from obsidian-bearing deposits

that are high and/or variable in water content. My results show that pursuing water content measurement should not imply or dictate the abandonment of trace element "sourcing". Instead, variation in water content should be included in the consideration of source-attribution pursued during obsidian hydration dating. Analysis of elements and water composition together on the same obsidian specimens, whether artifacts or geological samples, will be highly productive in determining whether obsidians with characteristic trace element profiles are more or less variable in water content. When combined with knowledge of the eruptive origin of the obsidian-bearing deposits, it should be possible to predict and then test the robustness of the association of low and less variable water contents with extrusive obsidian sources and high and more variable water contents with explosive pyroclastic obsidian sources.

Table 8-12. Individual FTIR measures (i.e. replicated measures at multiple locations on an individual specimen); water content calculations use Ihinger and Stolper 1994.

Measure	A 5200	A 4500	Thick (*d*) cm	Density (ρ)	IS 1994 5200 (ε)	IS 1994 4500 (ε)	H_2O	OH	H_2O + OH
CDM302-1-0	0.0049	0.0090	0.01980	2362.3	1.86	1.5	0.102%	0.231%	0.333%
CDM302-1-1	0.0050	0.0092	0.01980	2362.3	1.86	1.5	0.103%	0.237%	0.340%
CDM302-2-0	0.0053	0.0094	0.01980	2362.3	1.86	1.5	0.110%	0.243%	0.353%
CDM302-2-1	0.0053	0.0097	0.01980	2362.3	1.86	1.5	0.111%	0.249%	0.360%
CDM302-3-0	0.0062	0.0094	0.01980	2362.3	1.86	1.5	0.128%	0.241%	0.369%
CDM302-3-1	0.0062	0.0095	0.01980	2362.3	1.86	1.5	0.128%	0.243%	0.371%
CDM304-1-0	*0.0095*	*0.0225*	*0.01903*	*2323.8*	*1.86*	*1.5*	*0.209%*	*0.611%*	*0.820%*
CDM304-1-1	*0.0098*	*0.0225*	*0.01903*	*2323.8*	*1.86*	*1.5*	*0.214%*	*0.610%*	*0.824%*
CDM304-1-2	*0.0097*	*0.0226*	*0.01903*	*2323.8*	*1.86*	*1.5*	*0.213%*	*0.614%*	*0.828%*
CDM304-2-0	*0.0099*	*0.0232*	*0.01903*	*2323.8*	*1.86*	*1.5*	*0.217%*	*0.631%*	*0.848%*
CDM304-2-1	*0.0106*	*0.0229*	*0.01903*	*2323.8*	*1.86*	*1.5*	*0.231%*	*0.623%*	*0.854%*
CDM304-3-0	*0.0097*	*0.0235*	*0.01903*	*2323.8*	*1.86*	*1.5*	*0.213%*	*0.639%*	*0.852%*
CDM304-3-1	*0.0096*	*0.0235*	*0.01903*	*2323.8*	*1.86*	*1.5*	*0.210%*	*0.639%*	*0.850%*
CDM304-4-0	*0.0096*	*0.0234*	*0.01903*	*2323.8*	*1.86*	*1.5*	*0.211%*	*0.635%*	*0.847%*
CDM304-5-0	*0.0103*	*0.0240*	*0.01903*	*2323.8*	*1.86*	*1.5*	*0.227%*	*0.651%*	*0.878%*
CDM304-5-1	*0.0105*	*0.0241*	*0.01903*	*2323.8*	*1.86*	*1.5*	*0.229%*	*0.654%*	*0.883%*
CTD10-301-1-0	0.0097	0.0132	0.02730	2313.8	1.86	1.5	0.149%	0.251%	0.400%
CTD10-301-1-1	0.0094	0.0135	0.02730	2313.8	1.86	1.5	0.145%	0.257%	0.402%
CTD10-301-2-0	0.0095	0.0129	0.02730	2313.8	1.86	1.5	0.145%	0.245%	0.391%
CTD10-301-2-1	0.0091	0.0129	0.02730	2313.8	1.86	1.5	0.139%	0.246%	0.385%
CTD10-301-3-0	0.0127	0.0141	0.02730	2313.8	1.86	1.5	0.195%	0.268%	0.463%
CTD10-301-3-1	0.0125	0.0142	0.02730	2313.8	1.86	1.5	0.191%	0.270%	0.461%
CTD10-302-	*0.0058*	*0.0141*	*0.01937*	*2311.6*	*1.86*	*1.5*	*0.125%*	*0.378%*	*0.503%*
CTD10-302-1-0	*0.0056*	*0.0144*	*0.01937*	*2311.6*	*1.86*	*1.5*	*0.121%*	*0.386%*	*0.507%*
CTD10-302-1-1	*0.0056*	*0.0146*	*0.01937*	*2311.6*	*1.86*	*1.5*	*0.122%*	*0.391%*	*0.513%*
CTD10-302-3-0	*0.0057*	*0.0143*	*0.01937*	*2311.6*	*1.86*	*1.5*	*0.124%*	*0.384%*	*0.508%*
CTD10-302-3-0	*0.0057*	*0.0145*	*0.01937*	*2311.6*	*1.86*	*1.5*	*0.124%*	*0.388%*	*0.511%*
CTD10-302-4-0	*0.0057*	*0.0145*	*0.01937*	*2311.6*	*1.86*	*1.5*	*0.124%*	*0.388%*	*0.511%*
CTD10-302-4-1	*0.0048*	*0.0138*	*0.01937*	*2311.6*	*1.86*	*1.5*	*0.104%*	*0.370%*	*0.474%*
CTD10-303-1-0	0.0056	0.0117	0.01835	2311.2	1.86	1.5	0.128%	0.330%	0.458%
CTD10-303-1-1	0.0057	0.0117	0.01835	2311.2	1.86	1.5	0.131%	0.331%	0.462%
CTD10-303-2-0	0.0060	0.0131	0.01835	2311.2	1.86	1.5	0.136%	0.372%	0.508%
CTD10-303-2-1	0.0060	0.0129	0.01835	2311.2	1.86	1.5	0.138%	0.367%	0.504%
CTD10-303-3-0	0.0064	0.0133	0.01835	2311.2	1.86	1.5	0.147%	0.376%	0.523%
CTD10-303-3-1	0.0066	0.0132	0.01835	2311.2	1.86	1.5	0.151%	0.373%	0.524%
CTD10-305-1-0	*0.0068*	*0.0180*	*0.03060*	*2315.3*	*1.86*	*1.5*	*0.093%*	*0.305%*	*0.398%*
CTD10-305-1-1	*0.0069*	*0.0180*	*0.03060*	*2315.3*	*1.86*	*1.5*	*0.094%*	*0.305%*	*0.399%*
CTD10-305-2-0	*0.0063*	*0.0184*	*0.03060*	*2315.3*	*1.86*	*1.5*	*0.087%*	*0.313%*	*0.400%*
CTD10-305-2-1	*0.0068*	*0.0186*	*0.03060*	*2315.3*	*1.86*	*1.5*	*0.093%*	*0.316%*	*0.408%*
CTD10-305-3-0	*0.0063*	*0.0168*	*0.03060*	*2315.3*	*1.86*	*1.5*	*0.087%*	*0.284%*	*0.371%*
CTD10-305-3-1	*0.0064*	*0.0169*	*0.03060*	*2315.3*	*1.86*	*1.5*	*0.088%*	*0.286%*	*0.374%*
CTD12-302-1-0	0.0525	0.0440	0.02090	2307.8	1.86	1.5	1.054%	1.096%	2.150%
CTD12-302-2-0	0.0524	0.0440	0.02090	2307.8	1.86	1.5	1.053%	1.095%	2.148%
CTD12-302-3-0	0.0485	0.0424	0.02090	2307.8	1.86	1.5	0.974%	1.056%	2.030%

Table 8-13. Continued: Individual FTIR measures.

Measure	A 5200	A 4500	Thick (*d*) cm	Density (ρ)	IS 1994 5200 (ε)	IS 1994 4500 (ε)	H_2O	OH	H_2O + OH
CTD12-302-3-1	0.0484	0.0423	0.02090	2307.8	1.86	1.5	0.973%	1.053%	2.026%
CTD12-302-4-0	0.0476	0.0400	0.02090	2307.8	1.86	1.5	0.955%	0.996%	1.951%
CTD12-302-4-1	0.0475	0.0401	0.02090	2307.8	1.86	1.5	0.955%	0.998%	1.953%
CTD12-302-5-0	0.0503	0.0399	0.02090	2307.8	1.86	1.5	1.011%	0.993%	2.004%
CTD12-302-6-0	0.0499	0.0397	0.02090	2307.8	1.86	1.5	1.002%	0.989%	1.990%
CTD12-303-1-0	*0.0320*	*0.0404*	*0.01837*	*2311.2*	*1.86*	*1.5*	*0.731%*	*1.143%*	*1.874%*
CTD12-303-1-1	*0.0310*	*0.0405*	*0.01837*	*2311.2*	*1.86*	*1.5*	*0.709%*	*1.146%*	*1.855%*
CTD12-303-2-0	*0.0369*	*0.0426*	*0.01837*	*2311.2*	*1.86*	*1.5*	*0.843%*	*1.206%*	*2.049%*
CTD12-303-2-1	*0.0377*	*0.0422*	*0.01837*	*2311.2*	*1.86*	*1.5*	*0.861%*	*1.195%*	*2.056%*
CTD12-303-2-2	*0.0387*	*0.0429*	*0.01837*	*2311.2*	*1.86*	*1.5*	*0.883%*	*1.214%*	*2.096%*
CTD12-303-2-3	*0.0375*	*0.0427*	*0.01837*	*2311.2*	*1.86*	*1.5*	*0.855%*	*1.209%*	*2.064%*
CTD12-303-3-0	*0.0319*	*0.0396*	*0.01837*	*2311.2*	*1.86*	*1.5*	*0.727%*	*1.122%*	*1.849%*
CTD12-303-3-1	*0.0332*	*0.0400*	*0.01837*	*2311.2*	*1.86*	*1.5*	*0.758%*	*1.132%*	*1.889%*
CTD5-307-1-0	0.0698	0.0597	0.03357	2305.0	1.86	1.5	0.874%	0.926%	1.800%
CTD5-307-1-1	0.0694	0.0599	0.03357	2305.0	1.86	1.5	0.869%	0.930%	1.799%
CTD5-307-2-0	0.0508	0.0472	0.03357	2305.0	1.86	1.5	0.636%	0.733%	1.369%
CTD5-307-2-1	0.0495	0.0470	0.03357	2305.0	1.86	1.5	0.620%	0.730%	1.350%
CTD5-307-3-0	0.0687	0.0587	0.03357	2305.0	1.86	1.5	0.860%	0.911%	1.771%
CTD5-307-3-1	0.0682	0.0589	0.03357	2305.0	1.86	1.5	0.854%	0.914%	1.768%
CTD6-301-1-0	*0.0186*	*0.0336*	*0.03693*	*2314.0*	*1.86*	*1.5*	*0.211%*	*0.473%*	*0.684%*
CTD6-301-1-1	*0.0181*	*0.0339*	*0.03693*	*2314.0*	*1.86*	*1.5*	*0.205%*	*0.476%*	*0.681%*
CTD6-301-2-0	*0.0200*	*0.0350*	*0.03693*	*2314.0*	*1.86*	*1.5*	*0.227%*	*0.492%*	*0.720%*
CTD6-301-2-1	*0.0205*	*0.0348*	*0.03693*	*2314.0*	*1.86*	*1.5*	*0.233%*	*0.489%*	*0.722%*
CTD6-301-3-0	*0.0212*	*0.0353*	*0.03693*	*2314.0*	*1.86*	*1.5*	*0.241%*	*0.497%*	*0.737%*
CTD6-301-3-1	*0.0212*	*0.0353*	*0.03693*	*2314.0*	*1.86*	*1.5*	*0.240%*	*0.496%*	*0.736%*
CTD6-301-x-0	*0.0213*	*0.0351*	*0.03693*	*2314.0*	*1.86*	*1.5*	*0.242%*	*0.493%*	*0.735%*
CTD6-302-2-0	0.0105	0.0275	0.03557	2313.2	1.86	1.5	0.123%	0.401%	0.525%
CTD6-302-2-1	0.0104	0.0276	0.03557	2313.2	1.86	1.5	0.123%	0.403%	0.526%
CTD6-302-4-0	0.0108	0.0275	0.03557	2313.2	1.86	1.5	0.127%	0.401%	0.528%
CTD6-302-4-1	0.0105	0.0275	0.03557	2313.2	1.86	1.5	0.123%	0.402%	0.525%
CTD6-302-5-0	0.0110	0.0281	0.03557	2313.2	1.86	1.5	0.129%	0.410%	0.539%
CTD6-302-5-1	0.0111	0.0279	0.03557	2313.2	1.86	1.5	0.130%	0.408%	0.538%
CTD7-302-1-0	*0.0256*	*0.0402*	*0.03387*	*2309.1*	*1.86*	*1.5*	*0.317%*	*0.618%*	*0.935%*
CTD7-302-1-1	*0.0251*	*0.0401*	*0.03387*	*2309.1*	*1.86*	*1.5*	*0.310%*	*0.616%*	*0.927%*
CTD7-302-2-0	*0.0254*	*0.0408*	*0.03387*	*2309.1*	*1.86*	*1.5*	*0.314%*	*0.626%*	*0.940%*
CTD7-302-2-1	*0.0249*	*0.0410*	*0.03387*	*2309.1*	*1.86*	*1.5*	*0.309%*	*0.630%*	*0.938%*
CTD7-302-3-0	*0.0232*	*0.0350*	*0.03387*	*2309.1*	*1.86*	*1.5*	*0.287%*	*0.538%*	*0.826%*
CTD7-302-3-1	*0.0229*	*0.0349*	*0.03387*	*2309.1*	*1.86*	*1.5*	*0.283%*	*0.535%*	*0.819%*
CTDRM-301-1-0	0.0067	0.0078	0.02127	2317.6	1.86	1.5	0.131%	0.191%	0.322%
CTDRM-301-1-1	0.0066	0.0078	0.02127	2317.6	1.86	1.5	0.129%	0.191%	0.320%
CTDRM-301-2-0	0.0080	0.0065	0.02127	2317.6	1.86	1.5	0.157%	0.159%	0.316%
CTDRM-301-3-0	0.0067	0.0072	0.02127	2317.6	1.86	1.5	0.131%	0.176%	0.307%
CTDRM-301-3-1	0.0065	0.0078	0.02127	2317.6	1.86	1.5	0.129%	0.189%	0.318%
CTDRM-3-1-2-1	0.0078	0.0069	0.02127	2317.6	1.86	1.5	0.154%	0.167%	0.321%
CTN302-1-0	*0.0062*	*0.0062*	*0.02000*	*2315.4*	*1.86*	*1.5*	*0.130%*	*0.161%*	*0.292%*
CTN302-2-0	*0.0047*	*0.0051*	*0.02000*	*2315.4*	*1.86*	*1.5*	*0.099%*	*0.132%*	*0.231%*

Table 8-14. Continued: Individual FTIR measures.

Measure	A 5200	A 4500	Thick (*d*) cm	Density (ρ)	IS 1994 5200 (ε)	IS 1994 4500 (ε)	H_2O	OH	H_2O + OH
CTN302-3-0	*0.0039*	*0.0051*	*0.02000*	*2315.4*	*1.86*	*1.5*	*0.081%*	*0.133%*	*0.214%*
CTN302-3-1	*0.0040*	*0.0051*	*0.02000*	*2315.4*	*1.86*	*1.5*	*0.084%*	*0.132%*	*0.217%*
CTN302-3-2	*0.0041*	*0.0054*	*0.02000*	*2315.4*	*1.86*	*1.5*	*0.085%*	*0.140%*	*0.225%*
CTN304-1-0	0.0125	0.0186	0.01750	2309.4	1.86	1.5	0.300%	0.552%	0.852%
CTN304-1-1	0.0126	0.0188	0.01750	2309.4	1.86	1.5	0.303%	0.559%	0.862%
CTN304-2-0	0.0240	0.0228	0.01750	2309.4	1.86	1.5	0.575%	0.679%	1.254%
CTN304-2-1	0.0244	0.0229	0.01750	2309.4	1.86	1.5	0.586%	0.682%	1.267%
CTN304-3-0	0.0218	0.0221	0.01750	2309.4	1.86	1.5	0.522%	0.655%	1.177%
CTN304-3-1	0.0216	0.0219	0.01750	2309.4	1.86	1.5	0.518%	0.650%	1.168%
CTN304-x-0	0.0280	0.0236	0.01750	2309.4	1.86	1.5	0.671%	0.701%	1.372%
CTN304-x-1	0.0275	0.0239	0.01750	2309.4	1.86	1.5	0.658%	0.709%	1.367%
CTN308-2-0	*0.0099*	*0.0199*	*0.01945*	*2308.4*	*1.86*	*1.5*	*0.214%*	*0.532%*	*0.745%*
CTN308-2-1	*0.0099*	*0.0201*	*0.01945*	*2308.4*	*1.86*	*1.5*	*0.214%*	*0.539%*	*0.753%*
CTN308-3-0	*0.0092*	*0.0195*	*0.01945*	*2308.4*	*1.86*	*1.5*	*0.199%*	*0.521%*	*0.721%*
CTN308-3-1	*0.0091*	*0.0194*	*0.01945*	*2308.4*	*1.86*	*1.5*	*0.197%*	*0.518%*	*0.715%*
CTN308-4-0	*0.0099*	*0.0199*	*0.01945*	*2308.4*	*1.86*	*1.5*	*0.214%*	*0.532%*	*0.745%*
CTN308-4-1	*0.0099*	*0.0197*	*0.01945*	*2308.4*	*1.86*	*1.5*	*0.214%*	*0.526%*	*0.740%*
GS10-1-1-0	0.0058	0.0140	0.01880	2311.7	1.86	1.5	0.129%	0.387%	0.516%
GS10-1-1-1	0.0059	0.0138	0.01880	2311.7	1.86	1.5	0.132%	0.382%	0.514%
GS10-1-2-0	0.0055	0.0135	0.01880	2311.7	1.86	1.5	0.122%	0.372%	0.494%
GS10-1-2-1	0.0054	0.0136	0.01880	2311.7	1.86	1.5	0.119%	0.376%	0.495%
GS10-1-3-0	0.0064	0.0137	0.01880	2311.7	1.86	1.5	0.142%	0.378%	0.520%
GS10-1-3-1	0.0063	0.0135	0.01880	2311.7	1.86	1.5	0.141%	0.374%	0.515%
GS10-1-4-0	0.0060	0.0138	0.01880	2311.7	1.86	1.5	0.134%	0.380%	0.515%
GS10-1-4-1	0.0061	0.0135	0.01880	2311.7	1.86	1.5	0.135%	0.374%	0.509%
GS7-1-1-0	*0.0102*	*0.0204*	*0.01817*	*2309.2*	*1.86*	*1.5*	*0.235%*	*0.585%*	*0.821%*
GS7-1-1-1	*0.0103*	*0.0205*	*0.01817*	*2309.2*	*1.86*	*1.5*	*0.238%*	*0.588%*	*0.827%*
GS7-1-2-0	*0.0110*	*0.0210*	*0.01817*	*2309.2*	*1.86*	*1.5*	*0.253%*	*0.602%*	*0.855%*
GS7-1-2-1	*0.0107*	*0.0213*	*0.01817*	*2309.2*	*1.86*	*1.5*	*0.247%*	*0.611%*	*0.858%*
GS7-1-3-1	*0.0103*	*0.0207*	*0.01817*	*2309.2*	*1.86*	*1.5*	*0.237%*	*0.594%*	*0.831%*
GS7-1-3-2	*0.0104*	*0.0205*	*0.01817*	*2309.2*	*1.86*	*1.5*	*0.240%*	*0.587%*	*0.827%*
GS7B1-1-	0.0152	0.0241	0.01835	2308.5	1.86	1.5	0.348%	0.683%	1.031%
GS7B1-1-0	0.0154	0.0242	0.01835	2308.5	1.86	1.5	0.352%	0.686%	1.038%
GS7B1-1-1	0.0154	0.0239	0.01835	2308.5	1.86	1.5	0.353%	0.676%	1.030%
GS7B1-2-0	0.0145	0.0230	0.01835	2308.5	1.86	1.5	0.332%	0.652%	0.984%
GS7B1-2-1	0.0143	0.0230	0.01835	2308.5	1.86	1.5	0.326%	0.653%	0.979%
GS7B1-3-0	0.0159	0.0243	0.01835	2308.5	1.86	1.5	0.363%	0.690%	1.053%
GS7B1-3-1	0.0163	0.0242	0.01835	2308.5	1.86	1.5	0.373%	0.688%	1.061%
GS8-1-1-0	*0.0146*	*0.0215*	*0.01823*	*2311.5*	*1.86*	*1.5*	*0.337%*	*0.612%*	*0.948%*
GS8-1-1-1	*0.0146*	*0.0214*	*0.01823*	*2311.5*	*1.86*	*1.5*	*0.336%*	*0.611%*	*0.946%*
GS8-1-1-2	*0.0146*	*0.0225*	*0.01823*	*2311.5*	*1.86*	*1.5*	*0.336%*	*0.641%*	*0.977%*
GS8-1-2-1	*0.0148*	*0.0224*	*0.01823*	*2311.5*	*1.86*	*1.5*	*0.340%*	*0.639%*	*0.980%*
GS8-1-3-0	*0.0150*	*0.0224*	*0.01823*	*2311.5*	*1.86*	*1.5*	*0.344%*	*0.639%*	*0.984%*
GS8-1-3-1	*0.0147*	*0.0224*	*0.01823*	*2311.5*	*1.86*	*1.5*	*0.338%*	*0.639%*	*0.978%*

CHAPTER 9
CONCLUSIONS

This dissertation has been an exploration of the interplay between glass composition and the environmental transformation of obsidian by the processes of heat and hydration. At the outset of the project I made the decision to focus on the material in which the variable and extreme transformations occur—obsidian—rather than on the burning event represented by the Dome forest fire. This focus on glass composition led me to frame different kinds of questions about fire effects *and* geochemical analyses than usually are asked in studies where fire, obsidian sourcing, or obsidian hydration alone are the focus of research. This difference in perspective has been productive, leading to significant considerations that will help frame new strategies for integrating obsidian geochemical research and obsidian hydration dating practices. Below I summarize the studies I conducted and results obtained. Following the summary, I discuss implications of these results for archaeological formation processes, for the management of cultural resources, and for the validity of archaeological methods of obsidian analysis.

Summary of Research and Results

Three broad goals of the research have been: 1) to understand how fires alter archaeological artifacts and the obsidian hydration chronometric information contained in these assemblages, 2) to provide baseline information needed to better preserve obsidian artifact assemblages where fires are part of the forest ecology, and 3) to contribute to the on-going development of an important chronometric technique by enhancing our understanding of the role of glass composition in the obsidian hydration process. In the introduction I defined five objectives to pursue these goals:

1. Identify how archaeologists may recognize fire effects on obsidian artifacts by describing the variability in fire effects observed at Capulin Quarry.
2. Evaluate the impact of forest fires for obsidian hydration dating by examining the presence and characteristics of hydration rinds in burned artifacts associated with greater and lesser degrees of burn severity across Capulin Quarry.

3. Consider the role of obsidian elemental composition for variable fire effects, especially vesiculation, by measuring major, minor, and trace element composition within the Cerro Toledo Rhyolite obsidian-bearing deposits burned during the Dome fire, and then comparing elemental composition to nearby obsidian sources to assess intrasource vs. intersource compositional variation.
4. Develop appropriate archaeological methodology for measuring water in obsidian by testing alternative techniques for determining obsidian water content.
5. Determine the variation of volatile composition within this geochemical source by measuring obsidian water content within the Cerro Toledo Rhyolite and comparing to water content in nearby obsidian sources.

To meet the first objective I created a suite of descriptive categories to organize the variability in obsidian fire effects observed at Capulin Quarry. Recent archaeological discussions of obsidian fire effects have stated a need for standardized descriptions of visual indicators of heat exposure. The fire effects categories described in Chapter 3 using both narrative and graphic illustration provide a set of tools to meet this need, as well as to introduce the macroscopic appearance of fire effects to archaeologists unfamiliar with obsidian heat alteration, and to foster comparison and communication for others working with burned collections. These descriptive categories will be equally valuable for archaeologists seeking to recognize and identify obsidian altered by heat under numerous other cultural and natural circumstances.

For the second objective I examined heat alteration of obsidian artifacts at the microscopic scale. The analyses in Chapter 4 of obsidian hydration bands on Capulin Quarry artifacts demonstrated that significant loss and alteration of hydration bands (40 to 100 percent) occurred in artifacts burned during the Dome Fire and that these effects to OH increased with the degree of burn severity. My results strongly bolster the concerns raised in previous post-fire research: forest fires can have a substantial impact to the chronometric information contained in surface assemblages, and the role of forest fires as a secondary hydration variable must be given greater attention in managing archaeological resources in forested environments and when using OHD in these assemblages. My research also provides baseline observations to address these concerns.

I show that the presence of macroscopic fire effects attributes serve as valid indicators of OH alteration or loss in assemblages where burning was moderate to severe. This research also indicates that diffuse hydration is a useful indicator of recent fire exposure. I conducted an intensive analysis of individual specimens with crazing or partial vesiculation employing multiple OH cuts on individual artifacts. This unusual approach revealed that, when examined closely, burned artifacts can have intact obsidian hydration and may exhibit complex patterns of OH alteration that defy ready explanation. These results demonstrate the potential complexity of the hydration diffusion process in heated obsidian, and further suggest that research into obsidian dehydration and rehydration may be an important avenue to elucidate the diffusion processes that are central to the obsidian hydration dating model.

The last three objectives explore the role of obsidian composition for vesiculation and for the methodology of obsidian hydration dating. In Chapters 6 and 8, I employed multiple analyses to measure three components of obsidian composition: trace elements, minor and major elements, and water content. The approach taken in this study differs from most current standard obsidian analyses in that I focused on geochemical variation rather than characterization, and because I integrated the analyses of all three compositional components on the same samples. My goal in this comprehensive analysis of rhyolitic glass composition was to evaluate and compare the relative variation in these three components—within the obsidian-bearing deposits burned during the Dome Fire as well as among geologically related and unrelated obsidian sources included for comparison. I employed two techniques, LOI and FTIR, to investigate the water content of obsidian samples, and demonstrated that both are effective for archaeological applications. The discussion in Chapters 7 and 8 of the tradeoffs in accuracy, difficulty, cost, and destructiveness of each technique helps demystify the pursuit of obsidian water content measurement and will enable archaeologists seeking to utilize these or other techniques to compare both their methods and results.

My emphasis on composition analyses led to results that are instructive both for understanding the variation in fire effects observed following the Dome Fire and for broader application to practices of obsidian geochemical analyses and the obsidian hydration dating model. First, the trace element analyses confirm that the CTD obsidians

burned during the Dome Fire are a single chemical group. Thus, trace elements can be ruled out as a source of variation in the fire effects observed across this geological deposit. Second, analysis of minor and major elements reveals substantial variation within the CTD deposits or among the comparison deposits at CTN and CDM only in iron and magnesium. The results for iron are particularly intriguing and demonstrate that this major/minor element can vary substantially despite relative homogeneity in trace elements. Future analyses should explore how the unexpected results for ferrous and ferric iron content, alone or in conjunction with water content, may contribute to fire effects or to hydration.

Finally, I discuss in Chapter 5 how water content may play a role in obsidian hydration and vesiculation, and I consider how volcanic origin and eruptive history could contribute to variation in obsidian water content. Overall, high and variable water contents are more likely to result from explosive than extrusive volcanic activity, and thus obsidians in pyroclastic tephra deposits (i.e., CTD and CTN) are more likely to be high and variable in water content than obsidians found in extrusive domes or flows (e.g., CDM). The obsidian water content results I obtained conform to these expectations. In this study, the pyroclastic CTD and CTN obsidians were found to include a large proportion of samples that are high in water content (LOI greater than 0.5%, up to 1.3%) compared to previous results in the geological and archaeological literature. The pyroclastic CTD obsidians also were shown to be more variable in water content (LOI: 0.3% to 1.3%) than samples from the extrusive source, CDM (LOI: 0.2% to 0.6%). These results, in conjunction with observations made in the geological literature (see also data presented in Appendix C), strongly support the possibility that high and variable obsidian water content can contribute to variation in the susceptibility of obsidian artifacts to vesiculation when exposed to heat during forest fires. The simple muffle furnace experiments I conducted to test this association in high and low water CTD samples (Appendix E) provide additional preliminary support for the role of water content in lowering the temperature at which obsidian vesiculates.

The water content results I obtained in this study are similar to those found by Stevenson and colleagues in their study of obsidians from Coso quarries in California. Those results, in conjunction with later analyses, led the researchers to conclude that

hydration rates are related to water content: water-rich obsidians hydrate at faster rates than low-water obsidians. This possibility is tremendously important for the obsidian hydration dating method because it adds a compositional variable, water, to the current working OHD model. While much more research is needed, this modification has the potential to enhance the performance and productivity of this archaeological dating technique by improving the accuracy of dating outcomes and increasing the robustness of its application. The results of my study contribute to this possibility 1) by demonstrating the occurrence of water content variability in another geochemical source, 2) by considering the geological contexts that may be involved in high and variable obsidian water contents, and 3) by evaluating the performance of two techniques that archaeologists may use for measuring obsidian water content.

However, my conclusions about this combined body of results are different from Stevenson's. Whereas Stevenson and colleagues have advocated the abandonment of elemental composition analyses, I conclude that analysis of water content and elemental composition should be conducted in tandem. I have taken a variational approach to examining obsidian composition in which 1) I explored rather than assumed the relationship between trace element source characterization and potential variation in the minor and major elements *and* volatile composition that may affect hydration rates, and 2) I measured water content as part of comprehensive analysis of composition in obsidian samples from within and among obsidians of shared and differing chemical groups as well as variable geological contexts. The results of this examination of heat alteration of obsidian hydration in combination with these compositional analyses compel a reexamination of OHD practice and pursuit of hypotheses that test various aspects of the obsidian hydration model. In sum, rather than advocating a particular set of techniques or rejecting established practices, my conclusions call for active evaluation and enhancement of the OH model and OHD methods.

Applications and Implications

Fire and the Formation of the Archaeological Record

Exposure to forest fires is a natural transformation process of the archaeological record in forested environments (Connor and Cannon 1991). Little attention has been paid to forest fires outside the gray literature of federal lands cultural resource management, as demonstrated by the lack of treatment of the subject in Schiffer's (1987, 1995) treatises on archaeological formation processes. However, heat alteration of lithic materials could be a useful observation for diverse questions about prehistory, ranging from identification of the earliest hominid use of fire (e.g., Goren-Unbar et al. 2004), to unraveling the complexity of human behavior at the scale of site (e.g., Nakazawa 1998), to understanding aboriginal control of the landscape through the cultural use of fire (Deal and McLemore 2002; see also Vale 2002). The potential of fire to alter chronometric information contained in the archaeological record (including not just obsidian hydration dating, but also dendrochronology, thermoluminescence, archaeomagnetic and radiocarbon dating techniques[1]) lends additional relevance to the accurate and widespread identification of obsidian artifacts altered by fire. The descriptive categories I present in Chapter 3 can be used for recognition and identification of heat alteration in obsidian in any archaeological or geological context in addition to those where forest fires are the source of heat exposure.

As discussed in Chapter 2, low intensity fires with short return intervals characterize the natural fire regime in the Ponderosa and mixed-conifer forests characteristic of the Dome area, other areas in the Jemez Mountains, and throughout many parts of the American Southwest and elsewhere. All artifact assemblages on present and past surfaces within this and similar forested environments can be expected to have experienced the occurrence of wildland fires repeatedly. To consider how such fire exposure may have affected surface obsidian artifact assemblages in the past requires consideration of changing biotic and climatic conditions, and reconstruction of the history of exposure versus burial of assemblages. While the latter is often treated as self-evident,

[1] Alteration of dates by forest fires also has been implicated in a geological chronometric method, apatite and zircon (U-Th)/He dating (Mitchell and Reiners 2003).

with currently exposed surfaces treated as long-exposed and subsurface deposits treated as long-buried, observation of the extreme sheet erosion and subsequent exposure of buried artifacts across large areas at Capulin Quarry in the years immediately following the Dome Fire is an object lesson in the potential mutability of the surface vs. subsurface dichotomy. Determining what are the average or common fire effects for artifact assemblages is a complex enterprise with numerous variables and interacting factors to consider.

This work is a unique contribution to this effort because the Dome Fire and the outcomes observed at Capulin Quarry offer a case that appears to be well outside the norm—both in terms of the severity of the fire and the obsidian that was affected. The Dome Fire was the first large crown fire in the Jemez Mountains since the La Mesa Fire in 1977. At the time the Dome Fire burned in 1996 it was considered an extraordinary event and a potential harbinger of future catastrophic fire events (as realized by the subsequent Cerro Grande Fire). When abundant vesiculated obsidian was discovered by archaeologists at Capulin Quarry following the Dome Fire, this extreme fire effect was considered a powerful indicator of the unusual intensity of this fire. The severity of the Dome Fire was considered potentially anthropogenic, caused by the decades of fire suppression, logging, and grazing in the Jemez Mountains. The ignition of the fire was, in fact, due to human rather than nature agency.

I saw these circumstances as an important opportunity as a case study in the maximum impact of forest fires on obsidian artifacts, in a setting with the uppermost density and abundance of obsidian assemblages because it is a large obsidian quarry. The effects observed at Capulin Quarry following the Dome Fire are not an analog for past "normal" fire history or for average obsidian assemblages: I assumed instead that this is the worst case with the most stuff in the most exposed context. Here it was possible to observe a full range of macroscopic fire effects to obsidian, to examine what the (microscopic) effects were to obsidian hydration in such an assemblage, and thus to provide a case study that potentially encompassed the range of all other more normal events and conditions of fire exposure. This broad range would allow extrapolation not only to other natural contexts of burning but also to human behavioral contexts involving

high heat, such as hearths, swidden agriculture, structure fires, roasting pits, refuse burning, and cremations.

Given a context where the fire itself could be assumed to represent the extreme, it was possible to focus instead on the material that had been affected by the fire. I examined whether the extreme effects observed at Capulin Quarry were due to the, now assumed, severity of the forest fire or to characteristics of the glass composition. Could variation in fire effects observed in the assemblage be attributed to the known complexity of landscape-scale fires or to variation in the material subjected to heat exposure? My analyses of obsidian composition in samples drawn from the Cerro Toledo Rhyolite deposits indicated that this material is, in fact, potentially unusual in that it contains high and variable water content. In this regard, it appears that the obsidian burned in this fire may be "unusual" just as was the Dome Fire itself. However, the incidence and distribution of obsidians that are high and variable in water content has not been investigated sufficiently to determine whether CTR glasses are actually uncommon, or simply one of the few cases where the analyses to describe water content characteristics of obsidian-bearing deposits have been conducted. As it stands, the obsidian fire effects observed following the Dome fire have provided a productive case study for describing a broad range of fire effects that can be anticipated--from the extremes of vesiculation and fire fracture to the subtleties of crazing and surface sheen--to indicate that fire alteration has played a role in the formation processes operating in given archaeological record, whatever the natural or cultural contexts of those fires.

Fire and the Management of Cultural Resources

The active goal in managing cultural resources is to protect archaeological properties from undue damage from forest fires. In the terminology of Section 106 of the National Historic Preservation Act (NHPA), managers must evaluate whether there is a potential for an undertaking (e.g., a prescribed burn) to reach the severity required to compromise the OHD chronometric information potential of the surface assemblage that qualifies a site as eligible for inclusion on the National Register of Historic Places (NRHP), and thus whether a prescribed fire would constitute a potential adverse effect to historic properties. In considering adverse effects from future fires, cultural resource

managers have to assess the potential extent of damage from heat and combustion, as well as how great is the risk that damage may occur. When assessing fires after they have occurred, archaeologists often must be able to accurately evaluate what kinds of damage have occurred based on rapid field inspections. In terms of policy and planning, management decisions aimed at preserving the archaeological record must be both practical and well-informed. Expectations about potential threats to the archaeological record must be based on actual scientific observation, and knowledge of how to recognize effects must be shared broadly among those archaeologists tasked with assessing post-fire effects. The current study was designed to provide information relevant to all of these considerations.

Practicality is important in developing pre-fire site treatments because it is not feasible to simply avoid all archaeological sites when planning prescribed fires, nor is that approach effective for the long term protection of sites from unplanned fires. Archaeologists must identify what characteristics of cultural resources actually will be adversely affected by fire (rather than just inconsequentially altered), and then determine how to protect these specified values. In the case of obsidian artifacts, loss of artifact form is one important characteristic while the other high value is the potential chronometric information contained in intact unaltered artifact hydration rinds. Usually the threat to obsidian hydration dating potential is the only adverse effect considered. However, the extreme fire effects observed following the Dome Fire revealed the potential for forest fires to fully or partially destroy obsidian artifacts by vesiculation. While obsidian vesiculation was known to occur following forest fires (e.g., Trembour 1990), the extent of vesiculation damage observed at Capulin Quarry far exceeded the prior perception of merely anecdotal damage. Here vesiculated artifacts were abundant and the numerous clusters of vesiculated items demonstrated that loss of artifacts to vesiculation was sufficient to affect the contents of an assemblage.

The judgmental and systematic sampling I conducted at Capulin Quarry indicated that the extent of damage from partial and complete vesiculation of artifacts is proportionally low (e.g., 1.2 percent of artifacts in the systematic sampling unit). If extrapolated across the entire quarry, the total number of artifacts affected by vesiculation could be quite large but only because of the abundance of artifacts in this large quarry site.

Overall, the potential for loss of artifact form due to vesiculation appears to be relatively low and thus not a substantial concern for fire management planning in quarry contexts. However, where assemblages are rich in shaped obsidian artifacts and tools, loss of information on artifact style and function could be expected to be higher than in quarry assemblages. Fire fracture, on the other hand, was observed to occur in higher frequencies (>16 percent) in the systematic sample examined. Loss of artifact form is a possibility with thermal fracture, offset somewhat by the fact that certain technological attributes of intentional human-caused reduction remain on the fractured pieces. The greater problem posed by fire fracture probably is in creating non-artifacts that have the appearance of artifacts, thus causing confusion or obscuring the technological attributes apparent across quarry assemblages that already are challenging for rapid and accurate characterization by archaeologists who are not specialists in describing the early reduction of cobble and nodule obsidians.

The first goal of this study was to provide visual and descriptive tools for the identification of macroscopic effects of fire to obsidian artifacts. At the most elementary level, identification of macroscopic fire effects in obsidian artifacts aids the archaeologist in determining or initially recognizing that heat alteration has played a role in the formation history of an assemblage. As it stands now, the full range of fire effects are not commonly included by archaeologists when describing the condition of obsidian artifacts. The categories presented in Chapter 3 will assist archaeologists unfamiliar with the appearance of fire effects to begin to recognize and report their occurrence in assemblages. For researchers already aware of obsidian fire effects, the categories will aid in describing the range of effects present in assemblages (e.g., Buenger 2003), and to communicate within the field as to the frequency or prevalence of various effects. Increased attention to such effects will contribute in the future to more accurately assessing whether fire effects are actually as unusual as the existing literature would suggest, or if they are perhaps more ubiquitous than currently appreciated.

In addition, accurate identification of heat-altered obsidian artifacts will benefit post-fire site condition assessment as conducted by federal interagency BAER (Burned Area Emergency Response) teams. Recognition of heat alterations such as crazing and fire fracture can serve as a readily-apparent cue that high ground temperatures were

reached at sites that otherwise may have few visual indicators of impact to artifact assemblages. The results of the quantitative analysis of obsidian hydration alteration in the systematic sample conducted for this study (Chapter 4) indicate strongly that the presence of fire effects such as crazing and fire fracture co-occur spatially with burning conditions that result in a very high proportion (>60 percent) of OH alteration across the sum of all artifacts with and without visible alteration. In this capacity, macroscopic fire effects are a powerful tool for recognizing when or where forest fires may have had a significant impact to the chronometric information potential of obsidian artifact assemblages, and thus for indicating that further evaluation of forest fire impact is warranted.

The obsidian hydration analyses of burned artifacts presented in Chapter 4 provide strong evidence that the damage to OH sustained in the obsidian artifact assemblage at Capulin Quarry is substantial. In the first study, 44 to 100 percent of specimens collected from a range of apparent burn severity contexts exhibited loss or alteration of OH with a demonstrated trend of higher alteration/loss with increasing burn severity. Viewed from the perspective of preserving the chronometric information content within sites, the alteration/loss of OH bands in nearly half to all of a surface assemblage is an extraordinarily high proportion and cannot help but raise concern that wildfires like the Dome Fire need be considered an adverse effect to be avoided or mitigated.

In the second study, a more in-depth analysis conducted within an area of moderate to high burn severity showed that loss and alteration of OH occurred in >60 percent of all artifacts analyzed. This study also indicated that the frequency of OH loss/alteration was *not* greater in artifacts with visible fire effects. The latter results are counter to expectation and are important for how visual examination for macroscopic fire effects is used in assessing the post-fire condition of sites and artifacts. While the presence of macroscopic effects can be used to infer an increased potential for impacts to the OH information in a burned assemblage, the absence of these attributes does not indicate lack of alteration on a given individual specimen. Indeed, the intensive analysis of selected individual specimens demonstrated that OH bands may be present even on artifacts with partial vesiculation. This suggests that while macroscopic effects are useful

in identifying that assemblages have been exposed to intense burning conditions, the absence of macroscopic effects on a given artifact may not offer assurance that the chronometric information in the specimen has not been compromised. To determine fully whether a forest fire has adversely affected an assemblage, artifact collection and subsequent OH analyses are needed

The import of these results for cultural resource managers and practitioners of obsidian hydration dating is twofold caution. First, the loss/alteration of OH at Capulin Quarry is not evenly distributed across the site. During post-fire site condition assessment, archaeologists need to examine a large portion of a given burned site to determine whether loci of moderate or high burn severity are in evidence. Second, during pre-fire planning cultural resource managers will need to assess not only the anticipated effects of the prescribed fire as planned, but also the preservation tolerance for potential effects if pockets of high burn severity occur despite a strategy that emphasizes low to moderate severity or if the burn prescription is breached inadvertently.

Finally, the analyses of obsidian composition I conducted demonstrate that different ranges in obsidian water content and variability of water contents can occur both within and among obsidian chemical groups. These results challenge the assumption that obsidian fire effects studies are universally applicable. My analyses suggest that the susceptibility of obsidian to vesiculation and the alteration of obsidian hydration are affected by a compositional variable, water content, which can be expected to vary among, and perhaps within, obsidian sources. If so, it is now unclear whether the results of obsidian fire effects studies obtained for obsidian at Yellowstone or Newberry Crater actually would be applicable to obsidian in the Modoc, Willamette, or Santa Fe National Forests.

Raising this question about the replicability of obsidian fire effects research may at first seem discouraging, but actually has the potential to resolve prior puzzling outcomes and to enhance the robusticity of this body of research. It is possible that the widely ranging results obtained in post-fire and prescribed-fire field studies (as discussed in Chapter 2) are due not simply to differences in burn conditions, as currently assumed, but are affected also by compositional differences. Analyses of obsidian composition could be conducted retroactively to determine whether water contents vary among or

within the chemical groups included in these previous studies. Certainly the role of composition should be further investigated where OH loss or alteration has been shown to occur at very low temperatures (e.g., Benson 2002; Solomon 2002). Until there is knowledge of the water content characteristics of a large number and wide range of obsidian sources, the next best solution to this problem will be to conduct heat experiments on obsidian samples from numerous sources to test for variable heat response. At the least, obsidian fire effects researchers are strongly urged to precisely document, to fully report, and to control or minimize variation in the geochemical sources of obsidian artifacts and materials under study.

The Validity of Archaeological Methods of Obsidian Analysis

The broadest implications of this research are for the methodology of obsidian hydration dating. The most direct concern is whether the potential of forest fires to alter obsidian hydration significantly diminishes the broad utility of the dating method or invalidates its utility for the surface archaeological record in forested environments. I do not believe this is case. First, the potential for heat alteration as a relevant concern for OHD is not new and was raised in the earliest discussions of the techniques. However, the results obtained in this study and in similar research demand the attention of OHD practitioners. The occurrence of modified OH in artifacts without accompanying macroscopic indicators is unexpected, as is the puzzling observation of variable OH resilience within individual specimens. And the overall analysis of artifact OH demonstrates that the Dome Fire had a substantial deleterious effect on OH information in the Capulin Quarry surface assemblage. Alteration/loss of OH ranging from 40 to 100 percent of specimens in various burned contexts is a remarkable outcome. However, as stated at the beginning of this study, the surface quarry assemblage at this site provided an example of the worst-case scenario for forest fire alteration: the density of obsidian artifacts and non-artifact material is unusually high, surface assemblages are especially exposed and without the insulation of surrounding sediments, and compositional analyses suggest that the obsidian in the deposits burned are especially susceptible to heat alteration. In sum, the outcomes of this study confirm the initial impression that Capulin Quarry is better understood as the worst case and not the norm for obsidian fire effects.

Further, where the basis of concern is more broadly methodological (that is, the issue that contemporary and prehistoric forest fires may alter the essential properties of the OH phenomenon: gradual, constant, and uninterrupted hydration), it should be noted that it is not yet determined that heat alteration "re-sets" the hydration clock. How obsidian surfaces "re-hydrate" following heat alteration has not yet understood. Studies that demonstrate altered or lost OH following contemporary forest fires or laboratory experimentation confirm the immediate but not the long term consequences of heat exposure. Nonetheless, these studies, as well as the current research, establish that heat alteration can affect the OHD information contained in some portion of burned assemblages.

If fire is recognized simply as one of the many formation processes that archaeologists must understand when interpreting the record, then observational tools and inferential arguments can be developed to recognize fire effects and to evaluate the relative effects of heat for a specific use of obsidian hydration dating. At the scale of assemblage, archaeologists can routinely look for macroscopic effects during field investigations and during post-field artifact analysis to evaluate whether there is evidence of fire exposure that warrants consideration in selecting appropriate dating techniques or in interpreting OHD results. At the scale of individual artifact, obsidian hydration analysts alert to indicators of potential OH alteration such as diffuse hydration or weathered appearance can evaluate whether OHD outcomes for specific specimens should be excluded. If fully appreciated, forest fire effects need not make obsidian hydration dating unreliable; rather, incorporating the evaluation of heat effects into each application of OHD has the potential to improve the overall performance of the dating technique.

The broader implications of this research are for the role of composition analyses in the methodology of obsidian hydration dating. As discussed in Chapter 5, all three approaches to OHD (relative, empirical, and experimental) must consider obsidian composition in some way because it is known that obsidian from different geological deposits develop differing depths of hydration over similar intervals. There are two issues: what variables in obsidian composition cause these differences in the rate of hydration, and how composition should be measured or understood. The work of

Stevenson and colleagues provides evidence that water content plays an important compositional role in hydration, and theoretical contributions by the SIMS researchers support this possibility. If water content is variable among geological deposits, then it should be considered a contender in explaining variable hydration rates among sources. Further, if water content is variable within geochemically-defined obsidian sources, then identification of a shared characteristic trace element profile in a given group of obsidian artifacts would not insure that all artifacts in that group hydrate at the same rate. The current study observed both within-source and between-source variation in water content in the Jemez obsidians sampled.

However, observing that variable water contents occur and recognizing the potential relevance for the obsidian hydration dating model do not directly inform how archaeologists should employ this information in compositional analyses that accompany OHD. Stevenson and colleagues (2000) have posited that trace element composition analysis for sourcing should be abandoned and that the only compositional analysis required for OHD is measurement of water content directly on the artifacts being dated. I think this recommendation is premature and more studies are needed in a variety of areas. First, further induced hydration experimental analysis should be conducted to demonstrate the relationship of water content and accelerated hydration rates. Alternately, further empirical studies combining archaeological cross-dating of OH in artifacts with direct water content measurement would better establish the relationship between water content and hydration rate over long intervals of archaeological time. Second, more work needs to be done to determine what form of water in rhyolitic glass is most relevant for archaeological hydration: how do the different water species, H_2O and OH, play a role, and is it necessary to use techniques that differentiate between the water species or is it sufficient simply to measure total water?

Finally, the results of the current study in conjunction with the Coso example provide compelling but not definitive evidence for the occurrence of high and variable water content. If high and variable water contents occur only rarely among the many obsidian deposits utilized in prehistory, then these results merely describe outliers of obsidian composition. If, however, water contents are variable at several archaeologically relevant sources, then incorporating water content analyses into obsidian

source characterization studies would be vital to the methodology of archaeological obsidian sourcing conducted in conjunction with OHD.

Assessing water content variation across the hundreds of obsidian sources worldwide is a daunting task to consider. However, the possibility that water content in obsidian-bearing deposits varies systematically by volcanic context and eruptive history, as discussed in Chapter 5 and supported by the current results, points the way to designing effective sampling of broadly distributed obsidian sources. Sources to be compared could be selected by volcanic context, much as in this study, so that the water content characteristics of a suite of pyroclastic obsidian sources can be compared to a suite of extrusive obsidian sources. Such a comparison of even a limited sample of case studies would provide evidence for whether this contrast is useful for identifying high vs. low water content obsidians. If it can be shown that the incidence of high and variable obsidian water content is not isolated or rare, or that the occurrence is concentrated in certain geographic regions where obsidian utilization in prehistory is important or where OHD is a critical dating method for archaeologists, then the addition of water content measurement to the methodology of obsidian sourcing and hydration dating may contribute significantly to improving the accuracy and reliability of the OHD technique across applications.

The archaeological record of the American Southwest provides an excellent setting to test the potential of water content analysis for improvement in the obsidian hydration dating method. Here, obsidian artifacts are frequently found in archaeological contexts that otherwise are well-dated by a variety of independent relative and absolute dating methods. Because Jemez Mountains obsidians are found commonly in sites that range from Paleoindian to Puebloan in age, the obsidian composition results obtained in this study of Cerro Toledo and Cerro del Medio obsidians create an ideal opportunity to design a case study to test the performance of obsidian hydration dating as an archaeological chronometer when water content is included in the equation.

LIST OF APPENDICES

APPENDIX A. Unpublished results of laboratory heating of hydrated obsidian, by Fred W. Trembour

APPENDIX B. Fractography analysis of fire fractures, by Are Tsirk

APPENDIX C. Unpublished data on experimental vesiculation of artificially hydrated silica glass; experiments conducted by H. R. Westrich, Sandia National Laboratory

APPENDIX D. ED-XRF Analyses: Original Letter Reports and Data from R. E. Hughes, Geochemical Laboratory

APPENDIX E. Experimental Heating of Obsidian with Known Water Contents

APPENDIX F. ED-XRF and WD-XRF Tables: Elemental Composition Data by Specimen

APPENDIX A:

Unpublished results of laboratory heating of hydrated obsidian by Fred W. Trembour

STANDARD FORM NO. 64

Office Memorandum • UNITED STATES GOVERNMENT

TO : Irving Friedman, USGS DATE: May 22, 1983

FROM : Fred Trembour, USGS

SUBJECT: Heating Effects on some Obsidians.

This report summarizes laboratory tests and conclusions that have been made at intervals between March, 1976 and May, 1983.

The observations concerned mainly refractive index, thermal surface crazing and vesiculation as products of experimental heating.

The chief findings are given as temperature-dependent plots for 8 different obsidians in the attached Figures 1A and 1B.

Experimental Procedures.

All of the presented data were derived from tests in small electric bench furnaces, and involved slow heating in ambient air to predetermined temperatures for times of 1/2 to 1 hour, followed by natural cooling in room air.

Fresh pieces from each parent chunk were used for each of the successive temperature runs. Test pieces were generally of 3 or 4 cm^2 of surface area. They were usually hung in nichrome wire cradles near the thermocouple bead in the furnace muffle chamber.

Preliminary tests conducted at length with samples of the Popayan, Colombia (PCA) material had shown that a) contact with wood ashes during heating had no effect on the onset of surface crazing or vesiculation, and b) that water quenching from the furnace caused deep cracking of the samples from all elevated temperatures. Hence air only was used as the heating and cooling medium.

A hand lens was adequate to detect the presence of superficial shallow crazing or crackling.

When vesiculation of the obsidian occurred the condition was self-evident as an expanded frothy, often cocoon-like mass.

Refractive index was measured in the microscope by the central focal masking technique and the use of a powder sample and a series of graduated immersion liquids. Observed values were adjusted to a standard 25.0°C.

The reproducibility of all recorded phenomena within close temperature limits was demonstrated a number of times by the use of sample pairs as well as repeat runs.

Surface Crazing.

Susceptible obsidians craze spontaneously when a sufficiently high minimum temperature is reached, T_c. All surfaces - hydrated, fresh and internal (as walls of deep cracks) - are affected

simultaneously. The incipient cracks are few, scattered and appear unrelated to preexisting surface features. As temperature is increased above T_c the shallow cracks multiply and meet and an ever denser network develops, with all intersections at right angles.. Common crack depths are 10 to 50 micrometers. The spread of the crazing process ends with the onset of vesiculation.

Three of the 8 tested obsidians showed incipient crazing temperatures, T_c, as follows: 550°C (PCA), 600°C (EZN) and 675°C (JMN). The other five exhibited no crazing up to the maximum temperature of 850 or 900°C employed in the furnace experiments.

Vesiculation.

This feature is the sudden bubbling up of volatile constituents throughout the bulk of the softening glass as rising temperature reaches a characteristic level, T_v. Three such values were found in the studies: 750°C (for PCA), 850°C (EZN) and 900°C (LBN). The last-named instance (LBN) indicated also that thermal crazing is not always a precursor to vesiculation; the sample developed no noticeable crazing at any temperature.

Four of the obsidians (GMA, ECN, OCN and NZN) experienced neither thermal crazing nor vesiculation within the temperature limits of the test program, ca. 900°C max. Some might have done so at a higher test temperature, but conceivably none would vesiculate if their volatile contents were very low.

Refractive Index (R.I.).

Laboratory measurement differences in this glass property can be significant to ± .001 or less when persistent. The declining trends of R.I. with rising heat treatment exhibited by all eight obsidians in Figures 1A & 1B are thus reliable and useful.

All specimens tested up to 850°C showed declines in R.I. varying from .001 (LBN) to .006 (EZN). Generally the most obvious drops occur near T_c and T_v, but even the obsidians that showed neither of these physical changes had R.I. declines of up to .0035 (GMA and OCN).

Tested in their original conditions, the 8 obsidians ranged from R.I. 1.483 to 1.490. Their spacings along the R.I. scale in most cases were useful for separation purposes; 6 of the 28 possible pairings were less than .0015 apart. After maximum heating this ratio was 5 of 28.

Miscellaneous Observations.

The effect of heating on the hydration rind of artifact specimen PCA was studied in the microscope. The original 10.7 um hydration depth increased by about 10% after heating to ca. 300°C, with some concomitant blurring of the boundary line. At about 430°C practical obliteration of the visible hydration layer had occurred in both polarized and plain illumination.

Specimen GMA showed a drastic color change from heating: from an initial bottle-green color to a pale, barely greenish gray color after exposure to 850°C.

Conclusions.

Two main points worth further attention seem to emerge from the experiments:

1. The widely differing changes produced in some physical properties of obsidians suggest applying them for differentiating obsidians by source. For example, simple lab tests for R.I. before and after heating to a specified temperature, and for Tc and T_v determination may yield discriminants sufficient for separation of sources (and hydration rates) for the obsidians within a geographic region of concern.

2. The set of 8 obsidians showed R.I. declines ranging from .001 to .0035 before other signs of heat damage set in. This puts in question the application of R.I. for the hydration dating method devised by Friedman and Long (1976). Extensive crazing (up to 15% of obsidian surface collections), presumably owing to prehistoric slash-and-burn cultivation, has been noted, e.g., on agricultural land in Colombia. Thus, a) many uncrazed flakes may have been heated to somewhat under T_c, and b) the hydration in the crack walls of crazed flakes might be used for dating the firing events. What R.I. values should be applied to the materials to achieve a correct age conversion of hydration depth in these two cases? This seems to point out a good direction for further research.

Att.: Figures

Effects of heating on some properties of eight obsidians.

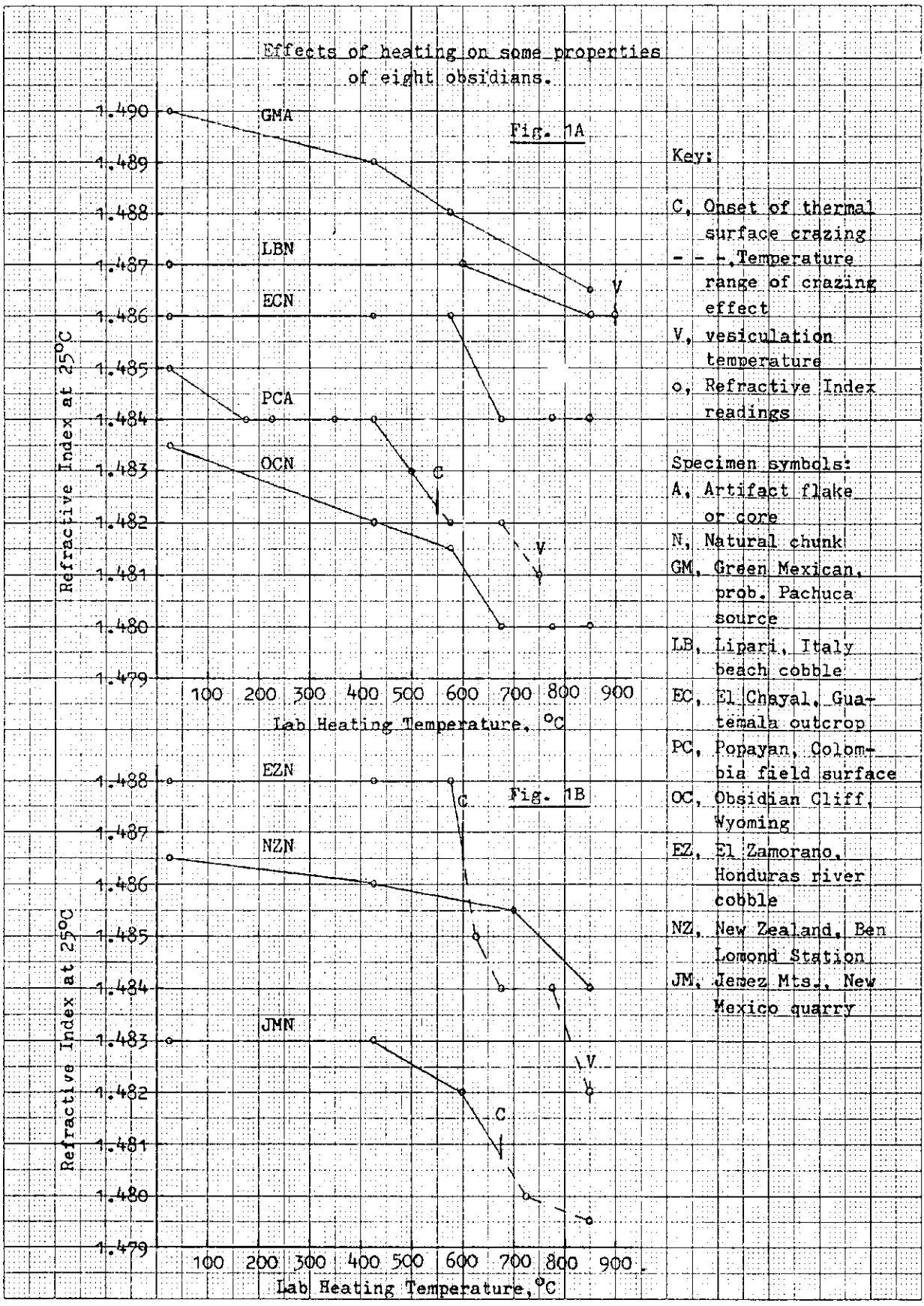

Key:

C, Onset of thermal surface crazing

- - -, Temperature range of crazing effect

V, vesiculation temperature

o, Refractive Index readings

Specimen symbols:

A, Artifact flake or core

N, Natural chunk

GM, Green Mexican, prob. Pachuca source

LB, Lipari, Italy beach cobble

EC, El Chayal, Guatemala outcrop

PC, Popayan, Colombia field surface

OC, Obsidian Cliff, Wyoming

EZ, El Zamorano, Honduras river cobble

NZ, New Zealand, Ben Lomond Station

JM, Jemez Mts., New Mexico quarry

Summary of Heating Experiments on Ponayan Obsidian.

(C, below, indicates test fragments all from one large piece of cultural obsidian, G from one geological cobble.)

Maximum Test Temperature, °Celsius	Test Conditions*	Results
700	C, 1 hr., ash, a.c. C, 1 hr., ash, f.c.	
		"Crazing" — evenly shallow, meandering and often intersecting cracks appeared on the fresh surface facets of all test pieces heated above 540°C.
	G, 1 hr., air, a.c.	
600	C, 1¼ hrs., air, f.c. G, 1¼ hrs., air, f.c. C, 3 hrs., air, f.c. C, 3 hrs., ash, f.c.	
		540°C
	C, 3/4 hrs., air, a.c. C, 2¼ hrs., air, f.c.	No crazing appeared on any pieces heated to below 540°C.
500	G, 2¼ hrs., ash, f.c. G, 2¼ hrs., air, f.c. C, 2 hrs., air, f.c.	
		Hydration interface obliterated in pieces heated above 430°C.
	G, 2 hrs., air, a.c.	
		430°C
400		Hydration interface altered and displaced in pieces heated up to 350°C.
	C, 3/4 hr., air, a.c.	— Interface blurred, moved deeper to 12.7 microns.
300		
	C, 2hrs., air, f.c.	— Interface moved deeper, to 11.3 microns.
200	C, 1-3/4 hrs., air, a.c.	— Interface moved deeper, to 11.1 microns.
100		
RT		— Original interface depth 10.7 micr.

* All test runs were made in an electric laboratory bench furnace from a room temperature start, the pieces hung in air unless ash (wood ash) is indicated. The given time is that near maximum temperature, a.c. means subsequent cooling in room air, and f.c. means furnace cooling to RT.

FWT 3/30/76

Table

The findings indicate that obsidians from different geologic sources may be distinguished in the laboratory by a vesiculation temperature at which the test piece changes suddenly to a frothy lump, and by a lower crazing temperature where characteristic shallow heating cracks first appear.

Summary of Heating Experiments*

Obsidian Source	Crazing** Temp. °F.	°C, conv.	Vesiculation Temp. °F	°C, conv.
Popayan, Colombia:				
Artifact "X"	1000	538	1400	760
River pebble, RN2	1080	588	1500	815
Soil pebble, RQ	1100	593	1550	843
River pebble, RM1	>1600	>871	>1600	>871
El Zamorano, Honduras:				
River Pebble	1100	593	1550-1600	843-871
(USGS) Mexico 1	<1150	<621	<1260	<682
(USGS) 3419-8B	<1150	<621	<1150	<621
" 3419-17D	>1550	>843	>1550	>843
Obsidian Cliff, Wyo.:				
nat. fragment	>1550	>843	>1550	>843
El Chayal, Guatemala:				
nat. fragment	>1550	>843	>1550	>843

* All tabulated results derive from heating runs made at USGS Denver in an electric laboratory bench furnace with the prevailing atmosphere. The ca. 2x1x0.5 cm. test fragments were freely suspended on iron wire, time at test temperature was ca. ½ to 1 hr., and cooling ensued by removal to room air.

Where the symbol "greater than" appears, the indicated feature was not observed at the given temperature, but was assumed to occur had a higher heating temperature been available than the ca. 1600°F (870°C) limit of the test furnace.

** The temperature of onset of typical crazing cracks, or thermal checks, was usually observed on the fresh fracture surfaces, but was also noted on some hydrated facets.

FWT, 7/28/76

Experimental Heating Effects on a Popayan Artifact Obsidian, "Block X". Test fragments were heated about an hour in an electric laboratory furnace.
(The conditions described below also occur among the field pieces of the Popayan surface collection.)

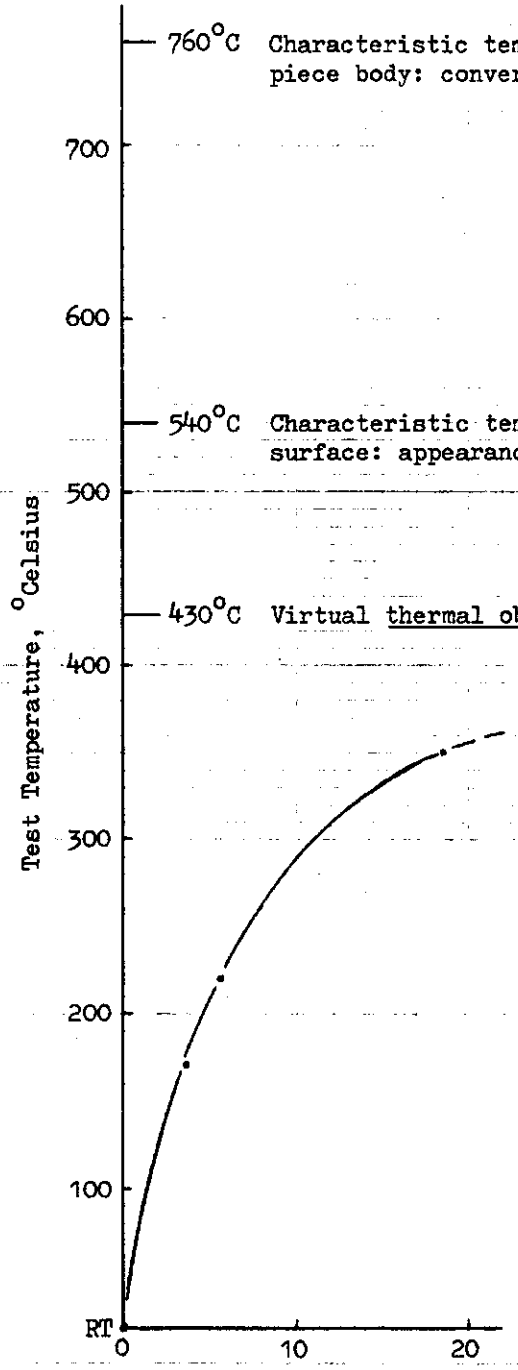

760°C Characteristic temperature for onset of vesiculation of the test piece body: conversion to an expanded frothy mass.

540°C Characteristic temperature for thermal crazing of the obsidian surface: appearance of a network of very shallow meandering cracks.

430°C Virtual thermal obliteration of the visible hydration layer.

Up to ca. 400°C.:

Temperature zone of increasing displacement and blurring of the interior hydration boundary by progressive thermal diffusion.

The curve shows the percentage increase of apparent hydration depth from an original value of 10.7 microns before heating.

FWT 6/13/76

APPENDIX B.

Fractography analysis of fire fractures

by Are Tsirk

Tsirk, A.
2003 *Obsidian Fractures from a Forest Fire Zone in Santa Fe National Forest*. Report No. 020607, submitted to A. Steffen, Santa Fe National Forest and University of New Mexico. Unpublished ms. in possession of the author.

Obsidian Fractures
from
a Forest Fire Zone in Santa Fe National Forest

Prepared
by
Are Tsirk, Ph.D.
Fractography Consultant
Upper Montclair, NJ 07043

Submitted
to
Anastasia Steffen
Department of Anthropology
University of New Mexico
Albuquerque, NM 87131
and
Santa Fe National Forest
Jemez District
Jemez Springs, NM 87025

Report No. 020607

March 14, 2003

Table of Contents

1. Introduction

2. Specimens Available

3. Observation and Photography

4. Fracture Markings Associated with Primary Fractures

5. Some Surface Alterations
    5.1 Contact Fractures
    5.2 Other Surface Fractures
    5.3 Some Other Surface Alterations

6. Fracture Origins, Velocities and Causes

7. Concluding Remarks

8. References

Tables

Captions for Figures

Figures

Appendix A: Original Photos
    - List of Photos
    - Copies of Photos
    - Original Color Photos

List of Tables and Figures

Tables:

1. Obsidian Specimens from Jemez Mountains, Santa Fe National Forest
2. Fracture Markings Observed
3. Locations for the More Unusual Fracture Markings Observed
4. Relative Fracture Velocities V_F/V_S from Gull Wings

Figures:

1. Sketch of Specimen 1
2. Sketch of Specimen 2
3. Sketch of Specimen 3
4. Sketch of Specimen 4
5. Mist Line, Gull Wings, Wallner Wake and Other Wallner Lines
6. Gull Wings and Wallner Wakes
7. Double Tails (with Mist Lines), Regions of Mist and Hackle
8. Detail of a Mist-Hackle Line
9. Detail of a Mist-Hackle Line
10. Scalar Chip Scars at an Inclusion
11. Incomplete Scalar Chip Formation at an Inclusion
12. Groove with "Butterfly Checks"
13. Chatter Marks and Other Surface Alterations
14. Chatter Marks and Other Surface Alterations
15. Abrasion Tracks, Striations and Mist Lines
16. Surface Fractures Due to Thermal Effects
17. Surface Fractures Due to Thermal Effects
18. Surface Fractures Due to Thermal Effects
19. Surface Alterations with Appearance of "Stacked Pancakes"
20. Surface Alterations Appearing as "Indentations"
21. Internal Inclusion at Fracture Origin
22. Internal Inclusion at Fracture Origin (Downstream Part)
23. Depletion Scarps
24. Depletion Scarps and Subcavitation Hackle or Its Counterpart
25. Depletion Scarps and Subcavitation Hackle or Its Counterpart

1. Introduction

During my March 16-19, 2002 visit to the University of New Mexico, Albuquerque, and the Jemez Mountains, Santa Fe National Forest, the effects of forest fire were observed on a number of obsidian specimens, including those from archaeological sites. Four such specimens were borrowed for further observation and study.

The primary objective of this investigation is to identify and document the fracture markings observed on the four obsidian specimens, to note some of their unusual characteristics, and to indicate their significance of potential interest to a broader study of the effects of forest fires on obsidian. This also serves to indicate that the markings are not features due to fire or other effects subsequent to the primary fractures.

A secondary objective is to identify some fracture features produced subsequent to the primary fractures, and to suggest their significance. Some of these fracture features are not understood presently, but are nevertheless noted for their potential future interest in fractography. A few of the numerous other kinds of surface alterations seen are also noted.

Finally, the report will also reflect on some of the fracture origins, velocities and causes.

2. Specimens Available

The four fracture specimens considered here are listed in Table 1, with the specimen numbers assigned here for convenient reference. The dimensions given in the table, as well as Figs. 1 to 4, identify the specimens by their number.

In subsequent documentation and discussion, it will be convenient to refer not only to a specimen but also to its different surfaces (facets). The identification of the facets is indicated on the rough sketches in Figures 1 to 4 for Specimens No. 1 to 4, respectively.

3. Observation and Photography

Observation of fracture markings on the primary fracture surfaces was partly obscured by various kinds of surface alteration, including some deposits or residues. Only some surfaces were wiped with a damp tissue paper prior to observation. During microscopic observation, the specimens were supported on green colored "modeling clay". Some specks of this material may still be adhering to the specimens after the observations were completed.

All of the fractures were inspected without magnification, and almost all of the fracture surfaces with an Olympus binocular microscope BHMJ, with internal lighting for brightfield and darkfield illumination. A magnification of 50X, and sometimes also 100X, was used.

Photographs were taken with an Olympus OM-2S camera attached to the microscope. Various facilitating accessories were used. Magnifications of 12.5X and 25X (onto a 35 mm film) were used. For the 31/2" X 5" photos, these correspond to about 46X and 93X, respectively.

4. Fracture Markings Associated with Primary Fractures

Most of the fracture markings observed on the primary fracture surfaces are listed in Table 2, along with their significance in a generic sense. The figures and photos (See Appendix A) illustrating some of these markings are indicated in the table, and references to explanation or discussion of the markings are provided as well. Occurrence of these markings in the context of knapping and accidental breakage of obsidian is also noted in the table.

"Hackle scars" in the table is a new term for fracture markings. For flakes encountered in knapping, the term "scars on flakes" has been used previously (Tsirk 1997) for these markings. They are the more generic counterparts of bulbar scars, occurring in various contexts in addition to the bulbar region of a flake. The previously used term is inappropriate for contexts not involving flakes. A hackle scar is essentially an extended lateral breakthrough (Tsirk 1997: Fig. 8.2) of a twist hackle.

The term "mist line" is taken here to include mist lines, mist-hackle lines and lines of recurrent hackle (Tsirk 1996). Based on the writer's previous observations on other obsidians, as the conditions for general mist region are approached, mist lines first appear as the trailing extensions to wake hackles or twist hackles. Closer to the conditions for general mist, mist lines replace or at least tend to replace wake hackles and twist hackles entirely. Under such conditions, mist lines nucleate directly from inclusions (or other flaws).

As seen from Table 2, all of the fracture markings observed can also be seen in the context of knapping and accidental breakage. However, markings or marking configurations No.7 through 12 occur rarely in knapping. This is especially the case for branching, which has been observed extremely rarely – and only with bending type fracture initiations where the fracture is extending laterally in the proximal region.

Table 3 documents the specimens and their facets on which the more unusual fracture markings were observed. The first six of these are indicative of relatively high (nominal) stresses during fracture, rarely encountered in knapping. One or more of these features were observed on seven primary fractures. Branching was observed on two of the four specimens. All of this fractographic evidence indicates that the stresses involved with the present specimens were sometimes higher than those normally encountered by archaeologists in knapping.

From a different perspective, it is clear from the evidence that fracture branching – and high levels of stress and available energy – contributed to the diminution of the obsidian nodules that resulted in at least two of the four specimens.

The last two markings in Tables 2 and 3 are indicative of very slow fracture velocity (less than about 10 cm/s) and of the presence of external liquid at the fracture front during the fracture. In a generic sense, liquid-induced fracture markings (LIFMs) may sometimes indicate also the type of liquid involved.

The types of scarps observed on Facet D of Specimen 4 (Figs. 23 to 25) are manifested characteristically with liquids such as water and human saliva (Tsirk 2001). The subcavitation hackle (or its counterpart), however, are more pronounced and more irregular than has characteristically been observed for the latter kinds of liquids in a number of obsidians. These unusual features of the fracture markings may perhaps be due to many inclusions, irregularities or inhomogeneities in this obsidian (Compare with Figs. 2a and 7 in Tsirk 2001).

The presence of the LIFMs together with their location indicates, for all practical purposes, that the facet on which they occurred was not produced in a context of knapping or accidental breakage in human activity. Although LIFMs can occur in knapping when the platform region is wetted, they have been observed to occur within a fraction of a millimeter or within several millimeters of a fracture origin (Tsirk and Parry 2000) in pressure flaking. Although never observed in percussion flaking, they would be expected to occur even closer to the fracture origin, if at all. The above statements relate to the fact that the fracture velocity must necessarily be be very low for a liquid to be able to follow a fracture front to cause manifestation of LIFMs (Fréchette 1990). The LIFMs on Facet D of Specimen 4 occur within about 3mm downstream from a ripple that is probably an arrest line. The distance involved precludes the possibility of percussion completing the flake detachment. The possibility of pressure flaking can also be precluded, unless one postulates a very slow application of pressure with a lever device.

It is of interest to ask what the sources of the liquid and the stress, both required for the LIFM, were. The liquid most likely is water from condensation at a pre-existing fracture front (probably at an arrest line) in the obsidian. The tensile stresses required for the fracture are probably due to thermal effects, not necessarily related to a forest fire. Such an explanation probably also holds for LIFMs that can sometimes be seen just downstream of an arrest line on obsidian fractures in a geological context. (If any liquid was used in firefighting, it is conceivable that such a liquid instead was associated with the LIFMs noted.)

Aside from the occurrence of the basic fracture markings noted (Table 2), a number of unusual characteristics of these markings were observed that have either not been encountered by the writer or are uncommon in the contexts of knapping and accidental breakage. These include the following:

a. Some mist and hackle regions exhibit features that seem to be unusual. Even if confirmed, the significance of this is unclear. It is not evident whether it relates to the particular obsidian or its conditions associated with the fractures.

b. A number of mist-hackle lines (streaks) are unusual, consisting primarily of larger recurrent hackles (Figs. 8 and 9). Somewhat similar features have been observed in knapping or accidental breakage contexts of other obsidians, but extremely rarely. Again, the significance of this is unclear, and it is not known whether or not it simply relates to the particular obsidian.

c. The lateral breakthroughs of twist hackles (See Tsirk 1997, Fig. 8.2) are sometimes rather unusual, exhibiting greater irregularities.

d. Some sizable hackle scars (extended lateral breakthroughs of twist hackles) seem to occur in unusual contexts. In particular, they were observed to occur in several cases at locations where no "higher" contour was apparent. Hackle scars in knapping are normally manifested at locally "higher" contours such as a bulb (on a flake), a large ripple or the ridge between adjacent flakes. Hackle scar formation is possible only in the presence of compression in the direction in which the lateral breakthrough of a twist hackle (usually normal to the twist hackle) extends. Without a "higher" contour, such compression is expected to be greater.

e. The secondary fracturing at numerous inclusions was observed to include relatively large "scalar chips" (Fig. 10), sometimes all around the inclusion (Fig. 11). In some other obsidians, such fracture features can also be encountered in knapping contexts, but relatively seldom and even then with relatively smaller

size of the "scalar chips". It is conceivable, though unlikely, that the scalar chips at some inclusions were produced due to thermal effects after the primary fractures. However, although this needs to be confirmed, it is likely that most of these features simply relate to the particular kind of obsidian involved.

5. Some Surface Alterations

Though not the primary focus of this study, some of the observed surface or near-surface alterations subsequent to the primary fractures are briefly noted here.

5.1 Contact Fractures

Subsequent to the primary fracturing that produced the facets of the four specimens, the surfaces have been subject to damage, usually microscopic, due to fractures from contact with some other objects. Some of these damage sites are linear, while others are more localized, "spot" features. Useful fractographic descriptions of contact fractures appear in Lawn and Marshall (1979) and Fréchette (1990: pp. 51-56).

The very common edge chipping, present on all the specimens, is mostly due to localized ("spot") contact at or very near the specimen edges. In some of the observed cases, the series of contiguous and partly overlapping edge chips suggests contact with a relatively blunt object.

The observed linear features of contact fracture are associated with various levels of contact pressure and a relative motion between the specimen and another object, sometimes sharp and sometimes blunt. Such features range from relatively wide, either continuous or discontinuous scratch marks from blunt contact to fine, light striations and more pronounced grooves and gouges. At least two of the grooves (on Specimen 1, Facet C) are associated with lateral scalar chips sometimes called butterfly checks (Fig. 12) (Fréchette 1990). (See also Photo 35 in Appendix A.)

Among the observed linear features well documented in literature (Lawn and Marshall 1979: pp. 70-72, Fréchette 1990: p. 56-57) are the chatter marks (Figs. 13 and 14). The object contacting the surface was moving, in a relative sense, towards the concave side of the markings. The ratio of the tangential to the normal contact force (equal to the effective coefficient of friction) was less in Fig. 14 than in Fig. 13 (See Fig. 6 in Lawn and Marshall 1979).

Various other linear damage tracks can be observed on the specimens, as those in Fig. 15, for example.

The localized, "spot" features of contact damage observed include various pecks and bruises.

5.2 Other Surface Fractures

Some of the observed surface or near-surface fractures from other than contact damage include those shown in Figs. 16, 17 and 18. These are due to thermal effects, probably associated with cooling. It is evident that some of these fractures have been affected by the presence of twist hackles and perhaps other fracture markings manifested during the primary fractures (Fig. 18).

5.3 Some Other Surface Alterations

Among other observed surface alterations are those associated with deposits or residues and indeterminate effects.

A rather curious feature is shown in Fig. 19. Such features, resembling "stacked pancakes", were observed only on Facet E of Specimen 4. Although their meaning is unclear, the writer suspects these to be associated with fracturing subsequent to the primary fractures.

Unclear is also the significance of the elongated, smooth "indentations" or dents seen in Fig. 20. They are not seen as being associated with brittle fracture. Possibly, they may be due to inelastic deformation of the material from contact, perhaps with the obsidian in a non-brittle state. These features were observed only on Facet A of Specimen 2.

6. Fracture Origins, Velocities and Causes

A number of the primary fractures associated with the four specimens had an origin well outside the facet in question. Only in one case (Facet A of Specimen 1) was the origin at an internal inclusion (Figs. 21 and 22), about 7.5 mm from the nearest specimen edge. It is judged unlikely that this fracture was caused by mechanical forces applied externally. In the latter case, a fracture would almost always start at some surface or near-surface flaw, even if significantly smaller. Such a flaw, combined with conceivable stress distributions from external forces, is normally more critical. (This may be verified by analysis, not considered here.) This fracture, therefore, is likely to be associated with thermal stresses. Most likely, the fracture occurred during heat-up rather than cooling, regardless of whether or not the temperatures outside the nodule were uniform or variable.

The fracture velocities V_F attained during the latter fracture, relative to the shear wave velocity V_S (constant for a material), were at least about $V_F/V_S = 0.634$, as indicated in Table 4 (No. 12). The first 12 cases in the table are for Facet A of Specimen 1; the last four, for Facet E of Specimen 3. All of these results are from angular measurements on gull wings. Incidentally, the gull wings in Fig. 5 (for Facet A of Specimen 1) gives $V_F/V_S = 0.54$. Relative fracture velocities as high as all of those in Table 4 are encountered extremely rarely, if ever, in knapping. The highest value measured previously by the writer for a knapping context, but for a Glass Buttes obsidian, was about 0.58.

The shear wave velocity V_S is unknown for the obsidian considered in this report, as well as that from Glass Buttes. The fracture velocities V_F given in the last column in Table 4 were obtained using an assumed shear wave velocity V_S = 3,548 m/s, based on the mean properties for obsidians in Speth (1972). Thus the highest fracture velocity V_F for Table 4, for $V_F/V_S = 0.634$ (No. 12), is about 2250 m/s.

Although the high relative fracture velocities measured do not necessarily preclude the possibility that the fractures were produced in knapping, they do make it extremely unlikely.

Based on fractographic evidence, above and in Section 4 together with an exercise of judgment from knapping experience, it can be concluded that Specimens 2, 3, 4, and most likely also Specimen 1 were not produced by knapping. In this regard, the one internal fracture origin on Specimen 1, and the presence and nature of fracture branching on Specimens 2 and 3 are of particular interest. From knapping experience, the nature of the flake scars or facets, the various edge angles and the location of fracture origins are relevant for the conclusion stated.

7. Concluding Remarks

A number of fracture markings or features observed on the four Jemez Mountain obsidian specimens were formed during the primary fractures, while others represented subsequent sites of surface damage (such as grooves, chatter marks, etc.). Simple experiments with this obsidian could render more meaning to the latter, as well as clarify the significance of some unusual features of the fracture markings manifested during the primary fractures. At least some of these unusual features may be due to the presence of transient or residual thermal stresses. Their better understanding may facilitate distinguishing thermal fractures from those caused by external mechanical forces.

Based only on the specific kinds of fractographic evidence discussed in Sections 4 and 6, is it possible to conclude that the fractures were not produced in knapping contexts, including accidental breakage? Considering all the facets on the four specimens, this fractographic evidence indicates that all the fractures were almost certainly not produced in such knapping contexts. This conclusion, however, cannot be drawn for each of the fractures that produced all the specimen facets. For a number of particular facets, it is extremely likely that the fractures were not produced by knapping (excluding accidental breakage). From fractographic evidence on the primary fractures alone, it was not possible to differentiate fire fractures from those due to other conceivable external forces, except in the one case suggested above (Facet A of Specimen 1).

Based on specific kinds of fractographic evidence of Sections 4 and 6 together with experience from knapping, it can be concluded that at least three and most likely all four of the specimens were not produced by knapping.

Some surface fracturing (Section 5.2) can serve as hard evidence for thermal effects. A further investigation of the latter may perhaps permit excluding thermal effects other than those due to fire.

Understanding the diminution processes of obsidian nodules by the effects of fire is of obvious interest. The effects of fire can lead to high (nominal) tensile stresses inside a nodule or near its outer portions. In at least most cases, these tensile stress locations are associated with heat-up or cooling of a nodule, respectively. Thus the location of a fracture origin can provide indications for distinguishing between these alternatives, regardless of whether the external temperatures were uniform or variable. For one of the observed primary fractures (Facet A of Specimen 1) with an internal origin, it is most likely that the fracture occurred during heat-up.

High tensile stresses can lead to fracture branching, usually at high fracture velocity, to promote diminution. Such fracture branching was in fact observed on two of the four Jemez Mountain specimens.

With regard to diminution by fire effects, it is of interest to note that the fractures occurring during cooling are usually most likely to originate near the corners of a nodule (having a square or a rectanguloid cross-section, for example). This is because the thermal tensile stresses are usually high, if not the highest, and the expectation for critical flaws is the greatest at such locations.

Finally, it should be noted that the effects of fire can lead to residual stresses in obsidian, with adverse effects on its workability. The presence of residual stresses tends to make fracturing unpredictable in knapping. In this sense, fire effects may

decrease the workability of obsidian or render it useless for knapping. Of course, the diminution of obsidian nodules by fire poses limits on the utility of the obsidian resource as well.

8. References

Beauchamp, Edwin K.
1995 "Crack Front Stability and Hackle Formation in High Velocity Glass Fracture", *Journal of the American Ceramic Society* 78 (3): 689-697.

1996 "Mechanisms for Hackle Formation and Crack Branching", pp. 409-445 in *Fractography of Glasses and Ceramics III*, edited by J.R. Varner, V.D. Fréchette and G.D. Quinn, The American Ceramic Society, Westerville.

Faulkner, Alaric
1972 "Mechanical Principles of Flintworking", Ph. D. Thesis, University of Washington, Pullman, Washington.

1974 "Mechanics of Eraillure Formation", *Newsletter of Lithic Technology* 2 (3): 4-12.

Fréchette, V.D.
1990 *Failure Analysis of Brittle Materials*, The American Ceramic Society, Westerville.

Hull, Derek
1999 *Fractography: Observing, Measuring and Interpreting Fracture Surface Topography*, Cambridge University Press, Cambridge.

Lawn, B.R. and D.B. Marshall
1979 "Mechanisms of Microcontact Fracture in Brittle Solids", pp. 63-82 in *Lithic Use-Wear Analysis*, edited by Brian Hayden, Academic Press, New York.

Michalske, Terry Arthur
1979 "Dynamic Effects of Liquids on Crack Growth Leading to Catastrophic Failure in Glass," Ph.D. Thesis, Alfred University, Alfred.

Poncelet, Eugene F.
1958 "The Markings on Fracture Surfaces", *Journal of the Society of Glass Technology* 42: 279T-288T.

Speth, John D.
1972 "Mechanical Basis of Percussion Flaking", *American Antiquity* 37 (1): 34-60.

Tsirk, Are
1988 "Formation and Utility of a Class of Anomalous Wallner Lines on Obsidian", pp. 57-69 in *Fractography of Glasses and Ceramics,* edited by J.R. Varner and V.D. Fréchette, The American Ceramic Society, Westerville.

1996 "Hackles Revisited", pp. 447-472 in *Fractography of Glasses and Ceramics III,* edited by J.R. Varner, V.D. Fréchette and G.D. Quinn, The American Ceramic Society, Westerville.

1997 "On Flintknapping", Unpublished manuscript on presentations at Tartu University, Tartu, Estonia.

2001 "An Exploration of Liquid-Induced Fracture Markings," pp. 87-101 in *Fractography of Glasses and Ceramics IV*, ed. by James R. Varner and George D. Quinn, The American Ceramic Society, Westerville.

Table 1 – Obsidian Specimens from Jemez Mountains, Santa Fe National Forest

Specimen No. *	Description on Label (as Received)	Approximate Size (cm)
1	AR 03-10-03-1691 Fire fracture from within burn area. No provenience.	4.8 x 3.4 x 2.7
2	AR 03-10-03-1691 Fire fracture from within burn area. No provenience.	4.8 x 4.4 x 4.0
3	Safety Zone Site FR 289 SFNF, Jemez Mtns.	3.5 x 3.0 x 1.8
4	Safety Zone Site FR 289 SFNF, Jemez Mtns.	5.0 x 3.9 x 3.8

*Note: Specimen No. assigned for reference in this report.

Table 2 – Fracture Markings Observed

Ref. No.	Fracture Marking	Significance	Occurrence in Knapping	Occurrence in Accidental Breakage	See Fig. No.	See Photo No.	Reference
1	Gull Wings	Obtain fracture direction & relative velocity	Yes	Yes	5, 6	1-3, 8-12, 14,18,21	Faulkner 1972, Fréchette 1990, Tsirk 1997
2	Wallner Wake	Fracture direction is towards the *concave* side; obtain lower bound estimate of relative fracture velocity.	Yes	Yes	5, 6	1-3, 8, 18	Tsirk 1986
3	Other Wallner Lines	Obtain clues to fracture front configurations & fracture directions	Yes	Yes	5, 6	8-11, 18,19,48	Fréchette 1990
4	Twist Hackles ("Striations")	Obtain fracture direction	Yes	Yes	-	32	Fréchette 1990
5	Tails (Sometimes as Wake Hackles)	Obtain fracture direction	Yes	Yes	22	48	Tsirk 1996
6	Hackle Scars (Eraillure Scars)	Indicates presence of compression in direction of the scar formation	Yes	Yes	-	-	Faulkner 1974, Tsirk 1997
7	Mist	High energy level available for fracture. Usually indicates high fracture velocity	Yes (Rarely)	Yes (Often)	7	6-17, 25	Beauchamp 1995, Fréchette 1990, Hull 1999
8	(Velocity) Hackle	Even higher energy level available for fracture. Usually indicates slightly higher fracture velocity than mist.	Yes (Rarely)	Yes (Often)	7	9-11, 25	Beauchamp 1995, Fréchette 1990, Hull 1999
9	Branching	Much higher energy level available for fracture. Usually indicates slightly higher fracture velocity than hackle.	Yes (Extremely rarely)	Yes (Often)	-	-	Beauchamp 1995, Fréchette 1990
10	Wallner Mist-Hackle Configuration	Conditions almost "ripe" for general mist & hackle formation. Fracture direction towards concave side.	Yes (Rarely)	Yes (Occasionally)	-	-	Beauchamp 1995, Tsirk 1996

11	Mist Lines (Streaks)	Conditions almost "ripe" for general mist & hackle formation. Indicates fracture direction.	Yes (Rarely)	Yes (Often)	5, 7	8-20	Beauchamp 1996, Tsirk 1996
12	Double Tails ("Parabolas") with mist lines	Bisector indicates fracture direction, towards the concave side. For trailing mist lines – see mist lines.	Yes (Rarely)	Yes (Often)	7	4-21, 24	Tsirk 1996, 1997
13	Depletion Scarp	External liquid was present at fracture front and being depleted, with wetted segment(s) becoming smaller. Extremely slow fracture velocity (less than about 10 cm/s). Sometimes indicates type of liquid involved.	Yes (when wetting platform)	No (But seen on geological fractures)	23, 24, 25	49-56	Fréchette 1990, Michalske 1979, Tsirk 2001
14	Subcavitation Hackle or Its Counterpart	External liquid was present at fracture front . Extremely slow fracture velocity (less than about 10 cm/s). Sometimes indicates type of liquid involved.	Yes (when wetting platform)	No	24, 25	51 - 56	Fréchette 1990, Michalske 1979, Tsirk 2001

Table 3 – Locations for the More Unusual Fracture Markings Observed

Fracture Marking or Feature	Specimen No.: Facet Identification
Mist	1: A 2: D* 3: B_1 3: E
(Velocity) Hackle	1: A 2: D 3: B_1 3: E
Branching	2: D → D_1 3: B_1 → B
Wallner Mist-Hackle Configuration	3: B_1
Mist Lines (Including Mist-Hackle Lines and Lines of Recurrent Hackle) (Streaks and Their Variants)	1: A 2: C (Seen as "arms" trailing double tails) 2: D 3:E 3:F
Double Tails ("Parabolas") with Mist Lines	1: A 2: C
Depletion Scarp	4: D
Subcavitation Hackle or Its Counterpart	4: D

* Note: Surface is obscured, but mist is inferred by (velocity) hackle and branching.

Table 4 – Relative Fracture Velocities V_F/V_S from Gull Wings

Fracture Location	Ref. No.	Sample Size	Relative Fracture Velocity V_F/V_S			Fracture Velocity V_F (m/s)
			Mean	Range	Std. Dev.	
Spec. 1, Facet A	1	6	0.5854	0.5616 - 0.6088	0.015	2,077
	2	3	0.6306	0.6134 - 0.6478	0.014	2,237
	3	1	0.5483	-	-	1,945
	4	1	0.6065	-	-	2,152
	5	1	0.5410	-	-	1,919
	6	3	0.5763	0.5610 - 0.6088	0.023	2,045
	7	1	0.5948	-	-	2,110
	8	2	0.6156	0.6053 – 0.6259	0.010	2,184
	9	7	0.5994	0.5896 – 0.6053	0.007	2,127
	10	4	0.6078	0.5843 – 0.6259	0.017	2,156
	11	2	0.6224	0.6088 – 0.6361	0.014	2,208
	12	2	0.6335	0.6293 – 0.6378	0.004	2,248
Spec. 3, Facet E	13	1	0.5931	-	-	2,104
	14	1	0.5556	-	-	1,971
	15	1	0.5188	-	-	1,840
	16	1	0.6225	-	-	2,209

Note: - All V_F/V_S are calculated from angular measurements on gull wings in or near mist regions, or at or near mist lines.
- V_F is based on mean V_F/V_S and assumed V_S = 3,548 m/s.

Captions for Figures

1. Sketch of Specimen 1

2. Sketch of Specimen 2: Fracture branching occurred from Facet D to D_1.

3. Sketch of Specimen 3: Fracture branching occurred from Facet B to B_1.

4. Sketch of Specimen 4

5. Mist Line, Gull Wings, Wallner Wake and Other Wallner Lines: Mist line extends downward from the inclusion with gull wings at its sides. Wallner wake is the concave downward arc. Fracture direction downward. Magnification 46X. Facet A of Specimen 1. The gull wings indicate an approximate relative fracture velocity $V_F/V_S = 0.54$ and a fracture velocity $V_F = 1900$ m/s approximately (See Section 6).

6. Gull Wings and Wallner Wakes: Gull wings at inclusions, many out of focus. The short arc at upper right and the wide arcs in the lower half of the photo, all concave downward, are Wallner wakes. Fracture direction downward. Magnification 46X. Facet A of Specimen 1.

7. Double Tails with Trailing Mist or Mist-Hackle Lines, Regions of Mist and Hackle: At least seven double tails, each resembling a parabola, are seen. Region of mist is at upper right and in the lighter part on the left. Hackle region appears at lower right. Fracture direction downward. Magnification 46X. Facet A of Specimen 1.

8. Detail of a Mist-Hackle Line: The mist-hackle line at the center is unusual in having large recurrent hackles. More detailed view of the mist-hackle line at the right is seen in Fig. 9. Fracture direction upward. Magnification 46X. Facet F of Specimen 3.

9. Detail of a Mist-Hackle Line: This mist-hackle line, also shown at the right in Fig. 8, is also unusual in having relatively few of the larger hackle marks combined with mist. Fracture direction upward. Magnification 93X. Facet F of Specimen 3.

10. Scalar Chip Scars at an Inclusion: Various other surface alterations subsequent to primary fractures are seen to obscure the surface. Fracture direction downward. Magnification 46X. Facet A of Specimen 2.

11. Incomplete Scalar Chip Formation at an Inclusion: The color pattern is due to the scalar chips formed around the inclusion but not released. Fracture direction downward. Magnification 46X. Facet B of Specimen 2.

12. Groove with "Butterfly Checks": Three pairs of scalar chips, known also as butterfly checks, are seen along the groove. Magnification 93X. Facet C of Specimen 1.

13. Chatter Marks and Other Surface Alterations: The track of recurrent small arcs, known as chatter marks, extends diagonally in the central part of the photo. The relative contact motion was upward along this diagonal track. Note other surface alterations. Fracture direction downward. Magnification 46X. Facet C of Specimen 3.

14. Chatter Marks and Other Surface Alterations: The track of chatter marks appears in the central part of the figure, with the relative motion downward during contact. Note other surface alterations. Magnification 93X. Facet F of Specimen 3.

15. Abrasion Tracks, Striations and Mist Lines: The abrasion tracks extend diagonally. Most of the vertical lines in the lower portion are fine striations, formed subsequent to primary fracture, that just happen to line up with the fracture direction downward. Mist lines, seen in the upper part of the photo, become indistinguishable from the striations in the lower part. The mist region in the upper portion is seen to vanish gradually downward. Magnification 46X. Facet A of Specimen 1.

16. Surface Fractures Due to Thermal Effects: Surface fracturing subsequent to the primary fractures. Magnification 93X. Facet C of Specimen 4.

17. Surface Fractures Due to Thermal Effects: Surface fracturing subsequent to the primary fractures. Magnification 93X. Facet C of Specimen 4.

18. Surface Fractures Due to Thermal Effects: Surface fracturing subsequent to the primary fractures. Magnification 93X. Facet C of Specimen 4.

19. Surface Alterations with Appearance of "Stacked Pancakes": Surface fracturing subsequent to the primary fractures. Magnification 93X. Facet E of Specimen 4.

20. Surface Alterations Appearing as "Indentations": Magnification 93X. Facet A of Specimen 2.

21. Internal Inclusion at Fracture Origin: The fracture originated from the inclusion at its left, re-entrant portion, as indicated by the hackle extending to the left and the two almost concentric Wallner lines. The fracture extended leftward at first, then downward as well as upward to sweep around the inclusion. See Fig. 22. Magnification 46X. Facet A of Specimen 1.

22. Internal Inclusion at Fracture Origin (Downstream Part): The two partial fracture fronts sweeping around the inclusion meet at the wake hackle (also known as a tail) extending upward at the center. Only part of the inclusion is seen at the bottom of the photo. Magnification 46X. Facet A of Specimen 1.

23. Depletion Scarps: Facet D of Specimen 4. Fracture direction upward. Magnification 46X. The region in on this and the next two figures has been obscured by alterations subsequent to the primary fracture.

24. Depletion Scarps and Subcavitation Hackle or Its Counterpart: The cusp-like features are the depletion scarps, and the linear features upstream of them are the other markings. This region is to the right of that in Fig.23. Fracture direction upward. Magnification 46X. Specimen 4, Facet D.

25. Depletion Scarps and Subcavitation Hackle or Its Counterpart: Fracture direction upward. Magnification 93X. Specimen 4, Facet D.

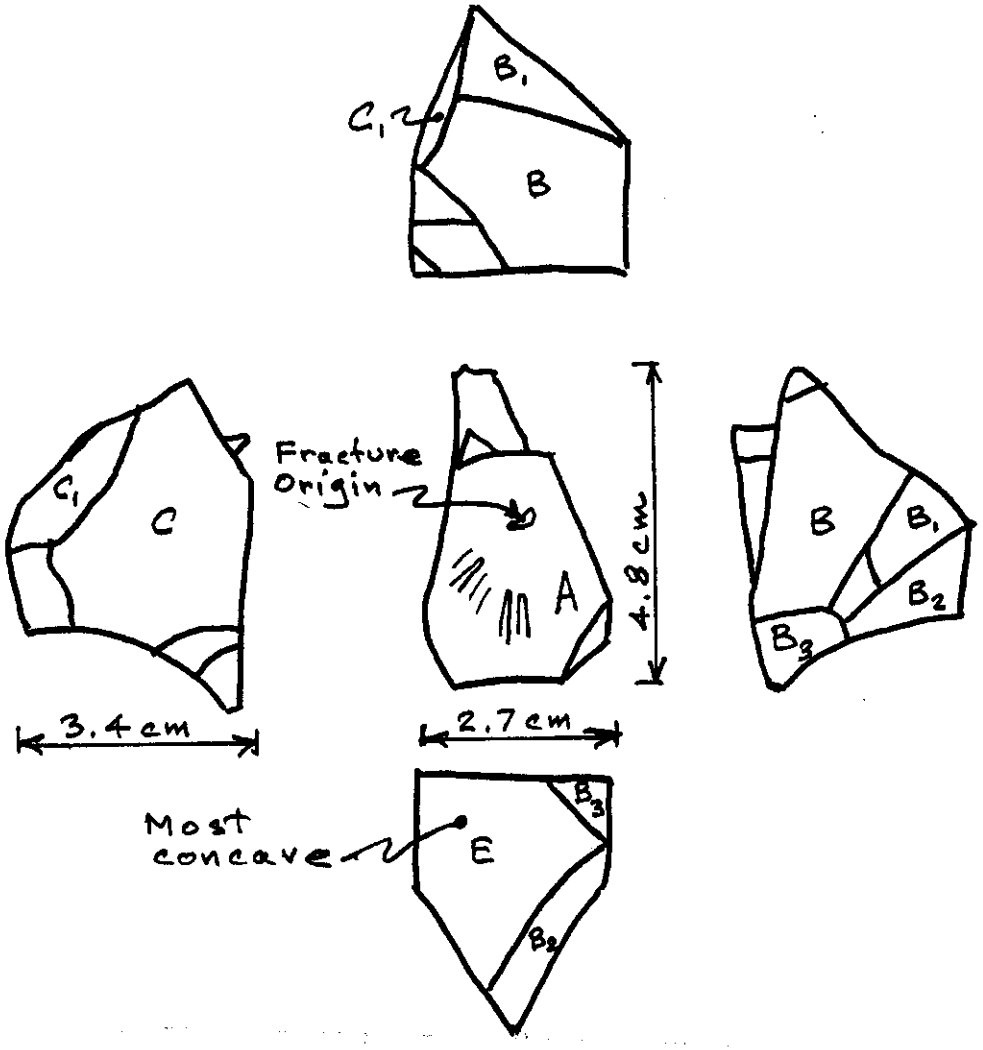

Figure 1 – Sketch of Specimen 1

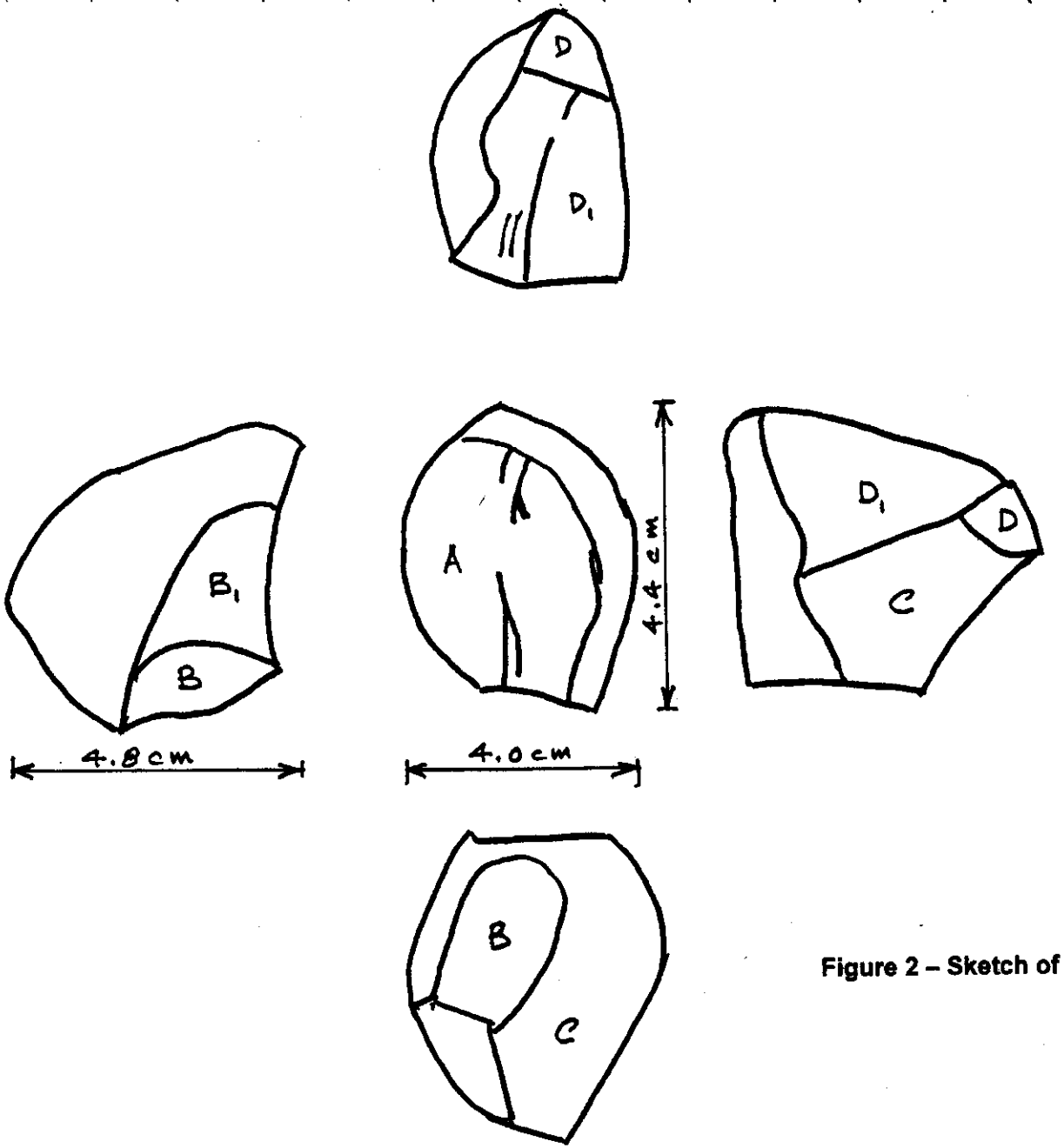

Figure 2 – Sketch of Specimen 2

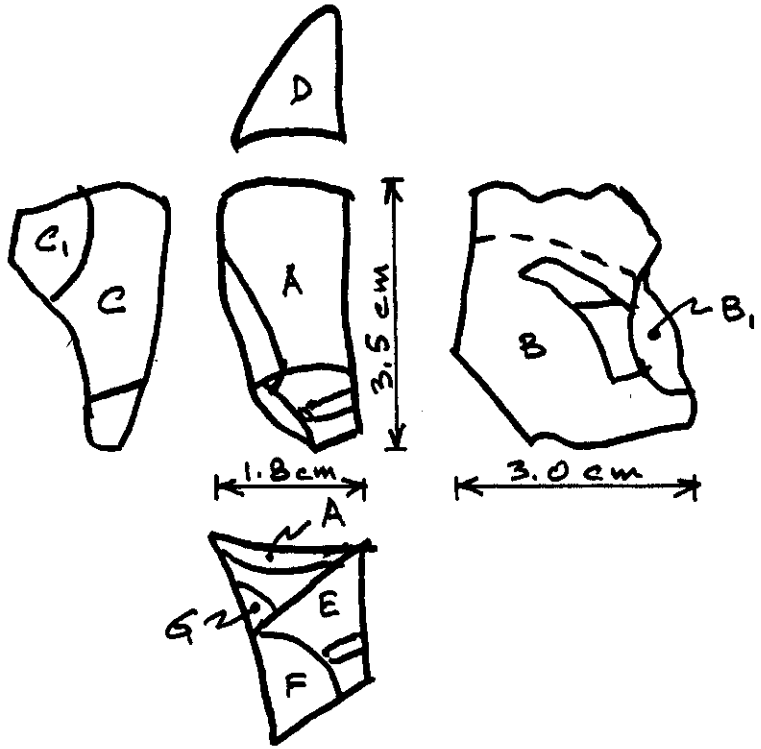

Figure 3 – Sketch of Specimen 3

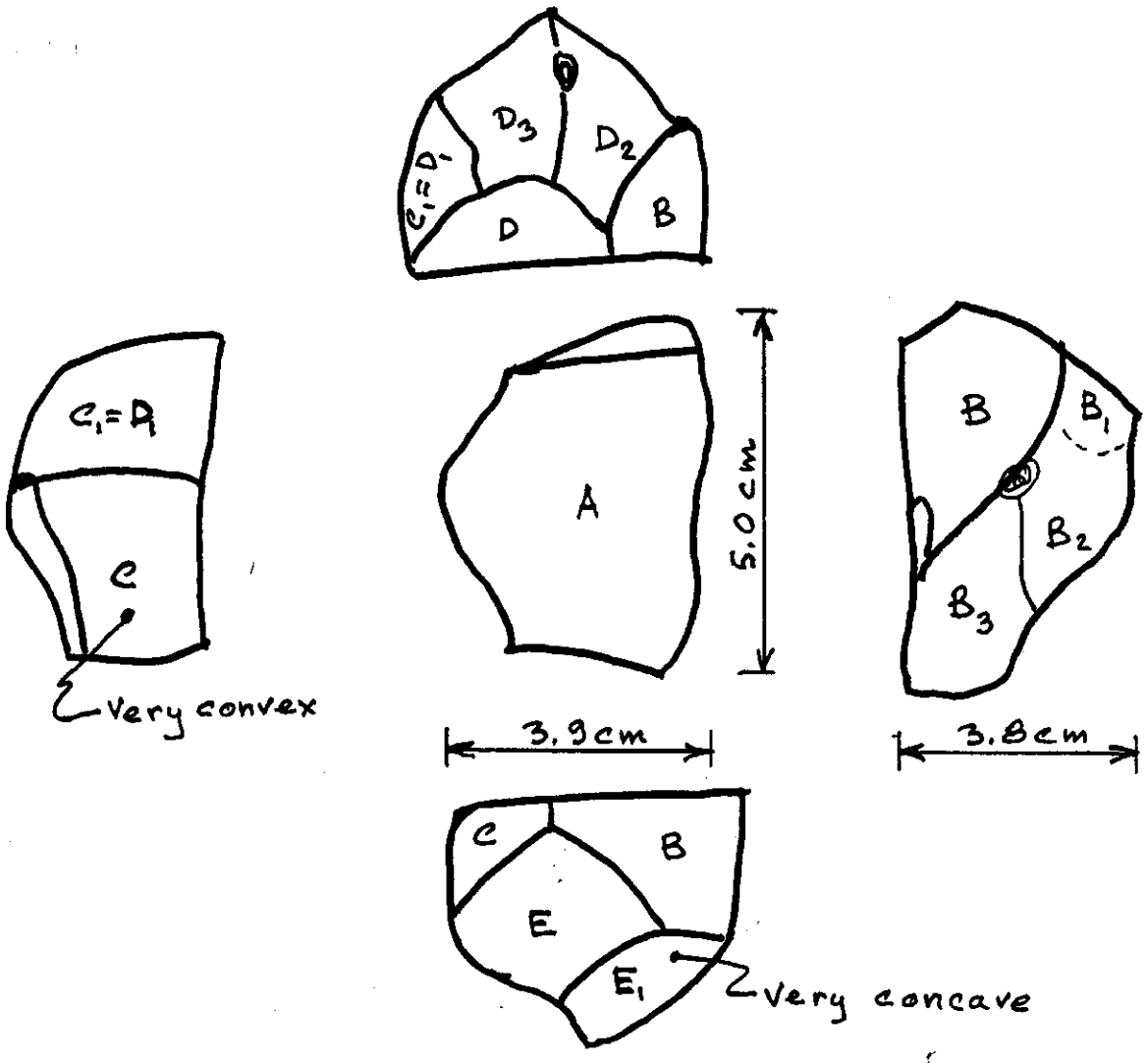

Figure 4 – Sketch of Specimen 4

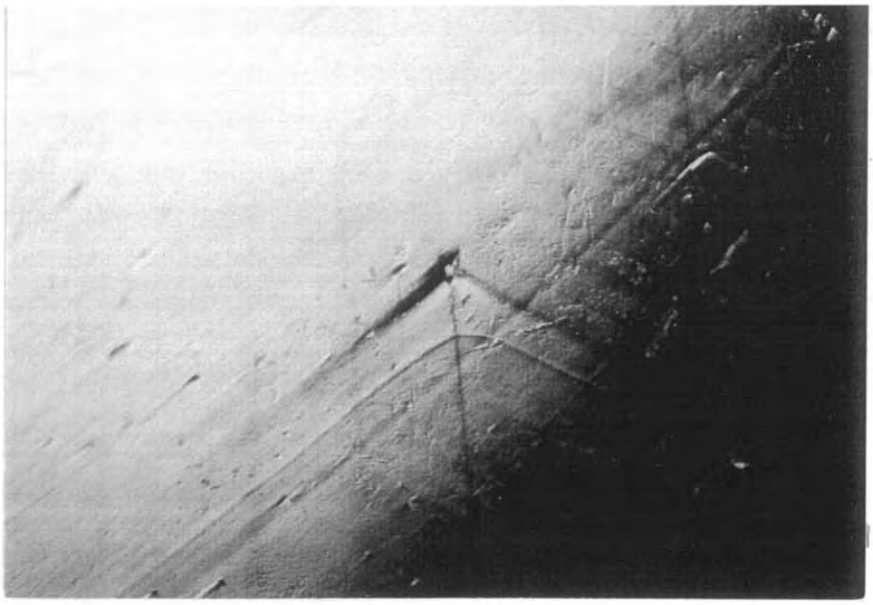

Figure 5

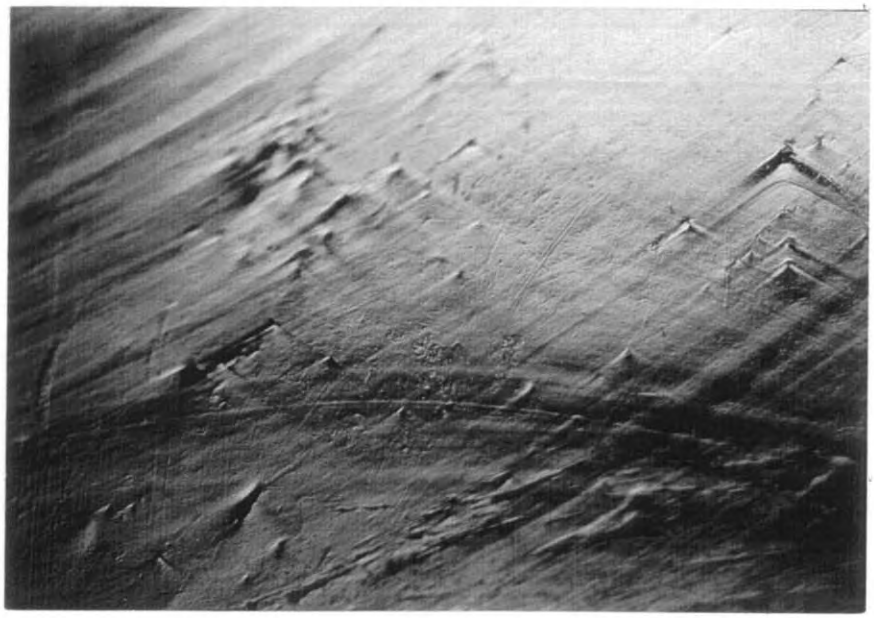

Figure 6

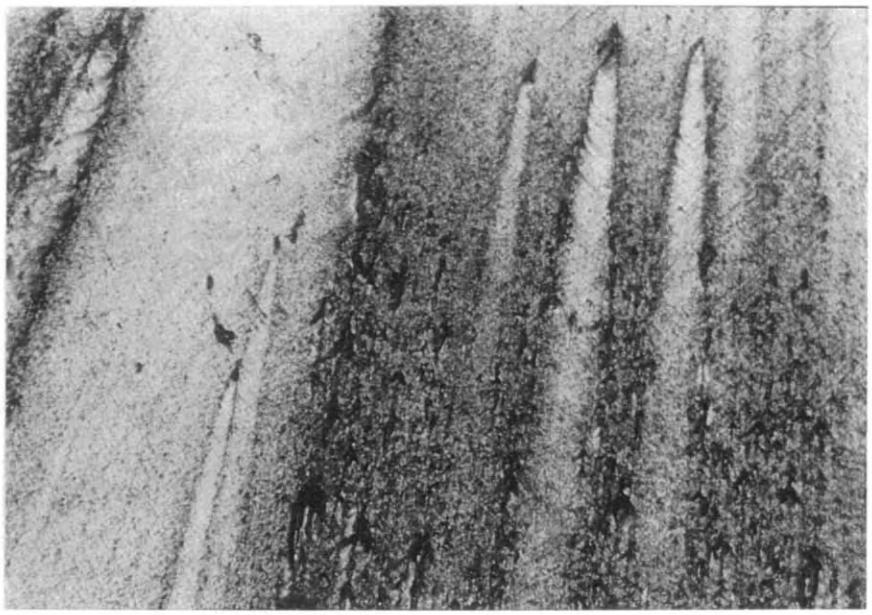

Figure 7

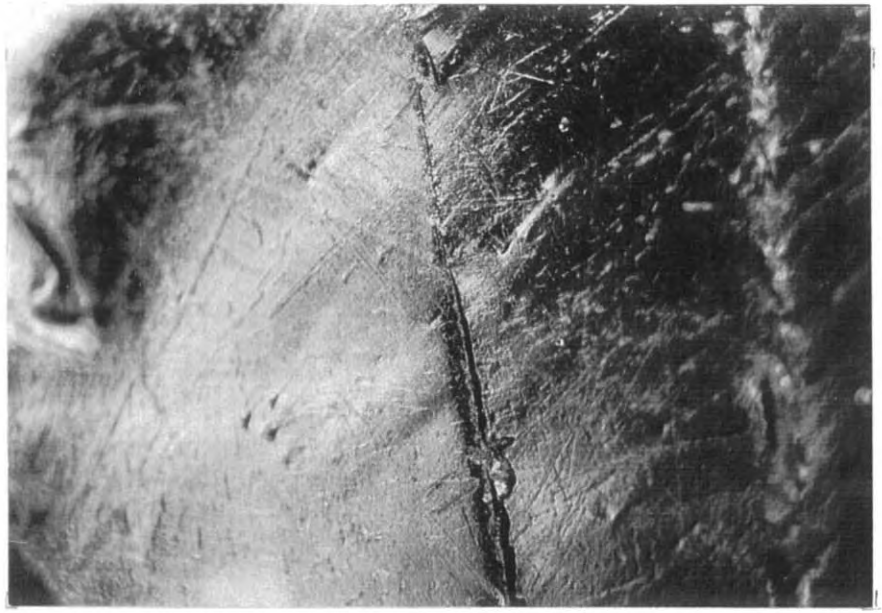

Figure 8

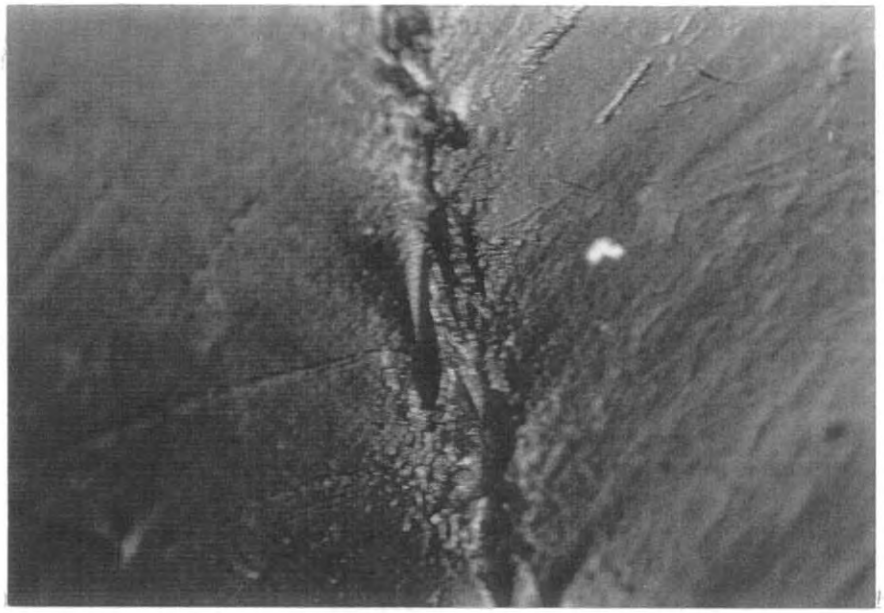

Figure 9

Figure 10

Figure 11

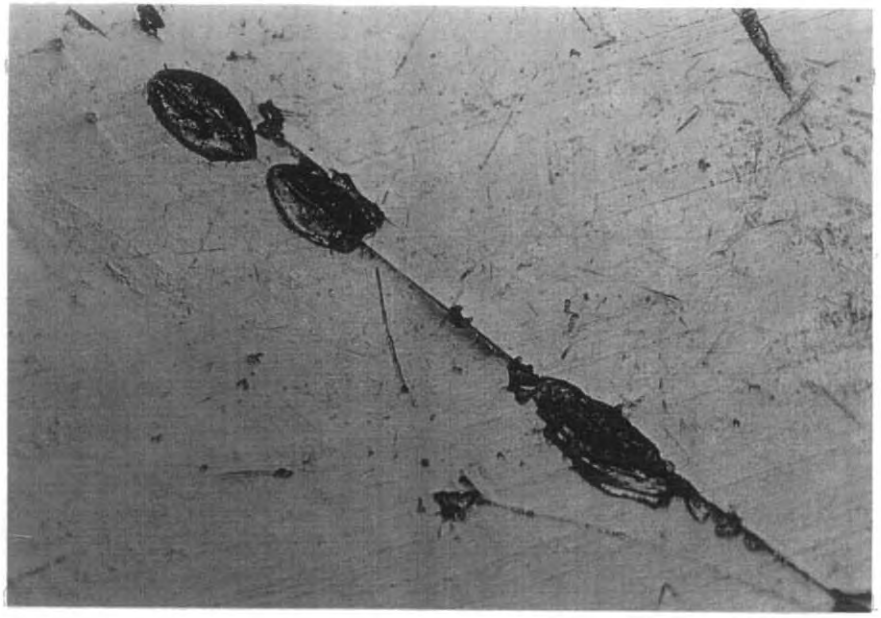

Figure 12

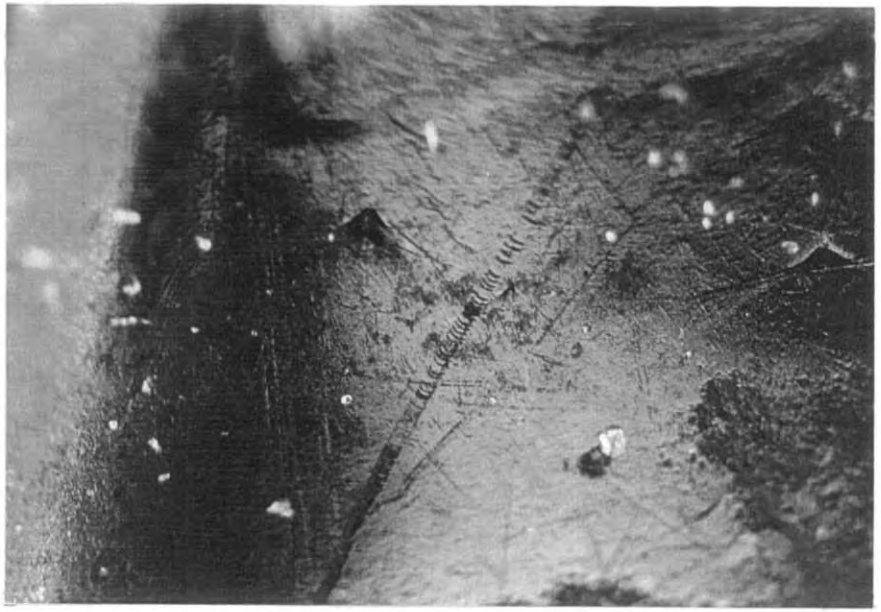

Figure 13

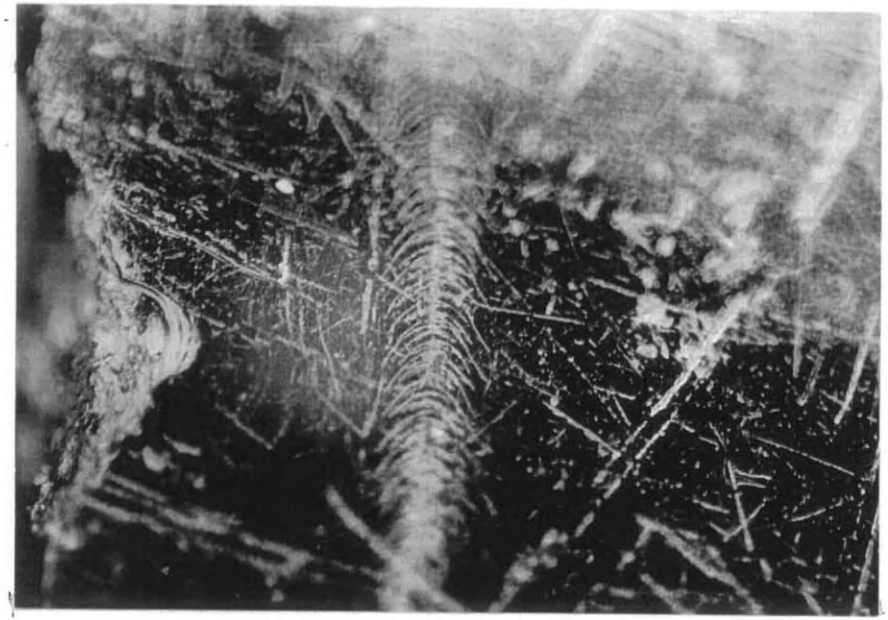

Figure 14

Figure 15

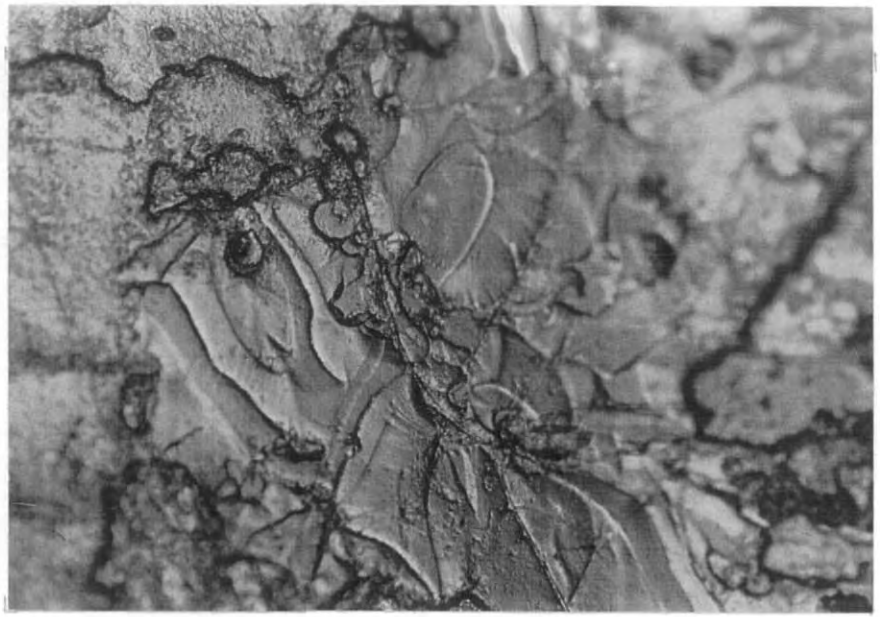

Figure 16

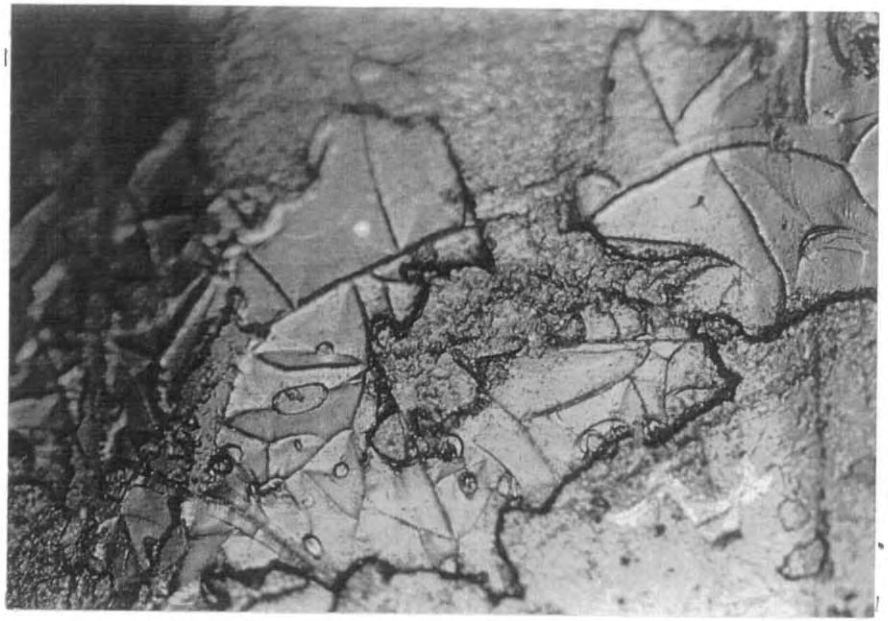

Figure 17

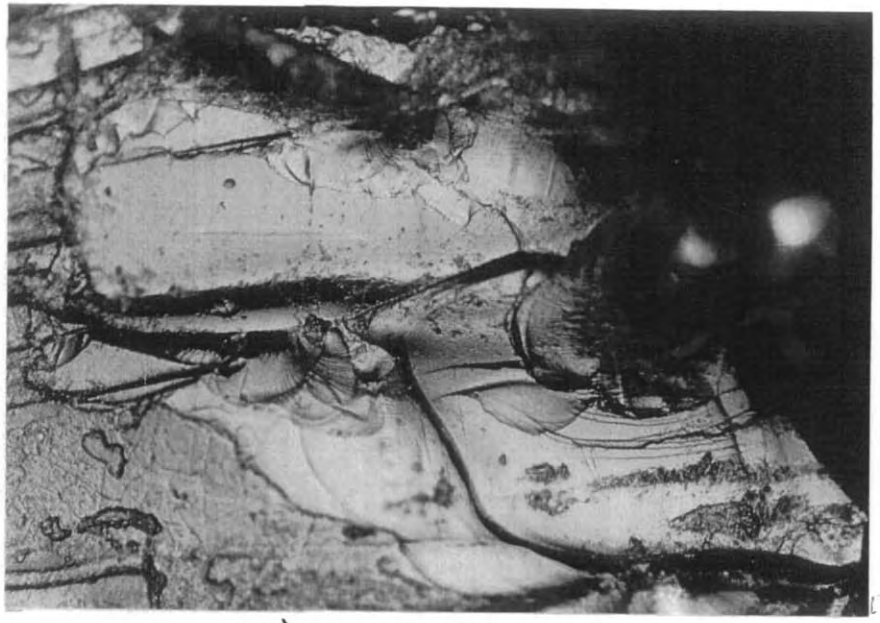

Figure 18

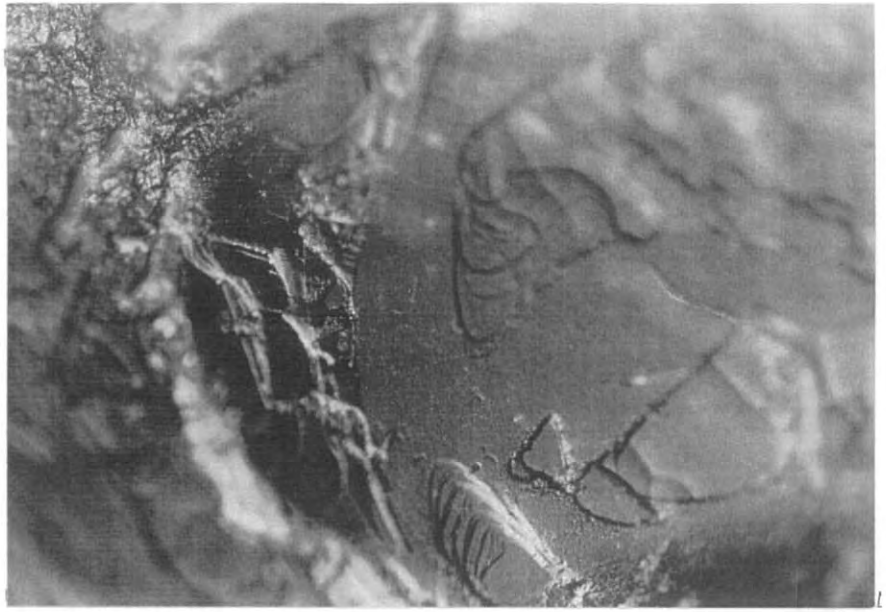

Figure 19

Figure 20

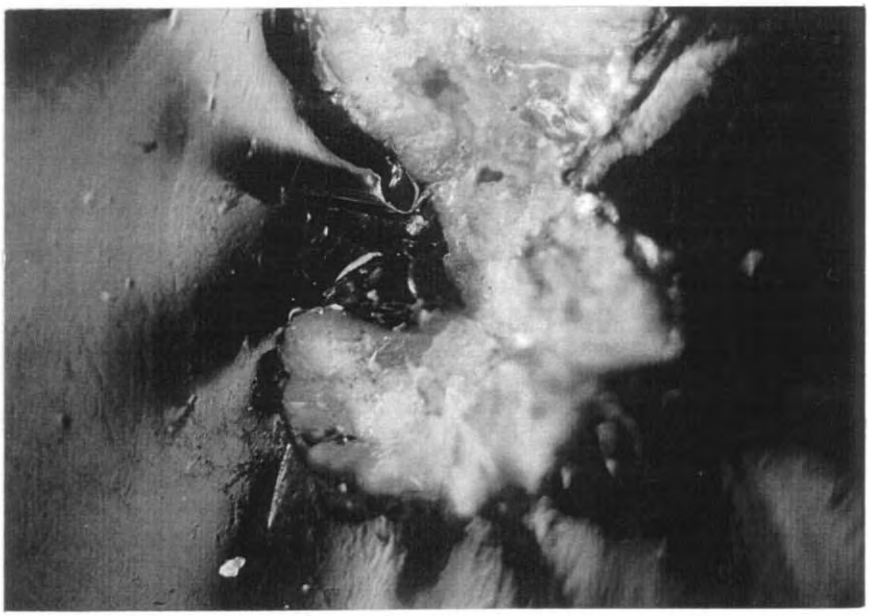

Figure 21

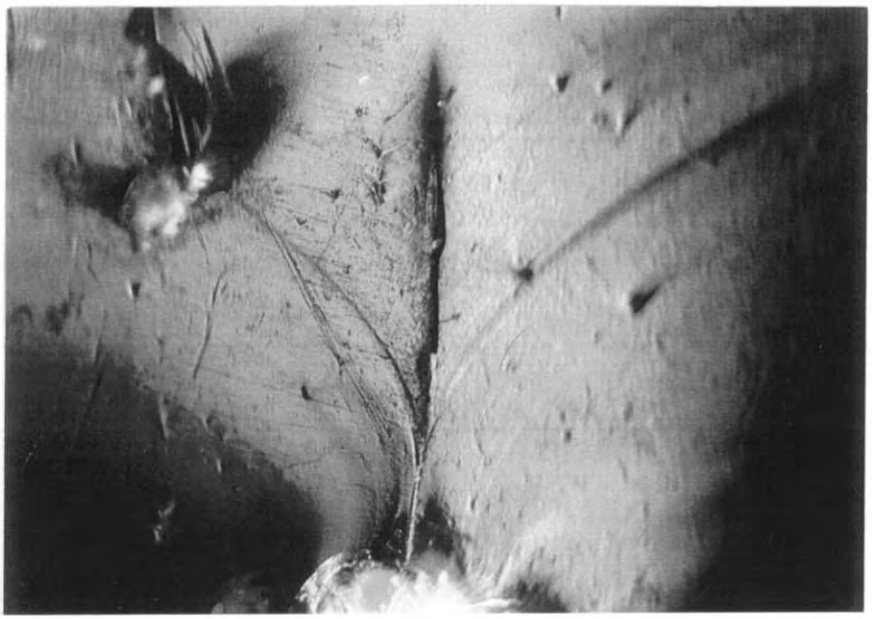

Figure 22

Figure 23

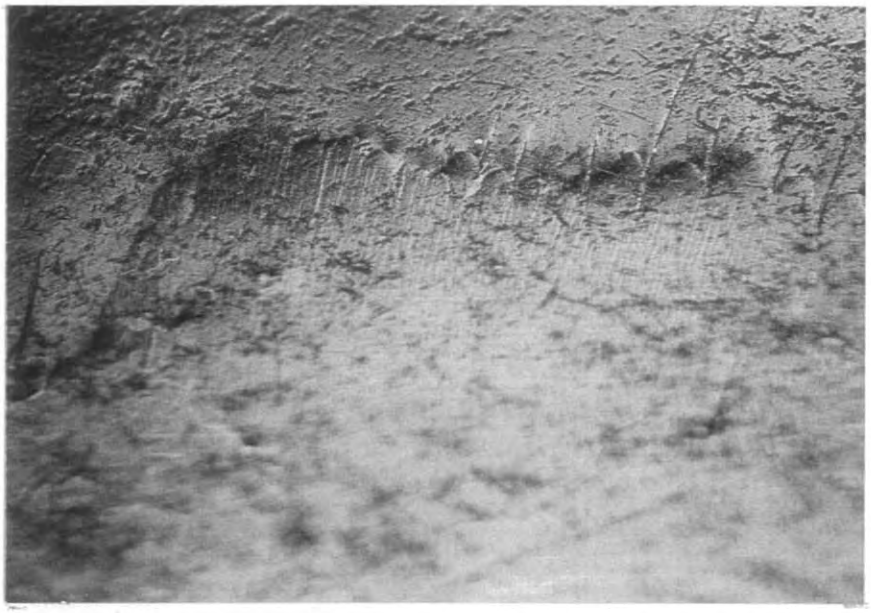

Figure 24

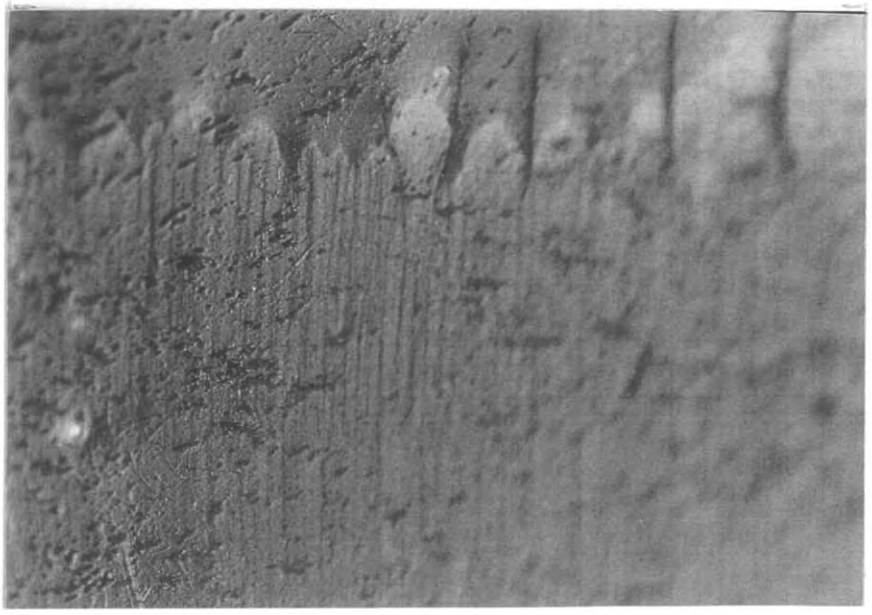

Figure 25

APPENDIX A: Original Photos

Includes:

- List of Photos
- Black and White Copies of Photos
- Original Color Photos

Note: Photo #8 is placed intentionally in front of #4.

List of Photos Attached

Photo No.	Reference No.	Specimen -Facet	Magnifi-cation	Fracture Direction	Description
1	31-17A	1 – A	46	Down	Same as Fig. 5
2	31-19A	1 – A	46	Down	Same as Fig. 6
3	28-17A	1 – A	46	Down	Mist lines, gull wings and Wallner wakes
4	31-22A	1 – A	46	Down	Same as Fig. 7
5	31-23A	1 – A	46	Down	As #4, but with different lighting
6	28-12A	1 – A	93	Down	As #4, at higher magnification
7	28-13A	1 – A	93	Down	As #5, at higher magnification
8	28-4A	1 – A	46	Down	Inclusion with triple tail, double tails, mist lines, gull wings and Wallner wakes
9	28-5A	1 – A	46	Down	Slightly downstream of #8: Double tails, mist lines, gull wings, mist (as at upper right), hackle at lower right
10	28-6A	1 – A	46	Down	Slighly downstream of #9: Double tails, mist lines, gull wings & other Wallner lines, mist becoming lighter (upper to lower part near center), hackle becoming less pronounced (upper to lower part at right)
11	28-7A	1 – A	46	Down	Slightly upstream of #10: Gull wings, double tails, mist lines, hackle becoming less pronounced to become mist at lower right
12	28-14A	1 – A	46	Down	Region left of #4-#7: Gull wings, double tails, mist lines. Note obscuring by surface alteration.
13	28-15A	1 – A	46	Down	As #12, but with different lighting: Double tails, mist lines
14	28-8A	1 – A	93	Down	Downstream of #4-#7: Gull wings, double tails, mist lines, mist
15	28-9A	1 – A	93	Down	As #14, but darkfield illumination: Double tails, mist lines, mist
16	28-18A	1 – A	46	Down	Just right of #8: Double tails, mist lines, Mist becoming more pronounced downward
17	28-19A	1 – A	46	Down	As #16, but darkfield illumination. Note surface obscuring, especially at upper part.
18	30-12	1 – A	46	Down	Multiple tails with mist lines at very large inclusions, with some white infill at the two mist lines at left. Gull wings, Wallner wakes and other Wallner lines.
19	30-13	1 – A	46	Down	Just right of #18, with similar features.
20	30-23	2 – C	46	Down	Double tail just left of center, and double tail with convergent arms just right of center. These are barely visible due to severe obscuring from surface alterations.
21	30-21A	2 – C	46	Down	Double tails and gull wings. Note severe surface obscuring.
22	30-21	2 – C	46	Down	Double tails and gull wings. Note surface obscuring.
23	30-24	2 – C	93	Down	Double tails. Note white infill, especially at left, and surface obscuring by deposits or residues.
24	30-20	2 – C	46	Down	Mist lines, double tails and hackle marks with white infill.
25	30-9	1 – A	93	Down	Double tail, mist (at left), hackle right of center with white infill.
26	30-10	1 – A	46	Down	As #25, but with darkfield illumination.
27	30-35A	2 – A	46	Up	Same as Fig. 8

28	30-36A	3 - F	93	Up	Same as Fig. 9
29	30-27A	2 – A	46	Up	Same as Fig. 10
30	30-26A	2 – A	93	Left	Enlarged view of #29.
31	30-25A	2 - B	46	Down	Same as Fig. 11
32	30-18	2 – C	46	Down	Large scalar chip at an inclusion, with Wallner lines and Twist hackles.
33	30-31A	3 – B_1	46	Down	Despite severe obsuring by surface alterations, the hackle region just upstream of branching (below bottom of photo) is evident. Mist just upstream of it can be inferred, but is not visible due to obscuring.
34	31-4A	1 – C	93	-	Same as Fig. 12
35	30-24A	2 – C	93	-	Scoring with scalar chipping ("butterfly checks").
36	30-30A	3 – C	46	Down	Same as Fig. 13
37	31-5A	3 – F	93	-	Same as Fig. 14
38	28-23A	1 – A	46	Down	Same as Fig. 15
39	31-10A	4 – C	93	-	Same as Fig. 16
40	31-9A	4 – C	93	-	Same as Fig. 17
41	31-12A	4 – C	93	-	Same as Fig. 18
42	31-16A	4 - E	93	-	Same as Fig. 19
43	31-15A	4 - E	93	-	Same as #42, with different lighting.
44	31-14A	4 - E	46	-	Same as #42 & #43, at lower magnification.
45	30-28A	2 – A	93	-	Same as Fig. 20
46	30-2	1 – A	46	Varies	Same as Fig. 21
47	28-2A	1 – A	46	Varies	Same region as on #46.
48	30-3	1 – A	46	Up	Same as Fig. 22
49	X–12A	4 - D	46	Up	Depletion scarps, just left of those in Photo 50.
50	X-13A	4 - D	46	Up	Depletion scarps. (Same as Figure 23.)
51	X-2A	4 – D	46	Up	Depletion scarps and subcavitation hackle or its counterpart. (Same as Figure 24.)
52	X-6A	4 - D	46	Up	Depletion scarps and subcavitation hackle or its counterpart. Region to the right of that in Photo 51.
53	X-23A	4 - D	93	Up	(Same as Figure 25.) Depletion scarps and subcavitation hackle or its counterpart. About the same region is shown on Photos 53 –55.
54	X-20A	4 - D	93	Up	Depletion scarps and subcavitation hackle or its counterpart.
55	X-21A	4 - D	93	Up	Depletion scarps and subcavitation hackle or its counterpart.
56	X-24A	4 - D	93	Up	Depletion scarps and subcavitation hackle or its counterpart. Region shown is to the right of that on Photos 53 –55.

Notes: - Photo numbers are marked at the bottom of the photos in green.
- Figure numbers are marked on the photos in red.
- Fracture direction is indicated by an arrow on some photos.
- See Figs. 1 to 4 for specimen and facet designations.
- Reference Nos. identify the film and negative, as follows:
  - The second number indicates the negative number, also printed on the back of the photo.
  - On Photos 1 - 48, the first number indicates the day of May 2002 printed on the back of the photo.
  - On Photos 49 –56, the first number is replaced by X (= Film #021217).

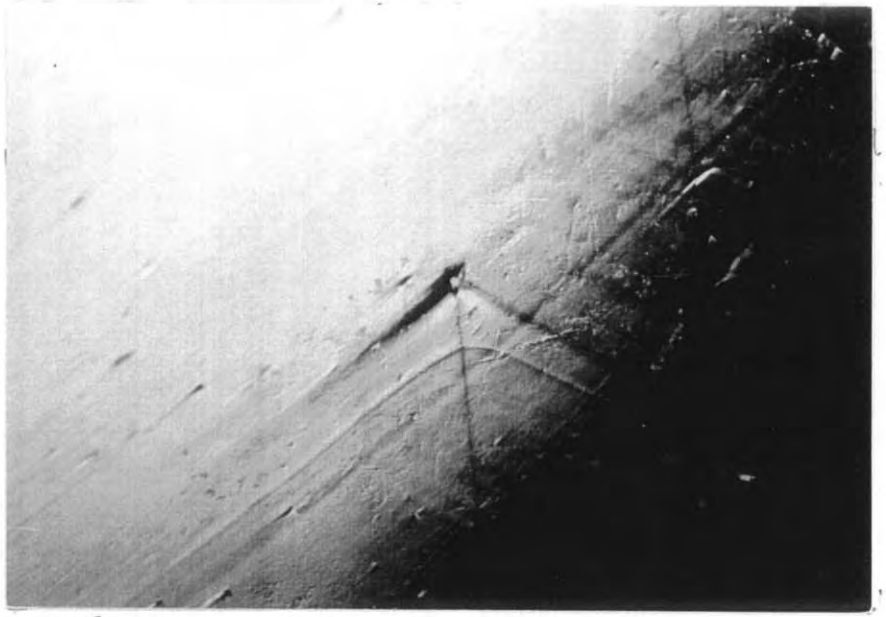

1

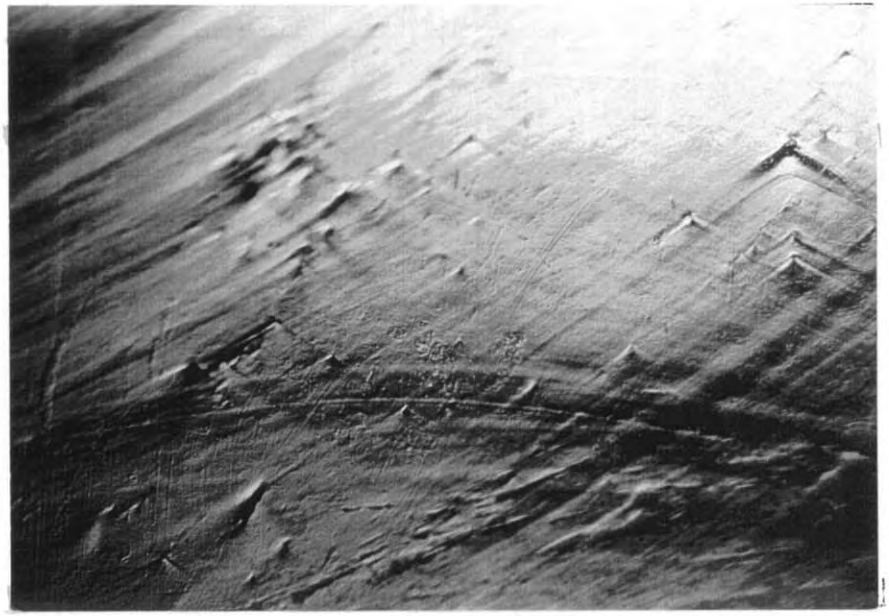

2

3

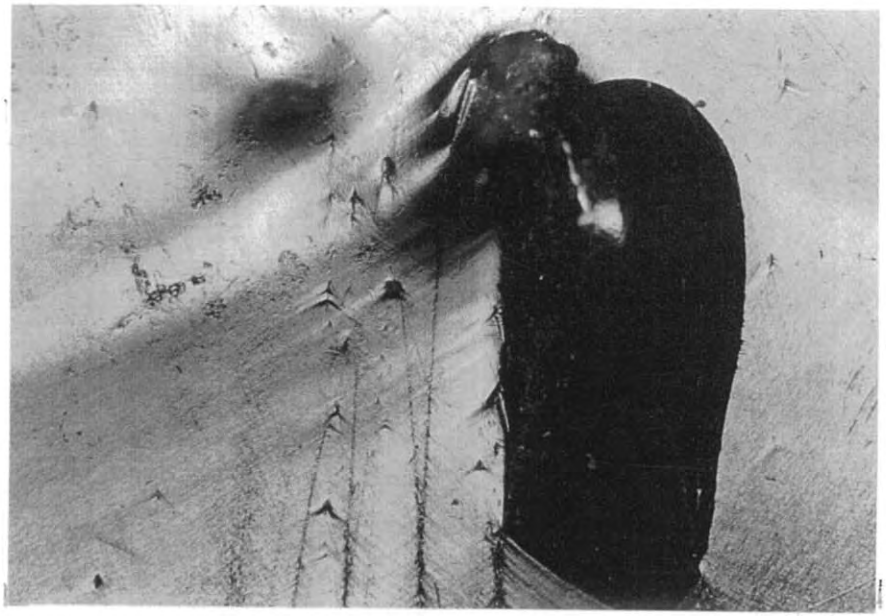

4

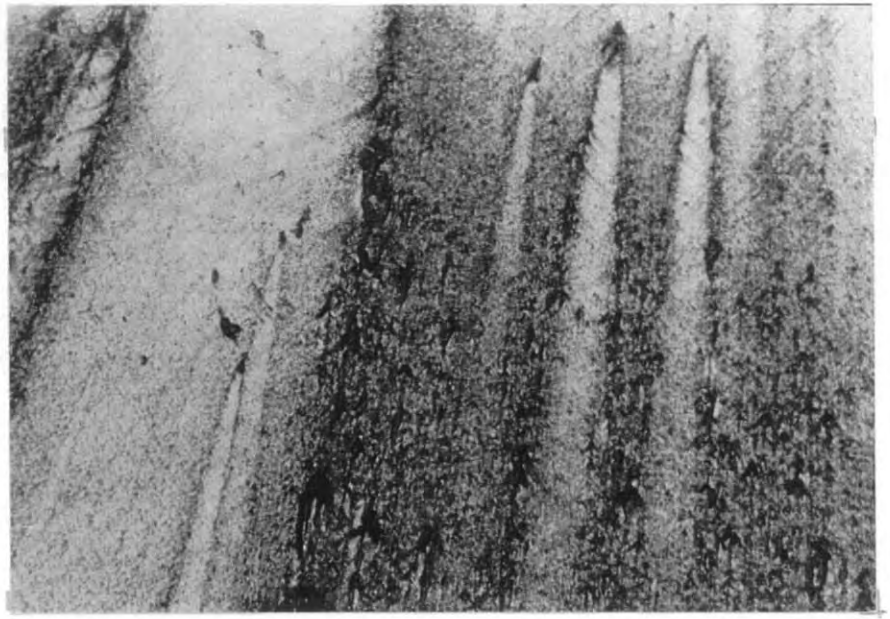

4

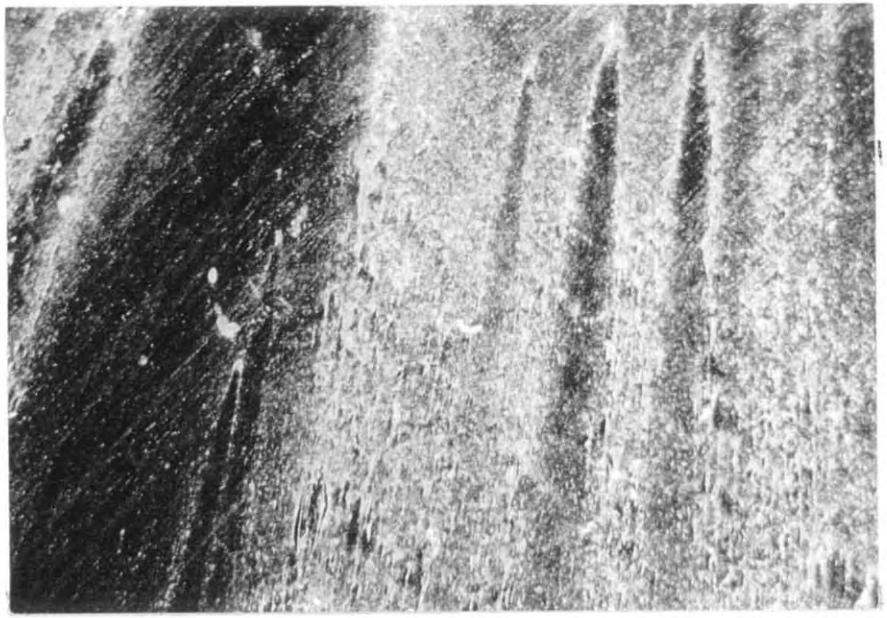

5

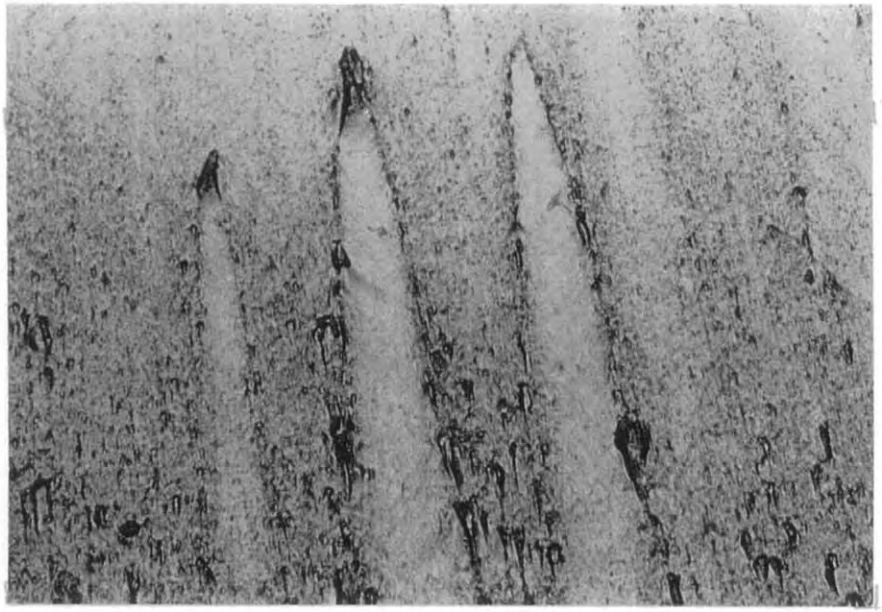

6

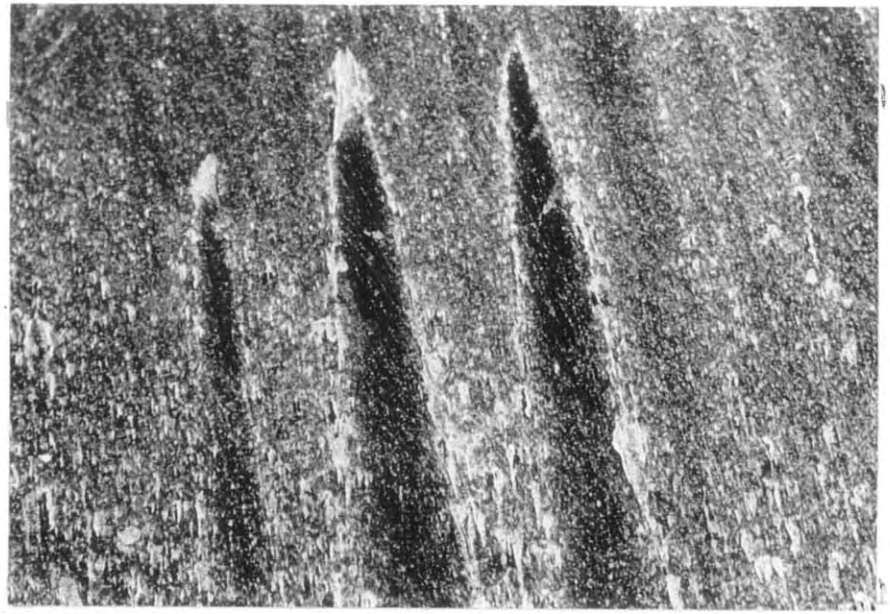

7

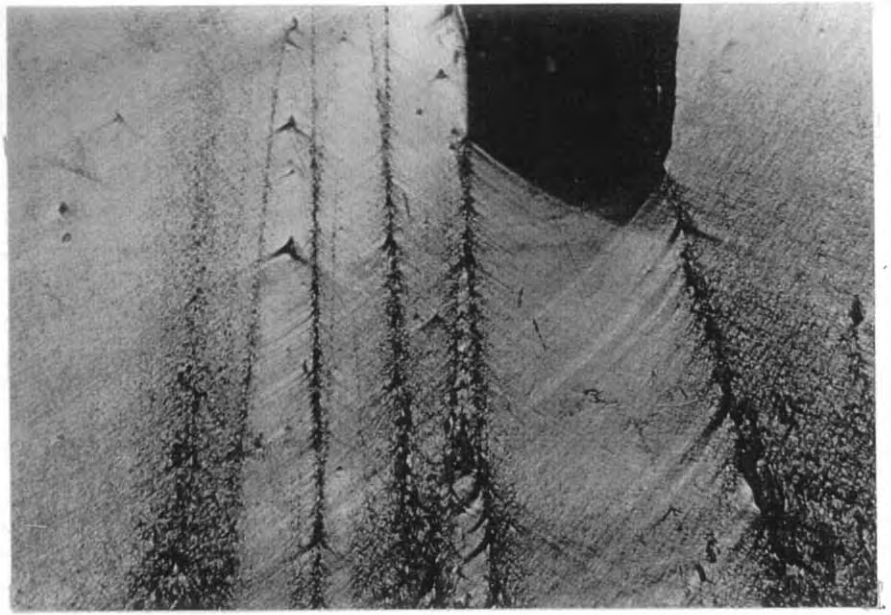

9

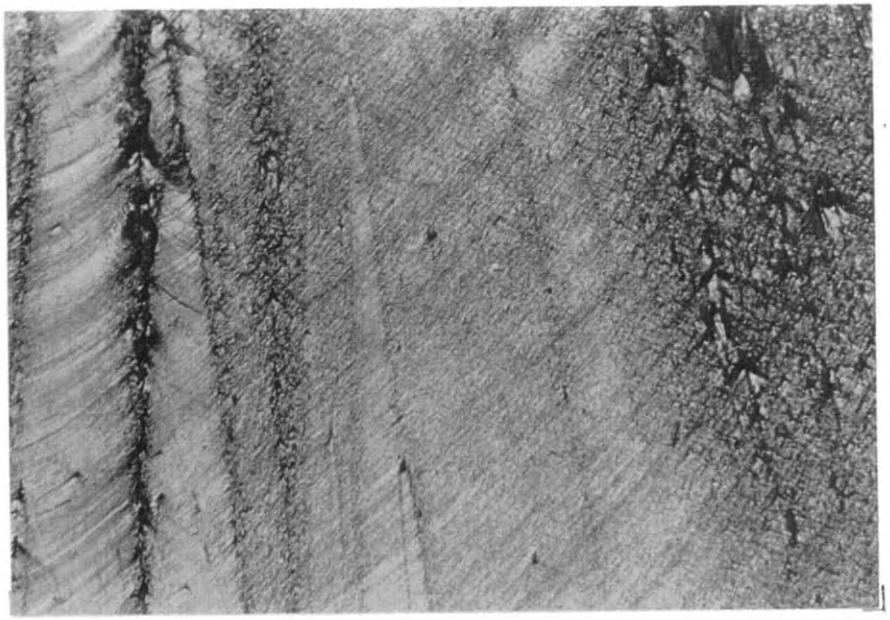

10

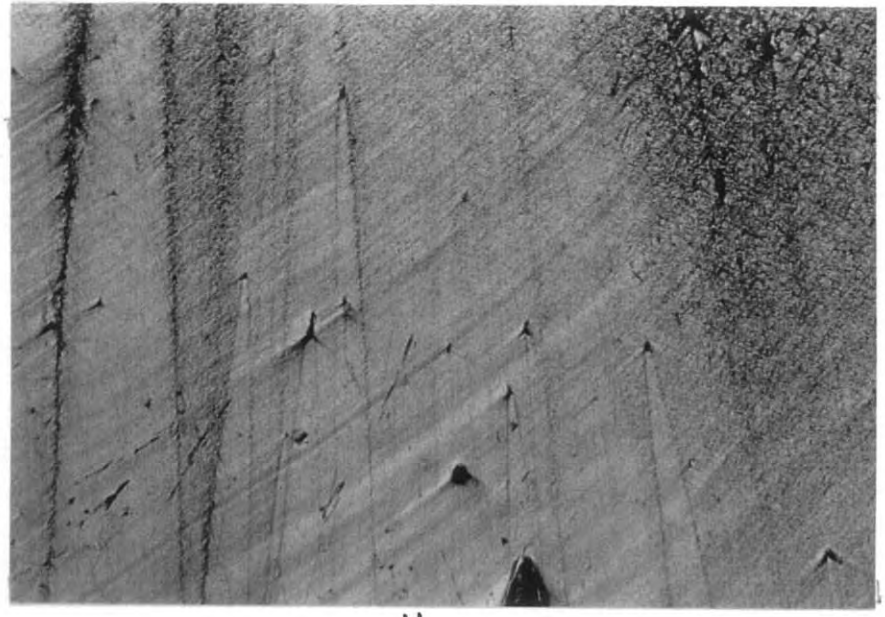

11

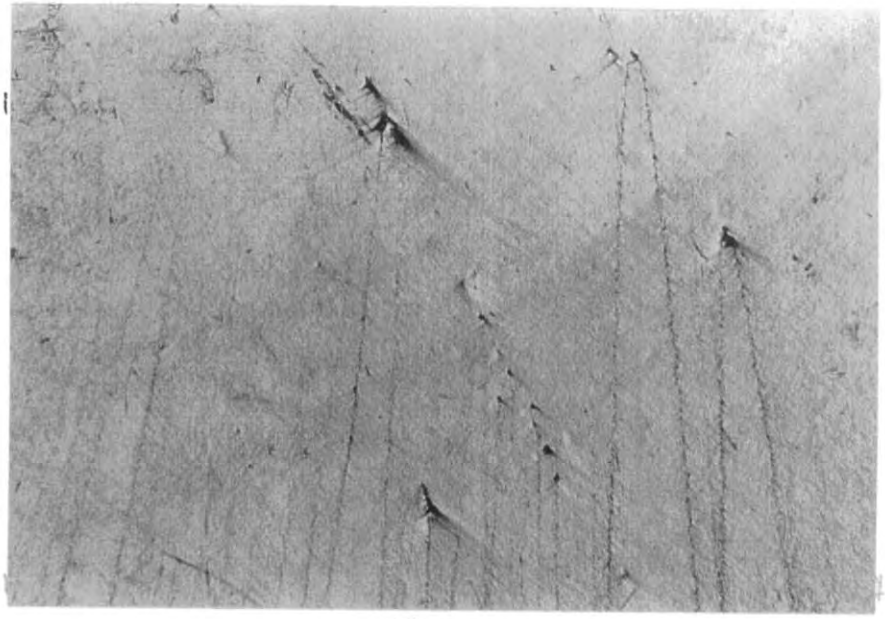

12

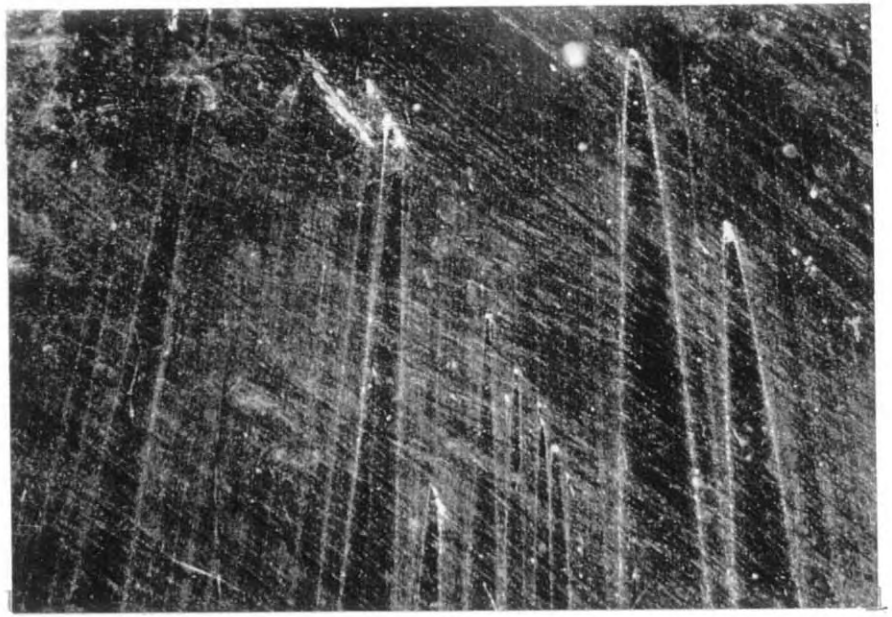

13

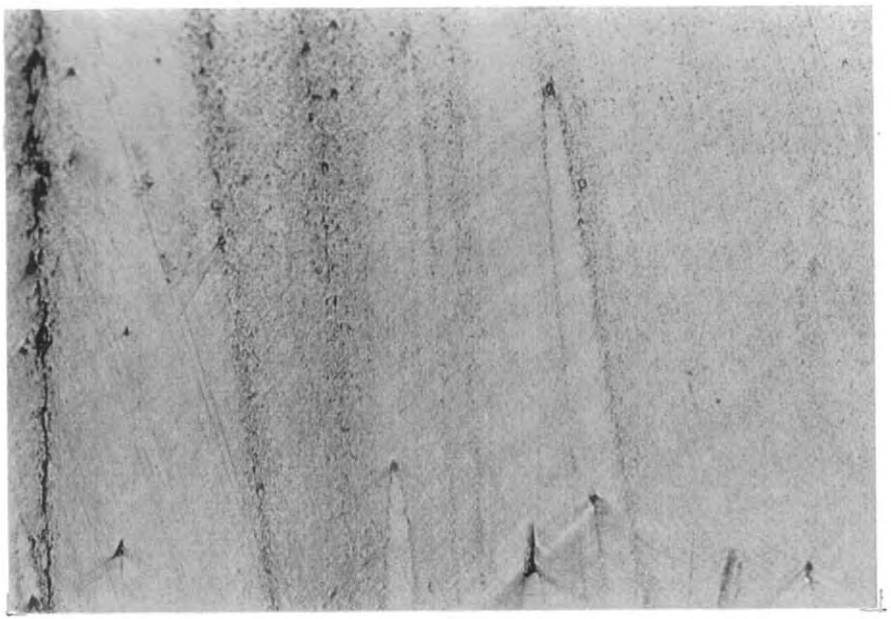

14

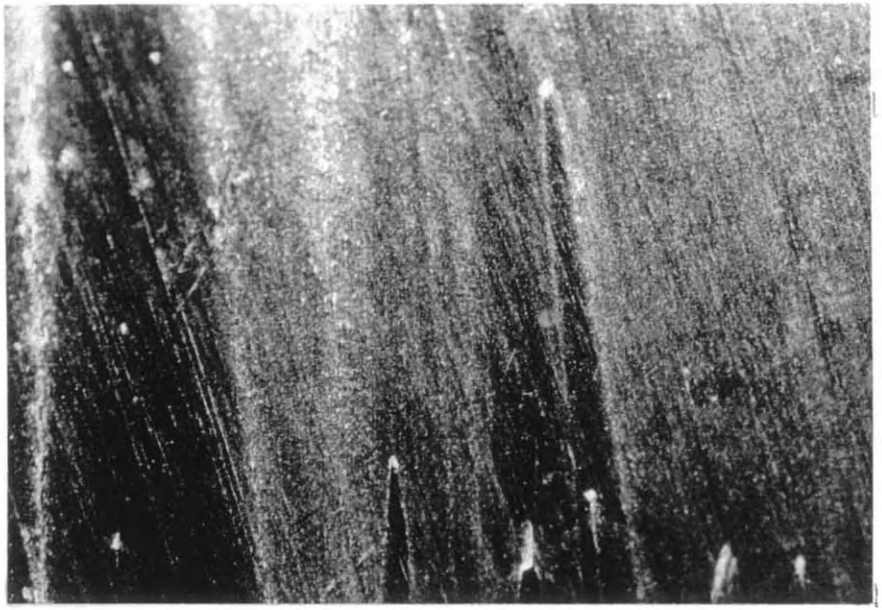

15

16

17

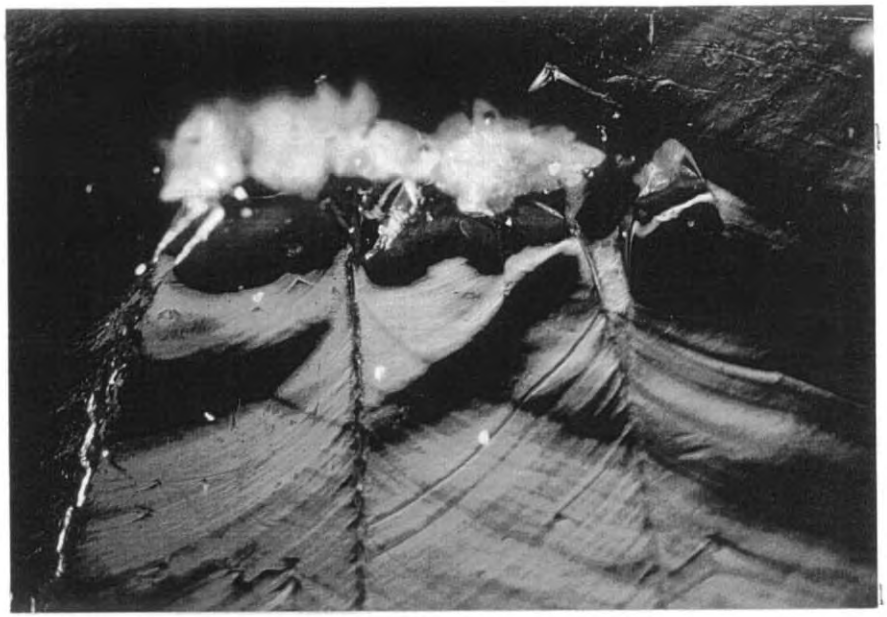

18

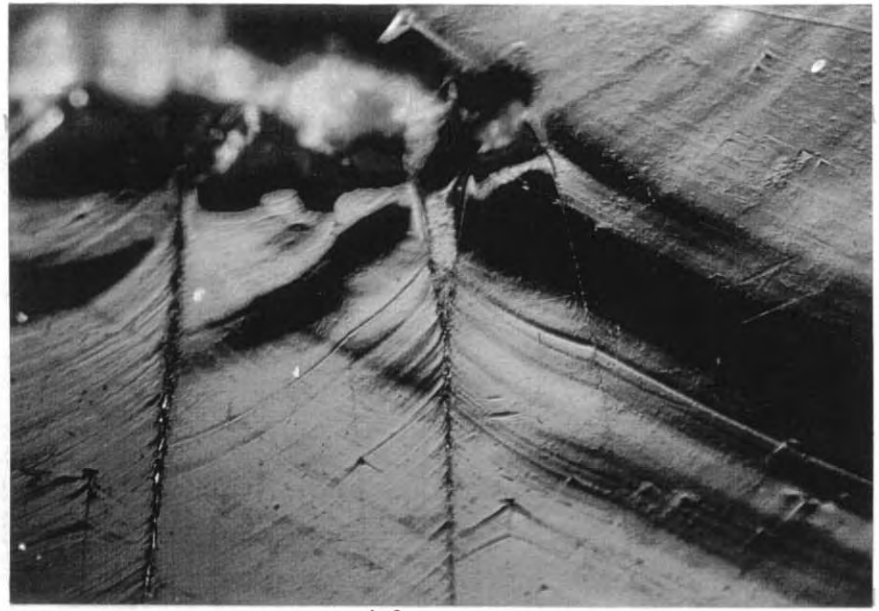

19

20

21

22

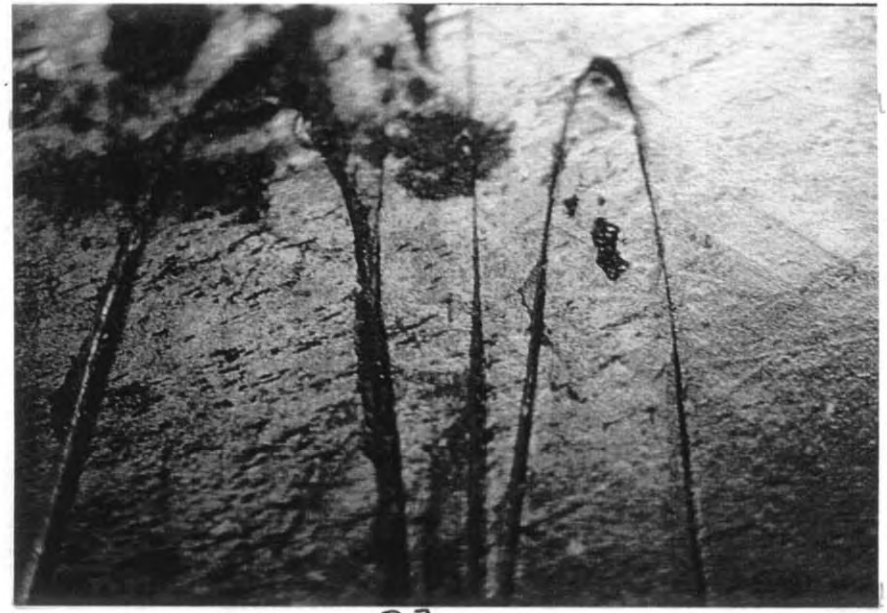

23

24

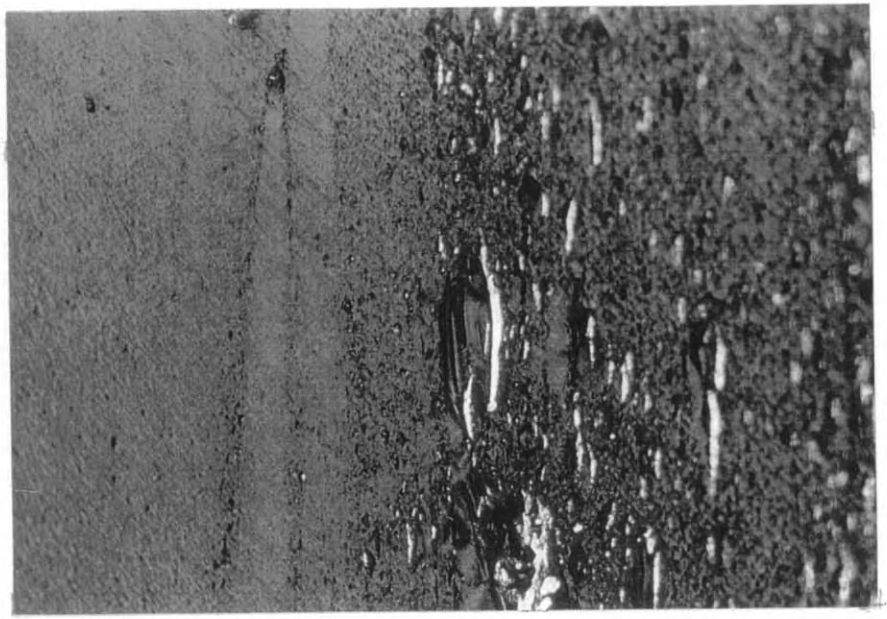

25

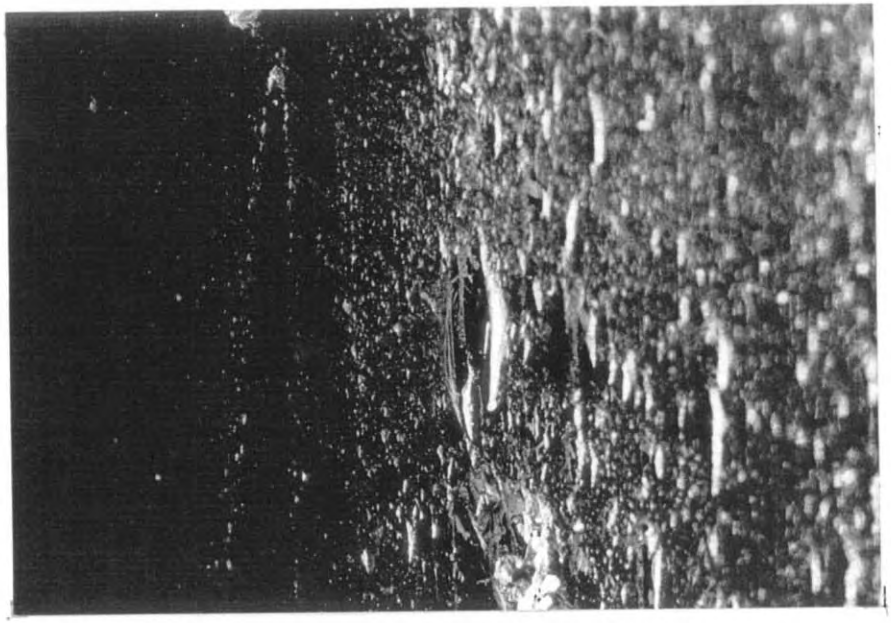

26

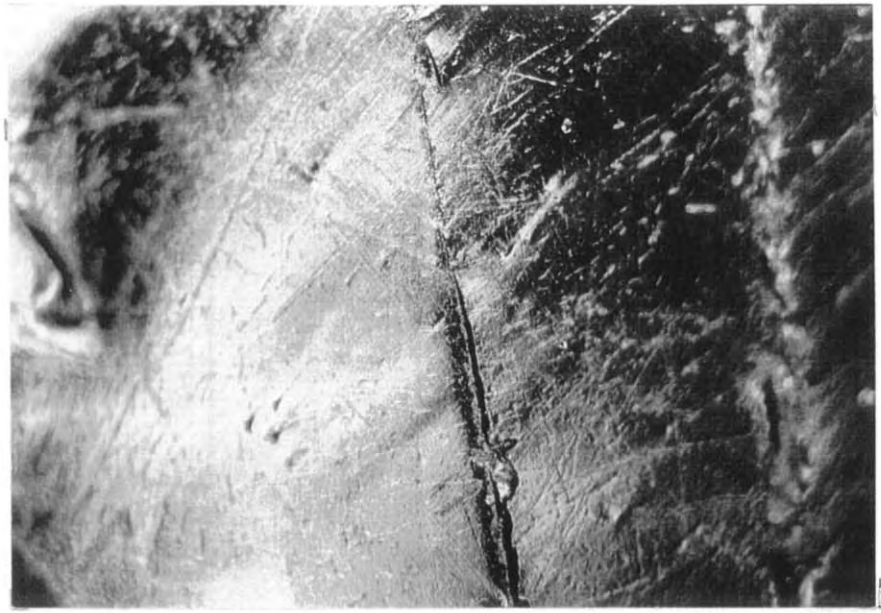

27

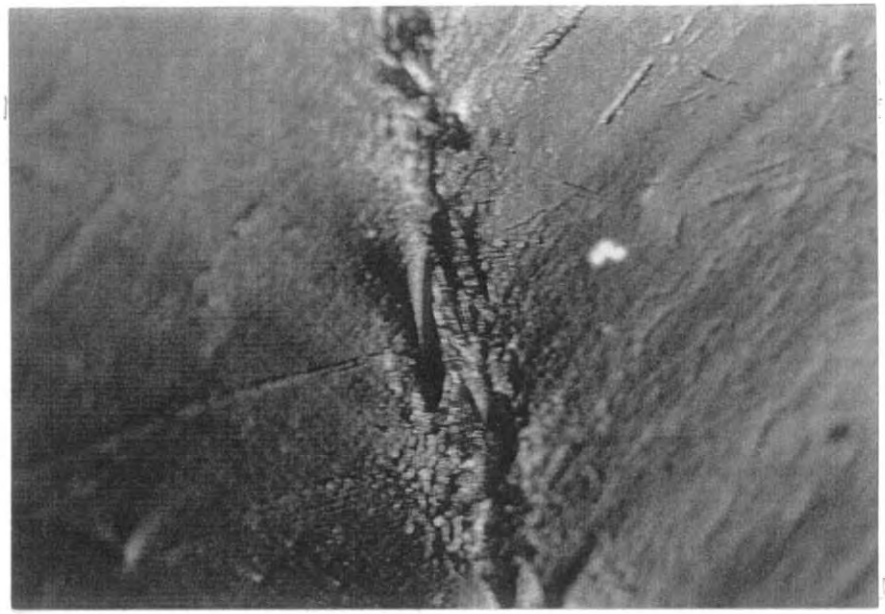

28

29

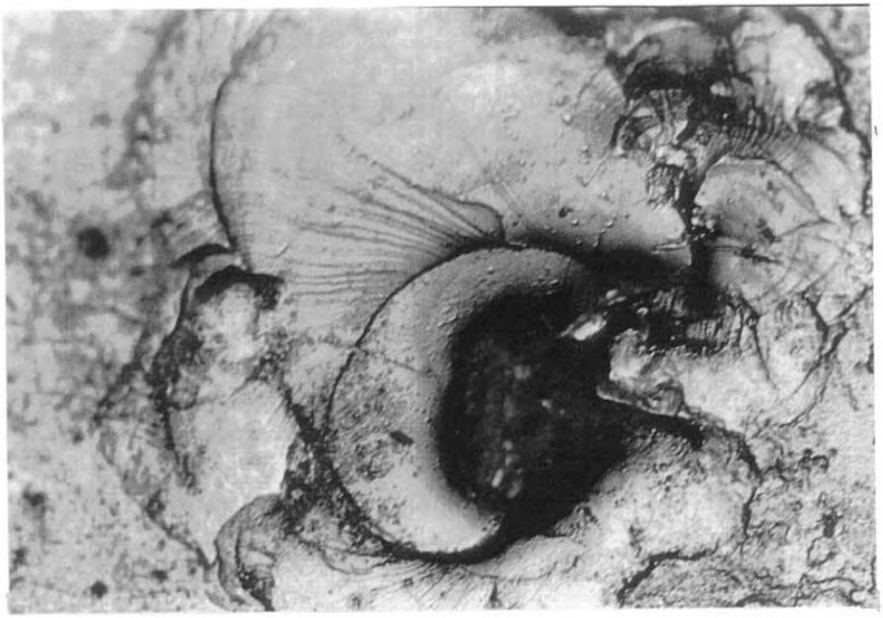

30

31

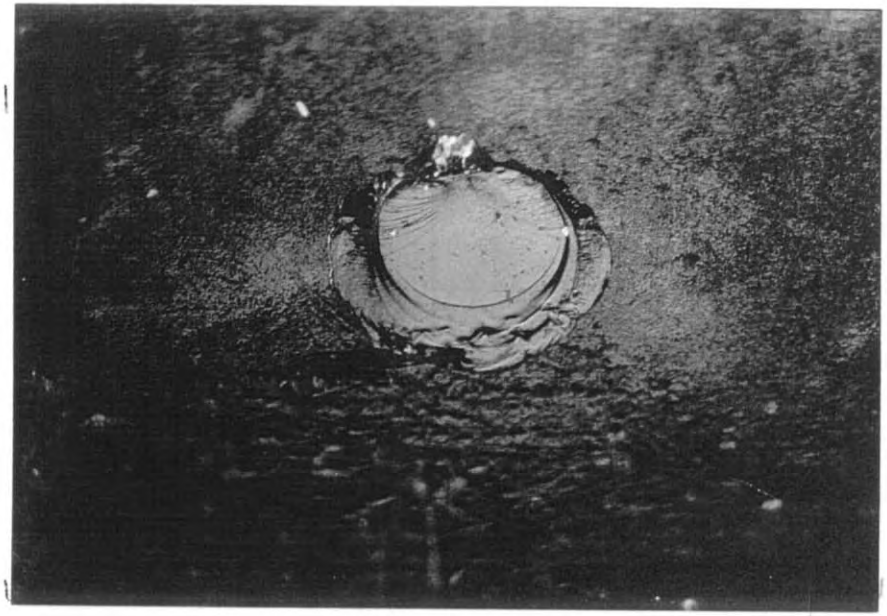

32

33

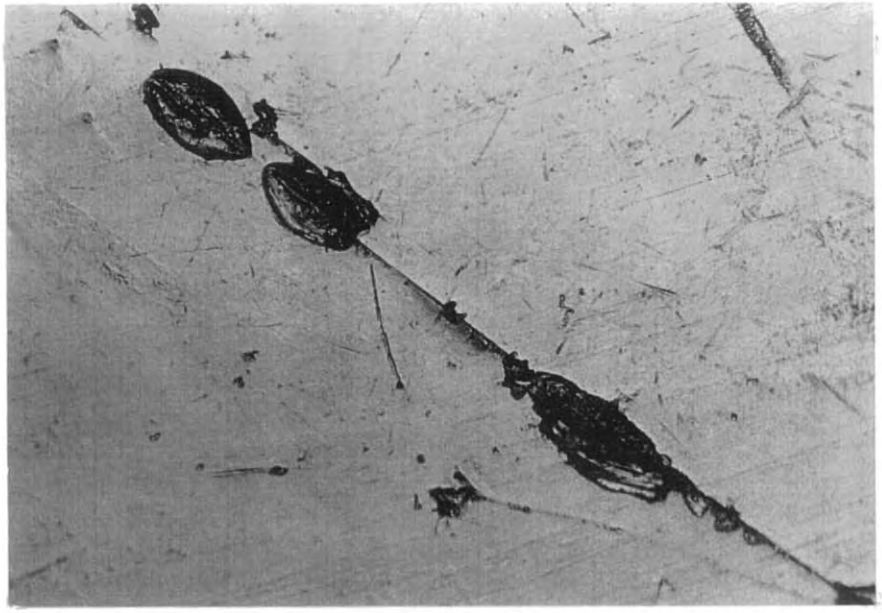

34

35

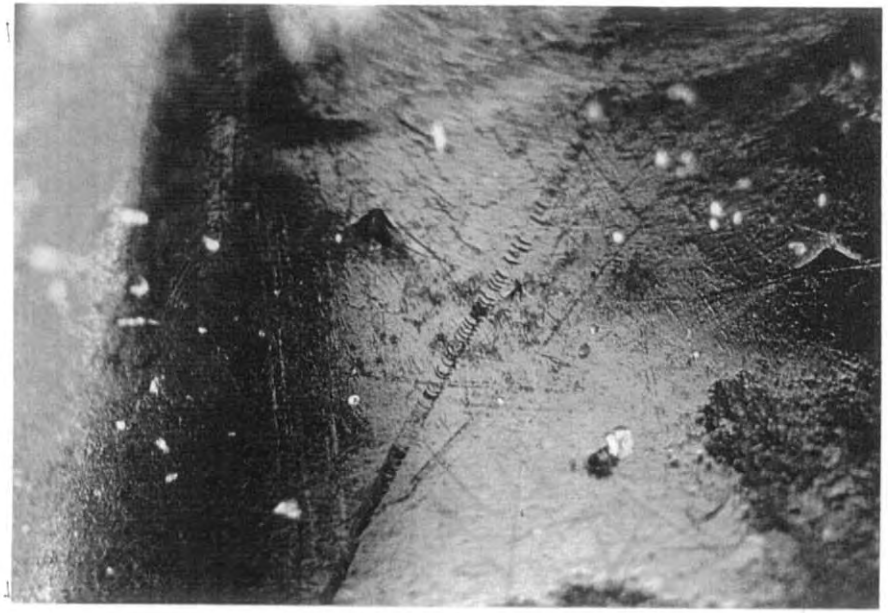

36

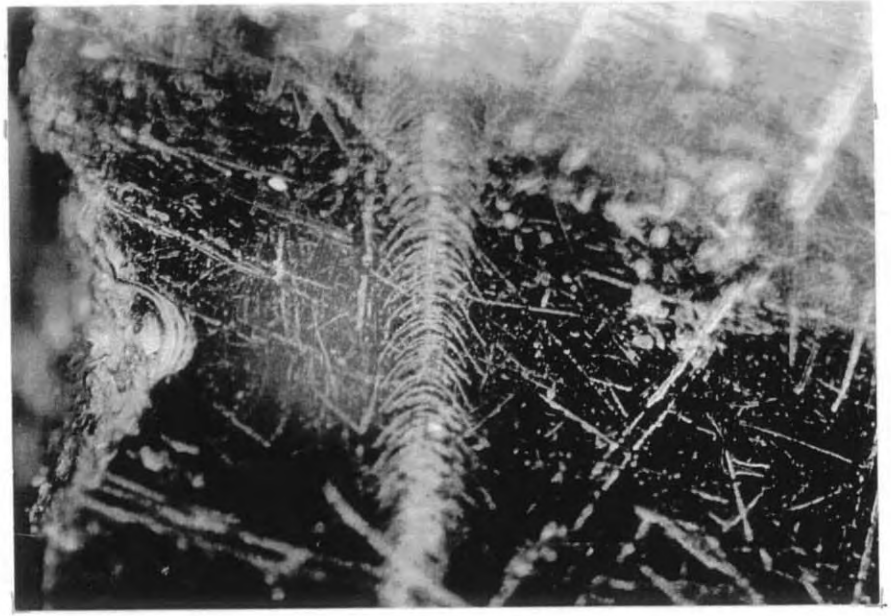

37

38

39

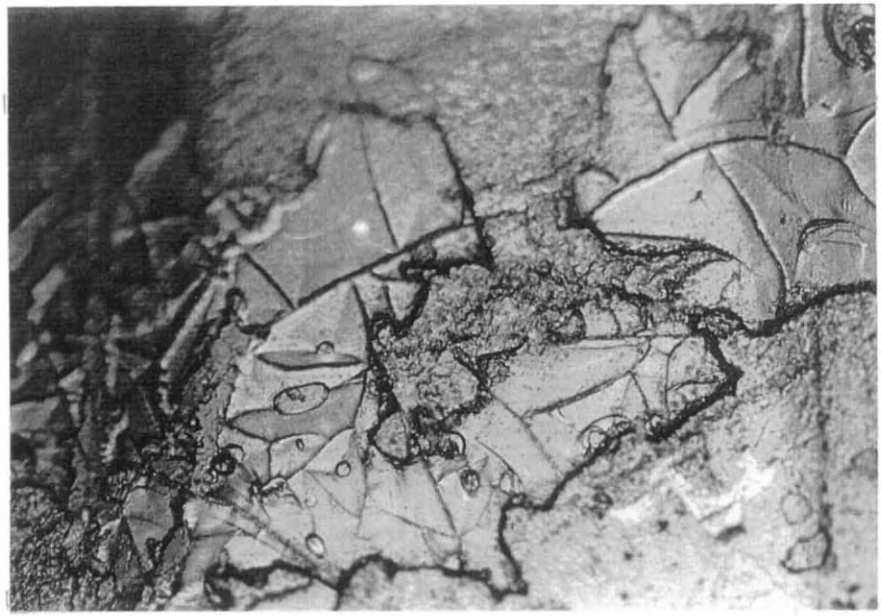

40

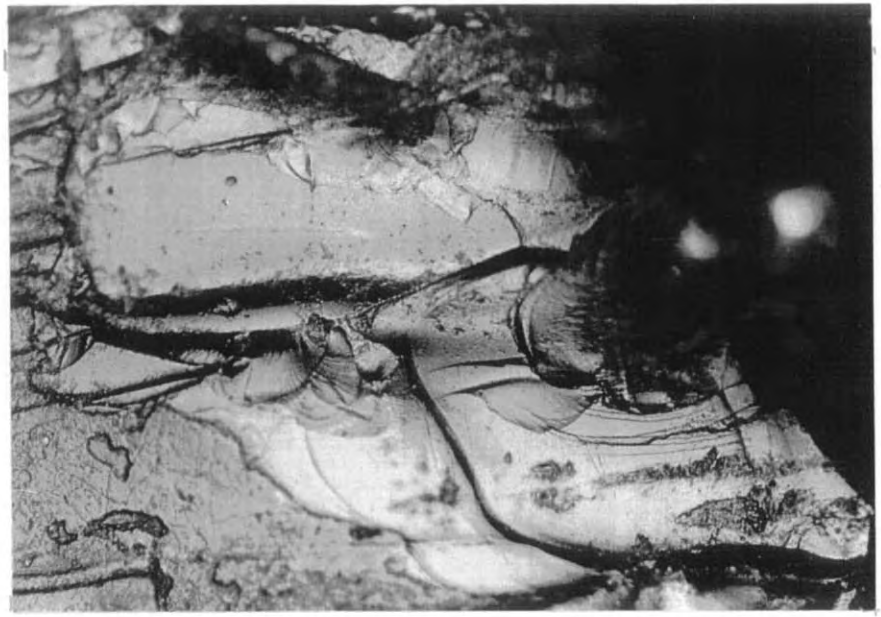

41

42

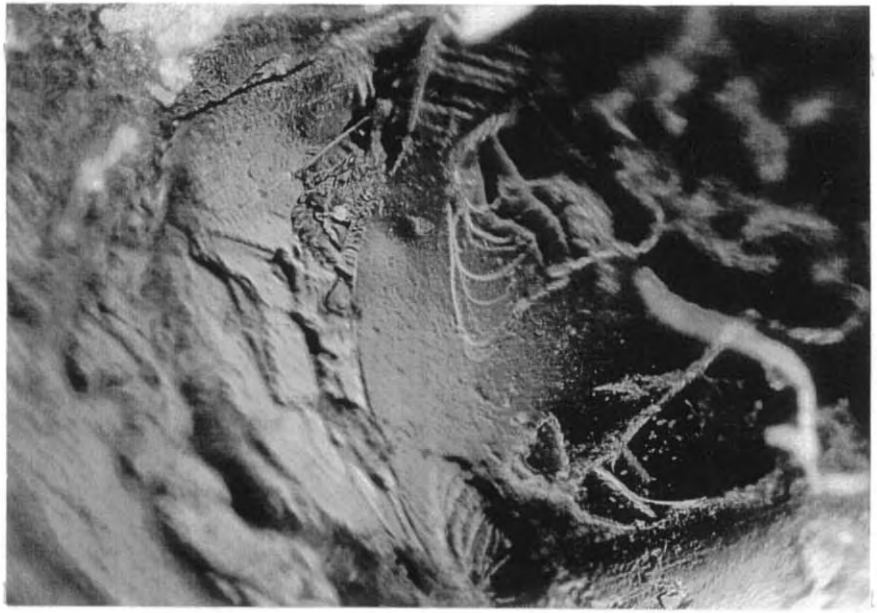

43

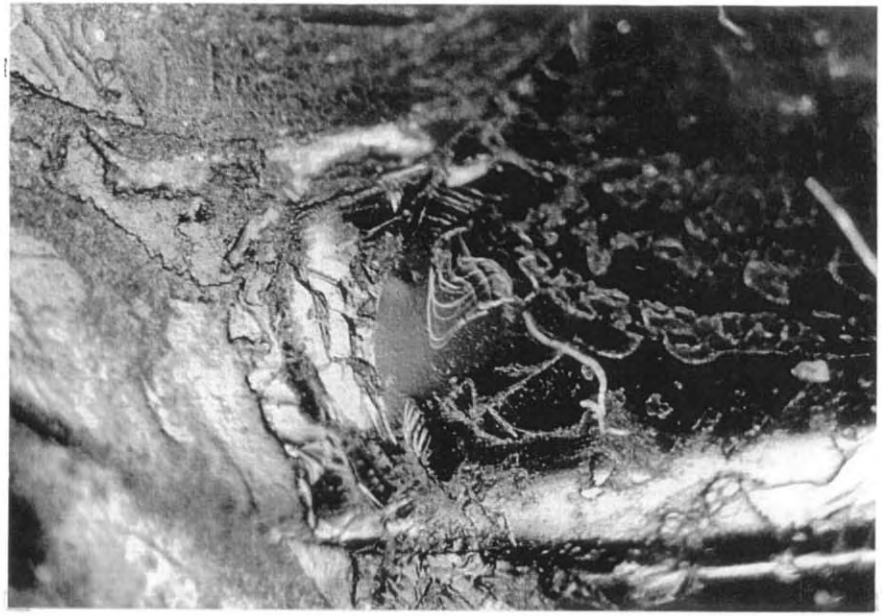

44

45

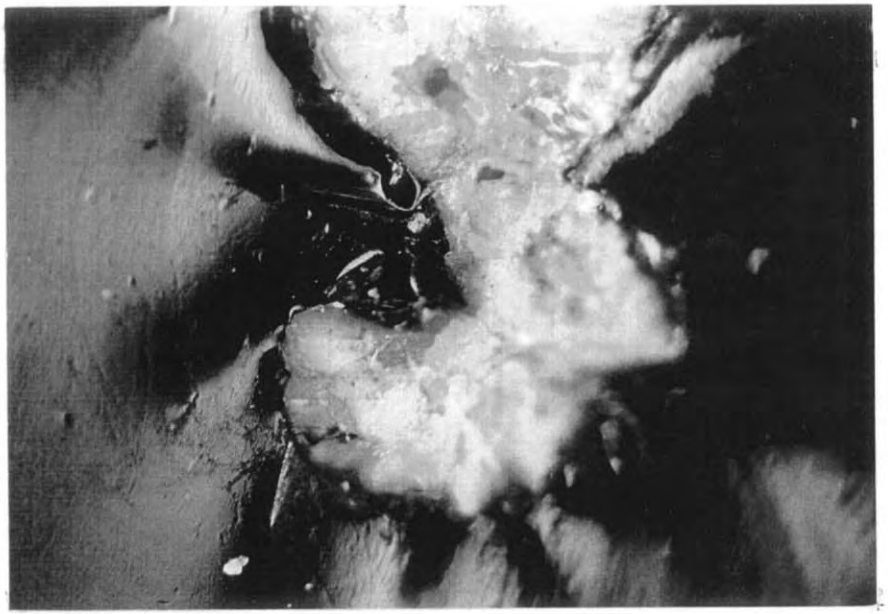

46

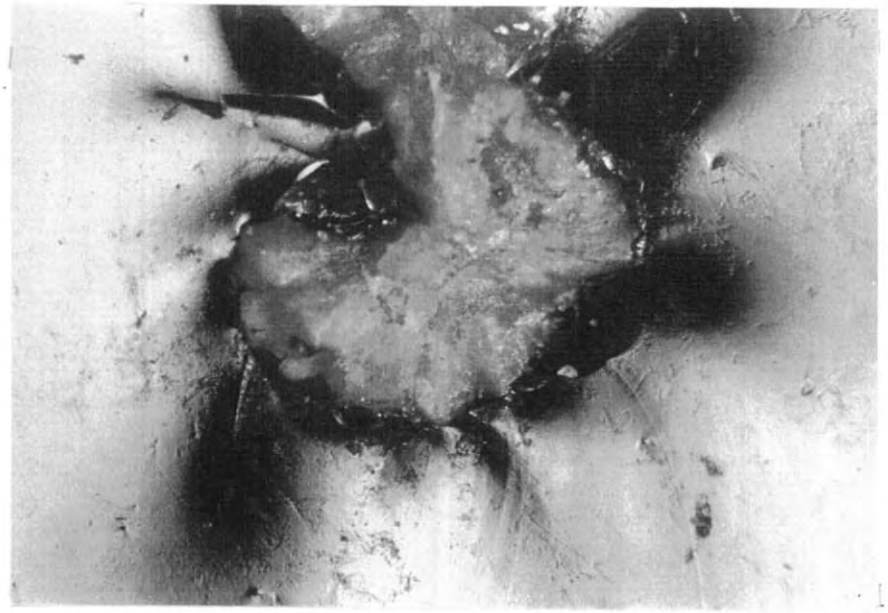

47

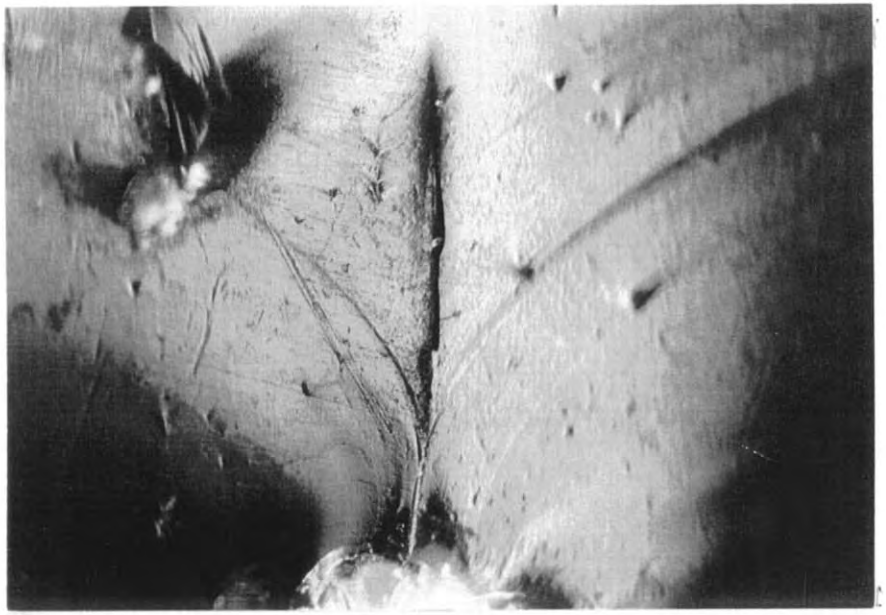

48

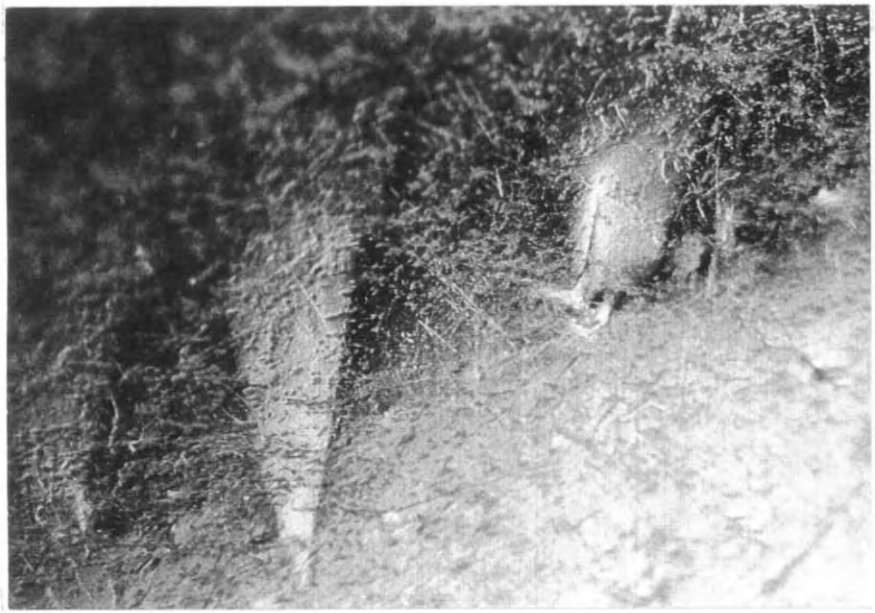

49

50

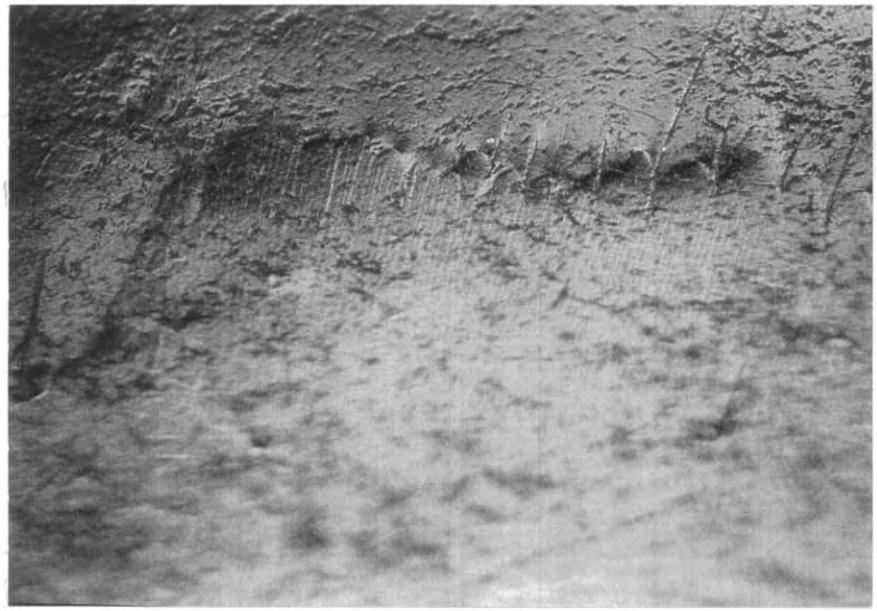

51

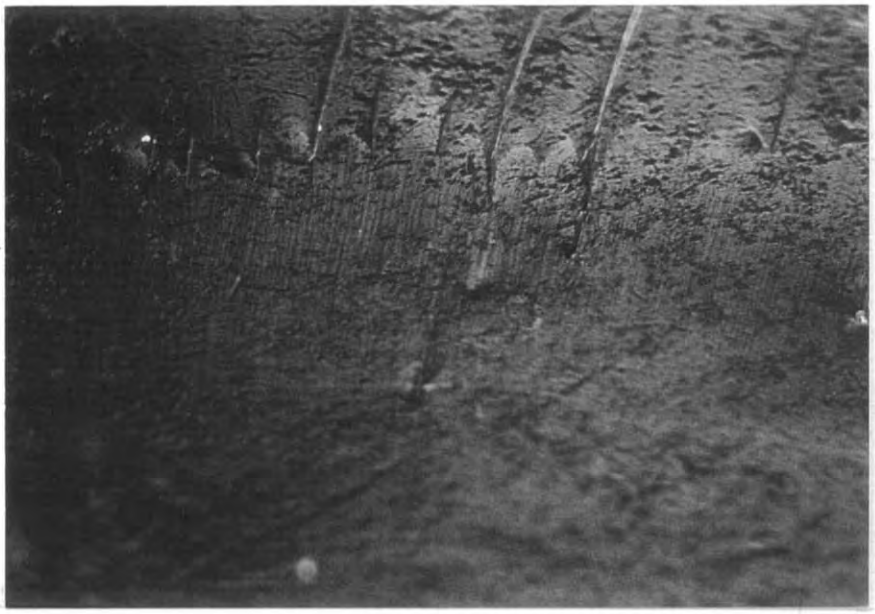

52

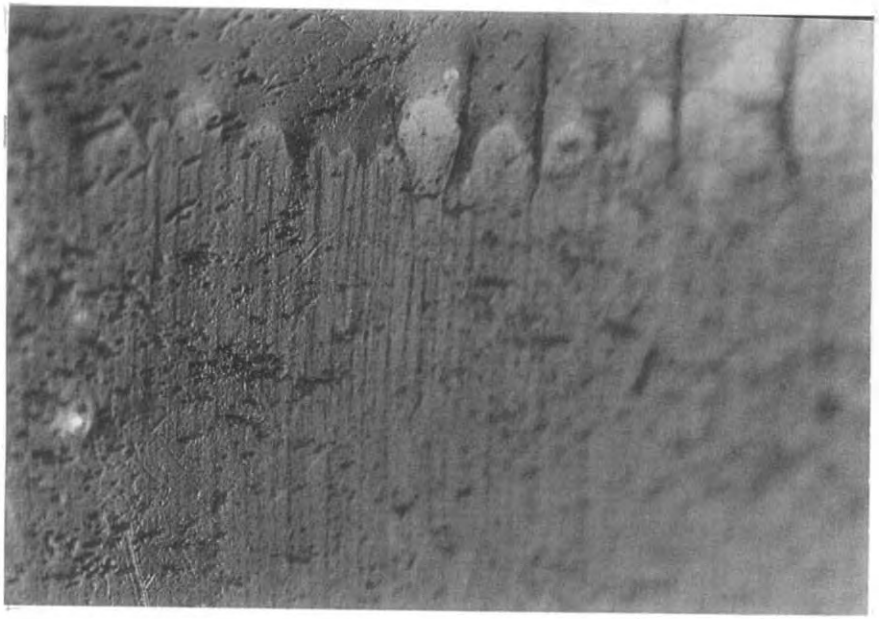

53

54

55

56

APPENDIX C.

Unpublished data on experimental vesiculation of artificially hydrated silica glass; experiments conducted by H. R. Westrich.
Sandia National Laboratory

Unpublished data on experimental vesiculation of artificially hydrated silica glass; experiments conducted by H. R. Westrich.
Sandia National Laboratory

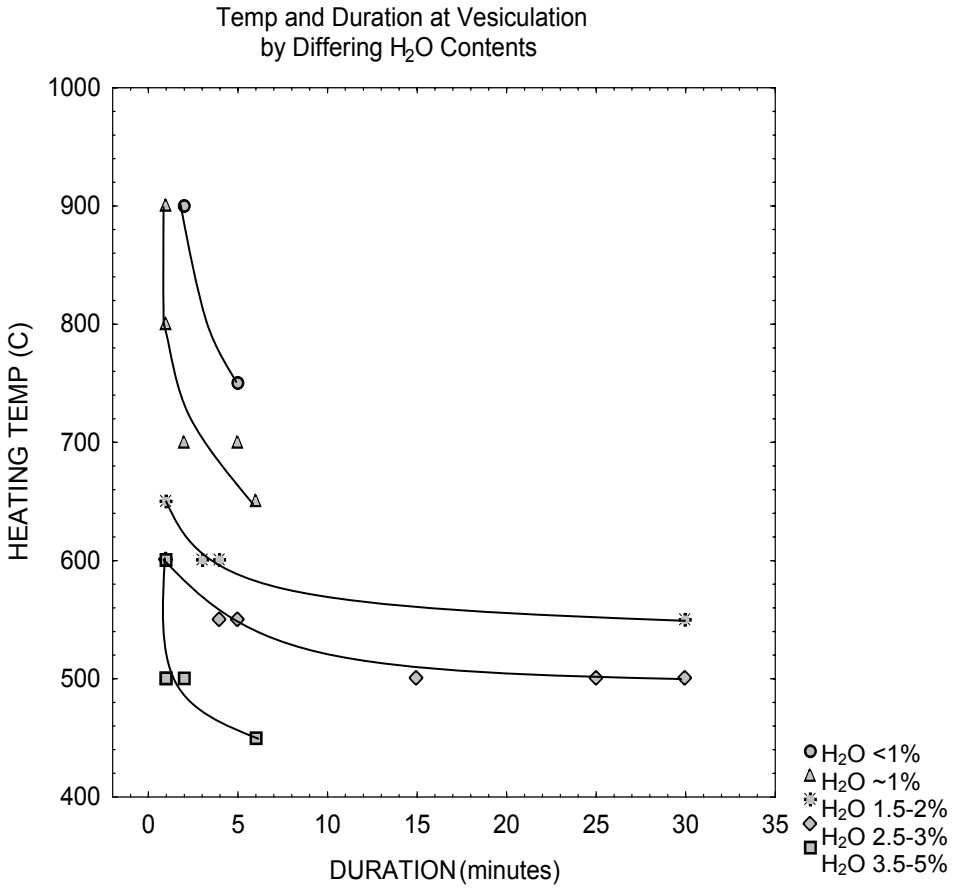

This graph is based on H. R. Westrich's unpublished data on heating experiments with glasses synthesized from natural obsidian that were artificially hydrated with water to several different weight % between 0.65 and 5.11%. Table on right shows Westrich's actual weight % (determined by K-F titration) and the five classes I created for the graph above.

H_2O wt%	H_2O class
0.65%	<1%
1.07% 1.09%	~1%
1.87% 1.91% 2.02%	1.5-2%
2.71% 2.94% 3.01%	2.5-3%
3.69% 4.50% 5.11%	3.5-5%

The purpose of the above graph is to demonstrate that the *time* to vesiculation decreases with increase in *temperature* of heating, and in samples with greater water content.

Points on the graph show the temperature and duration of heating at until vesiculation. I am not including all of the data on this graph, simply when full vesiculation occurs for each H_2O wt% class.

Westrich data summary			
Label	K-F Wt% H2O	H2O class	n
.05 S	0.65	<1%	4
0.5 S	0.65	<1%	11
1 N	1.07	1%	17
1 S	1.09	1%	9
1.05 S	1.87	1.5-2%	19
1.5 S	1.87	1.5-2%	1
2 S	1.91	1.5-2%	10
2 N	2.02	1.5-2%	9
3 S	2.71	2.5-3%	13
3 N	2.94	2.5-3%	2
3 N	3.01	2.5-3%	9
M3N	2.94	2.5-3%	5
4 S	3.69	3.5-5%	2
6 S	4.50	3.5-5%	3
M6N	5.11	3.5-5%	15
			129

Orig labels	label	Westrich 3/04/05
MV22-5	0.5%	0.5 S
MV22-2	1% N	1 N (natural)
MV22-19	1.5%	1.5 S
	2%	2 S
MV22-8	3%	3 S
MV22-20 (47)	4%	4 S
MV22-21	6%	6 S

Grey shading = calibration standards (Westrich 3/4/05)

Calibration standards used in FTIR analysis:

The glass chips used to create the standards were provided by H. R. Westrich, Sandia Labs, who had prepared the specimens over a decade ago using Karl-Fischer (K-F) titration analysis to measure total water content in glasses he altered to known water content values (see Westrich 1987 for description of K-F titration of glass). These results are not published, and this description of the specimens was provided directly to me by Westrich (personal communication, 2003, 2005).

The chips were determined by Westrich to have the following weight percents of total water: 0.65%, 1.07%, 1.87%, 1.91%, 2.71%, 3.69%, and 4.5%. Six of the seven standards were prepared from synthetic glass and are clear and without crystallites, while one of the seven standards (1.07%) was prepared from natural obsidian obtained from Panum Crater Dome (PCD) in California and is a darker color and may have crystallites present. This specimen is expected to differ in chemical composition from the other six glasses.

Determination of glass silica content using electron microprobe: After polishing and mounting, all seven standards were analyzed by electron probe microanalyzer (EPMA) to determine the silica content of the glass. Silica content and other chemical composition data is used to determine density for FTIR analysis. EPMA analysis was conducted September 10, 2003, at the UNM Department of Earth and Planetary Sciences, Institute of Meteoritics using a Jeol 8200 microprobe. The EPMA was operated by M. Spilde using a probe diameter of 10 microns and 20 nA beam current at 15 kV. The reference

standard used in the instrument was Smithsonian rhyolite glass standard #16 (Yellowstone National Park, Wyoming, USNM 72854 VG-568). Quantitative wavelength dispersive spectrometry (WDS) measurements were recorded as percent weight of oxides for nine elements (SiO_2, TiO_2, Al_2O_3, Fe_2O_3, MnO, MgO, CaO, Na_2O, and K_2O). Measurements were taken as a single transect across the piece beginning at 50-70 microns from an edge and continuing in a line across the surface at regular intervals of 150 microns, resulting in 11 to 14 measurements for each sample. The start and end locations of each transect was noted on a scanning electron image of the glass surface produced on the Jeol 8200 immediately prior to quantitative analysis.

Discussion of EPMA glass silica content results: Average values for each of the nine elements are compiled in Table C-1 below. Two aspects of these results are notable. First, the elemental values obtained for the 1% standard differ noticeably from the other standards for several elements, including SiO_2, TiO_2, Fe_2O_3, MnO, MgO, and CaO. These data have been examined and rechecked to determine that there was no error in data compilation or processing. The observed differences support the inference that the 1.07% specimen is the glass prepared by Westrich from natural Panum Crater Dome obsidian (as confirmed, personal communication, H. Westrich 2005).

Table C-1. Calibration standards: Average values for all 9 elements measured on EPMA.

Table C-1. Calibration standards: Average values for all 9 elements measured on EPMA											
Standard	n	SiO_2	TiO_2	Al_2O_3	Fe_2O_3	MnO	MgO	CaO	Na_2O	K_2O	Total
0.65%	13	75.419	0.015	14.812	0.045	0.010	0.865	0.963	3.784	4.922	100.837
1.07%	12	75.531	0.150	13.502	0.874	0.047	0.098	0.764	3.869	4.686	99.522
1.87%	11	73.872	0.013	14.513	0.032	0.005	0.850	0.952	3.617	4.809	98.664
1.91%	11	74.114	0.006	14.392	0.019	0.016	0.860	0.967	3.715	4.847	98.935
2.71%	11	72.656	0.011	14.289	0.050	0.023	0.853	0.943	3.640	4.783	97.247
3.69%	14	70.750	0.010	13.879	0.019	0.003	0.816	0.930	3.440	4.676	94.522
4.50%	12	70.557	0.018	13.610	0.030	0.018	0.800	0.915	3.168	4.607	93.721

Table C-2. Westrich data as scanned 10/2004.

row	Glass	Wt% H20	Temp C	Durations (m)	Result	Vesic
1	0.5 S	0.65	900	2	pumice	v
2	1.5 S	1.87	900	2	pumice	v
3	1 N	1.07	900	1	pumice	v
4	1 N	1.07	800	1	pumice	v
5	0.5 S	0.65	800	1	glass w many bubbles	pv
6	0.5 S	0.65	700	1	glass	n
7	0.5 S	0.65	700	3	glass	n
8	0.5 S	0.65	700	10	glass w bubbles?	?pv
9	0.5 S	0.65	700	20	glass w lots bubbles	pv
10	0.5 S	0.65	700	15	glass w bubbles	pv
11	1 S	1.09	700	5	pumice	v
12	1 S	1.09	700	1	glass w small bubbles	pv
13	1 S	1.09	700	2	glass w bubbles	pv
14	1 N	1.07	700	1	glass w lots bubbles	pv
15	1 N	1.07	700	2	glassy pumice	pv
16	M6N	5.11	600	2	pumice	v
17	M6N	5.11	600	1	pumice	v
18	M3N	2.94	600	1	pumice	v
19	2 N	2.02	600	1	glass	n
20	2 N	2.02	600	5	pumice	v
21	2 N	2.02	600	2	glass w lots bubbles	pv
22	2 N	2.02	600	3	pumice	v
23	3 N	3.01	600	1	pumice	v
24	1 N	1.07	600	5	glass	n
25	1 N	1.07	600	15	glass w tiny bubbles	pv
26	1 N	1.07	600	20	glass w bubbles	pv
27	1 N	1.07	600	30	glass bubbles	pv
28	1 N	1.07	600	10	glass	n
29	1 N	1.07	600	25	glass w bubbles	pv
30	1 N	1.07	600	35	glass w lots bubbles	pv
31	2 S	1.91	600	5	glass / pumice	pv
32	2 S	1.91	600	1	glass w small bubbles	pv
33	2 S	1.91	600	2	glass w small bubbles	pv
34	2 S	1.91	600	3	glass w lots bubbles	pv
35	2 S	1.91	600	4	glass w bubbles - pumice	v

Table C-2. Continued: Westrich data as scanned 10/2004.

row	Glass	Wt% H20	Temp C	Durations (m)	Result	Vesic
36	1.05 S	1.87	600	1	glass	n
37	1.05 S	1.87	600	5	glass w lots bubbles / pumice	pv
38	1.05 S	1.87	600	3	glass w tiny bubbles	pv
39	1.05 S	1.87	600	2	glass w lots bubbles	pv
40	1.05 S	1.87	600	4	glass w lots bubbles	pv
41	1 S	1.09	600	20	glass w few bubbles	pv
42	1 S	1.09	600	50	glass w bubbles	pv
43	1 S	1.09	600	60	glass w many bubbles	pv
44	1 S	1.09	600	30	glass w bubbles	pv
45	1 S	1.09	600	40	glass w bubbles	pv
46	1 S	1.09	600	80	glass / pumice	v
47	0.5 S	0.65	600	45	glass	n
48	0.5 S	0.65	600	120	glass w few. bubbles	pv
49	0.5 S	0.65	600	90	glass	n
50	0.5 S	0.65	600	180	glass w bubbles	pv
51	M6N	5.11	500	1	pumice	v
52	M6N	5.11	500	1	glass	n
53	M6N	5.11	500	6	glass	n
54	M6N	5.11	500	20	glass	n
55	M6N	5.11	500	60	glass (bulged?)	?n
56	M6N	5.11	500	120	glass (bulged?)	?n
57	6 S	4.50	500	1	pumice	v
58	4 S	3.69	500	1	cracked glass	?n
59	4 S	3.69	500	2	pumice/cracked glass w bubbles?	pv
60	3 S	2.71	500	5	glass w tlny bubbles	pv
61	3 S	2.71	500	10	glass w many bubbles	pv
62	3 S	2.71	500	1	glass w tiny bubbles	pv
63	3 S	2.71	500	2	glass w tiny bubbles	pv
64	3 S	2.71	500	3	glass w tiny bubbles	pv
65	3 S	2.71	500	4	glass w tiny bubbles	pv
66	3 S	2.71	500	15	glass w tiny bubbles	pv
67	3 S	2.71	500	20	glass w bubbles	pv
68	3 S	2.71	500	25	pumice	v
69	3 N	3.01	500	40	pumice	v
70	3 N	3.01	500	10	glass w many bubbles	pv
71	3 N	3.01	500	15	glass w lots bubbles almost pumice	pv
72	3 N	3.01	500	30	pumice	v
73	3 N	3.01	500	5	glass w bubbles	pv
74	3 N	3.01	500	3	glass w bubbles	pv
75	3 N	3.01	500	1	glass	n
76	3 N	3.01	500	2	glass w few bubbles	pv
77	M6N	5.11	450	1	glass	n
78	M6N	5.11	450	5	glass some bubbles	pv
79	M6N	5.11	450	10	glassy pumice	v
80	M6N	5.11	450	3	glass	n
81	M6N	5.11	450	7	glassy pumice	v
82	M6N	5.11	450	6	glassy pumice	v
83	M6N	5.11	450	4	glass	n
84	M3N	2.94	450	20	glass	n
85	M3N	2.94	450	30	glass	n
86	M3N	2.94	450	80	glass	n
87	M3N	2.94	450	120	glass	n

Table C-2. Continued: Westrich data as scanned 10/2004.

row	Glass	Wt% H20	Temp C	Durations (m)	Result	Vesic
88	6 S	5.11	450	10	glass pumice	v
89	6 S	5.11	450	6	pumice	v
90	3 S	2.71	550	10	pumice	v
91	3 S	2.71	550	4	pumice	v
92	3 S	2.71	550	1	glass w bubbles	pv
93	3 S	2.71	550	2	glass w lots bubbles pumice	pv
94	3 N	2.94	550	5	pumice	v
95	3 N	2.94	550	1	bubbly glass / almost pumice	pv
96	2 N	2.02	550	6	glass w lots bubbles	pv
97	2 N	2.02	550	4	glass w bubbles	pv
98	2 N	2.02	550	2	glass w tiny bubbles	pv
99	2 N	2.02	550	1	glass	n
100	2 N	2.02	550	8	glass w bubbles	pv
101	2 S	1.91	550	8	glass w bubbles	pv
102	2 S	1.91	550	10	glass w bubbles	pv
103	2 S	1.91	550	15	glass w bubbles	pv
104	2 S	1.91	550	30	glass w lots bubbles / almost pumice	pv
105	2 S	1.91	650	20	glass w bubbles	pv
106	1.05 S	1.87	550	10	glass w few bubbles	pv
107	1.05 S	1.87	550	5	glass w few bubbles	pv
108	1.05 S	1.87	550	15	glass w large bubbles	pv
109	1.05 S	1.87	550	3	glass w tiny bubbles	pv
110	1.05 S	1.87	550	7	glass w few bubbles	pv
111	1.05 S	1.87	550	20	glass w lots bubbles	pv
112	1.05 S	1.87	550	2	glass w tiny bubbles	pv
113	1.05 S	1.87	550	1	glass w tiny bubbles	pv
114	1.05 S	1.09	650	1	glassy pumice	pv
115	1.05 S	1.09	650	6	glass w tiny bubbles	pv
116	1.05 S	1.09	650	10	glass w large bubbles / pumice	pv
117	1.05 S	1.09	650	2	glass	n
118	1.05 S	1.09	650	8	glass w many tiny bubbles	pv
119	1.05 S	1.09	650	4	glass w tiny bubbles	pv
120	1 N	1.07	650	10	pumice	v
121	1 N	1.07	650	1	glass w tiny bubbles	pv
122	1 N	1.07	650	6	pumice	v
123	1 N	1.07	850	3	glass w bubbles	pv
124	1 N	1.07	850	4	glass w lots of bubbles	pv
125	1 N	1.07	650	2	glass w some bubbles	pv
126	.05 S	0.65	750	5	pumice / glassy	pv
127	.05 S	0.65	750	3	glass w lots of bubbles	pv
128	.05 S	0.65	750	1	glass	n
129	.05 S	0.65	750	2	glass w bubbles	pv

APPENDIX D:

ED-XRF Analyses: Original Letter Reports and Data from R. E. Hughes, Geochemical Laboratory

This appendix includes the letter reports and an additional data sheet from Richard Hughes, Geochemical Research Laboratory, for energy-dispersive X-ray fluorescence (ED-XRF) analysis conducted for this project. These data are discussed in Chapters 4 and 6 and reported as data tables in Appendix F. These letter reports also are referenced in the text as Hughes (1998b, 2004b). The letter reports provide details on the instrumentation and operating conditions (which differ between the two analyses) and discuss Hughes' conclusions concerning the chemical types of the specimens analyzed. Data in the 1998 letter report were previously discussed in Steffen (2002) as part of the Dome Fire pilot project. Analyses in the 2004 letter report were conducted on the same materials included in the WD-XRF analysis reported here in Chapter 6.

Geochemical Research Laboratory Letter Report 97-112

September 10, 1998

Anastasia Steffen
P.O. Box 340
Blue River, Oregon 97413

Dear Ana:

Enclosed with this letter you will find an five-page table presenting x-ray fluorescence (xrf) data generated from the analysis of obsidian samples from the Dome Fire Effects study, Jemez Ranger District, Santa Fe National Forest, New Mexico. This research was conducted pursuant to U.S.D.A. (Santa Fe National Forest) purchase order number 43-8379-7-0142.

Analyses of obsidian are performed at my laboratory on a Spectrace™ 5000 (Tracor X-ray) energy dispersive x-ray fluorescence spectrometer equipped with a rhodium (Rh) x-ray tube, a 50 kV x-ray generator, with microprocessor controlled pulse processor (amplifier) and bias/protection module, a 100 mHz analog to digital converter (ADC) with automated energy calibration, and a Si(Li) solid state detector with 160 eV resolution (FWHM) at 5.9 keV in a 30 mm^2 area. The x-ray tube is operated at 34.0 kV, .25 mA, using a .127 mm Rh primary beam filter in an air path to generate x-ray intensity data for elements zinc (Zn Kα), gallium (Ga Kα), rubidium (Rb Kα), strontium (Sr Kα), yttrium (Y Kα), zirconium (Zr Kα), and niobium (Nb Kα). Barium (Ba Kα) intensities are generated by operating the x-ray tube at 50.0 kV, .35 mA, with a .63 mm copper (Cu) filter, while those for titanium (Ti Kα), manganese (Mn Kα) and total iron ($Fe_2O_3^T$) are generated by operating the x-ray tube at 15.0 kV, .28 mA with a .127 mm aluminum (Al) filter. Iron vs. manganese (Fe Kα/Mn Kα) ratios are computed from data generated by operating the x-ray tube at 15.0 kV, .30 mA, with a .127 mm aluminum (Al) filter. Deadtime-corrected analysis time for each sample appears in the data table. X-ray spectra are acquired and elemental intensities extracted for each peak region of interest, then matrix correction algorithms are applied to specific regions of the x-ray energy spectrum to compensate for inter-element absorption and enhancement effects. After these corrections are made, intensities are converted to concentration estimates by employing a least-squares calibration line established for each element from analysis of up to 30 international rock standards certified by the U.S. Geological Survey, the U.S. National Institute of Standards and Technology, the Geological Survey of Japan, the Centre de Recherches Petrographiques et Geochimiques (France), and the South African Bureau of Standards. Further details pertaining to x-ray tube operating conditions and calibration appear in Hughes (1988a, 1994a). Extremely small/thin specimens are analyzed using a .25 mm^2 primary beam collimator, and resulting data normalized using a sample mass-correction algorithm. Deadtime-corrected analysis time is greatly extended in all instances when primary beam collimation is employed.

Trace element measurements in the xrf data table, except Fe/Mn ratios, are expressed in quantitative units (i.e. parts per million [ppm] and weight percent composition), and comparisons between the samples you sent and known obsidian chemical groups were made using trace element concentration values for Rb, Sr, Y, Zr, Nb and, as necessary, Ba, Ti , Mn, $Fe_2O_3^T$ and Fe/Mn ratios) that appear in Baugh and Nelson (1987), Hughes (1987; 1988b, c), Jack (1971), Macdonald et al. (1992), Nelson (1984), Newman and Nielsen (1985), Shackley (1991, 1992, 1995), and unpublished data in my possession on other Arizona, New Mexico, and Utah (e.g. Hughes 1994b) obsidians. Stevenson and Klimkiewicz (1990) have published quantitative concentration values for many of the samples in Shackley's (1995) study, but their measurements, like those in Stevenson and McCurry (1990), are not in particularly good agreement with values published for the same sources by others (see above). I consider artifact-to-obsidian source (i.e., geochemical type; *sensu* Hughes 1998) correspondences reliable if diagnostic mean measurements for artifacts fall within 2 standard deviations of mean values for source standards. The term "diagnostic" is used here to

specify those trace elements that are well-measured by x-ray fluorescence, and whose concentrations show low variability *within* a source and marked variability *across* sources. Diagnostic elements, then, are those whose concentration values allow one to draw the clearest geochemical distinctions between sources (see Hughes 1990, 1993). Although Zn and Ga ppm concentrations also were measured and reported for each specimen, they are not considered "diagnostic" because they don't usually vary significantly across obsidian sources (see Hughes 1982, 1984). This is particularly true of Ga, which occurs in concentrations between 10-30 ppm in many parent obsidians. Zn ppm values are infrequently diagnostic; they are always high in Zr-rich, Sr-poor peralkaline volcanic glasses, but otherwise they do not usually vary significantly between sources. The measurements presented in the enclosed table are reported to the nearest ppm to reflect the resolution capabilities of non-destructive energy dispersive x-ray fluorescence spectrometry. Resolution limits of the present x-ray fluorescence system for the determination of Zn is about 3 ppm; Ga about 2 ppm; for Rb about 4 ppm; for Sr about 3 ppm; Y about 2 ppm; Zr about 4 ppm; and for Nb about 3 ppm (see Hughes [1994a] for other elements). When counting and fitting error uncertainty estimates (the "±" value in the table) for a sample are greater than calibration-imposed limits of resolution, the larger number is a more conservative reflection of composition variation and measurement error arising from differences in sample size, surface and x-ray reflection geometry.

All of the samples analyzed-- burned artifacts and source samples-- have the same trace element composition as Obsidian Ridge (a.k.a. Cerro Toledo Rhyolite [Macdonald et al. 1992: Appendix I, p. 148]; cf. Baugh and Nelson 1987: Table 1) volcanic glass from the Jemez Mountains in northern New Mexico. While this is hardly surprising, given the samples came from the immediate proximity of Rabbit Mountain, the standards were collected and analyzed to serve as a baseline for comparisons with the fire-altered specimens. When such comparisons are made, there appears to be no significant difference in trace and selected minor element composition-- specifically, Rb, Sr, Y, Zr, Nb, Ti, Mn, $Fe_2O_3^T$ concentration and Fe/Mn ratios-- between the majority of artifacts subjected to varying degrees of fire-alteration and (apparently) unheated source samples. No differences in Fe/Mn ratios were observed, which might have been anticipated from the pilot study of Jackson (1986: 180). Instances of *possible* enhancement/depletion have been highlighted in the data table but, although every attempt was made to use a suitably flat surface for xrf analysis, in some cases surface irregularities caused by burning probably altered the x-ray reflection geometry, skewing derived concentration values. More suggestive results were obtained with the suite of specimens from your laboratory controlled burning experiment. Although in this small sample (n=4) there appears to be no significant difference between unaltered samples and those heated to 425°C and 625°C, in half the cases (i.e. in samples GS8 and GS7B), Rb and $Fe_2O_3^T$ concentrations are greater at 875°C than at lower temperatures. Interestingly, this trend is *not* evident in the other two samples (GS7 and GS10) subjected to the same heating conditions. After heating to 875°C sample GS10 appears macroscopically unaltered, while sample GS7B shows pronounced strain cracks and fire-induced "frothing" bubbles. Neither macroscopic variation appears to have effected the concentrations of chemical elements measured in this study on samples GS7B and GS10. In any case, more laboratory experiments could help establish chemical heat-tolerance limits which may correlate with presence/absence of hydration rinds.

Please contact me at my laboratory ([650] 851-1410) if I can be of further assistance.

Sincerely,

Richard

Richard E. Hughes, Ph.D.
Director, Geochemical Research Laboratory

cc: Rita Skinner, Jemez Ranger District

References

Baugh, Timothy G., and Fred W. Nelson, Jr.
1987 New Mexico Obsidian Sources and Exchange on the Southern Plains. **Journal of Field Archaeology** 14: 313-329.

Hughes, Richard E.
1982 Age and Exploitation of Obsidian from the Medicine Lake Highland, California. **Journal of Archaeological Science** 9: 173-185.

1984 Obsidian Sourcing Studies in the Great Basin: Problems and Prospects. *In* Richard E. Hughes (ed.) Obsidian Studies in the Great Basin. **Contributions of the University of California Archaeological Research Facility**, No. 45: 1-19. Berkeley.

1987 X-ray Fluorescence Analysis of Geologic Obsidian Samples from the Mt. Floyd - Round Mountain Area, Arizona. Letter report submitted to Larry Lesko, Kaibab National Forest, February 11, 1987.

1988a The Coso Volcanic Field Reexamined: Implications for Obsidian Sourcing and Hydration Dating Research. **Geoarchaeology** 3: 253-265.

1988b Archaeological Significance of Geochemical Contrasts Among Southwestern New Mexico Obsidians. **Texas Journal of Science** 40: 297-307.

1988c Notes on Obsidian from the Fort Hood Area of Central Texas. **Bulletin of the Texas Archeological Society** 59: 193-199.

1990 Obsidian Sources at James Creek Shelter, and Trace Element Geochemistry of Some Northeastern Nevada Volcanic Glasses. *In* Robert G. Elston and Elizabeth E. Budy (eds.), The Archaeology of James Creek Shelter. **University of Utah Anthropological Papers** No. 115, pp. 297-305.

1993 Trace Element Geochemistry of Volcanic Glass from the Obsidian Cliffs Flow, Three Sisters Wilderness, Oregon. **Northwest Science** 67: 199-207.

1994a Intrasource Chemical Variability of Artefact-Quality Obsidians from the Casa Diablo Area, California. **Journal of Archaeological Science** 21: 263-271.

1994b X-ray Fluorescence Analysis of Geologic Obsidian Samples and Artifacts from the Kern River Gas Transmission Project, Utah. *In* Kern River Pipeline Cultural Resources Data Recovery Report: Utah. Volume I, Research Context and Data Analysis. Report submitted by Dames & Moore to Kern River Gas Transmission Company, January 31, 1994.

1998 On Reliability, Validity, and Scale in Obsidian Sourcing Research. *In* Ann F. Ramenofsky and Anastasia Steffen (eds.), **Unit Issues in Archaeology: Measuring Time, Space and Material**, pp. 103-114. University of Utah Press, Salt Lake City.

Jack, Robert N.
1971 The Source of Obsidian Artifacts in Northern Arizona. **Plateau** 43: 103-114.

Jackson, Thomas L.
1986 Late Prehistoric Obsidian Exchange in Central California. Unpublished Ph.D. Dissertation, Department of Anthropology, Stanford University.

References (continued)

Macdonald, Ray, Robert L. Smith, and John E. Thomas
1992 Chemistry of the Subalkalic Silicic Obsidians. **U.S. Geological Survey Professional Paper** 1523.

Nelson, Fred W., Jr.
1984 X-ray Fluorescence Analysis of Some Western North American Obsidians. *In* Richard E. Hughes (ed.) Obsidian Studies in the Great Basin. **Contributions of the University of California Archaeological Research Facility**, No. 45: 27-62. Berkeley.

Newman, Jay R., and Roger L. Nielsen
1985 Initial Notes on the X-ray Fluorescence Sourcing of Northern New Mexico Obsidians. **Journal of Field Archaeology** 12: 377-383.

Shackley, M. Steven
1991 Tank Mountains Obsidian: A Newly Discovered Archaeological Obsidian Source in East-Central Yuma County, Arizona. **Kiva** 57: 17-25.

1992 The Upper Gila River Gravels as an Archaeological Obsidian Source Region: Implications for Models of Exchange and Interaction. **Geoarchaeology** 7: 315-326.

1995 Sources of Archaeological Obsidian in the Greater American Southwest: An Update and Quantitative Analysis. **American Antiquity** 60: 531-551.

Stevenson, Christopher M., and Maria Klimkiewicz
1990 X-ray Fluorescence Analysis of Obsidian Sources in Arizona and New Mexico. **Kiva** 55: 235-243.

Stevenson, Christopher M., and Michael O. McCurry
1990 Chemical Characterization and Hydration Rate Development for New Mexican Obsidian Sources. **Geoarchaeology** 5: 149-170.

Cat. Number	Trace and Selected Minor Element Concentrations											Ratio	Obsidian Source (Chemical Type)
	Zn	Ga	Rb	Sr	Y	Zr	Nb	Ba	Ti	Mn	$Fe_2O_3^T$	Fe/Mn	
GS1-001	89 ±6	19 ±3	201 ±4	3 ±4	56 ±3	159 ±4	87 ±3	0 ±15	431 ±14	597 ±9	1.20 ±.08	nm	Obsidian Ridge (Cerro Toledo Rhyolite)
GS1-002	92 ±5	26 ±3	212 ±4	4 ±3	62 ±3	175 ±4	90 ±3	0 ±15	438 ±14	620 ±8	1.22 ±.08	nm	Obsidian Ridge (Cerro Toledo Rhyolite)
GS1-003	81 ±5	19 ±3	213 ±4	3 ±8	60 ±3	168 ±4	86 ±3	0 ±14	420 ±14	611 ±8	1.23 ±.08	21	Obsidian Ridge (Cerro Toledo Rhyolite)
GS1-004	96 ±5	23 ±3	202 ±4	4 ±3	61 ±3	167 ±4	89 ±3	0 ±14	436 ±13	607 ±8	1.19 ±.08	nm	Obsidian Ridge (Cerro Toledo Rhyolite)
GS1-005	97 ±5	22 ±3	200 ±4	4 ±3	63 ±3	164 ±4	89 ±3	0 ±14	433 ±14	611 ±9	1.19 ±.08	nm	Obsidian Ridge (Cerro Toledo Rhyolite)
GS1-006	90 ±6	22 ±3	205 ±4	3 ±5	59 ±3	170 ±4	87 ±3	0 ±15	453 ±15	640 ±9	1.26 ±.08	nm	Obsidian Ridge (Cerro Toledo Rhyolite)
GS2-001	88 ±5	23 ±3	196 ±4	4 ±3	56 ±3	160 ±4	87 ±3	0 ±14	421 ±14	581 ±8	1.17 ±.08	nm	Obsidian Ridge (Cerro Toledo Rhyolite)
GS2-002	93 ±5	22 ±3	212 ±4	4 ±3	62 ±3	168 ±4	89 ±3	0 ±15	435 ±13	600 ±8	1.21 ±.08	nm	Obsidian Ridge (Cerro Toledo Rhyolite)
GS2-003	89 ±5	23 ±3	199 ±4	3 ±9	60 ±3	164 ±4	83 ±3	0 ±13	441 ±13	600 ±8	1.21 ±.08	nm	Obsidian Ridge (Cerro Toledo Rhyolite)
GS2-004	101 ±5	2 ±3	206 ±4	3 ±4	59 ±3	163 ±4	86 ±3	0 ±14	448 ±14	610 ±9	1.22 ±.08	nm	Obsidian Ridge (Cerro Toledo Rhyolite)
GS3-001	90 ±6	22 ±3	200 ±4	4 ±3	56 ±3	160 ±4	83 ±3	0 ±14	417 ±14	602 ±9	1.21 ±.08	nm	Obsidian Ridge (Cerro Toledo Rhyolite)
GS3-002	87 ±5	24 ±3	202 ±4	0 ±5	58 ±3	163 ±4	85 ±3	0 ±15	440 ±13	581 ±8	1.15 ±.08	nm	Obsidian Ridge (Cerro Toledo Rhyolite)
GS3-003	98 ±5	17 ±3	196 ±4	3 ±6	59 ±3	165 ±4	89 ±3	0 ±15	430 ±13	575 ±8	1.16 ±.08	nm	Obsidian Ridge (Cerro Toledo Rhyolite)
GS3-004	91 ±5	21 ±3	207 ±4	3 ±9	58 ±3	170 ±4	89 ±3	0 ±14	450 ±14	623 ±8	1.24 ±.08	nm	Obsidian Ridge (Cerro Toledo Rhyolite)
GS3-005	94 ±5	20 ±3	207 ±4	3 ±3	60 ±3	164 ±4	88 ±3	0 ±15	490 ±14	603 ±8	1.20 ±.08	nm	Obsidian Ridge (Cerro Toledo Rhyolite)
GS4-002	81 ±6	20 ±3	193 ±4	3 ±14	58 ±3	160 ±4	84 ±3	0 ±14	431 ±14	610 ±9	1.21 ±.08	nm	Obsidian Ridge (Cerro Toledo Rhyolite)
GS4-003	85 ±5	21 ±3	190 ±4	3 ±3	55 ±3	157 ±4	83 ±3	0 ±13	429 ±14	571 ±9	1.15 ±.08	nm	Obsidian Ridge (Cerro Toledo Rhyolite)

Values in parts per million (ppm) except total iron (in weight percent) and Fe/Mn ratios; ± = pooled estimate (in ppm and wt. % composition) of x-ray counting uncertainty and regression fitting error at 300 seconds livetime; nm = not measured.

Cat. Number	Trace and Selected Minor Element Concentrations											Ratio	Obsidian Source (Chemical Type)
	Zn	Ga	Rb	Sr	Y	Zr	Nb	Ba	Ti	Mn	$Fe_2O_3^T$	Fe/Mn	
GS4-004	88 ±5	18 ±3	192 ±4	4 ±3	56 ±3	157 ±4	84 ±3	0 ±14	413 ±14	588 ±8	1.16 ±.08	nm	Obsidian Ridge (Cerro Toledo Rhyolite)
GS6A-1	86 ±6	18 ±3	191 ±4	4 ±3	56 ±3	159 ±4	82 ±3	nm	440 ±14	596 ±9	1.17 ±.08	20	Obsidian Ridge (Cerro Toledo Rhyolite)
GS8-2	87 ±5	20 ±3	193 ±4	4 ±3	58 ±3	156 ±4	84 ±3	nm	451 ±14	600 ±8	1.19 ±.08	21	Obsidian Ridge (Cerro Toledo Rhyolite)
GS8-A Unburned	86 ±5	16 ±3	191 ±4	3 ±5	55 ±3	161 ±4	52 ±3	nm	403 ±13	571 ±8	1.12 ±.08	20	Obsidian Ridge (Cerro Toledo Rhyolite)
GS8-A 425°C	87 ±5	20 ±3	185 ±4	3 ±4	54 ±3	160 ±4	80 ±3	nm	368 ±13	574 ±8	1.10 ±.08	20	Obsidian Ridge (Cerro Toledo Rhyolite)
GS8-A 625°C	93 ±6	23 ±3	202 ±4	0 ±4	57 ±3	158 ±4	82 ±3	nm	408 ±14	622 ±8	1.18 ±.08	20	Obsidian Ridge (Cerro Toledo Rhyolite)
GS8-A 875°C	139 ±7	27 ±3	**243** ±4	4 ±3	66 ±3	173 ±4	89 ±3	nm	483 ±15	662 ±9	**1.31** ±.08	20	Obsidian Ridge (Cerro Toledo Rhyolite)
GS10-C Unburned	84 ±5	24 ±3	190 ±4	3 ±3	55 ±3	153 ±4	82 ±3	nm	389 ±14	589 ±8	1.14 ±.08	20	Obsidian Ridge (Cerro Toledo Rhyolite)
GS10-C 425°C	89 ±5	16 ±3	202 ±4	3 ±3	58 ±3	163 ±4	83 ±3	nm	422 ±13	603 ±8	1.15 ±.08	20	Obsidian Ridge (Cerro Toledo Rhyolite)
GS10-C 625°C	90 ±5	21 ±3	203 ±4	3 ±8	62 ±3	169 ±4	86 ±3	nm	406 ±13	595 ±8	1.13 ±.08	20	Obsidian Ridge (Cerro Toledo Rhyolite)
GS10-C 875°C	86 ±5	20 ±3	195 ±4	3 ±3	54 ±3	155 ±4	83 ±3	nm	405 ±14	591 ±8	1.14 ±.08	20	Obsidian Ridge (Cerro Toledo Rhyolite)
GS7-B Unburned	87 ±5	23 ±3	192 ±4	4 ±3	54 ±3	159 ±4	84 ±3	nm	363 ±14	571 ±8	1.11 ±.08	20	Obsidian Ridge (Cerro Toledo Rhyolite)
GS7-B 425°C	80 ±6	21 ±3	187 ±4	3 ±4	55 ±3	153 ±4	80 ±3	nm	397 ±14	578 ±8	1.10 ±.08	20	Obsidian Ridge (Cerro Toledo Rhyolite)
GS7-B 625°C	83 ±5	19 ±3	188 ±4	4 ±3	55 ±3	158 ±4	82 ±3	nm	390 ±14	568 ±8	1.08 ±.08	19	Obsidian Ridge (Cerro Toledo Rhyolite)
GS7-B 875°C	91 ±6	25 ±3	199 ±4	3 ±4	58 ±3	163 ±4	83 ±3	nm	472 ±19	626 ±9	1.24 ±.08	20	Obsidian Ridge (Cerro Toledo Rhyolite)
GS7B-D Unburned	78 ±5	19 ±3	190 ±4	3 ±5	55 ±3	158 ±4	81 ±3	nm	362 ±14	575 ±8	1.12 ±.08	20	Obsidian Ridge (Cerro Toledo Rhyolite)
GS7B-D 425°C	86 ±5	21 ±3	190 ±4	4 ±3	55 ±3	156 ±4	82 ±3	nm	393 ±14	576 ±8	1.11 ±.08	20	Obsidian Ridge (Cerro Toledo Rhyolite)

Values in parts per million (ppm) except total iron (in weight percent) and Fe/Mn ratios; ± = pooled estimate (in ppm and wt. % composition) of x-ray counting uncertainty and regression fitting error at 300 seconds livetime; nm = not measured.

Cat. Number	Trace and Selected Minor Element Concentrations											Ratio	Obsidian Source (Chemical Type)
	Zn	Ga	Rb	Sr	Y	Zr	Nb	Ba	Ti	Mn	$Fe_2O_3^T$	Fe/Mn	
GS7B-D	85	17	189	3	54	156	80	nm	423	593	1.14	20	Obsidian Ridge
625°C	±6	±3	±4	±5	±3	±4	±3		±14	±9	±.08		(Cerro Toledo Rhyolite)
GS7B-D	116	27	**227**	3	62	167	89	nm	502	661	1.27	20	Obsidian Ridge
875°C	±6	±3	±4	±4	±3	±4	±3		±15	±9	±.08		(Cerro Toledo Rhyolite)
1665-1	90	21	191	4	59	160	81	nm	510	574	1.17	21	Obsidian Ridge
	±5	±3	±4	±3	±3	±4	±3		±14	±8	±.08		(Cerro Toledo Rhyolite)
1665-2	88	23	201	3	57	163	85	nm	464	599	1.20	21	Obsidian Ridge
	±5	±3	±4	±3	±3	±4	±3		±14	±8	±.08		(Cerro Toledo Rhyolite)
1691-1a	87	20	196	4	56	166	87	nm	449	564	1.14	nm	Obsidian Ridge
	±5	±3	±4	±3	±3	±4	±3		±14	±8	±.08		(Cerro Toledo Rhyolite)
1691-1b	94	22	202	0	60	169	86	nm	480	613	1.21	nm	Obsidian Ridge
	±5	±3	±4	±3	±3	±4	±3		±14	±8	±.08		(Cerro Toledo Rhyolite)
1691-1c	89	21	196	3	56	159	80	nm	438	612	1.22	nm	Obsidian Ridge
	±6	±3	±4	±6	±3	±4	±3		±15	±9	±.08		(Cerro Toledo Rhyolite)
1691-2a	96	16	189	3	57	159	83	nm	429	582	1.17	nm	Obsidian Ridge
	±5	±3	±4	±12	±3	±4	±3		±14	±8	±.08		(Cerro Toledo Rhyolite)
1691-2b	134	19	203	0	59	166	86	nm	500	611	1.22	nm	Obsidian Ridge
	±6	±3	±4	±5	±3	±4	±3		±14	±8	±.08		(Cerro Toledo Rhyolite)
1691-3a	89	16	193	3	58	159	81	nm	430	603	1.20	nm	Obsidian Ridge
	±5	±3	±4	±5	±3	±4	±3		±14	±8	±.08		(Cerro Toledo Rhyolite)
1691-4a.1	88	20	196	3	55	160	80	nm	467	607	1.21	nm	Obsidian Ridge
	±5	±3	±4	±3	±3	±4	±3		±14	±8	±.08		(Cerro Toledo Rhyolite)
1691-4a.2	107	18	213	3	62	174	92	nm	457	615	1.23	nm	Obsidian Ridge
	±5	±3	±4	±7	±3	±4	±3		±14	±8	±.08		(Cerro Toledo Rhyolite)
1691-4b.1	92	23	199	3	59	162	87	nm	490	597	1.22	nm	Obsidian Ridge
	±5	±3	±4	±3	±3	±4	±3		±14	±8	±.08		(Cerro Toledo Rhyolite)
1691-4b.2	92	19	193	3	59	162	83	nm	591	620	1.21	nm	Obsidian Ridge
	±5	±3	±4	±5	±3	±4	±3		±14	±8	±.08		(Cerro Toledo Rhyolite)
1691-5a	84	21	197	0	57	165	86	nm	429	582	1.16	nm	Obsidian Ridge
	±5	±3	±4	±5	±3	±4	±3		±14	±8	±.08		(Cerro Toledo Rhyolite)
1691-6a	100	17	199	4	58	166	85	nm	557	584	1.20	nm	Obsidian Ridge
	±5	±3	±4	±3	±3	±4	±3		±15	±8	±.08		(Cerro Toledo Rhyolite)
1691-7a	133	32	230	19	63	194	86	nm	**955**	740	1.58	nm	Obsidian Ridge
	±6	±3	±4	±3	±3	±4	±3		±17	±9	±.08		(Cerro Toledo Rhyolite)

Values in parts per million (ppm) except total iron (in weight percent) and Fe/Mn ratios; ± = pooled estimate (in ppm and wt. % composition) of x-ray counting uncertainty and regression fitting error at 300 seconds livetime; nm = not measured.

Cat. Number	Trace and Selected Minor Element Concentrations											Ratio	Obsidian Source (Chemical Type)
	Zn	Ga	Rb	Sr	Y	Zr	Nb	Ba	Ti	Mn	$Fe_2O_3^T$	Fe/Mn	
1691-7b	84 ±6	2 ±3	199 ±4	5 ±3	61 ±3	163 ±4	84 ±3	nm	**880** ±16	590 ±8	1.39 ±.08	nm	Obsidian Ridge (Cerro Toledo Rhyolite)
1691-8a	85 ±6	20 ±3	193 ±4	6 ±3	55 ±3	158 ±4	83 ±3	nm	**672** ±16	569 ±9	1.23 ±.08	nm	Obsidian Ridge (Cerro Toledo Rhyolite)
1691-9a	91 ±5	20 ±3	201 ±4	0 ±5	58 ±3	166 ±4	86 ±3	nm	435 ±14	604 ±8	1.19 ±.08	nm	Obsidian Ridge (Cerro Toledo Rhyolite)
1691-9b	90 ±5	20 ±3	187 ±4	4 ±3	58 ±3	160 ±4	83 ±3	nm	607 ±15	599 ±8	1.23 ±.08	nm	Obsidian Ridge (Cerro Toledo Rhyolite)
1691-10a	101 ±5	25 ±3	218 ±4	12 ±3	62 ±3	172 ±4	87 ±3	nm	**892** ±16	667 ±8	1.26 ±.08	19	Obsidian Ridge (Cerro Toledo Rhyolite)
1691-11a.1	103 ±6	27 ±3	220 ±4	5 ±3	60 ±3	172 ±4	90 ±3	nm	598 ±15	669 ±9	1.27 ±.08	nm	Obsidian Ridge (Cerro Toledo Rhyolite)
1691-11a.2	94 ±6	22 ±3	207 ±4	3 ±6	57 ±3	162 ±4	86 ±3	nm	518 ±16	654 ±9	1.27 ±.08	nm	Obsidian Ridge (Cerro Toledo Rhyolite)
1691-11a.3	95 ±5	23 ±3	199 ±4	6 ±3	59 ±3	163 ±4	85 ±3	nm	579 ±15	622 ±8	1.23 ±.08	nm	Obsidian Ridge (Cerro Toledo Rhyolite)
1691-11b.1	95 ±5	20 ±3	199 ±4	3 ±7	58 ±3	163 ±4	86 ±3	nm	488 ±14	608 ±8	1.24 ±.08	nm	Obsidian Ridge (Cerro Toledo Rhyolite)
1691-11b.2	88 ±6	20 ±3	196 ±4	0 ±5	57 ±3	161 ±4	86 ±3	nm	453 ±14	595 ±8	1.20 ±.08	nm	Obsidian Ridge (Cerro Toledo Rhyolite)
1691-12a.1	90 ±5	19 ±3	199 ±4	4 ±3	58 ±3	163 ±4	86 ±3	nm	520 ±14	578 ±8	1.21 ±.08	nm	Obsidian Ridge (Cerro Toledo Rhyolite)
1691-14b	87 ±5	19 ±3	189 ±4	4 ±3	54 ±3	151 ±4	80 ±3	nm	532 ±14	558 ±8	1.15 ±.08	21	Obsidian Ridge (Cerro Toledo Rhyolite)
1691-15e	87 ±6	18 ±3	199 ±4	3 ±4	57 ±3	164 ±4	86 ±3	nm	454 ±14	603 ±9	1.21 ±.08	20	Obsidian Ridge (Cerro Toledo Rhyolite)
1691-18	83 ±6	22 ±3	192 ±4	3 ±4	56 ±3	161 ±4	83 ±3	nm	402 ±14	593 ±8	1.14 ±.08	20	Obsidian Ridge (Cerro Toledo Rhyolite)
1691-21	81 ±5	17 ±3	176 ±4	4 ±3	49 ±3	149 ±4	77 ±3	nm	371 ±14	560 ±9	1.08 ±.08	20	Obsidian Ridge (Cerro Toledo Rhyolite)
1691-22	92 ±6	25 ±3	199 ±4	3 ±3	61 ±3	166 ±4	83 ±3	nm	437 ±14	605 ±8	1.12 ±.08	19	Obsidian Ridge (Cerro Toledo Rhyolite)
1691-23	83 ±6	19 ±3	191 ±4	3 ±3	54 ±3	158 ±4	81 ±3	nm	443 ±14	592 ±8	1.15 ±.08	20	Obsidian Ridge (Cerro Toledo Rhyolite)

Values in parts per million (ppm) except total iron (in weight percent) and Fe/Mn ratios; ± = pooled estimate (in ppm and wt. % composition) of x-ray counting uncertainty and regression fitting error at 300 seconds livetime; nm = not measured.

Cat. Number	Trace and Selected Minor Element Concentrations											Ratio	Obsidian Source (Chemical Type)
	Zn	Ga	Rb	Sr	Y	Zr	Nb	Ba	Ti	Mn	$Fe_2O_3^T$	Fe/Mn	
1691-25a	94 ±5	23 ±3	199 ±4	4 ±3	55 ±3	161 ±4	82 ±3	nm	435 ±14	593 ±8	1.16 ±.08	19	Obsidian Ridge (Cerro Toledo Rhyolite)
1691-25b	80 ±6	17 ±3	190 ±4	3 ±4	56 ±3	153 ±4	80 ±3	nm	397 ±14	576 ±8	1.13 ±.08	20	Obsidian Ridge (Cerro Toledo Rhyolite)
1691-26a	110 ±6	27 ±3	**231** ±4	4 ±3	65 ±3	185 ±4	96 ±3	nm	546 ±16	685 ±9	**1.32** ±.08	19	Obsidian Ridge (Cerro Toledo Rhyolite)
1691-26b	83 ±6	20 ±3	190 ±4	4 ±3	54 ±3	158 ±4	77 ±3	nm	434 ±14	591 ±8	1.13 ±.08	20	Obsidian Ridge (Cerro Toledo Rhyolite)
1691-27	90 ±6	17 ±3	186 ±4	5 ±3	52 ±3	156 ±4	80 ±3	nm	**982** ±19	557 ±9	1.27 ±.08	24	Obsidian Ridge (Cerro Toledo Rhyolite)
1691-28	91 ±5	18 ±3	202 ±4	5 ±3	58 ±3	165 ±4	87 ±3	nm	468 ±14	591 ±8	1.18 ±.08	20	Obsidian Ridge (Cerro Toledo Rhyolite)
1691-31	92 ±5	21 ±3	197 ±4	3 ±3	58 ±3	159 ±4	83 ±3	nm	435 ±13	590 ±8	1.13 ±.08	20	Obsidian Ridge (Cerro Toledo Rhyolite)
1691-33	81 ±6	20 ±3	190 ±4	0 ±4	55 ±3	156 ±4	78 ±3	nm	398 ±15	597 ±9	1.16 ±.08	20	Obsidian Ridge (Cerro Toledo Rhyolite)
1691-35	85 ±6	17 ±3	197 ±4	4 ±3	56 ±3	158 ±4	80 ±3	nm	448 ±14	596 ±8	1.18 ±.08	20	Obsidian Ridge (Cerro Toledo Rhyolite)
1691-36	79 ±5	25 ±3	191 ±4	4 ±3	55 ±3	156 ±4	81 ±3	nm	408 ±14	567 ±8	1.14 ±.08	20	Obsidian Ridge (Cerro Toledo Rhyolite)
1691-39	90 ±6	21 ±3	198 ±4	4 ±3	57 ±3	157 ±4	85 ±3	nm	487 ±15	632 ±9	1.23 ±.08	20	Obsidian Ridge (Cerro Toledo Rhyolite)
1691-41	91 ±6	16 ±3	191 ±4	3 ±3	56 ±3	162 ±4	79 ±3	nm	401 ±15	623 ±9	1.17 ±.08	20	Obsidian Ridge (Cerro Toledo Rhyolite)
1691-42	89 ±5	23 ±3	195 ±4	5 ±3	57 ±3	162 ±4	82 ±3	nm	429 ±14	596 ±8	1.17 ±.08	20	Obsidian Ridge (Cerro Toledo Rhyolite)
1691-45	84 ±6	15 ±3	190 ±4	0 ±4	53 ±3	154 ±4	82 ±3	nm	574 ±16	594 ±9	1.25 ±.08	22	Obsidian Ridge (Cerro Toledo Rhyolite)
1691-47	92 ±6	18 ±3	206 ±4	0 ±4	59 ±3	169 ±4	88 ±3	nm	455 ±15	638 ±9	1.25 ±.08	19	Obsidian Ridge (Cerro Toledo Rhyolite)
9999-1a	37 ±6	13 ±3	166 ±4	70 ±3	8 ±3	74 ±4	4 ±3	428 ±14	439 ±15	322 ±8	.59 ±.08	21	Unknown, from Popayan, Colombia
9999-1b	39 ±6	10 ±3	143 ±4	67 ±3	7 ±3	70 ±4	7 ±3	521 ±15	422 ±17	267 ±8	.48 ±.08	20	Unknown, from Popayan, Colombia

Values in parts per million (ppm) except total iron (in weight percent) and Fe/Mn ratios; ± = pooled estimate (in ppm and wt. % composition) of x-ray counting uncertainty and regression fitting error at 300 seconds livetime; nm = not measured.

Geochemical Research Laboratory Letter Report 2003-69

March 8, 2004

Ms. Ana Steffen
2118 Central SE # 4
Albuquerque, NM 87106

Dear Ana:

Enclosed with this letter you will find a table presenting energy dispersive x-ray fluorescence (edxrf) data generated from the analysis of obsidian samples for your dissertation research in the Valles Caldera, New Mexico.

Analyses of obsidian are performed at my laboratory on a QuanX-EC™ (Thermo Electron Corporation) edxrf spectrometer equipped with a rhodium (Rh) x-ray tube, a 50 kV x-ray generator, digital pulse processor with automated energy calibration, and a Peltier cooled solid state detector with 145 eV resolution (FWHM) at 5.9 keV. The x-ray tube was operated at 40.0 kV using a 127 mm palladium (Pd) primary beam filter in an air path to generate x-ray intensity data for elements rubidium (Rb Kα), strontium (Sr Kα), yttrium (Y Kα), zirconium (Zr Kα), and niobium (Nb Kα). Barium (Ba Kα) intensities were generated by operating the x-ray tube at 50.0 kV with a.38 mm copper (Cu) filter, while those for potassium (Kα), calcium (Ca Kα), titanium (Ti Kα), manganese (Mn Kα) and total iron ($Fe_2O_3^T$) were generated by operating the x-ray tube at 30.0 kV using a .025 mm Pd filter. Iron vs. manganese (Fe Kα/Mn Kα) ratios were computed from data generated by operating the x-ray tube at 30.0 kV with a .025 mm Pd filter. Each subroutine was run at 200 deadtime-corrected seconds, with tube current (mA) scaled to the physical size of each specimen.

X-ray spectra are acquired and elemental intensities extracted for each peak region of interest, then matrix correction algorithms are applied to specific regions of the x-ray energy spectrum to compensate for inter-element absorption and enhancement effects. After these corrections are made, intensities are converted to concentration estimates by employing a least-squares calibration line established for each element from analysis of up to 30 international rock standards certified by the U.S. Geological Survey, the U.S. National Institute of Standards and Technology, the Geological Survey of Japan, the Centre de Recherches Petrographiques et Geochimiques (France), and the South African Bureau of Standards. Further details pertaining to calibration appear in Hughes (1988a, 1994b).

Trace element measurements in the xrf data table are expressed in quantitative units (i.e. parts per million [ppm] by weight), and comparisons between unknowns and known obsidian chemical groups are made on the basis of correspondences (at the 2-sigma level) in diagnostic trace element concentration values (in this case, ppm values for Rb, Sr, Y, Zr, Nb, Ba, Ti, Mn and $Fe_2O_3^T$) that appear in Anderson et al. (1986), Baugh and Nelson (1987, 1988), Glascock et al. (1999), Hughes (1984, 1988b), Hughes and Nelson (1987), Jack (1971), Nelson (1984), Shackley (1995, 1998), and unpublished data on other obsidians (e.g. Hughes 1994a; 1995a, b; 1997). Artifact-to-obsidian source (geochemical type, *sensu* Hughes 1998) correspondences were considered reliable if diagnostic mean measurements for artifacts fell within 2 standard deviations of mean values for source standards. I use the term "diagnostic" to specify those trace elements

that are well-measured by x-ray fluorescence, and whose concentrations show low intra-source variability and marked variability across sources. In short, diagnostic elements are those concentration values allowing one to draw the clearest geochemical distinctions between sources (Hughes 1990, 1993).

The trace element composition measurements in the enclosed table are reported to the nearest ppm to reflect the resolution capabilities of non-destructive edxrf spectrometry. The resolution limit of the present x-ray fluorescence instrument for the determination of Rb is about 4 ppm; for Sr about 3 ppm; Y about 2 ppm; Zr about 4 ppm; Nb about 2 ppm; and Ba about 10 ppm (see Hughes [1994b] for other elements). When counting and fitting error uncertainty estimates (the "±" value in the table) for a sample are greater than calibration-imposed limits of resolution, the larger number is a more conservative indicator of composition variation and measurement error arising from differences in sample size, surface and x-ray reflection geometry.

These results show that the vast majority of specimens represent the two dominant chemical types; Cerro del Medio (a.k.a. Valles Rhyolite), and the entity you have referred to as Cerro Toledo Dome (Obsidian Ridge and Rabbit Mountain). Of particular interest, however, are two specimens (CTN-301 and CTN-302) from Cerro Toledo North, which appear to be chemically distinct from Cerro Toledo Dome and Cerro del Medio obsidians. But because only two samples were analyzed, these results should be considered provisional until additional well-provenienced specimens can be collected anal analyzed. Nonetheless, if upheld by further analyses, these preliminary results may signal the existence of a "new" chemical type in the Jemez.

I hope this information will help in your analysis and interpretation of materials from these collection localities. Please contact me at my laboratory ([650] 851-1410; e-mail: rehughes@silcon.com) if I can be of further assistance.

Sincerely,

Richard E. Hughes, Ph.D., RPA
Director, Geochemical Research Laboratory

encl.

REFERENCES

Anderson, Duane C., Joseph A. Tiffany, and Fred W. Nelson
1986 Recent Research on Obsidian from Iowa Archaeological Sites. American Antiquity 51: 837-852.

Baugh, Timothy G., and Fred W. Nelson
1987 New Mexico Obsidian Sources and Exchange on the Southern Plains. **Journal of Field Archaeology** 14: 313-329.

1988 Archaeological Obsidian Recovered from Selected North Dakota Sites and Its Relationship to Changing Exchange Systems in the Plains. Journal of the North Dakota Archaeological Association 3: 74-94.

Church, Tim
2000 Distribution and Sources of Obsidian in the Rio Grande Gravels of New Mexico. Geoarchaeology 15: 649-678.

Glascock, Michael D., Raymond Kunselman, and Daniel Wolfman
1999 Intrasource Chemical Differentiation of Obsidian in the Jemez Mountains and Taos Plateau, New Mexico. Journal of Archaeological Science 26: 861-868.

Hughes, Richard E.
1982 Age and Exploitation of Obsidian from the Medicine Lake Highland, California. Journal of Archaeological Science 9: 173-185.

Hughes, Richard E.
1984 Obsidian Sourcing Studies in the Great Basin: Problems and Prospects. In Richard E. Hughes (ed.) Obsidian Studies in the Great Basin. Contributions of the University of California Archaeological Research Facility No. 45: 1-19.

1988a The Coso Volcanic Field Reexamined: Implications for Obsidian Sourcing and Hydration Dating Research. Geoarchaeology 3: 253-265.

1988b Archaeological Significance of Geochemical Contrasts Among Southwestern New Mexico Obsidians. Texas Journal of Science 40: 297-307.

1990 Obsidian Sources at James Creek Shelter, and Trace Element Geochemistry of Some Northeastern Nevada Volcanic Glasses. In Robert G. Elston and Elizabeth E. Budy (eds.), The Archaeology of James Creek Shelter. University of Utah Anthropological Papers No. 115, pp. 297-305.

1993 Trace Element Geochemistry of Volcanic Glass from the Obsidian Cliffs Flow, Three Sisters Wilderness, Oregon. Northwest Science 67: 199-207.

1994a X-ray Fluorescence Analysis of Geologic Obsidian Samples and Artifacts from the Kern River Gas Transmission Project, Utah. In Kern River Pipeline Cultural Resources Data Recovery Report: Utah. Volume I, Research Context and Data Analysis. Report submitted by Dames & Moore to Kern River Gas Transmission Company, January 31, 1994.

1994b Intrasource Chemical Variability of Artefact-Quality Obsidians from the Casa Diablo Area, California. Journal of Archaeological Science 21: 263-271.

1998 On Reliability, Validity, and Scale in Obsidian Sourcing Research. In Ann F. Ramenofsky and Anastasia Steffen (eds.), Unit Issues in Archaeology: Measuring Time, Space, and Material, pp. 103-114. University of Utah Press, Salt Lake City.

REFERENCES (continued)

Hughes, Richard E., and Fred W. Nelson
1987 New Findings on Obsidian Source Utilization in Iowa. Plains Anthropologist 32 (117): 313-316.

Jack, Robert N.
1971 The Source of Obsidian Artifacts in Northern Arizona. Plateau 43: 103-114.

Macdonald, Ray, Robert L. Smith, and John E. Thomas
1992 Chemistry of the Subalkalic Silicic Obsidians. U.S. Geological Survey Professional Paper 1523.

Nelson, Fred W., Jr.
1984 X-ray Fluorescence Analysis of Some Western North American Obsidians. In Richard E. Hughes (ed.) Obsidian Studies in the Great Basin. Contributions of the University of California Archaeological Research Facility No. 45: 27-62.

Shackley, M. Steven
1995 Sources of Archaeological Obsidian in the Greater American Southwest: An Update and Quantitative Analysis. American Antiquity 60: 531-551.

1998 Geochemical Differentiation and Prehistoric Procurement of Obsidian in the Mount Taylor Volcanic Field, Northwest New Mexico. Journal of Archaeological Science 25: 1073-1082.

Cat. Number	Trace and Selected Minor Element Concentrations K	Ca	Rb	Sr	Y	Zr	Nb	Ba	Ti	Mn	$Fe_2O_3^T$	Ratio Fe/Mn	Obsidian Source (Chemical Type)
CDM-301	3.82 ±.02	.21	143 ±.02	10 ±4	42 ±3	153 ±3	49 ±4	nm ±3	541	462 ±15	1.09 ±12	27 ±.10	CDM
CDM-302	3.69 ±.02	.17 ±.02	157 ±4	10 ±3	44 ±3	160 ±4	50 ±3	nm	457 ±14	507 ±12	1.18 ±.10	26	CDM
CDM-303	3.58 ±.02	.18 ±.02	156 ±4	6 ±3	40 ±3	156 ±4	47 ±3	nm	431 ±15	502 ±12	1.19 ±.10	27	CDM
CDM-304	3.56 ±.02	.19 ±.02	150 ±4	9 ±3	40 ±3	152 ±4	50 ±3	nm	443 ±15	489 ±12	1.18 ±.10	28	CDM
CDM-305	3.47 ±.02	.16 ±.02	161 ±4	6 ±3	41 ±3	158 ±4	48 ±3	nm	375 ±15	576 ±12	1.33 ±.10	25	CDM
CDM-306	3.74 ±.02	.19 ±.02	148 ±4	7 ±3	40 ±3	153 ±4	52 ±3	nm	502 ±15	501 ±12	1.18 ±.10	26	CDM
CDM-307	3.79 ±.02	.20 ±.02	138 ±4	10 ±3	37 ±3	144 ±4	43 ±3	nm	530 ±15	472 ±12	1.08 ±.10	26	CDM
CDM-308	3.75 ±.02	.17 ±.02	151 ±4	40 ±3	41 ±3	150 ±4	44 ±3	nm	414 ±15	515 ±12	1.19 ±.10	26	CDM
CDM-309	3.82 ±.02	.18 ±.02	150 ±4	6 ±3	45 ±3	162 ±4	51 ±3	nm	488 ±15	499 ±12	1.15 ±.10	25	CDM
CDM-310	3.73 ±.02	.19 ±.02	153 ±4	9 ±3	42 ±3	155 ±4	53 ±3	nm	460 ±15	506 ±12	1.16 ±.10	24	CDM
CDM-311	3.52 ±.02	.17 ±.02	151 ±4	9 ±3	41 ±3	147 ±4	42 ±3	nm	416 ±15	510 ±12	1.20 ±.10	25	CDM
CDM-312	3.70 ±.02	.18 ±.02	152 ±4	6 ±3	38 ±3	146 ±4	49 ±3	nm	484 ±15	468 ±12	1.12 ±.10	25	CDM
CDM-413	3.82 ±.02	.18 ±.02	162 ±4	8 ±3	43 ±3	157 ±4	48 ±3	nm	429 ±15	524 ±12	1.28 ±.10	24	CDM
CDM-414	3.75 ±.02	.21 ±.02	139 ±4	9 ±3	42 ±3	173 ±4	45 ±3	nm	578 ±15	547 ±12	1.09 ±.10	21	CDM
CDM-415	3.72 ±.02	.20 ±.02	142 ±4	6 ±3	43 ±3	167 ±4	50 ±3	nm	597 ±15	547 ±12	1.09 ±.10	21	CDM
CDM-416	3.45 ±.02	.16 ±.02	153 ±4	7 ±3	38 ±3	173 ±4	45 ±3	nm	492 ±15	584 ±12	1.16 ±.10	21	CDM
CTD5.	3.71	.13	214	3	60	175	91	nm	415	691	1.32	18	OR

Values in parts per million (ppm) except K, Ca, and total iron (in weight percent) and Fe/Mn ratios; ± = estimate (in ppm and wt. %) of x-ray counting uncertainty and regression fitting error at 200 seconds livetime; nm = not measured.

Cat. Number	Trace and Selected Minor Element Concentrations K	Ca	Rb	Sr	Y	Zr	Nb	Ba	Ti	Mn	$Fe_2O_3^T$	Ratio Fe/Mn	Obsidian Source (Chemical Type)
301	±.02	±.02	±4	±3	±3	±4	±3		±15	±12	±.10		
CTD5,	3.58	.14	187	6	59	158	85	nm	411	667	1.21	19	OR
302	±.02	±.02	±4	±3	±3	±4	±3		±15	±12	±.10		
CTD5,	4.95	.23	209	6	65	177	96	nm	654	658	1.30	17	OR
303	±.02	±.02	±4	±3	±3	±4	±3		±15	±12	±.10		
CTD5,	3.44	.13	198	4	60	168	81	nm	364	695	1.28	18	OR
304	±.02	±.02	±4	±3	±3	±4	±3		±15	±12	±.10		
CTD5,	3.73	.13	194	3	60	165	85	nm	433	648	1.20	20	OR
305	±.02	±.02	±4	±3	±3	±4	±3		±16	±11	±.10		
CTD5,	4.98	.32	193	6	60	167	94	nm	719	614	1.19	20	OR
307	±.02	±.02	±4	±3	±3	±4	±3		±16	±12	±.10		
CTD5,	3.40	.12	218	6	66	175	96	nm	326	727	1.41	19	OR
308	±.02	±.02	±4	±3	±3	±4	±3		±15	±1	±.10		
CTD5,	3.17	.11	208	4	61	173	88	nm	285	767	1.38	20	OR
309	±.02	±.02	±4	±3	±3	±4	±3		±16	±12	±.10		
CTD6,	4.85	.29	197	4	61	163	88	nm	676	618	1.18	20	OR
301	±.02	±.02	±4	±3	±3	±4	±3		±16	±12	±.10		
CTD6,	3.66	.14	204	3	61	165	85	nm	416	680	1.26	20	OR
302	±.02	±.02	±4	±3	±3	±4	±3		±15	±12	±.10		
CTD6,	3.76	.13	193	4	59	159	77	nm	425	673	1.21	20	OR
303	±.02	±.02	±4	±3	±3	±4	±3		±15	±12	±.10		
CTD6,	3.72	.16	188	4	60	162	86	nm	456	609	1.14	18	OR
304	±.02	±.02	±4	±3	±3	±4	±3		±15	±12	±.10		
CTD7,	3.44	.13	222	4	67	178	93	nm	361	695	1.39	20	OR
301	±.02	±.02	±4	±3	±3	±4	±3		±15	±12	±.10		
CTD7,	5.06	.28	198	6	63	167	93	nm	721	597	1.17	20	OR
302	±.02	±.02	±4	±3	±3	±4	±3		±16	±12	±.10		
CTD8,	3.65	.13	205	4	62	160	90	nm	398	679	1.28	20	OR
301	±.02	±.02	±4	±3	±3	±4	±3		±15	±12	±.10		
CTD8,	3.58	.13	217	4	61	163	82	nm	381	682	1.33	19	OR
302	±.02	±.02	±4	±3	±3	±4	±3		±15	±12	±.10		
CTD8S,	3.66	.14	195	5	61	158	85	nm	414	645	1.22	19	OR
301	±.02	±.02	±4	±3	±3	±4	±3		±15	±12	±.10		

Values in parts per million (ppm) except K, Ca, and total iron (in weight percent) and Fe/Mn ratios; ± = estimate (in ppm and wt. %) of x-ray counting uncertainty and regression fitting error at 200 seconds livetime; nm = not measured.

Cat. Number	Trace and Selected Minor Element Concentrations K	Ca	Rb	Sr	Y	Zr	Nb	Ba	Ti	Mn	$Fe_2O_3^T$	Ratio Fe/Mn	Obsidian Source (Chemical Type)
CTD8S, 302	3.57 ±.02	.13 ±.02	210 ±4	3 ±3	60 ±3	171 ±4	88 ±3	nm	383 ±16	385 ±12	1.28 ±.10	19	OR
CTD10, 301	3.74 ±.02	.14 ±.02	194 ±4	4 ±3	60 ±3	165 ±4	88 ±3	nm	427 ±15	671 ±12	1.25 ±.10	19	OR
CTD10, 302	3.66 ±.02	.14 ±.02	189 ±4	5 ±3	58 ±3	167 ±4	86 ±3	nm	424 ±16	644 ±12	1.20 ±.10	18	OR
CTD10, 303	3.66 ±.02	.14 ±.02	180 ±4	5 ±3	55 ±3	149 ±4	75 ±3	nm	459 ±15	616 ±12	1.11 ±.10	18	OR
CTD10, 304	3.80 ±.02	.15 ±.02	173 ±4	5 ±3	57 ±3	160 ±4	85 ±3	nm	461 ±15	595 ±12	1.14 ±.10	19	OR
CTD10, 305	3.62 ±.02	.14 ±.02	206 ±4	4 ±3	62 ±3	169 ±4	88 ±3	nm	394 ±15	688 ±12	1.28 ±.10	21	OR
CTD10, 306	3.39 ±.02	.12 ±.02	210 ±4	4 ±3	61 ±3	175 ±4	94 ±3	nm	381 ±15	681 ±12	1.32 ±.10	20	OR
CTD12, 301	3.69 ±.02	.15 ±.02	180 ±4	5 ±3	58 ±3	160 ±4	81 ±3	nm	428 ±16	652 ±12	1.21 ±.10	19	OR
CTD12, 302	3.38 ±.02	.12 ±.02	208 ±4	3 ±3	64 ±3	167 ±4	85 ±3	nm	346 ±15	705 ±12	1.33 ±.10	19	OR
CTD12, 303	4.94 ±.02	.29 ±.02	213 ±4	4 ±3	63 ±3	173 ±4	99 ±3	nm	686 ±16	636 ±13	1.29 ±.10	20	OR
CTDRM, 301	3.77 ±.02	.14 ±.02	202 ±4	3 ±3	59 ±3	161 ±4	90 ±3	nm	419 ±15	654 ±12	1.21 ±.10	20	OR
CTDRM, 302	4.46 ±.02	.18 ±.02	194 ±4	4 ±3	59 ±3	158 ±4	83 ±3	nm	472 ±16	648 ±12	1.22 ±.10	18	OR
CTDRM, 303	3.66 ±.02	.12 ±.02	195 ±4	4 ±3	59 ±3	167 ±4	89 ±3	nm	398 ±15	640 ±12	1.23 ±.10	18	OR
CTDRM, 304	3.65 ±.02	.14 ±.02	177 ±4	6 ±3	60 ±3	152 ±4	78 ±3	nm	438 ±15	636 ±12	1.16 ±.10	21	OR
CTN-301	4.10 ±.02	.16 ±.02	149 ±4	8 ±3	47 ±3	133 ±4	65 ±3	nm	480 ±15	555 ±12	.98 ±.10	18	
CTN-302	3.74 ±.02	.15 ±.02	148 ±4	11 ±3	46 ±3	133 ±4	67 ±3	nm	468 ±15	547 ±12	.99 ±.10	18	
CTN-303	3.65 ±.02	.14 ±.02	188 ±4	6 ±3	62 ±3	148 ±4	80 ±3	nm	421 ±15	675 ±12	1.18 ±.10	17	OR

Values in parts per million (ppm) except K, Ca, and total iron (in weight percent) and Fe/Mn ratios; ± = estimate (in ppm and wt. %) of x-ray counting uncertainty and regression fitting error at 200 seconds livetime: nm = not measured.

Cat. Number	Trace and Selected Minor Element Concentrations K	Ca	Rb	Sr	Y	Zr	Nb	Ba	Ti	Mn	Ratio $Fe_2O_3^T$	Fe/Mn	Obsidian Source (Chemical Type)
CTN-304	3.62	.13	201	4	57	156	88	nm	400	687	1.20	17	OR
	±.02	±.02	±4	±3	±3	±4	±3		±15	±12	±.10		
CTN-305	3.53	.18	163	9	41	153	48	nm	428	531	1.28	25	
	±.02	±.02	±4	±3	±3	±4	±3		±15	±12	±.10		
CTN-305A	3.52	.12	201	4	61	163	82	nm	554	531	1.27	19	OR
	±.02	±.02	±4	±3	±3	±4	±3		±26	±16	±.10		
CTN-306	3.72	.15	193	4	65	158	87	nm	442	635	1.12	18	OR
	±.02	±.02	±4	±3	±3	±4	±3		±16	±12	±.10		
CTN-307	3.59	.14	206	6	61	161	89	nm	405	673	1.24	20	OR
	±.02	±.02	±4	±3	±3	±4	±3		±15	±12	±.10		
CTN-308	3.60	.14	202	4	63	168	91	nm	400	689	1.27	19	OR
	±.02	±.02	±4	±3	±3	±4	±3		±15	±12	±.10		

Values in parts per million (ppm) except K, Ca, and total iron (in weight percent) and Fe/Mn ratios; ± = estimate (in ppm and wt. %) of x-ray counting uncertainty and regression fitting error at 200 seconds livetime; nm = not measured.

Additional Hughes ED-XRF data on selected burned artifacts (discussed in Chapter 4).

January 3, 2005 **Valles Caldera, NM, Xrf Data**
R. E. Hughes, Analyst **Page 1 of 1**

Cat. Number	Trace and Selected Minor Element Concentrations											Ratio	Obsidian Source (Chemical Type)
	K	Ca	Rb	Sr	Y	Zr	Nb	Ba	Ti	Mn	$Fe_2O_3^T$	Fe/Mn	
601	3.74 ±.02	.20 ±.02	201 ±4	4 ±3	58 ±3	165 ±4	91 ±3	nm	497 ±24	607 ±10	1.25 ±.02	nm	OR
603	3.52 ±.02	.18 ±.02	194 ±4	6 ±3	60 ±3	161 ±4	81 ±3	nm	451 ±21	655 ±10	1.33 ±.02	nm	OR
H2-10	3.74 ±.02	.21 ±.02	199 ±4	6 ±3	56 ±3	163 ±4	89 ±3	nm	527 ±21	561 ±10	1.17 ±.02	nm	OR
I4-1	3.82 ±.02	.21 ±.02	216 ±4	4 ±3	61 ±3	169 ±4	92 ±3	nm	616 ±24	565 ±10	1.17 ±.02	nm	OR
J1-10	3.93 ±.02	.23 ±.02	191 ±4	7 ±3	64 ±3	167 ±4	90 ±3	nm	639 ±24	604 ±10	1.27 ±.02	nm	OR
J4-1	3.71 ±.02	.23 ±.02	162 ±4	6 ±3	54 ±3	151 ±4	88 ±3	nm	635 ±24	584 ±10	1.26 ±.02	nm	OR
J5-B10	3.87 ±.02	.24 ±.02	195 ±4	2 ±3	60 ±3	164 ±4	89 ±3	nm	603 ±21	649 ±10	1.30 ±.02	nm	OR
~~J5-B12~~	~~3.77~~ ±.02	~~.19~~ ±.02	~~201~~ ±4	5 ±3	62 ±3	~~164~~ ±4	~~94~~ ±3	~~nm~~	~~490~~ ±22	~~597~~ ±10	~~1.23~~ ±.02	~~nm~~	~~OR~~
J5-E13	3.54 ±.02	.18 ±.02	191 ±4	6 ±3	59 ±3	159 ±4	88 ±3	nm	510 ±21	612 ±11	1.27 ±.02	nm	OR
J5-F14	3.66 ±.02	.18 ±.02	188 ±4	5 ±3	61 ±3	165 ±4	87 ±3	nm	499 ±24	557 ±10	1.17 ±.02	nm	OR
J5-G15	3.82 ±.02	.20 ±.02	189 ±4	6 ±3	60 ±3	165 ±4	92 ±3	nm	508 ±24	582 ±10	1.18 ±.02	nm	OR

Values in parts per million (ppm) except K, Ca, and total iron (in weight percent) and Fe/Mn ratios; ± = estimate (in ppm and wt. %) of x-ray counting uncertainty and regression fitting error at 120 seconds livetime; nm = not measured.

APPENDIX E:

Experimental Heating of Obsidian with Known Water Contents

In order to examine causes of fire-induced vesiculation in obsidian, I conducted several preliminary laboratory heating experiments (see also, Steffen 2002). The problem with such heating experiments is that they require precise control of physical characteristics of samples such as size, thickness, and surface area in order to be valid to compare differences in heat response across glasses of different composition and texture. Such precision in sample preparation proved to be beyond the scope of the current study and were not pursued further. Instead I refer to Appendix C which presents unpublished data by H. Westrich, Sandia National Laboratory, of glass heating experiments that control for sample physical characteristics, glass composition, and water content conducted to assess the role of heating temperature, rate, and duration for the onset of vesiculation.

The results presented in this appendix are considered a preliminary, initial attempt to examine whether higher water content in obsidian causes vesiculation at lower temperature. The results represent only a crude indicator of this relationship, with only rough control over the experimental conditions (e.g. firing duration, rate of heating, specimen shape, specimen size). The simple goal is to compare temperature of vesiculation among samples with greater and lesser water contents, as measured for this dissertation project (see Chapter 8). Results from these heating tests, while preliminary and poorly controlled, give some indication of the temperatures required for vesiculation, variability in the response to heat by obsidian from within the Cerro Toledo Dome (CTD) source, and trace element measurements before and after heating.

Samples are all from CTD locations within the Dome area. Elemental compositions are reported in Chapter 6. All experimental heating was conducted on a small electric bench furnace, donated to me by Fred Trembour. The furnace is a Thermolyne electric muffle furnace--the same one that Trembour used for his heating experiments following the 1977 La Mesa Fire (Trembour 1979, 1990).

Specimens were heated in three runs. No attempt was made to control the duration of heating. Heating runs 1 and 3 were started from an oven at room temperature. Runs 2 and 4 were started from a hot oven (approximately 600°C).

Tables E-1 and E-2 present information on the elemental composition and water content of each specimen, along with results of heating (Table E-1).

Heating outcomes indicate that specimens with water contents at LOI 0.80% or greater are more prone to vesiculation upon heating. Specimens with water contents at 0.70% to 0.73% have mixed results. Only a single specimen with <0.60% (CTD10-305) vesiculated in this experiment.

Data on iron content of specimens is included here because it may be that this constituent provides an interacting effect with water content. Interpretation of these data is not attempted at this time because further experimentation and analysis are needed.

Overall, these results provide preliminary data to support a trend to greater susceptibility to vesiculation with higher water content. While this test is not rigorous in control of heat conditions, it is suggestive. Further research is warranted.

Table E-1. Description of heated specimens including LOI water content and results.

Sample	Color	Run	Temp (C°) at change (or max temp reached)	Heating result	LOI H2O-	LOI H20+	**Total LOI**
CTD10-301	semi-opaque grey, with bands	2	(910)	no vesic	0.00%	0.63%	**0.56%**
CTD06-302	clear black	2	(910)	no vesic	0.06%	0.75%	**0.69%**
CTD10-303	clear black	1	(900)	no vesic	0.00%	0.78%	**0.72%**
CTD05-302	aphyric clear black	3	(900)	no vesic	0.22%	0.73%	**0.73%**
CTD10-305	clear black, faint bands	1,4	900, 910	no vesic, bubbles present	0.08%	0.57%	**0.52%**
CTD08-302	dark grey, pleochroic	3	900	vesic	0.06%	0.76%	**0.70%**
CTD12-303	opaque blue/brown	1	875	vesic	0.06%	0.90%	**0.84%**
CTD05-305	cloudy grey, bubbles	4	900	vesic	0.06%	0.95%	**0.89%**
CTD08-301	clear black, faint bands	4	900	vesic	0.02%	1.07%	**0.98%**
CTD8S-302	semi-opaque grey with swirled bands	3	875	vesic	0.04%	1.12%	**1.06%**
CTD12-302	opaque tobacco brown	4	900	vesic	0.16%	1.16%	**1.10%**
CTD05-303	grey cloudy and banded	2	910	vesic	0.00%	1.17%	**1.11%**
CTD8S-301	semi-opaque green-grey	1,2	850, 910	vesic	0.08%	1.33%	**1.26%**
CTD06-303	irregular browns, semi-opaque	3	900	vesic	0.15%	1.36%	**1.30%**

Table E 2. Additional composition data on heated specimens.

Sample	FTIR H2O	FTIR OH	FTIR Total water	Titration Fe2O3	Titration FeO	WD-XRF Total Fe	EDXRF Total Iron
CTD10-301	0.19%	0.22%	0.41%	0.40%	0.64%	1.11%	1.25
CTD06-302	0.15%	0.35%	0.50%	0.50%	0.58%	1.14%	1.26
CTD10-303	0.16%	0.31%	0.47%	0.47%	0.57%	1.10%	1.11
CTD05-302	nm	nm	nm	0.76%	0.74%	1.31%	1.21
CTD10-305	0.10%	0.26%	0.37%	0.60%	0.49%	1.14%	1.28
CTD08-302	nm	nm	nm	0.48%	0.57%	1.13%	1.33
CTD12-303	0.97%	0.98%	1.95%	0.57%	0.51%	1.14%	1.29
CTD05-305	nm	nm	nm	0.56%	0.56%	1.18%	1.20
CTD08-301	nm	nm	nm	0.61%	0.78%	1.48%	1.28
CTD8S-302	nm	nm	nm	0.48%	0.58%	1.13%	1.28
CTD12-302	1.15%	0.91%	2.06%	0.51%	0.55%	1.12%	1.33
CTD05-303	nm	nm	nm	0.50%	0.57%	1.13%	1.30
CTD8S-301	nm	nm	nm	0.48%	0.61%	1.16%	1.22
CTD06-303	nm	nm	nm	0.49%	0.58%	1.13%	1.21

APPENDIX F:

ED-XRF and WD-XRF Tables: Elemental Composition Data by Specimen

Table F- 1. 1998 Analysis: ED-XRF ppm values for trace elements and element weight percent values for K and Ca, CTD only (data by individual specimen).

Table F-2. 2004 Analysis: ED-XRF ppm values for trace elements and element weight percent values for K and Ca, includes all three source areas: CTD, CTN, and CDM (data by individual specimen) [shaded rows are excluded samples].

Table F-3. WD-XRF ppm values for trace elements (data by individual specimen).

Table F-4. WD-XRF oxide weight percent values for major and minor elements (data by individual specimen).

Table F-5. WD-XRF computed element weight percent and ppm values for selected major and minor elements (data by specimen).

Table F-6. WD-XRF summary of means for computed element weight % and ppm values for selected major and minor elements.

Table F-1. 1998 Analysis: ED-XRF ppm values for trace elements and element weight percent values for K and Ca, CTD only (data by individual specimen).

Specimen	Source	Color	Analysis	K el wt%	Ca el wt%	Rb ppm	Sr ppm	Y ppm	Zr ppm	Nb ppm	Ba ppm	Ti ppm	Mn ppm	$Fe_2O_3^T$ el wt%	Fe/Mn ratio	Type REH	Zn ppm	Ga ppm	ED_issues?
GS1-001	CTD	0	ed-xrf	nm	nm	201	3	56	159	87	nm	431	597	1.20	nm	OR	89	19	good
GS1-002	CTD	0	ed-xrf	nm	nm	212	4	62	175	90	nm	438	620	1.22	nm	OR	92	26	good
GS1-003	CTD	0	ed-xrf	nm	nm	213	3	60	168	86	nm	420	611	1.23	21	OR	81	19	good
GS1-004	CTD	0	ed-xrf	nm	nm	202	4	61	167	89	nm	436	607	1.19	nm	OR	96	23	good
GS1-005	CTD	0	ed-xrf	nm	nm	200	4	63	164	89	nm	433	611	1.19	nm	OR	97	22	good
GS1-006	CTD	0	ed-xrf	nm	nm	205	3	59	170	87	nm	453	640	1.26	nm	OR	90	22	good
GS2-001	CTD	0	ed-xrf	nm	nm	196	4	56	160	87	nm	421	581	1.17	nm	OR	88	23	good
GS2-002	CTD	0	ed-xrf	nm	nm	212	4	62	168	89	nm	435	600	1.21	nm	OR	93	22	good
GS2-003	CTD	0	ed-xrf	nm	nm	199	3	60	164	83	nm	441	600	1.21	nm	OR	89	23	good
GS2-004	CTD	0	ed-xrf	nm	nm	206	3	59	163	86	nm	448	610	1.22	nm	OR	101	2	good
GS3-001	CTD	0	ed-xrf	nm	nm	200	4	56	160	83	nm	417	602	1.21	nm	OR	90	22	good
GS3-002	CTD	0	ed-xrf	nm	nm	202	0	58	163	85	nm	440	581	1.15	nm	OR	87	24	good
GS3-003	CTD	0	ed-xrf	nm	nm	196	3	59	165	89	nm	430	575	1.16	nm	OR	98	17	good
GS3-004	CTD	0	ed-xrf	nm	nm	207	3	58	170	89	nm	450	623	1.24	nm	OR	91	21	good
GS3-005	CTD	0	ed-xrf	nm	nm	207	3	60	164	88	nm	490	603	1.20	nm	OR	94	20	good
GS4-002	CTD	0	ed-xrf	nm	nm	193	3	58	160	84	nm	431	610	1.21	nm	OR	81	20	good
GS4-003	CTD	0	ed-xrf	nm	nm	190	3	55	157	83	nm	429	571	1.15	nm	OR	85	21	good
GS4-004	CTD	0	ed-xrf	nm	nm	192	4	56	157	84	nm	413	588	1.16	nm	OR	88	18	good
GS6A-1	CTD	0	ed-xrf	nm	nm	191	4	56	159	82	nm	440	596	1.17	20	OR	86	18	good
GS6A-2	CTD	0	ed-xrf	nm	nm	208	5	62	170	93	nm	460	605	1.22	20	OR	92	27	good
GS6A-4	CTD	0	ed-xrf	nm	nm	200	3	60	167	87	nm	449	617	1.22	20	OR	91	26	good
*GS8-1a	CTD	0	ed-xrf	nm	nm	200	4	59	164	87	nm	513	625	1.28	20	OR	86	18	good
GS8-2	CTD	0	ed-xrf	nm	nm	193	4	58	156	84	nm	451	600	1.19	21	OR	87	20	good
GS8-3	CTD	0	ed-xrf	nm	nm	196	5	60	166	91	nm	469	604	1.21	20	OR	77	27	good
*GS10-1a	CTD	0	ed-xrf	nm	nm	212	0	65	173	90	nm	489	633	1.28	20	OR	95	25	good
GS10B-2	CTD	0	ed-xrf	nm	nm	201	0	58	173	89	nm	470	595	1.22	19	OR	86	24	good
GS10-1	CTD	0	ed-xrf	nm	nm	190	3	55	153	82	nm	389	589	1.14	20	OR	84	24	good
*GS7-1	CTD	0	ed-xrf	nm	nm	192	4	54	159	84	nm	363	571	1.11	20	OR	87	23	good
*GS7B-1	CTD	0	ed-xrf	nm	nm	190	3	55	158	81	nm	362	575	1.12	20	OR	78	19	good
*GS8-1	CTD	0	ed-xrf	nm	nm	191	3	55	161	81	nm	403	571	1.12	20	OR	86	16	good
*Names of samples changed slightly to clarify those called GS10-1, GS7-1, GS7B-1, GS8-1 in the heat experiments (Appendix E) and in the analyses conducted after 1998																			

Table F-2. 2004 Analysis: ED-XRF ppm values for trace elements and element weight percent values for K and Ca, includes all three source areas: CTD, CTN, and CDM (data by individual specimen) [shaded rows are excluded samples].

Specimen	Source	Color	Analysis	K el wt%	Ca el wt%	Rb ppm	Sr ppm	Y ppm	Zr ppm	Nb ppm	Ba ppm	Ti ppm	Mn ppm	$Fe_2O_3^T$ el wt%	Fe/Mn ratio	REH Type	ED_issues?
CTD5-301	CTD	0	ed-xrf	3.71%	0.13%	214	3	60	175	91	nm	415	691	1.32	18	OR	good
CTD5-302	CTD	0	ed-xrf	3.58%	0.14%	187	6	59	158	85	nm	411	667	1.21	19	OR	good
CTD5-303	CTD	0	ed-xrf	4.95%	0.23%	209	6	65	177	96	nm	654	658	1.30	17	OR	poor data
CTD5-304	CTD	0	ed-xrf	3.44%	0.13%	198	4	60	168	81	nm	364	695	1.28	18	OR	good
CTD5-305	CTD	0	ed-xrf	3.73%	0.13%	194	3	60	165	85	nm	433	648	1.20	20	OR	good
CTD5-307	CTD	bt	ed-xrf	4.98%	0.32%	193	6	60	167	94	nm	719	614	1.19	20	OR	non-fresh surface
CTD5-308	CTD	0	ed-xrf	3.40%	0.12%	218	6	66	175	96	nm	326	727	1.41	19	OR	good
CTD5-309	CTD	0	ed-xrf	3.17%	0.11%	208	4	61	173	88	nm	285	767	1.38	20	OR	good
CTD6-301	CTD	0	ed-xrf	4.85%	0.29%	197	4	61	163	88	nm	676	618	1.18	20	OR	spherulite present
CTD6-302	CTD	0	ed-xrf	3.66%	0.14%	204	3	61	165	85	nm	416	680	1.26	20	OR	good
CTD6-303	CTD	b	ed-xrf	3.76%	0.13%	193	4	59	159	77	nm	425	673	1.21	20	OR	good
CTD6-304	CTD	0	ed-xrf	3.72%	0.16%	188	4	60	162	86	nm	456	609	1.14	18	OR	good
CTD7-301	CTD	0	ed-xrf	3.44%	0.13%	222	4	67	178	93	nm	361	695	1.39	20	OR	good
CTD7-302	CTD	0	ed-xrf	5.06%	0.28%	198	6	63	167	93	nm	721	597	1.17	20	OR	non-fresh surface
CTD8-301	CTD	0	ed-xrf	3.65%	0.13%	205	4	62	160	90	nm	398	679	1.28	20	OR	good
CTD8-302	CTD	0	ed-xrf	3.58%	0.13%	217	4	61	163	82	nm	381	682	1.33	19	OR	good
CTD8S-301	CTD	0	ed-xrf	3.66%	0.14%	195	5	61	158	85	nm	414	645	1.22	19	OR	good
CTD8S-302	CTD	0	ed-xrf	3.57%	0.13%	210	3	60	171	88	nm	383	385	1.28	19	OR	good
CTD10-301	CTD	0	ed-xrf	3.74%	0.14%	194	4	60	165	88	nm	427	671	1.25	19	OR	good
CTD10-302	CTD	0	ed-xrf	3.66%	0.14%	189	5	58	167	86	nm	424	644	1.20	18	OR	good
CTD10-303	CTD	0	ed-xrf	3.66%	0.14%	180	5	55	149	75	nm	459	616	1.11	18	OR	poor reflection geometry
CTD10-304	CTD	0	ed-xrf	3.80%	0.15%	173	5	57	160	85	nm	461	595	1.14	19	OR	good
CTD10-305	CTD	0	ed-xrf	3.62%	0.14%	206	4	62	169	88	nm	394	688	1.28	21	OR	good
CTD10-306	CTD	0	ed-xrf	3.39%	0.12%	210	4	61	175	94	nm	381	681	1.32	20	OR	poor reflection geometry
CTD12-301	CTD	t	ed-xrf	3.69%	0.15%	180	5	58	160	81	nm	428	652	1.21	19	OR	good
CTD12-302	CTD	b	ed-xrf	3.38%	0.12%	208	3	64	167	85	nm	346	705	1.33	19	OR	good
CTD12-303	CTD	b	ed-xrf	4.94%	0.29%	213	4	63	173	99	nm	686	636	1.29	20	OR	poor reflection geometry

Table F-2. Continued: 2004 Analysis: ED-XRF trace and minor elements for CTD, CTN, and CDM individual specimens.

Specimen	Source	Color	Analysis	K el wt%	Ca el wt%	Rb ppm	Sr ppm	Y ppm	Zr ppm	Nb ppm	Ba ppm	Ti ppm	Mn ppm	$Fe_2O_3^T$ el wt%	Fe/Mn ratio	REH Type	ED_issues?
CTD13-301	CTD	0	nm	nm	nm	nm	nm	nm	nm	nm	nm	nm	nm	nm	nm	nm	
CTDRM-301	CTD	0	ed-xrf	3.77%	0.14%	202	3	59	161	90	nm	419	654	1.21	20	OR	good
CTDRM-302	CTD	0	ed-xrf	4.46%	0.18%	194	4	59	158	83	nm	472	648	1.22	18	OR	non-fresh surface
CTDRM-303	CTD	m	ed-xrf	3.66%	0.12%	195	4	59	167	89	nm	398	640	1.23	18	OR	good
CTDRM-304	CTD	0	ed-xrf	3.65%	0.14%	177	6	60	152	78	nm	438	636	1.16	21	OR	poor reflection geometry
GS10-1	CTD	0	ed-xrf	nm	nm	190	3	55	153	82	nm	389	589	1.14	20	OR	data from 1998 analysis
GS7-1	CTD	0	ed-xrf	nm	nm	192	4	54	159	84	nm	363	571	1.11	20	OR	data from 1998 analysis
GS7B-1	CTD	0	ed-xrf	nm	nm	190	3	55	158	81	nm	362	575	1.12	20	OR	data from 1998 analysis
GS8-1	CTD	0	ed-xrf	nm	nm	191	3	55	161	*81	nm	403	571	1.12	20	OR	data from 1998 analysis
CDM-301	CDM	0	ed-xrf	3.82%	0.21%	143	10	42	153	49	nm	541	462	1.09	27	CDM	good
CDM-302	CDM	0	ed-xrf	3.69%	0.17%	157	10	44	160	50	nm	457	507	1.18	26	CDM	good
CDM-303	CDM	m	ed-xrf	3.58%	0.18%	156	6	40	156	47	nm	431	502	1.19	27	CDM	good
CDM-304	CDM	0	ed-xrf	3.56%	0.19%	150	9	40	152	50	nm	443	489	1.18	28	CDM	good
CDM-305	CDM	0	ed-xrf	3.47%	0.16%	161	6	41	158	48	nm	375	576	1.33	25	CDM	good
CDM-306	CDM	0	ed-xrf	3.74%	0.19%	148	7	40	153	52	nm	502	501	1.18	26	CDM	good
CDM-307	CDM	0	ed-xrf	3.79%	0.20%	138	10	37	144	43	nm	530	472	1.08	26	CDM	good
CDM-308	CDM	m	ed-xrf	3.75%	0.17%	151	40	41	150	44	nm	414	515	1.19	26	CDM	good
CDM-309	CDM	0	ed-xrf	3.82%	0.18%	150	6	45	162	51	nm	488	499	1.15	25	CDM	good
CDM-310	CDM	0	ed-xrf	3.73%	0.19%	153	9	42	155	53	nm	460	506	1.16	24	CDM	good
CDM-311	CDM	0	ed-xrf	3.52%	0.17%	151	9	41	147	42	nm	416	510	1.20	25	CDM	good
CDM-312	CDM	0	ed-xrf	3.70%	0.18%	152	6	38	146	49	nm	484	468	1.12	25	CDM	good
CTN-301	CTN	0	ed-xrf	4.10%	0.16%	149	8	47	133	65	nm	480	555	0.98	18	unk	phenocrysts present
CTN-302	CTN	0	ed-xrf	3.74%	0.15%	148	11	46	133	67	nm	468	547	0.99	18	unk	phenocrysts present
CTN-303	CTN	0	ed-xrf	3.65%	0.14%	188	6	62	148	80	nm	421	675	1.18	17	OR	poor reflection geometry
CTN-304	CTN	t	ed-xrf	3.62%	0.13%	201	4	57	156	88	nm	400	687	1.20	17	OR	good
CTN-305a	CTN	0	ed-xrf	3.53%	0.12%	201	4	61	163	82	nm	554	531	1.27	19	OR	good

Table F-2. Continued: 2004 Analysis: ED-XRF trace and minor elements for CTD, CTN, and CDM individual specimens.

Specimen	Source	Color	Analysis	K el wt%	Ca el wt%	Rb ppm	Sr ppm	Y ppm	Zr ppm	Nb ppm	Ba ppm	Ti ppm	Mn ppm	$Fe_2O_3^T$ el wt%	Fe/Mn ratio	REH Type	ED_issues?
CTN-306	CTN	0	ed-xrf	3.72%	0.15%	193	4	65	158	87	nm	442	635	1.12	18	OR	good
CTN-307	CTN	t	ed-xrf	3.59%	0.14%	206	6	61	161	89	nm	405	673	1.24	20	OR	good
CTN-308	CTN	0	ed-xrf	3.60%	0.14%	202	4	63	168	91	nm	400	689	1.27	19	OR	good

Data for specimens in 11 shaded rows excluded from summary analyses due to poor sample configuration or condition, or because the sample was inadvertently excluded from the sample group submitted for analysis (CTD13-301). Nine CTD sample specimens excluded from this analysis of ED-XRF results are as follows: CTD5-303, CTD5-307, CTD6-301, CTD7-302, CTD10-303, CTD10-306, CTD12-303, CTDRM-302, and CTDRM-304. Because only a single sample was included from locations RM2 and RM4, removal of the samples CTDRM-302 and CTDRM-304 effectively excludes both of the sample locations from the analysis, decreasing the total number of CTD locations from 14 to 12. One specimen from CTN also was excluded for the same reasons (CTN-303).

* Nb value for sample GS8-1 is here corrected to 81 ppm because the original value of 52 ppm is believed to be an error (see Steffen 2002:174; discussion in text and Table 4).

Table F-3. WD-XRF ppm values for trace elements (data by individual specimen).

Specimen	Source	Color	Analysis	Ba ppm	Cr ppm	Rb ppm	Sr ppm	Y ppm	Zr ppm	Nb ppm	Co ppm	Ni ppm	Cu ppm	Zn ppm
CDM-301	CDM	0	wd-xrf	58	<1	163	8	46	167	82	<1	0	1	59
CDM-302	CDM	0	wd-xrf	40	14	161	7	44	159	81	30	1	5	75
CDM-303	CDM	m	wd-xrf	<1	<1	163	8	45	164	83	13	1	2	82
CDM-304	CDM	0	wd-xrf	36	1	164	7	45	164	82	7	2	2	73
CDM-305	CDM	0	wd-xrf	65	1	164	8	45	166	82	<1	1	3	77
CDM-306	CDM	0	wd-xrf	93	4	164	8	45	164	82	6	1	3	76
CDM-307	CDM	0	wd-xrf	45	<1	164	8	46	164	82	<1	1	2	65
CDM-308	CDM	m	wd-xrf	75	<1	164	7	45	164	83	<1	1	2	78
CDM-309	CDM	0	wd-xrf	73	<1	164	8	45	163	83	<1	2	2	76
CDM-310	CDM	0	wd-xrf	51	1	164	8	45	164	82	9	2	5	75
CDM-311	CDM	0	wd-xrf	51	<1	163	8	45	163	82	5	<1	3	74
CDM-312	CDM	0	wd-xrf	88	<1	164	8	46	164	83	17	1	3	77
CTD10-301	CTD	0	wd-xrf	17	1	205	5	66	178	147	18	3	1	144
CTD10-302	CTD	0	wd-xrf	18	0	205	4	66	178	147	23	2	0	139
CTD10-303	CTD	0	wd-xrf	<1	0	205	4	66	177	146	4	3	1	140
CTD10-304	CTD	0	wd-xrf	26	0	206	4	66	179	146	<1	3	0	140
CTD10-305	CTD	0	wd-xrf	<1	0	205	4	66	178	146	3	1	3	143
CTD10-306	CTD	0	wd-xrf	60	0	205	4	66	178	146	6	1	2	141
CTD12-301	CTD	t	wd-xrf	26	1	205	4	66	178	146	33	2	3	141
CTD12-302	CTD	b	wd-xrf	<1	0	206	5	66	177	145	29	3	0	139
CTD12-303	CTD	b	wd-xrf	<1	0	205	4	66	179	147	23	2	1	143
CTD13-301	CTD	0	wd-xrf	<1	29	199	4	63	172	140	13	5	6	140
CTD5-301	CTD	0	wd-xrf	<1	17	200	4	64	172	141	7	3	4	140
CTD5-302	CTD	0	wd-xrf	<1	16	201	4	64	173	143	16	3	5	138
CTD5-303	CTD	0	wd-xrf	13	4	205	4	66	178	147	18	3	6	142
CTD5-304	CTD	0	wd-xrf	45	<1	205	4	66	178	147	16	3	2	140
CTD5-305	CTD	0	wd-xrf	25	<1	205	4	65	178	147	22	2	2	142
CTD5-307	CTD	bt	wd-xrf	9	<1	206	4	65	179	147	<1	2	0	140
CTD5-308	CTD	0	wd-xrf	<1	<1	205	4	66	178	146	<1	3	1	140
CTD5-309	CTD	0	wd-xrf	72	<1	206	4	65	179	147	12	2	1	140

Table F-3. Continued: WD-XRF ppm values for trace elements (data by individual specimen).

Specimen	Source	Color	Analysis	Ba ppm	Cr ppm	Rb ppm	Sr ppm	Y ppm	Zr ppm	Nb ppm	Co ppm	Ni ppm	Cu ppm	Zn ppm
CTD6-301	CTD	0	wd-xrf	12	1	205	4	66	178	148	5	2	1	142
CTD6-302	CTD	0	wd-xrf	21	<1	205	4	65	178	145	34	2	1	181
CTD6-303	CTD	b	wd-xrf	<1	<1	205	4	66	178	146	7	1	2	146
CTD6-304	CTD	0	wd-xrf	9	<1	206	4	65	177	146	22	2	2	146
CTD7-301	CTD	0	wd-xrf	1	<1	203	4	65	175	144	29	2	1	143
CTD7-302	CTD	0	wd-xrf	25	<1	205	4	66	178	147	5	1	1	127
CTD8-301	CTD	0	wd-xrf	<1	22	199	4	63	171	138	<1	4	5	139
CTD8-302	CTD	0	wd-xrf	39	1	205	4	66	179	146	13	2	0	141
CTD8S-301	CTD	0	wd-xrf	28	0	205	4	65	178	146	26	2	2	140
CTD8S-302	CTD	0	wd-xrf	19	<1	205	4	65	178	146	30	2	1	143
CTDRM-301	CTD	0	wd-xrf	<1	1	205	4	65	177	146	11	1	1	128
CTDRM-303	CTD	m	wd-xrf	2	<1	204	4	65	177	146	7	1	1	126
CTDRM-304	CTD	0	wd-xrf	33	<1	205	4	66	178	147	4	1	2	130
GS10-1	CTD	0	wd-xrf	<1	19	200	4	64	172	142	12	3	3	139
GS7-1	CTD	0	wd-xrf	<1	18	200	4	64	171	141	14	3	3	140
GS7B-1	CTD	0	wd-xrf	12	27	200	4	63	173	141	<1	5	5	141
GS8-1	CTD	0	wd-xrf	<1	22	200	5	64	174	141	5	3	4	140
CTN-301	CTN	0	wd-xrf	81	<1	167	10	47	149	111	4	1	3	84
CTN-302	CTN	0	wd-xrf	70	<1	166	11	48	152	111	<1	1	2	75
CTN-303	CTN	0	wd-xrf	20	<1	208	4	66	173	149	5	3	2	142
CTN-304	CTN	t	wd-xrf	20	1	209	4	67	173	150	38	1	1	144
CTN-305	CTN	0	wd-xrf	29	<1	209	4	67	172	150	14	1	1	142
CTN-306	CTN	0	wd-xrf	24	1	209	4	67	175	150	36	2	2	142
CTN-307	CTN	t	wd-xrf	2	<1	209	4	67	173	151	22	2	2	144
CTN-308	CTN	0	wd-xrf	33	<1	208	4	66	172	150	17	2	8	141

All ppm values reported as <1 were changed to 0 for summary analyses

Table F-4. WD-XRF oxide weight percent values for major and minor elements (data by individual specimen).

Specimen	Source	Color	SiO_2	TiO_2	Al_2O_3	Fe_2O_3	FeO	MnO	MgO	CaO	Na_2O	K_2O	H_2O-	H_20+	Total	Total Fe ((as Fe_2O_3)	LOI
CTD5-301	CTD	0	76.01%	0.080%	11.94%	0.51%	0.74%	0.074%	0.040%	0.41%	4.23%	4.31%	0.180%	1.33%	99.85%	1.330%	1.25%
CTD5-302	CTD	0	75.56%	0.081%	11.73%	0.76%	0.74%	0.074%	0.040%	0.41%	4.28%	4.31%	0.220%	0.73%	99.02%	1.310%	0.73%
CTD5-303	CTD	0	76.64%	0.081%	12.07%	0.50%	0.57%	0.077%	0.060%	0.41%	4.34%	4.36%	0.001%	0.00%	100.30%	1.130%	1.11%
CTD5-304	CTD	0	76.55%	0.081%	12.11%	0.52%	0.55%	0.076%	0.060%	0.41%	4.40%	4.36%	0.040%	0.73%	99.89%	1.130%	0.67%
CTD5-305	CTD	0	76.41%	0.083%	12.26%	0.56%	0.56%	0.075%	0.060%	0.41%	4.31%	4.32%	0.060%	0.95%	100.10%	1.180%	0.89%
CTD5-307	CTD	bt	75.09%	0.080%	11.83%	0.46%	0.59%	0.074%	0.001%	0.41%	4.34%	4.37%	0.001%	1.31%	98.55%	1.120%	1.24%
CTD5-308	CTD	0	76.94%	0.082%	12.11%	0.44%	0.59%	0.075%	0.030%	0.42%	4.33%	4.37%	0.090%	0.93%	100.40%	1.100%	0.86%
CTD5-309	CTD	0	75.70%	0.082%	11.95%	0.53%	0.56%	0.076%	0.070%	0.41%	4.33%	4.36%	0.100%	0.93%	99.27%	1.150%	0.87%
CTD6-301	CTD	0	76.07%	0.082%	12.58%	0.55%	0.55%	0.076%	0.059%	0.41%	4.28%	4.34%	0.039%	0.84%	99.97%	1.160%	0.78%
CTD6-302	CTD	0	76.72%	0.082%	12.24%	0.50%	0.58%	0.076%	0.050%	0.41%	4.33%	4.37%	0.060%	0.75%	100.20%	1.140%	0.69%
CTD6-303	CTD	b	75.44%	0.081%	12.14%	0.49%	0.58%	0.076%	0.060%	0.41%	4.30%	4.34%	0.150%	1.36%	99.43%	1.130%	1.30%
CTD6-304	CTD	0	76.56%	0.081%	12.24%	0.51%	0.56%	0.076%	0.060%	0.41%	4.31%	4.37%	0.078%	0.74%	100.00%	1.135%	0.68%
CTD7-301	CTD	0	76.34%	0.081%	12.13%	0.50%	0.57%	0.076%	0.060%	0.42%	4.32%	4.35%	0.020%	1.22%	100.10%	1.130%	1.16%
CTD7-302	CTD	0	76.18%	0.082%	11.99%	0.50%	0.57%	0.075%	0.070%	0.41%	4.32%	4.34%	0.001%	1.04%	99.58%	1.130%	0.98%
CTD8-301	CTD	0	76.27%	0.081%	11.98%	0.61%	0.78%	0.074%	0.040%	0.41%	4.23%	4.30%	0.020%	1.07%	99.86%	1.480%	0.98%
CTD8-302	CTD	0	76.61%	0.082%	12.18%	0.48%	0.57%	0.075%	0.070%	0.42%	4.33%	4.34%	0.060%	0.76%	99.99%	1.130%	0.70%
CTD8S-301	CTD	0	76.70%	0.080%	12.05%	0.48%	0.61%	0.075%	0.030%	0.41%	4.32%	4.33%	0.080%	1.33%	100.61%	1.160%	1.26%
CTD8S-302	CTD	0	76.28%	0.081%	12.08%	0.48%	0.58%	0.075%	0.070%	0.41%	4.32%	4.32%	0.040%	1.12%	99.86%	1.130%	1.06%
CTD10-301	CTD	0	76.72%	0.084%	12.10%	0.40%	0.64%	0.074%	0.030%	0.42%	4.31%	4.37%	0.001%	0.63%	99.78%	1.110%	0.56%
CTD10-302	CTD	0	76.74%	0.080%	12.02%	0.46%	0.58%	0.074%	0.030%	0.41%	4.30%	4.36%	0.170%	0.72%	99.94%	1.100%	0.66%
CTD10-303	CTD	0	76.54%	0.080%	12.08%	0.47%	0.57%	0.074%	0.030%	0.41%	4.31%	4.34%	0.001%	0.78%	99.68%	1.100%	0.72%
CTD10-304	CTD	0	76.70%	0.081%	12.06%	0.46%	0.58%	0.074%	0.030%	0.41%	4.33%	4.35%	0.020%	1.02%	100.10%	1.100%	0.96%
CTD10-305	CTD	0	76.83%	0.082%	12.14%	0.60%	0.49%	0.076%	0.064%	0.41%	4.35%	4.37%	0.075%	0.57%	100.10%	1.140%	0.52%
CTD10-306	CTD	0	76.62%	0.081%	12.18%	0.54%	0.54%	0.077%	0.056%	0.41%	4.34%	4.38%	0.015%	0.69%	99.93%	1.140%	0.63%
CTD12-301	CTD	t	76.43%	0.082%	12.10%	0.46%	0.58%	0.074%	0.030%	0.41%	4.31%	4.32%	0.020%	1.34%	100.20%	1.100%	1.28%
CTD12-302	CTD	b	76.07%	0.082%	12.00%	0.51%	0.55%	0.076%	0.090%	0.42%	4.31%	4.35%	0.160%	1.16%	99.78%	1.120%	1.10%
CTD12-303	CTD	b	76.26%	0.081%	12.10%	0.57%	0.51%	0.076%	0.060%	0.41%	4.31%	4.34%	0.060%	0.90%	99.68%	1.140%	0.84%
CTD13-301	CTD	0	76.26%	0.080%	11.92%	0.57%	0.82%	0.074%	0.040%	0.41%	4.27%	4.32%	0.130%	0.82%	99.71%	1.480%	0.73%

Table F-4. Continued: WD-XRF oxide weight percent values for major and minor elements (data by individual specimen).

Specimen	Source	Color	SiO_2	TiO_2	Al_2O_3	Fe_2O_3	FeO	MnO	MgO	CaO	Na_2O	K_2O	H_2O-	H_20+	Total	Total Fe ((as Fe_2O_3)	LOI
CTDRM-301	CTD	0	76.87%	0.083%	12.09%	0.66%	0.45%	0.076%	0.055%	0.41%	4.24%	4.45%	0.001%	0.40%	99.78%	1.160%	0.35%
CTDRM-303	CTD	m	76.20%	0.083%	11.95%	1.09%	0.04%	0.076%	0.061%	0.41%	4.07%	4.71%	0.060%	0.28%	99.15%	1.130%	0.28%
CTDRM-304	CTD	0	75.26%	0.080%	11.80%	0.39%	0.59%	0.075%	0.059%	0.41%	4.32%	4.35%	0.001%	1.38%	98.71%	1.050%	1.32%
GS10-1	CTD	0	74.83%	0.080%	11.72%	0.51%	0.73%	0.073%	0.040%	0.41%	4.18%	4.29%	0.018%	1.15%	98.03%	1.320%	1.07%
GS7-1	CTD	0	76.48%	0.082%	12.02%	0.55%	0.72%	0.074%	0.050%	0.42%	4.28%	4.33%	0.060%	1.38%	100.40%	1.350%	1.30%
GS7B-1	CTD	0	75.70%	0.076%	11.91%	0.52%	0.58%	0.074%	0.040%	0.41%	4.27%	4.28%	0.100%	1.85%	99.81%	1.170%	1.79%
GS8-1	CTD	0	75.51%	0.080%	11.81%	0.53%	0.80%	0.077%	0.060%	0.42%	4.28%	4.33%	0.460%	1.36%	99.72%	1.420%	1.27%
CDM-301	CDM	0	76.75%	0.100%	12.49%	0.49%	0.57%	0.055%	0.072%	0.47%	4.20%	4.57%	0.030%	0.38%	100.20%	1.120%	0.32%
CDM-302	CDM	0	76.33%	0.098%	12.28%	0.55%	0.75%	0.054%	0.050%	0.47%	4.14%	4.53%	0.080%	0.32%	99.65%	1.380%	0.24%
CDM-303	CDM	m	76.16%	0.099%	12.71%	1.04%	0.07%	0.055%	0.080%	0.47%	4.16%	4.53%	0.060%	0.29%	99.72%	1.110%	0.28%
CDM-304	CDM	0	76.04%	0.098%	12.36%	1.00%	0.61%	0.056%	0.001%	0.47%	4.20%	4.52%	0.001%	0.98%	100.30%	1.680%	0.91%
CDM-305	CDM	0	77.40%	0.099%	12.63%	0.52%	0.55%	0.056%	0.080%	0.48%	4.18%	4.54%	0.001%	0.33%	100.90%	1.130%	0.27%
CDM-306	CDM	0	76.08%	0.100%	12.36%	0.48%	0.58%	0.055%	0.090%	0.48%	4.18%	4.56%	0.180%	0.42%	99.84%	1.120%	0.36%
CDM-307	CDM	0	76.59%	0.099%	12.31%	0.48%	0.58%	0.055%	0.070%	0.48%	4.16%	4.61%	0.001%	0.42%	99.85%	1.120%	0.36%
CDM-308	CDM	m	75.94%	0.099%	12.30%	1.02%	0.08%	0.056%	0.070%	0.47%	4.18%	4.66%	0.130%	0.48%	99.68%	1.110%	0.47%
CDM-309	CDM	0	76.30%	0.098%	12.34%	0.44%	0.61%	0.055%	0.071%	0.47%	4.18%	4.53%	0.160%	0.50%	99.99%	1.120%	0.43%
CDM-310	CDM	0	75.82%	0.099%	12.67%	0.46%	0.60%	0.056%	0.120%	0.48%	4.17%	4.53%	0.000%	0.66%	99.67%	1.130%	0.59%
CDM-311	CDM	0	75.73%	0.099%	12.30%	0.47%	0.59%	0.056%	0.080%	0.48%	4.19%	4.57%	0.310%	0.25%	99.12%	1.130%	0.18%
CDM-312	CDM	0	76.34%	0.098%	12.42%	0.41%	0.63%	0.056%	0.080%	0.48%	4.21%	4.56%	0.020%	0.41%	99.71%	1.110%	0.34%
CTN-301	CTN	0	76.36%	0.113%	12.20%	0.70%	0.22%	0.063%	0.084%	0.46%	3.66%	5.13%	0.020%	0.49%	99.50%	0.950%	0.47%
CTN-302	CTN	0	75.32%	0.112%	11.97%	0.71%	0.23%	0.065%	0.087%	0.47%	4.00%	4.75%	0.001%	0.48%	98.19%	0.970%	0.45%
CTN-303	CTN	0	75.49%	0.081%	11.92%	0.63%	0.43%	0.076%	0.070%	0.41%	4.34%	4.33%	0.001%	1.19%	98.97%	1.110%	1.14%
CTN-304	CTN	t	76.33%	0.081%	12.07%	0.46%	0.58%	0.077%	0.060%	0.41%	4.33%	4.33%	0.060%	0.98%	99.77%	1.110%	0.92%
CTN-305	CTN	0	76.25%	0.081%	12.35%	0.50%	0.56%	0.076%	0.061%	0.41%	4.32%	4.34%	0.036%	1.10%	100.10%	1.120%	1.03%
CTN-306	CTN	0	75.21%	0.081%	11.83%	0.50%	0.57%	0.076%	0.060%	0.41%	4.33%	4.34%	0.020%	1.06%	98.49%	1.130%	1.00%
CTN-307	CTN	t	76.53%	0.081%	12.34%	0.44%	0.60%	0.077%	0.057%	0.41%	4.30%	4.30%	0.001%	1.28%	100.40%	1.110%	1.21%
CTN-308	CTN	0	75.36%	0.079%	11.93%	0.47%	0.57%	0.075%	0.070%	0.42%	4.34%	4.29%	0.160%	1.09%	98.85%	1.100%	1.03%

Table F-5. WD-XRF computed element weight percent and ppm values for selected major and minor elements (data by specimen).

Specimen	Source	Color	Analysis	TiO_2 ox wt%	Ti elwt%	Ti ppm	MnO ox wt%	Mn el wt%	Mn ppm	CaO ox wt%	Ca el wt%	Ca ppm	K2O ox wt%	K el wt%	K ppm
CTD5-301	CTD	0	wd-xrf	0.080%	0.048%	479	0.074%	0.057%	573	0.41%	0.293%	2932	4.31%	3.577%	35773
CTD5-302	CTD	0	wd-xrf	0.081%	0.049%	485	0.074%	0.057%	573	0.41%	0.293%	2932	4.31%	3.577%	35773
CTD5-303	CTD	0	wd-xrf	0.081%	0.049%	485	0.077%	0.060%	596	0.41%	0.293%	2932	4.36%	3.619%	36188
CTD5-304	CTD	0	wd-xrf	0.081%	0.049%	485	0.076%	0.059%	588	0.41%	0.293%	2932	4.36%	3.619%	36188
CTD5-305	CTD	0	wd-xrf	0.083%	0.050%	497	0.075%	0.058%	581	0.41%	0.293%	2932	4.32%	3.586%	35856
CTD5-307	CTD	bt	wd-xrf	0.080%	0.048%	479	0.074%	0.057%	573	0.41%	0.293%	2932	4.37%	3.627%	36271
CTD5-308	CTD	0	wd-xrf	0.082%	0.049%	491	0.075%	0.058%	581	0.42%	0.300%	3003	4.37%	3.627%	36271
CTD5-309	CTD	0	wd-xrf	0.082%	0.049%	491	0.076%	0.059%	588	0.41%	0.293%	2932	4.36%	3.619%	36188
CTD6-301	CTD	0	wd-xrf	0.082%	0.049%	491	0.076%	0.059%	588	0.41%	0.293%	2932	4.34%	3.602%	36022
CTD6-302	CTD	0	wd-xrf	0.082%	0.049%	491	0.076%	0.059%	588	0.41%	0.293%	2932	4.37%	3.627%	36271
CTD6-303	CTD	b	wd-xrf	0.081%	0.049%	485	0.076%	0.059%	588	0.41%	0.293%	2932	4.34%	3.602%	36022
CTD6-304	CTD	0	wd-xrf	0.081%	0.049%	485	0.076%	0.059%	588	0.41%	0.293%	2932	4.37%	3.627%	36271
CTD7-301	CTD	0	wd-xrf	0.081%	0.049%	485	0.076%	0.059%	588	0.42%	0.300%	3003	4.35%	3.611%	36105
CTD7-302	CTD	0	wd-xrf	0.082%	0.049%	491	0.075%	0.058%	581	0.41%	0.293%	2932	4.34%	3.602%	36022
CTD8-301	CTD	0	wd-xrf	0.081%	0.049%	485	0.074%	0.057%	573	0.41%	0.293%	2932	4.30%	3.569%	35690
CTD8-302	CTD	0	wd-xrf	0.082%	0.049%	491	0.075%	0.058%	581	0.42%	0.300%	3003	4.34%	3.602%	36022
CTD8S-301	CTD	0	wd-xrf	0.080%	0.048%	479	0.075%	0.058%	581	0.41%	0.293%	2932	4.33%	3.594%	35939
CTD8S-302	CTD	0	wd-xrf	0.081%	0.049%	485	0.075%	0.058%	581	0.41%	0.293%	2932	4.32%	3.586%	35856
CTD10-301	CTD	0	wd-xrf	0.084%	0.050%	503	0.074%	0.057%	573	0.42%	0.300%	3003	4.37%	3.627%	36271
CTD10-302	CTD	0	wd-xrf	0.080%	0.048%	479	0.074%	0.057%	573	0.41%	0.293%	2932	4.36%	3.619%	36188
CTD10-303	CTD	0	wd-xrf	0.080%	0.048%	479	0.074%	0.057%	573	0.41%	0.293%	2932	4.34%	3.602%	36022
CTD10-304	CTD	0	wd-xrf	0.081%	0.049%	485	0.074%	0.057%	573	0.41%	0.293%	2932	4.35%	3.611%	36105
CTD10-305	CTD	0	wd-xrf	0.082%	0.049%	491	0.076%	0.059%	588	0.41%	0.293%	2932	4.37%	3.627%	36271
CTD10-306	CTD	0	wd-xrf	0.081%	0.049%	485	0.077%	0.060%	596	0.41%	0.293%	2932	4.38%	3.635%	36354
CTD12-301	CTD	t	wd-xrf	0.082%	0.049%	491	0.074%	0.057%	573	0.41%	0.293%	2932	4.32%	3.586%	35856
CTD12-302	CTD	b	wd-xrf	0.082%	0.049%	491	0.076%	0.059%	588	0.42%	0.300%	3003	4.35%	3.611%	36105
CTD12-303	CTD	b	wd-xrf	0.081%	0.049%	485	0.076%	0.059%	588	0.41%	0.293%	2932	4.34%	3.602%	36022
CTD13-301	CTD	0	wd-xrf	0.080%	0.048%	479	0.074%	0.057%	573	0.41%	0.293%	2932	4.32%	3.586%	35856

Table F-5. Continued: WD-XRF computed element weight percent and ppm values for selected major and minor elements.

Specimen	Source	Color	Analysis	TiO_2 ox wt%	Ti elwt%	Ti ppm	MnO ox wt%	Mn el wt%	Mn ppm	CaO ox wt%	Ca el wt%	Ca ppm	K2O ox wt%	K el wt%	K ppm
CTDRM-301	CTD	0	wd-xrf	0.083%	0.050%	497	0.076%	0.059%	588	0.41%	0.293%	2932	4.45%	3.694%	36935
CTDRM-303	CTD	m	wd-xrf	0.083%	0.050%	497	0.076%	0.059%	588	0.41%	0.293%	2932	4.71%	3.909%	39093
CTDRM-304	CTD	0	wd-xrf	0.080%	0.048%	479	0.075%	0.058%	581	0.41%	0.293%	2932	4.35%	3.611%	36105
GS10-1	CTD	0	wd-xrf	0.080%	0.048%	479	0.073%	0.057%	565	0.41%	0.293%	2932	4.29%	3.561%	35607
GS7-1	CTD	0	wd-xrf	0.082%	0.049%	491	0.074%	0.057%	573	0.42%	0.300%	3003	4.33%	3.594%	35939
GS7B-1	CTD	0	wd-xrf	0.076%	0.046%	455	0.074%	0.057%	573	0.41%	0.293%	2932	4.28%	3.552%	35524
GS8-1	CTD	0	wd-xrf	0.080%	0.048%	479	0.077%	0.060%	596	0.42%	0.300%	3003	4.33%	3.594%	35939
CDM-301	CDM	0	wd-xrf	0.100%	0.060%	599	0.055%	0.043%	426	0.47%	0.336%	3361	4.57%	3.793%	37931
CDM-302	CDM	0	wd-xrf	0.098%	0.059%	587	0.054%	0.042%	418	0.47%	0.336%	3361	4.53%	3.760%	37599
CDM-303	CDM	m	wd-xrf	0.099%	0.059%	593	0.055%	0.043%	426	0.47%	0.336%	3361	4.53%	3.760%	37599
CDM-304	CDM	0	wd-xrf	0.098%	0.059%	587	0.056%	0.043%	433	0.47%	0.336%	3361	4.52%	3.752%	37516
CDM-305	CDM	0	wd-xrf	0.099%	0.059%	593	0.056%	0.043%	433	0.48%	0.343%	3432	4.54%	3.768%	37682
CDM-306	CDM	0	wd-xrf	0.100%	0.060%	599	0.055%	0.043%	426	0.48%	0.343%	3432	4.56%	3.785%	37848
CDM-307	CDM	0	wd-xrf	0.099%	0.059%	593	0.055%	0.043%	426	0.48%	0.343%	3432	4.61%	3.826%	38263
CDM-308	CDM	m	wd-xrf	0.099%	0.059%	593	0.056%	0.043%	433	0.47%	0.336%	3361	4.66%	3.868%	38678
CDM-309	CDM	0	wd-xrf	0.098%	0.059%	587	0.055%	0.043%	426	0.47%	0.336%	3361	4.53%	3.760%	37599
CDM-310	CDM	0	wd-xrf	0.099%	0.059%	593	0.056%	0.043%	433	0.48%	0.343%	3432	4.53%	3.760%	37599
CDM-311	CDM	0	wd-xrf	0.099%	0.059%	593	0.056%	0.043%	433	0.48%	0.343%	3432	4.57%	3.793%	37931
CDM-312	CDM	0	wd-xrf	0.098%	0.059%	587	0.056%	0.043%	433	0.48%	0.343%	3432	4.56%	3.785%	37848
CTN-301	CTN	0	wd-xrf	0.113%	0.068%	676.9	0.063%	0.049%	488	0.46%	0.329%	3289	5.13%	4.258%	42579
CTN-302	CTN	0	wd-xrf	0.112%	0.067%	670.9	0.065%	0.050%	503	0.47%	0.336%	3361	4.75%	3.943%	39425
CTN-303	CTN	0	wd-xrf	0.081%	0.049%	485	0.076%	0.059%	588	0.41%	0.293%	2932	4.33%	3.594%	35939
CTN-304	CTN	t	wd-xrf	0.081%	0.049%	485	0.077%	0.060%	596	0.41%	0.293%	2932	4.33%	3.594%	35939
CTN-305	CTN	0	wd-xrf	0.081%	0.049%	485	0.076%	0.059%	588	0.41%	0.295%	2953	4.34%	3.602%	36022
CTN-306	CTN	0	wd-xrf	0.081%	0.049%	485	0.076%	0.059%	588	0.41%	0.293%	2932	4.34%	3.602%	36022
CTN-307	CTN	t	wd-xrf	0.081%	0.049%	485	0.077%	0.060%	596	0.41%	0.293%	2932	4.30%	3.569%	35690
CTN-308	CTN	0	wd-xrf	0.079%	0.047%	473	0.075%	0.058%	581	0.42%	0.300%	3003	4.29%	3.561%	35607

Table F-6. WD-XRF summary of means for computed element weight % and ppm values for selected major and minor elements.

LOCATION		Ti el wt%/100	Ti ppm	Mn el wt%/100	Mn ppm	Ca el wt%/100	Ca ppm	K el wt%/100	K ppm
CDM	N	12	12	12	12	12	12	12	12
	Min	0.00059	587	0.000418	418	0.00336	3,361	0.0375	37,516
	Max	0.00060	599	0.000433	433	0.00343	3,432	0.0387	38,678
	Mean	0.0005920	592.01	0.0004289	428.93	0.0033963	3,396.25	0.0378411	37,841.08
	SD	0.00000430	4.299	0.00000517	5.175	0.00003734	37.340	0.00033846	338.461
	CV	0.73	0.73	1.21	1.21	1.10	1.10	0.89	0.89
CTD	N	35	35	35	35	35	35	35	35
	Min	0.00046	455	0.000565	565	0.00293	2,932	0.0355	35,524
	Max	0.00050	503	0.000596	596	0.00300	3,003	0.0391	39,093
	Mean	0.0004860	486.05	0.0005814	581.38	0.0029458	2,945.80	0.0361406	36,140.57
	SD	0.00000824	8.237	0.00000835	8.347	0.00002902	29.018	0.00057338	573.377
	CV	1.69	1.69	1.44	1.44	0.99	0.99	1.59	1.59
CTN	N	6	6	6	6	6	6	6	6
	Min	0.00047	473	0.000581	581	0.00293	2,932	0.0356	35,607
	Max	0.00049	485	0.000596	596	0.00300	3,003	0.0360	36,022
	Mean	0.0004832	483.19	0.0005895	589.53	0.0029470	2,946.99	0.0358698	35,869.83
	SD	0.00000489	4.891	0.00000583	5.826	0.00002875	28.749	0.00017737	177.369
	CV	1.01	1.01	0.99	0.99	0.98	0.98	0.49	0.49
CTNo	N	2	2	2	2	2	2	2	2
	Min	0.00067	671	0.000488	488	0.00329	3,289	0.0394	39,425
	Max	0.00068	677	0.000503	503	0.00336	3,361	0.0426	42,579
	Mean	0.0006739	673.88	0.0004954	495.36	0.0033248	3,324.75	0.0410020	41,002.00
	SD	0.00000424	4.236	0.00001095	10.946	0.00005056	50.558	0.00223021	2,230.215
	CV	0.63	0.63	2.21	2.21	1.52	1.52	5.44	5.44
Total	N	55	55	55	55	55	55	55	55
	Min	0.00046	455	0.000418	418	0.00293	2,932	0.0355	35,524
	Max	0.00068	677	0.000596	596	0.00343	3,432	0.0426	42,579
	Mean	0.0005157	515.68	0.0005459	545.88	0.0030580	3,057.99	0.0366588	36,658.84
	SD	0.00005438	54.380	0.00006494	64.943	0.00019628	196.283	0.00125613	1,256.125
	CV	10.55	10.55	11.90	11.90	6.42	6.42	3.43	3.43

REFERENCES

Acklen, J. C. (editor)
1993 *Archaeological Site Testing for the Ojo Line Extension 345kV Transmission Project in the Jemez Mountains, New Mexico.* SFNF Report 1990-10-030G. Mariah Associates, Inc. Report MAI 527-9. Public Service Company of New Mexico, Albuquerque.

Aldrich, M. J., Jr.
1986 Tectonics of the Jemez Mountains and the Rio Grande Rift. *Journal of Geophysical Research* 91(B2):1753-1762.

Allen, C. D.
2001 Fire and Vegetation History of the Jemez Mountains. In *Water, Watersheds, and Land Use in New Mexico: Impacts of Population Growth on Natural Resources, Santa Fe Region, 2001*, edited by P. S. Johnson, pp. 29-33. New Mexico Decision Makers-Field Guide No. 1. New Mexico Bureau of Mines and Mineral Resources, Socorro.

Ambrose, W. R.
1976 Intrinsic Hydration Rate Dating of Obsidian. In *Advances in Obsidian Glass Studies: Archaeological and Geochemical Perspectives*, edited by R. E. Taylor, pp. 81-105. Noyes Press, New Jersey.

1998 Obsidian Hydration Dating at a Recent Age Obsidian Mining Site in Papua, New Guinea. In *Archaeological Obsidian Studies: Method and Theory*, edited by M. S. Shackley, pp. 205-222. Advances in Archaeological and Museum Science, Vol. 3, M. J. Aitken, E. V. Sayre and R. E. Taylor, general editor. Plenum Press, New York.

Ander, M. E., G. Heiken, J. C. Eichelberger, A. W. Laughlin, and S. Husetis
1981 *Geological and Geophysical Investigations of the Zuni Volcanic Field, New Mexico*. Los Alamos National Lab Report LA-8827-MS, Los Alamos, New Mexico. From website: http://volcano.und.nodak.edu/vwdocs/volc_images/ north_america/ mccartys_flow.html.

Anderson, J., and T. M. Origer
1997 Adding a Little Fuel to the Fire: Some Thoughts on Fire and Obsidian Hydration. *International Association for Obsidian Studies Bulletin* 19:17-20.

Anovitz, L. M., J. M. Elam, L. R. Riciputi, and D. R. Cole
1999 The Failure of Obsidian Hydration Dating: Sources, Implications, and New Directions. *Journal of Archaeological Science* 26:735-752.

2004 Isothermal Time-Series Determination of the Rate of Diffusion of Water in Pachuca Obsidian. *Archaeometry* 46(2):301-326.

Baldwin, A. R., J. M. Bremer, and M. L. Elliott
2002 Connecting the Dots: Recent Fire Sequencing, Fire Effects to Heritage Resources and Archaeological Interpretation on the East Side of the Jemez Mountains, New Mexico: The La Mesa, Dome, Oso, and Cerro Grande Fires. Paper presented at the 67th Annual Meeting of the Society for American Archaeology, Denver.

Baugh, T. G., and F. W. Nelson, Jr.
1987 New Mexico Obsidian Sources and Exchange on the Southern Plains. *Journal of Field Archaeology* 14:313-329.

Beck, C., and G. T. Jones
1994 Dating Surface Assemblages Using Obsidian Hydration. In *Dating in Exposed and Surface Contexts*, edited by C. Beck, pp. 47-76. University of New Mexico, Albuquerque.

2000 Obsidian Hydration Dating, Past and Present. In *It's About Time: A History of Archaeological Dating in North America,* edited by S. E. Nash, pp. 124-151. The University of Utah Press, Salt Lake City.

Bennett, P. S., and M. Kunzmann
1985 *Effects of Heating on Artifacts: A Brief Report of Work Conducted at the Western Archeological and Conservation Center, Tucson*. Preliminary Report: Not for Citation or Publication. Draft Ms. on File, NPS Western Archeological and Conservation Center, Tucson.

Benson, A.
2002 Meadow Canyon Prescribed Burn: Effects of Fire on Obsidian Hydration Bands. In *The Effects of Fire and Heat on Obsidian*, edited by J. Loyd, T. M. Origer and D. A. Fredrickson, pp. 95-112. US DOI, Bureau of Land Management. Cultural Resources Publication, Anthropology-Fire History.

Bowen, B. M.
1989 *Los Alamos Climatology*. Los Alamos National Laboratory, Los Alamos, New Mexico.

Buenger, B. A.
2003 The Impact of Wildland and Prescribed Fire on Archaeological Resources. Unpublished Ph.D. Dissertation, Department of Anthropology, University of Kansas.

Cartledge, T. R.
1987 *Proposed Changes to Dome Unit Data Recovery Plan*. USDA Forest Service, Santa Fe National Forest Report 1982-10-011H. Copies available from SFNF, Supervisor's Office, Santa Fe.

1996 Heritage Resources and Fire Management: A Resource Management Crossroads. In *Fire Effects in Southwestern Forests: Proceedings of the Second La Mesa Fire Symposium*, edited by C. D. Allen, pp. 206-214. General Technical Report RM-GTR-286. USDA Forest Service, Rocky Mountain Forest and Range Experimental Station, Fort Collins, Colorado.

Connolly, J. R., and J. W. Husler
1990 *NWRT Department Technical Procedure TP-61: Procedures for Laboratory Sample Bulk Chemical Determination, Rev. A*. Sandia National Laboratory.

Connor, M. A., and K. P. Cannon
1991 Forest Fires as a Site Formation Process in the Rocky Mountains of Northwestern Wyoming. *Archaeology in Montana* 32(2):1-14.

Davis, L. B., S. A. Aaberg, and J. G. Schmitt
1995 Archaeological Fieldwork at Yellowstone's Obsidian Cliff. *Park Science: A Resource Management Bulletin,* Spring 1992. USDI National Park Service.

Deal, K.
1997 Fire Histories, Fuel Loads, and Obsidian: Preliminary Results of a Prescribed Burn Experiment on the Eldorado National Forest. Paper presented at the California Fuels Committee Meeting, Placerville, California.

1999 Draft: Fire Effects to Flaked Stone, Ground Stone, and Other Stone Artifacts. In *USDA Rainbow Series Publication: Fire Effects to Cultural Resources: IN PREPARATION*.

Deal, K., and D. McLemore
2002 Effects of Prescribed Fire on Obsidian and Implications for Past Landscape Condition. In *The Effects of Fire and Heat on Obsidian*, edited by J. M. Loyd, T. M. Origer and D. A. Fredrickson, pp. 15-43. US DOI, Bureau of Land Management. Cultural Resources Publication, Anthropology-Fire History.

DeBano, L. F., P. H. Dunn, and D. E. Conrad
1977 Fire's Effects on Physical and Chemical Properties of Chaparral Soils. In *Environmental Consequences of Fire and Fuel Management in Mediterranean Ecosystems*, pp. 65-74. USDA Forest Service General Technical Report WO-3.

Doell, R. G., G. G. B. Dalrymple, R. L. Smith, and R. A. Bailey
1968 Paleomagnetism, Potassium-Argon, and the Geology of Rhyolites and Associated Rocks of the Valles Caldera, New Mexico. In *Studies in Volcanology, Geological Society of America Memoir 116*, edited by R. A. Coats, R. L. Hay and C. A. Anderson, pp. 211-248.

Dunbar, N. W., and P. R. Kyle
1986 H_2O and Cl Contents, and Temperature of Taupo Volcanic Zone Rhyolitic Magmas. In *International Volcanological Congress, Abstracts*, pp. 148, New Zealand.

1992 Volatile contents of obsidian clasts in tephra from the Taupo Volcanic Zone, New Zealand: Implications to eruptive processes. *Journal of Volcanology and Geothermal Research* 49:127-145.

Duncan, F.
1990 *Long Mesa Fire 1989, Fire Effects and Cultural Resources: An Annotated Bibliography*. Long Mesa Fire Series, Publication No. 2. National Park Service, Division of Research and Cultural Resource Management, Mesa Verde National Park, Colorado.

Dunnell, R. C.
1971 *Systematics in Prehistory*. Reprint of the 1st edition: Blackburn Press, Caldwell, New Jersey.

Dunnell, R. C., and W. S. Dancey
1983 The Siteless Survey: A Regional Scale Data Collection Strategy. In *Advances in Archaeological Method and Theory*, edited by M. B. Schiffer, pp. 267-287. vol. 6. Academic Press, New York.

Eichelberger, J. C., and H. R. Westrich
1983 Behavior of Water in Rhyolitic Magmas at Shallow Depth. *EOS* 64:338.

Elliott, M. L.
1999 The Dome Fire Archaeology Project of 1996-7: A Summary Report. Bandelier National Monument. Copies available from Santa Fe National Forest, Santa Fe.

Elliott, M. L., L. C. Schub, M. M. Ensey, and M. J. Brennan
1998 Appendix C. Dome Fire Cultural Resources Damage Assessment and Treatment Project - 1997 Progress Report. In *1996 Dome Fire Emergency Fire Rehabilitation: A Draft Report*, edited by C. Sydoriak, E. Matic, M. L. Elliott and E. Ruby. Bandelier National Monument.

Ericson, J. E.
1975 New Results in Obsidian Hydration Dating. *World Archaeology* 7:151-159.

1981 *Exchange and Production Systems in California Prehistory: The Results of Hydration Dating and Chemical Characterization of Obsidian Sources*. BAR International Series 110. B.A.R., Oxford, England.

1988 Obsidian Hydration Rate Development. In *Materials Research Society*

Symposium Proceedings, Vol. 123, edited by E. V. Sayre, P. Vandiver, J. Druzik, and C. M. Stevenson, pp. 215-224. Materials Research Society, Pittsburgh.

Ericson, J., and R. Berger
1976 Physics and Chemistry of the Hydration Process in Obsidians, II: Experiments and Measurements. In *Advances in Obsidian Glass Studies, edited by R. E. Taylor*, pp. 46-62. Noyes Press, Park Ridge, New Jersey.

Ericson, J., J. MacKenzie, and R. Berger
1976 Physics and Chemistry of the Hydration Process in Obsidians, I: Theoretical Implications. In *Advances in Obsidian Glass Studies*, edited by R. E. Taylor, pp. 25-45. Noyes Press, Park Ridge, New Jersey.

Foley, R.
1981 Off-Site Archaeology: An Alternative Approach for the Short-Sited. In *Patterns of the Past: Essays in Honor of David Clarke*, edited by I. Hodder, G. Isaac and G. Hammond, pp. 157-183. Cambridge University Press, London.

Foxx, T. S., and L. D. Potter
1978 *Fire Ecology at Bandelier National Monument*. Unpublished report on file, Bandelier National Monument, New Mexico.

Fréchette, V. D.
1990 *Failure Analysis of Brittle Materials*. Advances in Ceramics Vol. 28. The American Ceramic Society, Westerville, Ohio.

Fredrickson, D. A.
1984 The Use of Obsidian Analyses to Establish "Units of Contemporaneity", Paper presented at Annual Meeting of the Society for American Archaeology, Portland, April 1984.

Freter, A.
1993 Obsidian-Hydration Dating: Its past, present, and future application in Mesoamerica. *Ancient Mesoamerica* 4:285-303.

Friedman, I.
1989 Are extrusive rhyolites produced from permeable foam eruptions? *Bulletin of Volcanology* 51:69-71.

Friedman, I., and W. Long
1976 Hydration Rate of Obsidian. *Science* 191:347-352.

Friedman, I., and R. L. Smith
1955 Water and Other Volatiles in Volcanic Glasses. *American Mineralogist* 40:1071-1089.

1958 The deuterium content of water in some volcanic glasses. *Geochimica et Cosmochimica Acta* 15:218-228.

1960 A New Dating Method Using Obsidian: Part 1, The Development of the Method. *American Antiquity* 25:476-493.

Friedman, I., and F. W. Trembour
1978 Obsidian: The Dating Stone. *American Scientist* 66:44-51.

1983 Obsidian Hydration Dating Update. *American Antiquity* 48(3):544-547.

Friedman, I., W. Long, and R. L. Smith
1963 Viscosity and Water Content of Rhyolitic Glass. *Journal of Geophysical Research* 68(24):6523-6535.

Friedman, I., R. L. Smith, and W. D. Long
1966 Hydration of Natural Glass and Formation of Perlite. *Geological Society of America Bulletin* 77:323-328.

Friedman, I., F. W. Trembour, and R. E. Hughes
1997 Obsidian Hydration Dating. In *Chronometric Dating in Archaeology*, edited by R. E. Taylor and M. J. Aitken, pp. 297-321. Advances in Archaeological and Museum Science. vol. 2, M. J. Aitken, E. V. Sayre, and R. E. Taylor, general editor. Plenum Press, New York.

Friedman, I., F. W. Trembour, F. L. Smith, and G. I. Smith
1994 Is Obsidian Hydration Dating Affected by Relative Humidity? *Quaternary Research* 41:185-190.

Gardner, J. N., and F. Goff
1996 Geology of the Northern Valles Caldera and Toledo Embayment, New Mexico. In *New Mexico Geological Society Handbook, 47th Field Conference, Jemez Mountains Region*, edited by F. Goff, B. S. Kues, M. A. Rogers, L. D. McFadden and J. N. Gardner, pp. 225-230. New Mexico Geological Society.

Gardner, J. N., F. Goff, S. Garcia, and R. C. Hagan
1986 Stratigraphic Relations and Lithologic Variation in the Jemez Volcanic Field. *Journal of Geophysical Research* 91(B2):1763-1778.

Glascock, M. D., G. E. Braswell, and R. H. Cobean
1998 A Systematic Approach to Obsidian Source Characterization. In *Archaeological Obsidian Studies: Method and Theory*, edited by M. S. Shackley, pp. 15-65. Plenum Press, New York.

Glascock, M. D., R. Kunselman, and D. Wolfman
1999 Intrasource Chemical Differentiation of Obsidian in the Jemez Mountains

and Taos Plateau, New Mexico. *Journal of Archaeological Science* 26:861-868.

Goeksu, H. Y.
1991 Obsidian Hydration Dating. In *Scientific Dating Methods*, edited by H. Y. Goeksu, M. Oberhofer, and D. Regulla, pp. 301-317. Advanced Scientific Techniques. vol. 1. Kluwer Academic Publishers, Dordrecht, The Netherlands.

Goff, F., J. N. Gardner, and S. L. Reneau
2002 Geology of the Frijoles 7.5-minute Quadrangle, Los Alamos and Sandoval Counties, New Mexico. Open-file Digital Geologic Map OF-GM 42, 1:24,000. New Mexico Bureau of Geology and Mineral Resources.

Goff, F., J. N. Gardner, and G. Valentine
1990 Geology of the St. Peter's Dome area, Jemez Mountains, New Mexico. Geologic Map 69, 1:24,000. New Mexico Bureau of Mines and Mineral Resources.

Goff, F., G. Heiken, S. Tamanyu, J. N. Gardner, S. Self, R. Drake, and M. Shafiqullah
1984 Location of the Toledo Caldera and Formation of the Toledo Embayment. *EOS Transactions, American Geophysical Union* 65:1145.

Goffer, Z.
1980 *Archaeological Chemistry: A Sourcebook on the Applications of Chemistry to Archaeology*. Chemical Analysis 55. John Wiley and Sons, Inc.

Goren-Unbar, N., N. Alperson, M. E. Kislev, O. Simchoni, Y. Melamed, A. Ben-Nun, and E. Werker
2004 Evidence of Hominin Control of Fire at Gesher Benot Ya'aqov, Israel. *Science* 304(5671):725-727.

Green, D. F., K. Bordwell, R. Hall, and A. Goheen
1997 *Effects of Prescribed Fire on Obsidian Hydration Rates.* Report on file, Warner Mountain Ranger District, Modoc National Forest, Cedarville, California.

Halford, K., and A. S. Halford
2002 The Trench Canyon Prescribed Burn: An Analysis of Fire Effects on Archaeological Resources Within the Sagebrush Steppe Community Type. In *The Effects of Fire and Heat on Obsidian*, edited by J. Loyd, T. M. Origer, and D. A. Fredrickson, pp. 45-67. US DOI, Bureau of Land Management. Cultural Resources Publication, Anthropology-Fire History.

Hall, R. J.
1989 Obsidian Hydration Dates in California. In *Current Directions in California Obsidian Studies*, edited by R. E. Hughes, pp. 31-58. Contributions of the University of California Archaeological Research Facility, No. 48, Berkeley.

Hatch, J. W., J. W. Michels, C. M. Stevenson, B. E. Scheetz, and R. A. Geidel
1990 Hopewell Obsidian Studies: Behavioral Implications of Recent Sourcing and Dating Research. *American Antiquity* 55(3):461-479.

Heiken, G., F. Goff, J. Stix, S. Tamanyu, M. Shafiqullah, S. Garcia, and R. Hagan
1986 Intracaldera Volcanic Activity, Toledo Caldera and Embayment, Jemez Mountains, New Mexico. *Journal of Geophysical Research* 91(B2):1799-1815.

Hughes, R. E.
1982 Age and Exploitation of Obsidian from the Medicine Lake Highland, California. *Journal of Archaeological Science* 9:173-185.

1984 Obsidian Sourcing Studies in the Great Basin: Problems and Prospects. In *Obsidian Studies in the Great Basin*, edited by R. E. Hughes, pp. 1-19. Contributions of the University of California Archaeological Research Facility, No. 45, Berkeley.

1988 The Coso Volcanic Field Reexamined: Implications for Obsidian Sourcing and Hydration Dating. *Geoarchaeology* 3:253-265.

1993 Trace Element Geochemistry of Volcanic Glass from the Obsidian Cliffs Flow, Three Sisters Wilderness, Oregon. Northwest Science 67(3):199-207.

1994 Intrasource Chemical Variability of Artefact-Quality Obsidians from the Casa Diablo Area, California. *Journal of Archaeological Science* 21:263-271.

1998a On Reliability, Validity, and Scale in Obsidian Sourcing Research. In *Unit Issues in Archaeology: Measuring Time, Space, and Material*, edited by A. F. Ramenofsky and A. Steffen, pp. 103-114. Foundations of Archaeological Inquiry, J. M. Skibo, general editor. University of Utah Press, Salt Lake City.

1998b *Geochemical Research Laboratory Letter Report 97-112*. Conducted pursuant to USDA Santa Fe National Forest PO 43-8379-0142.

2004a Appendix C: Geochemical Laboratory Letter Report 2004-3. In *Cultural Resources Data Recovery Program at Selected Archaeological Sites Along the PNM-DOE Pipeline in the Santa Fe National Forest and the Valles Caldera National Preserve, New Mexico*., by A. Schilz, et al. **DRAFT REPORT**: Prepared for Public Service Company of New Mexico (PNM) by LopezGarca Group, Albuquerque.

2004b *Geochemical Research Laboratory Letter Report 2003-69*.

Hughes, R. E., and R. L. Smith
1993 Archaeology, Geology, and Geochemistry in Obsidian Provenance Studies. In *Effects of Scale on Archaeological and Geoscientific Perspectives*, edited by J.

K. Stein, and A. R. Linse, pp. 79-91. Geological Society of America Special Paper 283, Boulder, Colorado.

Hull, K., L.
2001 Reasserting the Utility of Obsidian Hydration Dating: A Temperature-Dependent Empirical Approach to Practical Temporal Resolution with Archaeological Obsidians. *Journal of Archaeological Science* 28:1025-1040.

Ihinger, P. D., and E. M. Stolper
1994 *No title* (data is presented in Ihinger et al. 1994, Table 2, p. 105, but referenced there as "Ihinger and Stolper 1994"). In Analytical Methods for Volatiles in Glass, Chapter 2, *Volatiles in Magma*, edited by M. R. Carroll, and J. R. Holloway, pp. 67-121. Reviews in Mineralogy. vol. 30, P. H. Ribbe, general editor. Mineralogical Society of America, Washington D. C.

Ihinger, P. D., R. L. Hervig, and P. F. McMillan
1994 Analytical Methods for Volatiles in Glass. In *Volatiles in Magma*, edited by M. R. Carroll and J. R. Holloway, pp. 67-121. Reviews in Mineralogy. vol. 30, P. H. Ribbe, general editor. Mineralogical Society of America, Washington D. C.

Jackson, R.
1984 Current Problems in Obsidian Hydration Analysis. In *Obsidian Studies in the Great Basin*, edited by R. E. Hughes, pp. 103-116. Contributions of the University of California Archaeological Research Facility, No. 45, Berkeley.

Jackson, T. L.
1986 *Late Prehistoric Obsidian Exchange in Central California*. Unpublished Ph.D. Dissertation, Department of Anthropology, Stanford University.

Jones, T.
2002 The Effect of Heat on Obsidian Density. In *The Effects of Fire and Heat on Obsidian*, edited by J. Loyd, T. M. Origer and D. A. Fredrickson, pp. 113-116. Cultural Resources Publication, Anthropology-Fire History. US DOI, Bureau of Land Management.

Justet, L.
1996 *The Geochronology and Geochemistry of the Bearhead Rhyolite, Jemez Volcanic Field, New Mexico.* Unpublished M.S. Thesis, Department of Geoscience, University of Nevada, Las Vegas.

Justet, L., and T. J. Spell
2001 Effusive eruptions from a large silicic magma chamber: the Bearhead Rhyolite, Jemez volcanic field, NM. *Journal of Volcanology and Geothermal Research* 107:241-264.

Kelly, R.

2002 An Overview of Obsidian Studies within Western United States Parks. In *The Effects of Fire and Heat on Obsidian*, edited by J. Loyd, T. M. Origer, and D. A. Fredrickson, pp. 11-14. Cultural Resources Publication, Anthropology-Fire History. US DOI, Bureau of Land Management.

Kimberlin, J.
1976 Obsidian Hydration Rate Determinations on Chemically Characterized Samples. In *Advances in Obsidian Glass Studies*, edited by R. E. Taylor, pp. 63-80. Noyes Press, Park Ridge, New Jersey.

King, P. L., T. W. Venneman, J. R. Holloway, R. L. Hervig, J. B. Lowenstern, and J. F. Forneris
2002 Analytical techniques for volatiles: A case study using intermediate (andesitic) glasses. *American Mineralogist* 87(1077-1089).

Klug, C.
1997 *Vesiculation and Fragmentation of Silicic Magma as Recorded in Volcanic Pumice.* Unpublished PhD Dissertation, Department of Geosciences, Princeton University.

Kuhn, T. S.
1970 *The Structure of Scientific Revolutions*. 2nd ed., enlarged. The University of Chicago.

Larson, T. K., D. M. Penny, R. G. Hilman, and P. H. Sanders
1988 *A Data Recovery Program for Sites in the Dome Unit, Santa Fe National Forest*. Larson-Tibesar Associates. Submitted to USDA Forest Service, Santa Fe National Forest Report 1982-10-011K. Copies available from SFNF Supervisor's Office, Santa Fe.

Layton, T. N.
1973 Temporal Ordering of Surface-Collected Obsidian Artifacts by Hydration Measurement. *Archaeometry* 15:129-132.

Lentz, S. C.
1996 Lithic Artifact Analysis. In *Fire Effects on Archaeological Resources, Phase 1: The Henry Fire, Jemez Mountains, New Mexico*, edited by S. C. Lentz, J. K. Gaunt, and A. Willmer, pp. 65-73. Rocky Mountain Forest and Range Experiment Station, General Technical Report, RM-GTR-273, Fort Collins, CO.

Lentz, S. C., J. K. Gaunt, and A. Willmer
1996 *Fire Effects on Archaeological Resources, Phase 1: The Henry Fire, Jemez Mountains, New Mexico*. Rocky Mountain Forest and Range Experiment Station, General Technical Report, RM-GTR-273.

LeTourneau, P. D.

2000 Folsom Toolstone Procurement in the Southwest and Southern Plains. Unpublished Ph.D. Dissertation, Department of Anthropology, University of New Mexico.

LeTourneau, P. D., and A. Steffen
2002 Field Investigations at a Likely Source for New Mexico Obsidian Folsom Artifacts. *Current Research on the Pleistocene* 19:57-59.

LeTourneau, P. D., S. Aby, and R. Kunselman
1997 Lithic Resources of the Jemez Mountains. In *OLE, Volume II: Artifacts*, edited by J. C. Acklen, pp. 1-29. Public Service Company of New Mexico.

Linderman, C.
1991 The Effects of Fire on Obsidian Artifacts, 1989 Regional Forester's Challenge Grant Study. McKenzie Ranger District, Willamette National Forest, McKenzie Bridge, OR.

1992 *The Effects of Fire on Prehistoric Lithic Sites: A Problem in Obsidian Hydration Dating in a Woodland Environment*. Senior Honors Paper, Department of Anthropology, University of Oregon, Eugene.

Liritzis, I., and M. Diakostamatiou
2002 Toward a New Method of Obsidian Hydration Dating with Secondary Ion Mass Spectrometry via a Surface Saturation Approach. *Journal of Mediterranean Archaeology and Archaeometry* 2(1):3-20.

Liritzis, I., M. Diakostamatiou, C. M. Stevenson, and I. Abdelrehim
2004 Dating of Hydrated Surfaces by SIM-SS. *Journal of Radioanalytical and Nuclear Chemistry* 261(1):51-60.

Loyd, J.
1999 Abstracts and Annotations of Reports and Publications. *International Association for Obsidian Studies Bulletin* 23(Winter):3-5.

2002 Rehydration of Burned Obsidian. In *The Effects of Fire and Heat on Obsidian*, edited by J. Loyd, T. M. Origer, and D. A. Fredrickson, pp. 135-140. Cultural Resources Publication, Anthropology-Fire History. US DOI, Bureau of Land Management.

Loyd, J. M., T. M. Origer, and D. A. Fredrickson (editors)
2002 *The Effects of Fire and Heat on Obsidian*. Cultural Resources Publication, Anthropology-Fire History. US DOI, Bureau of Land Management.

Macdonald, R., R. L. Smith, and J. E. Thomas
1992 *Chemistry of the Subalkalic Silicic Obsidians*. Professional Paper 1523. U. S. Geological Survey, Washington D. C.

Mazer, J. J., C. M. Stevenson, W. L. Ebert, and J. K. Bates
1991 The Experimental Hydration of Obsidian as a Function of Relative Humidity and Temperature. *American Antiquity* 56(3):504-513.

McMillan, P. F.
1994 Water Solubility and Speciation Models. In *Volatiles in Magma*, edited by M. R. Carroll and J. R. Holloway, pp. 131-156. Reviews in Mineralogy. vol. 30, P. H. Ribbe, general editor. Mineralogical Society of America, Washington D. C.

Michels, J. W., and I. S. T. Tsong
1980 Obsidian Hydration Dating: A Coming of Age. In *Advances in Archaeological Method and Theory*, edited by M. B. Schiffer, pp. 405-444. vol. 3. Academic Press, New York.

Mitchell, S. G., and P. W. Reiners
2003 Influence of wildfires on apatite and zircon (U-Th)/He ages. *Geology* 31(12):1025-1028.

Moore, G., A. Chizmeshya, and P. F. McMillan
2000 Calibration of a reflectance FTIR method for determination of dissolved CO_2 concentration in rhyolitic glasses. *Geochimica et Cosmochimica Acta* 64(20):3571-3579.

Moore, R. A.
1987 *The Santa Fe National Forest Dome Unit Mitigation Project: Testing and Evaluation of Sites 03-1163, 03-1171, 03-1172 for the Santa Fe National Forest*. Division of Conservation Archaeology, Studies in Archaeology No. 4, San Juan County Archaeological Research Center and Library. Submitted to USDA Forest Service, Santa Fe National Forest Report 1982-10-011I. Copies available from SFNF Supervisor's Office, Santa Fe.

Muceus, C.
1982 *Dome Unit Timber Sales Mitigation Research*. USDA Forest Service, Santa Fe National Forest Report 1982-10-011B. Copies available from SFNF, Supervisor's Office, Santa Fe.

NMBGMR
2000 Satellite Map of New Mexico. Resource Map 23,1:500,000. New Mexico Bureau of Geological and Mineral Resources.

Nakazawa, Y.
1998 Thermal Alteration of Obsidian Flakes and Its Archaeological Implications. Unpublished Master's Thesis (in English), Hokkaido University.

2002 An Experimental Examination for Detecting Thermal Traits on Obsidian

Artifacts. In *The Effects of Fire and Heat on Obsidian*, edited by J. M. Loyd, T. M. Origer, and D. A. Fredrickson, pp. 203-219. US DOI, Bureau of Land Management. Cultural Resources Publication, Anthropology-Fire History.

National Park Service
1996 *Dome Fire Burned Area Rehabilitation (BAER) Plan*. Department of the Interior, Northern States, Burned Area Rehabilitation Team, May 19, 1996.

Newman, J. R., and R. L. Nielsen
1985 Initial Notes on the X-ray Fluorescence Sourcing of Northern New Mexico Obsidians. *Journal of Field Archaeology* 12:377-383.

Newman, S., S. Epstein, and E. M. Stolper
1988 Water, Carbon Dioxide, and Hydrogen Isotopes in Glasses from the ca. 1340 A.D. Eruptions of the Mono Craters, California: Constraints on Degassing Phenomena and Initial Volatile Content. *Journal of Volcanology and Geothermal Research* 35:75-96.

Newman, S., E. M. Stolper, and S. Epstein
1985 Variations in Hydrogen Isotopic Ratios of Obsidians Erupted 1400 A.D. at Mono Craters, California. *EOS* 66:391.

1986 Measurement of water in rhyolitic glasses: Calibration of an infrared spectroscopic technique. *American Mineralogist* 71:1527-1541.

O'Neil, J. R., and B. E. Taylor
1985 Degassing of Obsidian Dome Magma: Hydrogen and Oxygen Isotope Studies in the Inyo Dome Chain, Long Valley Area, California. *EOS* 66:387.

Origer, T. M.
1996 Obsidian Hydration. In *Fire Effects on Archaeological Resources, Phase 1: The Henry Fire, Jemez Mountains, New Mexico*, edited by S. C. Lentz, J. K. Gaunt, and A. Willmer, pp. 81-83. Rocky Mountain Forest and Range Experiment Station, General Technical Report, RM-GTR-273.

Origer, T. M., and J. Anderson
1994 Preliminary Results on an Assessment of the Effects of Fire on Obsidian Specimens from CA-SON-48, Salt Point State Park, Sonoma County, California. *International Association for Obsidian Studies Bulletin* 12.

Picha, P. R., S. A. Ahler, R. D. Sayler, and R. W. Seabloom
1991 Effects of Prairie Fire on Selected Artifact Classes. *Archaeology in Montana* 32(2):15-28.

Pollard, A. M., and C. Heron
1996 *Archaeological Chemistry*. The Royal Society of Chemistry, Cambridge,

UK.

Purdy, B. A.
1975 Fractures for the Archaeologist. In *Lithic Technology: Making and Using Stone Tools*, edited by E. Swanson, pp. 133-141. Mouton Publishers, The Hague.

1974 Investigations Concerning the Thermal Alteration of Silica Minerals: An Archaeological Approach. *Tebiwa* 17:37-66.

Purdy, B. A., and H. K. Brooks
1971 Thermal Alteration of Silica Materials: An Archaeological Approach. *Science* 173:322-325.

Ramenofsky, A. F., and A. Steffen
1998 Units as Tools of Measurement. In *Unit Issues in Archaeology: Measuring Time, Space, and Material*, edited by A. F. Ramenofsky and A. Steffen, pp. 3-17. Foundations of Archaeological Inquiry, J. M. Skibo, general editor. University of Utah Press, Salt Lake City.

Riciputi, L. R., J. M. Elam, L. M. Anovitz, and D. R. Cole
2002 Obsidian Diffusion Dating by Secondary Ion Mass Spectrometry: A Test Using Results from Mound 65, Chalco, Mexico. *Journal of Archaeological Science* 29:1055-1075.

Ridings, R.
1991 Obsidian Hydration Dating: The Effects of Mean Exponential Ground Temperature and Depth of Artifact Recovery. *Journal of Field Archaeology* 18:77-85.

1996 Where in the World Does Obsidian Hydration Work? *American Antiquity* 61(1):136-148.

Rosen, S. A., R. H. Tykot, and M. Gottesman
in press Long Distance Trinket Trade: Early Bronze Age Obsidian from the Negev. *Journal of Archaeological Science*.

Ross, C. S., and R. L. Smith
1955 Water and other Volatiles in Volcanic Glasses. *American Mineralogist* 40(11-12):1071-1089.

Ruscavage-Barz, S. M.
1999 Fire in the Hole: The Effects of Fire on Subsurface Archaeological Materials. Ms. in preparation, Bandelier National Monument.

Rust, A. C.
2003 *Viscosity, Deformation and Permeability of Bubbly Magma: Applications*

to Flow and Degassing in Volcanic Conduits. Ph.D. Dissertation, University of Oregon.

Rust, A. C., K. V. Cashman, and P. J. Wallace
2004 Magma Degassing Buffered by Vapor flow Through Brecciated Conduit Margins. *Geology* 32(4):349-352.

SPSS
2002 SPSS for Windows. Release 11.5.0 (6 Sep 2002) ed. SPSS, Inc.

Schiffer, M. B.
1987 *Formation Processes of the Archaeological Record*. University of New Mexico Press, Albuquerque.

1995 *Behavioral Archaeology: First Principles*. University of Utah Press, Salt Lake City.

Schilz, A., H. P. Lawrence, K. Harbour, T. G. Baugh, S. A. Sundermeyer, S. N. DeFreece, C. D. Neel, and G. Smith
2004 *Cultural Resources Data Recovery Program at Selected Archaeological Sites Along the PNM-DOE Pipeline in the Santa Fe National Forest and the Valles Caldera National Preserve, New Mexico*. **DRAFT REPORT**: Prepared for Public Service Company of New Mexico (PNM) by LopezGarca Group, Albuquerque.

Schroder, S.
2002 A Synthesis of Previous Studies that Explored the Effects of Fire on Obsidian: Where We've Been and Where We're Going. In *The Effects of Fire and Heat on Obsidian*, edited by J. Loyd, T. M. Origer, and D. A. Fredrickson, pp. 5-9. Cultural Resources Publication, Anthropology-Fire History. US DOI, Bureau of Land Management.

Schub, L. C., and M. L. Elliott
1998 Appendix B. Dome Fire Cultural Resource Damage Assessment and Treatment Project - 1996 Progress Report. In *1996 Dome Fire Emergency Fire Rehabilitation: A Draft Report*, edited by C. Sydoriak, E. Matic, M. L. Elliott, and E. Ruby. Bandelier National Monument.

Self, S., F. Goff, J. N. Gardner, J. V. Wright, and W. M. Kite
1986 Explosive Rhyolitic Volcanism in the Jemez Mountains: Vent Locations, Caldera Development and Relation to Regional Structure. *Journal of Geophysical Research* 91(B2):1779-1798.

Shackley, M. S.
2002 Unpublished website: http://obsidian.pahma.berkely.edu (with date of last revision: March 12, 2004).

Shackley, M. S., and C. Dillian
2002 Thermal and Environmental Effects on Obsidian Geochemistry: Experimental and Archaeological Evidence. In *The Effects of Fire/Heat on Obsidian*, edited by J. M. Loyd, T. M. Origer, and D. A. Fredrickson, pp. 117-134. Cultural Resources Publication, Anthropology - Fire History. United State Department of Interior, Bureau of Land Management.

Silver, L. A., and E. M. Stolper
1989 Water in Albitic Glasses. *Journal of Petrology* 30:667-709.

Silver, L. A., P. D. Ihinger, and E. M. Stolper
1990 The Influence of Bulk Composition on the Speciation of Water in Silicate Glasses. *Contributions to Mineralogy and Petrology* 104:142-162.

Skinner, C. E., J. J. Thatcher, and M. K. Davis
1997 *X-Ray Fluorescence Analysis and Obsidian Hydration Rim Measurement of Artifact Obsidian from 35-DS-193 and 35-DS-201, Surveyor Fire Rehabilitation Project, Deschutes National Forest, Oregon*. Northwest Research Obsidian Studies Laboratory Report 96-33.

Smith, L. D.
1984 *Dome Unit Timber Sales Data Recovery Plan*. USDA Forest Service, Santa Fe National Forest Report 1982-10-011C. Copies available from SFNF, Supervisor's Office, Santa Fe.

Smith, R. L., R. A. Bailey, and C. S. Ross
1970 Geologic Map of the Jemez Mountains, New Mexico. Miscellaneous Investigation Series Map I-571, 1:125,000. United States Geological Survey.

Sokal, R. R., and F. J. Rohlf
1970 *Biometry: The Principles and Practice of Statistics in Biological Research, 2nd Edition*. W. H. Freeman and Company, New York.

Solomon, M.
2002 Fire and Glass: Effects of Prescribed Burning on Obsidian Hydration Bands. In *The Effects of Fire and Heat on Obsidian*, edited by J. Loyd, T. M. Origer, and D. A. Fredrickson, pp. 69-93. US DOI, Bureau of Land Management. Cultural Resources Publication, Anthropology-Fire History.

Spell, T. J., P. R. Kyle, and J. Baker
1996 Geochronology and Geochemistry of the Cerro Toledo Rhyolite. In *New Mexico Geological Society Handbook, 47th Field Conference, Jemez Mountains Region*, edited by F. Goff, B. S. Kues, M. A. Rogers, L. D. McFadden and J. N. Gardner, pp. 263-268. New Mexico Geological Society.

Statistica
2001 STATISTICA for Windows. 6.0 ed. StatSoft, Inc., Tulsa, OK; email: info@statsoft.com; http://www.statsoft.com.

Steffen, A.
2002 The Dome Fire Pilot Project: Extreme Obsidian Fire Effects in the Jemez Mountains. In *The Effects of Fire and Heat on Obsidian*, edited by J. Loyd, T. M. Origer, and D. A. Fredrickson, pp. 159-201. Cultural Resources Publication, Anthropology-Fire History. US DOI, Bureau of Land Management.

Stevenson, C. M.
n.d. Unpublished website: http://members.aol.com/obsidlab/index.html.

1994 Appendix 3. Hydration Analysis of Obsidian Artifacts from Sites 60372, 3840, 3852, 50972, 60550. In *Jemez Mountains Chronology Study*, edited by D. Wolfman. Santa Fe National Forest. USDA Forest Service Contract No. 53-8379-9-14.

Stevenson, C. M., and Klimkiewicz
1990 X-ray Fluorescence Analysis of Obsidian Sources in Arizona and New Mexico. *Kiva* 55:235-243.

Stevenson, C. M., and M. O. McCurry
1990 Chemical Characterization and Hydration Rate Development for New Mexico Obsidian Sources. *Geoarchaeology* 5:149-170.

Stevenson, C. M., I. Abdelrehim, and S. W. Novak
2001 Infra-red Photoacoustic and Secondary Ion Mass Spectrometry Measurements of Obsidian Hydration Rims. *Journal of Archaeological Science* 28:109-115.

2004 High Precision Measurement of Obsidian Hydration Layers on Artifacts from the Hopewell Site Using Secondary Ion Mass Spectrometry. *American Antiquity* 69(3):555-568.

Stevenson, C. M., M. Gottesman, and M. Macko
2000 Redefining the Working Assumptions of Obsidian Hydration Dating. *Journal of California and Great Basin Anthropology* 22(2):223-236.

Stevenson, C. M., E. Knaus, J. J. Mazer, and J. K. Bates
1993 Homogeneity of water content in obsidian from the Coso Volcanic Field: Implication for obsidian hydration dating. *Geoarchaeology* 8(5):371-384.

Stevenson, C. M., J. J. Mazer, and B. E. Sheetz
1998 Laboratory Obsidian Hydration Rates: Theory, Method, and Application. In *Archaeological Obsidian Studies: Method and Theory*, edited by M. S.

Shackley, pp. 181-204. Advances in Archaeological and Museum Science, Vol. 3, M. J. Aitken, E. V. Sayre, and R. E. Taylor, general editors. Plenum Press, New York.

Stevenson, C. M., P. J. Sheppard, D. G. Sutton, and W. R. Ambrose
1996 Advances in Hydration Dating of New Zealand Obsidian. *Journal of Archaeological Science* 23:233-242.

Stevenson, R. J., N. S. Bagdassarov, and C. Romano
1997 Vesiculation processes in a water-rich calc-alkaline obsidian. *Earth and Planetary Science Letters* 146:555-571.

Stix, J., F. Goff, M. P. Gorton, G. Heiken, and S. R. Garcia
1988 Restoration of Compositional Zonation in the Bandelier Silicic Magma Chamber Between Two Caldera-Forming Eruptions: Geochemistry and Origin of the Cerro Toledo Rhyolite, Jemez Mountains, New Mexico. *Journal of Geophysical Research* 93(B6):6129-6147.

Stolper, E. M.
1982 Water in Silicate Glasses: An Infrared Spectroscopic Study. *Contributions to Mineralogy and Petrology* 81:1-17.

Swetnam, T. W., and C. H. Baisan
1996 Historical Fire Regime patterns in the Southwestern United States Since SD 1700. In *Fire Effects in Southwestern Forests: Proceedings of the Second La Mesa Fire Symposium*, edited by C. D. Allen, pp. 11-32. General Technical Report RM-GTR-286. USDA Forest Service, Rocky Mountain Forest and Range Experimental Station, Fort Collins, Colorado.

Taylor, B. E., J. C. Eichelberger, and H. R. Westrich
1983 Hydrogen Isotopic Evidence of Rhyolitic Magma Degassing During Shallow Intrusion and Eruption. *Nature* 306:541-545.

Touchan, R., C. D. Allen, and T. W. Swetnam
1996 Fire History and Climatic Patterns in Ponderosa Pine and Mixed-Conifer Forests of the Jemez Mountains, Northern New Mexico. In *Fire Effects in Southwestern Forests: Proceedings of the Second La Mesa Fire Symposium*, edited by C. D. Allen, pp. 33-46. General Technical Report RM-GTR-286. USDA Forest Service, Rocky Mountain Forest and Range Experimental Station, Fort Collins, Colorado.

Traylor, D., L. Hubbell, N. Wood, and B. Fiedler
1979 *The 1977 La Mesa Fire Study: An Investigation of Fire and Fire Suppression Impact on Cultural Resources in Bandelier National Monument*. Submitted by F. Broilo, P. I., Office of Contract Archaeology, to the National Park Service, Southwest Cultural Resources Center, Santa Fe, New Mexico.

1990 *The 1977 La Mesa Fire Study: An Investigation of Fire and Fire Suppression Impact on Cultural Resources in Bandelier National Monument*. Southwest Cultural Resources Center Professional Paper No. 28.

Tremaine, K. J., and D. A. Fredrickson
1988 Induced Obsidian Hydration Experiments: An Investigation in Relative Dating. *Materials Research Society Symposium Proceedings* 123:271-278.

Trembour, F. W.
1979 *Appendix F. A Hydration Study of Obsidian Artifacts, Burnt vs. Unburnt by the La Mesa Fire*, The 1977 La Mesa Fire Study: An Investigation of Fire and Fire Suppression Impact on Cultural Resources in Bandelier National Monument, edited by D. Traylor, L. Hubbell, N. Wood, and B. Fiedler. Submitted by F. Broilo, P. I., Office of Contract Archaeology, to the National Park Service, Southwest Cultural Resources Center, Santa Fe, New Mexico.

1990 Appendix F. A Hydration Study of Obsidian Artifacts, Burnt vs. Unburnt by the La Mesa Fire. In *The 1977 La Mesa Fire Study: An Investigation of Fire and Fire Suppression Impact on Cultural Resources in Bandelier National Monument*, edited by D. Traylor, L. Hubbell, N. Wood, and B. Fiedler, pp. 174-190. Southwest Cultural Resources Center Professional Paper No. 28.

Trembour, F. W., and I. Friedman
1984 Obsidian Hydration Dating and Field Site Temperature. In *Obsidian Studies in the Great Basin*, edited by R. E. Hughes. Contributions of University of California Research Facility, No. 45.

Tsirk, A.
2005 Personal communication: correspondence in possession of the author.

2003 *Obsidian Fractures from a Forest Fire Zone in Santa Fe National Forest*. Report No. 020607, submitted to A. Steffen, Santa Fe National Forest and University of New Mexico. Unpublished ms. in possession of the author.

Vale, T. R. (editor)
2002 *Fire, Native Peoples, and the Natural Landscape*. Island Press, Washington D.C.

Vierra, B. J.
1993 Part 2. Explaining Long-Term Change in Lithic Procurement and Reduction Strategies (Chapters 6-10). In *Across the Colorado Plateau: Anthropological Studies for the Transwestern Pipeline Expansion Project*, edited by B. J. Vierra, T. W. Burchett, K. L. Brown, M. E. Brown, P. T. Kay and C. J. Phagan, pp. 141-381. vol. XVII. Office of Contract Archaeology and Maxwell Museum, University of New Mexico, Albuquerque.

Westrich, H. R.
1987 Determination of Water in Volcanic Glasses by Karl-Fischer Titration. *Chemical Geology* 63:335-340.

White, W. B.
1988 Glass Hydration Mechanisms with Application to Obsidian Hydration Dating. In *Materials Research Society Symposium Proceedings, Vol. 123*, edited by E. V. Sayre, P. Vandiver, J. Druzik, and C. M. Stevenson, pp. 225-236. Materials Research Society, Pittsburgh.

Winter, J. D.
2001 *An Introduction to Igneous and Metamorphic Petrology*. Prentice-Hall, New Jersey.

Yokelson, R. J., R. Susott, D. E. Ward, J. Reardon, and D. W. T. Griffith
1997 Emissions from Smoldering Combustion of Biomass Measured by Open-Path Fourier Transform Infrared Spectroscopy. *Journal of Geophysical Research* 102(D15):18,865-18,877.

Zhang, Y., and H. Behrens
2000 H_2O Diffusion in Rhyolitic Melts and Glasses. *Chemical Geology* 169:243-262.

Zhang, Y., E. M. Stolper, and G. J. Wasserburg
1991 Diffusion of Water in Rhyolitic Glasses. *Geochimica et Cosmochimica* Acta 55:441-456.

Zhang, Y., R. Belcher, P. D. Ihinger, L. Wang, Z. Xu, and S. Newman
1997 New calibration of infrared measurement of dissolved water in rhyolitic glasses. *Geochimica et Cosmochimica Acta* 61(15):3089-3100.